

Paine, Kevin Andrew (1998) Steel fibre reinforced concrete for prestressed hollow core slabs. PhD thesis, University of Nottingham.

**Access from the University of Nottingham repository:**

<http://eprints.nottingham.ac.uk/11095/1/287190.pdf>

**Copyright and reuse:**

The Nottingham ePrints service makes this work by researchers of the University of Nottingham available open access under the following conditions.

This article is made available under the University of Nottingham End User licence and may be reused according to the conditions of the licence. For more details see:  
[http://eprints.nottingham.ac.uk/end\\_user\\_agreement.pdf](http://eprints.nottingham.ac.uk/end_user_agreement.pdf)

**A note on versions:**

The version presented here may differ from the published version or from the version of record. If you wish to cite this item you are advised to consult the publisher's version. Please see the repository url above for details on accessing the published version and note that access may require a subscription.

For more information, please contact [eprints@nottingham.ac.uk](mailto:eprints@nottingham.ac.uk)

**UNIVERSITY OF NOTTINGHAM**



**STEEL FIBRE REINFORCED CONCRETE  
FOR PRESTRESSED HOLLOW CORE SLABS**

by

**Kevin Andrew Paine, B.Eng**

**September 1998**

**Thesis submitted to the University of Nottingham for the degree of  
Doctor of Philosophy**

**SCHOOL OF CIVIL ENGINEERING**

## ABSTRACT

An investigation of prestressed concrete containing steel fibres as secondary reinforcement to improve performance in shear, flexure and bond is reported. Emphasis is placed on the use of steel fibres in prestressed extruded hollow core slabs, since these common precast elements have intrinsic difficulty in incorporating traditional secondary reinforcement due to their unique shape and manufacturing method.

Two separate studies were carried out. The first study involved laboratory investigations into the bond between fibre reinforced concrete (FRC) and the prestressing strand, and the shear behaviour of laboratory-cast prestressed fibre reinforced concrete (PFRC) beams. The second part involved the factory production of fibre reinforced hollow core slabs in co-operation with a local manufacturer. The fibre reinforced hollow core slabs were subjected to conventional full-width shear tests, concentrated load shear tests, and to transverse flexure. For all laboratory cast elements, cubes, cylinders and prisms were cast to investigate compressive, tensile and flexural properties, respectively. Two types of steel fibre were investigated: hooked-end steel fibres at fibre volume fractions ( $V_f$ ) of 0.5%, 1.0% and 1.5%; and amorphous metal fibres at  $V_f$ 's of 0.28% and 0.56%.

The trial production of fibre reinforced hollow core slabs necessitated the investigation of the effect of steel fibres on the extrusion manufacturing process. It was shown that fibre reinforced hollow core slabs could be adequately compacted with only slight increases in mixing water. Fibres were found to distribute randomly throughout the cross-section. However, the rotation of the augers affected the orientation of fibres, with fibres tending to align vertically in the web.

It was shown that the addition of steel fibres to prestressed concrete has a negative effect on the bond between matrix and tendon, leading to longer transfer lengths. The effect of the increase in transfer length was to reduce cracking shear strengths by 4%. Shear tests showed that the incorporation of steel fibres could increase shear strength by as much as 45% for  $V_f = 1.5\%$ . This increase in shear strength, known as the fibre contribution, was shown to be due to fibres bridging across the crack and an increased compressive resistance due to fibres arresting the propagation of cracks into the compressive zone.

A semi-empirical equation for shear strength of PFRC elements is developed. It is given in two forms, one compatible with the present equations for prestressed concrete given in BS 8110 and Eurocode 2, and a second form compatible with that advocated for fibres in reinforced concrete. The equation makes use of equivalent flexural strength which is recognised as the most useful material property for design of FRC. The equation was found to give good correlation with the shear strength of single web beams cast both in the laboratory and under factory conditions. However, a overall strength reduction factor is required for full-width hollow core slabs to account for uneven load distribution and inconsistent web widths. This is consistent with tests on plain hollow core slabs found in the literature.

# PUBLICATIONS

Parts of the results from this study have been published :-

1. Peaston, C.H., Elliott, K.S., & Paine, K.A., "Steel Fibres in Extruded Precast Concrete Hollow Core Flooring," Nottingham University - Osaka University Joint Symposium. New Frontiers in Materials Science and Related Engineering Applications, Nottingham, 7-8 September 1995.
2. Paine, K.A., "Trial Production of Fibre Reinforced Hollow Core Slab," *Research Report SR96007*, Department of Civil Engineering, University of Nottingham, 1996, 38 pp
3. Peaston, C.H., Elliott, K.S., & Paine, K.A., "Steel Fibre Reinforcement for Extruded Prestressed Hollow Core Slabs," Paper presented at the ACI Spring Convention, Seattle, Washington, USA, 5-10 April 1997. To be published in ACI special publication - Structural Applications of FRC
4. Paine, K.A., Elliott, K.S., & Peaston, C.H., "Increasing the Shear Strength and Ductility of Prestressed Hollow Core Slabs using Metal Fibres," The 4th International Symposium on Noteworthy Developments in Prestressing and Precasting, Singapore, 3-4 July 1997, pp 116-124

# ACKNOWLEDGEMENTS

I gratefully acknowledge all the support, encouragement and assistance given throughout this work by my supervisors Dr. Chris Peaston and Dr. Kim Elliott; for this my sincere thanks.

I also wish to thank each of the technicians, Charlie Lambert, Bal Loyla, Geoff Mitchell, Melvyn Ridal and Brian Whitehouse, and Mike Bettison (Experimental Officer) for all their assistance with the experimental work.

This work would not have been possible without the generous support of Richard Lees Ltd. who manufactured all of the hollow core slabs used in the testing free of charge. My sincere thanks go to all the work force, and in particular to Geoff Bailey (Technical Manager) for organising the trials and for much valuable discussion.

I must also offer my many thanks to Dirk Nemegeer and John Greenhalgh (N.V. Bekaert), and Jean-Marc Boucharet (Seva) for supplying all the fibres used in this work free of charge.

Likewise, I must thank David Johnson (Pozament Ltd.) and Les Hodgkinson (W.R.Grace Ltd., Cormix Division) for their generous free supplies of silica fume and superplasticizer, respectively.

On a different note, I would to like thank all my friends in Nottingham for all their support, and in particular I wish to thank Nicol for her never-ending encouragement. Special thanks also to Jackie and Mat.

Finally, but certainly not least, thanks to my parents for all their support and love.

# DECLARATION

I declare that this thesis is the result of my own work. No part of this thesis has been submitted to any other University or other educational establishment for a Degree, Diploma or other qualification (except for publication)

A handwritten signature in black ink, appearing to read 'K. Paine', is written above a horizontal line.

(Kevin Paine)

# NOTATION

## Roman upper case letters

$A_c$	Concrete area
$A_p$	Cross-sectional area of prestressing strand
✓ $E_f$	Youngs modulus of fibre
✓ $E_m$	Youngs modulus of matrix
$E_s$	Youngs modulus of steel
$F$	Fibre factor
✓ $I$	Second-moment of area
✓ $I_5, I_{10}, I_{20}$	ASTM toughness indices
$P$	Prestressing force
$R_{0.3-1.0}$	Ratio of average load between 0.3mm and 1mm deflection and cracking load
$R_{1.0-2.0}$	Ratio of average load between 1mm and 2mm deflection and cracking load
$R_{5,10}$	ASTM C1018 residual strength factor, $20(I_{10}-I_5)$
$R_{10,20}$	ASTM C1018 residual strength factor, $20(I_{20}-I_{10})$
$V_b$	Fibre contribution to shear capacity
$V_c$	Concrete contribution to shear capacity
$V_{co}$	Theoretical shear capacity of plain prestressed concrete failing in flexurally uncracked region
$V_{cou}$	Theoretical shear capacity of PFRC failing in flexurally uncracked region
$V_{cr}$	Cracking shear capacity
✓ $V_f$	Fibre volume fraction
✓ $V_{f,crit}$	Critical fibre volume fraction
$V_{ult}$	Ultimate shear capacity
$W_{cr}$	Cracking load
$W_{ult}$	Ultimate load
$Z_b$	Section modulus (bottom)
$Z_t$	Section modulus (top)

## Roman lower case letters

a	shear span
b	beam width
$b_w$	web width
c	strand/wire slip
d	effective depth
$d_f$	fibre diameter
$f_b$	compressive strength at bottom of section due to prestress
$f_c'$	cylinder compressive strength
$f_{ci}$	initial cube compressive strength (at release of prestress)
$f_{cr,sp}$	cracking splitting tensile strength
✓ $f_{ct}$	concrete tensile strength
$f_{ct,sp}$	ultimate splitting tensile strength
✓ $f_{cu}$	cube compressive strength
✓ $f_{fl,cr}$	cracking flexural tensile strength
$f_{fl,eq,150}$	equivalent flexural tensile strength upto span/150
$f_{fl,eq,300}$	equivalent flexural tensile strength upto span/300
✓ $f_{fl,ult}$	ultimate flexural tensile strength
$f_{fu}$	ultimate tensile strength of fibre
$f_{pu}$	ultimate tensile strength of prestressing strand
$f_t$	compressive strength at top of section due to prestress
h	height of section
$l_{crit}$	critical fibre length
$l_d$	development length of prestressing strand/wire
✓ $l_f$	fibre length
$l_s$	bearing length
$l_t$	transfer length of prestressing strand/wire
r	ratio of fibre cross-section to fibre perimeter
w	crack width
x	depth to neutral axis
z	moment lever arm



## **Greek lower case letters**

✓ $\delta$	deflection
$\delta_i$	initial strand/wire slip
$\phi$	diameter of prestressing wire/strand
$\eta_b$	fibre bond factor
$\eta_l$	fibre length factor
✓ $\eta_\theta$	fibre orientation factor
$\lambda_f$	fibre aspect ratio
$\sigma_{cp}$	effective prestress at centroid of section
$\sigma_{cpx}$	effective prestress at centroid of section within transfer length
$\sigma_p$	effective prestress in steel (after all losses)
$\sigma_{pi}$	initial prestress in steel
$\sigma_{ps}$	fibre prestress due to matrix-fibre load sharing
$\sigma_{tu}$	post-cracking fibre bridging strength
$\tau_f$	fibre-matrix interfacial bond strength

# CONTENTS

ABSTRACT.....	ii
PUBLICATIONS.....	iii
ACKNOWLEDGEMENTS.....	iv
DECLARATION .....	v
NOTATION.....	vi

## CHAPTER 1 INTRODUCTION

1.1 Introduction.....	1
1.2 Fibres for prestressed hollow core slabs .....	3
<i>1.2.1 Prestressed hollow core slabs</i> .....	3
<i>1.2.2 Possible benefits of using fibres in hollow core slabs</i> .....	5
1.3 Types of steel fibre.....	6
<i>1.3.1 Hooked-end steel fibres</i> .....	7
<i>1.3.2 Amorphous metal fibres</i> .....	7
1.4 Objectives of research.....	8
1.5 Methodology.....	9A
1.6 Notation .....	9D
1.7 Layout of thesis.....	9E

## CHAPTER 2 MATERIAL CHARACTERISTICS OF FRC

2.1 Introduction.....	16
<i>2.1.1 Orientation</i> .....	17
<i>2.1.2 Length efficiency</i> .....	19
<i>2.1.3 Fibre-matrix bond</i> .....	20
2.2 Tension.....	22
<i>2.2.1 General</i> .....	22
<i>2.2.2 Theoretical methods</i> .....	23

2.2.3	<i>Direct measurement of tensile strength</i> .....	27
2.2.4	<i>Indirect measurement of tensile strength</i> .....	28
2.3	Compression .....	32
2.4	Flexure .....	33
2.4.1	<i>Introduction</i> .....	33
2.4.2	<i>Flexural strength</i> .....	33
2.4.3	<i>Energy-based dimensionless indices</i> .....	35
2.4.4	<i>Load-based dimensionless indices</i> .....	36
2.4.5	<i>Energy absorption capacity</i> .....	37
2.4.6	<i>Equivalent flexural strength</i> .....	38
2.4.7	<i>Residual strength</i> .....	38
2.4.8	<i>Specific issues related to flexural toughness</i> .....	39
2.5	Material property based design .....	41

## CHAPTER 3 REVIEW OF HOLLOW CORE SLABS AND PFRC

3.1	Introduction.....	55
3.2	Testing and design of hollow core slabs .....	56
3.2.1	<i>General</i> .....	56
3.2.2	<i>Flexural strength</i> .....	57
3.2.3	<i>Web shear tension failure</i> .....	58
3.2.4	<i>Anchorage failure</i> .....	68
3.3	Testing and design of PFRC elements .....	71
3.3.1	<i>Shear tests on fibre reinforced prestressed hollow core slabs</i> .....	71
3.3.2	<i>Shear tests on PFRC</i> .....	71
3.3.3	<i>Predictive equations for ultimate shear capacity of PFRC beams</i> .....	74
3.3.4	<i>Direct shear</i> .....	80
3.3.5	<i>Flexural testing and design of PFRC</i> .....	85
3.3.6	<i>FRC on bond properties</i> .....	87

## CHAPTER 4 MIX DESIGN AND MATERIAL TESTS ON FRC

4.1 Introduction.....	105
4.2 Pull-out bond test mix.....	106
4.2.1 <i>Materials</i> .....	106
4.2.2 <i>Test specimen and mixing</i> .....	106
4.3 Material test results for pull-out bond test.....	107
4.3.1 <i>Compressive strength</i> .....	107
4.3.2 <i>Splitting tensile strength</i> .....	108
4.3.3 <i>Flexural strength/toughness</i> .....	109
4.4 Shear test mix .....	110
4.4.1 <i>Mix design</i> .....	110
4.4.2 <i>Mixing and placing of concrete</i> .....	112
4.5 Material test results for shear test mix.....	114
4.5.1 <i>Slump</i> .....	114
4.5.2 <i>Compressive strength</i> .....	114
4.5.3 <i>Splitting tensile strength</i> .....	115
4.5.4 <i>Flexural strength/toughness</i> .....	116

## CHAPTER 5 BOND AND SHEAR TESTS ON PFRC

5.1 Introduction.....	131
5.2 Pull-out bond tests .....	131
5.2.1 <i>General</i> .....	131
5.2.2 <i>Test set-up</i> .....	132
5.3 Results of pull-out bond tests .....	133
5.3.1 <i>Axial steel strains</i> .....	133
5.3.2 <i>Loaded-end strand movement</i> .....	134
5.3.3 <i>Remote-end strand movement</i> .....	135
5.3.4 <i>Transfer length</i> .....	135
5.4 Shear tests .....	137

5.4.1 <i>General</i> .....	137
5.4.2 <i>Prestressing</i> .....	138
5.4.3 <i>Testing</i> .....	139
5.5 <i>Results</i> .....	140
5.5.1 <i>Prestress and transfer length</i> .....	140
5.5.2 <i>General behaviour of test beams</i> .....	142
5.5.3 <i>Shear capacity</i> .....	144
5.5.4 <i>Ductility</i> .....	145
5.5.5 <i>Steel strains</i> .....	146
5.5.6 <i>Crack widths</i> .....	148
5.5.7 <i>Wire slip</i> .....	148

## CHAPTER 6 MANUFACTURE OF FIBRE REINFORCED HOLLOW CORE SLAB

6.1 <i>Introduction</i> .....	182
6.2 <i>Laboratory Investigation</i> .....	183
6.2.1 <i>Plain mix</i> .....	183
6.2.2 <i>FRC mix</i> .....	183
6.3 <i>Trial Production of FRC hollow core slabs</i> .....	185
6.3.1 <i>General</i> .....	185
6.3.2 <i>Mixing procedure</i> .....	186
6.3.3 <i>Extrusion</i> .....	186
6.4 <i>Production of FRC hollow core slabs</i> .....	187
6.5 <i>Fibre distribution</i> .....	188
6.5.1 <i>Wash-out tests</i> .....	188
6.5.2 <i>Crushed cores</i> .....	189
6.6 <i>Fibre orientation</i> .....	190
6.6.1 <i>Method</i> .....	190
6.6.2 <i>Results and discussion</i> .....	192
6.7 <i>Concrete density of slabs</i> .....	194

## CHAPTER 7 TESTING OF FIBRE REINFORCED HOLLOW CORE SLABS

7.1 Introduction.....	209
7.2 Shear tests on full width hollow core slabs.....	210
7.2.1 Test set-up.....	210
7.2.2 General behaviour of test specimens.....	211
7.2.3 Shear capacity .....	213
7.2.4 Ductility .....	214
7.2.5 Crack widths .....	214
7.2.6 Wire slip.....	215
7.3 Factory Produced x-beam tests .....	215
7.3.1 Test set-up.....	215
7.3.2 General behaviour of test beams .....	216
7.3.3 Flexural capacity.....	217
7.3.4 Shear capacity .....	218
7.3.5 Strand slip.....	219
7.4 Transverse flexural tests .....	219
7.4.1 Test set-up.....	219
7.4.2 Behaviour of transverse tests.....	220
7.4.3 Transverse flexural capacity .....	221
7.4.4 Ductility .....	221
7.5 Concentrated load tests .....	222
7.5.1 Test set-up.....	222
7.5.2 Results of centric concentrated load tests .....	223
7.5.3 Results of eccentrically loaded tests over span of 1900 mm .....	224

## CHAPTER 8 THEORETICAL ANALYSIS OF PFRC IN SHEAR

8.1 Introduction.....	259
8.2 Contributions to shear strength.....	260
8.2.1 Plain concrete contribution.....	260

8.2.2 <i>Fibre bridging component</i> .....	261
8.2.3 <i>Calculation of compressive resistance</i> .....	263
8.3 <i>Theoretical equation</i> .....	265
8.3.1 <i>Splitting tensile strength</i> .....	265
8.3.2 <i>Development of semi-empirical equation</i> .....	268

## CHAPTER 9 ANALYSIS AND DISCUSSION OF RESULTS

9.1 <i>Introduction</i> .....	276
9.2 <i>Prestress transfer</i> .....	276
9.2.1 <i>Introduction</i> .....	276
9.2.2 <i>Transfer length in plain concrete</i> .....	277
9.2.3 <i>Transfer length in FRC</i> .....	278
9.3 <i>Shear</i> .....	279
9.3.1 <i>Introduction</i> .....	279
9.3.2 <i>Shear strength of plain beams and hollow core slabs</i> .....	280
9.3.3 <i>Shear strength of FRC beams</i> .....	281
9.3.4 <i>Shear strength of FRC hollow core slabs</i> .....	282
9.3.5 <i>Fibre shear supplement</i> .....	283
9.4 <i>Flexure</i> .....	284
9.4.1 <i>Flexural cracking strength</i> .....	284
9.4.2 <i>Transverse flexural cracking strength</i> .....	286
9.5 <i>Implications for the design of FRC hollow core slabs</i> .....	287
9.5.1 <i>Transverse and flexural reinforcement</i> .....	287
9.5.2 <i>Shear reinforcement</i> .....	287

## CHAPTER 10 CONCLUSIONS AND FUTURE WORK

10.1 <i>Introduction</i> .....	301
10.2 <i>Manufacture</i> .....	302
10.2.1 <i>Manufacture of extruded FRC slabs</i> .....	302
10.2.2 <i>Fibre orientation</i> .....	303

10.2.3 Fibre distribution.....	303
10.3 Testing .....	304
10.3.1 Bond.....	304
10.3.2 Shear.....	304
10.3.3 Transverse flexure .....	306
10.3.4 Anchorage and flexural cracking.....	306
10.4 Design equation .....	307
10.5 Future work.....	309
 REFERENCES .....	 310

## APPENDICES

APPENDIX A FIBRE CHARACTERISTICS

APPENDIX B FLEXURAL TOUGHNESS TEST RESULTS

APPENDIX C MIX PROPORTIONS FOR MAIN TRIAL HOLLOW CORE SLABS

APPENDIX D GRILLAGE ANALYSIS OF HOLLOW CORE SLABS

APPENDIX E NET DEFLECTION OF SHEAR TESTS

APPENDIX F LOAD TEST ON SPREADER BEAM



## LIST OF TABLES

Table 1-1 Major hollow core slab systems .....	11
Table 3-1 Results of sensitivity study by Åkesson (1994) showing absolute values and relative changes in percent, compared with a standard slab, for transfer length and draw-in. ....	90
Table 3-2 Shear test results from plain and fibre reinforced "cut-out beams" from a Dy-Core slab.....	90
Table 4-1 Plain Concrete Mix (by weight of cement) for Pull-out Tests .....	119
Table 4-2 Compression and Splitting Tension Test Results at Test Age (7 days) for Pull-Out Bond Specimens .....	119
Table 4-3 Compression and Splitting Tension Tests at 28 days for Pull-Out Bond specimens .....	119
Table 4-4 Mean ASTM C 1018 Toughness Indices for HS fibre pull-out bond test mixes .....	120
Table 4-5 Mean Cracking, ultimate and equivalent flexural strengths for HS pull-out test bond mixes.....	120
Table 4-6 Mix design for plain shear test concrete mixes (by weight of cement).....	120
Table 4-7 Mean Compression and Splitting Tension Test and Slump Results for HS fibre reinforced beams tested over $a/d = 2.8$ .....	121
Table 4-8 Mean Compression and Splitting Tension Test and Slump Results for HS fibre reinforced beams tested over $a/d = 2.0$ .....	121
Table 4-9 Mean Compression and Splitting Tension Test and Slump Results for AM fibre reinforced beams .....	122
Table 4-10 Mean ASTM C 1018 Toughness Indices for plain and HS fibre shear test mixes.....	122
Table 4-11 Mean Cracking, ultimate and equivalent flexural strengths for plain and HS fibre shear test mixes .....	123
Table 4-12 Mean ASTM C 1018 Toughness Indices for AM fibre shear test mixes.....	123
Table 4-13 Mean Cracking, ultimate and equivalent flexural strengths for AM fibre shear test mixes.....	123
Table 5-1 Calculated transfer lengths from pull-out tests.....	150
Table 5-2 Schedule of prestressed beam tests.....	150
Table 5-3 Shear Test Results $a/d = 2.8$ .....	151
Table 5-4 Shear Test Results $a/d = 2$ .....	151

Table 6-1 Mix Proportions used in Preliminary Trials ( $\text{kg/m}^3$ ).....	196
Table 6-2 Section properties based on nominal properties of hollow core slab .....	196
Table 6-3 Concrete Mix used in Trial Production of Hollow Core Slab.....	197
Table 6-4 Result of cube compression tests on preliminary trial slab mix.....	197
Table 6-5 Specimens produced at each of the main FRC trials.....	198
Table 6-6 Geometrical properties and reinforcement details for plain concrete slabs .....	199
Table 6-7 Compressive strength and measured in situ fibre volume fraction .....	200
Table 6-8 Density of FRC slabs and calculated density of the matrix.....	201
Table 7-1 Programme for factory cast slabs and x-beams .....	227
Table 7-2 Test programme for shear tests on hollow core slabs.....	229
Table 7-3 Shear Tests over $a/d = 2.0$ .....	230
Table 7-4 Shear Tests over $a/d = 2.8$ .....	231
Table 7-5 Shear Tests over $a/d = 3.5$ .....	232
Table 7-6 Test programme for factory-produced x-beams .....	233
Table 7-7 Flexural test results of factory-produced x-beams .....	234
Table 7-8 Results of factory-produced x-beams failing in shear .....	235
Table 7-9 Average dimensions of transverse test specimens.....	236
Table 7-10 Ultimate strength of transverse bending tests.....	236
Table 7-11 Results of Centric Concentrated Load Tests .....	237
Table 7-12 Results of Eccentric Concentrated Load Tests.....	237
Table 8-1 Average results from analysis of compressive resistance.....	270
Table 9-1 Comparison of measured transfer lengths for 12.5 mm strand and 7 mm wire in plain concrete with predictive equations .....	291
Table 9-2 Comparison of theoretical equation with average ultimate shear strength of plain slabs and x-beams.....	292
Table 9-3 Comparison of theoretical equations with average ultimate shear strength of FRC x-beams .....	293
Table 9-4 Comparison of theoretical equations with average ultimate shear strength of FRC hollow core slabs.....	294
Table 9-5 Comparison of observed and theoretical cracking moments for factory-produced plain concrete x-beams .....	295
Table 9-6 Comparison of observed and theoretical cracking moments for factory-produced FRC x-beams.....	296
Table 9-7 Comparison of observed and theoretical cracking moments for laboratory-cast x-beams .....	297
Table 9-8 Increases in slab properties to attain same increase in ultimate shear strength as adding a fibre volume fraction of 1.0%.....	298

## LIST OF FIGURES

Figure 1-1 ‘Spiroll’ machine used in the manufacture of extruded hollow core slabs.....	12
Figure 1-2 Typical extruded hollow core slab cross-sections.....	13
Figure 1-3 700 mm deep slide-formed hollow core slabs.....	14
Figure 1-4 Manufacturing methods for steel fibres .....	15
Figure 2-1 Three dimensional orientation of fibres .....	45
Figure 2-2 Idealised bond shear stress-slip relationship for fibre pullout.....	45
Figure 2-3 Load - slip curves of a HS fibre and straight fibre in concrete, and a waxed HS fibre in epoxy resin.....	46
Figure 2-4 The composite tensile stress-strain curve for fibre-reinforced matrices.....	46
Figure 2-5 Load - extension curve of a pre-cracked FRC specimen in tension .....	47
Figure 2-6 Idealised load - extension curve for a FRC specimen in tension .....	47
Figure 2-7 Simplified tensile load -extension curve of FRC assuming constant post-cracking bridging stress .....	48
Figure 2-8 Individual contributions of aggregate bridging action, fibre bridging action and fibre prestress to the tensile stress - crack width curve .....	48
Figure 2-9 Influence of Cook-Gordon effect and bond weakening on tensile stress - crack width curve.....	49
Figure 2-10 The splitting tensile test and horizontal stress distribution.....	49
Figure 2-11 Schematic representation of a FRC beam under flexural loading.....	50
Figure 2-12 Measurement of toughness by ASTM C1018 .....	50
Figure 2-13 Definition of strength based dimensionless indices with proposed toughness parameters R0.5-1.5 and R1.5-3.0 .....	51
Figure 2-14 Determination of first crack strength .....	51
Figure 2-15 Load - deflection curves with the same absolute toughness as derived by the JCI Method.....	52
Figure 2-16 Typical load - deflection curves with and without extraneous deformations .....	52
Figure 2-17 Yoke system used at University of Nottingham.....	53
Figure 3-1 Possible flexural failures.....	91
Figure 3-2 Possible shear failures.....	91

Figure 3-3 Computation of ultimate flexural strength of prestressed hollow core slab .....	92
Figure 3-4 Mohr's circle for shear in prestressed concrete.....	92
Figure 3-5 Parabolic distribution of prestress transfer.....	93
Figure 3-6 Critical transfer-development envelope according to ACI-318 .....	93
Figure 3-7 Development of anchorage and pretensioning force.....	94
Figure 3-8 Flexural cracking and anchorage capacity along development length .....	94
Figure 3-9 Free body diagram for anchorage failure .....	95
Figure 3-10 Geometry of FRC hollow core slabs used by Bernander (1986).....	95
Figure 3-11 Cracking shear strength $v A_v/A_{v(ACI)}$ .....	96
Figure 3-12 Ultimate shear strength $v A_v/A_{v(ACI)}$ .....	96
Figure 3-13 Shear forces and reactions .....	97
Figure 3-14 Comparison of the equations of Mansur <i>et al.</i> (1986) and Dramix Guidelines (1995) for the shear resistance supplement due to adding steel fibres .....	97
Figure 3-15 State of stress in an element cracked in shear .....	98
Figure 3-16 Comparison of BS 8110 (1985) and Marshall (1974) equations for predicting splitting tensile strength of plain concrete from compressive cube strengths.....	98
Figure 3-17 Localised crack opening (dilatancy) associated with shear displacement .....	99
Figure 3-18 Shear stress as a function of shear displacement and crack opening for three specimens at different fibre volume fractions .....	99
Figure 3-19 Schematic representation of increase in shear strength due to concrete strength for various fibre volume fraction and fibre aspect ratio .....	100
Figure 3-20 Idealised shear stress - shear displacement curve for FRC .....	100
Figure 3-21 Idealised tensile stress - strain curve for FRC assumed by Valle and Buyukozturk (1994) .....	101
Figure 3-22 Effect of fibre volume fraction on flexural strength and cracking shear strength of a x-beam.....	101
Figure 3-23 Observed failure modes for RFRC beams.....	102
Figure 3-24 Stress and strain blocks for a RFRC beam in flexure .....	102
Figure 3-25 Bond stress $v$ slip for reinforcement bar and prestressing strand.....	103
Figure 3-26 Transfer curves for beams with $V_f = 0\%$ , $0.5\%$ and $1\%$ at various prestressing forces.....	104

Figure 4-1 Splitting tensile strength v fibre volume fraction for pull-out control test specimens.....	124
Figure 4-2 Small scale pull-out test arrangement .....	124
Figure 4-3 Force v pull-in for small-scale bond tests .....	125
Figure 4-4 Dosage of superplasticizer used with increasing fibre volume fraction.....	125
Figure 4-5 Compressive strength gain with age (PB5).....	126
Figure 4-6 Splitting cube and cylinder tensile strength v fibre volume fraction (HS fibres).....	126
Figure 4-7 Typical load v deflection curves for both fibre types and each fibre volume fraction in flexure.....	127
Figure 4-8 Relationship between ASTM toughness indices and fibre volume fraction.....	127
Figure 4-9 Increase in average flexural cracking strength and average ultimate flexural strength with fibre volume fraction.....	128
Figure 4-10 Increase in average equivalent flexural strength with fibre volume fraction .....	128
Figure 4-11 Relationship between strength based dimensionless indices and fibre volume fraction for both fibre types.....	129
Figure 5-1 Test specimen for Pull-out tests .....	153
Figure 5-2 Pull-out test arrangement .....	154
Figure 5-3 Axial stress v steel strain for specimen B-0.0A .....	155
Figure 5-4 Axial stress v steel strain for test specimens at 200 mm embedded strain gauge .....	155
Figure 5-5 Axial stress v steel strain for test specimens at 400 mm embedded strain gauge .....	156
Figure 5-6 Axial stress v steel strain for test specimens at 600 mm embedded strain gauge .....	156
Figure 5-7 Axial stress v steel strain for test specimens at 800 mm embedded strain gauge .....	157
Figure 5-8 Axial stress v loaded-end strand movement.....	157
Figure 5-9 Axial stress v loaded-end strand movement for specimens B-2.0 and B-0.0B up to ultimate.....	158
Figure 5-10 Axial stress v remote-end strand movement for specimens B-2.0 and B-0.0B .....	158
Figure 5-11 Axial stress at “transfer” of stress v embedment length of strain gauge.....	159
Figure 5-12 Effect of fibre volume fraction on calculated transfer length .....	159

Figure 5-13 Strain at 1328 N/mm <sup>2</sup> v embedment length of strain gauge .....	160
Figure 5-14 X-beam test specimen, (a) PB1-PB4, (b) PB5-PB22 .....	160
Figure 5-15 Test set-up for X-beam tests (A Test) .....	161
Figure 5-16 Test set-up for X-beam tests (B Test) .....	161
Figure 5-17 Experimentally measured prestress transfer curve for plain wires.....	162
Figure 5-18 Experimentally measured prestress transfer curve for indented wires.....	162
Figure 5-19 Prestress attained at 750 mm from end of beam v fibre volume fraction.....	163
Figure 5-20 Comparison of experimental transfer curves with BS 8110 and Eurocode 2.....	163
Figure 5-21 Shear force v deflection for PB1 - PB4 .....	164
Figure 5-22 Shear force v deflection for $V_f = 0\%$ at $a/d = 2.0$ .....	164
Figure 5-23 Shear force v deflection for $V_f = 0\%$ at $a/d = 2.8$ .....	165
Figure 5-24 Shear force v deflection for $V_f = 0.5\%$ (HS) at $a/d = 2.0$ .....	165
Figure 5-25 Shear force v deflection for $V_f = 1\%$ (HS) at $a/d = 2.0$ .....	166
Figure 5-26 Shear force v deflection for $V_f = 1.5\%$ (HS) at $a/d = 2.0$ .....	166
Figure 5-27 Shear force v deflection for $V_f = 0.5\%$ (HS) at $a/d = 2.8$ .....	167
Figure 5-28 Shear force v deflection for $V_f = 1\%$ (HS) at $a/d = 2.8$ .....	167
Figure 5-29 Shear force v deflection for $V_f = 1.5\%$ (HS) at $a/d = 2.8$ .....	168
Figure 5-30 Shear force v deflection for $V_f = 0.28\%$ (AM) at $a/d = 2.8$ .....	168
Figure 5-31 Shear force v deflection for $V_f = 0.56\%$ (AM) at $a/d = 2.8$ .....	169
Figure 5-32 Cracking shear strength v fibre volume fraction (HS fibres) .....	169
Figure 5-33 Cracking shear strength v fibre volume fraction (AM fibres).....	170
Figure 5-34 Ultimate shear strength v fibre volume fraction (HS fibres).....	170
Figure 5-35 Ultimate shear strength v fibre volume fraction (AM fibres) .....	171
Figure 5-36 Definition of ductility term $V_{lim}/V_{cr}$ .....	171
Figure 5-37 $V_{lim}/V_{cr}$ v fibre volume fraction (HS fibres) at $a/d = 2.0$ .....	172
Figure 5-38 $V_{lim}/V_{cr}$ v fibre volume fraction (HS fibres) at $a/d = 2.8$ .....	172
Figure 5-39 Shear load v steel strain for $V_f = 0\%$ (PB18B) .....	173
Figure 5-40 Shear load v steel strain for $V_f = 0.5\%$ (PB19B) .....	173
Figure 5-41 Shear load v steel strain for $V_f = 1.0\%$ (PB16).....	174
Figure 5-42 Shear load v steel strain for $V_f = 1.5\%$ (PB15).....	174
Figure 5-43 Shear load v diagonal shear crack width ( $a/d = 2.0$ ) .....	175
Figure 5-44 Shear load v diagonal shear crack width ( $a/d = 2.8$ ).....	175
Figure 5-45 Typical wire slip v deflection curves .....	176
Figure 5-46 Wire slip/deflection gradient for $a/d = 2.0$ and span = 1900 mm .....	176
Figure 5-47 Wire slip/deflection gradient for $a/d = 2.0$ and span = 1350 mm .....	177

Figure 5-48 Wire slip/deflection gradient for $a/d = 2.8$ and span = 1900 mm .....	177
Figure 5-49 Wire slip/deflection gradient for $a/d = 2.8$ and span = 1350 mm .....	178
Figure 6-1 Rotation of augers in 'Spiroll' extrusion.....	202
Figure 6-2 Wash-Out test results: a) Preliminary trial (0.6% HS), b) Trial 1 (0.5% HS), c) Trial 2 (1% HS), d) Trial 3 (0.28% AM).....	203
Figure 6-3 Orientation factor for the three orthogonal directions throughout depth of slab (HS fibre slabs) .....	204
Figure 6-4 Orientation factor for fibres crossing shear planes angled at $45^\circ$ and $35^\circ$ to the longitudinal.....	204
Figure 6-5 Orientation factor for the three orthogonal directions throughout depth of slab (AM fibre slabs).....	205
Figure 6-6 Orientation factor through vertical depth of slab for laboratory cast specimens PB5, PB16 and PB15.....	206
Figure 6-7 Orientation factor through across $45^\circ$ shear plane for laboratory cast specimens PB5, PB16 and PB15. ....	207
Figure 7-1 General arrangement of shear test set-up on full width slabs.....	238
Figure 7-2 Shear load v deflection curves for plain $P= 806$ kN reinforced slabs at $a/d = 2.0$ .....	239
Figure 7-3 Shear load v deflection curves for FRC $P= 806$ kN reinforced slabs at $a/d = 2.0$ .....	239
Figure 7-4 Shear load v deflection curves for $P = 518$ kN reinforced slabs at $a/d = 2.0$ .....	240
Figure 7-5 Shear load v deflection curves for plain $P= 806$ kN reinforced slabs at $a/d = 2.0$ .....	240
Figure 7-6 Shear load v deflection curves for $P = 806$ kN reinforced slabs at $a/d = 2.8$ .....	241
Figure 7-7 Shear load v deflection curves for $P = 518$ kN reinforced slabs at $a/d = 2.8$ .....	241
Figure 7-8 Effect of fibre volume fraction on $V_{cr}$ .....	242
Figure 7-9 Effect of fibre volume fraction on $V_{ult}$ .....	242
Figure 7-10 $V_{lim}/V_{cr}$ v $V_f$ for HS fibre slabs .....	243
Figure 7-11 Moment v deflection curves for x-beams reinforced with 7 mm wire and 9.3 mm strand at $a/d = 2.0$ .....	243
Figure 7-12 Moment v deflection curves for x-beams reinforced with 7 mm wire and 9.3 mm strand at $a/d = 2.8$ .....	244
Figure 7-13 Moment v deflection curves for x-beams reinforced with 12.5 mm strand at different $a/d$ .....	244
Figure 7-14 Effect of $a/d$ on $M_{cr}$ .....	245

Figure 7-15 Effect of precompression in soffit on $M_{cr}$ .....	245
Figure 7-16 Strand slip v deflection for 9.3 mm strands in plain concrete and FRC.....	246
Figure 7-17 Strand slip v deflection for 12.5 mm strands .....	246
Figure 7-18 Test set-up for transverse bending tests .....	247
Figure 7-19 Load v deflection curves for plain concrete transverse bending tests .....	247
Figure 7-20 Load v deflection curves for FRC transverse bending tests.....	248
Figure 7-21 Relationship between longitudinal width of slab and transverse cracking load.....	248
Figure 7-22 Test set-up for centric concentrated load test.....	249
Figure 7-23 Test set-up for eccentric concentrated load test .....	250
Figure 7-24 Typical load v deflection curves from centrally loaded punching shear tests .....	251
Figure 7-25 Typical wedge shaped cracking from centrally loaded punching shear tests.....	251
Figure 7-26 Failure pattern in eccentric load tests.....	252
Figure 7-27 Load v deflection curves for eccentric load tests .....	252
Figure 7-28 Load v deflection curves for the four LPs across the width of Test F7 .....	253
Figure 7-29 Load v strain on the soffit for Test F7.....	253
Figure 7-30 Strand slip v deflection curve for all strands in eccentric load Test P16 .....	254
Figure 8-1 Shear strength of plain prestressed concrete with increasing crack width .....	271
Figure 8-2 Theoretical V-w relationship for FRC ( $V_f = 1.0\%$ ) formed from combination of fibre bridging, fibre prestress and plain concrete contribution in comparison with actual V-w relationships. ....	271
Figure 8-3 Improvement in dowel contribution to shear resistance with increasing fibre volume fraction in prestressed x-beams according to Equation 3-19.....	272
Figure 8-4 Computation of average additional shear force carried by compressive zone due to fibre crack arrest.....	272
Figure 8-5 Proposed stress block for analysis of compressive resistance.....	273
Figure 8-6 Variation of average tensile stress component ( $f_{tM}$ ) with deflection .....	273
Figure 8-7 Relationship between $\tau_f$ and $f_{cu}$ as calculated from splitting tensile tests .....	274



Figure 8-8 Comparison of  $f_{ct,sp}$  with Equation 8-9.....274

Figure 9-1 Comparison of ultimate shear stress ( $v_{ult}$ ) for FRC x-beams with  
theoretical equation for  $v_{cou}$  .....299

Figure 9-2 Increase in shear strength with fibre volume fraction for  
laboratory-cast x-beams compared with predictive equations for  
fibre shear supplement.....299

Figure 9-3 Increase in shear strength with fibre volume fraction for hollow  
core slabs compared with predictive equations for fibre shear  
supplement.....300

## LIST OF PLATES

Plate 2-1 Yoke system used at University of Nottingham .....	54
Plate 4-1 Small scale pull-out test arrangement.....	130
Plate 4-2 Poor compaction of concrete in specimen PB13 .....	130
Plate 5-1 Failure of specimen PB2.....	179
Plate 5-2 Failure pattern for plain beam at $a/d = 2.0$ .....	179
Plate 5-3 Failure pattern for plain beam at $a/d = 2.8$ .....	180
Plate 5-4 Typical failure of PFRC beam at end of test (PB11B).....	180
Plate 5-5 "Soffit crack" in beam PB10B.....	181
Plate 6-1 Compaction of the three batches at the preliminary trial.....	208
Plate 7-1 Shear test set-up for tests with two spreader beams .....	255
Plate 7-2 Typical web shear failure at $a/d = 2.0$ .....	255
Plate 7-3 Typical web shear failure at $a/d = 2.8$ .....	256
Plate 7-4 Typical anchorage failure (Test F12A).....	256
Plate 7-5 Non-Symmetry of the factory-produced x-beams (Beam F9/2) .....	257
Plate 7-6 Transverse flexural failure from test F200 .....	257
Plate 7-7 Test set-up for centric concentrated load test .....	258
Plate 7-8 Typical failure in centric concentrated load test (Slab 10).....	258
Plate 8-1 Dowel action in plain concrete at large deflections.....	275

# CHAPTER 1

## INTRODUCTION

### 1.1 Introduction

Modern development of steel fibre reinforced concrete (FRC) began in the 1960s and has been the subject of considerable research since this time. It was initially hoped that fibres would be able to significantly increase the tensile strength, however, it transpired that with the practical fibre contents that were available due to mixing considerations only insignificant increases could be attained. Instead it was found that FRC could considerably improve ductility, particularly in tensile regions, and prevent sudden, catastrophic failures. It is now recognised that the purpose of adding steel fibres to concrete should be to convert the brittle character of concrete into a tough, ductile material. The benefits of FRC over plain concrete can be summarised as follows:

- (i) retarded or delayed growth of cracking
- (ii) ability to resist tensile load after cracking by fibres resisting pullout and fibres bridging across cracks
- (iii) increased shear strength
- (iv) increased flexural strength
- (v) improved impact resistance
- (vi) increased fatigue strength under cyclic loading
- (vii) reduction of shrinkage and creep

These properties of FRC are presently utilised in a number of non-structural applications. The largest use of FRC is in industrial floors where the homogeneous reinforcement, which is a characteristic of FRC, is utilised to resist dynamic wheel

loads and static rack loads. In this application the fibres are able to replace and eliminate all traditional mesh reinforcement and reduce slab thickness. There is therefore an economic advantage in using steel fibres

Steel fibres are also becoming increasingly common in sprayed concrete for mine and tunnel lining, rock stabilisation, thin shell dome construction and repair of surfaces. In this application fibres are once again able to eliminate the mesh reinforcement, and reduce the considerable steel fixing time. In addition, fibres are able to improve toughness, increase resistance to abrasion and possibly reduce thickness of section (Austin and Robins 1995).

However, despite considerable research into the use of steel fibres in structural elements, the only wide-scale use is in precast tunnel linings. Here, in a similar manner to sprayed concrete tunnel linings, the fibres are able to replace the mesh reinforcement and additionally reduce the amount of waste caused by accidental damage during the construction phase.

A prime reason for fibres not being widely used in structural elements is the absence of design procedures for FRC in structural concrete design codes such as BS 8110 (1985), Eurocode 2 (1993) and ACI 318 (1992). This is largely as a consequence of the lack of the following four interrelated requirements (Criswell 1994): a relevant measure of FRC properties; accurate models and equations for FRC; formulation of design equations and procedures; and assurance of the reliability of the fibre structural contribution.

However, each of these four points has been widely discussed and researched, and many contradictory and subsequently confusing suggestions for designing FRC in structural elements can be found throughout the literature. A further obstruction to the acceptance of a design procedure for FRC is the increasing numbers of fibres on the market. This means that in contrast to steel reinforcement which has known and recognised properties, there are no properties for steel fibres which are consistently defined from which design values could be derived. This is fully discussed in Section 2.5.

Additionally, there is a further, perhaps more important, reason why fibres have not been introduced into structural design codes. This is that much of the research carried out has shown fibres to be less effective in providing strength and ductility than traditional reinforcement. There is therefore no reason why structural

engineers should wish to utilise steel fibres in their structures. However, despite steel fibres generally being less effective than traditional reinforcement, there have been some areas highlighted where fibres are more efficient than traditional reinforcement. One example is the improvement in ductility in seismic connections and hinging areas (Criswell 1994). Further, there are some structural elements in which it is difficult or even impossible to place traditional types of reinforcement in which steel fibres could be efficiently used. It is the author's opinion, that research should concentrate on the application of steel fibres in such structural elements, where fibres are the only viable form of reinforcement, either for economic or practical reasons.

The use of fibres in these elements and the knowledge accrued from design equations specifically set-up for such elements may eventually lead to the wider use of fibres in more conventional structural elements. This thesis studies the feasibility of using fibres in one of these promising applications - prestressed hollow core slabs.

## **1.2 Fibres for prestressed hollow core slabs**

### **1.2.1 Prestressed hollow core slabs**

Prestressed hollow core slabs are the most common form of precast flooring used world-wide, with an annual production in Europe of about 20 million m<sup>2</sup>; which represents about 40 to 60% of the precast flooring market (Elliott 1996). They are used in commercial, industrial and residential buildings as well as for car parks and sports stadiums. They have continuous voids to reduce weight, and due to the low self weight and prestressing (which is in the longitudinal direction only) they can span as far as 20 m.

Slabs are designed on the basis of a nominal 1200 mm grid, and over 95% of slabs have a nominal width of 1200 mm. The actual width of about 1197 mm allows for construction tolerances and the prevention of overrunning due to cumulative errors. Most slabs produced are between 100 mm and 400 mm in depth, although in recent years there has been an increase in the manufacture of deeper slabs

Hollow core slabs are cast on long line beds, normally 90 m to 180 m long, and saw-cut to the appropriate length for each intended project. The slabs can be

manufactured by a variety of wet-cast and dry-cast methods, the most common of which are listed in Table 1-1. The dry-cast methods of extrusion and slip-forming are the only two methods used in the UK.

In the extrusion process the concrete is pressed out by screws during compaction into the required cross-section. A typical 'Spiroll' machine is shown in Figure 1-1. Since the cores are circular, the thickness of the web at mid-height can be as little as 30 mm to optimise the cross-sectional properties. Typical extruded cross-sections are shown in Figure 1-2.

The most popular method of producing hollow core slabs is slip-forming, where the concrete is fed around steel formers. This profiled form is moved during placement and the concrete is vibrated around the forms under little pressure. It is usual for the concrete to be laid in three layers - the bottom flange, web and top flange.

The concrete used in dry cast units has a zero slump (hence the term dry cast), with water/cementitious material ratios as low as 0.3. 10 mm coarse aggregate gravel or crushed limestone is usually used in combination with medium grade sand. Recycled aggregate at not more than 9% of the total aggregate content can also be used. Lightweight aggregate is not used, however, because of excess wear on the machinery.

Although in 95 per cent of cases hollow core slabs would fail due to mid-span flexure, much attention is paid to the shear capacity. This is largely because shear failures are catastrophic, and both extrusion and slip-forming restrict the placement of secondary transverse and shear reinforcement. The shear capacity of the slabs is therefore largely dependant on the tensile strength of concrete in resisting shear and torsion.

Shear is a problem in slabs with short spans ( $< 3\text{m}$ ) or heavily loaded spans, particularly where large line loads (e.g.,  $>100\text{ kN/m}$ ) are present (Elliott 1996). Concentrated loads can also cause concern and need to be dealt with on an individual basis. Additionally, in many applications slabs need to be notched in order to control the crack path in coupled ends or to fix the slabs to other members. In such situations the shear capacity can be significantly reduced (Girhammar and Pajari 1995).

Further, the problem of shear has been highlighted, recently, due to a number of problems with slabs supported on flexible beams (Pajari and Lin Yang 1994). In

such situations stresses caused by transverse bending of slabs lead to complementary shear stresses in addition to those from longitudinal loading. A FIP Committee has been set up to deal specifically with this problem (FIP Recommendations 1996).

Recent developments in Italy, have lead to the production of a 700 mm deep slab, as shown in Figure 1-3. One of the most important innovations in the production of these slabs is that it is possible to incorporate vertical reinforcement in the two outer webs prior to casting, as reinforcement against shear (Della Bella and Querin 1997).

In the more commonly used smaller slabs the placement of shear links is extremely difficult, particularly in dry-cast systems and is therefore not a viable strength enhancing method. An alternative method for increasing shear capacity in dry-cast hollow core slabs is to reduce the number of cores. This may be done by either leaving out a core for the entire length of the production, or by locally breaking into the cores and filling with solid whilst the concrete is still in a plastic state (PCI 1991). With the latter method shear links can also be added, but this is uncommon.

Both the placement of shear links and local filling of cores are time consuming and labour intensive activities. Leaving out cores for the entire length of slab reduces the beneficial low weight of hollow core systems, which is also true of increasing the slab depth to overcome shear and torsion problems. Other solutions are to increase the level of prestress or the tensile strength. Given that high-strength concrete is already utilised in hollow core slabs the latter solution is unlikely to yield any significant increases and it is known that increasing prestress for shear is uneconomical (Elliott 1996). It is also likely to lead to alternative problems such as excessive bursting stresses at the end of the member.

It is for this reason in particular that the inclusion of discrete steel fibres in hollow core slabs may be a viable alternative. The possible benefits of using steel fibres in hollow core slab are discussed in the following section.

### **1.2.2 Possible benefits of using fibres in hollow core slabs**

As discussed above, the inclusion of traditional secondary reinforcement in hollow core slabs is both time consuming and expensive. Because steel fibres can be

added directly to mixes, there is no need for any additional work on the slabs after casting which would lead to savings in labour expenses. Further, at the fibre contents typically used in structural components (40-80 kg/m<sup>3</sup>) the increased weight is only 2.5% which compares favourably with the alternative of missing out cores. The ability of fibres to increase shear strength is reviewed extensively in Chapter 3, and the use of steel fibres as shear and torsion reinforcement in hollow core slabs is potentially a very-useful application of fibres.

The addition of fibres to hollow core slabs could also be favourable in a number of other areas. For example, use of fibres in other precast structural elements such as tunnel segments have shown significant reductions in damage due to handling, transporting and building-in. It is possible that similar reductions in accidental damage could occur in hollow core slabs. An economic feasibility study in Denmark (Glavind *et al.* 1994) has suggested that the use of fibres could be a cost-effective solution to this problem. In a similar way, the increased impact resistance of FRC could be utilised to resist the dynamic stresses imparted by the use of shotfired ceiling fixers, which are commonly used in the construction industry but are severely restricted on hollow cores slabs.

A further benefit of fibres could be in increased bond between the concrete and strands. This may result in a shortened transmission length and subsequently increases in shear capacity. A more consistent transfer of stresses may reduce differential camber.

In addition, fibres increase stiffness and delay initial cracking. This results in reduced deflections and may allow the use of smaller sections or larger spans in areas where deflections govern. Further, there is evidence that fibres reduce shrinkage and creep strains. This could have the effect of reducing prestress losses, and allow a reduction in the number of prestressing wires.

### **1.3 Types of steel fibre**

Steel fibres are generally between 6 mm and 75 mm in length, with an aspect ratio (ratio of length to diameter) of between 20 and 100. Fibres are manufactured by a variety of methods, and are supplied in various shapes and forms. ASTM A-820



(1985) classifies steel fibres in four categories depending on the manufacturing process (see Figure 1-4):

Type I	cold drawn wire
Type II	cut sheet
Type III	melt extracted
Type IV	other methods (e.g., milling, filing, quenching)

To improve the mechanical anchorage between fibres and the matrix, drawn wires and cut sheet fibres are often enhanced by adding deformations such as crimps or deformed-ends. Fibres produced by milling or melt extraction intrinsically have irregular surfaces which aids bond. In this thesis, two types of fibre were used: hooked-end steel fibres and amorphous metal fibres. Hooked-end fibres were used since they are generally regarded world-wide as the most efficient fibre type. However, some fabrication concerns were raised about this fibre by the hollow core manufacturer, and therefore amorphous metal fibres were introduced into the study as a possible alternative. These two fibres are described in detail below (and properties are given in Appendix A):

### **1.3.1 Hooked-end steel fibres**

The hooked-end steel fibres (HS) used in this study, are produced by the Bekaert company in Belgium and are distributed under the name Dramix. They are made from drawn wire and are hooked at the end to provide anchorage in the concrete. The hooked-end offers a strong mechanical anchorage, which leads to a higher crack resistance, toughness and fatigue resistance. Equivalent levels of toughness can therefore be achieved with a lower quantity of HS fibres than straight steel fibres.

For general applications HS fibres are made of uncoated wire, but occasionally for specialist applications stainless steel fibres are used or the fibres can be coated with a corrosion protective layer. To ease mixing, HS fibres can be glued together in small bundles with a water soluble adhesive. This compact bundle form offers the

opportunity to mix longer steel fibres at higher fibre contents. As soon as the mixing process commences these bundles spread out throughout the entire mass and separate due to the action of the moisture and the scouring action of the aggregate.

### **1.3.2 Amorphous metal fibres**

Amorphous metal (AM) fibres are in the form of thin ribbons of varying length and widths, and are obtained by the quenching process shown in Figure 1-4, in which a jet of molten metal is quenched on a water-cooled wheel rotating at high speed at a quenching rate of one million degrees Celsius per second. The liquid metal solidifies in an amorphous state, which gives the fibres high flexibility and strong mechanical characteristics (Boucharet 1994). In addition, the presence of chromium and the amorphous state makes the fibres highly resistant to acid or chloride induced corrosion. The fibres have a high specific surface ( $10 \text{ m}^2/\text{kg}$  for 30 mm long fibres) which provides excellent adhesion along the length of the fibre, and is almost as effective in providing anchorage as the geometrical deformations provided for fibres with a circular cross-section (Peiffer 1994). The geometry of AM fibres also results in a lower average fibre spacing than other fibre types, resulting in a dense mesh distributed throughout the concrete.

## **1.4 Objectives of Research**

The objectives of the work presented in this thesis are listed below:

1. To investigate the performance of prestressed concrete in combination with steel fibres, particularly in areas where the improved post-cracking strength and ductility of FRC over plain concrete is most beneficial. These areas include:
  - shear
  - flexure
  - bond

2. To relate improvements in strength and ductility into possible design equations for PFRC. It is particularly important that any equations should be in common with equations currently used for prestressed concrete, or equations being developed for FRC in other structural elements. In this respect the use of a flexural toughness parameter for quantifying FRC is important.

3. To study the possibility of using FRC in prestressed hollow core slabs to improve performance in areas where traditional reinforcement is not an adequate solution. This may lead to a potentially new application for the use of FRC. To fulfil this objective it is necessary to:

- investigate mixing procedures for use with fibres in dry-cast, extrudable concrete
- manufacture fibre reinforced hollow core slabs
- investigate the compaction of the FRC slabs, and examine the distribution and orientation of fibres throughout the cross-section.

## **1.5 Methodology**

The objectives described in Section 1.4 were set and achieved through a number of phases of work which are described in the following section.

The work commenced in October 1994, and the first phase involved identifying a suitable field of research, representing the interests of my supervisors, FRC and precast concrete, with the potential of forwarding the current state-of-the-art. This goal was achieved through consultation with practitioners and industry, and through perusal of the most recent journals and research papers. In particular a paper by Marvin Criswell (Criswell 1994) identifying a number of requirements for future research in FRC was especially helpful in identifying a suitable area of research. The current state of the art was identified through papers by Balaguru (1994) and Batson (1994). It became clear to the author that although FRC was useful in providing enhanced performance to a number of structural elements it was not widely used in the field, and was confined mainly to research and laboratory studies. This was mainly because traditional reinforcement is generally more efficient and is better

understood. It was seen as important, therefore, that elements in which there was difficulty in placing traditional reinforcement should be prioritised for research in FRC, particularly where the lack of traditional reinforcement leads to problems in the use of the element. Such an element is the prestressed hollow core slab where web shear tension is a particular concern due to the difficulty in incorporating shear links and the expense of alternative options. It was decided therefore that a possible area of study was the use of FRC in hollow core slabs as shear reinforcement.

It was recognised that such a study would require a number of field trials and, in addition, the need to study the behaviour of prestressed fibre reinforced concrete (PFRC) in general. A comprehensive literature review on FRC was carried out which showed that there had previously been only limited research on PFRC. It was therefore decided that in addition to field trials an extensive series of laboratory testing of PFRC would be required. It was concluded from the literature that tests on the bond and shear performance of PFRC would be of most importance.

Having decided upon this area of research it was important to make links with both a steel fibre supplier and a hollow core manufacturer. In late 1994, N.V.Bekaert and Richard Lees Ltd. both agreed to contribute significantly 'in kind' to the project.

Before finalising a programme of work for the entire study it was important to be sure at an early stage whether it was actually possible for steel fibres to be successfully added to hollow core slabs. In early 1995, Richard Lees supplied samples of the raw materials used in hollow core slab production for an investigation into different mixing procedures and mix design methods for using FRC in hollow core slabs. At the same time, they supplied a number of 150 mm deep hollow core slabs to provide the means for development of test procedures for testing hollow core slabs. The result of these developmental slab tests can be found elsewhere (Paine 1995).

Following the laboratory mixing study, a preliminary trial manufacturing fibre reinforced hollow core slabs was performed in June 1995 at the premises of Richard Lees near Derby. This trial was used to provide detailed data on the levels of compaction, the orientation and distribution of fibres and any required changes to the mix design. The resulting slabs were brought to Nottingham for testing, and were used to further develop the test procedures. Since they were only trial slabs, and had

flaws, the results are not included in this thesis, but can be found elsewhere (Paine 1996).

Following this successful preliminary trial, a programme of work consisting of a laboratory study, and the production of further FRC hollow core slabs was formulated. The laboratory studies were intended to allow fundamental knowledge of the behaviour of PFRC to be acquired, and to allow semi-empirical equations for predicting the strength of PFRC to be developed. Although the laboratory study was to some extent general in nature to allow application of the results to all prestressed concrete beams, the nature of the tests performed and the size and shape of elements used was directly related to the slabs that were to be produced in the factory trials.

In line with the review of the literature, the laboratory study incorporated both bond and shear tests. In addition, the literature showed the use of flexural toughness parameters to be the most promising approach to designing FRC structural elements, and therefore all laboratory cast mixes included the determination of flexural toughness properties.

The study of laboratory cast FRC was commenced in October 1995. The first series of tests carried out were bond tests using seven-wire helical strand embedded in FRC of varying fibre volume fractions. The tests showed no benefit in adding fibres and therefore the laboratory study from this point concentrated on shear.

The shear tests were performed on beams cast in the shape of hollow core slab webs to allow comparison of the results with those attained from slabs. It was always clear that it would not be possible to produce beams in the laboratory using a hollow core slab mix. Therefore a plastic mix was chosen which had a similar strength development, and final strength to concrete used in hollow core slabs. Use of this plastic mix also allowed higher fibre volume fractions to be used than could have been incorporated into a factory mix. All shear tests were set-up to force a web shear tension failure. In addition to shear load, deflections (gross and net), steel strains, concrete strains, wire slip and crack widths were recorded throughout the tests to obtain a thorough understanding of the nature of shear failure in PFRC.

The results of these shear tests and the knowledge attained through the on-going review of the literature was then used to assess the post-cracking behaviour of the beams, and to develop a semi-empirical equation for predicting shear failure in PFRC.

The parallel factory study incorporating steel fibres into hollow core slabs was commenced towards the end of the second year of work. Three full-scale trials were organised and were carried out in the autumn of 1996. In addition to using the Bekaert HS fibre, additional fibres were supplied by Seva who were asked to join the study in the summer of 1996, after concerns relating to the safety of HS fibres were brought up by Richard Lees. This fibre was additionally incorporated into the laboratory study at the same time. The majority of the slabs produced from these three trials were used to assess the shear capacity, with the tests performed in a similar manner to the tests on the laboratory-cast beams. In addition, single web beams were cut from the slabs to allow a more direct comparison with the laboratory cast beams. It was also deemed necessary to test a number of the slabs for transverse strength and for transverse and longitudinal load distribution since the developmental tests had shown that hollow core slabs do not behave in a purely two-dimensional manner.

The final step of the work involved a comparison of the results of the tests on hollow core slabs with the semi-empirical formulations from the laboratory study. Methods for specifying and predicting the strength of fibre reinforced hollow core slabs were developed.

## **1.6 Notation**

The notation used in this thesis is based on recommendations by Criswell (1994). The term FRC has been used to indicate the use of small, discrete steel fibres to reinforce the inherently tension-weak concrete matrix. Prestressed fibre reinforced concrete (PFRC) describes FRC which has been reinforced with prestressed wires or strands, and likewise reinforced fibre reinforced concrete (RFRC) refers to FRC reinforced with conventional steel bar reinforcement.

## 1.7 Layout of thesis

Chapters 2 and 3 of this thesis are essentially reviews of the current literature on FRC and PFRC relevant to the research. Chapter 2 is a review of the effects of FRC on the standard concrete control tests which are used in the later experimental chapters, and also deals in some detail on the theoretical methods for determining the reinforcing ability of fibres. The models for FRC in tension proposed by Lim *et al.* (1987a) and Li *et al.* (1993) are dealt with in some detail. In the final section of the chapter, consideration is given to each of the standard material control tests and theoretical methods as a potential means of characterising material properties for use in design.

The present literature on hollow core slabs and PFRC beams is reviewed in Chapter 3. This review primarily concentrates on shear and in particular web shear, because this type of failure is of most concern in the design of hollow core slabs. The chapter is in two parts: testing and design of hollow core slabs; and testing and design of PFRC elements.

Chapters 4 and 5 deal with laboratory-based experiments by the author on the behaviour of FRC in prestressed concrete and the interaction with prestressing strand. The main tests are dealt with in Chapter 5, and consist of bond tests and shear tests. Chapter 4 reports on the mix designs, materials and mix procedures used for both sets of tests. In addition, Chapter 4 presents and discusses the results of the standard material control tests which were carried out on the plain concrete and FRC to measure and compare the strength, toughness and workability of each of the mixes used.

In Chapter 6 the trial manufacture of extruded fibre reinforced hollow core slabs which took place in a total of four trials at the premises of Richard Lees Ltd. is reported. In addition to the mixing and compaction of FRC hollow core slabs, this chapter also deals with the effects of extrusion on the distribution and orientation of fibres within the slabs. The tests performed on the manufactured FRC slabs are presented in Chapter 7, and took the form of shear tests on full-width slabs, shear tests on single web beams (known as x-beams), concentrated load tests to stimulate three-dimensional behaviour, and transverse bending tests.

A discussion of the post-cracking shear behaviour of the prestressed fibre reinforced x-beams and the separate contributions to strength and ductility provided by the dowel action, aggregate interlock, fibre bridging and compressive resistance is presented in Chapter 8. In the latter part of the chapter a semi-empirical equation for predicting the shear strength based on these effects is developed.

Finally, analysis of each of the main series of tests is given in Chapter 9, with discussion on the implications of the results of the tests on the use of steel fibres in hollow core slabs, and the implications towards the design of FRC hollow core slabs. Consideration is also given to the situations in which fibres may best be utilised with regard to hollow core slabs. The conclusion of the thesis and recommendations for future work are given in Chapter 10.



**Table 1-1 Major hollow core slab systems  
(after PCI 1991 and Elliott 1996)**

Manufacturer	Machine Type	Concrete Type	Slump	Core Forms
Dy-Core	extruder	dry	low	tubes
Flexicore	fixed form	wet	normal	pneumatic tubes
Span Deck	slip form	wet	normal	filler aggregate
Roth	slip form	dry	low	tubes
Spiroll	extruder	dry	low	augers
Spancrete	extruder	dry	low	tubes
Dynaspan	slip form	wet	normal	tubes

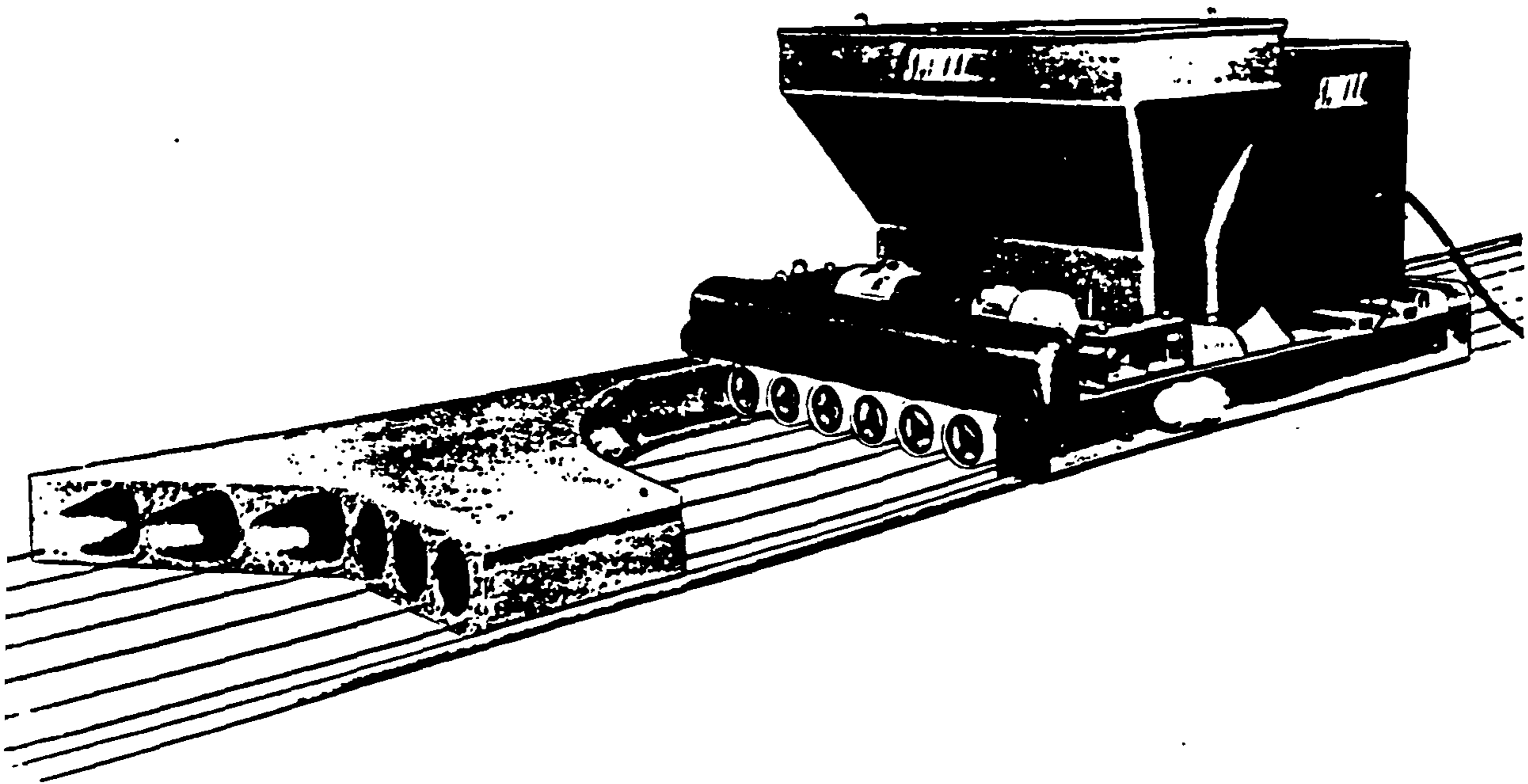


**Figure 1-1 'Spiroll' machine used in the manufacture of extruded hollow core slabs (Richardson 1973)**

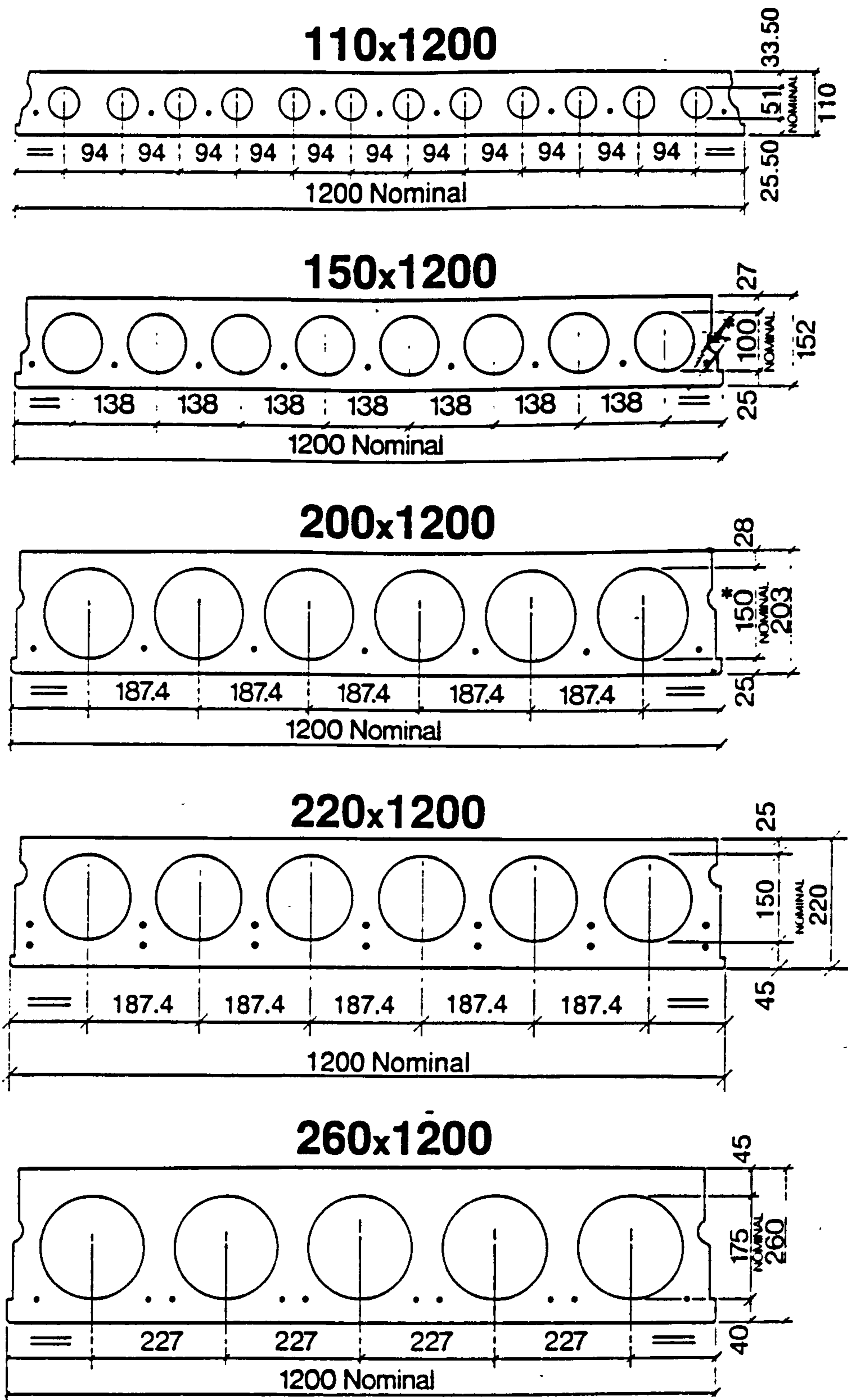
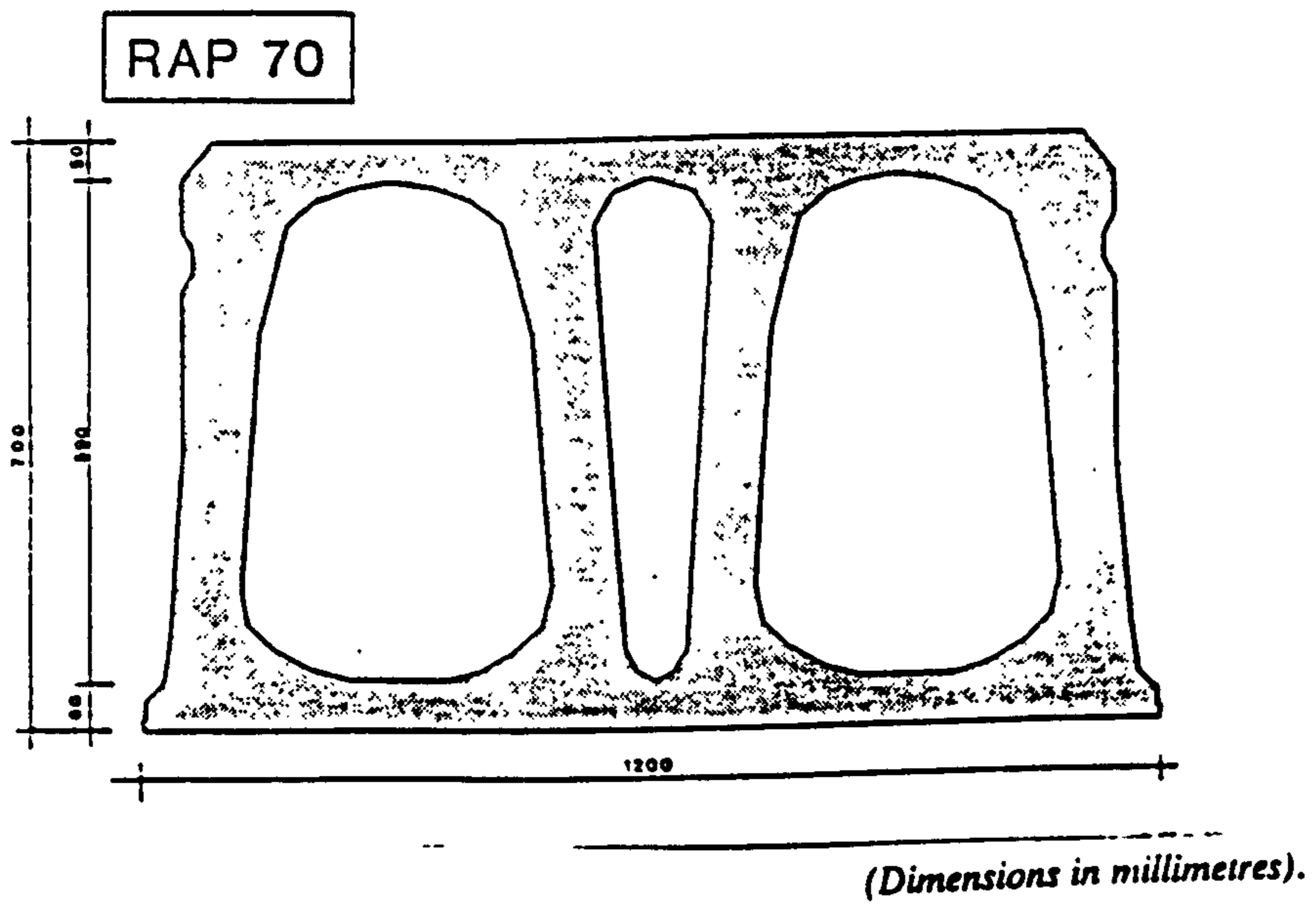
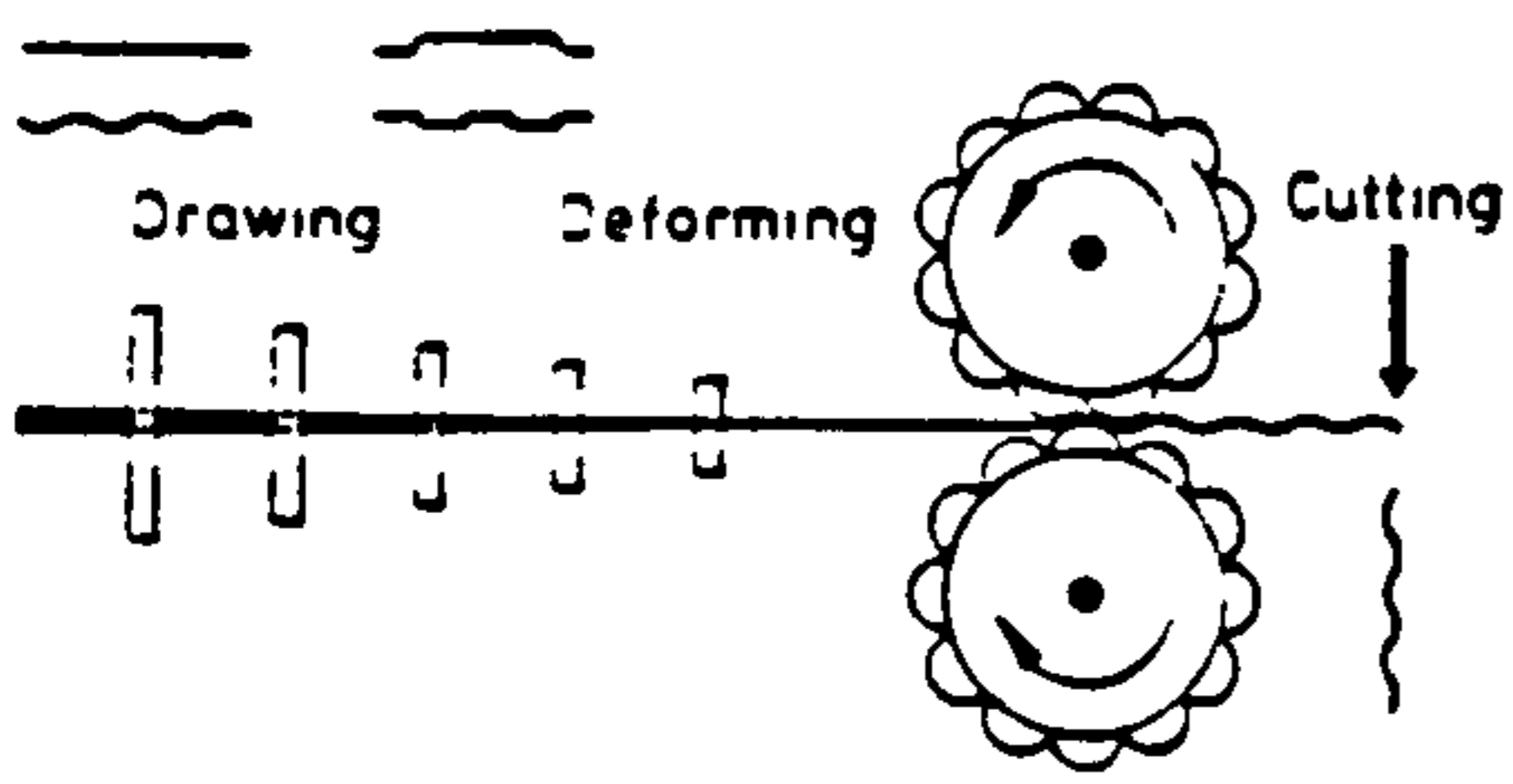


Figure 1-2 Typical extruded hollow core slab cross-sections (Richard Lees Ltd.)

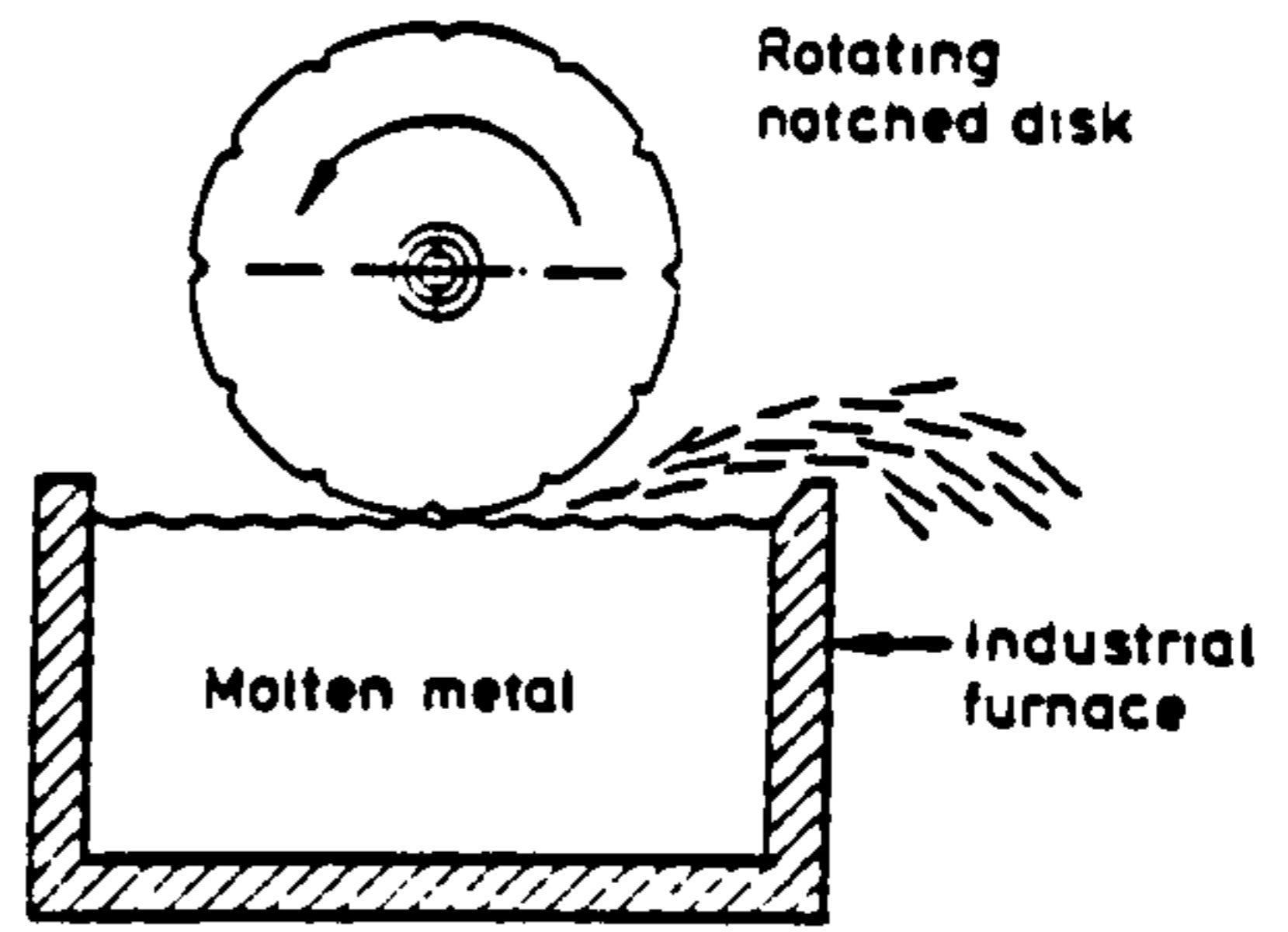


**Figure 1-3 700 mm deep slide-formed hollow core slabs (Sparrow 1992)**

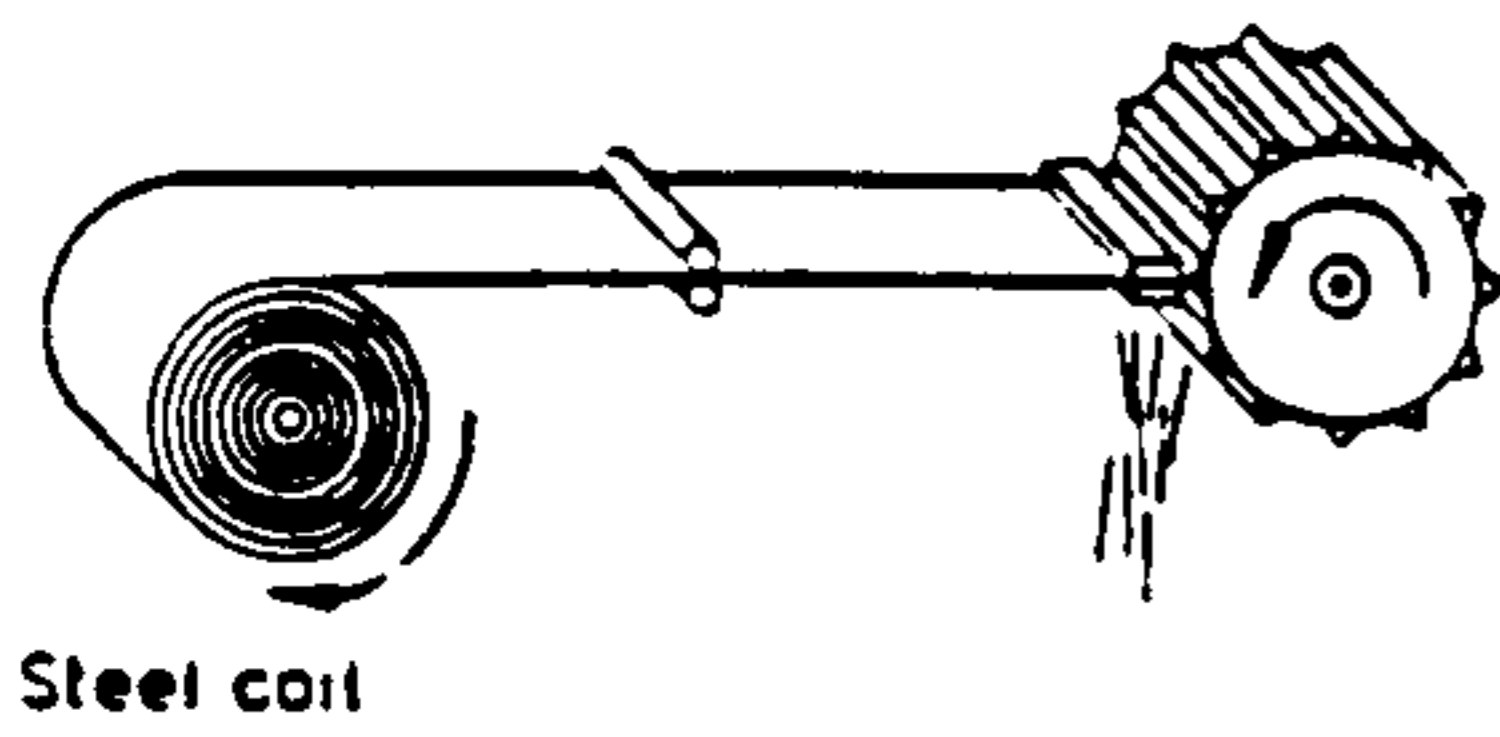
Possible fibre forms



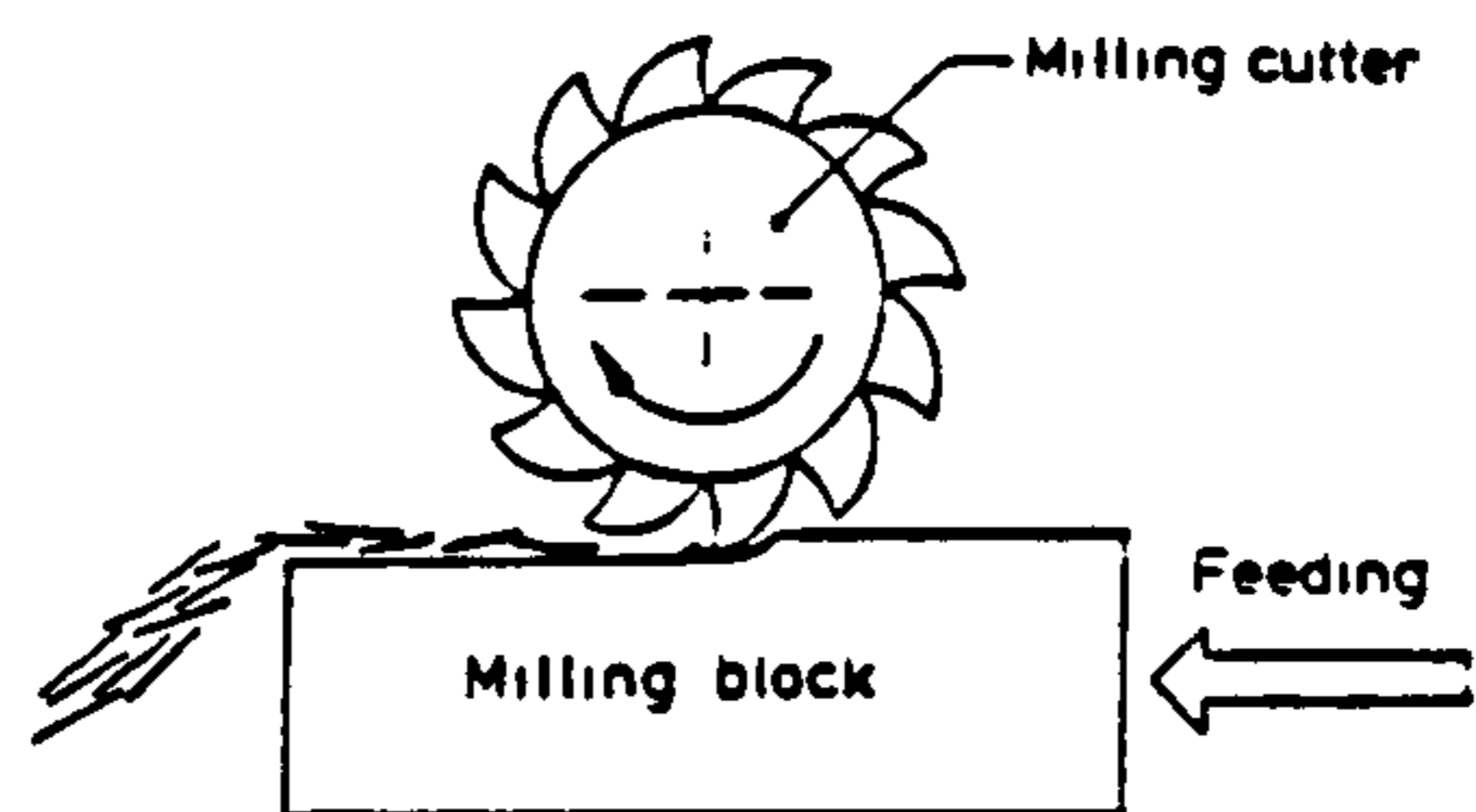
cold drawn wire process



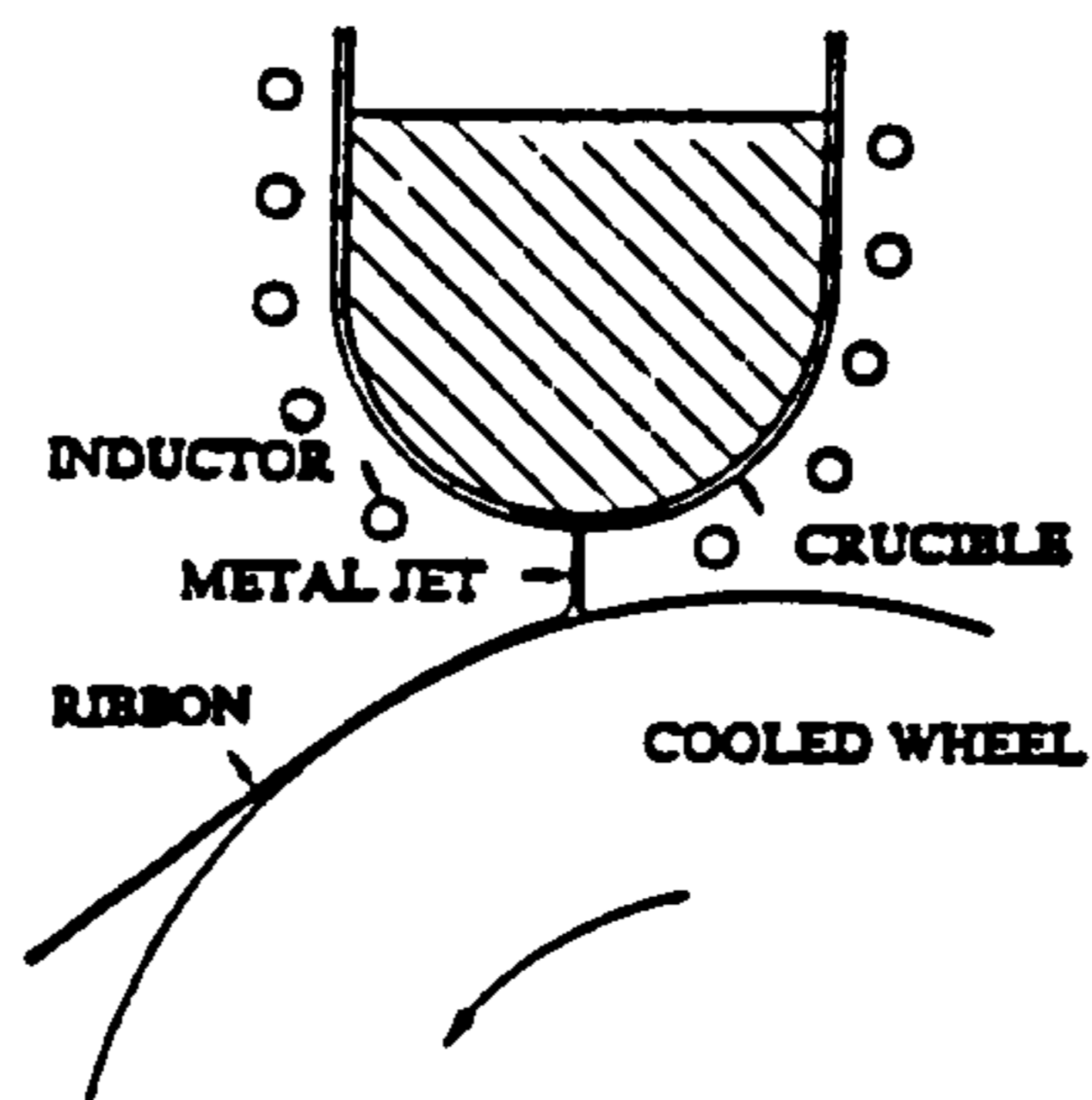
melt extraction



slitting sheets



milling process



wheel quenching process

Figure 1-4 Manufacturing methods for steel fibres (from Maidl 1995 and Boucharet 1994)

## CHAPTER 2

### MATERIAL CHARACTERISTICS OF FRC

#### 2.1 Introduction

In this chapter the effects of FRC on the standard concrete control tests, used for the experimental chapters of this thesis are reviewed. The reinforcing mechanism of the fibres in each of the tests is described and discussed. Much of the chapter deals with characterisation of flexural toughness; this is because flexural toughness is generally considered the most suitable and feasible material control test for characterising FRC. The final section of the chapter, considers each of the material control tests as a potential means of characterising material properties for use in design.

As an alternative to determining the fibre reinforcing ability empirically from control tests, it may be more practical to use theoretical tools. This is particularly true for tension where direct measurement is difficult. The tension section of this chapter therefore deals with theoretical methods for determining the reinforcing ability of fibres, and concentrates in some detail on the models proposed by Lim *et al.* (1987a) and Li *et al.* (1993).

For use in these theoretical models it is necessary to understand the fundamentals behind the fibre reinforcement mechanism, with regard to: geometry of the fibre; surface characteristics of the fibre; orientation of the fibres and fibre volume fraction. The following section concentrates on these factors which are essential for understanding theoretical treatments, and are also important for understanding the experimental results.

### 2.1.1 Orientation

Fibre orientation is an important consideration for fibre reinforced concrete because only those fibres favourably aligned with respect to the tensile stress will be effective in resisting tension. For modelling FRC an orientation factor,  $\eta_\theta$ , is often used in conjunction with the fibre volume fraction to give an effective fibre volume fraction resisting the tensile stresses. Orientation factors have been derived by many researchers (Maidl 1995) and can be summarised as (Lanu 1996):

- |  |                             |
|--|-----------------------------|
| 1. fibres aligned in direction of stress       | $\eta_\theta = 1.0$         |
| 2. fibres randomly distributed in 2-dimensions | $\eta_\theta = 1/3 - 2/\pi$ |
| 3. fibres randomly distributed in 3-dimensions | $\eta_\theta = 1/6 - 1/2$   |

where the actual orientation factor is affected by the shape and dimensions of the mould.

A commonly used value for the orientation factor is that corresponding to the average ratio for all possible fibre orientations, of the projected fibre length in the direction of stress to the actual fibre length. For the random, three-dimensional case where the fibre has an equal probability of orienting in any direction, this is calculated as (see Figure 2-1)

$$\eta_\theta = \frac{1}{\pi^2 l_f} \int_{-\pi/2}^{\pi/2} \int_{-\pi/2}^{\pi/2} l_f \cos \phi \cos \theta d\phi d\theta = 0.405$$

.. 2-1

However, boundaries which restrict the freedom of the fibres affect this orientation factor. Equations for the orientation factor of fibres within the presence of parallel boundaries are given by Soroushian and Lee (1990).

The above value of  $\eta_\theta = 0.41$  has been used by many authors (Romualdi and Mandel 1964, Lim *et al.* 1987a, *etc.*) because it relates to the pull-out behaviour of fibres, in which the efficiency of the fibre is directly related to the total fibre length resisting tension in the direction of stress.

There is evidence to suggest, however, that fibres perfectly aligned in the direction of stress are not at the optimum orientation for increasing the post-cracking strength of FRC (Bentur and Mindess 1990). This is because fibres which are askew to tensile stress are reoriented in the direction of the stress at the crack. This local bending causes flexural stresses in the fibre and local compressive stresses in the matrix. The flexural stresses lead to yielding of the fibre, and subsequently a substantial amount of the fracture energy is required to plastically deform that part of the fibre not parallel to the direction of stress. Additionally, the compressive stresses in the matrix, may lead to matrix spalling and more inelastic energy absorption. However, this spalling may reduce the fibre tension resulting in a reduction in the bridging stress. For composites with a high fibre aspect ratio or fibre-matrix interfacial bond strength these effects are not all that significant with regard to the maximum fibre bridging stress (Li and Maalej 1996). More significant, is a local friction effect known as “snubbing”, which can be visualised by regarding the fibre as acting like a rope passing over a friction pulley.

Li *et al.* (1993) have adopted this snubbing effect in their models by use of a snubbing factor,  $g$ . This factor which is greater than unity, has the opposite effect to  $\eta_\theta$  in that it has a multiplying effect on the fibre bridging stress. This is because snubbing is directly related to the fibre aspect ratio and fibre-matrix interfacial bond strength, and as either of these values increases so does the amount of energy absorption due to snubbing (Li and Maalej 1996). A value of  $g = 1.9$  is given for stiff steel fibres (Li *et al.* 1993), and a value of  $g = 1.5$  for more flexible spectra (high-modulus polyethylene) fibres (Li 1992).

Because steel fibres reorient across the crack, it has been additionally suggested by Li *et al.* (1993) that an orientation factor of  $\eta_\theta = 1.0$  is applicable to the post-cracking phase since all fibres crossing the crack will be aligned with respect to the tensile stress. However, this is likely to exaggerate the efficiency of the fibres, since the embedded length of the fibre which resists pull-out by means of bond, is still randomly oriented with respect to the stress.



### 2.1.2 Length efficiency

The ability of a fibre to effectively resist tension has to be studied with respect to a parameter known as the critical fibre length,  $l_{crit}$ . This length is the minimum fibre length required for the fibre to achieve its full tensile capacity, and is intrinsically related to the fibre-matrix interfacial bond strength ( $\tau_f$ ). Fibres shorter than  $l_{crit}$  will pullout of the matrix, whilst fibres longer than  $l_{crit}$  may fracture. The latter failure allows greater composite strengths to be attained, but has the negative effect of increasing the fracture energy and thus loses the beneficial post-cracking ductility obtained during fibre pull-out. By approximating constant shear resistance along a fibre,  $l_{crit}$  can be estimated as

$$l_{crit} = \frac{2r \cdot f_{fu}}{\tau_f} \quad .. 2-2$$

where  $f_{fu}$  is the ultimate tensile strength of a single fibre and  $r$  is the ratio of the fibre cross-sectional area to the fibre perimeter.

For any fibre under stress within the concrete, the axial stress along the length varies from zero at the end portions to a maximum in the middle. Therefore not all of the fibre length is equally effective in resisting tensile forces. To account for this variation of fibre stress at the end portions, a fibre length efficiency factor,  $\eta_l$ , is used in models for FRC. It is defined as the ratio of the average fibre stress to the maximum fibre stress, and is given as (Lim *et al.* 1987a):

$$\eta_l = 0.5 \quad \text{for } l_f \leq l_{crit} \quad .. 2-3$$
$$\eta_l = 1 - \frac{l_{crit}}{2l_f} \quad \text{for } l_f > l_{crit}$$

### 2.1.3 Fibre-matrix bond

Bond is a major factor in fibre-matrix composite behaviour. In uncracked composites, the forces are transmitted from the matrix to the fibres through bond. In the post-cracking stage, the function of the bond changes as the role of the fibres is to transmit stresses into the uncracked part of the matrix. As the fibres are bridging the crack whilst the crack openings widen, the fibres are subjected to increasing tension that will eventually cause them to pull-out or fail.

The pull-out behaviour which is important in relation to this post-cracking phase can be experimentally investigated by means of direct fibre pull-out tests, in which either a single fibre, or an array of fibres is pulled out of the matrix. The results of such tests show the relationship between the bond shear stress and slip, as well as the peak bond shear stress. For theoretical purposes, this bond shear stress - slip relationship is usually approximated as elastic-perfectly frictional (Lim *et al.* 1987a, Nammur and Naaman 1989) as show in Figure 2-2. However, some researchers (Balaguru and Shah 1992) believe that the post-peak frictional component, although still constant is actually less than the peak shear stress - thus producing a tri-linear relationship. Li *et al.* (1993) assume that the bond gradually weakens from the peak stress with increasing crack width.

For theoretical models, it is usually necessary only to have a uniform interfacial bond strength,  $\tau_f$ , corresponding to the constant frictional component of the bond shear stress - slip curve. This is commonly taken as the maximum load from direct pull-out tests divided by the fibre contact area. Doubts do exist, however, as to whether direct pull-out tests are relevant to the actual bond behaviour within a structure.

The interfacial bond between the fibre and matrix is attributable to two mechanisms. The first is chemical adhesion at the interface due to the bonding of the cement paste to the steel, and the second is mechanical anchorage due to surface configurations and deformations of the fibres. Generally, anchorage is considered to play the greater part in fibre-matrix bond. The peak load from direct fibre pull-out tests, is intrinsically a combination of both effects.

Weiler and Grosse (1996) performed pull-out tests on HS fibres to try and separate the components due to anchorage and adhesion. To record just the anchorage effect, a 60 mm x 0.8 mm HS fibre was dipped in liquid wax and then embedded in a matrix composed of epoxy resin. In addition to eliminating the effect of fibre-matrix adhesion, this enabled the behaviour of the fibre to be observed during fibre pull-out. The anchorage effect was eliminated by cutting the ends of the fibre, to leave essentially a straight fibre, to be tested in concrete. A third pull-out test on a HS fibre in concrete was also performed. The results are shown in Figure 2-3, and the summation of the two lower curves relating to anchorage and adhesion approximate to the higher curve.

It is apparent that the anchorage is much more effective in resisting the pull-out forces than the adhesion. However, beyond a slip of approximately 6 mm the anchorage becomes less significant, which provides evidence that the influence of the fibre hook has ended due to fibre straightening (Weiler and Grosse 1996). Direct observation of the fibre within the epoxy resin showed that the large initial stiffness is due to elastic deformation of the straight part of the fibre and debonding from the matrix. Once the fibre starts to pull-out, there is plastic deformation of the fibre end and deformation of the surrounding matrix. The two "peaks" in strength (in the higher pull-out curve) can be attributed to the straightening of the two bends in the fibre as it pulls through the matrix.

Both the anchorage and adhesion contribution to bond are affected by the strength of the matrix. Therefore, any value for  $\tau_f$  calculated from direct pull-out tests is related only to the concrete from which it was obtained. However,  $\tau_f$  generally increases with compressive strength, and for simplicity can often be equated to the tensile strength of the concrete.

It is not necessary to describe the pull-out behaviour of the other fibre used in this study (AM fibres) because: the bond area of the fibre is so great, and the concretes used sufficiently strong that failure will always occur by fibre rupture. This is shown in Appendix A by putting the appropriate values into Equation 2-2.

Evidence suggests that a deformation at the end of a fibre is better than deformations throughout the length of a fibre. For example, in crimped fibres it appears that stress concentrations at the troughs and peaks lead to premature failure of

the interfacial bond along the length of the fibre, resulting in a wide de-bonded section allowing the fibre to pull out relatively easily (Paine and Peaston 1997).

## **2.2 Tension**

### **2.2.1 General**

It is the post-cracking tensile strength of FRC which most distinguishes it from plain concrete and, the behaviour of fibre reinforced composites in tension has been the subject of much research and testing.

In general the tensile failure strain of the concrete matrix is much less than that of the fibre. Therefore the matrix cracks before the fibre reaches its tensile strength. After the matrix has cracked the behaviour of the FRC composite can be described by one of the following modes:

(i) The composite fractures immediately because the fibre volume fraction ( $V_f$ ) of the composite is too low to carry the load after matrix cracking. See Figure 2-4(a). This behaviour is typical of very low fibre volume fractions.

(ii) The load-bearing capacity of the composite reduces after matrix cracking, but the fibres are able to sustain a certain proportion of the transferred stresses (Figure 2-4(b)). The capacity of the composite reduces with increasing strain as the fibres gradually pull-out of the cracked surface and the final failure occurs by a single fracture. If the fibres are sufficiently long failure can occur by fibre yielding.

(iii) The fibre volume fraction is greater than the critical fibre volume fraction ( $V_{f,crit}$ ) and so the load-bearing capacity of the fibres is greater than that of the composite at first crack. Additional load leads to further cracking (multiple cracking), and a reduction in stiffness due to the loss of the matrix contribution. The maximum load is reached once the fibres commence pulling out of the matrix, or yield. Figure 2-4(c).

Modes ii and iii have engineering applications, whilst mode iii gives the optimum use of fibres. However mode ii tension failures are relevant to the fibre volume fractions used throughout this work, where sufficient fibres are provided to sustain the load after cracking, but this fibre volume is less than  $V_{f,crit}$  (see example calculations in Appendix A). The tensile behaviour of FRCs within this range of fibre volume fraction are discussed in further detail below.

### 2.2.2 Theoretical methods

In the elastic range prior to cracking, the so-called “law of mixtures” can be used as a means of obtaining the fibre reinforced composite tensile response. This assumes that the strains in the matrix, the fibres and the composite are equal; i.e. there is no slip of the fibres within the composite, and that additionally, the load carried by the composite is a summation of the loads carried by the fibres and the matrix. The modulus of elasticity of the composite ( $E_c$ ) can therefore be expressed as

$$E_c = E_f V_f + V_m E_m \quad .. 2-4$$

where  $E_f$  and  $E_m$  are respectively the Young's moduli of elasticity for the fibres and matrix, and  $V_m$  is the matrix volume fraction. Since  $V_m + V_f = 1$ , Equation 2-4 can be expressed as

$$E_c = E_f V_f + (1 - V_f) E_m \quad .. 2-5$$

However, this expression is only valid for continuous fibres, aligned in the loading direction. For a matrix reinforced with discrete and randomly distributed fibres it is necessary to include factors to account for fibre orientation, bond and length (Section 2.1) as follows

$$E_c = \eta_\theta \eta_l E_f V_f + (1 - V_f) E_m \quad \text{.. 2-6}$$

Given the modulus of elasticity of the composite, the cracking strength can be expressed as

$$\sigma_c = E_c \varepsilon_c \quad \text{.. 2-7}$$

where  $\varepsilon_c$  is the cracking strain of the composite.  $\varepsilon_c$  is often taken as equal to the cracking strain of the matrix, however, experimental results have actually shown that cracking of the FRC occurs at a slightly greater strain (Lim *et al.* 1987a).

The law of mixtures approach has also been applied to model the tensile stress-strain behaviour of FRC after cracking but has been found to be applicable only when the composite can sustain additional load in the cracked range (mode iii behaviour above), which requires  $V_f > V_{f,crit}$ .  $V_{f,crit}$  can be estimated as (Bentur and Mindess 1990):

$$V_{f,crit} = \frac{E_m \sigma_c}{E_c \eta_\theta \eta_l f_{fu}} \quad \text{.. 2-8}$$

For fibre volume fractions less than  $V_{f,crit}$  as used throughout this study, alternative models are required to characterise the post-cracking strength.

Lim *et al.* (1987a) analysed the post-cracking tensile strength of FRC by considering the idealised response of a pre-cracked FRC specimen under a tensile load. The idealised load - extension (P- $\Delta$ L) curve of a pre-cracked specimen is shown in Figure 2-5, where the extension is a combination of the elastic deformation of the uncracked part of the specimen and the crack opening width. This curve represents the fibre bridging contribution to tensile strength. In the pre-peak region of this fibre bridging curve the fibres are being stressed under increasing load, while at the peak the tensile stress in the fibres is equal to the total frictional and anchorage bond stress

and fibre slip is activated. The maximum strength ( $\sigma_{tu}$ ) of the pre-cracked composite at the onset of pullout is given as

$$\sigma_{tu} = 2\eta_l\eta_\theta V_f \tau_f \lambda_f$$

.. 2-9

The descending portion of the load-extension curve is characteristic of the gradual pull-out of fibres from the concrete. The fibre bridging stress reaches zero when the last fibre has pulled out (i.e.  $\Delta L = l_f/2$ ). The average pull-out length at commencement of pull-out is thus  $l_f/4$ . As an approximation, Lim *et al.* assumed a bi-linear post-peak curve with the load dropping from  $P_{tu}$  to  $P_{tu}/2$  at an extension of  $l_f/8$ , and then more gradually from  $P_{tu}/2$  to zero at an extension of  $l_f/2$ .

An idealised load - extension curve (Figure 2-6) for an initially uncracked FRC specimen was then produced by combining the elastic behaviour of an initially uncracked specimen (using Equation 2-7) and the above post-crack behaviour. Using experimental tensile load - extension data, Lim *et al.* suggested that the post-crack tensile behaviour could be further simplified to that shown in Figure 2-7, provided the strain range is limited. A limit of about  $\Delta L = l_f/16$  was considered appropriate, which equates to a post-cracking strain of  $\epsilon_{tu} = l_f/16l^*$ , where  $l^*$  is a suitably chosen reference length.

A more advanced analytical model for the post-cracking behaviour of FRC was given by Li *et al.* (1993), in which the total post-cracking response is not only derived from the fibre bridging effect but by aggregate bridging and fibre prestress. The total post-crack response derived from these three contributions is shown in Figure 2-8.

The aggregate bridging contribution ( $\sigma_a$ ) can be expressed as a function of the crack-width opening,  $w$ , from an empirical model proposed by Stang (1992), given as

$$\sigma_a = \frac{\sigma_m}{1 + \left(\frac{w}{w_o}\right)^p}$$

.. 2-10

where  $\sigma_m$  is the cracking strength of the matrix,  $p$  characterises the softening process, and  $w_0$  is the crack opening which corresponds to  $\sigma_m/2$ .

The fibre prestress contribution ( $\sigma_{ps}$ ) considers that the fibres have been previously stretched before cracking due to load-sharing between the fibres and matrix in the uncracked state. This value is therefore effectively the fibre contribution to pre-cracking strength, and can be determined from Equation 2-6 and Equation 2-7 as

$$\sigma_{ps} = (\eta_\theta \eta_l V_f E_f) \epsilon_c \quad .. 2-11$$

It was assumed by Li *et al.* that this prestress will decrease linearly with  $w$ , and reach zero at the crack width at which fibre pullout commences.

For the fibre-bridging curve the pre-peak region of a cracked specimen was assumed to be similar to that given by Lim *et al.* (1987a) with the exception that the maximum fibre bridging stress is given as

$$\sigma_m = \frac{1}{2} g \tau_f V_f \lambda_f \quad .. 2-12$$

The value  $\frac{1}{2}$  is associated with  $\eta_l$  in Equation 2-9, and thus the difference between Equation 2-9 and Equation 2-12 exists in the difference between the snubbing factor,  $g$  and the factor,  $2\eta_\theta$ . Suggested values by the author for these factors, presented in Section 2.1.1 of respectively 1.9 and 0.82, show that Li *et al.* estimate the ultimate fibre bridging stress to be approximately 2.3 times that estimated by Lim *et al.* However, this difference is more than accounted for by Li *et al.*'s assumption that no orientation factor is necessary because all the fibres are reoriented to align with the tensile stress. Use of an orientation factor in Equation 2-12 may be necessary, and would bring the equation into line with Equation 2-9.

In addition, the post-peak behaviour of the fibre bridging effect was analysed by Li *et al.* with respect to a degenerative fibre-matrix interfacial bond with increasing slip (as opposed to plastic load-slip behaviour assumed by Lim *et al.* (1987)), and additionally a so-called Cook-Gordon debonding effect.



To describe the degenerative loss of interfacial bond strength with increasing crack width, a polynomial form was employed for the fibre pullout as follows

$$\tau(\delta) = \tau_f + a_1 \delta + a_2 \delta^2$$

.. 2-13

where  $\delta$  is the crack width associated with debonding, and  $\tau_f$  is the initial fibre-matrix interfacial bond strength. For 25 x 0.4 mm diameter steel fibres (geometry of fibre unknown)  $a_1$  and  $a_2$  have been found experimentally from pull-out tests to be approximately -4.0 and 1.0 (Li *et al.* 1993).

The Cook-Gordon effect considers a crack tip stress field, whereby a matrix crack approaching a fibre can cause interfacial debonding before the crack tip actually reaches the fibre-matrix interface. This has been observed experimentally by Bentur and Mindess (1993) using spectral electron microscopy. It is modelled by Li *et al.* by assuming that elastic stretching of the debonded length, defined by the Cook-Gordon parameter,  $\alpha$  (related to size and type of fibre) causes an additional crack displacement. Li *et al.* assume an arbitrary value of  $\alpha = 15d_f$ , with no experimental evidence. Figure 2-9 shows the relative importance of including the slip-weakening and Cook-Gordon effects on the total post-cracking response. By neglecting the Cook-Gordon effect it can be seen that the strength at small crack widths is overestimated, but that there is little effect at higher crack widths. The bond-weakening effect only becomes important at larger crack widths.

### 2.2.3 Direct measurement of tensile strength

There is at present no standard procedure for uniaxial tensile testing of plain concrete or FRC because it is difficult to perform. The main difficulty is in obtaining a uniform stress distribution across the specimen without introducing stress concentrations, which usually requires incorporating a "neck" into the specimen. This makes the moulds an inconvenient shape and there is an increased risk of eccentricities leading to false results.

In the most commonly used non-necked specimens, steel plates are glued to end surfaces. However, the adhesive and the concrete exhibit different lateral strains due to differences in Young's modulus and Poisson's ratio, which leads to shear stresses at the contact zone. Failure therefore tends to occur near the end of the specimens, and again "necking" of the specimen is the solution (Hansen 1996). In addition, specially designed grips which do not induce local stress concentrations are also required, which can lead to complicated test arrangements.

Successful testing of FRC in uniaxial tension is more difficult than testing of plain concrete because it is additionally necessary to be able to control the machine after matrix cracking in order to record the post-cracking curve and measure the post-cracking strength. This is particularly difficult when  $V_f < V_{f,crit}$  because of the large fall in load-carrying capacity after cracking. It is possible to record the post-cracking curve with some closed-loop control testing machines.

Further, because of the method in which most tensile test specimens are cast, the majority of fibres within the concrete tend to be aligned at right angles to the tensile stress. This leads to lower cracking and post-cracking tensile strengths, and a greater possibility of an uncontrolled failure.

Since uniaxial tests are difficult to perform, and research has led to the development of useful analytical tools for predicting the post-cracking response of FRC, no uniaxial tests were performed in this work. The cracking strength of the FRC can be estimated by indirect means like the splitting tensile test (Section 2.2.4) or the flexural test (Section 2.4.2).

#### **2.2.4 Indirect measurement of tensile strength**

The splitting tension test is the most popular indirect method of measuring the tensile strength of plain concrete. In its simplest form it consists of applying a load to a cylinder along two opposite generatrices as shown in Figure 2-9. This subjects the element to a vertical compressive stress along the loading plane and horizontal tensile stress normal to this plane. To reduce localised compressive stress directly under the

load, a loading strip of a width of about a tenth the diameter of the cylinder is interposed between the cylinder and platen.

The resulting horizontal elastic stress distribution along the vertical diameter is shown in Figure 2-10. The maximum tensile stress, which is approximately constant over 80% of the diameter (Nanni 1988), and maximum at the cylinder centre, can be expressed approximately as

$$f_{ct,sp} = \frac{2P}{\pi l D}$$

.. 2-14

where P is the compressive load on the cylinder, l is the length of the cylinder, and D is the diameter. The test can also be performed on cubes or prisms. In the case of cubes, the load is applied through semi-cylindrical platens resting against the cube on the centre line of two opposing faces. The load is assumed to act through a cylinder inscribed within the cube, and the dimension of the cube replaces l and D in the above equation.

However, tests on cubes are considered to be less reliable than those on cylinders, owing to uneven stress distribution (Neville 1981). Additionally, tests by Hansen (1996) have shown that cubes give higher splitting strengths than cylinders with the same cross-sectional dimension, and argues that for this reason, cubes should not be used as they possibly overestimate tensile strength.

The splitting tensile strength (corresponding with maximum load) has been observed as being about 5-12% greater than the actual direct tensile strength (Neville 1981) for plain concrete, and tests generally show the splitting tensile strength to be greater than that attained from direct uniaxial tests. Some tests do show the opposite behaviour. Hansen (1996) points out four aspects to consider when comparing the tensile strength from the two types of test. Three which give reasons why the direct strength would be expected to be give lower results than the splitting test, and one reason why the splitting test should give the lowest result. His reason for suspecting the splitting tensile strength to be lower is that within the failure zone of the splitting test there are both tensile and compressive stresses leading to greater strains within the concrete.

Hansen also reports that finite element analysis has shown that the ratio between the splitting strength and direct tensile strength is dependant on specimen size and concrete ductility. As the specimen size decreases or the ductility of the concrete increases, the splitting tensile strength increases more significantly than the direct tensile strength. For large, brittle high strength concrete specimens there is less difference between the two tests.

From the above evidence, it would appear that to obtain the best measure of the tensile strength of concrete from the splitting tension test it is necessary to use relatively large cylinders, and that the test works best for high strength concrete which is more brittle than normal strength concrete.

Splitting tension tests have been carried out on FRC by a number of researchers. They each note that there are two parameters of interest; first crack splitting strength ( $f_{cr,sp}$ ) and ultimate splitting tensile strength ( $f_{ct,sp}$ ). In tests by Nanni (1988) the first crack strength (defined as the point of non-linearity on a load-deflection curve) was found to be only slightly affected by fibres and strongly dependant on matrix characteristics; values of  $f_{cr,sp}$  between 0.95 and 1.1 of the splitting tensile strength of plain concrete being obtained. Since  $f_{cr,sp}$  approximately corresponds with onset of cracking in the matrix, it can probably be regarded as a measure of the direct tensile strength of FRCs in which  $V_f < V_{f,crit}$ .

In contrast, the ultimate splitting strength is strongly dependant on the fibre performance. The ultimate splitting tensile strength of FRC has often been dismissed (e.g. ACI Committee 544, 1988), because the stress distribution after cracking is unknown. Nanni (1988) reports, however, that finite element analysis shows the stress distribution up to ultimate does not differ substantially from that up to cracking. Equation 2-14 can still be used therefore to provide an indication of the ultimate strength of FRC - although, of course, it has no real physical meaning.

Even with low fibre volume fractions (e.g., 0.5%) the ultimate splitting strength of FRC is greater than the cracking strength, which differs markedly from the behaviour in direct tension. This confirms that the behaviour between cracking and ultimate is not solely due to tensile effects. However, it should be noted that by using normal casting methods the majority of fibres in a splitting cylinder test will be aligned favourably to the tensile stresses, whereas in a uniaxial direct tensile test they

are more likely to be aligned perpendicular to the direction of stress. For this reason it should be expected that the splitting cylinder test will give greater cracking and post-cracking strengths. However, these differences in alignment of fibres do not fully explain the differences in post-cracking behaviour in splitting tension and uniaxial tension tests.

Tests performed by Narayanan and Palanjian (1984) and Nanni (1988) on a total of six fibre types: straight round fibres; crimped fibres; indented (duoform) fibres; deformed-end wires; slit-sheet fibres and mill-cut fibres, have shown that  $f_{ct,sp}$  increases with  $V_f$  and  $\lambda_f$ . Additionally the mechanical anchorage provided by the deformed-end fibres gives much greater ultimate strength than alternatives such as mill-cut fibres.

An empirical equation was developed by Narayanan and Palanjian (1984), to predict the ultimate splitting tensile strength of plain concrete and FRC. It is given as

$$f_{ct,sp} = \frac{f_{cu}}{20 - \sqrt{F}} + 0.8 + 1\sqrt{F} \quad (\text{N/mm}^2) \quad .. 2-15$$

The factor  $F$ , known as the fibre factor, reflects the influence of  $V_f$  and  $\lambda_f$ , and also includes a bond factor  $\eta_b$  to account for the relative bonding capabilities of different fibre types, and is given as

$$F = \eta_b V_f \lambda_f \quad .. 2-16$$

Reported values of  $\eta_b$  were: 0.5 for straight round fibres; 0.75 for crimped fibres and 1.0 for indented fibres (Narayanan and Palanjian 1984). Imam *et al.* (1997) have extended this list by giving a value of 1.0 to HS fibres. For plain concrete (i.e.,  $F=0$ ), Equation 2-15 equates to that given by Marshall (1974).

## 2.3 Compression

Improvements in the compressive strength of concrete by adding steel fibres are small, and for design purposes can be assumed to be negligible (Balaguru and Shah 1992). However, given that compression tests are the most commonly used quality control tests for plain concrete, and that compressive strength is used in most design codes for concrete, it is important to consider the effect of fibres on this strength. A large number of tests by Narayanan and Palanjian (1984) has led to the development of an equation for the lower-bound compressive cube strength of FRC, where the increase in strength over an equivalent plain concrete matrix is given as  $f_{cu} \cdot F/10$  (N/mm<sup>2</sup>). This is consistent with their observation that fibre addition has a proportionally greater effect on the strength of high-strength concrete than normal strength concrete.

However, the addition of steel fibres can sometimes lead to lower compressive cube strengths, often because of difficulties in compacting FRC (e.g. Paine and Peaston 1997). This is consistent with observations that factors resulting in lower compressive strengths in plain concrete (i.e. water/cement ratio, percentage of air voids) have more effect on the compressive strength than the fibres.

Because of the small effect of the fibres, the compressive strength test is insufficient for determining the increased reinforcing ability of FRC. However, the test is still useful for quality control purposes to ensure adequate compaction and necessary strength development of the mix, e.g. sufficient strength for release of prestress in pretensioned concrete.

The toughness of FRC under compression is, however, much improved over that of plain concrete, and is related to the ability of fibres to resist lateral strains (Maidl 1995). The inclusion of fibres is therefore useful in reducing spalling and increasing post-cracking ductility and energy absorption. High-strength concrete has a much steeper descending branch to the compressive stress - strain curve than normal strength concrete. Taerwe (1991) has shown that the inclusion of only a small amount of fibres (30-40 kg/m<sup>3</sup>) to high-strength concrete makes the descending curve similar to that of normal strength concrete. For this reason the inclusion of fibres in high-strength concrete for traditional construction practice has been vaunted.

## 2.4 Flexure

### ✂ 2.4.1 Introduction

Flexural tests are generally regarded as the most practical methods of characterising the strength and ductility of FRC. The tests are usually performed on prisms subjected to either centre-point loading or symmetrical two-point loading (four-point flexure test). The latter arrangement is the most popular because it subjects a larger percentage of the span to the maximum bending moment. There is therefore a greater possibility of the weakest part of the element being subjected to the maximum stress. This leads to lower flexural strengths being recorded.

In addition to flexural strength, FRC prisms have been widely used for calculating toughness based on the load-deflection behaviour before and after cracking. Although toughness can also be calculated from tension and compression tests, flexural tests are by far the most popular.

### 2.4.2 Flexural Strength

The most common flexural strength measured for a plain concrete beam is the modulus of rupture ( $f_{fl,ult}$ ) which is calculated using ordinary elastic theory from the maximum bending moment borne by the beam. The modulus of rupture is often regarded as an indirect measure of the tensile strength of the concrete, but is in fact greater than the tensile strength because close to failure, tensile stresses in the concrete are not proportional to distance from the neutral axis (Neville 1983). The modulus of rupture for a prism tested under symmetrical four-point bending is

$$f_{fl,ult} = \frac{Pl}{bh^2}$$

.. 2-17

where P is the maximum total load on the beam, and l, b and h are respectively the span, width and depth of the beam.

For plain concrete, the ultimate load (and therefore the modulus of rupture) occurs almost simultaneously with the first crack. Therefore for plain concrete the first crack flexural strength ( $f_{fl,cr}$ ) is equal to the modulus of rupture. After cracking, the load-carrying capacity of a plain prism is significantly reduced and falls to zero almost immediately. However, with sufficiently stiff-testing machines the actual load - deflection behaviour can be recorded.

Considerable loads can be carried by FRC after cracking because of its ability to carry tensile stresses across the flexurally cracked region. As with tensile strength, once a critical fibre volume fraction is added to the concrete then the ultimate strength of the prism can exceed the cracking strength. The critical fibre volume in flexure ( $V_{f,crit,fl}$ ) is less than that in tension, because of inelastic behaviour, and can be estimated as  $0.41 V_{f,crit}$  (Lanu 1995).

A number of authors have attempted to model the ultimate flexural strength of FRC using various assumed stress distributions (Hannant (1978), Mangat and Gurusamy (1983) and Lim *et al* (1987b)). For composites with fibre volumes less than  $V_{f,crit,fl}$ , the law of mixtures for tension can be applied to elastic theory, with an adjustment to the composite strength to compensate for differences between flexural and tensile strength.

Where the composite can carry greater loads after cracking, Mangat and Gurusamy (1987) showed that it is essential to include the effects of both the matrix and fibres within the tensile region. Alternative approaches by Hannant (1978), which considered only the fibre contribution were shown to be inappropriate in their assumption of a fully cracked and ineffective matrix at ultimate load because this leads to unrealistically high values of  $\tau_f$ .

Ultimate flexural strength occurs at relatively small crack widths, and an analytical model based on a fictitious crack concept has shown ultimate flexure to occur when the fracture process zone is only partially developed (Maalej and Li 1994). The matrix contribution to flexural strength is therefore significant. Robins *et al.* (1995) showed that the tensile zone of a FRC beam under flexure can be schematically represented by four distinct zones (see Figure 2-11): an uncracked tensile zone; an aggregate bridging zone; a fibre bridging zone; and a traction free zone (where the fibres have completely pulled out of the matrix).



The tensile stress-strain block which is formed from the combination of these four zones constantly changes as the crack propagates. The flexural capacity of the beam at any crack length is therefore related to a number of factors, of which the fibre pull-out stress distribution is the principal parameter (Robins *et al.* 1995). Mangat and Gurusamy (1987) have shown experimentally that at ultimate load the neutral axis is about 0.75h from the tensile face, while in the descending portion of the load - deflection curve the neutral axis rises to a maximum height of 0.9h.

### 2.4.3 Energy-based dimensionless indices

The first methods adopted to characterise the flexural toughness of FRC were energy-based dimensionless indices. The first recommended procedure was given by ACI Committee 544 (1978), but this procedure is now obsolete.

The most familiar energy-based dimensionless indices are given in ASTM C 1018 (1994), and also currently recommended by the American Concrete Institute (ACI Committee 544, 1988), which are based on work by Johnston (1982).

These ASTM indices are computed as the ratio of the load under the load-deflection curve up to a specified multiple of the "first crack" deflection ( $\delta_{cr}$ ), to the area under the same curve up to  $\delta_{cr}$ .  $I_5$ ,  $I_{10}$ , and  $I_{20}$  are calculated at deflections of  $3 \delta_{cr}$ ,  $5.5 \delta_{cr}$  and  $10.5 \delta_{cr}$ , respectively, such that a perfectly elastic-plastic material would produce toughness values of 5, 10 and 20. See Figure 2-12.

The first crack deflection is defined in ASTM C1018 as the point on the load-deflection curve "at which the curvature first increases sharply and the slope of the curve exhibits a definite change". However many researchers have reported difficulties in actually identifying this point. ASTM C1018 (1994) recommends the use of a plotted scale on which the load scale corresponds to at least 25 mm for a stress of  $1 \text{ N/mm}^2$ , and a deflection scale where 25 mm corresponds to a deflection of 0.1 mm. Modern computer programs enable greater resolution to be achieved, in which the initial "linear" portion can appear as a smooth curve. This is because in reality there is no such thing as a first crack; microcracks occur in the matrix from the moment tensile stresses are first induced. The term "limit of proportionality" is

therefore often adopted as a more appropriate term for the point referred to by ASTM C1018 as the first crack. It is possible to estimate the deflection at the limit of proportionality using the following equation (Johnston 1985):-

$$\delta = \frac{23Pl^3}{1296EI} \left( 1 + \frac{216d^2(1+\mu)}{115l^2} \right)$$

.. 2-18

where  $\mu$  is Poisson's ratio,  $I$  is the uncracked second moment of area of the prism and  $E$  is Young's modulus for the composite.

The ASTM indices have been criticised for not distinguishing between FRCs made with different fibre types, fibre volumes and fibre aspect ratios. This is mainly because the indices are based on the area under the load-deflection curve up to small deflections where the performance of the beam is still largely governed by the matrix, and the fibres play only a secondary role. The load-deflection curves originally considered by Johnston (1982) were based on gross deflection in which extraneous deflections were included, see Section 2.4.9. Measuring gross deflection rather than net deflection may yield deflections of the order of three times the actual deflection. Therefore, when ASTM first accepted this procedure the indices were useful for distinguishing between different FRCs. With the use of net deflection, which is used to make the tests less machine dependent, their usefulness has diminished. Gopalaratnam *et al* (1991) showed that the indices were only useful at high deflections relating to indices of  $I_{30}$  and  $I_{50}$  (which are no longer required in ASTM C1018).

#### 2.4.4 Load-based dimensionless indices

To overcome the difficulties in locating the first crack deflection present in the energy-based method of ASTM C1018, Nemegeer and Tatnall (1995) have proposed a load-based dimensionless index. This is defined as the ratio of the average load present in the composite over a specified deflection limit to the load at first crack, see Figure 2-13. To overcome the same problem as in ASTM C1018 in locating the point

of first-crack on a load-deflection curve, the first-crack load has been defined objectively by the following method (see Figure 2-14):

A straight line is drawn parallel to the initial linear portion of the curve at a distance  $x$  mm from the origin (where  $x$  is taken as the theoretical first crack deflection from Equation 2-18). The first crack is then taken as the point where the load - deflection curve first shows a drop in load before crossing this line. If no drop in load is recorded then the first crack is taken as the intersection point.

Despite the index being dimensionless the influence of specimen dimensions is unknown. Nemegeer and Tatnall therefore recommend a fixed beam geometry, whilst test programmes examine size effects. The deflection intervals recommended are span/900 to span/300, and span/300 to span/150. The Belgian Standard implements three strength-based dimensionless indices based on deflection intervals of span/600, span/450, span/300 and span/150 (Gopalaratnam and Gettu 1994).

#### **2.4.5 Energy absorption capacity**

An approach to defining toughness based simply on the area under the load - deflection curve has been proposed by the Japan Concrete Institute (JCI SF4 1983b), where the measured toughness parameter,  $T_{JCI}$ , is taken as the area under the load - deflection curve up to a deflection of span/150. Studies have shown that this parameter is more sensitive to changes in fibre type and fibre content than the ASTM C1018 indices, and is therefore a more useful measure of the relative toughness of FRCs (Gopalaratnam *et al.* 1991).

A major criticism of JCI SF4 is that the toughness parameter is dependant on the specimen size and testing configuration. For fibres of length less than 30 mm, JCI SF4 recommends a 100 mm x 100 mm cross-section beam tested over a 300 mm span, and for FRCs with longer fibres a test beam of 150 mm x 150 mm cross-section over a span of 450 mm. This leads to obvious difficulties in comparing the toughness of FRCs made with different fibre lengths. A further criticism of the JCI toughness definition is that the limiting deflection of span/150 is large, and does not reflect a useful level of serviceability for many FRC applications.

Additionally, the JCI SF4 parameter does not reflect the shape of the load - deflection curve and can fail to distinguish between low fibre volume composites, where only toughening takes place, and high fibre volume composites where there is both strengthening and toughening (Trottier and Banthia 1994). FRCs with significantly different load - deflection curves can therefore be defined as having identical toughness (Johnston 1985), see Figure 2-15. However such load-deflection curves are extreme, and generally JCI SF4 adequately defines toughness.

#### **2.4.6 Equivalent flexural strength**

Equivalent flexural strengths can be derived from the JCI SF4 parameter,  $T_{JCI}$ , to dimension the parameter with respect to specimen size and test span. In JCI SF4, an equivalent flexural strength (or “flexural toughness factor”) is expressed as  $(T_{JCI} \times \text{span})/(\delta_{JCI}bd^2)$ , where  $\delta_{JCI}$  is span/150.

Similar equivalent flexural strength definitions appear in the Belgian and Dutch standards (Gopalaratnam and Gettu 1994). The Belgian standard defines two equivalent strengths at deflection limits of span/300 and span/150, whilst the Dutch code specifies identical limits of 1.5 mm and 3 mm for a test span of 450 mm.

An alternative approach is adopted in the German recommendations, where the area used to compute the equivalent flexural strength is taken as the area under the load - deflection curve up to a specified deflection, with the idealised contribution of an unreinforced beam subtracted (Nemegeer and Teutsch 1993).

#### **2.4.7 Residual strength**

In addition to the energy-based dimensionless indices, ASTM C 1018 (1994) requires the computation of dimensionless residual strength factors. These factors termed  $R_{5,10}$  and  $R_{10,20}$  are computed as  $20(I_{10} - I_5)$  and  $10(I_{20} - I_{10})$  respectively, and represent the average strength between the two cut-off deflections as a percentage of the first-crack strength.

As an alternative to residual strength factors, it is also possible to define the flexural toughness of FRC using residual strength values defined as the post-cracking strength at a particular deflection. This method is currently adopted in the EFNARC (1994) specification for sprayed concrete, which classifies FRCs by the strength remaining at deflections of 1mm and 3mm, for a 75 x 125 mm beam over a span of 450 mm. However, Morgan *et al.* (1995) have raised concerns with using actual values for the residual strength limits and suggest that they should be specified as a percentage of a required design flexural strength.

#### **2.4.8 Specific issues related to flexural toughness**

Sections 2.4.3 - 2.4.7 have indicated a number of methods for calculating and characterising the flexural toughness of FRC. Of primary importance, for use as a design and quality control parameter, is that toughness results are repeatable and the tests are machine independent. There are a number of issues which relate to each of the test methods described which need to be taken into account if meaningful toughness values are to be measured. Three of these issues are described in detail below: accurate measurement of deflection; specimen size; and stability of the test specimen.

In calculating the toughness of FRC it is important that the net deflection of the beam is measured, independent of extraneous deformations, so that tests performed on different machines may be compared. This is particularly true for toughness measures based on first crack deflection. Extraneous deformations to be avoided are: (El-Shakra and Gopalaratnam 1993)

- 1) Elastic and inelastic deformations of the loading fixtures and supports. About 80% of all extraneous deformations are due to elastic punching deformations at the supports.
- 2) Local deformations of the beam at the loading points.
- 3) Initial specimen rocking.

It has been shown that the gross deflection at first crack due to measuring extraneous deformations is generally about three times greater than the net deflection, and that the inclusion of extraneous deformations can lead to errors of up to 30% in the calculation of ASTM indices (Gopalaratnam *et al* 1991). The error is smaller (5%) in measuring JCI SF4 toughness, because the limiting deflection is much larger and the measuring error becomes gradually negligible with increasing deflection, see Figure 2-16.

A number of systems have been recommended for measuring net deflection, and a yoke system, similar to that originally recommended in JCI SF4 (1983b), has been adopted at the University of Nottingham and was used for flexural toughness testing throughout this thesis. This yoke system is shown in Figure 2-17 and Plate 2-1.

The cross-sectional size and test span also play an important role in generating toughness values. Measures based on absolute values such as the JCI Toughness parameter are wholly dependant upon the specimen size and are only meaningful when compared to identically sized specimens.

The ASTM indices were originally defined so as to be independent of specimen size (Johnston 1985), however this has since been shown to be true only when specimens are exactly geometrically proportionate (Chen *et al* 1994). Nemegeer and Tatnall (1995) are unsure of the effect of the specimen size on their strength based dimensionless indices. However, since the base level of their measure is the first crack strength, there is a probable size effect, because it is known that first crack strength decreases with specimen dimensions (Gopalaratnam and Gettu 1994).

The specimen size also affects test results because of the affect of shear. Most standard test beams are in the ratio of 1:1:3 (height: width: span), with a shear span to depth ratio of 1. This leads to high shear stresses similar to those occurring in deep beams, and the additional deformation due to shear can be as high as 25% of the total deflection.

The speed of test also possibly affects toughness values. However, it is generally believed that there is no significant effect if the speed is less than 0.5 mm/min (Nemegeer and Tatnall 1995). Recommended test speeds are specified in each standard, and are generally less than 0.5 mm/min.

A more significant problem in calculating and comparing toughness values is met in attempting to accurately measure load and deflection immediately after cracking. For FRCs with low fibre volume fractions, a momentary loss of test stability often occurs when the matrix cracks, making it impossible to record the actual specimen behaviour. The usual explanation is that an insufficiently tough FRC specimen has been tested in an insufficiently stiff testing machine (Morgan *et al* 1995) and that the problem can be overcome by using closed-loop servo-controlled testing machines. However, even with these machines loss of stability is likely when very high strength FRCs with low fibre volumes reach first crack (Gopalaratnam and Gettu 1994).

Since most testing laboratories do not have such sophisticated equipment and losses in stability can occur even with normal strength concretes there is a need to decide how load - deflection curves with areas of instability can be utilised - if at all. No test standards at present offer any guidance (Gopalaratnam and Gettu 1994).

Since the ASTM C1018 indices  $I_5$  and  $I_{10}$  often fall within this instability range, the validity of these indices is questionable - even before considering the problems in locating the first crack (see Section 2.4.3). The problems identified with instability become less important as the limiting deflection becomes larger. In fact calculation of the JCI toughness parameter is largely unaffected by problems of instability.

## **2.5 Material property based design**

The need to find a characteristic material property for FRC that can be used in the design of FRC, RFRC and PFRC structures has long been recognised. This task has proved difficult since the material property chosen must be consistently defined and well understood, applicable to all fibre types and above all adequately able to distinguish FRC from concrete without fibres. In addition the material property should be able to reflect the combined effects of many more basic parameters. For example parameters such as fibre aspect ratio, fibre-matrix interfacial bond strength and orientation factors have often been adopted in empirical design equations, but their

use in actual design procedures is possibly too detailed (Criswell 1994). One material property that measures all of these effects would be more useful in design.

Toughness is recognised as the property of FRC that most distinguishes it from plain concrete, and of the different measures of toughness, flexural toughness is probably the most useful in terms of devising FRC designs. Flexural toughness is well understood and requires little adaptation for use in present material testing machines. Its ability to provide consistent measures of FRC properties has led to its use in two specifications suitable for sprayed concrete to specify levels of deformation performance; the American specification (ASTM C 1116, 1995) uses ASTM C 1018 toughness indices, whilst the European specification (EFNARC 1996) uses residual strength classes.

In an attempt to consolidate research on FRC in structural elements N.V. Bekaert have worked out a guideline for the design of steel wire fibre reinforced concrete structures (Dramix Guideline 1995). This document, based on Eurocode 2 as a framework, almost exclusively details the fibre benefit in terms of flexural toughness, making use of equivalent flexural strengths and ratios between equivalent flexural strength and cracking flexural strength.

The benefits of using flexural toughness as a material property definition for FRC is that it is easy to measure, and the results are directly related to the benefits of fibres in increasing performance. A disadvantage is that the property is not uniquely and consistently defined, in addition to the problems outlined in Section 2.4.9. For flexural toughness to be generally accepted as a design property, consensus must be reached to which methods of characterising toughness are most useful. For example, the ASTM C 1018 toughness indices are unlikely to be any use for a structural design purpose, given that the many problems relating to location of the first crack deflection will make designs based on such a method unreliable.

The other major disadvantage with flexural toughness is that accurate load - deflection curves can only be achieved with closed loop strain controlled testing equipment due to the instabilities after first crack. Any properties calculated within the instability area are machine dependant and effectively useless as design parameters. Equipment which can overcome this problem is expensive and not commonly found in testing laboratories. Because of this some current feeling is that



deflection control should be discontinued and crosshead control taken as standard. Another solution is to use toughness characterisation parameters calculated away from the instability zone. Unfortunately the critical strains found in most structural FRC applications will relate to the strains and crack widths found within the instability zone of flexural toughness tests.

Some design reports and guidelines are now using flexural toughness to define the increased ductility and energy absorption of structural members due to fibre addition. To make the use of such procedures easy for designers and concrete specifiers the design equations are generally only slight modifications of those currently in practice.

Use of flexural toughness is opposed, however, by many researchers and designers. Criswell (1994) in particular points out that to completely describe toughness both first crack strength and index values are required, and makes use of the concept impractical. Use of a single equivalent flexural strength would of course overcome this problem.

In Criswell's opinion, any material test used must be well formulated and the behaviour of the FRC material within the test specimen well defined, whilst the single quantity measured must be both strength and ductility related. Use of ultimate strength and post-cracking strength values from direct tension, splitting strength and compression tests are therefore inadequate since these values are not related to ductility. This problem could be overcome by measuring deformations, and calculating a toughness related parameter. In the case of the splitting tension test, Nanni (1988) has shown that toughness values adequately describe the performance of FRC and can be considered as a viable alternative to the flexural test. A standard compression toughness test is given in JCI SF5 (JCI 1983c), and according to Gopalaratnam (1997) the parameters give good correlation with the post-cracking toughness of RFRC beams. However, both the splitting tension test and compression test fall foul of the stipulation that the behaviour of the FRC material within the test should be well defined and understood.

Criswell (1994) proposes a modified modulus of rupture test as a possible method of predicting a cracked FRC design strength directly related to RFRC applications. The test is essentially a standard flexural test on a 150 mm square cross-

section prism tested over a 450 mm span, except that a 9 or 10 mm diameter deformed bar is placed at the bottom at a cover of 19 mm. The principle is that this models a local region of a RFRC member, in the form of stirrups, ties or small flexural reinforcement. Possible property measures are the FRC flexural strength (estimated from the overall strength by subtracting the idealised contribution of the deformed bar) at a specified strain, or the minimum strength within a specified strain range.

The obvious problem with this proposal is that the material measure of FRC is not necessarily independent of the reinforcing bar, and therefore is unlikely to be directly relatable to more heavily reinforced beams. Additional discouragements to its use are that the specimen is not straightforward to produce, and the material property is not directly measured.

No suitable measure is therefore presently available for use in structural design of FRC, although flexural toughness appears to be the most promising approach. Throughout the tests reported in this thesis a number of prisms were therefore cast from each laboratory mix for assessment of flexural toughness, with the aim of finding a correlation with the main test results. In addition, standard ultimate splitting tension and compression tests were also performed.

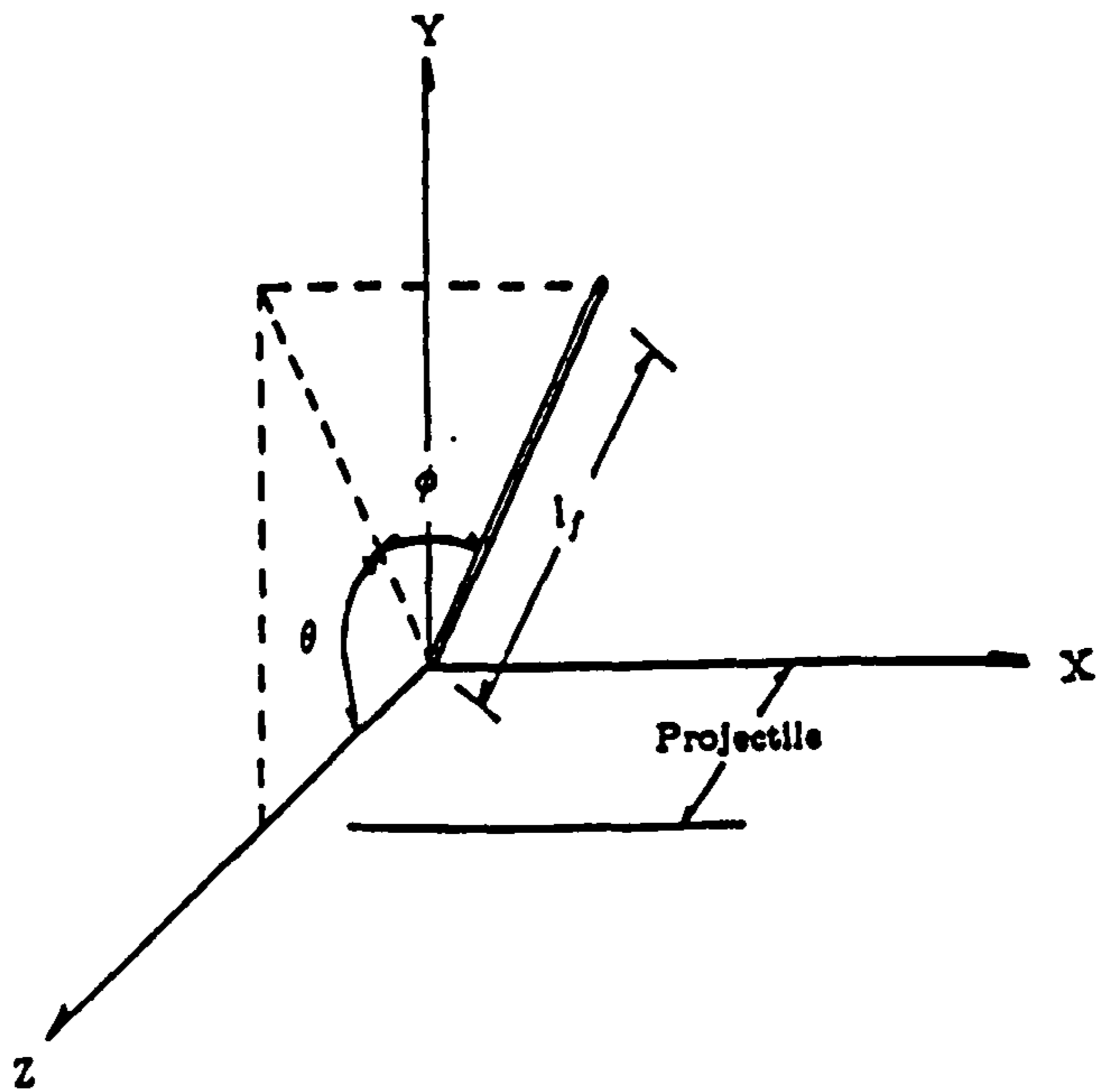


Figure 2-1 Three dimensional orientation of fibres (Soroushian and Lee 1990)

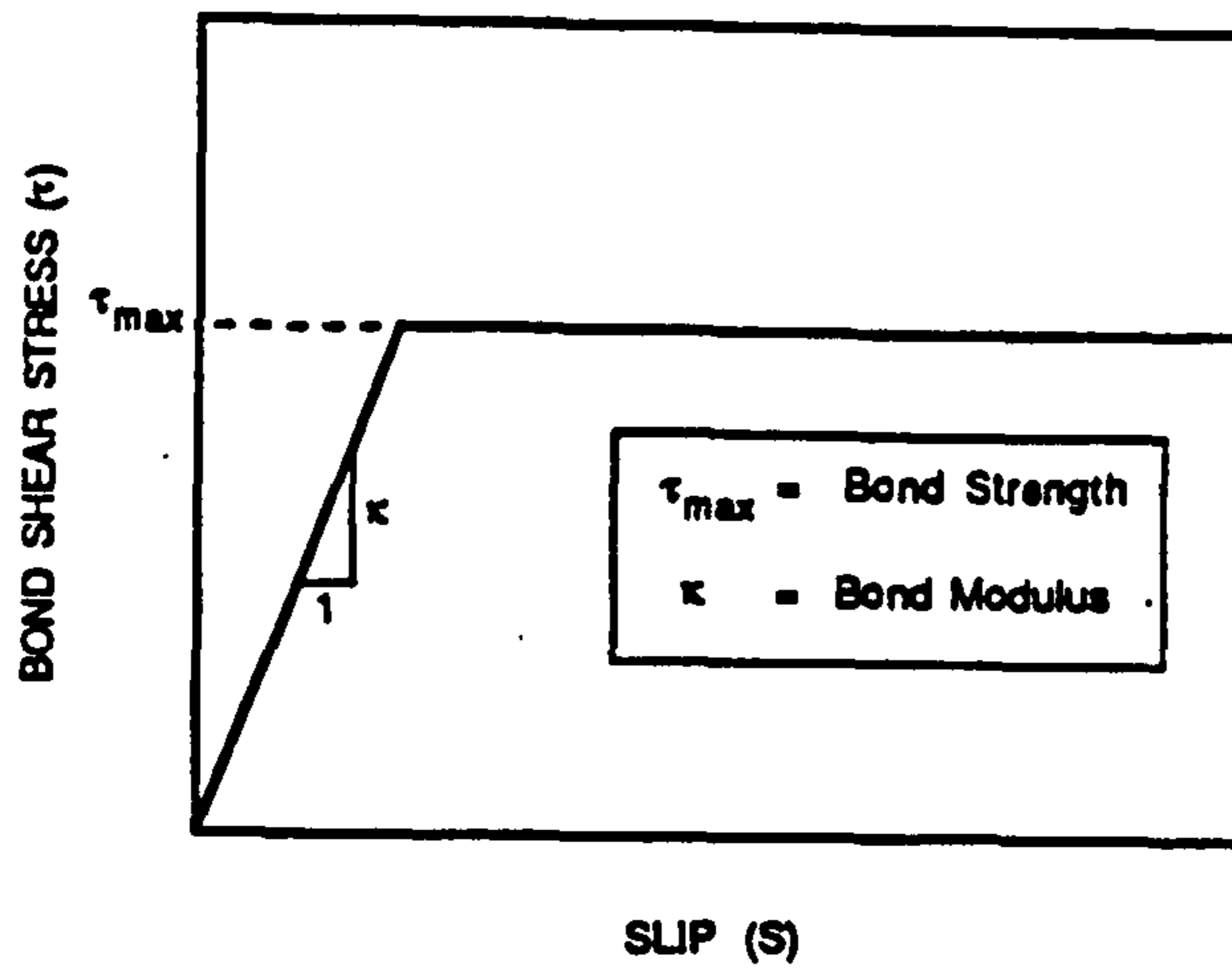


Figure 2-2 Idealised bond shear stress-slip relationship for fibre pullout (Nammur and Naaman 1989)

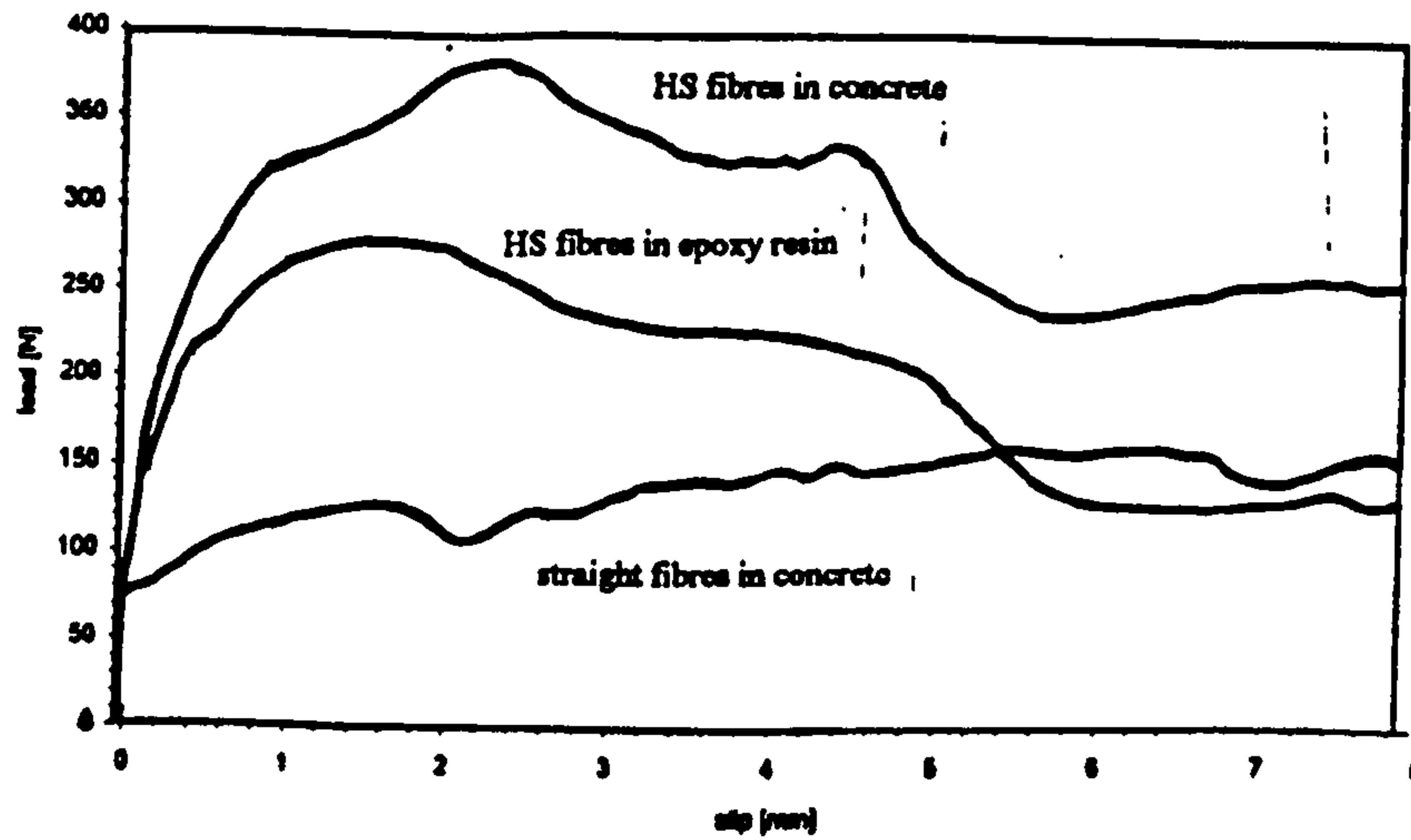


Figure 2-3 Load - slip curves of a HS fibre and straight fibre in concrete, and a waxed HS fibre in epoxy resin (Weiler and Grosse 1996)

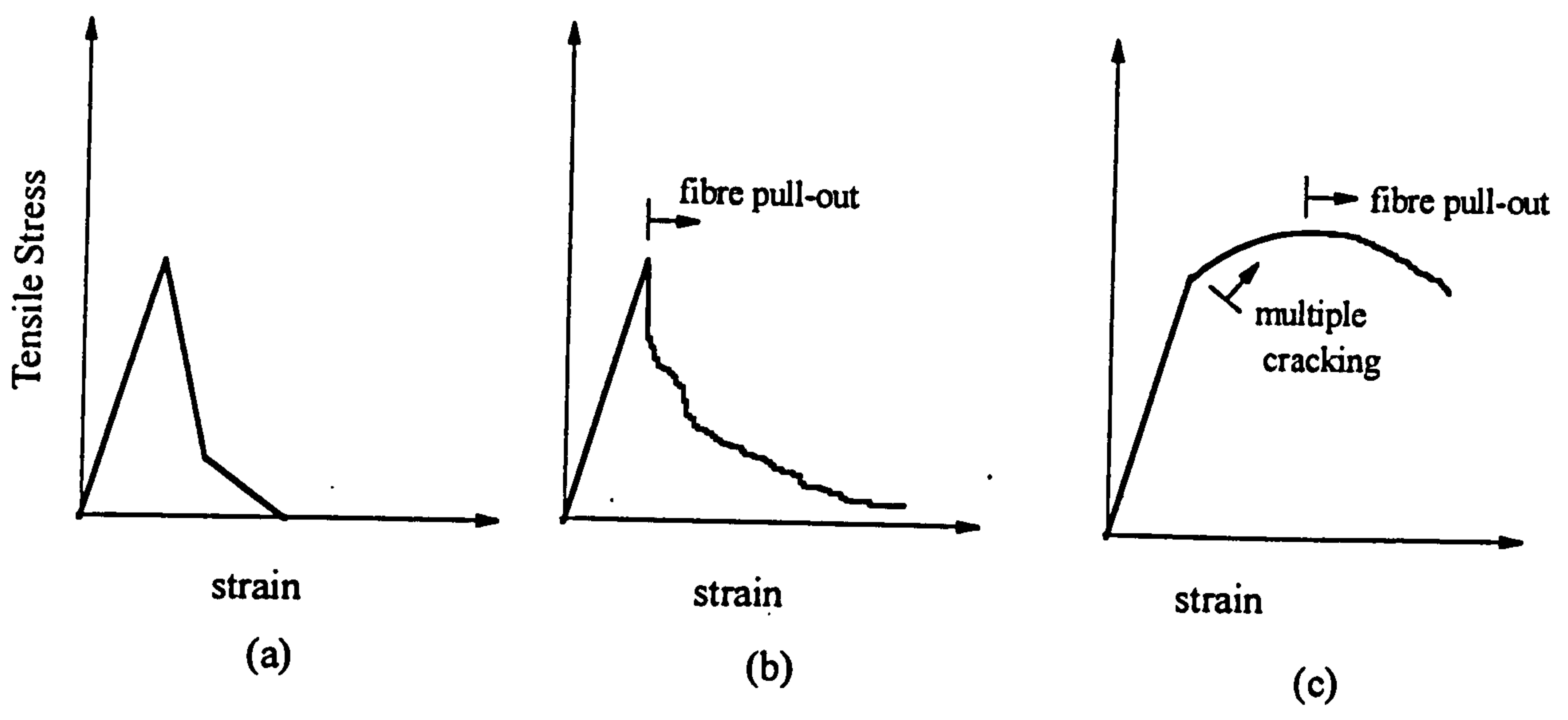
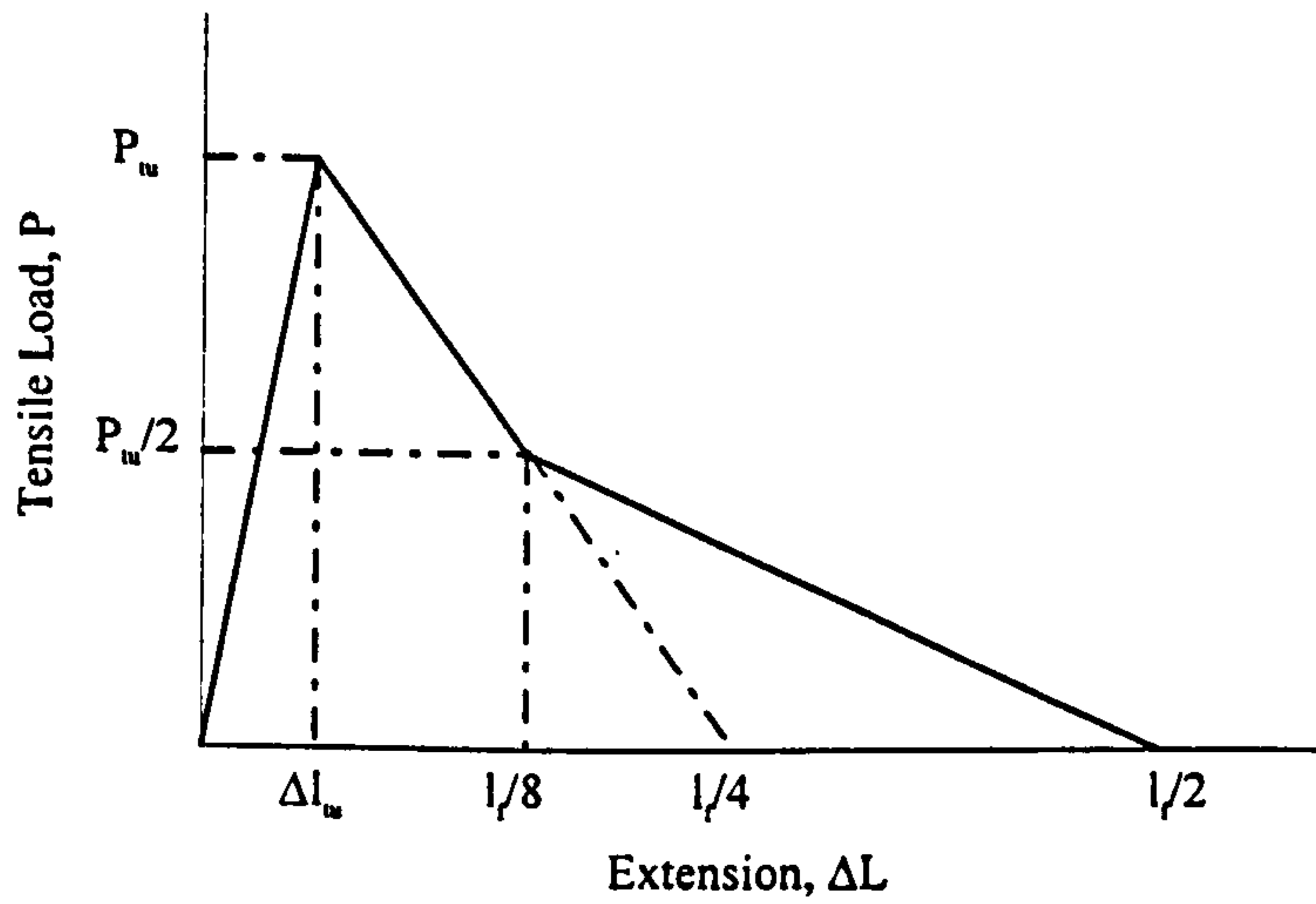
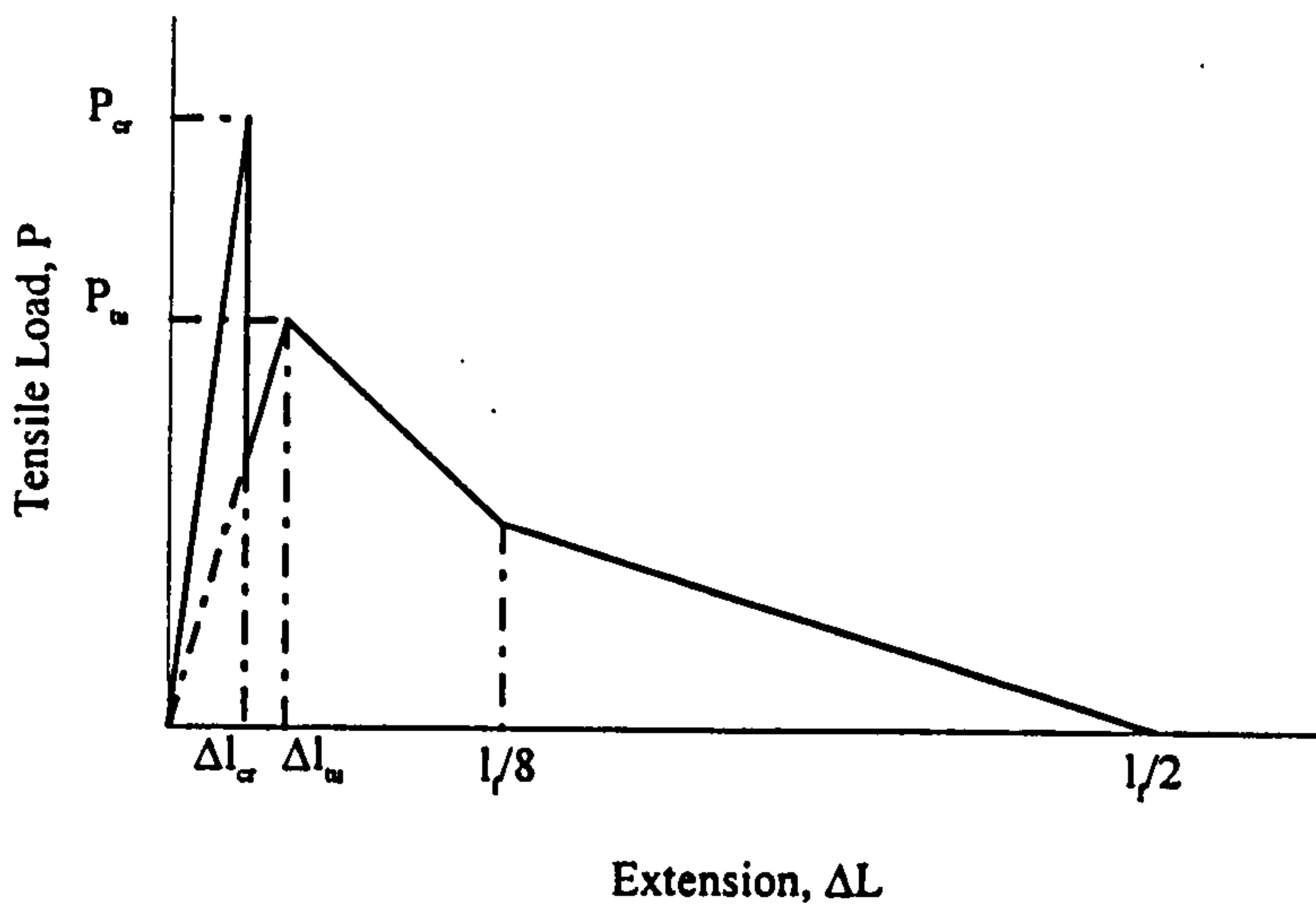


Figure 2-4 The composite tensile stress-strain curve for fibre-reinforced matrices: (a) low fibre volume fractions; (b) intermediate fibre volume fractions; (c) high fibre volume fractions



**Figure 2-5 Load - extension curve of a pre-cracked FRC specimen in tension**



**Figure 2-6 Idealised load - extension curve for a FRC specimen in tension (after Lim *et al.* 1987a)**

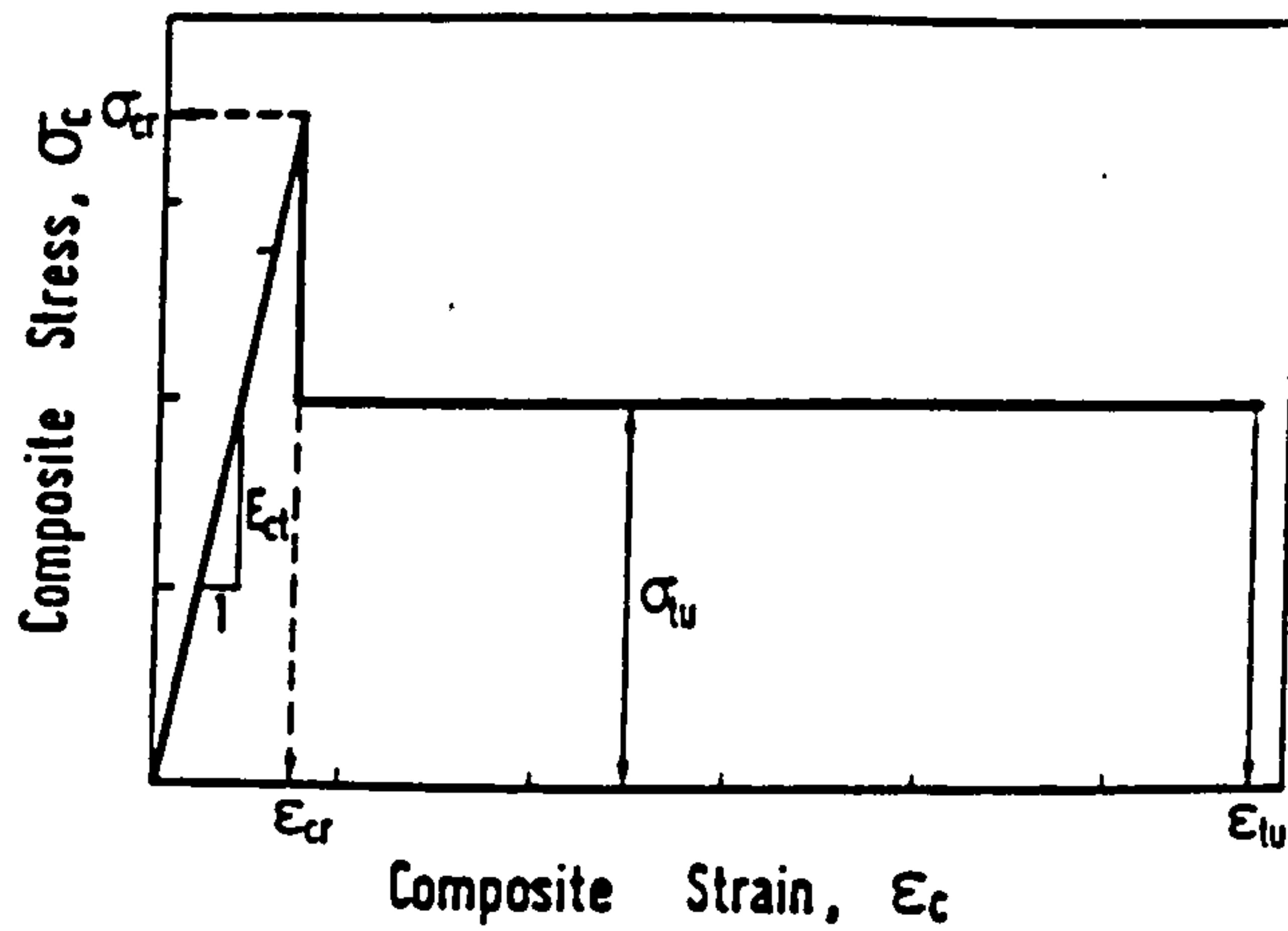


Figure 2-7 Simplified tensile load -extension curve of FRC assuming constant post-cracking bridging stress (Lim *et al.* 1987a)

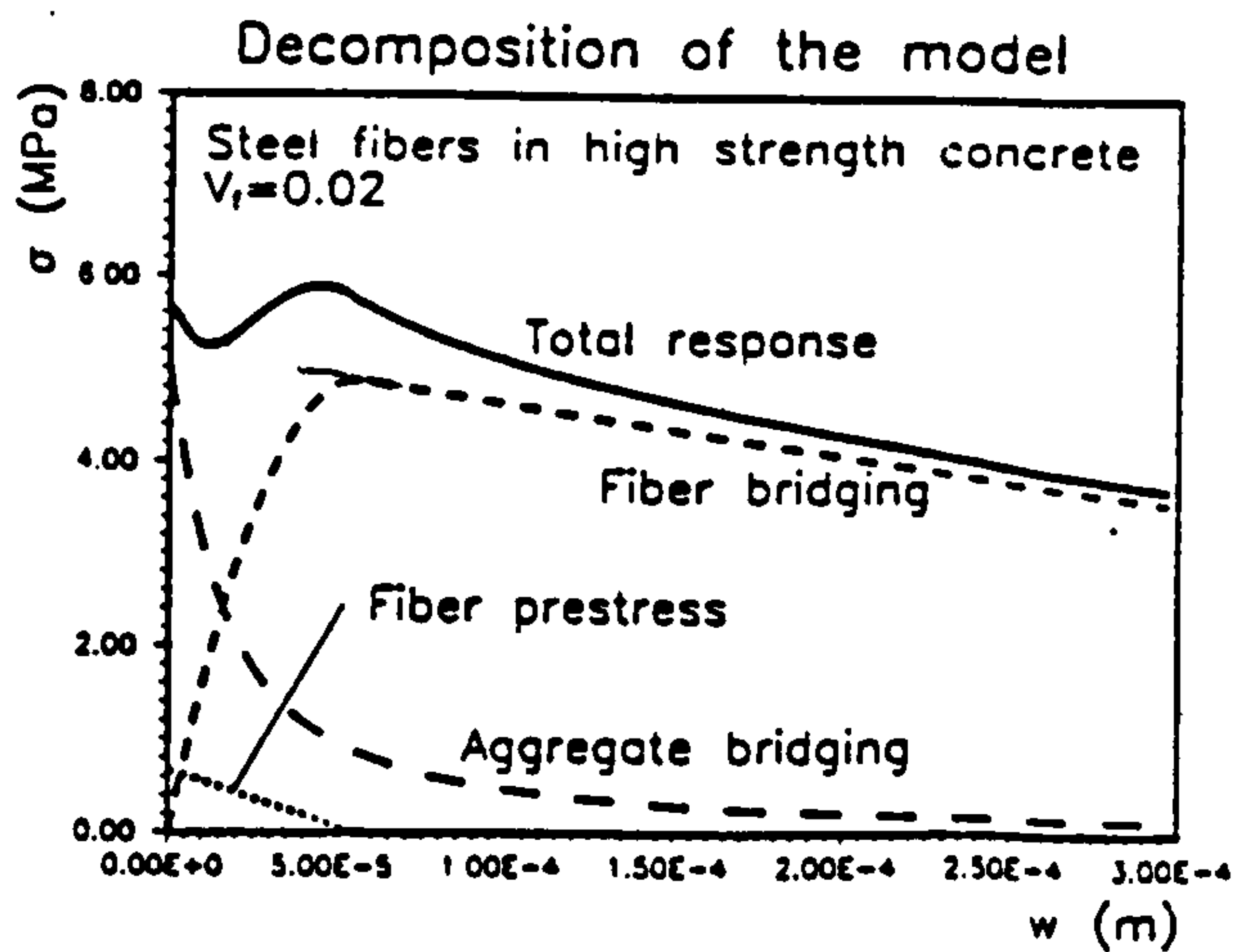


Figure 2-8 Individual contributions of aggregate bridging action, fibre bridging action and fibre prestress to the tensile stress - crack width curve (Li *et al.* 1993)

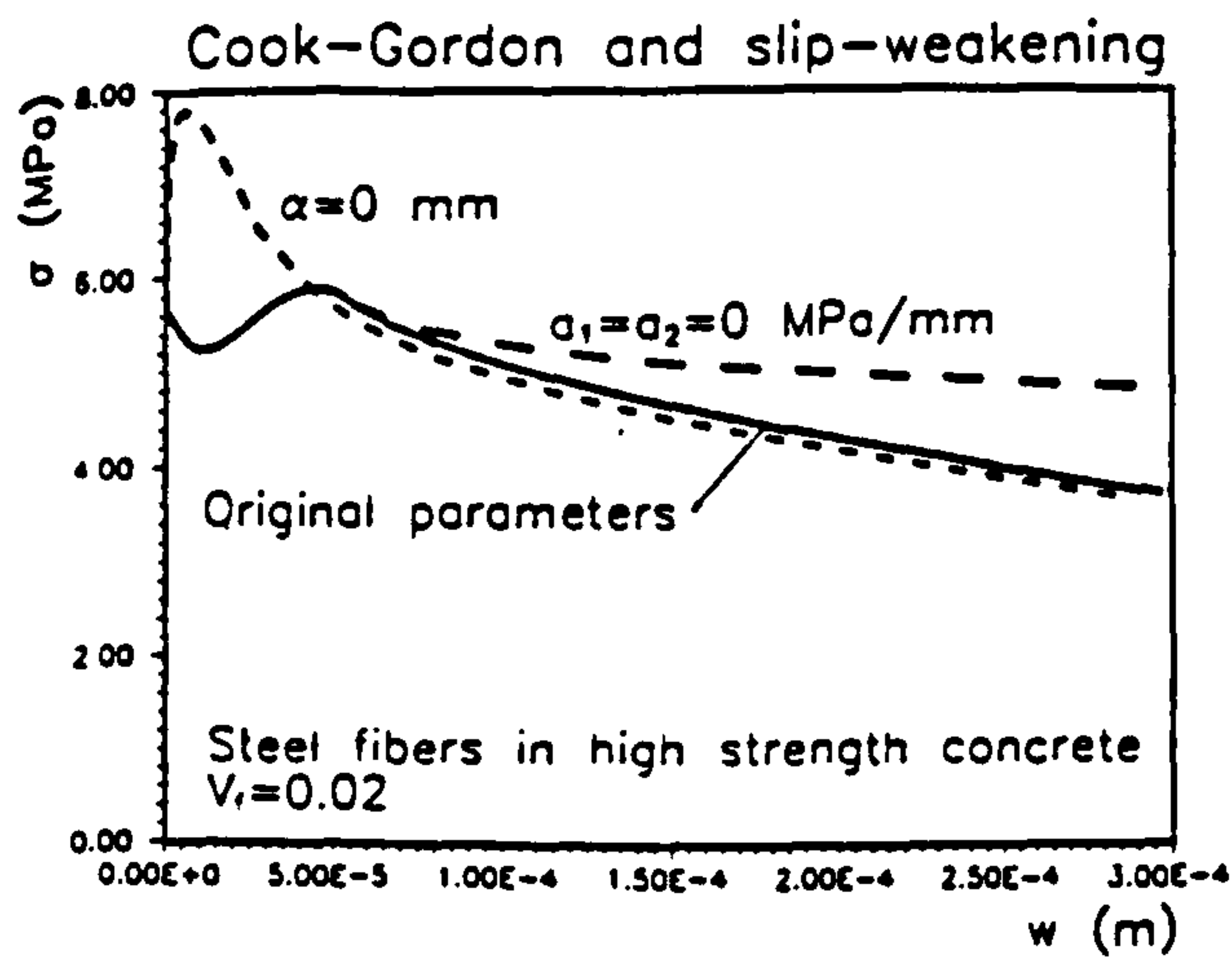


Figure 2-9 Influence of Cook-Gordon effect and bond weakening on tensile stress - crack width curve (Li *et al.* 1993)

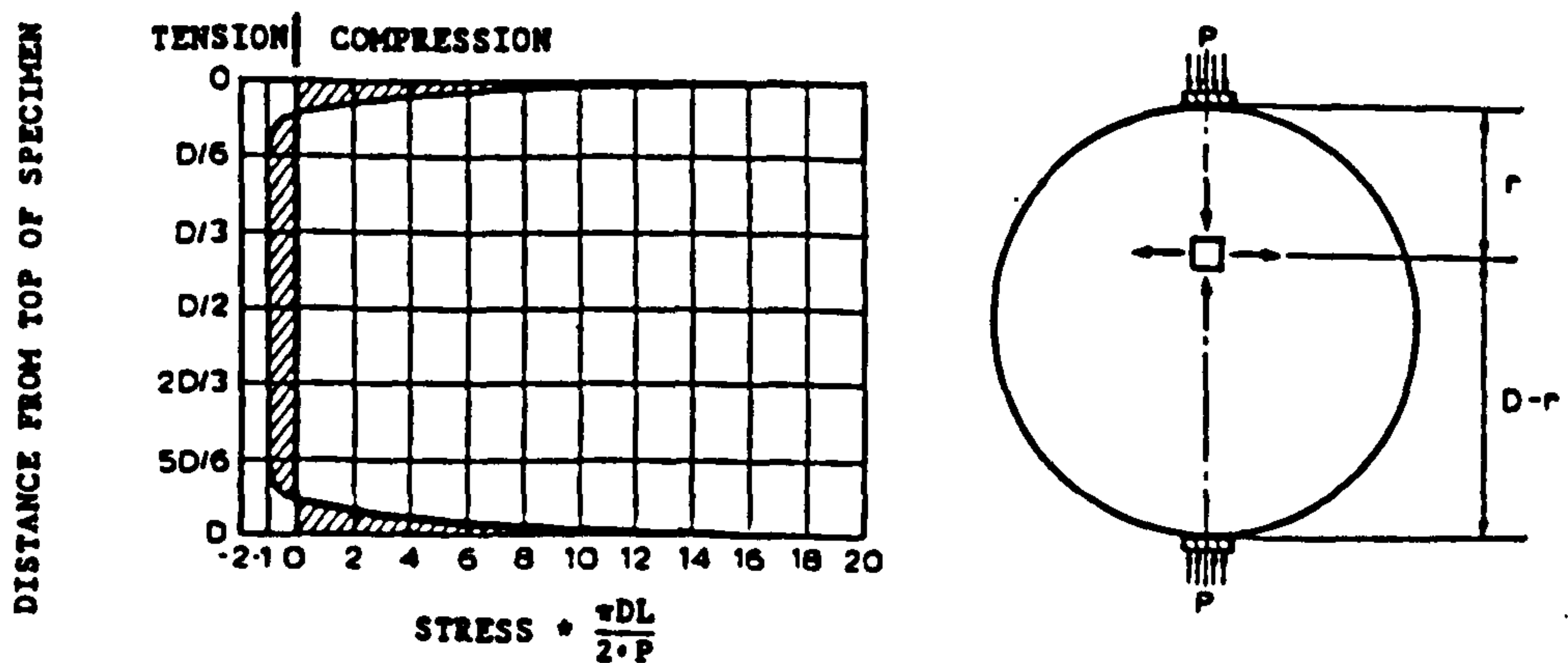


Figure 2-10 The splitting tensile test and horizontal stress distribution (Hansen 1996)

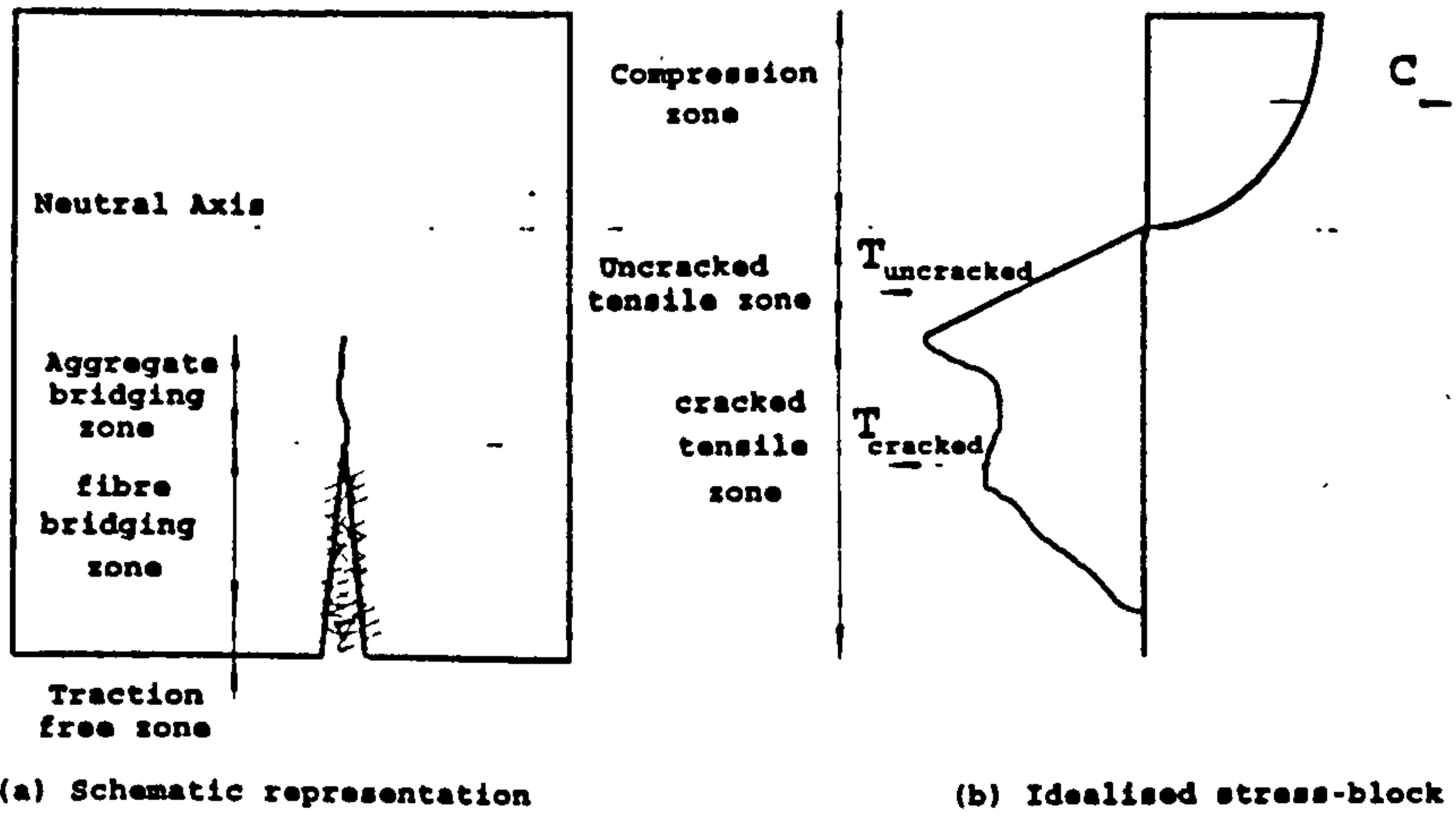


Figure 2-11 Schematic representation of a FRC beam under flexural loading (Robins *et al.* 1996)

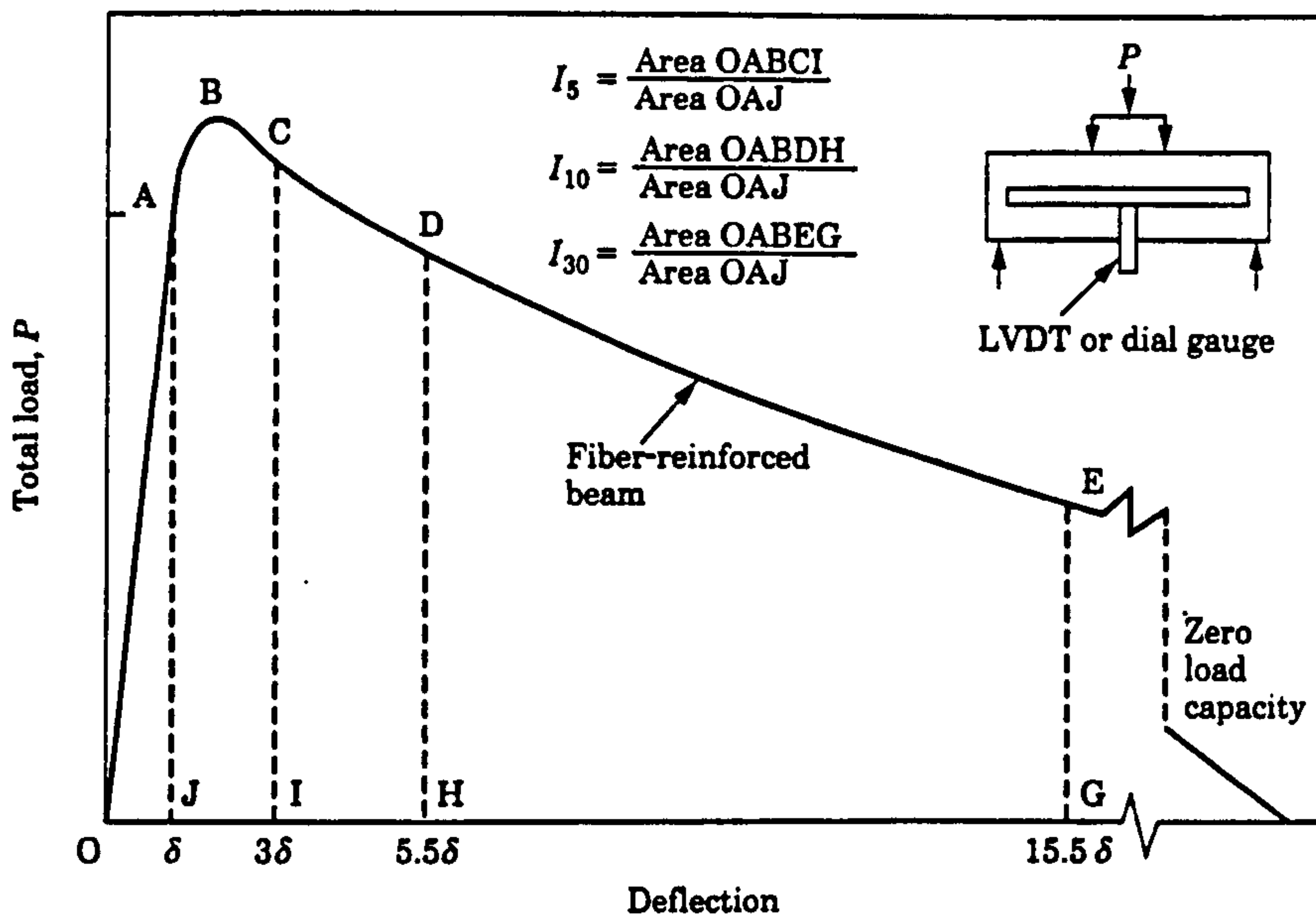
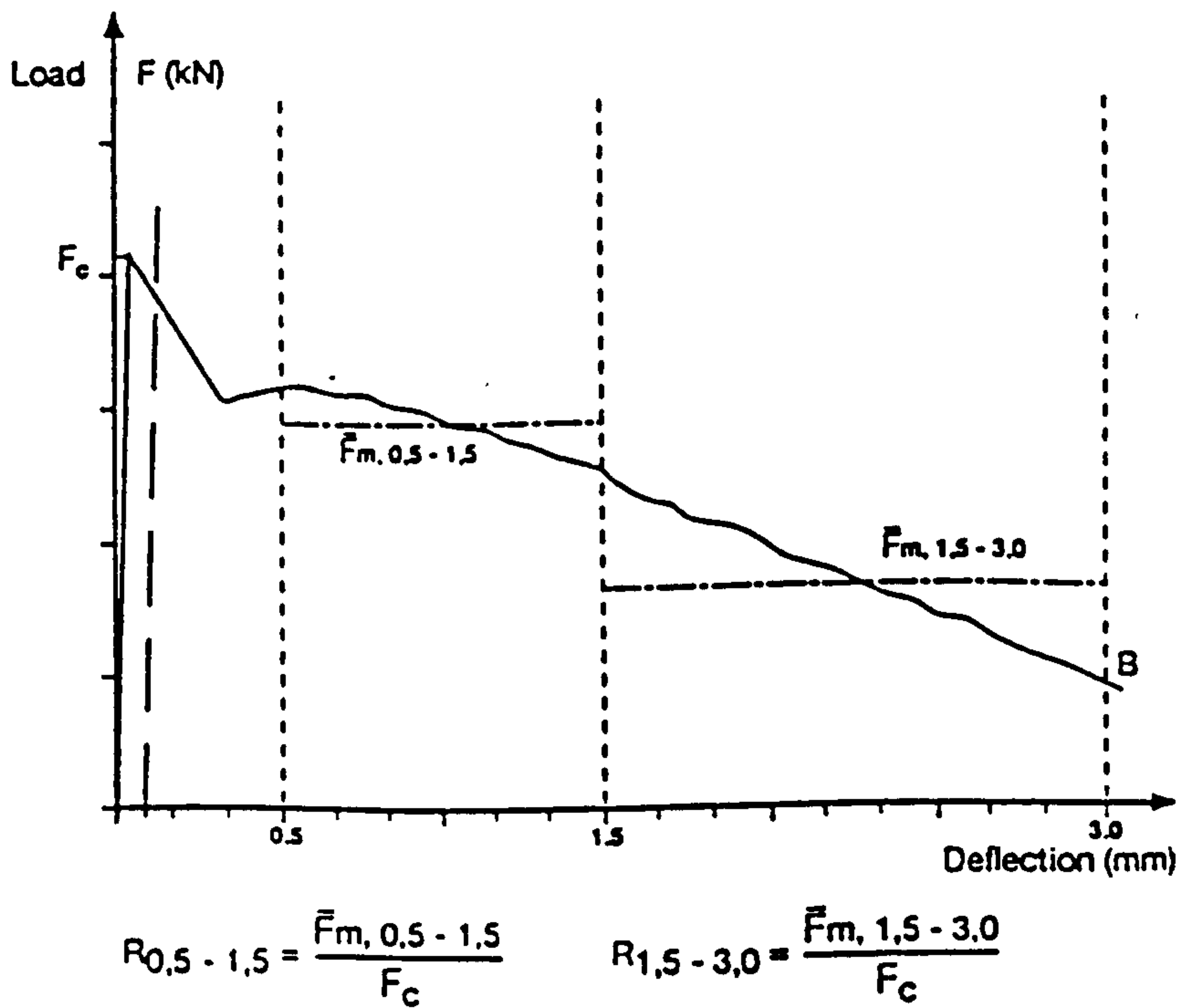
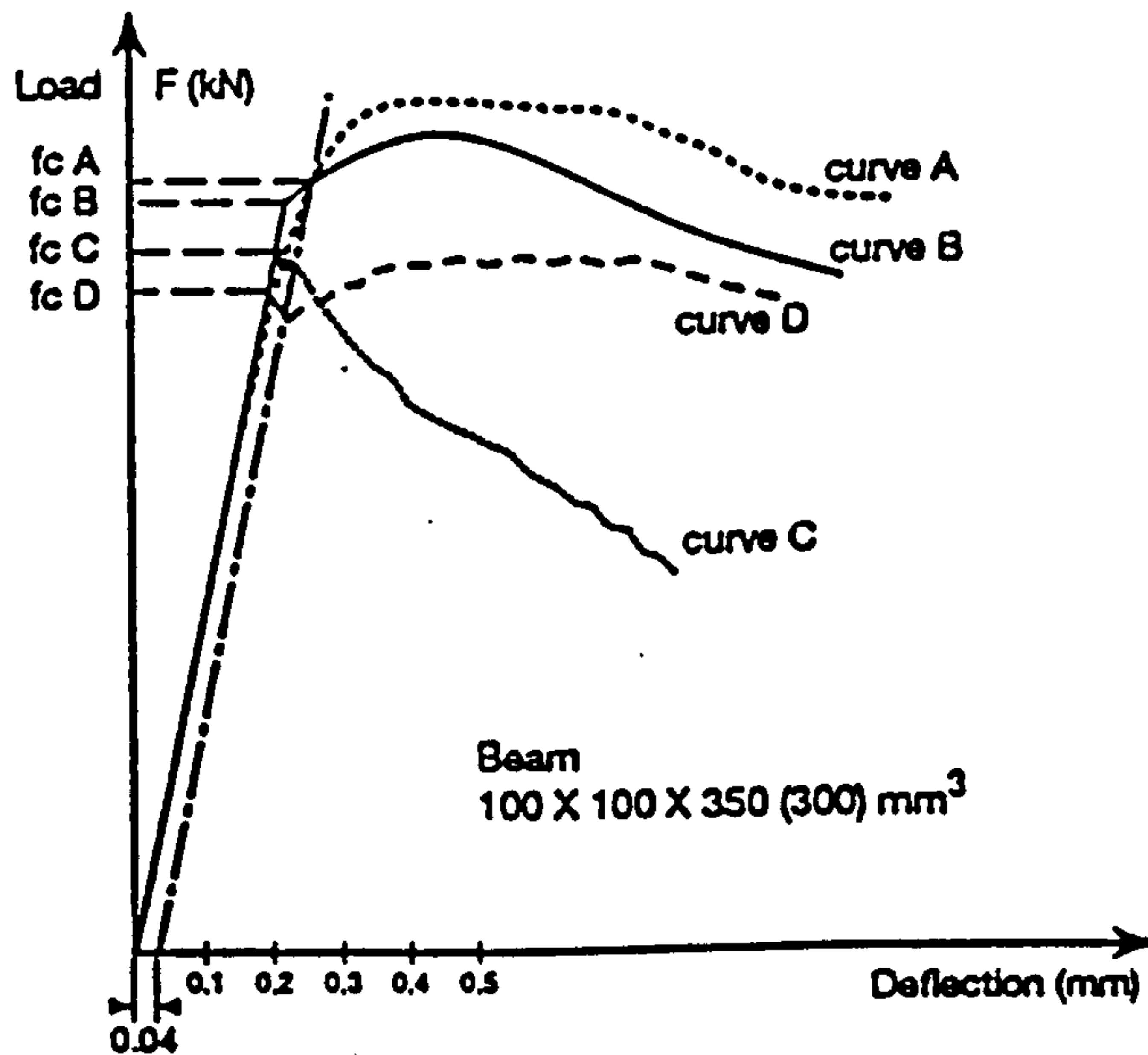


Figure 2-12 Measurement of toughness by ASTM C1018 (Balaguru and Shah 1992)





**Figure 2-13 Definition of strength based dimensionless indices with proposed toughness parameters  $R_{0.5-1.5}$  and  $R_{1.5-3.0}$  (Nemegeer and Tatnall 1995)**



**Figure 2-14 Determination of first crack strength (Nemegeer and Tatnall 1995)**

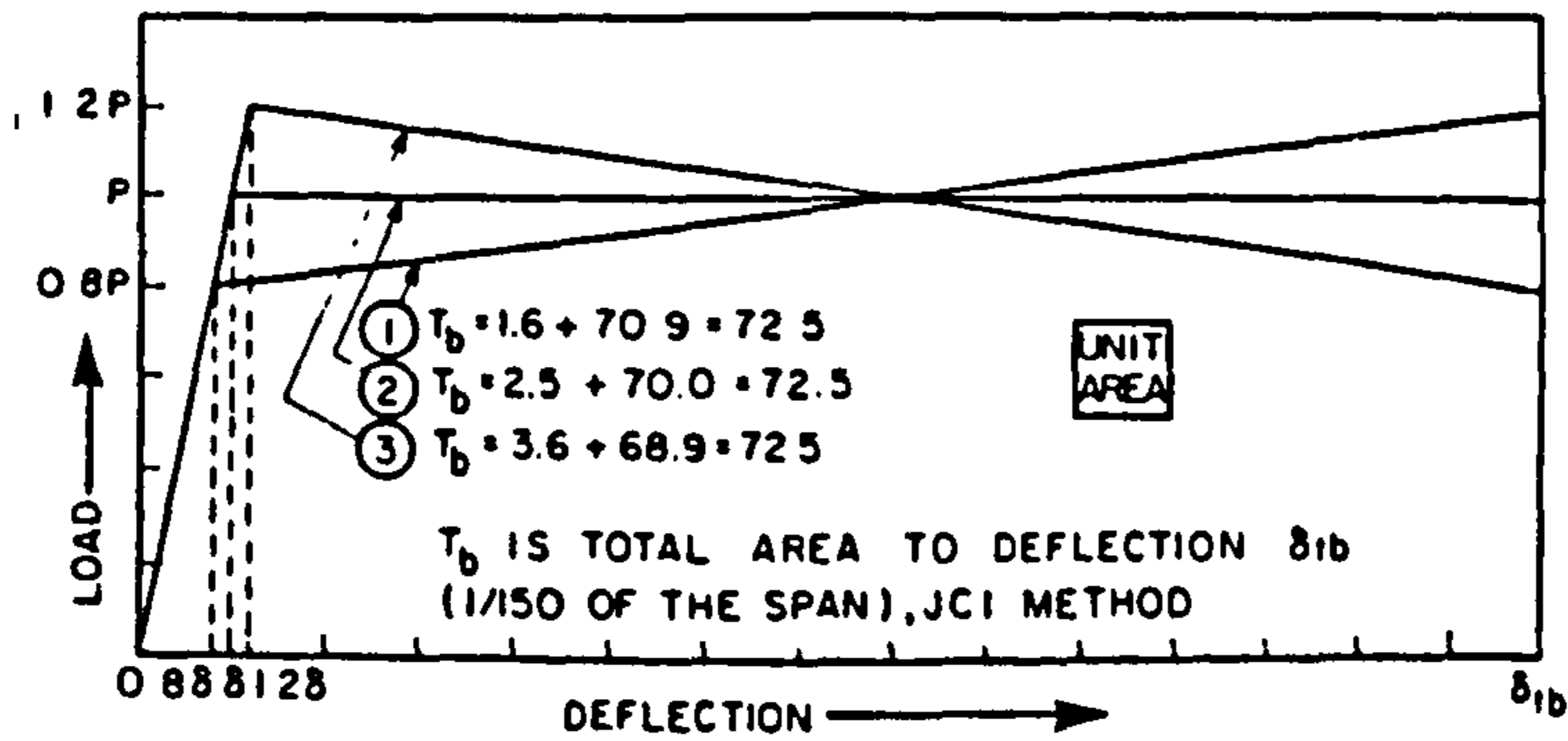


Figure 2-15 Load - deflection curves with the same absolute toughness as derived by the JCI Method (Johnston 1985)

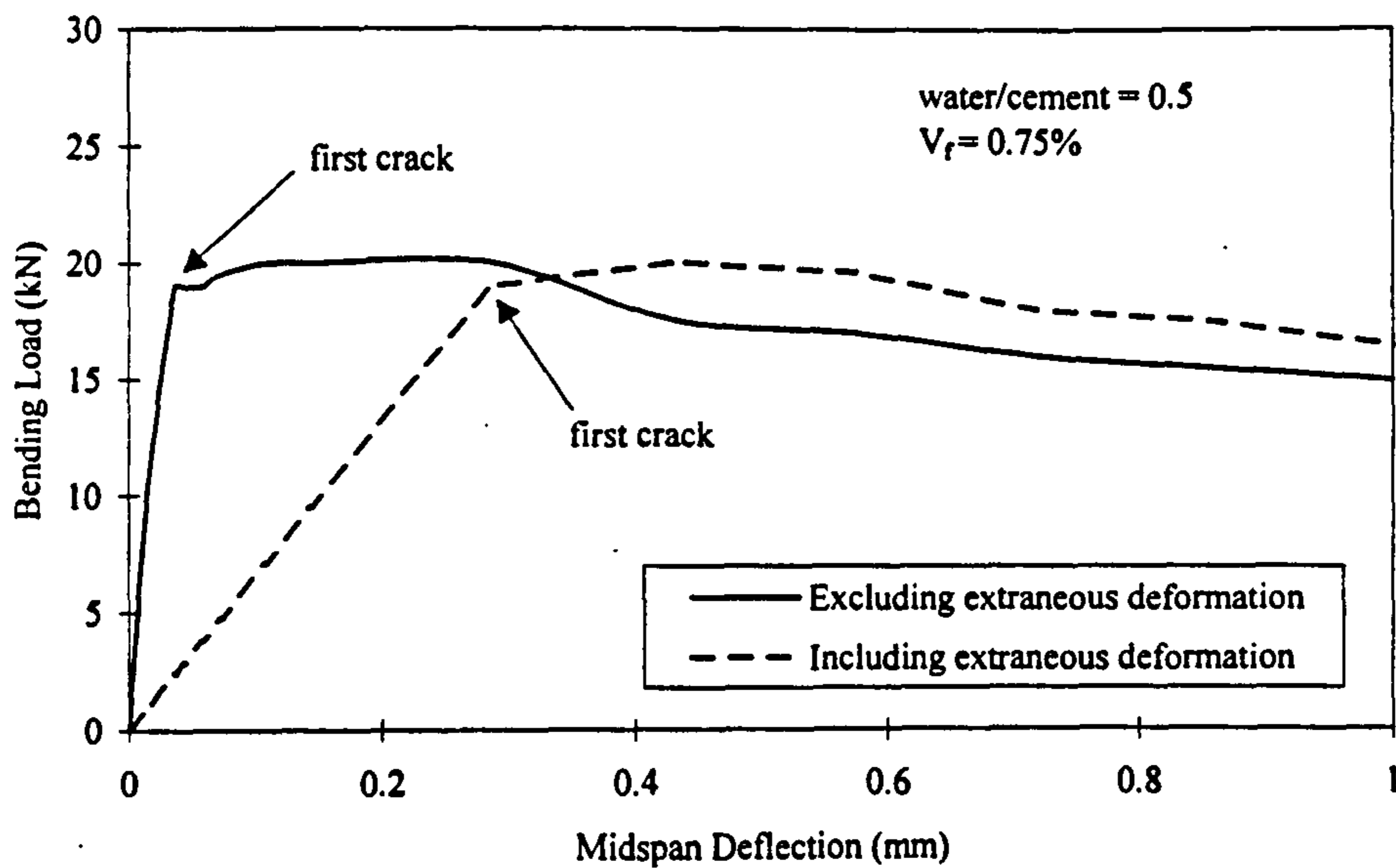
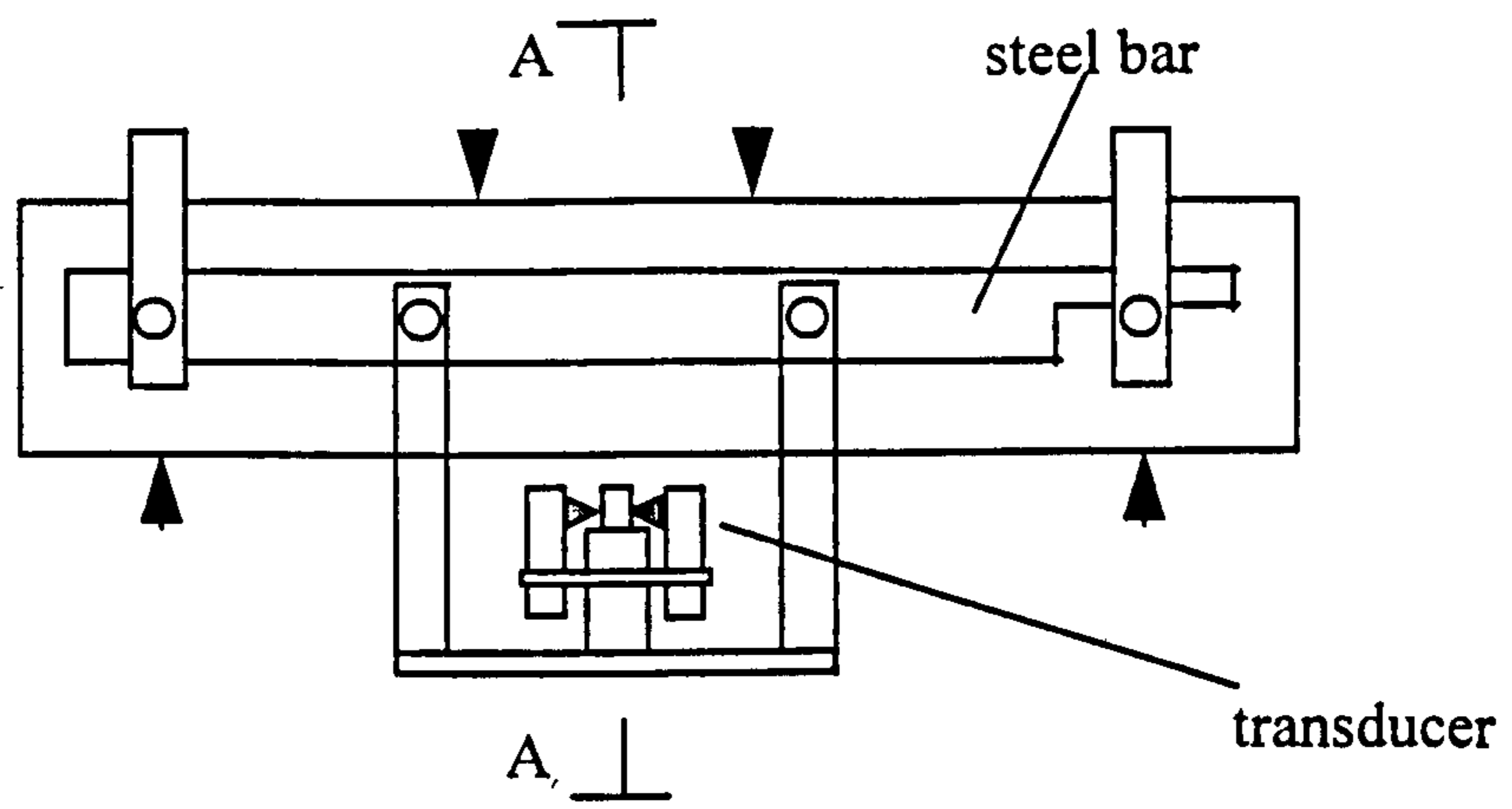
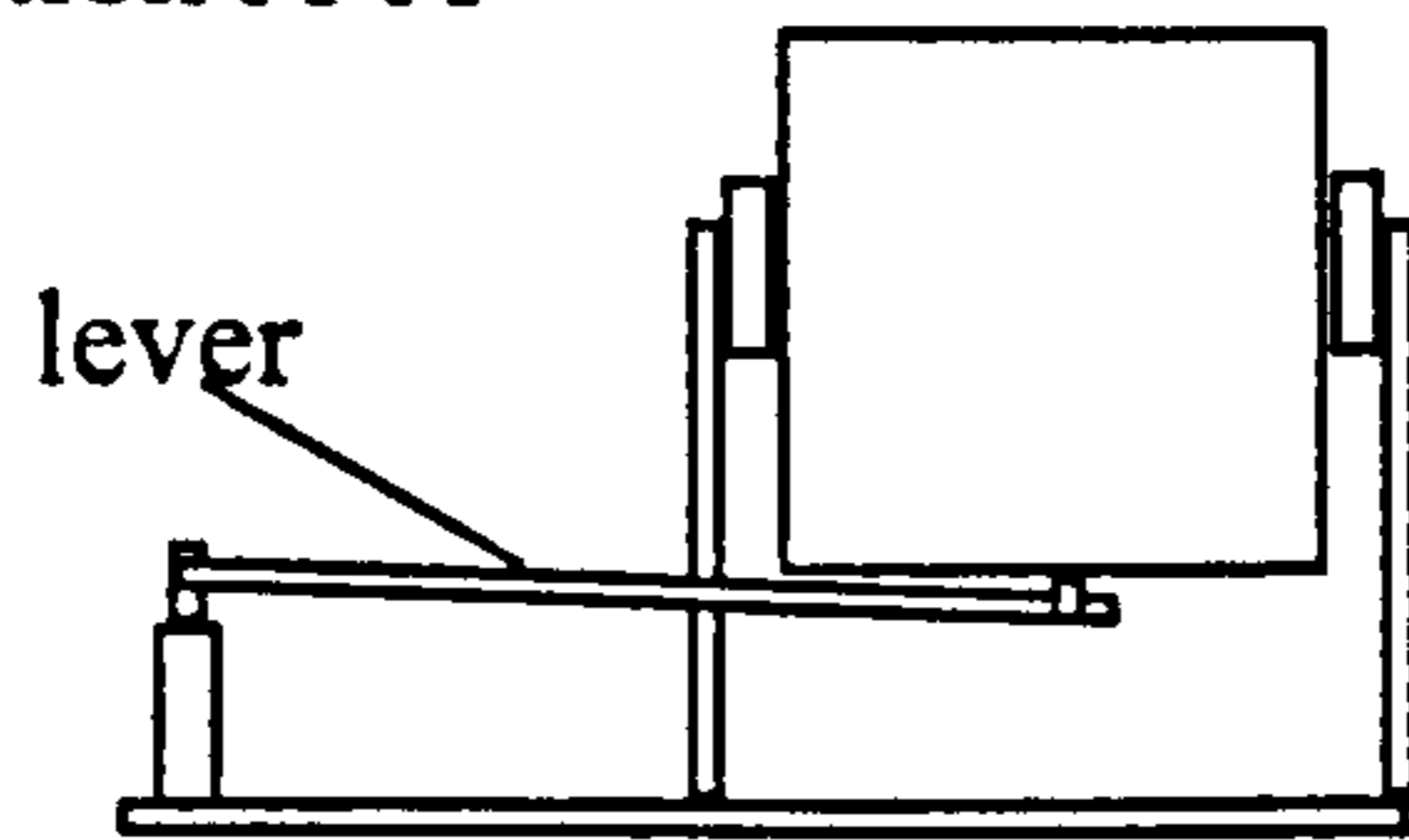


Figure 2-16 Typical load - deflection curves with and without extraneous deformations (Morgan *et al.* 1994).



Section A-A



cradle support system

**Figure 2-17 Yoke system used at University of Nottingham**

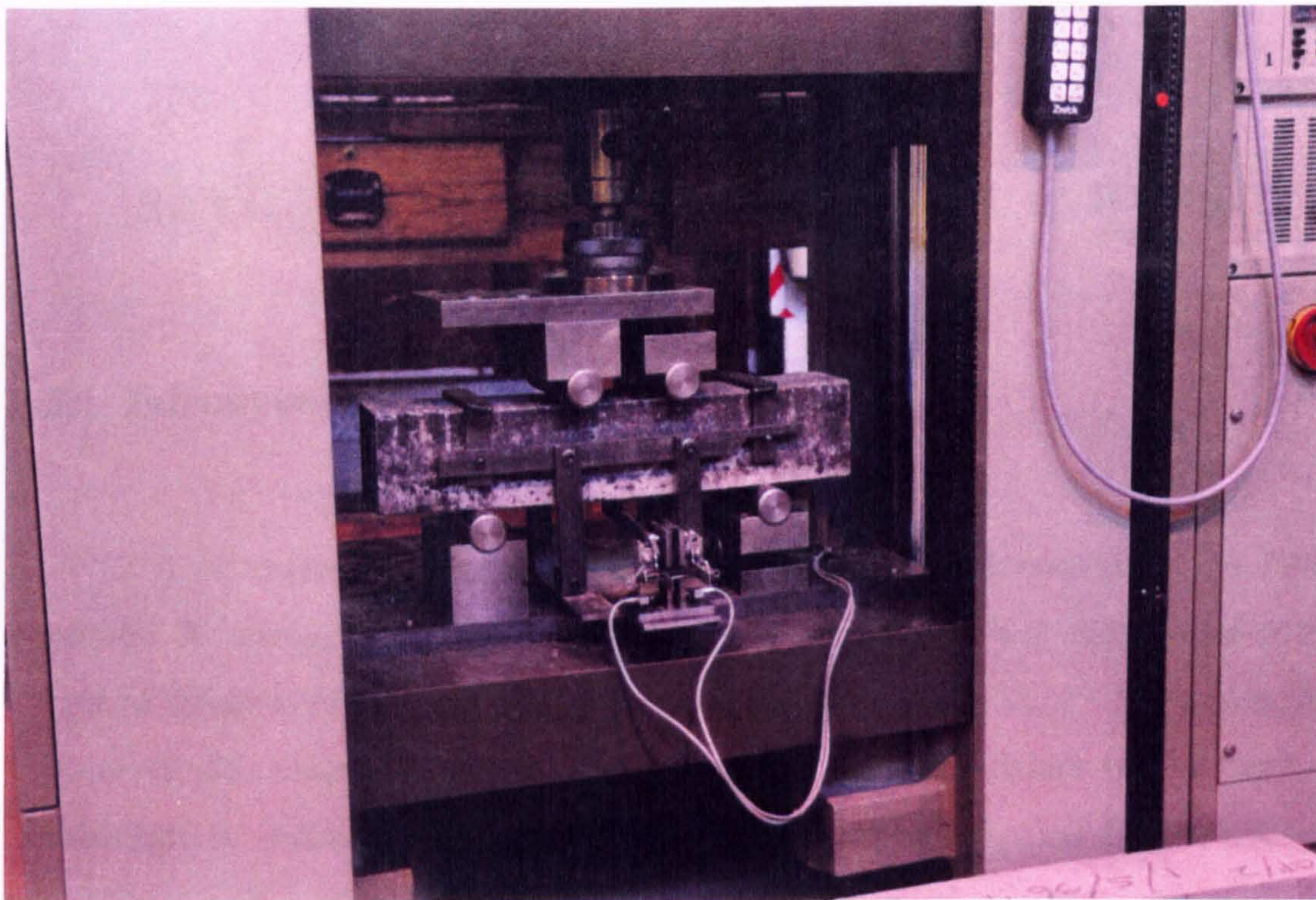


**Plate 2-1 Yoke system used at University of Nottingham**

## CHAPTER 3

### REVIEW OF HOLLOW CORE SLABS AND PFRC

#### 3.1 Introduction

This chapter reviews the present literature on hollow core slabs and PFRC beams. It concentrates, primarily, on shear and in particular web shear, because this type of failure is of most concern in the design of hollow core slabs. To be complete, however, this chapter also briefly describes flexural-shear failure (which tends to culminate in anchorage failure in hollow core slabs) and flexural failure. This is necessary because the interaction between shear and flexural type failures is of interest in the tests performed. Flexure is a much more favourable failure mode than shear, and it is possible that addition of fibres may produce flexural failure, or flexural cracking before the initiation of shear. In addition, many of the tests described in Chapters 4 and 6 suffered flexural cracking and therefore a review of present knowledge of these failure types is necessary to fully understand the test results.

This chapter is in two parts: testing and design of hollow core slabs; and testing and design of PFRC elements. The first section is essentially a review of design practice for hollow core slabs. Most of this section is also relevant to the design of normal prestressed beams. However, difficulties in the use of traditional design as a result of the unique shape of hollow core slabs, the dry concrete used and the manufacturing method are specifically mentioned, along with suggested changes to overcome these problems. Specific research is only referred to where there are differences in opinion in the perceived best method for characterising the strength and nature of failures.

The second section of the chapter is mostly a review of testing performed on PFRC beams. Due to the few tests performed, it has been necessary to refer to the

many tests on RFRC beams where it is felt the test results are relevant to both prestressed and reinforced concrete.

Since there are no standard design methods available for fibre reinforced structural elements (either RFRC or PFRC), some of the suggested equations and methods for characterising PFRC are described. As with the first section, testing on shear dominates.

With regard to web shear tension and anchorage failures in prestressed concrete the bond properties of the tendon to the concrete, and the development of the prestress are very important. It has been suggested that FRC has different bond properties with the steel reinforcement (bar or tendon) than plain concrete. A review of bond tests on reinforcing bar, and the two tentative studies on prestressing strand is given at the end of the chapter.

## **3.2 Testing and design of hollow core slabs**

### **3.2.1 General**

A comprehensive review of the ultimate flexural and shear failures, which can occur in hollow core slabs, can be found in Pajari (1989) and Girhammar (1992). Figure 3-1 and Figure 3-2 show the five bending failures and six shear failures, respectively. Although not an ultimate failure in its own right “excessive deflection” is included because it can be argued that the ultimate load corresponding to yielding of strands and concrete compression failure cannot be reached unless such secondary effects are limited. By a similar argument, “excessive crack width” could also be included. In most of the failure types, the tensile and flexural strength of the concrete play only a minor part. For the purposes of the testing reported in this thesis only the flexural tensile cracking, anchorage and web shear tension failures are of interest. These are described below. In this regard, this literature review to some extent anticipates the test results found in Chapter 5 and Chapter 7, by concentrating on those failures observed.

### 3.2.2 Flexural strength

The flexural cracking strength of a prestressed hollow core slab is dependant upon the prestressing force and the modulus of rupture of the concrete. If the flexural capacity is such that the capacity of the strands is not exceeded - the over-reinforced case - then the cracking capacity corresponds with ultimate capacity and a brittle failure ensues. In general, the opposite is true and there is a considerable amount of ductility available after cracking. Ultimate failure occurs when the tensile capacity of the strands, or the flexural compression capacity is reached.

Although the cracking capacity is dependant on the modulus of rupture of the concrete, this tensile capability of concrete is often neglected in structural design codes.

The ultimate moment of a hollow core slab, assuming the concrete to be fully strained in the compression zone at the ultimate limit state, can be calculated using traditional approaches (Figure 3-3).

Assuming the flexural crack reaches the upper flange of the slab, then the depth of the compression flange,  $x$ , is calculated from

$$A_p f_p = b \cdot x \cdot \lambda \cdot f_c \quad \text{.. 3-1}$$

where  $A_p$  is the nominal area of the prestressing tendon,  $f_p$  is the initial prestress force,  $b$  is the width of the slab,  $f_c$  is the concrete compressive strength and  $\lambda$  is the shape factor of the stress-strain diagram of concrete. Ultimate moment,  $M_{fu}$  is calculated as

$$M_{fu} = A_p f_p z \quad \text{.. 3-2}$$

where  $z$  is the inner lever arm, given as  $d - \beta x$ . In many case, hollow core slabs fail by rupture of the strands, which implies the inner lever arm is actually smaller than that

given above. However, the error in using this approach is only about 2% (Walraven and Mercx 1983).

### **3.2.3 Web shear tension failure**

Web shear tension failure takes place within regions of the span that are uncracked in flexure. The failure initiates when the principal tensile stress within the web equals the tensile strength of the concrete, this normally occurs close to the neutral axis. Theoretically, the crack also occurs close to the support at a distance of  $h/2$  from the edge of the bearing i.e. outside the area where vertical support pressure is active. Experimentally, the range of the critical crack location is large (Girhammar 1992) but usually lies within the transfer length, where the prestressing force is not fully developed.

The shear crack grows towards the flanges, and the failure is of the brittle type. Since the crack normally occurs close to the support, the anchorage capacity of the tendons is very low and strand slip can be severe. Generally, a crack in the web close to the support leads to an immediate failure. Occasionally load sharing will occur between webs, and in these cases the load can be slightly increased after cracking.

Web shear tension is a particular worry in hollow core slab design because of the excessively brittle nature of the failure. Since vertical and transverse reinforcement are difficult to place, the shear stresses must be carried by the prestressed concrete. It is not economical, however, to increase the number of prestressing tendons to satisfy shear. Increasing the area of prestressing reinforcement by a factor of 4 will increase flexural capacity by 2.5 and shear capacity by only 1.2 (Elliott 1996). Additionally, shear strength design equations for hollow core slabs are based on those used for conventional types of beam, with alterations to account for shape and design method. Of particular concern to designers is the bond between concrete and steel in the extrusion process, since a low level of prestress will place even more emphasis on the tensile strength of the concrete.



The cracking load corresponding to web shear tension is calculated in most design codes as the point when the principal tensile stress at the centroid equates to the tensile strength of the concrete, which can be represented by means of a Mohr's circle (Figure 3-4), and gives

$$\tau_{cpx} = \sqrt{f_{ct}^2 + \sigma_{cpx} f_{ct}}$$

.. 3-3

which leads to the basic internationally accepted equation for web shear tensile strength for prestressed concrete ( $V_{co}$ ) of

$$V_{co} = \frac{Ib}{Ay} \sqrt{f_{ct}^2 + \sigma_{cpx} f_{ct}}$$

.. 3-4

where  $f_{ct}$  is the concrete principal tensile strength,  $\sigma_{cpx}$  is the effective prestress in the concrete at the critical section,  $I$  is the second moment of area,  $Ay$  is static moment and  $b$  is the width of the section.

Hollow core slabs are designed for shear according to the same provisions as prestressed beams. For hollow core slabs, the parameter  $b$  in Equation 3-4 is taken as the sum of the width of all the webs,  $\Sigma b_w$ . Instead of  $Ib/Ay$ , BS 8110 (1985) adopts the more conservative value of  $0.67 bh$ , as evaluated from a rectangular section, thus neglecting the effect of the flanges.

An approximation to Equation 3-4 has been suggested by Girhammar (1992), in which the shear strength is given as two separate components relating to the concrete contribution and prestress contribution. This equation is given as

$$V_{co} = [f_{ct} + 0.3\sigma_{cpx}]bz$$

.. 3-5

The lever arm,  $z$ , can be replaced by the effective depth,  $d$ , as a further approximation. This is effectively identical to the equation given for hollow core slabs by PCI (1991),

which is extracted from the ACI-318 Building Code (1989). When translated for SI units this is given as

$$V_{co} = [0.3\sqrt{f'_c} + 0.3\sigma_{cp_x}]bd$$

. 3-6

where  $0.3\sqrt{f'_c}$  is a design approximation for the tensile strength of the concrete.

However, tests on hollow core slabs have failed to show the most effective and relevant procedures, and measures for the principal tensile strength, the manner in which this prestress is transferred into the element, and the most critical section for carrying out assessment of shear strength. Subsequently, the many design recommendations and codes of practice available for hollow core slabs use different procedures. Each of the above points is discussed below in more detail. In addition, recent concerns have been expressed about the shear capacity of hollow core slabs when placed on flexible supports (Pajari and Yang 1994), and when the slabs have notches cut out of the ends (Girhammar and Pajari 1995).

### ***Concrete tensile strength***

Consistent with design for most concrete, the design provisions in BS 8110 (1985) and Eurocode 2 (1994) empirically derive the maximum principal tensile strength of concrete for use in Equation 3-4 from the compressive strength. The formulae being,  $f_{ct} = 0.3\sqrt{f_{cu}}$  and  $f_{ct} = 0.21 f_{ck}^{2/3}$ , respectively, where  $f_{cu}$  is the mean cube compressive strength and  $f_{ck}$  is the characteristic cylinder compressive strength. For normal strength concrete ( $f_{cu} < 60 \text{ N/mm}^2$ ) experience has shown these formulae to be relatively reliable, and a maximum value of  $60 \text{ N/mm}^2$  is always assumed for  $f_{cu}$ , despite higher compressive strengths of concrete being used in the modern manufacture of hollow core slabs. However, traditional methods of measuring compressive strength of concrete using cubes and cylinders may not provide representative strengths due to difficulties in obtaining similar levels of compaction to that achieved in the slabs. Tests by Sebaratnam and Rangan (1992) showed that such

methods considerably overestimate the strength. As an alternative they suggest use of Schmidt Impact Hammer readings taken horizontally on the sawn faces and side faces of the flange area. However, their tests were based on 40 N/mm<sup>2</sup> strength concrete, and the unique relationships between hardness and strength that are required will not necessarily be applicable to high strength concrete. In addition this test is known to be susceptible to variations in local concrete quality (Neville 1981).

Various methods have been tried to assess the tensile strength directly from the flanges or web. Walraven and Mercx (1983) took a number of 75 mm diameter cylindrical cores sawn horizontally from the top flange, and vertically through the top flange and the top of the web, and subjected them to splitting tensile tests. Good correlation was found between the splitting tensile strength and cube crushing strength. The limitation of these cores is that they can only be taken from the top of the slab where strands are not present and where the quality of the concrete is superior to the rest of the slab. This is because compaction is applied to the top of the slab in the extrusion process. Additionally, representative cores can only be taken from deep slabs with large flange areas and web widths, due to the relative size effects and difficulties in testing small specimens.

Pisanty and Regan (1991) sawed a number of prismatic specimens from the flanges and webs of 200 mm and 300 mm deep hollow core slabs, to examine flexural tensile strength at different levels in the slab thickness. The specimens were taken from two webs specially cast free of strands, and they were either 100 mm or 150 mm high (depending on the depth of the slab). As expected, differences were found with the tensile strength through the web height with the highest strengths found at the top. However, these differences diminished as slab depth and web width increased. The average flexural strength was found to be about 8.5% of the characteristic cube crushing strength obtained by standard cube tests. The measured flexural strength was thought to be lower than the actual values because use of a powerful revolving disc to prepare the samples inevitably damages the microstructure of the concrete. Given that these results were consistent with code recommendations for the relationship between flexural tensile strength and compressive strength, Pisanty (1992) recommended that a

value of 0.55 of the flexural tensile strength, measured directly from sawn prisms, be taken as the characteristic principal tensile strength of the concrete.

### *Transfer of prestress*

At release of prestress in a pretensioned concrete member, the force initially maintained by the anchorages at the end of the prestressing bed is suddenly transferred into the end of the concrete member. As there is no anchorage at the end of a pretensioned concrete element there can be no force in the tendon there. Further along the tendon, the bond between steel and concrete enables the forces in the tendon to build up, until at some distance known as the *transfer or transmission length* ( $l_t$ ) the force in the tendons is equal to the initial prestress force.

The interfacial bond in the transfer zone between prestressing tendons and concrete is due to two mechanisms (Den Uijl 1995). The first is an initial bond due to adhesion and interlocking between the concrete and tendon surface. Adhesion is caused by chemical and mechanical connections at molecule level, whilst interlocking occurs due to “cement stone” sticking into the microscopically rough tendon surface (Åkesson 1994). After only a small slip this initial bond is broken and the remaining interfacial bond is due to friction.

Friction occurs due to the compressive stresses acting perpendicular to the tendon surface caused by (Vandewalle & Mortelmans 1994, Den Uijl 1995): shrinkage of the concrete; Poisson effect; wedging action caused by irregular shape of the tendon; pitch effect of strands (caused by the helical shape of the outer wires); and external compressive forces.

The distribution of the prestress into the transfer length is commonly accepted as following a parabolic shape. Equations for predicting the effective prestress within the transfer length where a parabolic distribution is assumed are given by BS 8110 (1985) and the FIP Recommendations (1992) for hollow core slabs. The equation given by BS 8110 is

$$\sigma_{cp_x} = \frac{x}{l_t} \left( 2 - \frac{x}{l_t} \right) \sigma_{cp}$$

.. 3-7

where  $\sigma_{cp_x}$  is the effective prestress at a distance  $x$  from the edge of the bearing, and  $\sigma_{cp}$  is the effective fully transferred prestress at the centroid.

It has been suggested, however, that due to slip of the strands at release, the transfer of prestress into ends of the slab is actually delayed. Pisanty (1992) recommends modifying Equation 3-7 to account for this by multiplying  $\sigma_{cp}$  by a factor of 0.8. The FIP Recommendations suggest that no prestress should be assumed until a distance equal to that between the centre of the bearing and the end of slab ( $l_s$ ). This equation has been adapted by Lin Yang (1995), who assumes no prestress until a distance of 5 tendon diameters ( $\phi$ ) from the end of the slab ( $5\phi \approx l_s$ ), to give (see Figure 3-5)

$$\sigma_{cp_x} = \left[ 1 - \left( \frac{l_t + 5\phi - x - l_s}{l_t} \right)^2 \right] \sigma_{cp}$$

.. 3-8

when,  $0 \leq x + l_s \leq 5\phi$ ,  $\sigma_{cp_x} = 0$ ; and when  $x + l_s \leq 5\phi + l_t$ ,  $\sigma_{cp_x} = \sigma_{cp}$ . As with the FIP Recommendations (1992) this equation is not representative for plain or indented prestressing wires.

According to Girhammar (1992) a distance of  $5\phi$  is only applicable to slow release, and that a distance of  $10\phi$  corresponds more accurately with saw cutting of slabs.

There are a variety of equations for calculating the transfer length of prestressing tendons available in the literature. A number of these are summarised below. The transfer length is generally dependent upon :

1. Concrete quality – usually expressed in terms of concrete compressive strength.
2. Initial stress in the tendon.

3. Bond properties of the tendon.
4. Cross-sectional area of the tendon.
5. Concrete cover to the tendon.

A sensitivity analysis by Åkesson (1994) using a 3-dimensional finite element model showed that the most important parameter influencing transfer length was the initial stress in the tendon ( $P_i$ ). It was found that this was over five times as influential as the next most important parameters, compressive strength and cross-sectional area of the tendon ( $A_p$ ). The results of this sensitivity study are shown in Table 3-1. Interestingly, it was found that reducing the cross-sectional area of the tendon, and therefore the diameter of the tendon, increased the transfer length. This is in direct contrast to most predictive equations. Other parameters studied were the radius of the core and the concrete cover.

The equation for transfer length given in BS 8110 is dependant on tendon diameter, and cube compressive strength at release of the prestress ( $f_{ci}$ ) and is given as

$$l_t = \frac{k_t \phi}{\sqrt{f_{ci}}} \quad \text{.. 3-9}$$

where  $k_t$  is a coefficient that represents the relative bonding capabilities of different tendon types. Values of  $k_t = 600$  and  $k_t = 240$  are given for plain or indented wire and helical 7 wire standard strand, respectively. Strand is therefore regarded as having over twice the bonding capability of wire. This equation, however, is not generally used in the design of hollow core slabs (Elliott 1996).

EC 2 (1994) and the European pre-standard for hollow core slabs, prEN 1168 (1995), adopt a similar but much simpler expression for transfer length, based on the concrete strength at transfer and diameter of the tendons. It is given as

$$l_t = \beta_b \phi \quad \text{.. 3-10}$$

where  $\beta_b$  is equal to  $100-0.8f_{ci}$ , for  $25 \text{ N/mm}^2 \leq f_{ci} \leq 50 \text{ N/mm}^2$ . No differentiation is given in the equation between the bonding capability of smooth wires, indented wires and strands. The values from this equation are consistent with suggested transfer lengths for hollow core slabs of  $55\phi$  for slow release of strands, and  $60\phi$  for saw-cutting of strands (Lin Yang 1995).

The PCI manual for design of hollow core slabs (1991) and the FIP recommendations for hollow core slabs (1988), use an identical expression for the transfer length based on tests performed in 1963 on Grade 250 stress-relieved strand. This is:

$$l_t = \frac{\sigma_p \phi}{21} \quad \text{(using N/mm}^2 \text{ and mm)} \quad \text{.. 3-11}$$

where  $\sigma_p$  is the effective prestress in the steel (after initial losses). There are concerns, however, that this equation is now unconservative, since modern industry uses Grade 270, low-relaxation strands. In addition, the 1963 tests were performed using a slow method of transfer release, whilst saw cutting is performed on most precast units, leading to the probability of longer transfer lengths (Martin and Scott 1976).

An alternative expression is also given in the FIP Recommendations (1988) based on experiments by Olesniewicz at the Research and Design Centre for Industrialised Building, Warsaw, Poland in 1976. This expression is

$$l_t = C_1 \phi \sqrt{\frac{\sigma_{pi}}{f_{cu}}} \quad \text{.. 3-12}$$

Where lower, mean and upper limits for  $C_1$  are given as 7, 10 and 13, and  $\sigma_{pi}$  is the stress in the tendons immediately after release. It is suggested by Den Uijl (1997a) that the lower bound limit of Equation 3-12 is the best method for predicting the transfer length of hollow core slabs reinforced with prestressing strand, since it is

simple to use and in his experience gives a very close approximation to the actual transfer length.

A more complete set of equations for calculating transfer length are given in the CEB-FIP Model Code 1990, summarised by Den Uijl (1997b), where the treatment of bond in reinforced concrete and prestressed concrete is harmonised.

The anchorage length of a non-pretensioned tendon cast at the bottom of an element ( $l_{bp}$ ) is given as

$$l_{bp} = \frac{A_p}{\pi\phi} \frac{f_{pd}}{\eta_{p1} f_{ct}} \quad \text{.. 3-13}$$

$\eta_{p1}$  is a constant given as 1.4 for indented wire and 1.2 for plain strand,  $f_{pd}$  is the design strength of the tendon. The transfer length is calculated as

$$l_t = \alpha_8 \alpha_{10} l_{bp} \frac{\sigma_p}{f_{pd}} \quad \text{.. 3-14}$$

$\alpha_8$  = gradual release 1.0, sudden release 1.25 and  $\alpha_{10}$  refers to the Poisson effect: strand = 0.5 and indented wire = 0.7.

Therefore, in addition to the different frictional bond characteristics used for the two types of tendon, represented by  $\eta_{p1}$  in Equation 3-13, the transfer length equation also refers to the enhancement of bond due to deformation of the tendon (Poisson effect) which is greater in strands because of the Hoyer effect.

Using typical values in Equation 3-13 and Equation 3-14, it can be calculated that the transfer length of a prestressed strand is expected to be between 40% to 50% of the anchorage length of a non-prestressed strand.

As a final point it is common practice in many hollow core slab production plants to measure the initial end tendon slip ( $\delta_i$ ) and use it as a measure of  $l_t$ . By accumulating the concrete and steel strains over the transfer zone, an estimate of the transfer length ( $l_t$ ) can be calculated as (Brooks *et al.* 1988)



$$l_t = 2\delta_t \frac{E_s}{\sigma_{p_i}}$$

.. 3-15

From measurements made on 85 pretensioned beams, Rose and Russell (1997) concluded that there is a very good correlation between initial end slip and transfer length using this equation. Initial end slips measured were between 1 mm and 4 mm.

Given that the transfer length of a 12.5 mm helical strand is approximately  $60\phi$  (i.e. 750 mm), it follows, from Equation 3-15 that the initial end slip of the tendon should be about 2.5 mm. However, slabs with such large initial end slips are usually regarded as rejects. Generally, in the author's experience, the average end slip of a 12.5 mm strand is about 0.7 mm, and can be as little as 0.1 mm. Walraven and Mercx (1983) felt that this anomaly was due to the sawing process, and that the initial slip was not merely due to the relative displacement between steel and concrete, but is actually smaller because of the comparatively thick layer of concrete lost during sawing. It was concluded that formulae relating transfer length to end slip did not apply to specimens where the end face was cut with a saw.

### ***Critical section for verification of shear***

Theoretical analysis using finite element calculations have shown that for hollow core slabs containing circular voids the most critical cross-section for web shear tension failure is at a distance of about  $h/2$  from the inner face of the bearing (Girhammar 1992) where  $h$  is the thickness of the slab. For slabs with non-circular voids the greatest principal tensile stress may occur closer to the support (Pajari 1991).

Additionally, the crack normally occurs close to the neutral axis. However, for circular voids, such as those formed from extrusion, the highest principle stress will be found at the height of the narrowest web width. It has been shown that cracking will initiate at this point even when a concrete topping greater than the slab depth is placed (Ueda and Stitmannathum 1991).

BS 8110, Eurocode 2 and prEN 1168 (1995) take the critical section as the intersection of a 45° line from the edge of the bearing and the centroidal axis of the element. Rather than the centroidal axis, the FIP (1988) recommendations for hollow core slabs uses the mid-height depth from the soffit. In all cases the assumption of the most unfavourable shear crack projecting at an inclination of 45° is very conservative. FEM analysis by Lin Yang, shows the critical angle to be about 35° with the critical crack occurring at 1.43 h from the centre of the bearing.

### **3.2.4 Anchorage failure**

If flexural cracking occurs too close to the support the anchored length of the strand may be too short to provide sufficient anchorage capacity. Transfer of stress to the steel after cracking therefore leads to the tendons slipping, widening of the cracks and large rotations (Walraven and Mercx 1983). However, it has been shown that anchorage failures are of the ductile type as long as the failure is by loss of bond, and no splitting or dowel action takes place (Girhammar 1992). Because the crack for such a failure initiates close to the support, the initial flexural crack is sometimes described as a flexural shear crack. Final failure will occur by crushing in the compression zone (flexural shear compression) or by yielding and rupture of the strands.

In determining anchorage capacity of tendons it is necessary to re-consider how the prestress force is introduced into the concrete at the end of the element. If cracking occurs within the transfer length, the limit-state of equilibrium will prevent any increase in the stress in the steel. The tendons will slip under further loading and a ductile failure will ensue.

If cracking occurs outside of the transfer length, an increase in stress in the steel is possible. In this case the additional forces in the steel will be transmitted over a certain length on both sides of the crack. If the increase in stress is large then the flexural bond wave created may invade the transfer area, disturb the equilibrium and cause tendons to slip.

When the distance from the crack to the end of the transfer length is large enough, the ultimate stress of the tendons can be reached before the flexural bond wave invades the transfer area. This distance is known as the flexural bond length, and the tendon is fully developed. The sum of the transfer length and the flexural bond length is the development length ( $l_d$ ).

The critical transfer-development envelope according to ACI-318 (1989), based on tests performed in 1963, and adopted by the FIP recommendations (1988) and PCI design manual (1991) for hollow core slabs is shown in Figure 3-6. The transfer length is given as Equation 3-11 and the development length is given as

$$l_d = l_t + \left( \frac{f_p - \sigma_p}{7} \right) \phi \quad (\text{N, mm}) \quad \text{.. 3-16}$$

$f_p$  is the ultimate strength of the tendon.

The difference in the gradient of the two curves reflects the different nature of the bond. Over the transfer length the tendons are in active frictional contact with the surrounding concrete. Over the flexural bond length the tendons are not acting in friction with the concrete, so only adhesion exists between the tendons and concrete. Subsequent frictional forces activated by sliding of the tendon under imposed loading are relatively small; because the stresses in the strand tend to reduce the diameter of the tendon and therefore reduce the effective bond.

However, Girhammar (1992) suggests that the effective stress that can be carried by the tendon-concrete bond in the transfer length during anchorage pull-out is slightly greater than at transfer of the prestress. Development curves for the anchorage and pretensioning force are shown in Figure 3-7.

Tests on 36 hollow core slabs (formed by three manufacturing methods) by Anderson and Anderson (1976) concluded that the ACI-318 provisions for development of strands were adequate, so long as the initial tendon slip at release of the prestress was limited. Slabs with excessive initial tendon slip ( $\delta_i > 2.5$  mm) were found to fail by bond failure even over spans of 5 m. As assurance against premature

anchorage failure, a maximum initial slip, equal to about  $\sigma_p/6500$  (N/mm<sup>2</sup>) was suggested, which is approximately 0.3% of the expected transfer length.

Given the transfer-development envelope, a lower bound for the pull-out capacity of any cross-section can be calculated. Over a certain length of the slab between the end face and a critical distance,  $l_{cr}$ , the anchorage capacity will be less than that of the flexural cracking moment (Figure 3-8). Therefore, upon cracking, anchorage failure will immediately occur. This critical length can be calculated by considering the free body diagram shown in Figure 3-9, where the lever arm,  $z$ , is taken as the distance from the mid-height of the compression flange to the centroid of the strands, using an identical compression flange to that used in calculating ultimate flexural capacity (Walraven and Mercx 1983). This is an approximation because the compressive zone at the end of a slab is not exactly the same as that at mid-span (Girhammar 1992).

The ultimate failure moment ( $M_{anch}$ ) which causes anchorage slip failure is therefore given as

$$M_{anch} = z(\sigma_p + \Delta\sigma_p) A_p \quad .. 3-17$$

Walraven and Mercx (1983), take  $M_{anch}$  as the 5% lower limit for flexural cracking moment ( $M_{cr}$ ) approximated as  $0.9 M_{cr}$ .  $l_{ct}$  can then be calculated from the critical transfer-development envelope, given the value of  $\Delta\sigma_p$ .

General flexural behaviour can be summarised as:

- (a)  $x > l_d$  the full flexural capacity can be reached
- (b)  $l_{cr} < x < l_d$  capacity is larger than the flexural cracking moment but less than the full flexural capacity and is limited by slip of the strands
- (c)  $x < l_{cr}$  the anchorage capacity is smaller than the flexural cracking moment, so failure immediately occurs upon flexural cracking
- (d)  $x < l_t$  in addition to (c), the flexural cracking moment is reduced due to incomplete development of prestressing force.

### **3.3 Testing and design of PFRC elements**

#### **3.3.1 Shear tests on fibre reinforced prestressed hollow core slabs**

In the authors knowledge, the only previous tests on fibre reinforced hollow core slabs were performed in co-operation between the Swedish hollow core slab manufacturer, AB Strängbetong, and the Royal Institute of Technology, Stockholm, Sweden in 1986. However, the tests, as reported by Bernander (1986), were not performed on full-scale slabs but on beam specimens sawn from the slabs. The slabs were 380 mm deep 4 cored extruded Dy-core slabs, and the geometry of the test beams are shown in Figure 3-10. Slit sheet fibres with enlarged ends (18 mm x 0.6 mm x 0.3 mm) were added to the mix at  $V_f = 1\%$ . The beams were tested with a shear span to effective depth ( $a/d$ ) ratio of 4, and the fibres were found to increase the ultimate web shear tension capacity by about 25%. Three plain and three fibre reinforced beams, were tested, and the variation in the test results was less for the fibre reinforced specimens. It was suggested that this may lead to less conservative strength reduction factors for design. The results of Bernander's tests are shown in Table 3-2, and it is interesting to note that both the web shear tension strength and splitting tensile strength increase by 25% over that of plain concrete with the addition of the fibres.

#### **3.3.2 Shear tests on PFRC**

A substantial number of shear tests have been performed on RFRC beams. A comprehensive review of shear tests on RFRC beams without shear links can be found elsewhere (Adebar *et al.* 1997). Within this section a review of shear tests on PFRC beams is given. Where the behaviour of PFRC is comparable with the behaviour of RFRC, some RFRC beam tests are briefly described.

The most extensive series of test performed on PFRC beams were carried out by Narayanan and Darwish (1987a). In total they tested 38 beams at a number of fibre

volume fractions (ranging from 0.3% to 3.0%), a/d ratios (2.0 and 3.0) and prestressing ratios. The fibres used were crimped steel fibres with a nominal aspect ratio of 100. In all but four of these tests, the beams were made partially-prestressed (i.e., the beams have both prestressed and non-prestressed longitudinal reinforcement) by adding 12 mm diameter un-tensioned bars. These bars were added with the sole intention of ensuring a shear failure by enhancing the flexural performance. However, it was found that beams which contained no bar reinforcement failed at lower loads than their counterparts. This difference in ultimate load diminished with increasing prestress.

Narayanan and Darwish's tests were performed on 150 mm x 85 mm rectangular beams over a 0.9 m span, and two types of failure were observed. Generally, at a/d = 2.0 web shear tension failures occurred, whilst at a/d = 3.0 flexural shear failures were observed. These flexural failures eventually failed by crushing of concrete in the compression zone.

For the beams failing in web shear tension, the plain concrete beams collapsed immediately after first cracking, while fibre reinforced beams, cracked at similar loads but were able to sustain considerable loads beyond the first crack. Typical increases in ultimate strength of about 40% were observed for a fibre volume fraction of 1%.

Similar increases were found by Lorentsen (1985) who observed a 50% increase in ultimate strength using  $V_f = 1.5\%$  on fully prestressed (i.e. no bar reinforcement) pretensioned I-beams tested over an a/d ratio of 3.7. The fibres used were HS fibres of length 40 mm and 0.4 mm in diameter.

Less favourable results were obtained by Balaguru and Ezeldin (1986) who tested five partially-prestressed T-beams in shear. In these tests, a 15.9 mm un-tensioned bar and minimum shear links were provided. HS fibres (30 mm x 0.5 mm) at varying fibre volume fractions from 0% to 1.5% were investigated, and it was found that adding  $V_f = 1.5\%$  gave only a marginal 6% increase in ultimate load. In fact there appeared to be an optimum fibre volume fraction of about 0.75%, beyond which there was an insignificant increase in strength.

It is likely that this low increase in shear strength observed by Balaguru and Ezeldin is due to the effect of the minimum shear links in their tests. Tests by Shin *et*

*al.* (1994) have shown that RFRC beams containing shear links do not attain the same increases in shear strength with increasing fibre volume fraction as those which do not contain shear links. Figure 3-11 and Figure 3-12 show how the shear contribution of fibres significantly reduces when shear links are provided. In both figures the ratio  $A_v/A_{v(ACI)}$  is the percentage of shear reinforcement provided in relation to that suggested in the ACI Building Code (1989). It can be concluded that links are much more effective at providing shear reinforcement than fibres, since even 50% of the required shear links renders fibre reinforcement ineffective. Little advantage is to be gained therefore from the combined use of links and fibres, or the use of fibres where shear links could be used. However, fibres could be more viable and economic in situations where links are difficult to place due to confined space, manufacturing method or time restrictions.

Although the increase in strength is not significant when shear links are present, Shin *et al.* (1994) showed that fibres did improve ductility, as was also observed by Balaguru and Ezeldin (1986). In addition, fibres perform better than shear links in limiting crack widths, since they can bind the crack wherever it may occur, whilst shear links are only effective where the crack actually crosses the vertical reinforcement bars. This leads to greater rigidity and greater ductility in PFRC beams compared with plain reinforced concrete beams (Casanova *et al.* 1997).

In contrast to the tests by Balaguru and Ezeldin, Rajagopal and Siddappa (1992) tested 8 partially-prestressed post-tensioned beams, and found significant increases in both the cracking shear strength and ultimate shear strength. No improvements in  $V_{cr}$  had previously been acknowledged by earlier researchers and yet these tests showed a 71% increase in  $V_{cr}$  despite using straight round steel fibres (aspect ratio = 100) at a maximum  $V_f$  of only 0.75%. This increase in  $V_{cr}$  was attributed to the crack arrest mechanism of fibres.

Increases in web cracking strength were also reported by Tan *et al.* (1995) who tested ten partially-prestressed T-beams. An increase of 23% was observed for 1% HS fibres (30 x 0.5 mm). The behaviour of these beams differed from all the other tests reported, however, in that the plain concrete beams had a considerable load-carrying capacity after web cracking. Values of  $V_{ult} = 1.8 V_{cr}$  were observed

independently of whether the beams failed by web crushing or diagonal tension. Tan *et al.* also showed that the load-carrying capacity of the beams increases with a decrease in the  $a/d$  ratio for the same type of failure. This had previously been observed in RFRC beams by Narayanan and Darwish (1987b) and Ashour *et al.* (1992), and is due to increased compressive strut action at these lower  $a/d$  ratios resulting in the beams acting more like deep beams.

### 3.3.3 Predictive equations for ultimate shear capacity of PFRC beams

From the various shear tests on PFRC beams, three different methods have been suggested for predicting the ultimate shear capacity.

A popular method for defining the increase in ultimate shear capacity for RFRC beams in diagonal shear has been to adopt an additive method, where a shear supplement due to the fibres,  $V_b$ , is added to conventional equations for plain reinforced concrete beams, such that the ultimate shear capacity of RFRC is given as (see Figure 3-13)

$$V_u = V_c + V_b$$

.. 3-18

where  $V_c$  is the concrete contribution to shear capacity, a combination of concrete compressive resistance ( $V_{cc}$ ) and dowel resistance ( $V_d$ ). Lorentsen (1985) suggested that this may also be a suitable method for calculating the ultimate shear resistance of PFRC beams although no definition of  $V_b$  was given other than that it was dependant on fibre type and fibre content. Given that after cracking, web shear tension in PFRC acts similarly to shear tension in RFRC (Narayanan and Darwish 1987a), it may be suitable to directly adopt measures of  $V_b$  previously defined for use in RFRC, which have largely concentrated on the tensile stresses which the fibres can provide across the shear crack.

In addition to this term,  $V_b$ , it has been suggested by some authors that fibres have an effect on the concrete compressive resistance and the dowel resistance.  $V_{cc}$  is



usually calculated using a formula involving the concrete compressive strength and to account for fibres, Sharma (1986) simply suggested using the compressive strength of FRC. However given that the effect of fibres in compression is only marginal, Narayanan and Darwish (1987b) and Shin *et al.* (1994) suggested that the ability of fibres to hold together the compressive zone may be best approximated from an empirical equation based on the ultimate tensile splitting strength. Likewise, Swamy and Bahia (1985) suggested using the ultimate flexural tensile strength.

The dowel contribution depends primarily on the tensile resistance of concrete to splitting and the bond strength of concrete. Results of tests by Swamy and Bahia (1979) suggest that fibres increase the stiffness of the dowel zone helping to contain dowel crack growth, resulting in more efficient dowel contribution. An equation for the dowel resistance to shear in FRC was presented by Swamy and Bahia (1979):

$$V_d = \rho_w b_n^2 (0.156 f_{ft,ult} - 0.25)$$

.. 3-19

where  $\rho_w$  is the percentage of tension steel, and  $b_n$  is the net concrete width at the level of the steel centroid.

However, in general the effect of fibres on the concrete contribution are small and it is generally accepted that the same value of  $V_c$  can be taken for both reinforced concrete and RFRC beams of the same geometry, concrete strength and longitudinal reinforcement. Therefore the term  $V_b$  is usually the sole measure of the improved shear resistance due to fibres. Methods of calculating  $V_b$  are discussed below.

In all these measures of  $V_b$ , the additional post-cracking shear resistance of RFRC is assumed to be due to the fibres transferring tensile stresses across the crack (i.e. stresses normal to the crack), and not due to any additional shearing effect on the fibres. Mansur *et al.* (1986) assumed that the fibre supplement was due to the post-cracking tensile strength of FRC ( $\sigma_{tu}$ ) acting across the entire length of the diagonal shear crack. As in tension this value can be regarded as the fibre bridging component. Similarly, Casanova *et al.* (1997) suggested calculating the fibre tensile stress across the crack directly from uniaxial tension tests by means of an equivalent post-cracking

residual stress at a critical crack width of  $w_{mu}$ . This is in fact the mean value of the post-cracking residual stress between zero crack width and  $w_{mu}$ , and could additionally be taken from analytical models such as that of Lim *et al.* (1992) described in Section 2.2.2. Casanova *et al.* define  $w_{mu}$  as 1% of the inner lever arm  $0.9d$ . Given that the simple equation for post-cracking tensile strength suggested by Lim *et al.* (1992) is valid over such small crack widths, it is suggested that this method of defining  $\sigma_{tu}$  is perfectly reasonable. This is in fact consistent with Mansur *et al.* (1986) who only suggested experimental values for  $\sigma_{tu}$  given that there were no satisfactory analytical models available at the time. For diagonal cracks inclined at  $45^\circ$  the equation for  $V_b$  simplifies as:

$$V_b = \sigma_{tu} bd \quad \dots 3-20$$

The parameter  $d$  in this equation denotes that the diagonal crack crossed by the fibres runs diagonally at  $45^\circ$  from the longitudinal reinforcement to the top of the beam. In fact due to the compression zone in the upper regions of the beam, the crack never actually reaches the top of the beam. The term  $0.9d$  is therefore used in preference to  $d$  by some researchers (Swamy *et al.* 1993, Casanova *et al.* 1997) for this reason.

An alternative form for  $V_b$  is given in the Dramix Guidelines (1995) where the fibre supplement is due to a constant tensile stress acting along a diagonal crack of vertical height  $0.9h$ . The term  $V_b$  is calculated by assuming the bending moment carried by the fibres to equal the bending moment due to an equivalent post-cracking flexural strength,  $f_{fl,eq,300}$ , using elastic theory. Using empirical relationships correlating flexural strengths to axial tensile strengths,  $V_b$  is given as:

$$V_b = 0.54 f_{ct,ax} R_t bd \quad \dots 3-21$$

$$R_t = \frac{1.1 W_f \lambda_f}{(180C + W_f \lambda_f)} \quad \dots 3-22$$

where  $W_f$  is the fibre content (in  $\text{kg/m}^3$ ) and  $C$  is a function of the anchorage effect of the fibres (given as 20 for HS fibres, and 35 for straight round fibres).  $R_t$  is intended to be the ratio of the tensile strength before cracking to the tensile strength after cracking (Nemegeer 1995), and can be calculated experimentally according to Bekaert (1995) from the ratio of cracking flexural strength,  $f_{fl,cr}$ , to the equivalent flexural strength to span/300,  $f_{fl,eq,300}$ .

A comparison between Equation 3-20 and Equation 3-21 is given in Figure 3-14. As the fibre volume fraction increases the shear supplement as given by Equation 3-21 can be seen to diminish. This is consistent with the result of the tests by Balaguru and Ezeldin (1986) where there appeared to be an optimum  $V_f$  of 0.75%. Similarly the tests on RFRC beams by Swamy and Bahia (1985), Narayanan and Darwish (1987b) and Ashour *et al.* (1992) showed an optimum  $V_f$  of 1%. The appearance of an optimum  $V_f$  is probably as a result of reduced concrete workability with increasing fibre content. This leads to reduced bond between the fibre and matrix and, therefore, lower fibre efficiency.

A problem with Equations 3-20 and 3-21 for calculating the ultimate shear capacity are that they both rely on fibre parameters which may not necessarily be applicable to different fibre types, especially those of an altogether different shape and profile. For example, the fibre aspect ratio of a fibre with a non-round cross-section is not uniquely defined. Additionally, it may not be practical in design to base predictive equations on a large number of parameters. Criswell (1994) noted that although these parameters may be useful in materials engineering they may be too detailed and involve quantities a structural designer would not want to try and specify. As an alternative to Equation 3-21, RILEM TC-162 (1997) suggested an equation which incorporates the equivalent flexural tensile strength over a deflection of span/150 as the sole measure of the shear performance of fibres. This is given as

$$V_b = (0.09 f_{fl,eq})bd$$

.. 3-23

This is consistent with the original expression given by the Dramix Guidelines (1995) since the term  $f_{ct,ax} \cdot R_t$  was derived from an empirical relationship between the shear strength and equivalent flexural strength (Bekaert 1995). Although Equation 3-23 is believed to work very well for rectangular beams, it is apparently too conservative for T-beams (RILEM TC-162, 1997).

Tan *et al.* (1995) derived a further form of the term  $V_b$  based on principal tensile stress-strain relationships, in which the state of stress in a cracked partially-prestressed element under bending and shear was assumed to be as shown in Figure 3-15. Given this condition and taking  $\sigma_y = 0$  and  $\rho_y = 0$ , i.e. no vertical prestressing or stirrups, the shear stress in the element,  $\tau_{xy}$ , can be written as

$$\tau_{xy} = \sigma_1 \cot \alpha \quad \dots 3-24$$

where  $\sigma_1$  is the principal tensile stress, which at ultimate equals the post-peak principal tensile strength,  $\sigma_r$ . The ultimate shear capacity of the section is  $V_u = \tau_{xy} \cdot b_w \cdot d$  and therefore the shear supplement due to adding fibres,  $V_b$  equals

$$V_b = [\sigma_{r(FRC)} \cot \alpha - \sigma_{r(plain)} \cot \alpha] b d \quad \dots 3-25$$

and again assuming the inclination of the shear crack,  $\alpha$ , is  $45^\circ$  simplifies as

$$V_b = [\sigma_{r(FRC)} - \sigma_{r(plain)}] b d \quad \dots 3-26$$

Tan *et al.* proposed a post-peak principal tensile strength, based on the work of Tan and Mansur (1990), which is given as  $(f_{cr} + \sqrt{\sigma_{tu}})/(1 + \sqrt{2})$ . Using this equation and taking the cracking principal tensile stress,  $f_{cr}$ , as equal for plain concrete and FRC, gives

$$V_b = 0.6\sigma_{tu}bd$$

.. 3-27

i.e. 0.6 of the term previously derived by Mansur *et al.* (1986).

Although these additive terms have proved suitable for estimating the shear capacity of RFRC and PFRC beams, they are inconsistent in their approach to shear when compared with methods presently in design codes for prestressed concrete; and equally for prestressed hollow core slabs.

Narayanan and Darwish (1987a) offer an alternative approach to calculating ultimate web shear capacity by suggesting a modification of the present BS 8110 equation. They considered that beams that fail in shear and torsion exhibit similar ultimate load characteristics to that of cylinders in the splitting tension test, and suggested replacing  $f_{ct}$  in Equation 3-4 with the ultimate splitting tensile strength,  $f_{ct,sp}$  as calculated using Equation 2-15 as an approximation to the tensile strength of FRC. This is of course inappropriate given the significant increases in  $f_{ct,sp}$  with increasing  $V_f$  compared to the small increases in the uniaxial tensile strength. However the equation gave very good correlation with the test results and is given as:

$$V_u = 0.67bh\sqrt{f_{ct,sp}^2 + f_{ct,sp}\sigma_{cp}}$$

.. 3-28

Rajagopal and Siddappa (1992) found that this equation also gave good correlation with their fibre reinforced post-tensioned beams. However, there is an inconsistency between Equation 3-28 and the original BS 8110 equation, because Equation 2-15 for plain concrete ( $F=0$ ) does not correspond with  $f_{ct} = 0.3\sqrt{f_{cu}}$  - the expression used in BS 8110 for the principal tensile splitting strength of plain concrete. A comparison between the BS 8110 expression and Equation 2-15, derived for plain concrete by Marshall (1974), is shown in Figure 3-16. It can be seen that they do not give similar tensile strengths for the compressive strengths used by Narayanan and Darwish (1987a) and Rajagopal and Siddappa (1992), i.e.,  $f_{cu} = 50$  to  $60 \text{ N/mm}^2$ .

Although not calculated or specifically mentioned in either reference, it seems sensible to presume that use of the first crack splitting strength of FRC in Equation 3-28 will correspond with the first crack shear capacity of a PFRC beam.

This appears therefore to be a more suitable method for calculating the ultimate shear capacity than the additive methods, since it can be used in calculation of both the cracking and ultimate capacity. In addition, it is based on the same principles as the present code design equations, which makes it more acceptable as a design formula as it will not lead to over-complication of design procedures and therefore confusion amongst designers. However, a problem with such an equation is that the use of  $f_{ct,sp}$  is purely empirical because the behaviour of FRC beyond cracking in the splitting tension test is not clearly understood, and is certainly not related purely to tension. On these grounds it is difficult to justify the use of  $f_{ct,sp}$ . None of the present approaches for estimating the ultimate shear capacity of RFRC and PFRC beams are therefore entirely satisfactory.

#### **3.3.4 Direct Shear**

A number of researchers have investigated the strength and ductility of FRC under conditions of direct shear. These investigations can be separated into two distinctly different problems: shear transfer across an initially cracked plane and shear transfer across an initially uncracked plane.

Tests on shear transfer in FRC across initially cracked planes, have been essentially empirical investigations of the shear friction along the existing crack. The relationships between the following four parameters are individually investigated: normal stress ( $\sigma$ ), shear stress ( $\tau$ ), crack width ( $w$ ) and shear displacement ( $\Delta$ ). In models, there is often assumed to be no direct relationship between one or more parameters (e.g. Divakar *et al.* 1987). It is also important to appreciate that shear displacement causes an additional local increase in the crack width by cutting-off protruding asperities and thus creating a lateral dilatancy (Tassios and Vintzeleou 1987), see Figure 3-17.

Van de Loock (1987) tested a number of FRC push-off specimens pre-cracked along the shear plane, with HS fibres (60 mm x 0.8 mm) providing the only reinforcement across the shear plane. Both crack width and dilatancy were measured with LVDTs and normal restraint across the crack was provided by external bars. The relationship between the increase in  $\sigma$  and  $w$  was dependant on the elastic stiffness of the bars, and could not be changed during the test. The parameters studied were fibre volume fraction (0%, 0.5% and 1%) and amount of normal restraint. Figure 3-18 shows the test results for each fibre volume fraction at similar levels of normal restraint stiffness. It can be seen that fibres have a significant influence on the maximum shear stress and ductility of the specimens. The cracking stress, however, is unaffected by fibres. Both crack width and shear displacement at ultimate shear stress increase with increasing fibre volume fraction, but ultimate stress still occurs at relatively small values, i.e.  $\Delta = 0.2$  mm and  $w = 0.3$  mm for  $V_f = 1\%$ . It was also noted that as the level of normal restraint increased, the effect of increasing the fibre content decreased.

Similar push-off tests performed by Hara (1984) using flat fibres (0.5 x 0.5 x 30 mm) with crimped ends found that there was no influence of fibres on shear strength until a fibre volume fraction of at least 1.5% was added.

An alternative arrangement for examining the influence of fibres in shear across a cracked plane was used by Holmgren (1985). Prisms were sawn from concrete boxes, and around the middle of these prisms one mm deep grooves were scored. The prisms were subjected to negative and positive flexure to develop a crack all the way through and pulled apart to create an initial crack width. Initial crack widths between 1 mm and 5 mm were tested. During testing, this initial crack width was kept constant whilst the two sides of the prisms were pushed in the opposite direction to each other. In all the tests Holmgren attempted to eliminate all effects of aggregate interlock to leave just the fibre contribution. In fact this only proved possible in tests with an initial crack width of at least 3 mm.

HS fibres (45 mm x 0.35 mm) were tested at fibre volume fractions of 1% and 1.5%, resulting in shear strengths of  $0.7 \text{ N/mm}^2$  and  $1.3 \text{ N/mm}^2$ , respectively. For both  $V_f$ 's maximum shear stress was achieved at a dilatancy of about 7 mm.

Interestingly, even at a dilatancy of  $l_f/2$  there was still some shear carrying capacity remaining even though the average fibre is completely pulled out.

Push-off tests on initially uncracked FRC specimens have been performed by Valle and Buyukozturk (1994), and by Khaloo and Kim (1997). The latter investigated the effects of two fibre lengths (16 mm and 32 mm) on direct shear strength and ductility, using fibres with an identical triangular cross-section with hooked-ends and twisted along the longitudinal axis. The tests were performed on matrices with four compressive strengths by testing nominally identical specimens at different ages - thus eliminating any differences attributable to changes in water-cement ratio, ratio of fine to coarse aggregate, *etc.* Valle and Buyukozturk's (1994) tests were performed with 30 mm x 0.5 mm crimp-ended fibres at a fibre volume fraction of 1% in high-strength and normal strength matrices.

In both series of tests, measurements were made of the average shear stress against shear displacement. Little or no affect of fibre aspect ratio or fibre volume fraction was found on the cracking shear stress, while increases in the ultimate shear stress were very significant. Khaloo and Kim (1997) found that a fibre volume fraction of 1.5% increased the shear strength by up to 100% compared with an equivalent plain concrete specimen. Significantly the ability of fibres to increase the shear strength improved with the concrete compressive strength, and this was attributed to greater fibre-matrix interfacial bond strength at higher concrete strengths. Figure 3-19 shows the fibre contribution to shear strength at the four concrete compressive strengths. It can be seen that the fibres with the greater aspect ratio provided the greatest shear resistance.

The observed failure in the plain concrete specimens was very brittle with no warning before collapse. The specimens lost their integrity and broke into several pieces. The FRC specimens failed by the development of a fine crack along the shear plane, although according to Valle and Buyukozturk (1994) this may be several small diagonal cracks which develop along the shear plane to form a crack band along the shear plane. The failure mechanism after cracking has similarities with that observed in pre-cracked specimens. Fibres are able to hold the integrity of the specimens, and



final failure occurs by fibre pullout or rupture depending on fibre characteristics and the strength of the matrix.

A model was proposed by Khaloo and Kim (1997) based on their results, in which the shear stress - slip behaviour was idealised as a bi-linear curve as shown in Figure 3-20.  $\tau_{cr}$  which corresponds to the shear stress at cracking is given as  $0.65 \sqrt{f'_c}$ . For FRC an alternative equation was given for  $\tau_{cr}$  based on  $V_f$ , but as explained above the cracking stress differs only slightly from that of plain concrete. The ultimate direct shear strength of FRC ( $\tau_{ult}$ ) is given as

$$\tau_{ult} - \tau_{cr} = G_{pc}(\delta_{ult} - \delta_{cr}) \quad \dots 3-29$$

where  $G_{pc}$  is the post-cracking shear modulus derived as

$$G_{pc} = 0.686 V_f^{0.62} \lambda_f^{0.37} f'_c^{0.165} \quad (\text{N/mm}^2) \quad \dots 3-30$$

To use this equation it is necessary to have information on the amount of post-cracking slip ( $\delta_{ult} - \delta_{cr}$ ) between cracking and ultimate. Study of the shear stress - slip curves presented by Khaloo and Kim show that this value is between 0.3 mm and 0.5 mm. Post-cracking slips to ultimate in the tests by Valle and Buyukozturk (1994) were approximately 0.2 mm to 0.3 mm. Figure 3-18 shows the slip in the precracked specimens of Van de Loock (1987) to be of similar magnitude. However, as with the shear supplements discussed in Section 3.3.3 the above equation for ultimate shear strength assumes a constant matrix shear strength after cracking. This does not correspond with the brittle plain concrete shear failures which were observed in the tests.

Valle and Buyukozturk modelled the shear transfer based on a truss model considering the softening of concrete in compression. However, they idealised the tension stress-strain curve for FRC as that shown in Figure 3-21, where  $f_{ct,ult}$  is given as:

$$f_{cr,ult} = f_{ct,cr} + \eta_0 \eta_l V_f f_{fu}$$

.. 3-31

However,  $f_{ct,ult} > f_{ct,cr}$  is only applicable when  $V_f > V_{f,crit}$ . For the fibres used by Valle and Buyukozturk,  $V_{f,crit}$  is approximately 2%, whilst only 1% was used in the tests. This basic material law for concrete used in the analysis therefore appears to be incorrect.

The toughness of the shear tests was also investigated in both series of tests by comparing the area under the measured stress-displacement curves. In general, the addition of fibres resulted in an improvement of toughness in all cases as did increases in the fibre aspect ratio. Interestingly, Khaloo and Kim found that the shear toughness increased with higher concrete compressive strength.

Push-off tests on initially uncracked FRC specimens containing steel stirrups across the shear plane have been performed by Tan and Mansur (1990) using slightly twisted 30 mm long fibres with a square cross-section (0.5 x 0.5 mm), and Valle and Buyukozturk (1994) using crimp-ended fibres (30 mm x 0.5 mm).

The failure, when steel stirrups are included across the plane, occurs by the formation of discrete diagonal cracks and well defined compressive struts in the concrete. In combination with the tensile forces in the stirrups this forms a truss-like action, and is therefore a distinctly different problem from that of shear friction (Tan and Mansur 1990). For all the tests the behaviour up to cracking was essentially the same, with only small tensile, compressive and shear strains at cracking. After cracking the fibres bridging the crack provided restraint to its widening and as a result those specimens with highest  $V_f$ 's exhibited smallest strains. Tan and Mansur found that because of the stirrups, even plain concrete specimens were able to carry greater post-cracking stresses than at cracking. The behaviour of the tests performed by Valle and Buyukozturk was essentially the same.

### 3.3.5 Flexural testing and design of PFRC

The flexural cracking strength of prestressed concrete is dependant on the prestressing force and flexural tensile cracking strength. Given that any effect of fibres on the prestressing force is likely to be small, any difference in flexural cracking strength between plain prestressed concrete and PFRC is solely dependant upon the difference in flexural cracking tensile strength of plain concrete and FRC.

Figure 3-22 shows the effect of increasing the fibre volume fraction on a typical x-shaped prestressing beam at  $a/d = 2.8$ , using Equation 3-28 for ultimate shear strength and the law of mixtures to estimate the increase in flexural tensile cracking strength. It can be seen that the influence of fibres on the ultimate shear strength is much greater than on the flexural cracking moment. At low  $V_f$ , shear is the most critical failure, but as  $V_f$  increases there is a critical fibre volume fraction at which flexural cracking occurs before shear cracking. This does not necessarily mean that shear failure will not occur, since after flexural cracking the load-carrying capacity of a beam can still increase. A similar curve, could be drawn showing ultimate shear and ultimate moment capacity with another critical fibre volume fraction indicating the change from shear to flexural failure.

The effect of increasing  $V_f$  is therefore similar to increasing the  $a/d$  ratio. Mansur *et al.* (1986) showed that there is a gradual deviation away from shear failure towards flexural failure with increasing  $a/d$  ratio and  $V_f$  for RFRC beams (see Figure 3-23). An extensive description of this shear-flexure interaction for RFRC is given by Imam *et al.* (1997).

As far as the author is aware, no extensive testing has been carried out on PFRC beams in flexure. However, the ultimate behaviour of prestressed concrete and reinforced concrete are essentially the same, and the ultimate strength of PFRC can be predicted using the same methods as those for RFRC.

In predicting the ultimate moment of resistance of reinforced concrete, the following assumptions are made:

1. Plane sections before bending remain plane after bending
2. The stress/strain curve for steel is known
3. The compressive stress/strain curve for concrete is known, defining the magnitude and distribution of compressive stresses.
4. The tensile strength of concrete can be neglected.

Since fibres are able to transfer considerable stresses across the section cracked in tension, assumption 4 is invalid. Stress blocks for use in calculating the ultimate flexural strength of RFRC beams can be found throughout the literature, and are essentially the same with the main distinctions being due to the different national standards for calculating flexure of plain reinforced concrete on which they are based. Figure 3-24 shows a possible stress block and forces for a PFRC section at ultimate based on that proposed by Mansur *et al.* (1986) for a RFRC section. A slight alteration has been made by the author to make the calculation of ultimate flexural strength consistent with BS 8110 (1985). Mansur *et al.* based their compressive strains and stresses on the provisions provided in ACI 318 (1989) for plain concrete with no alterations. The ultimate compressive strains and stresses shown in Figure 3-24 are exactly those present in BS 8110 for plain concrete.

The tensile stress block consists of tensile stresses provided by the longitudinal reinforcement and by the fibres. The longitudinal reinforcement contribution is consistent with that found in BS 8110, whilst the tensile stresses provided by the fibres are assumed to be equal to the post-cracking strength of fibres ( $\sigma_{tu}$ ). For small crack widths the expression derived by Lim *et al.* (1987a) for  $\sigma_{tu}$  is valid. This post-cracking stress is assumed by Mansur *et al.* and other researchers (e.g. Craig 1987) to act throughout the entire depth of region in tension. However, some researchers and guidelines favour utilising only those fibres between the neutral axis and the centroid of the reinforcement (e.g. Narayanan and Palanjian 1986, Dramix Guidelines 1995).

From Figure 3-24, the ultimate moment of the rectangular PFRC beam,  $M_u$ , can be calculated as

$$M_u = A_{ps}f_{pb}\left(d - \frac{0.9x}{2}\right) + \sigma_{tu}b(h-x)\left(0.1x + \frac{h}{2}\right) \quad .. 3-32$$

where the neutral axis depth,  $x$ , can be calculated by equilibrating the compressive and tensile forces, i.e.  $F_c = F_s + F_f$ . This calculation of  $M_u$  is only valid where there is a rectangular cross-section above the neutral axis at failure. For other shapes,  $x$ , must be determined by trial.

As mentioned above, the effect of fibres within the compressive zone is usually neglected, however, Swamy and Al-Ta'an (1981) tested a number of simply-supported RFRC beams in flexure with fibres only included in the bottom half, and it was found that there was no significant increase in shear strength or ductility. Similar results have been obtained elsewhere (Bentur and Mindess 1990). It may be that fibres in the compressive zone act as crack arresters, and restrict the migration of the neutral axis into the compression zone. This probably allows the fibres in the tension zone to be more effective.

### 3.3.6 FRC on bond properties

A few authors have experimentally investigated the effect of FRC on the bond properties of ribbed reinforcing bar and prestressing strand.

Ezeldin and Balaguru (1989) compared the pull-out behaviour of different bar diameters (9 mm, 16 mm, 19 mm and 25 mm) from both normal and high strength concrete containing various fibre contents ( $0 \text{ kg/m}^3$  to  $60 \text{ kg/m}^3$ ). The embedded length of the bar in the concrete, varied in relation to the bar diameter for each test, but was only small to prevent yielding of the bar and ensure bond failure. Two different failure types were observed.

The 9 mm diameter bars failed by friction pull-out, with no extensive internal cracking around the bar. The larger diameter bars failed by concrete splitting along the length of the bar, as a result of radial force components caused by deformation of the concrete. Because the splitting is tensile, failure in the plain concrete specimens was very brittle and immediate. FRC specimens were more ductile and post-crack stress-slip curves could be recorded. The ductility of the specimens improved with increasing fibre volume fraction and fibre aspect ratio.

Ezeldin and Balaguru found, however, that the effect of fibres on the bond strength of the concrete was very small and almost negligible. With the larger bars there was a slight improvement, which was attributed to the fibres slowing down the opening of the split tensile cracks. No noticeable differences in bond strength between FRC with differing fibre volume fractions or fibre aspect ratios was observed.

More encouraging results were obtained by the studies of Swamy and Al-Noori (1974) and Soroushian *et al.* (1994), which both observed a 33% increase in local bond strength for FRC over plain concrete. In the case of Swamy and Al-Noori this was obtained using straight steel fibres ( $\lambda_f = 65$ ) at  $V_f = 2.0\%$ . However, the latter study found that any increase in  $V_f$  beyond 0.5% did not lead to any further significant increases in bond strength.

In addition, Soroushian *et al.* investigated different aspect ratios (60, 80 and 100) and fibre types (HS, straight and crimped). They found that all FRC gave better performance than plain concrete, but that there was no significant differences in the strength as a result of varying fibre type or  $\lambda_f$ . Given that neither of these parameters has an effect, it would appear that bond strength is not related to fibre pull-out. It is more likely, as noted by Ezeldin and Balaguru (1989), that it is due to the crack arrest mechanism of fibres at a microcrack level - which is only slightly affected by fibre properties.

Whilst the effect of fibres on the bond properties of reinforcing bar are encouraging leading to greater strengths and ductility, Lorentsen (1985) showed that the effect of fibres on the bond properties of prestressing strand are less significant.

Figure 3-25 shows bond stress - slip curves for reinforcing bar and prestressing strand in plain concrete and 1.5% HS (40 x 0.4 mm) FRC.

A comparison of the draw-in and strain measurements on three pretensioned beams ( $V_f = 0\%$ ,  $0.5\%$  and  $1.0\%$ ) containing 12.9 mm seven-wire helical strand was carried out by Balázs *et al.* (1997). HS fibres (30 x 0.5 mm) were used, and the three beams were cast on the same strand. The beams measured 2 m in length and had a rectangular cross-section of 80 x 120 mm.

Release of the prestress after casting was by a slow method, and measurements of the draw-in were made in nine increments as the prestressing force at the end of the member was reduced to zero. According to Balázs *et al.* (1997) comparison of the three beams indicates that fibres produce lower draw-in of the prestressing strand. The specimen with  $V_f = 0.5\%$  actually gave the best response, although it was not significantly better than the  $V_f = 1\%$  specimen. This effect of fibre volume is consistent with the observation of Soroushian *et al.* (1994), but given only these three results there is insufficient information for any significant conclusions. The draw-in measurements indicate transfer lengths of 388 mm for 12.9 mm strand in plain concrete, and for FRC a transfer length in the range 310 - 336 mm.

The strain measurements were made on the compression face of the specimens at release to indicate the build-up of prestress along the transfer length. The curves for each specimen are shown in Figure 3-26. The difference in each of the curves appears to be insignificant, but Balázs *et al.* (1997) again suggest that they indicate the application of fibres leads to shorter transfer lengths. This improved bond is attributed to the steel fibres reducing micro-cracking in the interactional zone, consistent with observations on reinforcing bar.

**Table 3-1 Results of sensitivity study by Åkesson (1994) showing absolute values and relative changes in percent, compared with a standard slab, for transfer length and draw-in.**

Type	Transfer Length	Draw-in
Standard	329	0.75
1.10 $f_{cu}$	326 (-0.9%)	0.740 (-1.1%)
1.10 $P_i$	346 (+5.2%)	0.865 (+15.6%)
1.10 $r$	329	0.75
0.90 $A_p$	332 (+0.9%)	0.840 (+12.3%)
0.90 cover	327 (-0.6%)	0.746 (-0.3%)

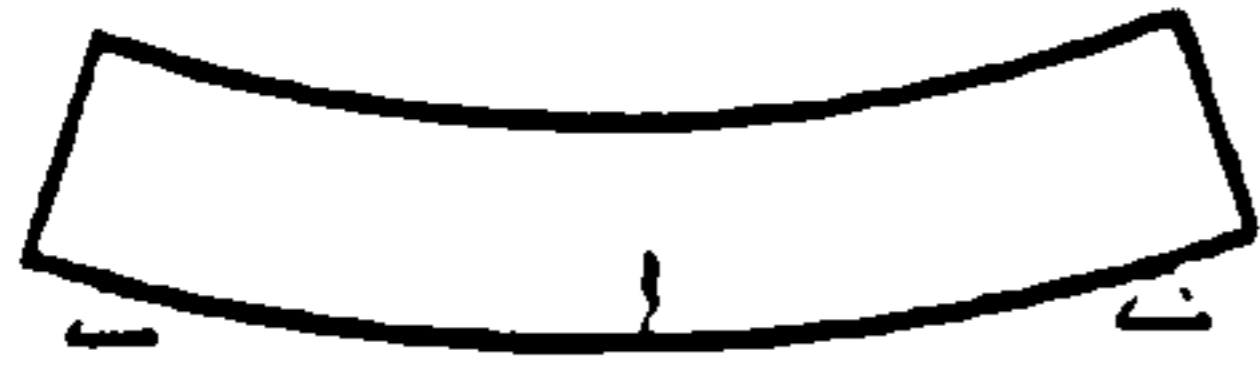
For standard:  $f_{cu} = 47.5 \text{ N/mm}^2$ ,  $P_i = 1000 \text{ N/mm}^2$ , radius of the hollow core  $r = 73.5 \text{ mm}$ ,  $A_p = 100 \text{ mm}^2$  and concrete cover = 34 mm

**Table 3-2 Shear test results from plain and fibre reinforced "cut-out beams" from a Dy-Core slab (Bernander 1986)**

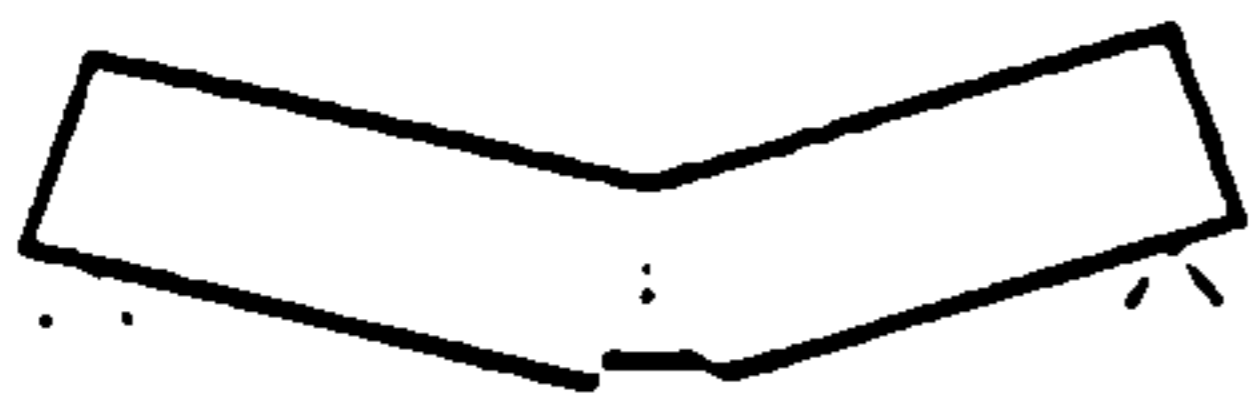
Beam No.	b (mm)	h (mm)	$f_{cu}$ ( $\text{N/mm}^2$ )	$f_{ct,sp}$ ( $\text{N/mm}^2$ )	$V_{ult}$ (kN)	$V_{ult}/bh$ ( $\text{N/mm}^2$ )
O2	73	376	62.8	5.1	105	3.93
O3	74	376	63.7	5.7	130	4.78
O4	82	379	68.6	5.4	115	3.8
mean values			65	5.4		4.17
F2	70	372	59.3	6.9	140	5.49
F3	69	376	67.2	8.7	135	5.32
F4	70	378	69.6	6.5	127.5	4.93
mean values			65.4	6.7		5.25
ratio F/O of mean values				1.24		1.26

O = plain concrete beam, F = fibre reinforced concrete beam  
 $f_{ct,sp}$  obtained from cylinders drilled horizontally out of top flange





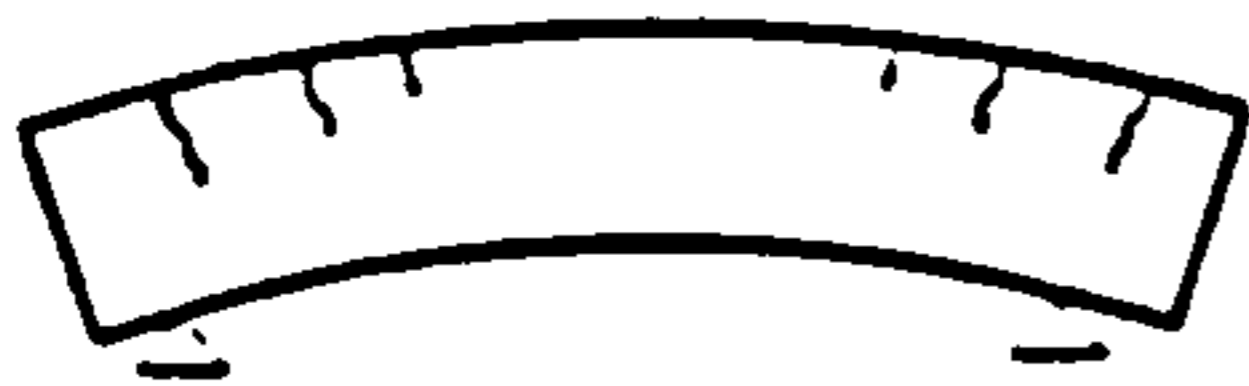
a) Flexural tensile cracking of concrete



b) Yielding (rupture) of strands



c) Flexural compression failure of concrete



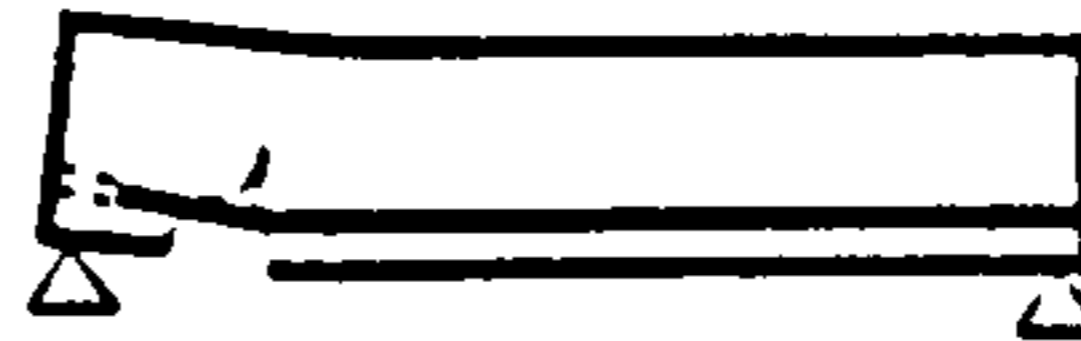
d) Flexural tensile cracking of top fibre



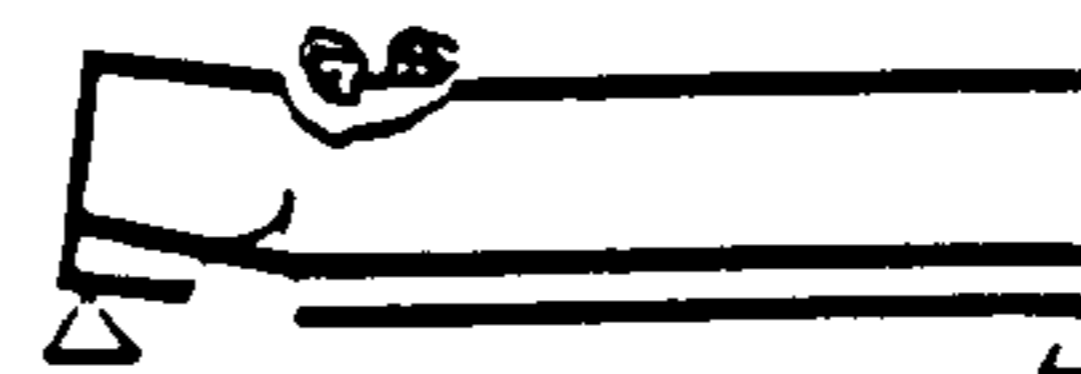
e) Excessive deflection



a) Flexural shear cracking of concrete



b) Anchorage failure of strands



c) Flexural shear compression failure of concrete



d) Web shear tension failure of concrete



e) Longitudinal web shear cracking of concrete or longitudinal shear cracking of concrete at strand level



f) Web shear compression failure of concrete

**Figure 3-1 Possible flexural failures**

**Figure 3-2 Possible shear failures**

(Girhammar 1992)

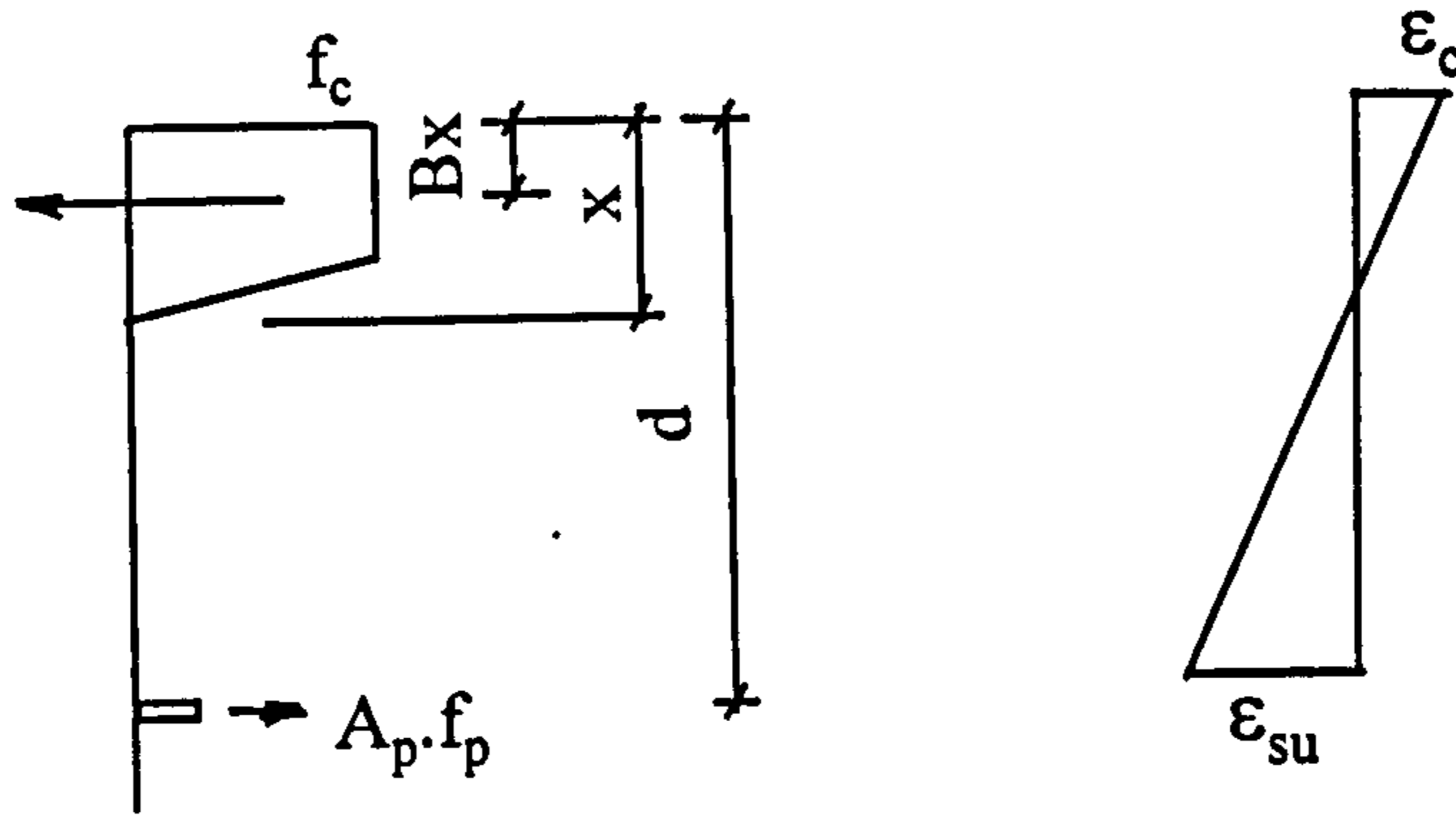


**Figure 3-3 Computation of ultimate flexural strength of prestressed hollow core slab**

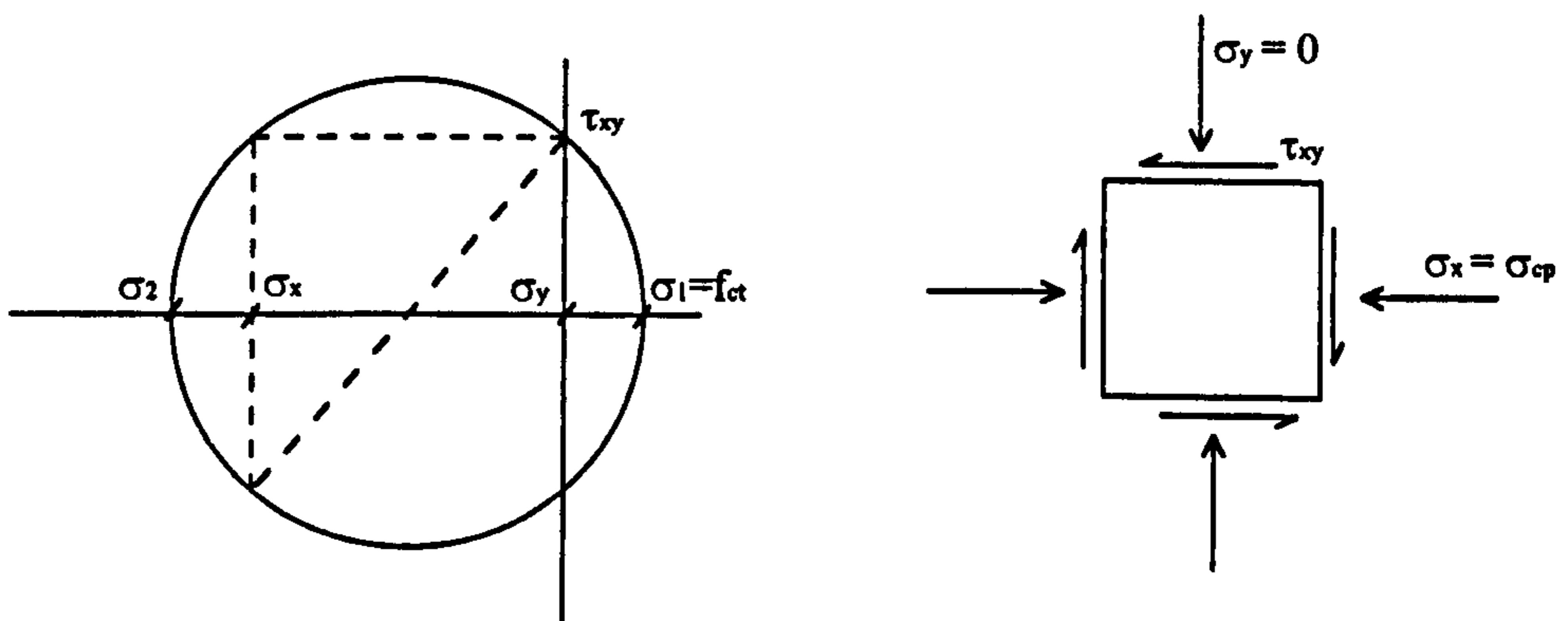


**Figure 3-4 Mohr's circle for shear in prestressed concrete**

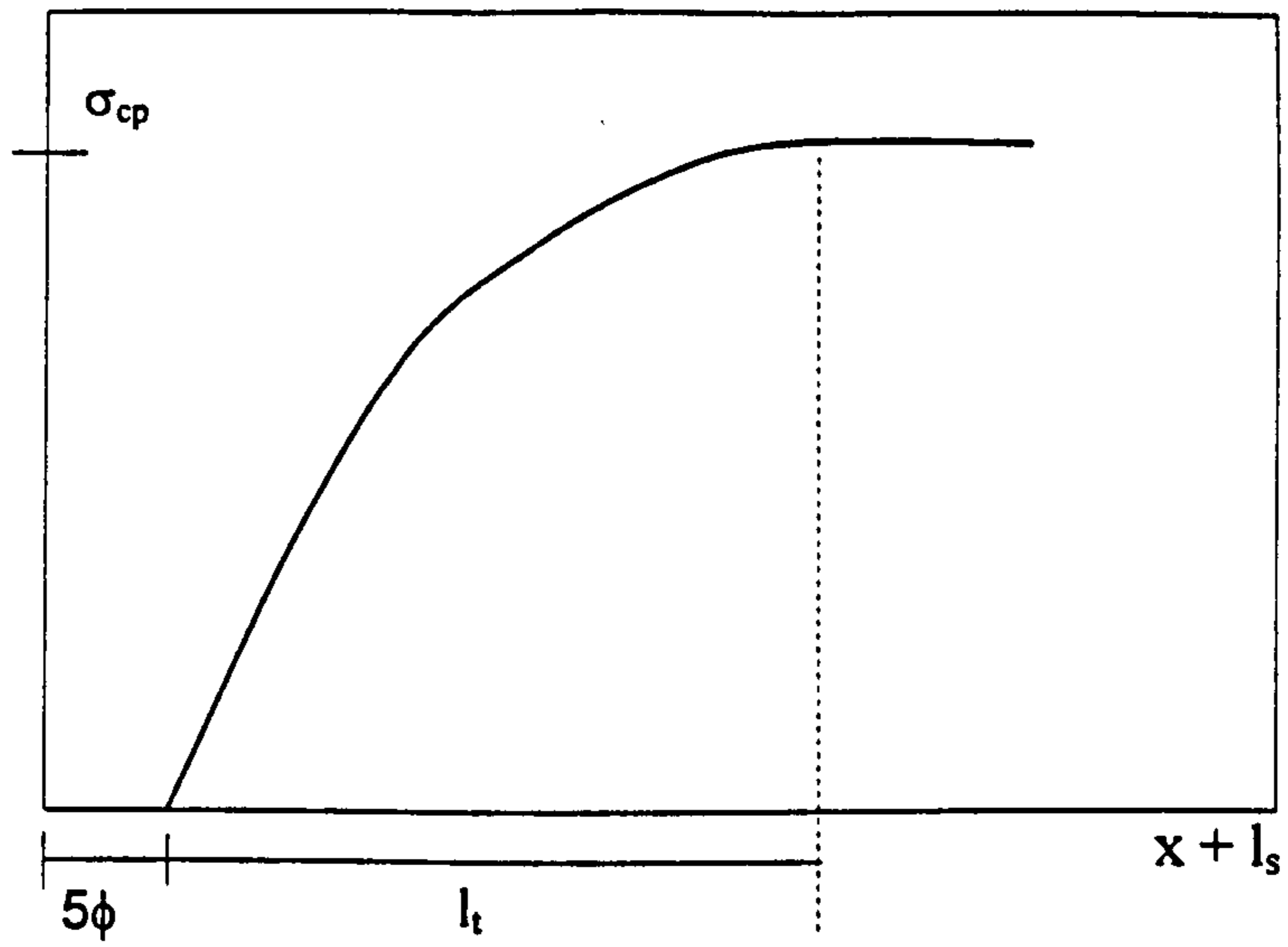


Figure 3-5 Parabolic distribution of prestress transfer (Lin Yang 1995)

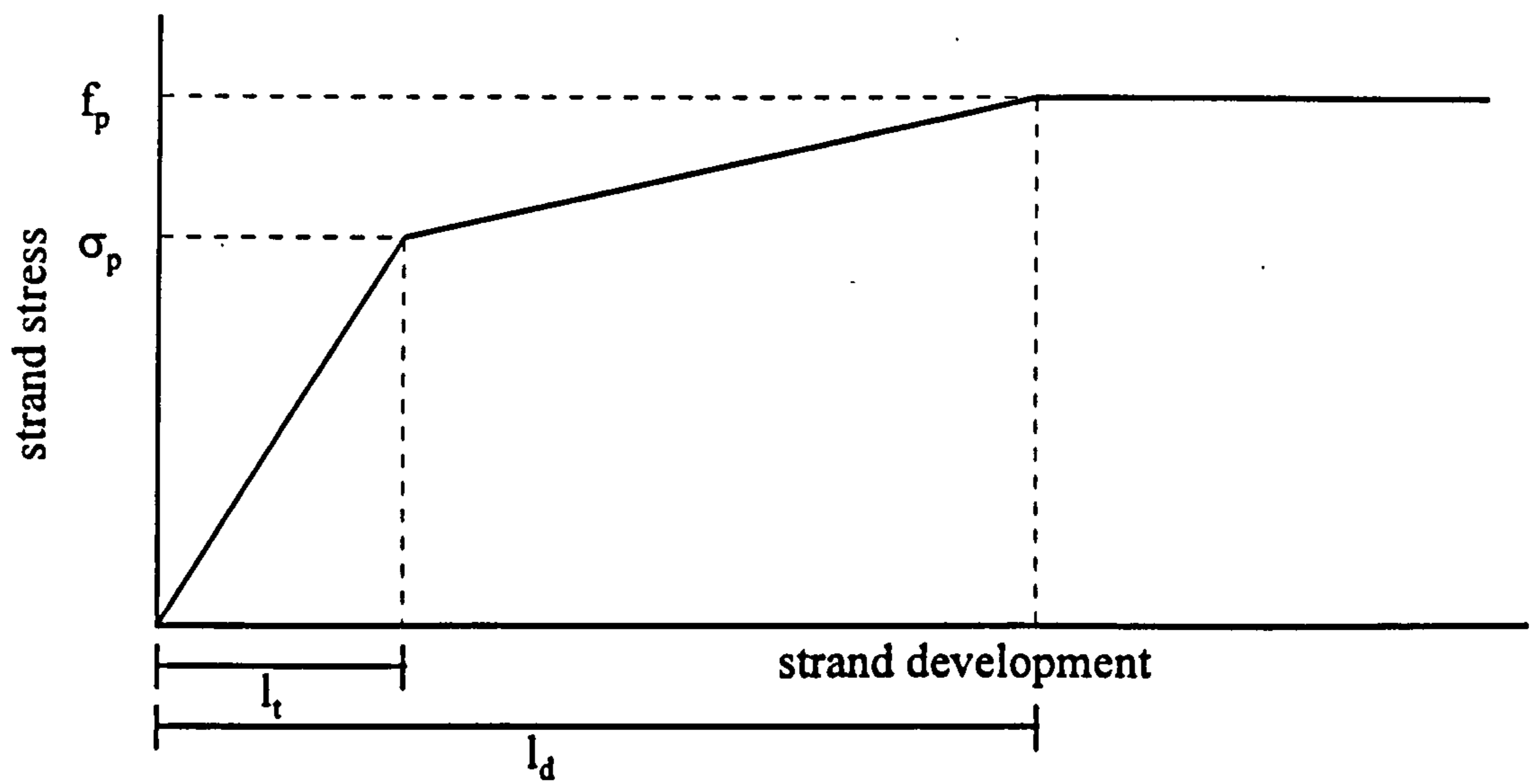


Figure 3-6 Critical transfer-development envelope according to ACI-318

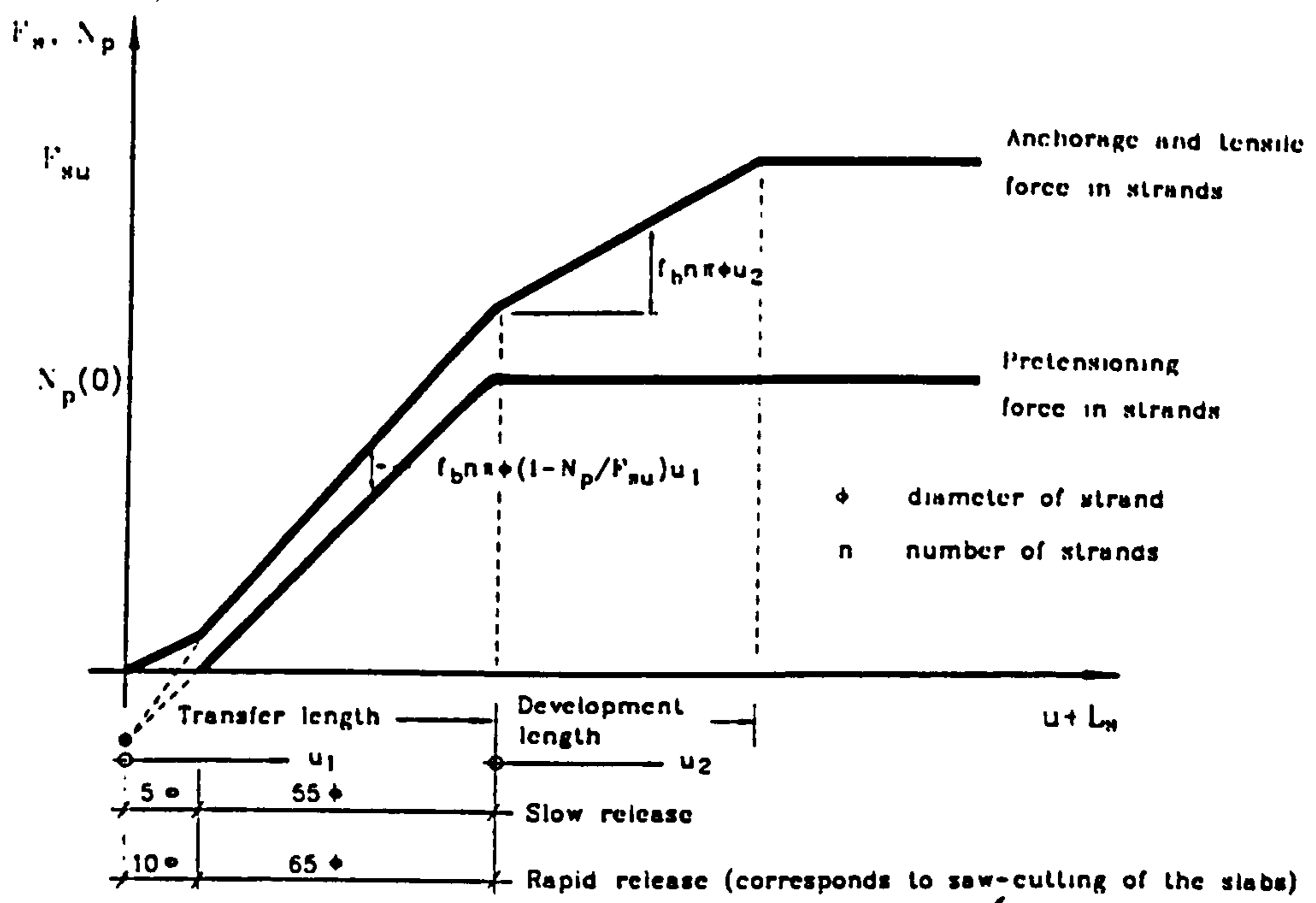


Figure 3-7 Development of anchorage and pretensioning force (Girhammar 1992)

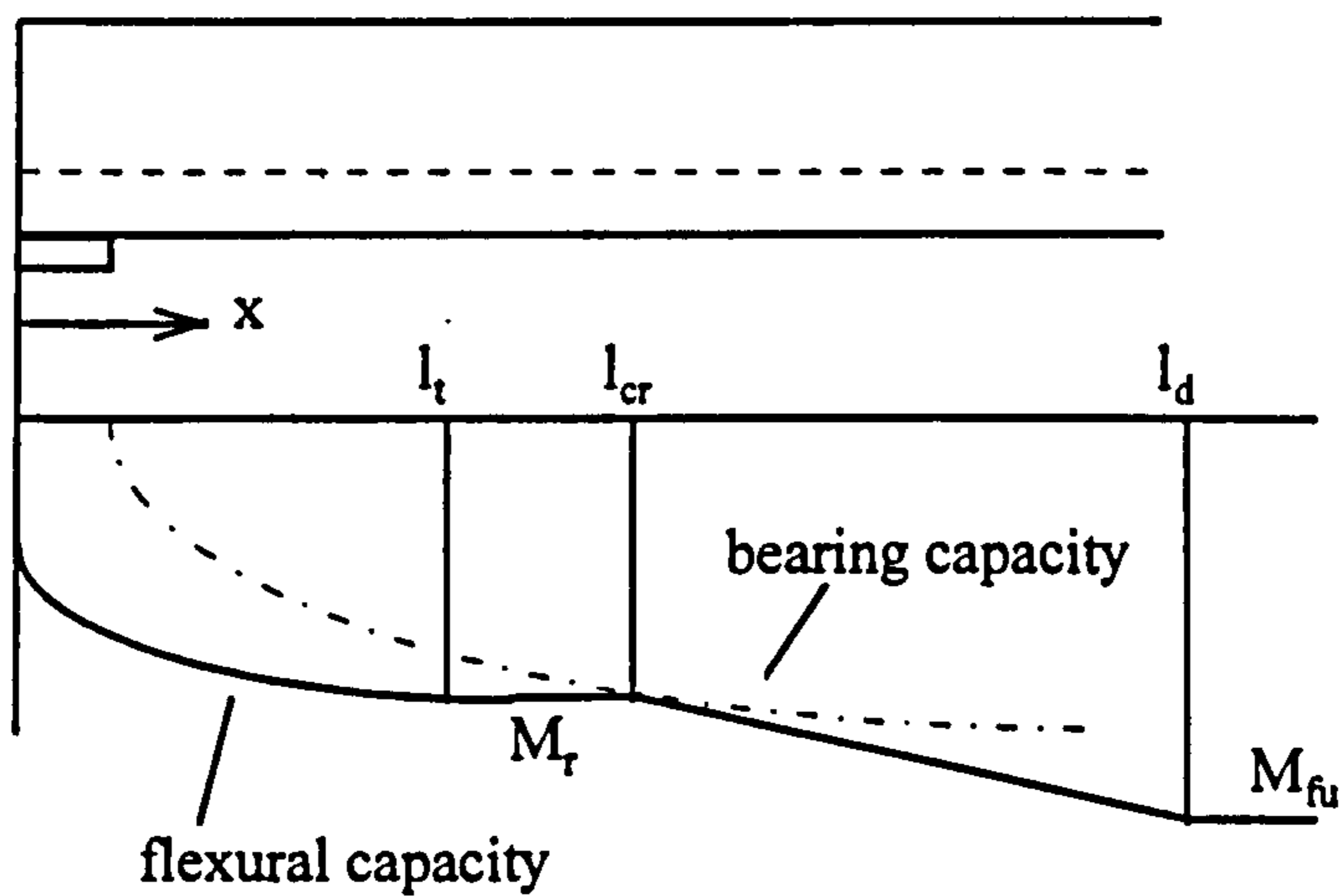
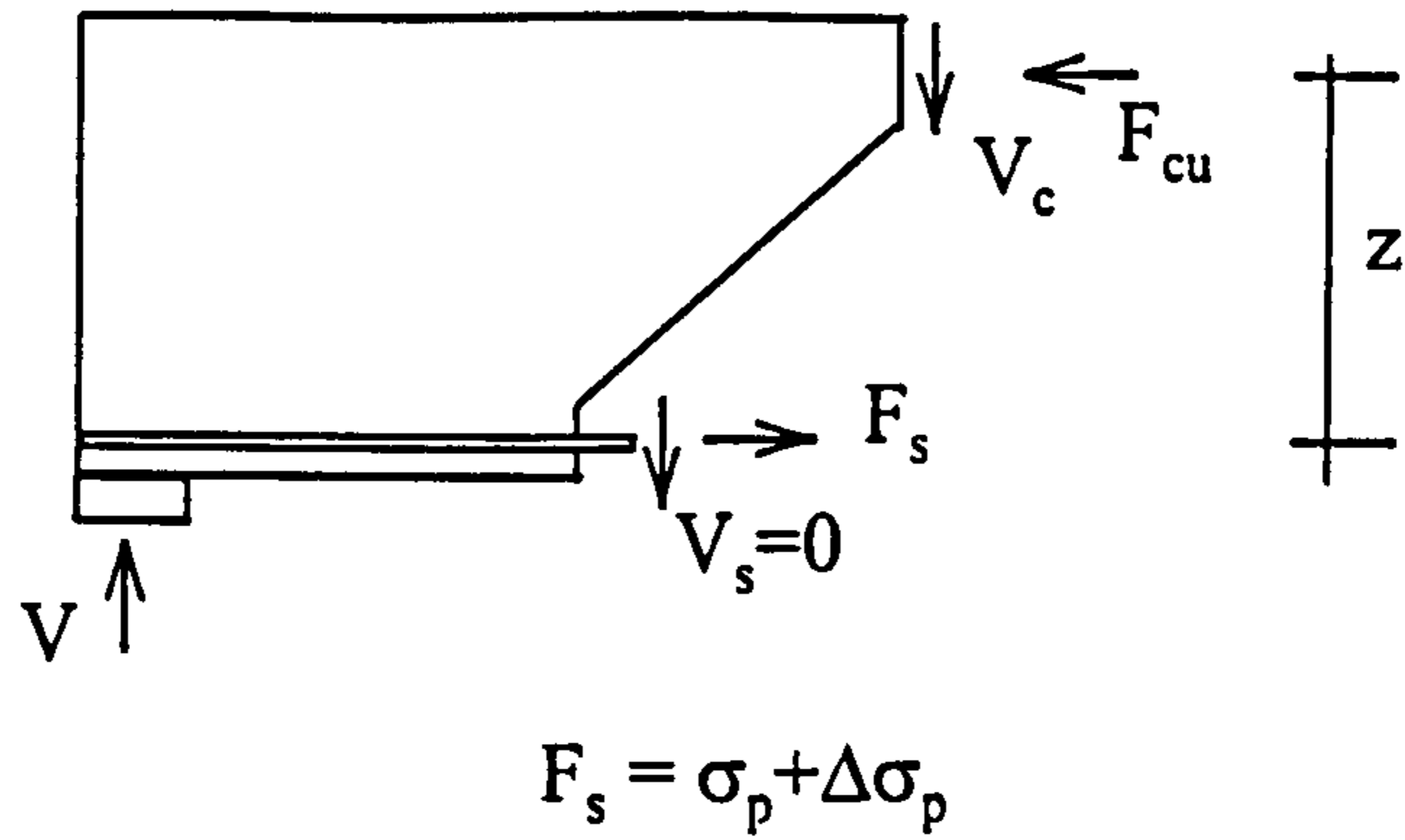
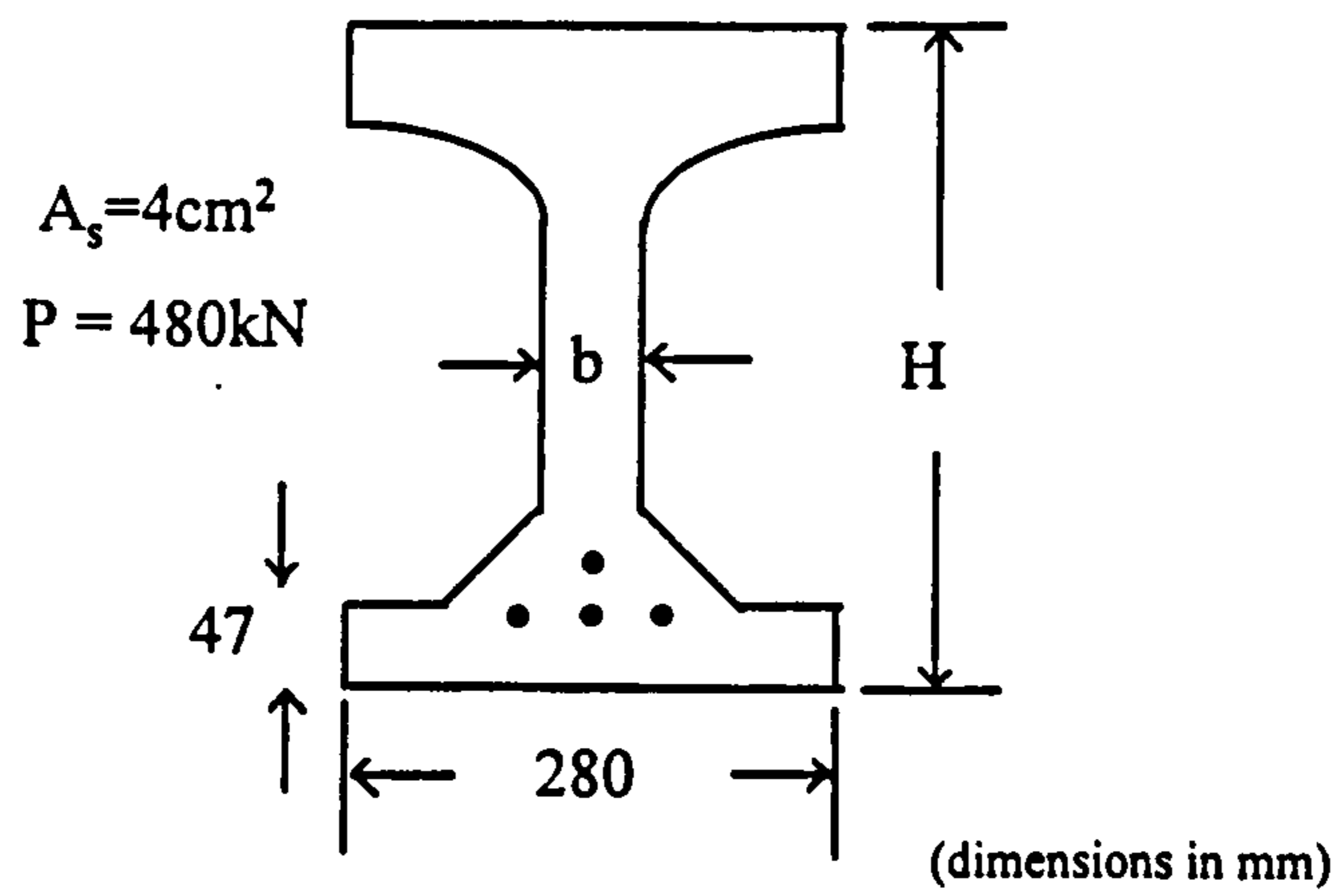


Figure 3-8 Flexural cracking and anchorage capacity along development length



**Figure 3-9 Free body diagram for anchorage failure**



**Figure 3-10 Geometry of FRC hollow core slabs used by Bernander (1986)**

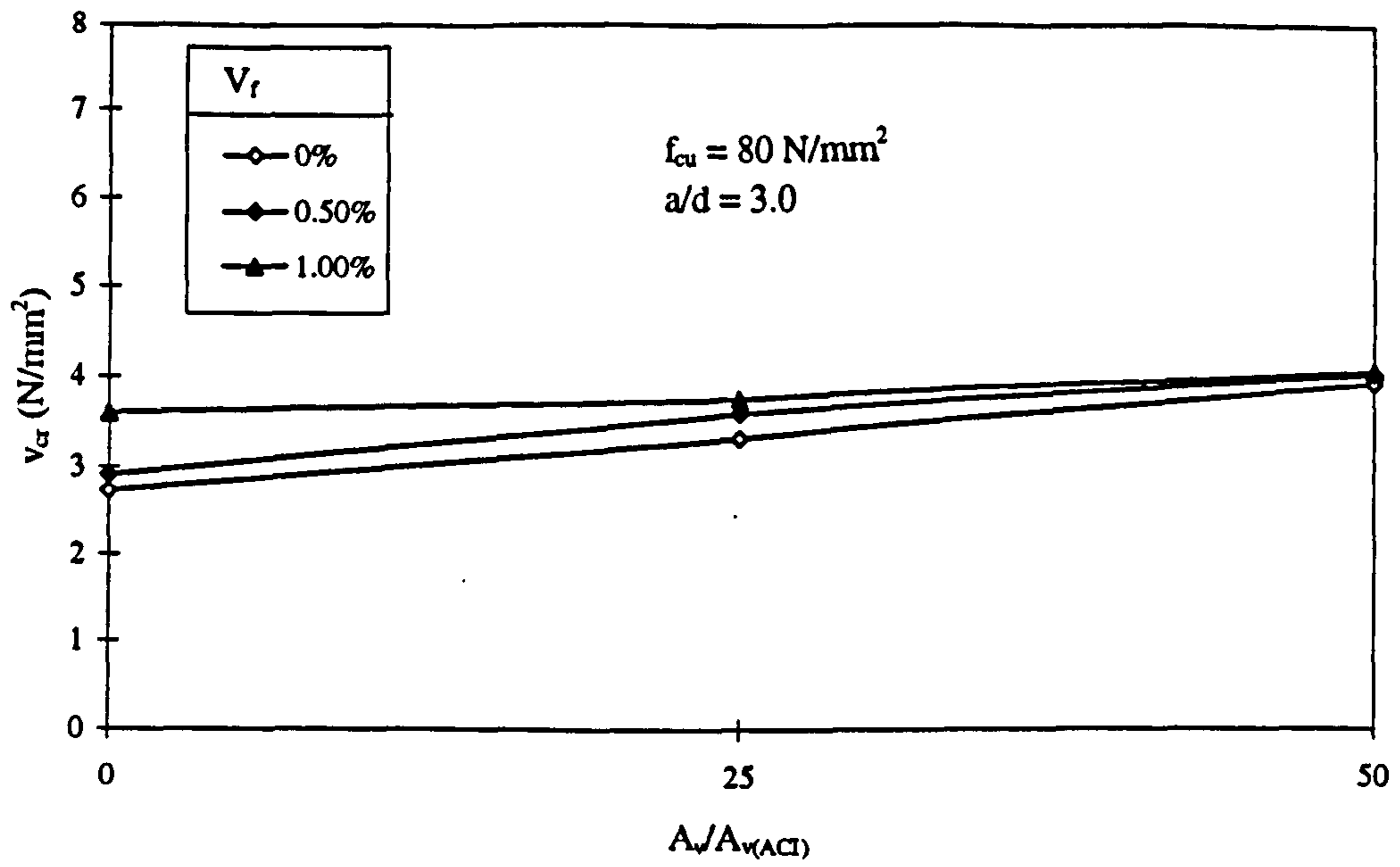


Figure 3-11 Cracking shear strength v  $A_v/A_{v(ACI)}$  (Shin *et al.* 1994)

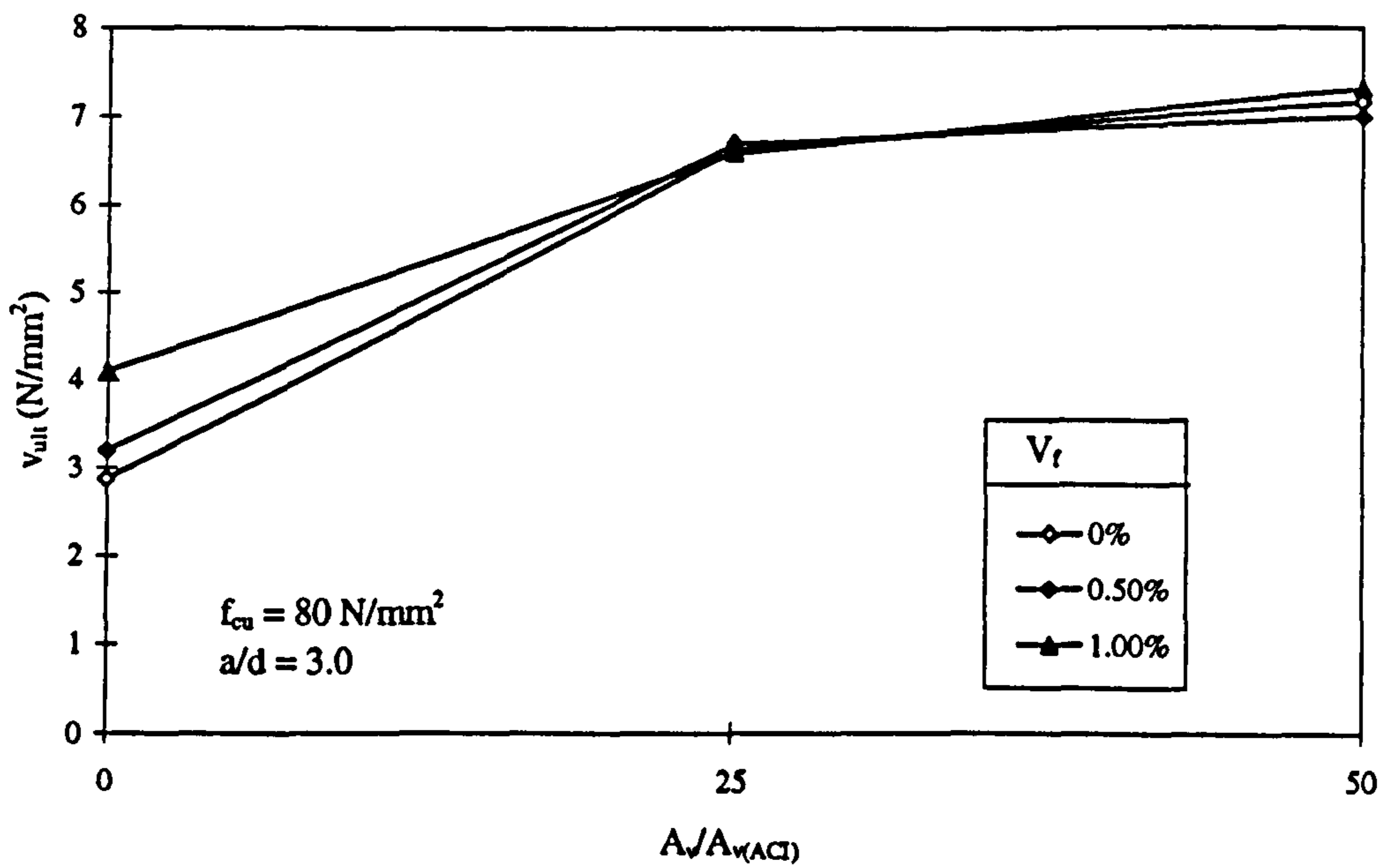


Figure 3-12 Ultimate shear strength v  $A_v/A_{v(ACI)}$  (Shin *et al.* 1994)

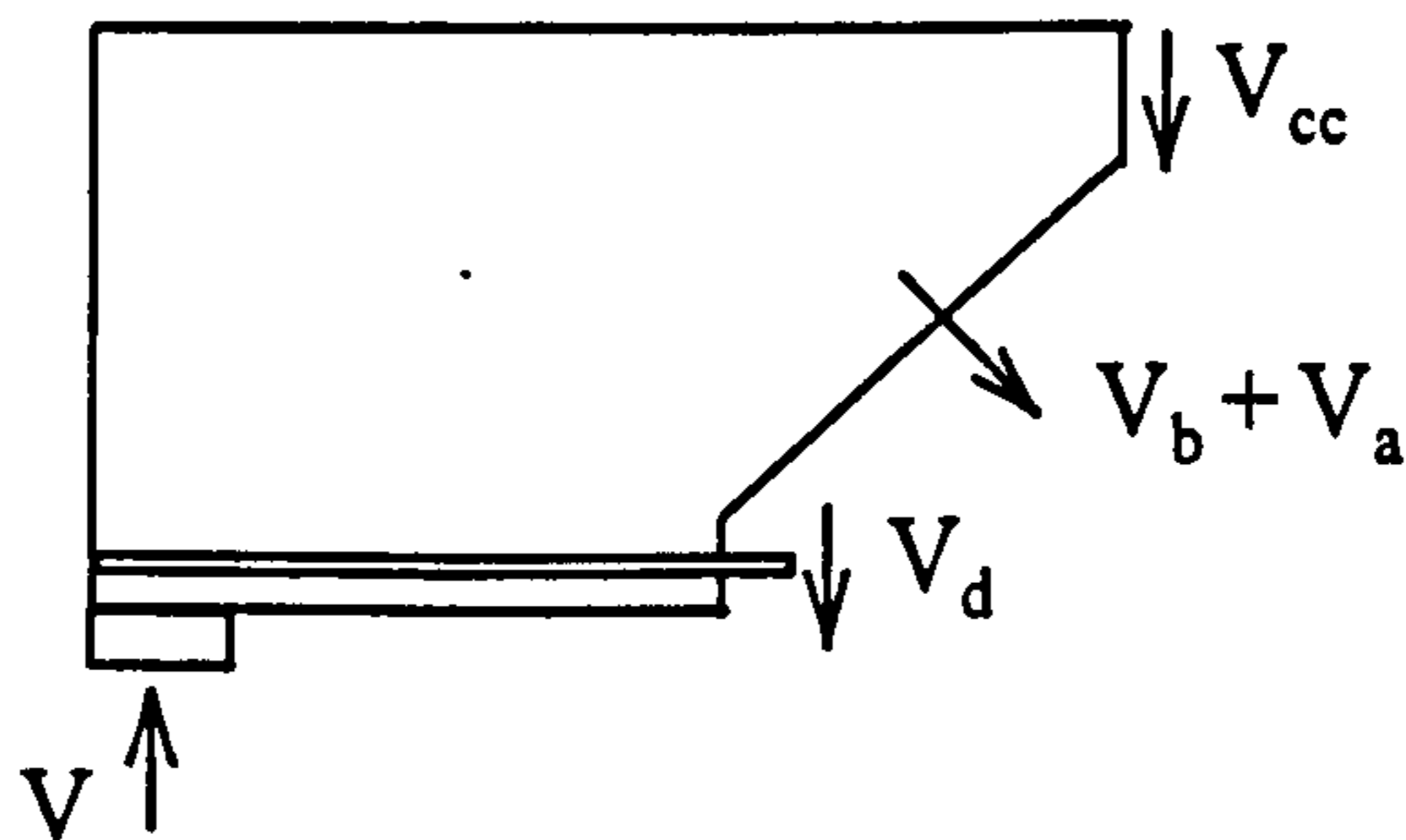


Figure 3-13 Shear forces and reactions

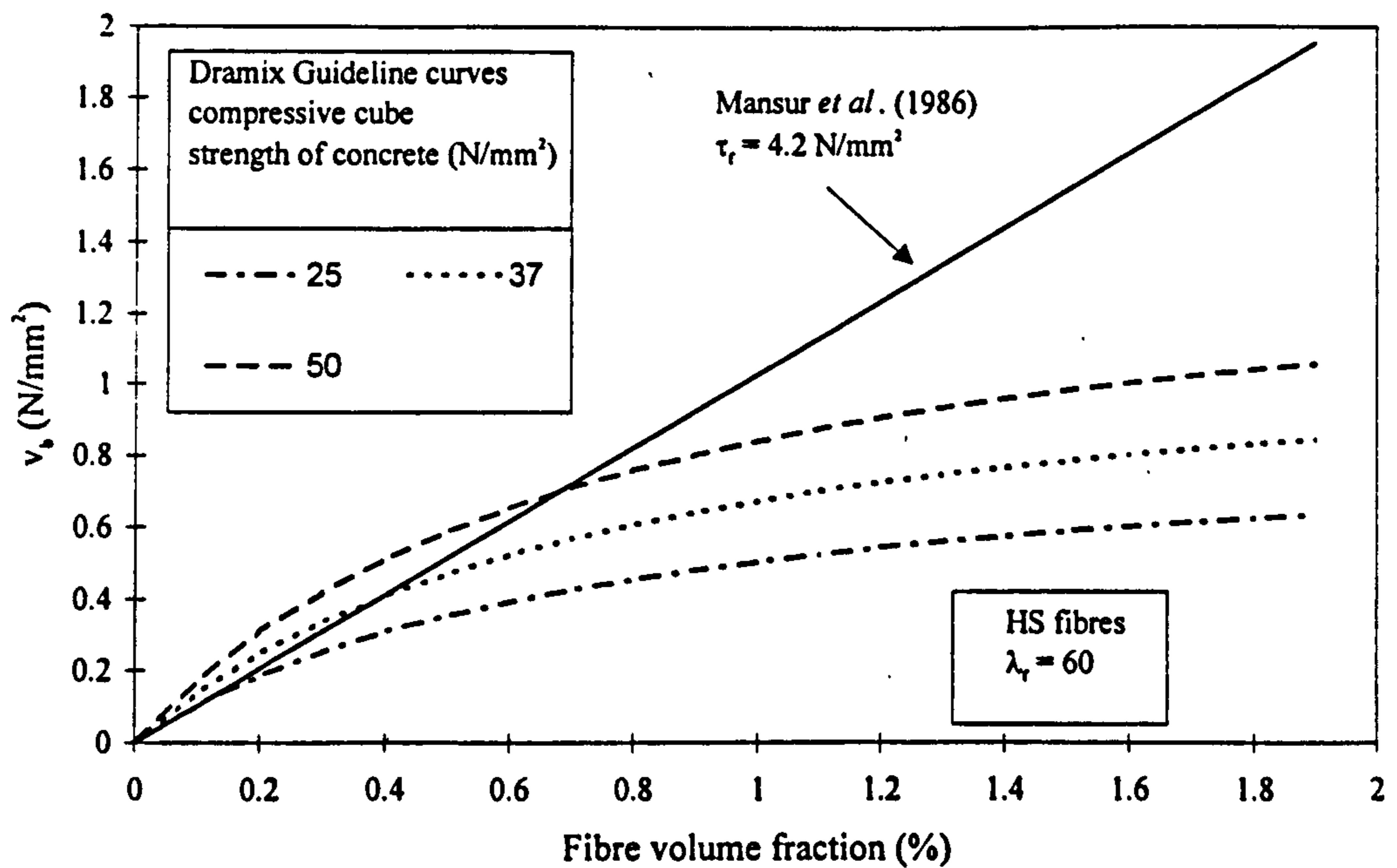


Figure 3-14 Comparison of the equations of Mansur *et al.* (1986) and Dramix Guidelines (1995) for the shear resistance supplement due to adding steel fibres

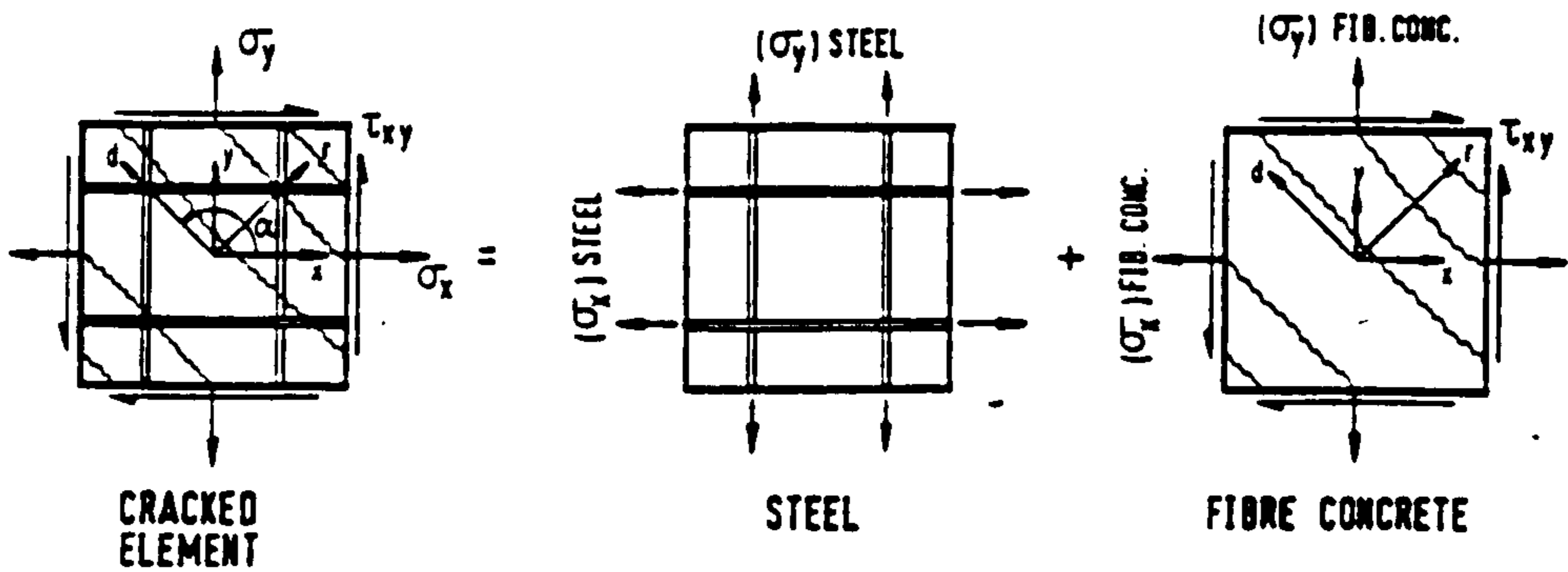


Figure 3-15 State of stress in an element cracked in shear (Tan *et al.* 1995)

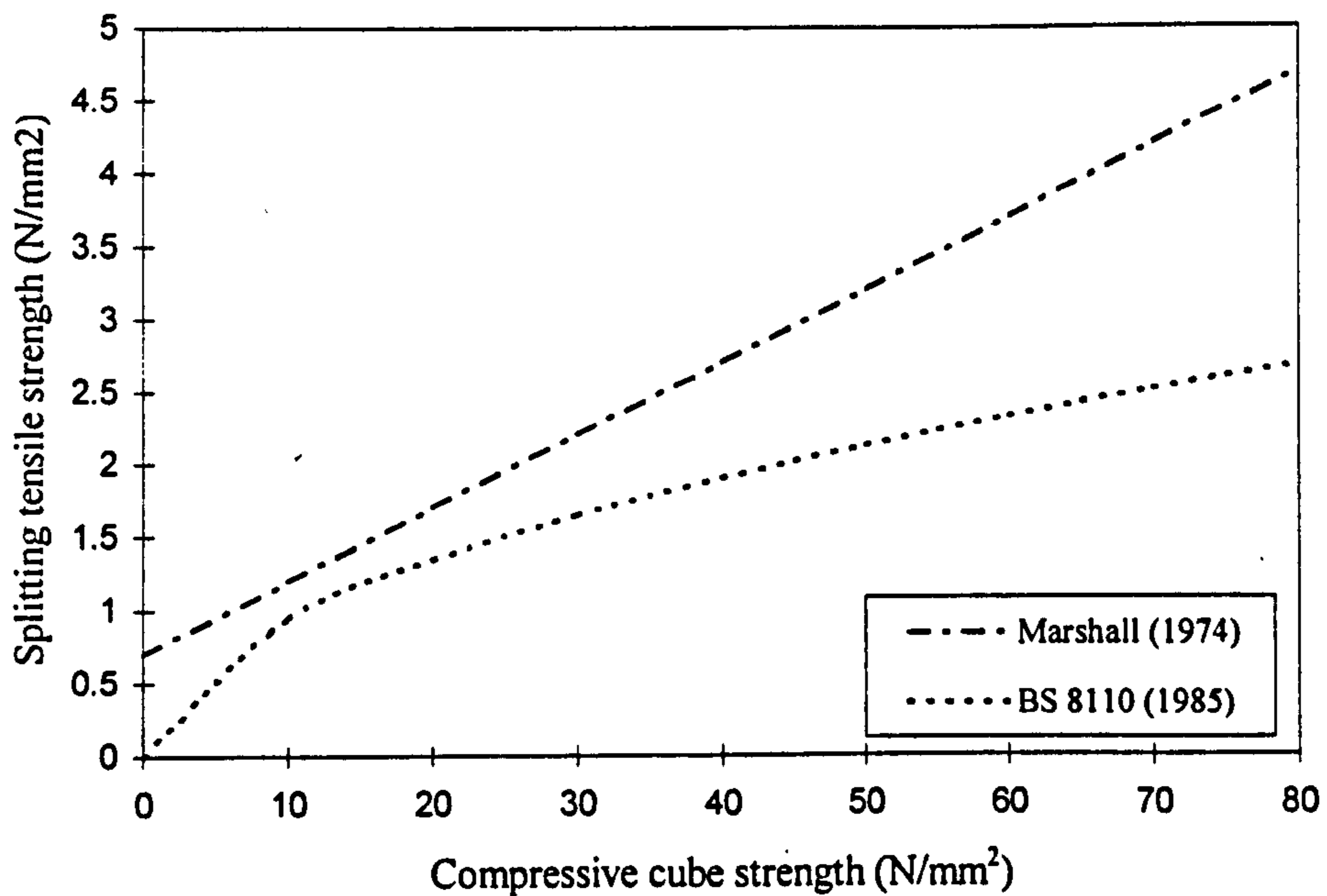


Figure 3-16 Comparison of BS 8110 (1985) and Marshall (1974) equations for predicting splitting tensile strength of plain concrete from compressive cube strengths



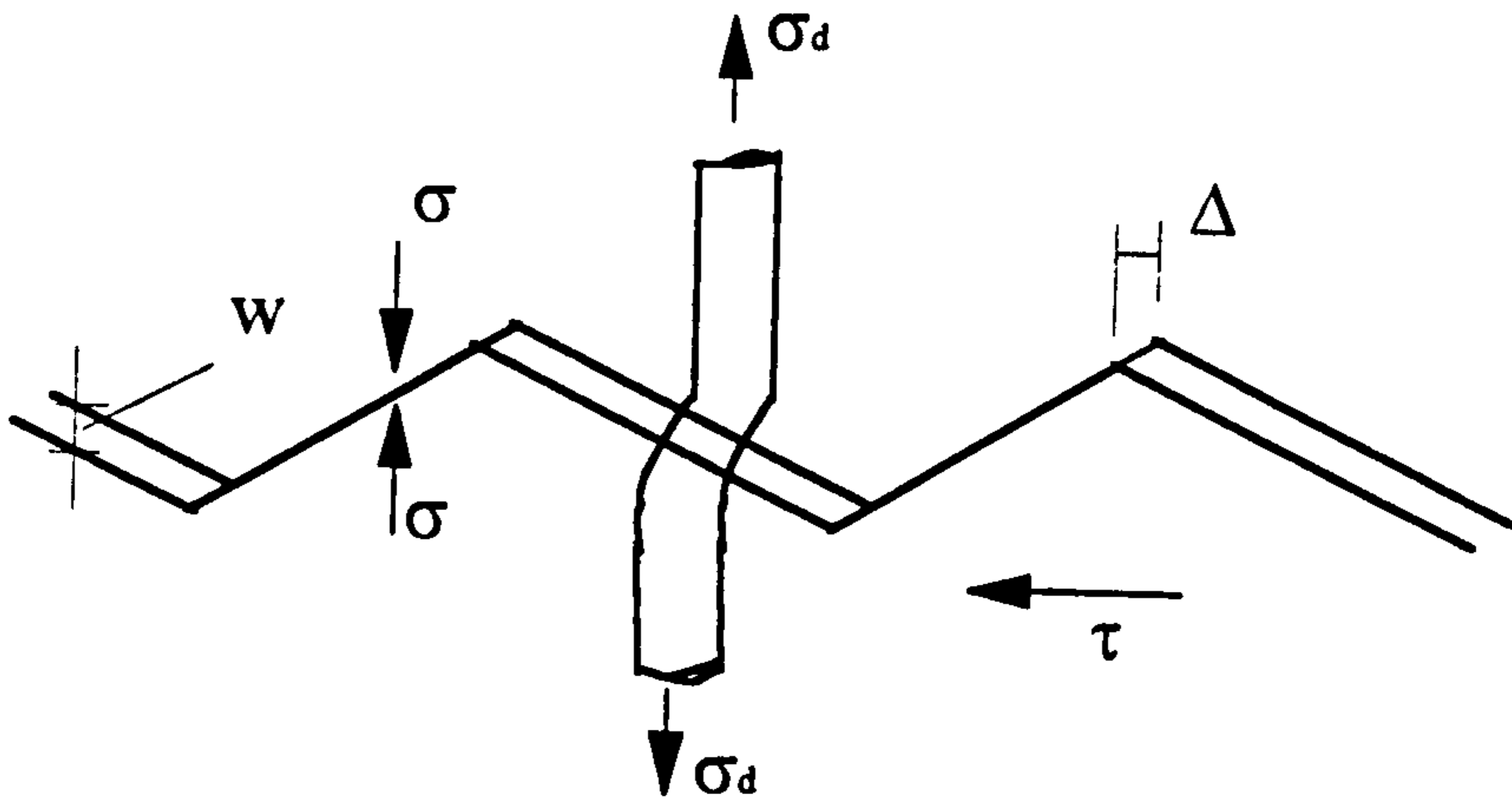


Figure 3-17 Localised crack opening (dilatancy) associated with shear displacement

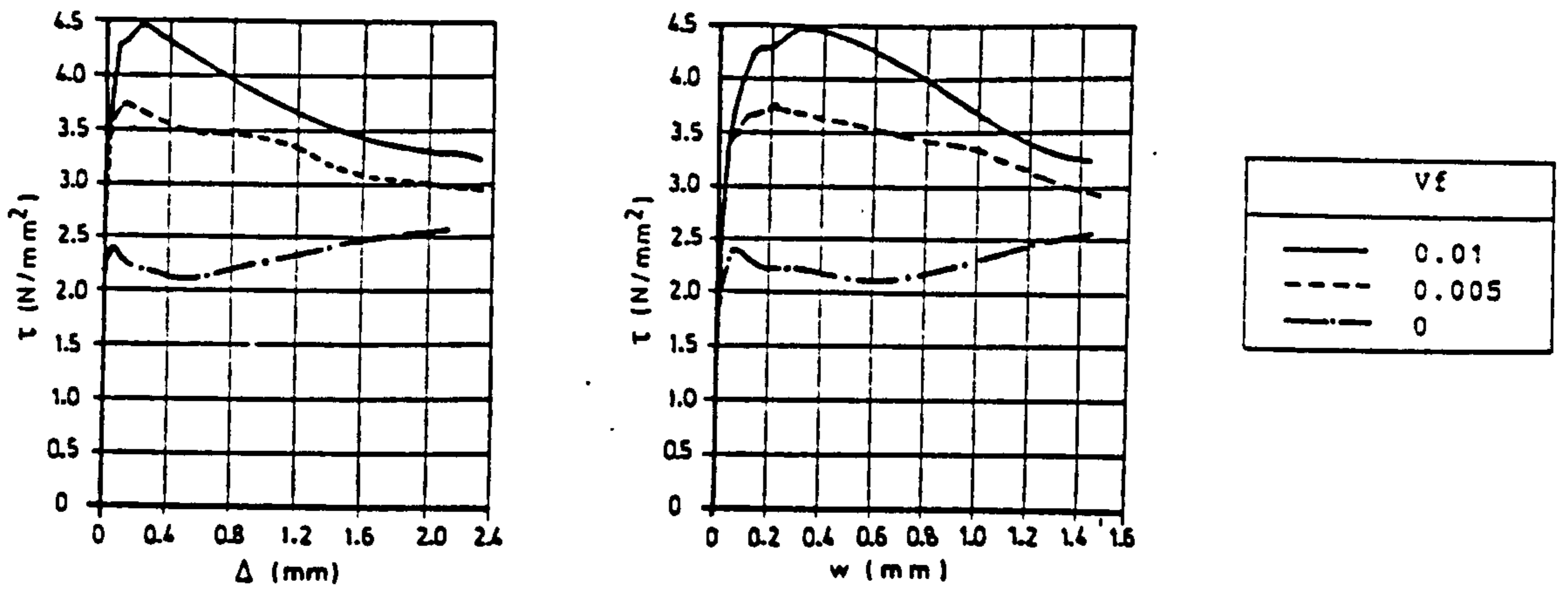


Figure 3-18 Shear stress as a function of shear displacement and crack opening for three specimens at different fibre volume fractions (Van de Loock 1987)

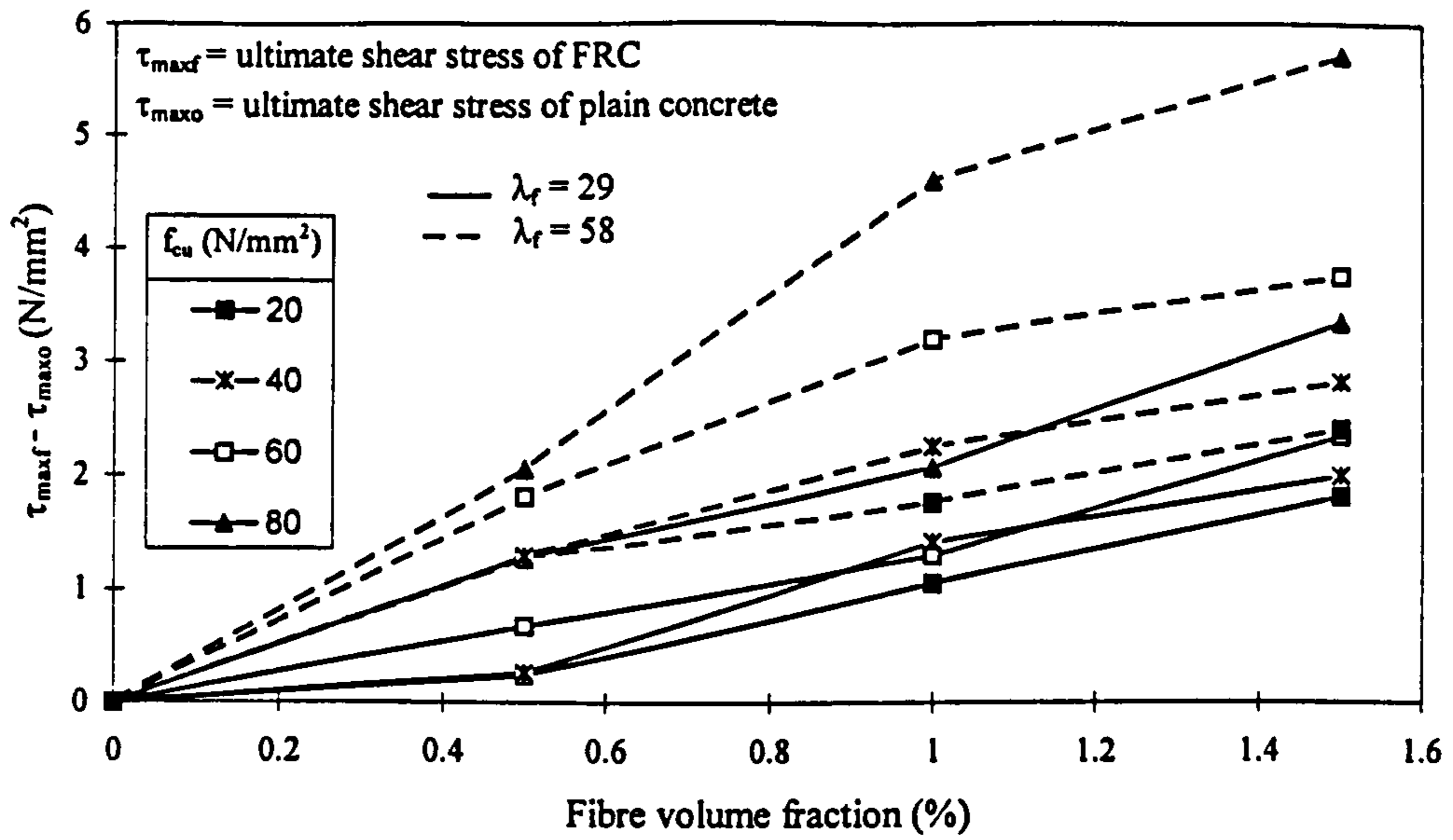


Figure 3-19 Schematic representation of increase in shear strength due to concrete strength for various fibre volume fraction and fibre aspect ratio (Khaloo and Kim 1997)

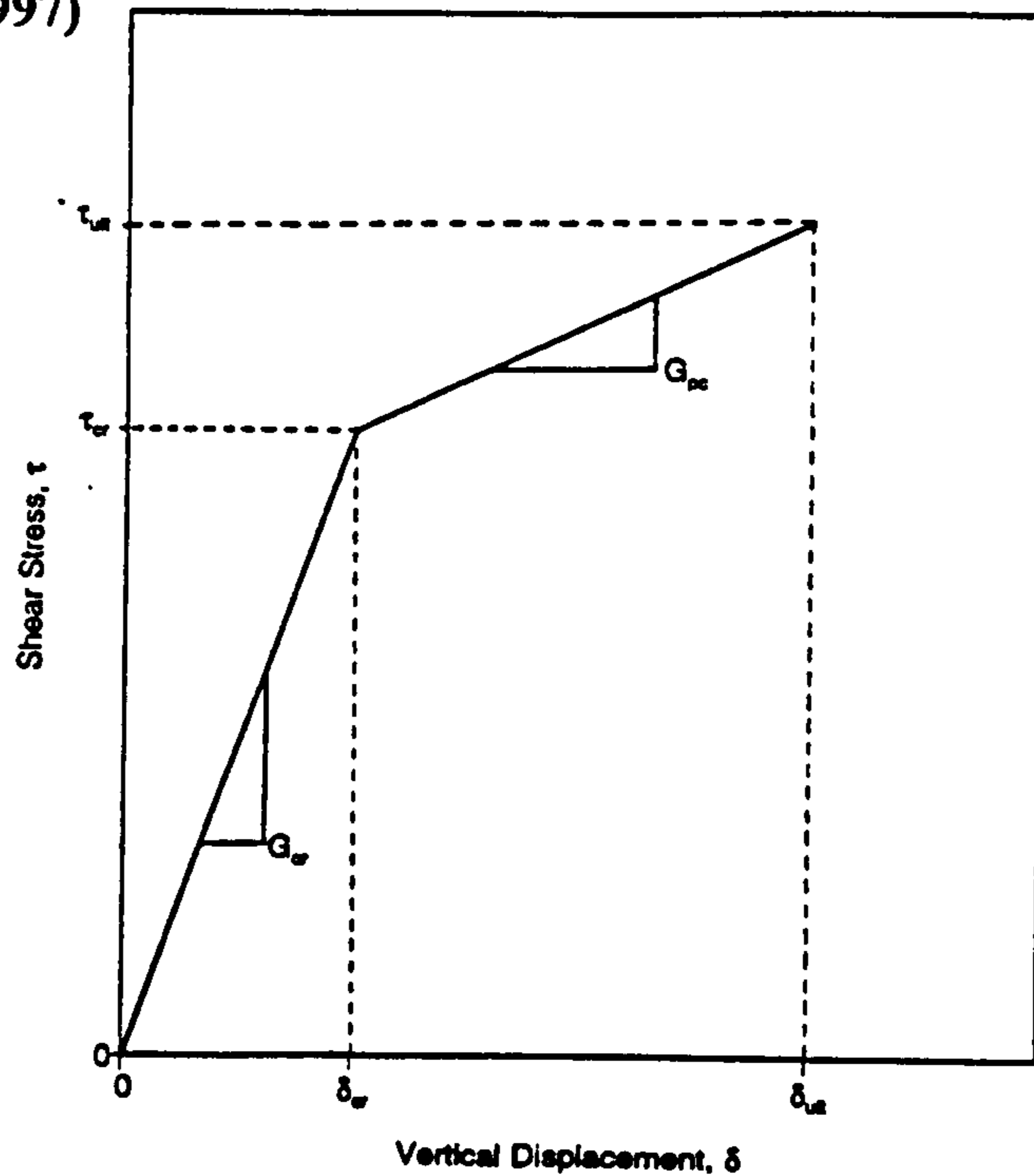


Figure 3-20 Idealised shear stress - shear displacement curve for FRC (Khaloo and Kim 1997)

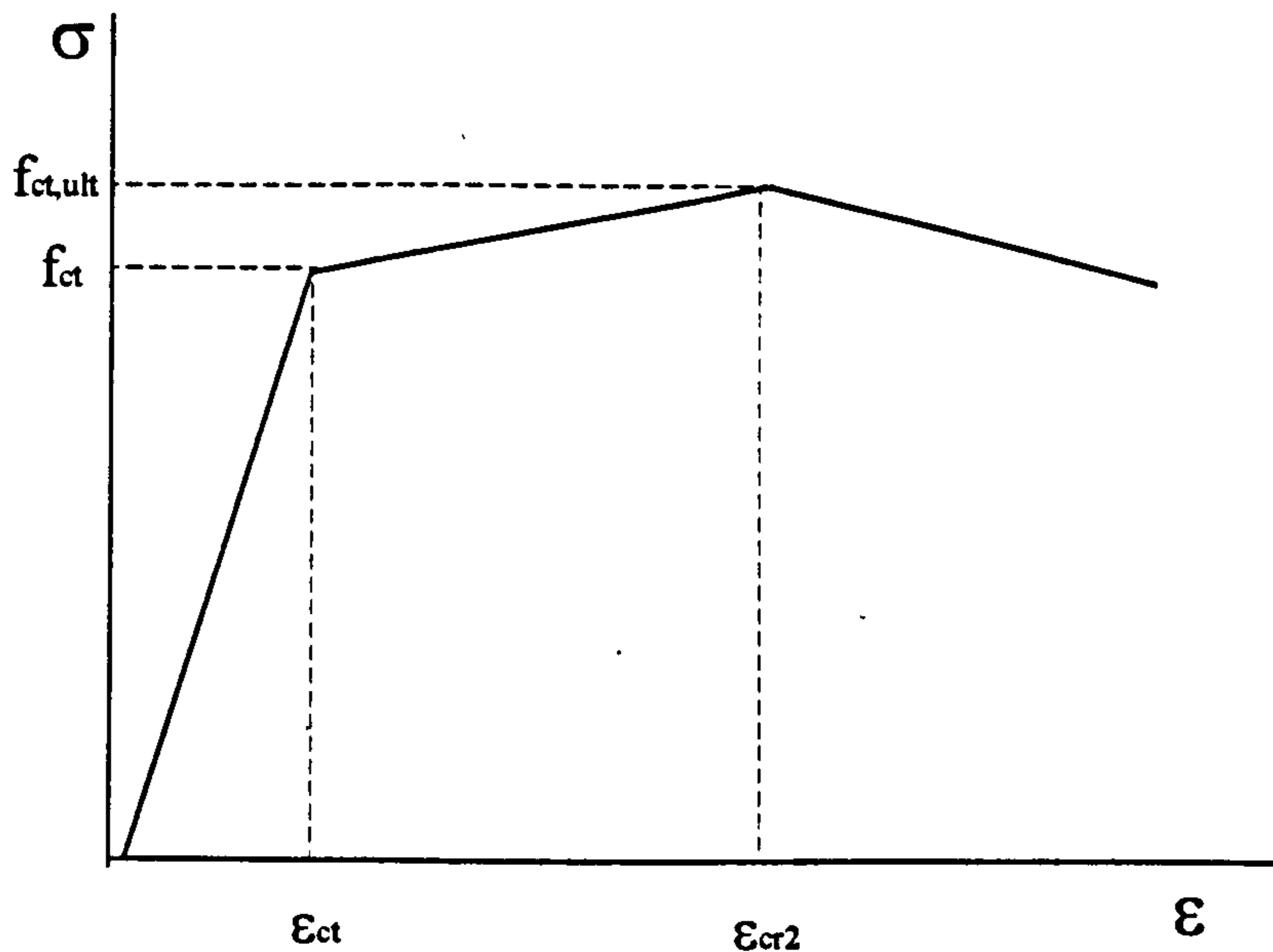


Figure 3-21 Idealised tensile stress - strain curve for FRC assumed by Valle and Buyukozturk (1994)

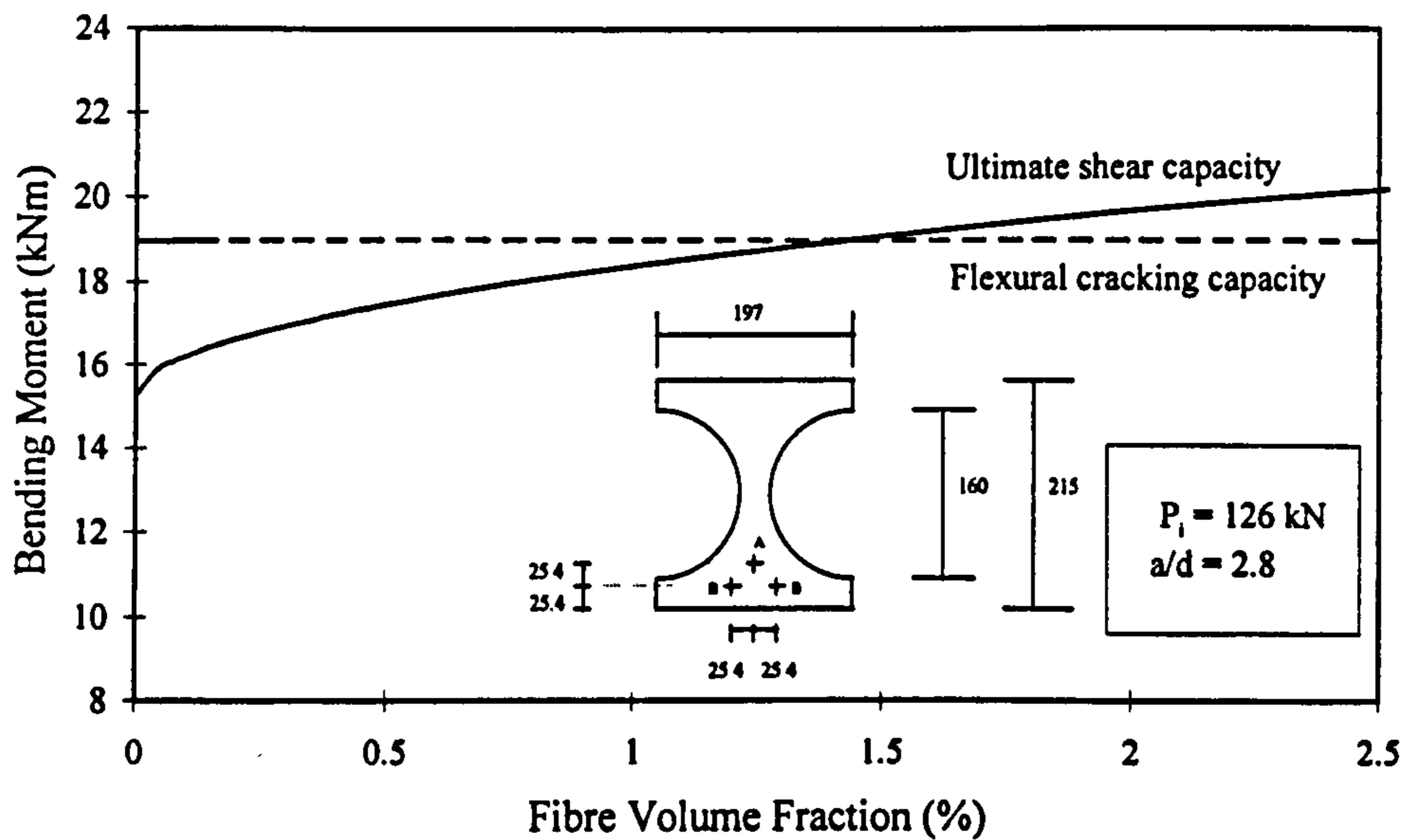


Figure 3-22 Effect of fibre volume fraction on flexural strength and cracking shear strength of a x-beam

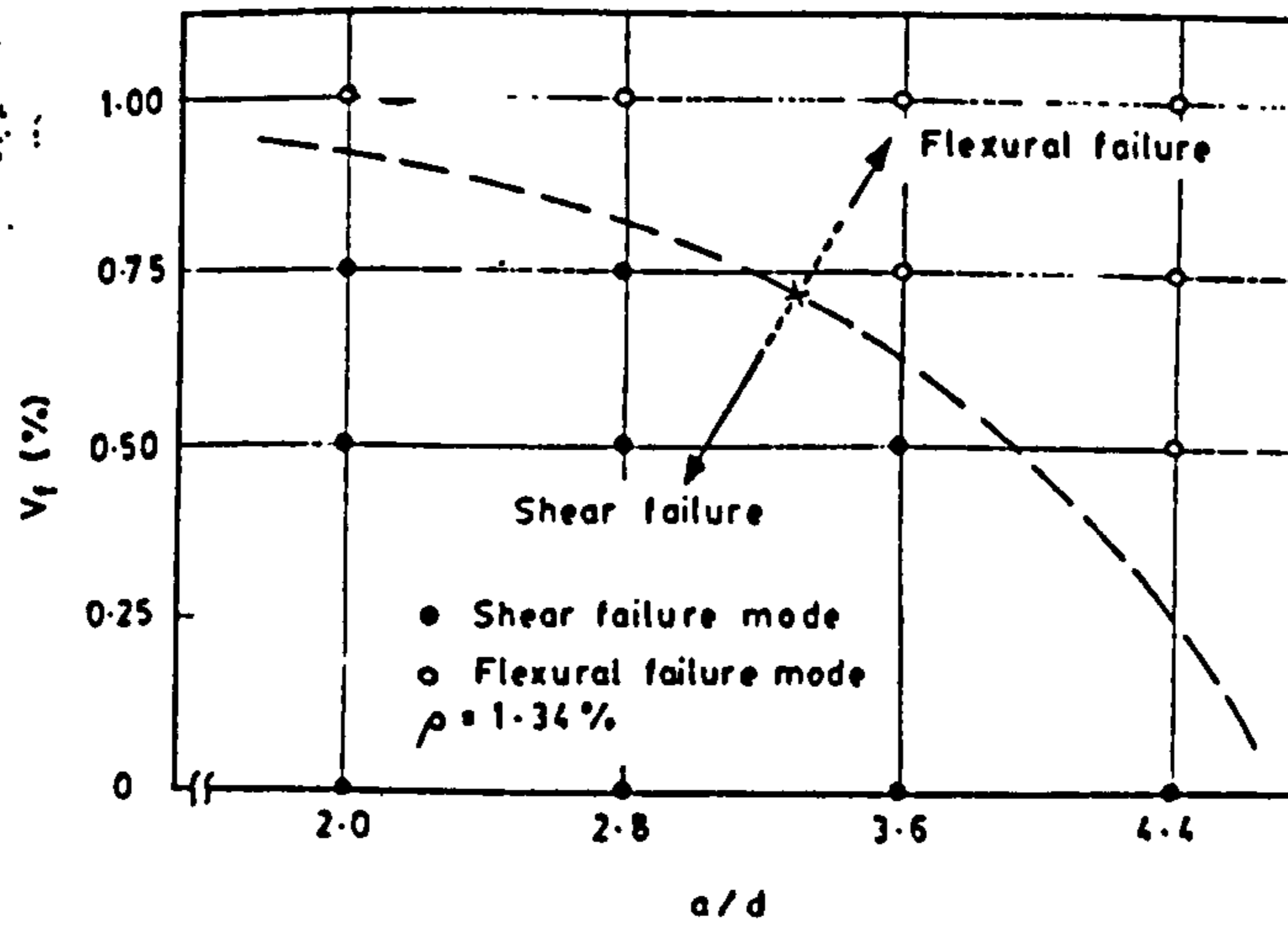


Figure 3-23 Observed failure modes for RFRC beams (Mansur *et al.* 1986)

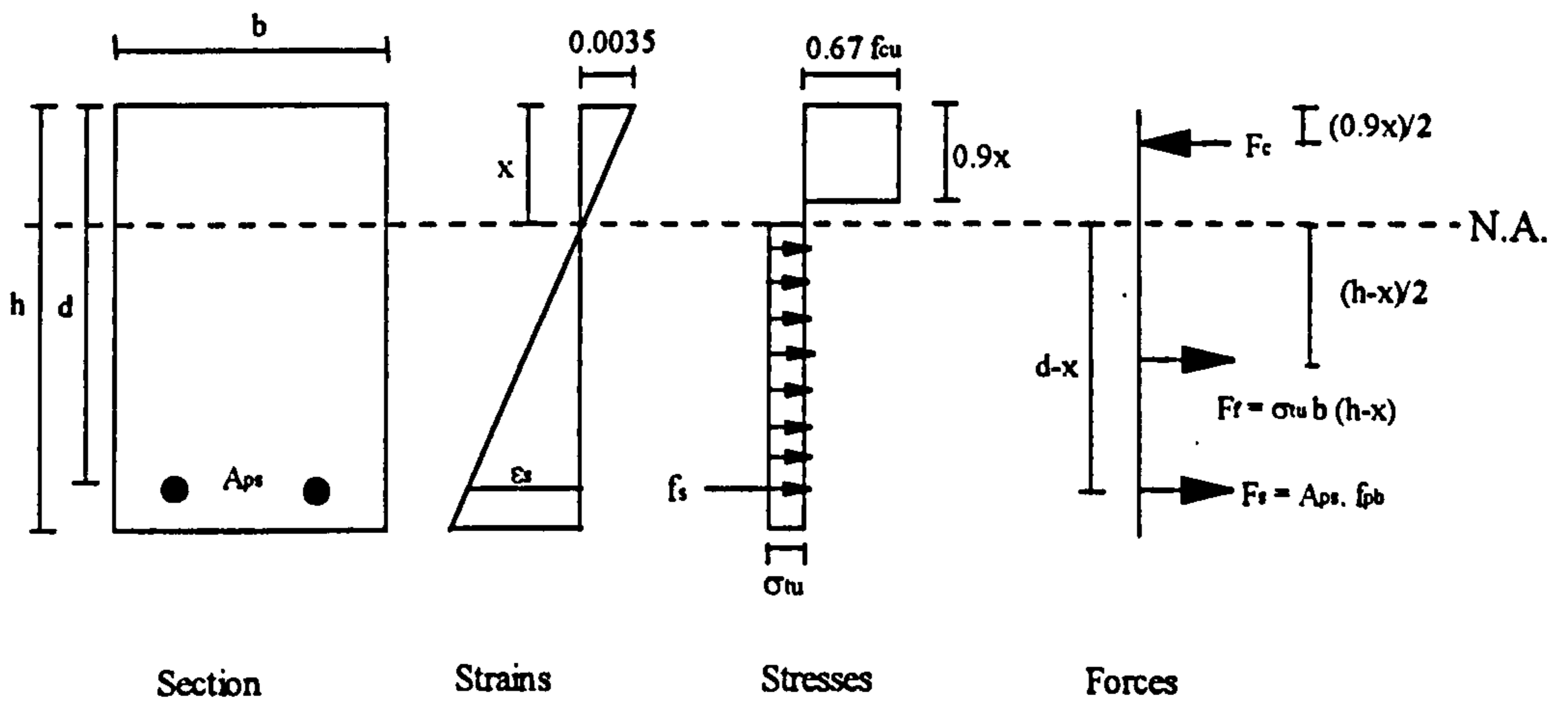
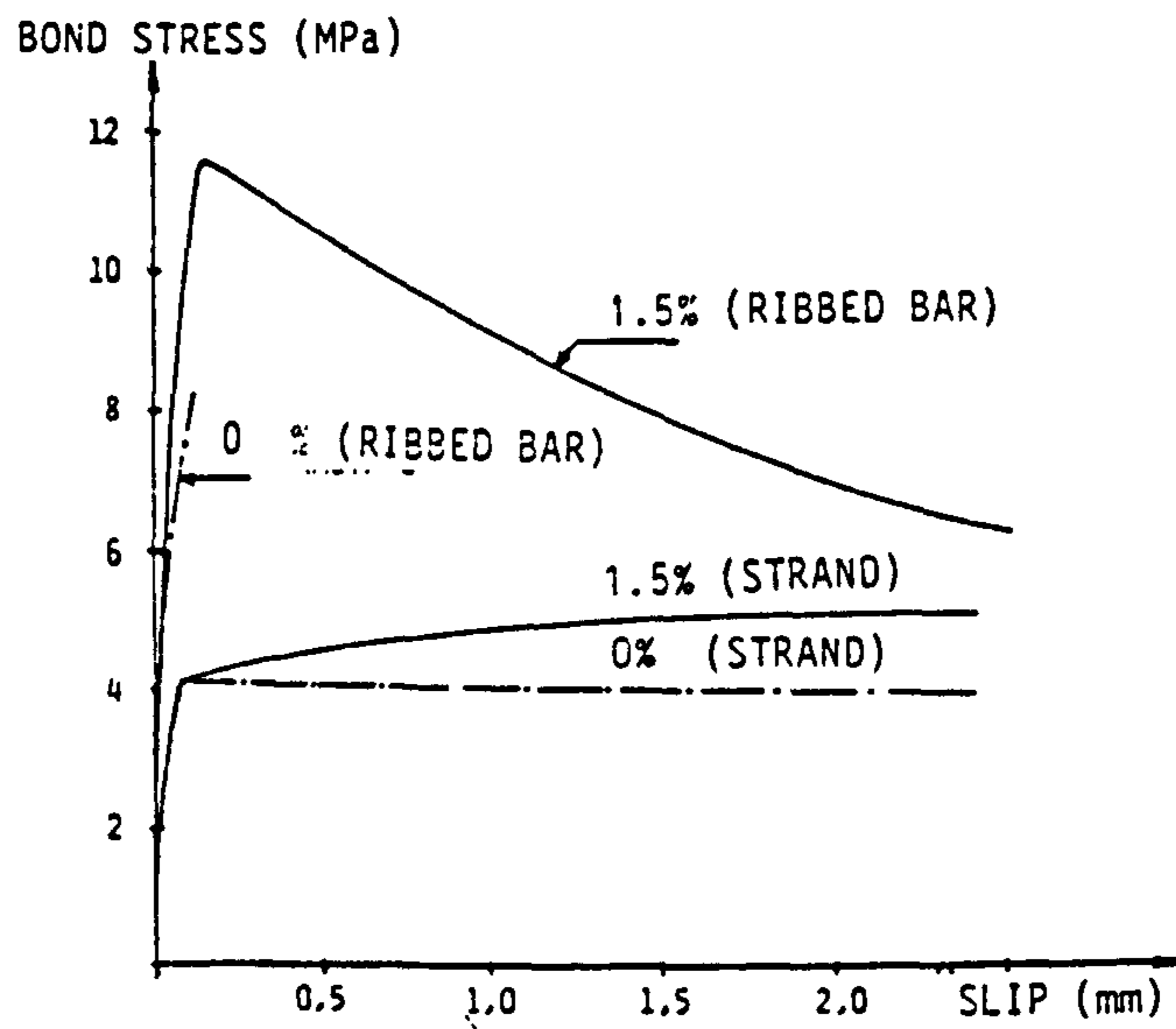


Figure 3-24 Stress and strain blocks for a RFRC beam in flexure



**Figure 3-25 Bond stress v slip for reinforcement bar and prestressing strand (Lorentsen 1985)**

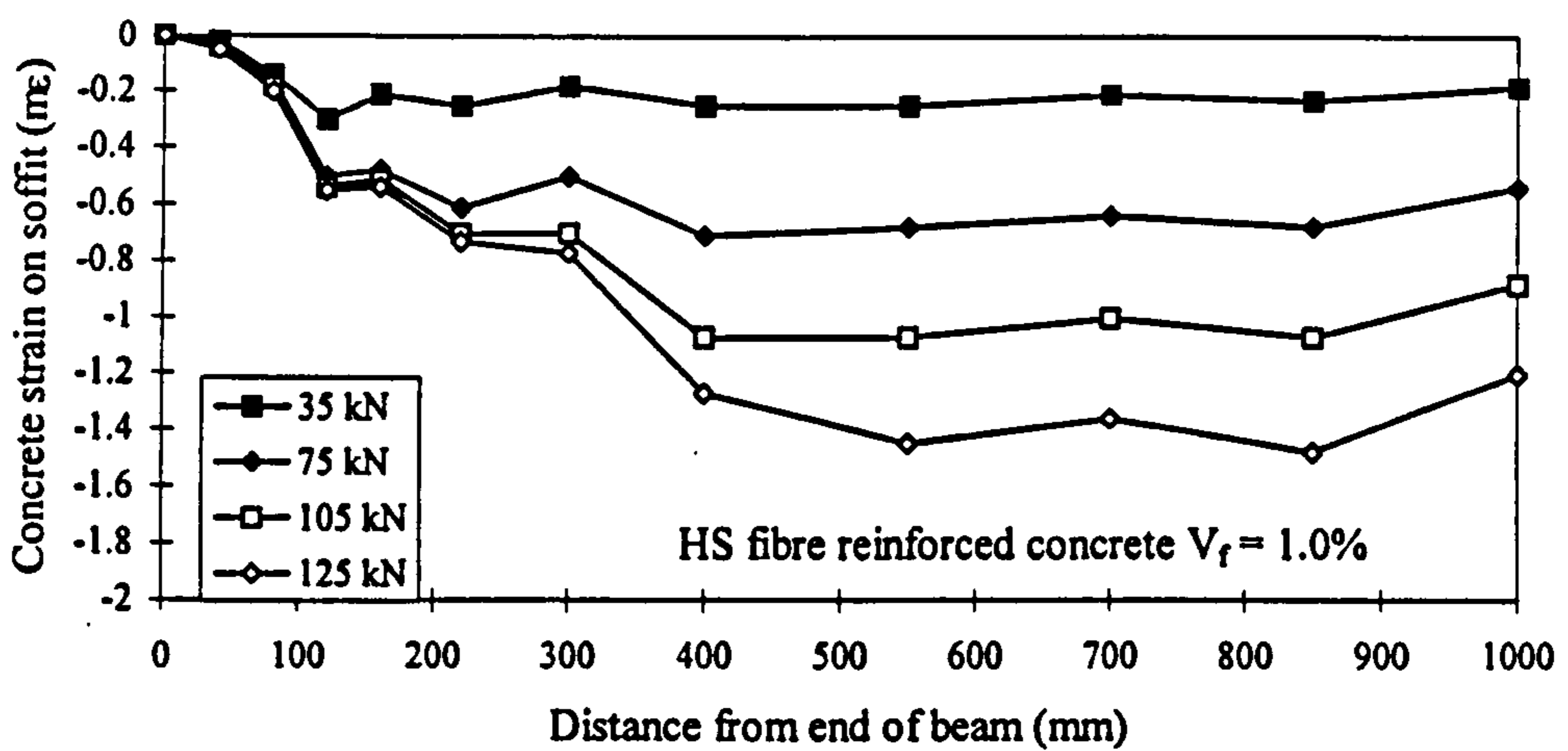
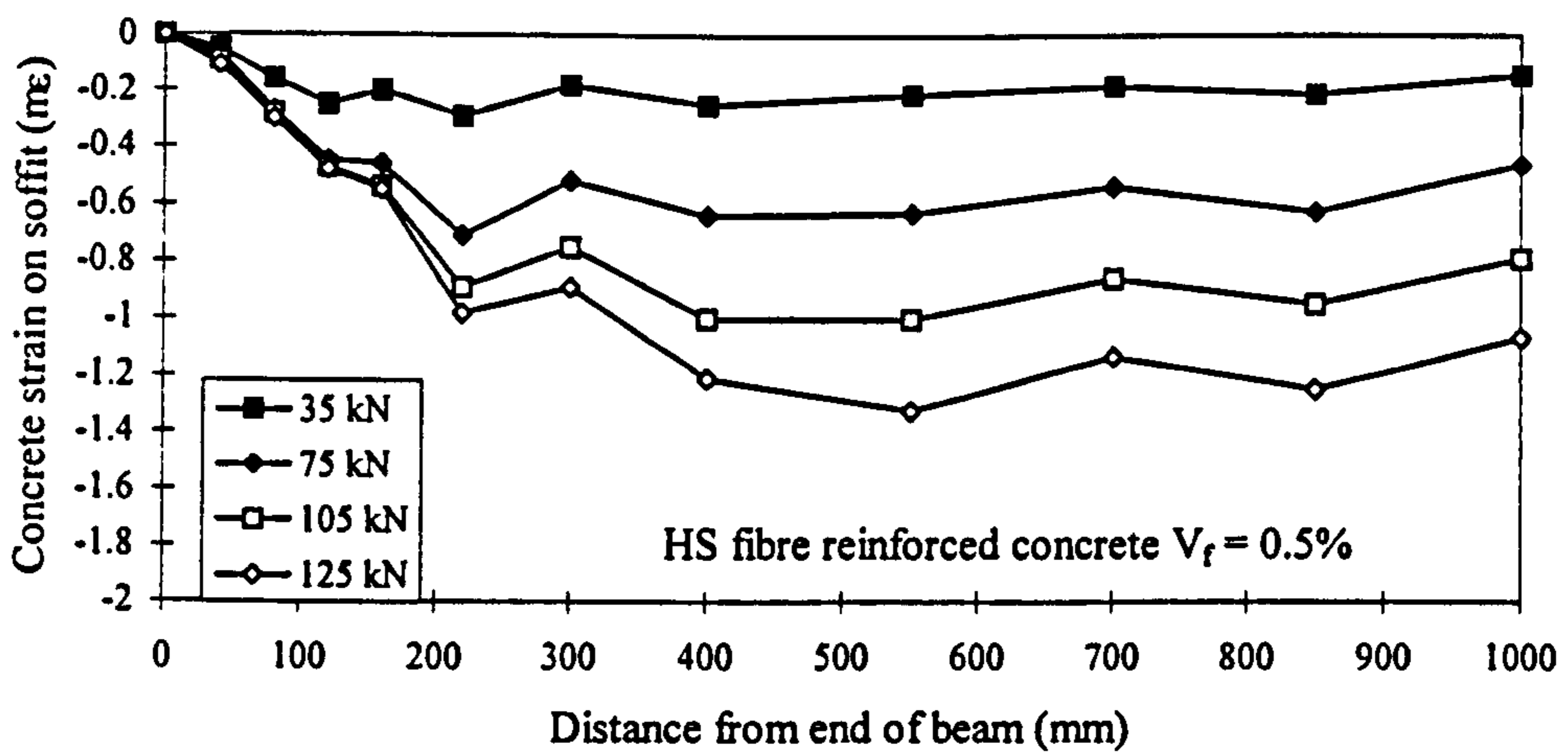
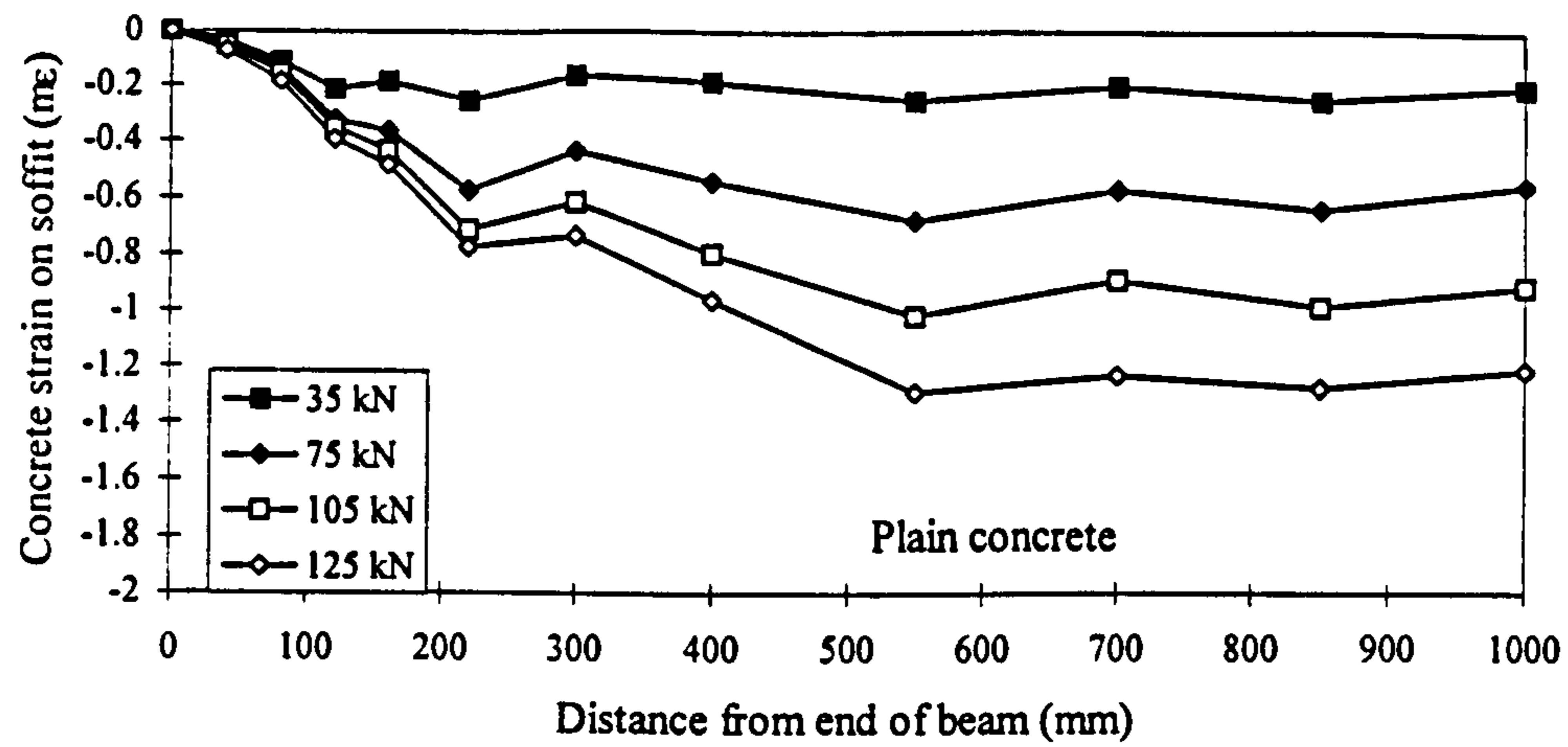


Figure 3-26 Transfer curves for beams with  $V_f = 0\%$ ,  $0.5\%$  and  $1\%$  (Balázs *et al.* 1997) at various prestressing forces

## CHAPTER 4

### MIX DESIGN AND MATERIAL TESTS ON FRC

#### 4.1 Introduction

An investigation into the effect of fibres on the bond between concrete and prestressing strand, and on the shear strength of prestressed concrete beams is described in Chapter 5. To simulate the materials used in practice, it was necessary to achieve relevant concrete material properties (i.e. strength, workability) for both series of tests. In addition, mix designs and mixing procedures had to be formulated to account for the inclusion of fibres to assure adequate compaction, whilst limiting the effect on other properties. This chapter reports on the mix designs, materials and mix procedures used for both sets of tests, → replace \*

Standard material control tests were carried out on the plain concrete and FRC to measure and compare the strength (compression, splitting tension and flexure), the toughness (flexure) and the workability (slump). The results of these tests are presented and discussed. Although there are obvious similarities between the results from the two separate concrete mixes used (pull-out bond test mix and shear test mix), they are described in separate sections for clarity. 100x

In the series of pull-out bond tests, 30 mm long HS fibres, commercially known as Dramix ZP 30/.5, were used. These fibres had a nominal length of 30 mm and a circular cross-section of 0.5 mm diameter. In the shear tests, as well as using these HS fibres, two beams were made which contained 30 mm long AM fibres (commercially known as Fibraflex FF30L6). These fibres which are in the shape of thin ribbons were 1.6 mm wide and 50  $\mu\text{m}$  thick. This gave an effective aspect ratio of 309 when an equivalent circular diameter was taken as four times the cross-sectional area divided by the fibre perimeter. The manufacturers literature (Fibraflex

1995) reports the thickness as 29  $\mu\text{m}$  but measurement of 38 fibres gave the above result of 50  $\mu\text{m}$  at a standard deviation of only 6  $\mu\text{m}$ .

## **4.2 Pull-Out Bond Test Mix**

### **4.2.1 Materials**

The materials used in this study consisted of ordinary Portland cement (OPC), and medium zone sand and river gravel with a maximum size of 10 mm both conforming to BS 882 (1992). The chosen plain concrete mix is given in Table 4-1, and had a water/cement ratio of 0.5. This mix was chosen both for its few ingredients, and because it gave a compressive strength of between 35 and 40  $\text{N/mm}^2$  at 7 days when the specimens were to be tested. This strength is typical for precast prestressed concrete units at release of the prestress. The basic mix proportions were kept constant with the addition of fibres, except for the specimen that contained a fibre volume fraction of 2%, in which the water/cement ratio was marginally increased to 0.52 in order to improve workability.

### **4.2.2 Test Specimen and Mixing**

Specimens were cast in a wooden mould with the strand situated towards the bottom of the specimen, with a concrete cover of 34 mm (Figure 5-1). In addition to the specimen, four cubes (100 mm), four cylinders (300 mm x 150 mm diameter) and three prisms (100 mm x 100 mm x 500 mm) were cast as control specimens to obtain cube compressive strengths, splitting tensile strengths and flexural strength and toughness properties, respectively.

Mixing was carried out in a 0.1  $\text{m}^3$  capacity pan mixer which was insufficient to produce all the required concrete in one batch. Therefore the specimen and control tests were made in two batches, with the first batch used to make two of each of the cube and cylinder control specimens, with one tested at 7 days and the other at 28 days. The first batch control results are most relevant to the pull-out test since it is the concrete from this batch that surrounds the strand.



The mixing procedure used for plain concrete was to add all the dry ingredients (sand, aggregate, OPC) together and mix for about two minutes, after which the water was added and mixing continued for a further three minutes. This basic mixing procedure was adhered for the FRC, with the fibres regarded as a dry ingredient. This proved to be the best method of separating the glue collated HS fibre bundles since it enabled all the free water to be available to disperse the fibres. Additionally it was found that some fibres separated during the dry mixing process due to the scouring action of the fibres. Different mixing methods for HS fibres are described in further detail in Chapter 6.

The pull-out specimens were compacted using an internal vibrator whilst the control specimens were compacted on vibrating tables. Curing of the control specimens was in accordance with BS 1881 (1983). The pull-out specimens were covered with plastic sheets and left at room temperature for 24 hours before being stripped off their moulds and left uncovered at room temperature until the day of testing.

Six pull-out test specimens were made in all, two plain specimens (given notation B-0.0A and B-0.0B) and one each at a fibre volume fraction of 0.5%, 1.0%, 1.5% and 2.0% (notated B-0.5, B-1.0, B-1.5 and B-2.0, respectively).

## **4.3 Material Test Results for Pull-out Bond Test**

### **4.3.1 Compressive Strength**

Cubes were tested in compression in accordance with BS 1881 (1983) using a 2500 kN capacity compression testing machine. Load was applied at a rate of 160 kN/min.

The results of the compressive cube tests are shown in Table 4-2 and Table 4-3, for 7 days and 28 days respectively. For the important first batch mixes it can be seen that the first five test specimens were consistently between 40 N/mm<sup>2</sup> and 42 N/mm<sup>2</sup> at the pull-out test age. Specimen B-0.0B was slightly weaker at 36 N/mm<sup>2</sup>.

### 4.3.2 Splitting Tensile Strength

Splitting cylinder tests were performed under load-control using a Denison testing machine to obtain the ultimate splitting cylinder tensile strength ( $f_{ct,sp}$ ). The results are given in Table 4-2 and Table 4-3, and shown graphically in Figure 4-1. Ultimate strengths were calculated using the theory of linear-elasticity and as discussed in Section 2.2.4 have no actual physical meaning.

Although the cracking strength of the FRC specimens was not measured it is expected that this strength would have been similar to the ultimate splitting strength of the plain concrete cylinders. The post-cracking benefit of the fibres is, therefore, approximately equal to the difference between the ultimate strength of FRC specimens and the strength of the plain concrete specimen. The plain concrete splitting strength approximated to  $0.49 \sqrt{f_{cu}}$  for both 7 day and 28 day old specimens.

As can be seen Figure 4-1, there is a clear linear relationship between the ultimate splitting strength and the fibre volume fraction. However, it could possibly be argued that a bi-linear curve would better fit the data if no increase in  $f_{ct,sp}$  is acknowledged for  $V_f < 0.4\%$ . The best fit linear relationships between the ultimate splitting cylinder strength of FRC and fibre volume fraction are given below, for the 7 day and 28 day tests respectively.

$$f_{ct,sp} = 0.49\sqrt{f_{cu}} + 109V_f \quad (\text{N/mm}^2) \quad \dots 4-1$$

$$f_{ct,sp} = 0.49\sqrt{f_{cu}} + 141V_f \quad (\text{N/mm}^2) \quad \dots 4-2$$

Also shown in Figure 4-1 is the line corresponding with the equation for predicting the splitting tensile strength empirically derived by Narayanan and Palanjian (1984) - Equation 2.15. It can be seen that the equation only gives valid results at small fibre volume fractions and significantly underestimates the splitting strength at higher fibre volume fractions.

### 4.3.3 Flexural Strength/Toughness

The prisms were tested in a 200 kN capacity screw driven Zwick Universal Testing Machine (UTM), in four-point flexure over a span of 300 mm, in accordance with ASTM C 1018 (1994) and JCI SF4 (1983b). The yoke arrangement shown in Plate 2-1 was used to obtain the net mid-span deflection, independent of extraneous deformations. The tests were carried out under closed-loop deflection control at a rate of specimen deflection of 0.1 mm/min, and terminated at a total deflection of 2 mm.

A number of problems existed with the control system for this series of tests, which resulted in imperfect results. For the  $V_f = 0.5\%$  specimens there was a substantial amount of instability after the first crack due to poor gain control, which lead to the test aborting almost immediately on cracking.

A further problem existed with the automatic storage interval within the UTM which meant that it was not possible to record any data beyond a specimen deflection of about 1.6 mm. No toughness values in accordance with JCI SF4 (1983b) have therefore been calculated.

The mean flexural strength and toughness values for each set of prisms which were measured are presented in Table 4-4 and Table 4-5. In each case, the mean value has been calculated from tests on three prisms at an age of about 28 days. The results of all prisms are given in Appendix B.

Each of the strength and toughness parameters presented in Table 4-4 and Table 4-5 are described fully in Section 2.4, and are: the ASTM toughness indices ( $I_5$ ,  $I_{10}$  and  $I_{20}$ ); ASTM residual strength indices ( $R_{5,10}$  and  $R_{10,20}$ ); first crack strength ( $f_{fl,cr}$ ) as calculated using the method proposed by Nemegeer and Tatnall (1995) - see section 2.4.4; ultimate flexural strength ( $f_{fl,ult}$ ); equivalent flexural strength based on the average strength up to a deflection of  $l/300$  ( $f_{fl,eq300}$ ); and the ratio ( $R_{0.3-1.0}$ ) of the average load between the deflections of  $l/900$  and  $l/300$  to the first crack load.

A discussion of the results is given in Section 4.5.4 where they are compared with the flexural test on the prisms cast from the shear test mix.

## 4.4 Shear Test Mix

### 4.4.1 Mix Design

It was recognised that due to the short length of the prestressing bed and the limited time available in the laboratory, that a rapid hardening mix would be required to enable a rapid turnover of test specimens. The main requirement for the tests, being that the mix should achieve a cube compressive strength of  $35 \text{ N/mm}^2$  within 24 hours so that detensioning and stripping of the mould could take place; such a procedure making it possible to cast two specimens each week. The notation given to each of these laboratory-cast single web prestressed beams (known as x-beams) was simply the initials PB followed by a number referring to the order in which the beam was cast. A list of all the x-beams is given in Table 5-2.

The initial plain mix chosen for beams PB1 and PB2 is shown in Table 4-6. To obtain the necessary strength it was very cement rich. Although the mix did not quite meet the strength development criterion - it took about 29 hours to achieve a compressive strength of  $35 \text{ N/mm}^2$  - these plain mix proportions were used to make the first four beams (PB1-PB4).

Apart from the unsatisfactory development of strength, it became apparent that there were other problems with this mix. Firstly, due to its high cement content the mix was very “sticky”, which made both placing and compaction very difficult. It was clear that such a mix would not be used in practice and questions were also raised about the validity of the results which would be obtained. Secondly, at the release of the prestress each of the strain gauges that were attached to the wire (see Section 5.4.2) tore off, which suggested that there was excessive wire slip as a result of poor bond between the wire and the concrete. The level of prestress within the concrete was therefore unknown and seemed likely to be low.

The test behaviour of these four specimens (PB1-PB4) is described fully in Section 5.5.2, but it should be noted that none of the specimens failed in web shear as had been hoped. The reason behind this poor behaviour was almost certainly due to lack of prestress caused partly by the lack of bond. In addition, the initial prestressing force had been low, anyway, because only one prestressing wire had been used. For later beams (PB5-PB22) three prestressing wires were used.

Following these problems it was decided to develop a new mix. To aid strength development silica fume was used as a partial cement replacement, and to maintain workability whilst limiting the amount of water in the mix a superplasticizer was used. The basic mix design was based on one used by den Uijl (1995) in tests studying transfer length in high performance concrete (in particular hollow core slabs). A number of different superplasticizers were tried out, and a suitable mix using the superplasticizer Cormix 2000 obtained (Table 4-6).

Because of the previously suspected problems with bond between concrete and wire two small-scale bond tests were performed to compare the new mix (to be used for PB5) and the mix used in PB1.

The details of the test set-up for these bond tests are shown in Figure 4-2 and Plate 4-1. Both specimens were tested at one day with the compressive strength of the mixes equal to  $37.5 \text{ N/mm}^2$  and  $36.5 \text{ N/mm}^2$  for the PB1 mix and prospective PB5 mix, respectively. Figure 4-3 shows the force versus pull-in curves for both tests. It can be seen that at a force of 2 kN pull-in occurs from the unloaded end of the PB1 mix specimen. There is a slight additional resistance up to a force of 3.3 kN beyond which the wire pulls out at an average bond stress ( $P/l\pi\phi$ ) of  $0.43 \text{ N/mm}^2$ .

The prospective PB5 mix performed much better with the first signs of slip at a force of about 5.6 kN, but no significant movement until 9 kN with a maximum force of 9.5 kN being obtained - which is almost three times greater than the force taken by the PB1 mix. Beyond the maximum load the wire pulls out quite freely at a average bond stress of  $0.92 \text{ N/mm}^2$ , indicating that the frictional bond is twice as effective in this mix as the PB1 mix.

From these simple tests it was felt that the new mix would be much more effective in holding the prestress as the implication is that the transfer length for the PB5 mix is between two and three times shorter. The reasons for the improved initial bond performance are possibly due to the smaller particle size of the silica fume which provides better interlock with the microscopically rough wire surface, and the enhanced workability of the new mix which allowed better compaction, and therefore less air voids, around the wire.

The test specimen PB5 was cast using this mix. The concrete was easy to place and compact, and the strains measured at the release of prestress suggested a

good bond between the concrete and wires as expected from the small-scale bond tests.

All future specimens had to be manufactured using Cormix 2001 superplasticizer due to the non-availability of Cormix 2000 used in the trial. The plain mix for future specimens (PB7, PB18 and PB20) was modified to that shown in Table 4-6. The slightly higher superplasticizer content was suggested by the manufacturers (Hodgkinson 1996).

Various alterations were made to the plain mix to allow for the addition of HS fibres. Originally the mix proportions were kept constant for each fibre content, but at a fibre volume fraction of 1.5% the mix proved unworkable in the mixer. Additional water was added to this mix (PB10) which adversely affected the hardened concrete properties. As described later the results from the beam PB10 are unrepresentative.

For future beams (PB11-PB22) the difficulties in mixing FRC were overcome by using increasingly higher dosages of superplasticizer with increasing fibre contents. This is shown graphically by the thick line in Figure 4-4. The mixes which do not follow this general trend are marked separately on the figure.

Previous research using the Baron-Lesage Method of mix design (Rossi 1992), had shown that the superplasticizer requirements for a 2% volume fraction HS fibre mix were comparable with that of a 0.5% volume fraction AM fibre mix, with sand/aggregate and water/cement ratios about constant. Therefore, for the 0.56% AM fibre mix in this study the superplasticizer content was taken as 0.015 by weight of cement (equal to that used for 2% HS fibres), and for the 0.28% AM fibre mix the superplasticizer content was taken as equal to that used for 1% HS fibres.

#### **4.4.2 Mixing and placing of concrete**

Mixing was carried out in a 0.1 m<sup>3</sup> capacity pan mixer, following a similar procedure to that used for the pull-out bond specimens. Silica fume was added as a dry ingredient and the superplasticizer was added along with the water.

As with the Pull-Out Bond Tests, the collated HS fibres were added as part of the dry ingredients. However, it was not possible to add the AM fibres directly into the pan along with the dry ingredients since they tend to form "balls" which fail to

separate during mixing. The method adopted was to add the fibres through the grill-covered observation port in the mixer lid whilst mixing was taking place. The actual mix procedure was as follows:

1. Mix dry ingredients
2. after 2 minutes, add 1/2 water
3. continue mixing and add 1/2 of AM fibres
4. add rest of water and superplasticizer
5. continue mixing and add rest of AM fibres

All beams were compacted using an external shutter vibrator. Occasionally for the higher fibre volume fractions it was necessary to use a poker vibrator but this was used sparingly so as to avoid the formation of "fibreless chimneys" within the mix. Adequate compaction was achieved in all the beams except PB12 and PB13 at 1.5% fibre volume fraction. In both these cases, it was difficult to use a poker vibrator for fear of damaging the strain gauges. Subsequently, there was hardly any compaction around the wires in these beams, which lead to a large wire pull-in at release, little or no stress in the wires and a very low quality severely 'honeycombed' concrete (Plate 4-2).

For control purposes eight cubes (100 mm), three prisms (100 x 100 x 500 mm) and two cylinders (150 mm diameter x 300 mm) were cast from each mix and compacted on vibrating tables.

The shear test beams were cured in air under polythene and wet hessian up to detensioning and then left uncovered in air at room temperature until testing. The control specimens were cured in air under polythene for 24 hours and then transferred to water and cured in accordance with BS 1881.

## **4.5 Material Test Results for Shear Test Mix**

### **4.5.1 Slump**

Slump is useful in detecting variations in the consistency of concrete mixes and is often used on plain concretes as an indirect measure of the workability. For FRC's such a relationship is invalid and unreliable, however the test can still be used as a quality control check on the relative consistency of each mix (ACI Committee 544, 1988). The results of slump tests were therefore useful in this study because of the different concentrations of superplasticizer used to counteract the mixing problems at high fibre contents.

The measured slumps of each mix as measured in accordance with BS 1881 are given in Table 4-7 to Table 4-9. It can be seen that the three nominally identical plain mixes (PB7, PB18, PB20) gave slumps varying between 50 mm and 140 mm, and that the plain mix with a lower superplasticizer content (PB5) gave a high slump of 100 mm.

The effect of the superplasticizer is more noticeable on the HS FRC's. An increase in superplasticizer content from 0.6% to 0.8% by weight of cement increased slump from 15 mm to 40 mm (100 mm in the case of PB17) at a fibre volume fraction of 0.5%; and an increase in superplasticizer from 0.8% to 1.1% by weight of cement increased slump from 5 mm to 40 mm at a fibre volume fraction of 1%. It is clear therefore that increasing superplasticizer content in HS FRCs increases the slump. FRC's of fibre volume fraction 1.5% gave effectively zero slump concretes (values of 0 mm and 5 mm measured) independent of superplasticizer content.

For the two mixes containing AM fibres the slump was 20 mm.

### **4.5.2 Compressive Strength**

The compressive strength of each beam was tested by crushing of 100 mm cubes in identical fashion to that for the pull-out test mixes. Cubes were tested in pairs at 24 hours to measure the strength before detensioning, age of the first test known as the A Test (see Section 5.4.3), and at 28 days. The results are shown in



Table 4-7 to 4-9, which are separated to distinguish between fibre type and the a/d ratio over which the prestressed beam was tested.

The aim of the mix was to attain a concrete with a strength of 35 N/mm<sup>2</sup> within 24 hours to ensure adequate strength for detensioning as well as a speedy turn-over of test specimens. In all cases this was achieved.

A curve showing the gain of compressive strength against age for the plain mix (PB7) is shown in Figure 4-5. It can be seen that at the age of the A Test the compressive strength is about 94% of the 28 day strength. The ratio between test strength and 28 day strength was similar for both the plain and FRC cubes. In general, the compressive strength of the plain mix at the A test was 71 N/mm<sup>2</sup> and the 28 day strength was 75 N/mm<sup>2</sup>.

Addition of HS fibres in almost all cases increased the compressive strength with a maximum strength of 90 N/mm<sup>2</sup> being achieved at a fibre volume fraction of 1.5% (PB15). However where compaction was difficult much lower strengths were achieved (e.g., 76 N/mm<sup>2</sup> for PB10).

The effect of adding extra superplasticizer to the later mixes had no noticeable effect on the strength at testing or at 28 days, but does appear to have had a slightly detrimental effect on the strength at 24 hours.

### 4.5.3 Splitting Tensile Strength

Splitting tensile tests were performed in pairs on the day of the A test. As with the control tests for the pull-out bond tests, these were carried out under load-control using a Denison testing machine. Both cylinders and cubes were split and two strengths, the ultimate cylinder splitting strength and the ultimate cube splitting strength ( $f_{ct,spc}$ ), calculated. The results are given in Table 4-7 to Table 4-9, and shown graphically in Figure 4-6. Notably the fibres have a greater effect on the ultimate splitting strength obtained from the cylinder tests than the dimensionally smaller cube tests. The relationship between cylinder splitting tensile strength and cube compressive strength is about  $f_{ct,sp} = 0.48\sqrt{f_{cu}}$  (N/mm<sup>2</sup>) for the plain mixes at test age. This is consistent with the observation for the pull-out test mixes in Section 4.3.2.

The linear relationship between the ultimate splitting cylinder strength of FRC and fibre volume fraction at 28 days is given below. Both results differ from that obtained on the control tests for the pull-out bond tests (see Section 4.3.2). The influence of fibres on splitting strength is therefore not matrix independent.

$$f_{ct,sp} = 0.48\sqrt{f_{cu}} + 237V_f \quad (\text{N/mm}^2) \quad \text{.. 4-3}$$

As with the pull-out test mixes, Equation 2.15 underestimates the splitting strength at fibre volume fractions greater than 0.5%. The equivalent equation derived from the splitting tests on AM fibre reinforced concrete cylinders is:

$$f_{ct,sp} = 0.48\sqrt{f_{cu}} + 336V_f \quad (\text{N/mm}^2) \quad \text{.. 4-4}$$

#### 4.5.4 Flexural Strength/Flexural Toughness

The average results of the flexural strength and toughness tests for each mix are given in Table 4-10 and Table 4-11 for the plain concrete and HS fibre reinforced concrete, and in Table 4-12 and Table 4-13 for the AM fibre reinforced concrete (results of all prisms are given in Appendix B). The parameters presented are the same as those described in Section 4.3.3, with two additions which are: the equivalent flexural strength based on the average strength up to a deflection of 1/150 ( $f_{fl,eq150}$ ) as specified by JCI SF4 (1983b); and the ratio ( $R_{1.0-2.0}$ ) of the average load between the deflections of 1/300 and 1/150 to the first crack load.

Typical load - deflection curves from the shear test mixes for each fibre volume fraction and fibre type are shown in Figure 4-7. It can be seen that for each of the HS fibre specimens there is a considerable load-bearing capacity after cracking, but that the post-cracking capacity of the AM fibre specimens is not all that much better than the plain concrete. Due to the stiffness of the UTM and use of satisfactory gain control, it was possible to record the descending portion of the load-deflection curve for plain concrete prisms.

Comparison of each of the parameters with increasing fibre volume fraction are shown in Figure 4-8 to Figure 4-11. The results of the tests from the pull-out bond mix are also shown to compare the toughness between different matrices.

Figure 4-8 shows the relationship between each of the toughness indices ( $I_5$ ,  $I_{10}$  and  $I_{20}$ ) and the fibre volume fraction. Similar to Peaston (1993), best fit second-order polynomial lines have been drawn through each index for both matrices, i.e., all mixes. It can be seen from Table 4-4 and Table 4-10, and Figure 4-8 that the index  $I_5$  is unable to significantly distinguish between different fibre contents and fibre types. This is because this index is based on the behaviour of the concrete up to a relatively small deflection of approximately 0.1 mm. The other indices are able to show the benefit of fibre addition more effectively.

The toughness index for the two separate matrix types can be seen to give very similar results at each fibre volume fraction, and the curves drawn have very similar shapes. This would appear to suggest that the ASTM indices are largely matrix independent.

Figure 4-9 compares the average cracking strength and average ultimate strength of each set of specimens with fibre volume fraction. The  $f_{fl,cr}$  results show two almost parallel linear relationships for both matrix types. The lower flexural cracking strength of the pull-out test mix is consistent with the lower compressive strength of the matrix.

The ultimate flexural strength curve can be expressed as a bi-linear relationship. At low fibre volume fractions,  $f_{fl,ult} = f_{fl,cr}$  whilst at higher fibre volume fractions the prisms are able to bear greater load than at cracking. The junction of the two linear lines indicates the critical fibre volume fraction in flexure. For the shear mix this is about  $V_f = 0.8\%$ , whilst a lower value of  $V_f = 0.65\%$  can be interpolated for the pull-out test mix.

Comparison of the AM fibre test results with those of the HS fibre shear test mixes, show that the AM fibre reinforced concrete gave greater first cracking and ultimate strengths. This is attributable to the shape of the AM fibres which have eight times the surface contact area of an HS fibre for the same fibre volume (Boucharet 1994), which leads to closer spaced fibre reinforcement. Microcracks are therefore bound together more effectively at a material level before crack localisation, leading to the higher strengths observed (Rossi 1992). The critical fibre volume fraction in

flexure for these fibres can be seen to lie between 0.28% and 0.56%. Theoretically it can be calculated as just greater than 0.3%, using Equation 2-8 and assuming the critical fibre volume fraction in flexure to be 0.41 times that in tension (Lanu 1995).

The relationships between the equivalent flexural strengths and fibre volume fraction are shown in Figure 4-10. Each of the relationships is typically linear. The two lines for the shear test mix representing the equivalent flexural strength up to 1/300 and 1/150, and the line representing the pull-out test mix are almost parallel. This suggests that the relative increases in strength with increasing fibre volume fraction are matrix independent. The slope of these curves is therefore directly a function of the effectiveness of the fibres.

Figure 4-11 shows the load based dimensionless indices,  $R_{0.3-1.0}$  and  $R_{1.0-2.0}$  relative to the fibre volume fraction for the two matrix types. For both mixes, linear relationships exist. It is clear, however, that for the same fibre content, the pull-out mix produces higher ratios than the shear test mix. This shows that the pull-out mix is less brittle than the shear test mix. This can probably be attributed to the different matrix failure mechanisms between the two concretes, which was evident from inspection of the cracked faces of the prisms after testing. For the prisms from the pull-out test mix, the failure was by aggregate pull-out from the cement paste. While for the prisms from the shear test mix which bore a greater load, there was evidence of aggregate splitting which gives rise to more brittle failures .

The load based dimensionless indices can distinguish between fibre types, however. In Figure 4-11, the AM results have also been included. It can be seen that the AM fibre results are lower than the HS results by as much as an order of ten. For comparative purposes, the fibre volume fractions, of 0.28% and 0.56% have been placed at the 1% and 2% HS positions, because of similar mixing requirements (Section 4.4.1).

**Table 4-1 Plain Concrete Mix (by weight of cement) for Pull-out Tests**

Sand <sup>1</sup>	1.75
10 mm aggregate	2.75
OPC <sup>2</sup>	1
Water	0.5

<sup>1</sup>Medium zone sand, complying with BS 882 (1992), <sup>2</sup>Ordinary Portland cement, complying with BS 12 (1991)

**Table 4-2 Compression and Splitting Tension Test Results at Test Age (7 days) for Pull-Out Bond Specimens**

V <sub>f</sub> (%)	Test No.	f <sub>cu</sub>	f <sub>cu</sub>	f <sub>ct,sp</sub>	f <sub>ct,sp</sub>
		(N/mm <sup>2</sup> ) batch 1	(N/mm <sup>2</sup> ) batch 2	(N/mm <sup>2</sup> ) batch 1	(N/mm <sup>2</sup> ) batch 2
0	B-0.0A	42.0	45.5	3.15	3.45
0.5	B-0.5	40.0	45.5	3.20	3.55
1	B-1.0	42.0	40.0	3.95	4.10
1.5	B-1.5	42.0	35.0	4.65	4.45
2	B-2.0	40.0	-	5.40	-
0	B-0.0B	36.0	37.0	2.90	3.10

**Table 4-3 Compression and Splitting Tension Tests at 28 days for Pull-Out Bond specimens**

V <sub>f</sub> (%)	Test No.	f <sub>cu</sub>	f <sub>cu</sub>	f <sub>ct,sp</sub>	f <sub>ct,sp</sub>
		(N/mm <sup>2</sup> ) batch 1	(N/mm <sup>2</sup> ) batch 2	(N/mm <sup>2</sup> ) batch 1	(N/mm <sup>2</sup> ) batch 2
0	B-0.0A	57.0	57.5	3.90	3.70
0.5	B-0.5	52.5	60.0	3.90	4.10
1	B-1.0	52.5	52.0	4.70	4.60
1.5	B-1.5	52.5	54.5	5.60	5.50
2	B-2.0	55.5	-	6.45	-
0	B-0.0B	52.0	50.5	3.35	3.40

**Table 4-4 Mean ASTM C 1018 Toughness Indices for HS fibre pull-out bond test mixes**

$V_f$ (%)	Specimen	$I_5$	$I_{10}$	$I_{20}$	$R_{5,10}$	$R_{10,20}$
1	B-1.0	4.5	9.4	19.0	98.3	96.1
1.5	B-1.5	5.1	9.9	20.1	105.6	101.3
2	B-2.0	5.3	12.2	26.0	137.7	137.6

**Table 4-5 Mean Cracking, ultimate and equivalent flexural strengths for HS pull-out test bond mixes**

$V_f$ (%)	Beam	$f_{fl,cr}$ (N/mm <sup>2</sup> )	$f_{fl,ult}$ (N/mm <sup>2</sup> )	$f_{fl,eq,300}$ (N/mm <sup>2</sup> )	$R_{0.3-1.0}$
1	B-1.0	5.57	6.61	5.54	0.96
1.5	B-1.5	5.72	7.25	6.34	1.12
2	B-2.0	6.10	9.57	8.54	1.42

**Table 4-6 Mix design for plain shear test concrete mixes (by weight of cement)**

*PB1-4*

	PB1 & PB2	PB5	PB7, PB18 & PB20
Sand <sup>1</sup>	1.5	1.66	1.66
10 mm aggregate	1	2.11	2.11
RHPC <sup>2</sup>	1	1	1
Silica fume	-	0.05	0.05
Water	0.38	0.4	0.4
Superplasticizer	-	0.006 <sup>†</sup>	0.008 <sup>‡</sup>

<sup>1</sup>Medium zone sand, complying with BS 882 (1992), <sup>2</sup>Rapid hardening Portland cement, complying with BS 12 (1991), <sup>†</sup> Cormix 2000, <sup>‡</sup> Cormix 2001

**Table 4-7 Mean Compression and Splitting Tension Test and Slump Results for HS fibre reinforced beams tested over  $a/d = 2.8$**

$V_f$ (%)	Beam	Slump (mm)	Detension		Test age		28 days
			$f_{ci}$ (N/mm <sup>2</sup> )	$f_{cu}$ (N/mm <sup>2</sup> )	$f_{ct,sp}$ (N/mm <sup>2</sup> )	$f_{ct,spc}$ (N/mm <sup>2</sup> )	$f_{cu}$ (N/mm <sup>2</sup> )
0	PB5	100	35.0	71.0	3.85		73.0
0	PB7	50	46.0	73.0	4.20	4.50	78.0
0.5	PB6	15	44.0	77.0	5.25	4.70	72.0
0.5	PB8	40	43.5	75.5	5.50	4.70	78.5
1	PB9	5	49.0	79.5	7.45	5.60	86.0
1	PB11	5	46.5	75.5	7.05	5.70	82.5
1.5	PB10	0	39.0	67.0	7.40	5.90	76.0
1.5	PB12	0	37.5	68.5	7.15	4.00	80.5

**Table 4-8 Mean Compression and Splitting Tension Test and Slump Results for HS fibre reinforced beams tested over  $a/d = 2.0$**

$V_f$ (%)	Beam	Slump (mm)	Detension		Test age		28 days
			$f_{ci}$ (N/mm <sup>2</sup> )	$f_{cu}$ (N/mm <sup>2</sup> )	$f_{ct,sp}$ (N/mm <sup>2</sup> )	$f_{ct,spc}$ (N/mm <sup>2</sup> )	$f_{cu}$ (N/mm <sup>2</sup> )
0	PB18	140	40.5	71.0	4.30	4.50	77.0
0	PB20	60	34.5	71.0	4.05	4.10	74.0
0.5	PB17	100	35.0	73.5	5.20	4.40	79.5
0.5	PB19	40	36.5	69.5	5.15	4.20	77.0
1	PB14	40	38.5	75.0	7.05	5.75	82.0
1	PB16	30	37.5	77.0	6.65	6.20	86.0
1.5	PB13	0	45.0	82.5	7.85	6.70	88.5
1.5	PB15	5	42.0	82.0	7.45	7.45	90.0

**Table 4-9 Mean Compression and Splitting Tension Test and Slump Results for AM fibre reinforced beams**

$V_f$ (%)	Beam	Slump (mm)	Detension		Test age		28 days
			$f_{ci}$ (N/mm <sup>2</sup> )	$f_{cu}$ (N/mm <sup>2</sup> )	$f_{ct,sp}$ (N/mm <sup>2</sup> )	$f_{ct,spc}$ (N/mm <sup>2</sup> )	$f_{cu}$ (N/mm <sup>2</sup> )
0.28	PB21	20	43.0	69.5	4.55	4.00	74.0
0.56	PB22	20	40.0	71.0	6.20	5.65	77.0

**Table 4-10 Mean ASTM C 1018 Toughness Indices for plain and HS fibre shear test mixes**

$V_f$ (%)	Specimen	$I_5$	$I_{10}$	$I_{20}$	$R_{5,10}$	$R_{10,20}$
0	PB20	2.5	3.2	3.7	14.1	4.7
0.5	PB17	4.1	8.1	15.7	79.1	76.4
0.5	PB19	4.1	7.5	13.6	68.2	61.2
1	PB9	4.3	9.1	18.1	95.8	91.0
1	PB11	5.1	11.0	23.6	119.3	125.4
1	PB14	4.8	9.9	20.1	104.2	101.7
1	PB16	4.7	8.5	17.6	75.6	91.7
1.5	PB10	4.6	10.2	20.4	112.2	102.3
1.5	PB12	5.3	11.0	22.6	113.0	116.3
1.5	PB13	5.0	11.4	23.1	127.8	116.8
1.5	PB15	4.9	11.3	23.3	127.3	120.1



**Table 4-11 Mean Cracking, ultimate and equivalent flexural strengths for plain and HS fibre shear test mixes**

$V_f$ (%)	Beam	$f_{fl,cr}$ (N/mm <sup>2</sup> )	$f_{fl,ult}$ (N/mm <sup>2</sup> )	$f_{fl,eq,150}$ (N/mm <sup>2</sup> )	$f_{fl,eq,300}$ (N/mm <sup>2</sup> )	$R_{0.3-1.0}$	$R_{1.0-2.0}$
0	PB18	6.85	6.85	-	-	0	0
0	PB20	7.62	7.62	-	-	0	0
0.5	PB17	6.03	6.03	3.90	4.56	0.75	0.56
0.5	PB19	7.99	7.99	3.86	4.74	0.55	0.37
1	PB9	8.24	8.25	5.08	6.45	0.75	0.45
1	PB11	7.04	7.64	5.29	6.41	0.89	0.58
1	PB14	7.40	8.50	5.90	6.85	0.90	0.66
1	PB16	7.57	7.57	4.96	5.85	0.75	0.74
1.5	PB10	7.87	8.68	6.40	7.24	0.91	0.7
1.5	PB12	8.11	9.60	6.48	7.85	0.95	0.63
1.5	PB13	8.55	10.28	7.63	8.48	0.99	0.79
1.5	PB15	8.10	10.09	7.26	8.49	1.05	0.74

Do these  
not have  
(read)  
values

**Table 4-12 Mean ASTM C 1018 Toughness Indices for AM fibre shear test mixes**

$V_f$ (%)	Specimen	$I_5$	$I_{10}$	$I_{20}$	$R_{5,10}$	$R_{10,20}$
0.28	PB21	4.1	6.6	9.7	47.7	28.4
0.56	PB22	4.5	9.3	14.4	95.1	51.1

**Table 4-13 Mean Cracking, ultimate and equivalent flexural strengths for AM fibre shear test mixes**

$V_f$ (%)	Beam	$f_{fl,cr}$ (N/mm <sup>2</sup> )	$f_{fl,ult}$ (N/mm <sup>2</sup> )	$f_{fl,eq,150}$ (N/mm <sup>2</sup> )	$f_{fl,eq,300}$ (N/mm <sup>2</sup> )	$R_{0.3-1.0}$	$R_{1.0-2.0}$
0.28	PB21	8.34	8.34	1.23	2.22	0.09	0.02
0.56	PB22	8.75	8.94	2.40	3.99	0.29	0.09

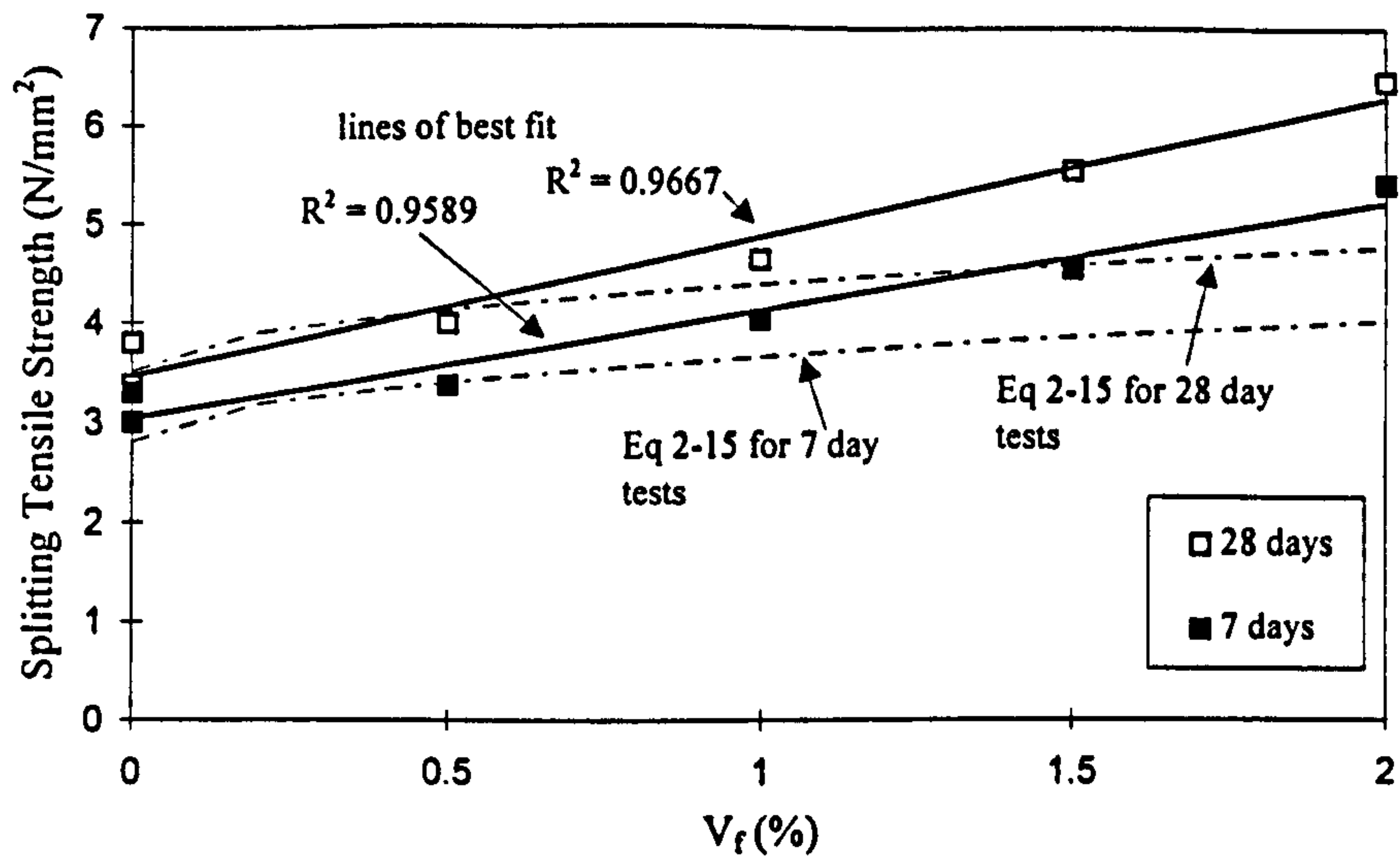


**Figure 4-1 Splitting tensile strength v fibre volume fraction for pull-out control test specimens**

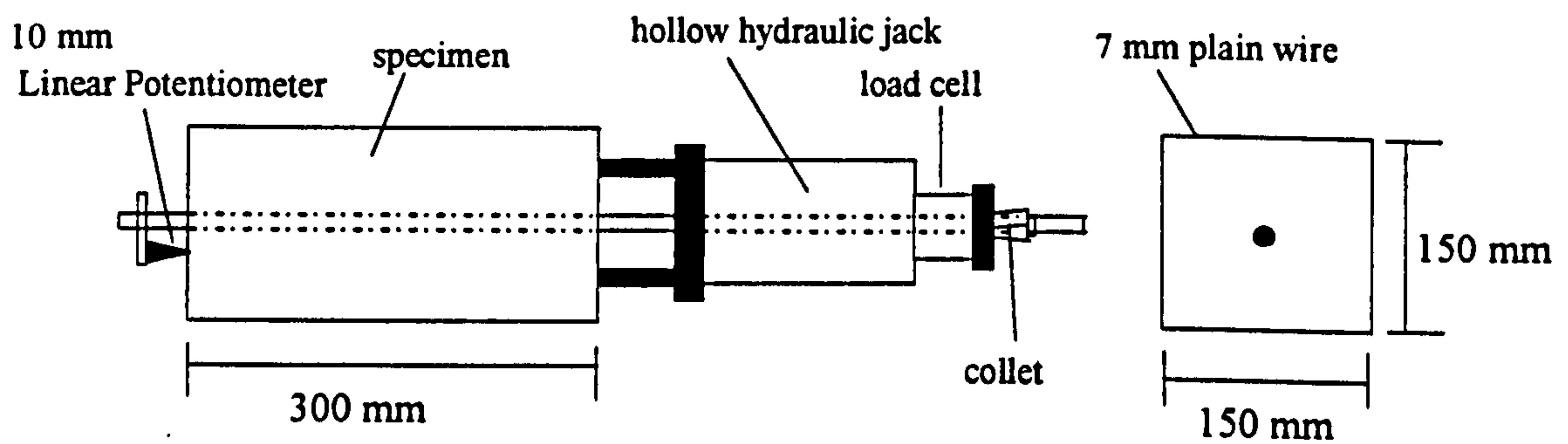


**Figure 4-2 Small scale pull-out test arrangement**

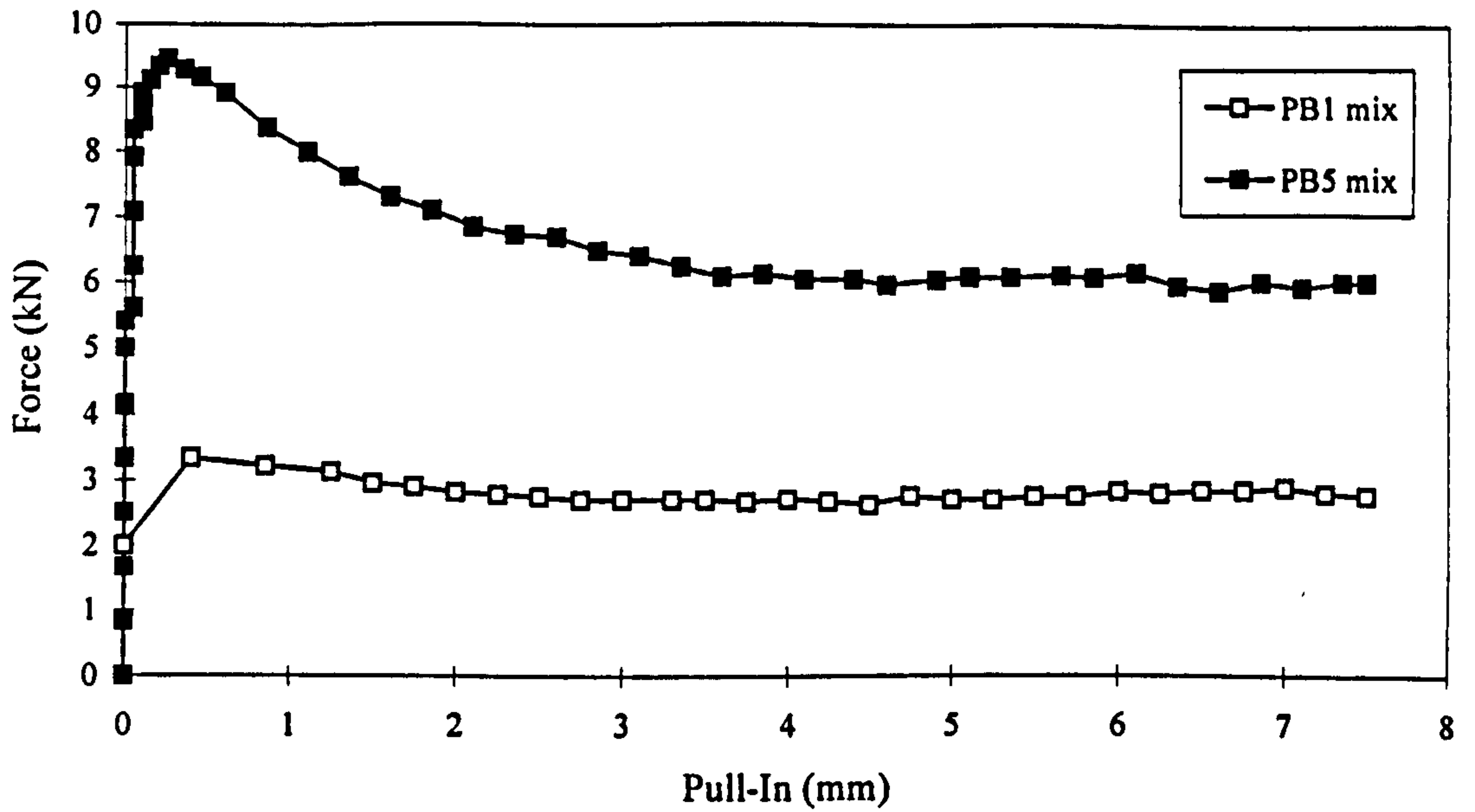


Figure 4-3 Force v pull-in for small-scale bond tests

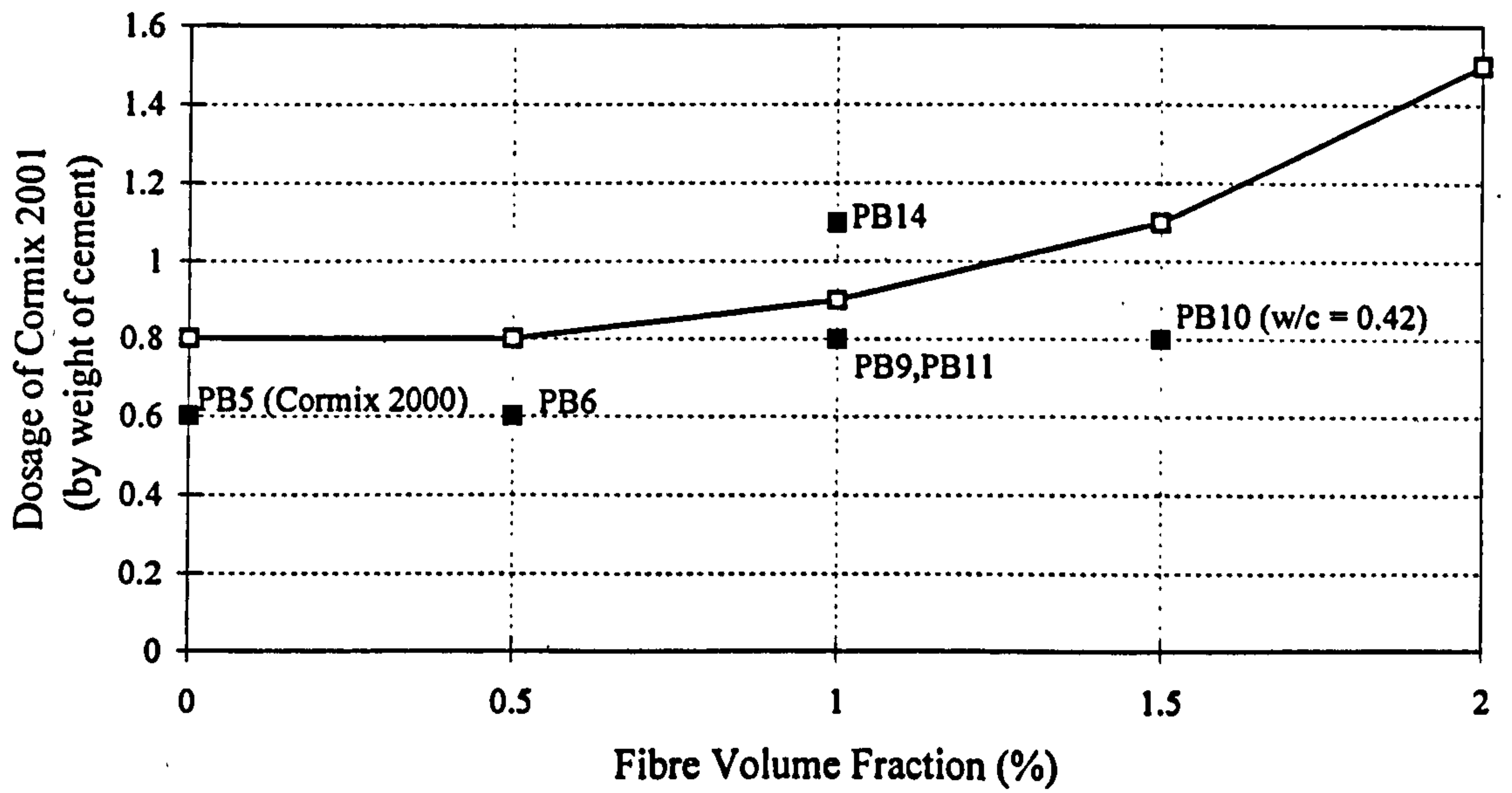


Figure 4-4 Dosage of superplasticizer used with increasing fibre volume fraction

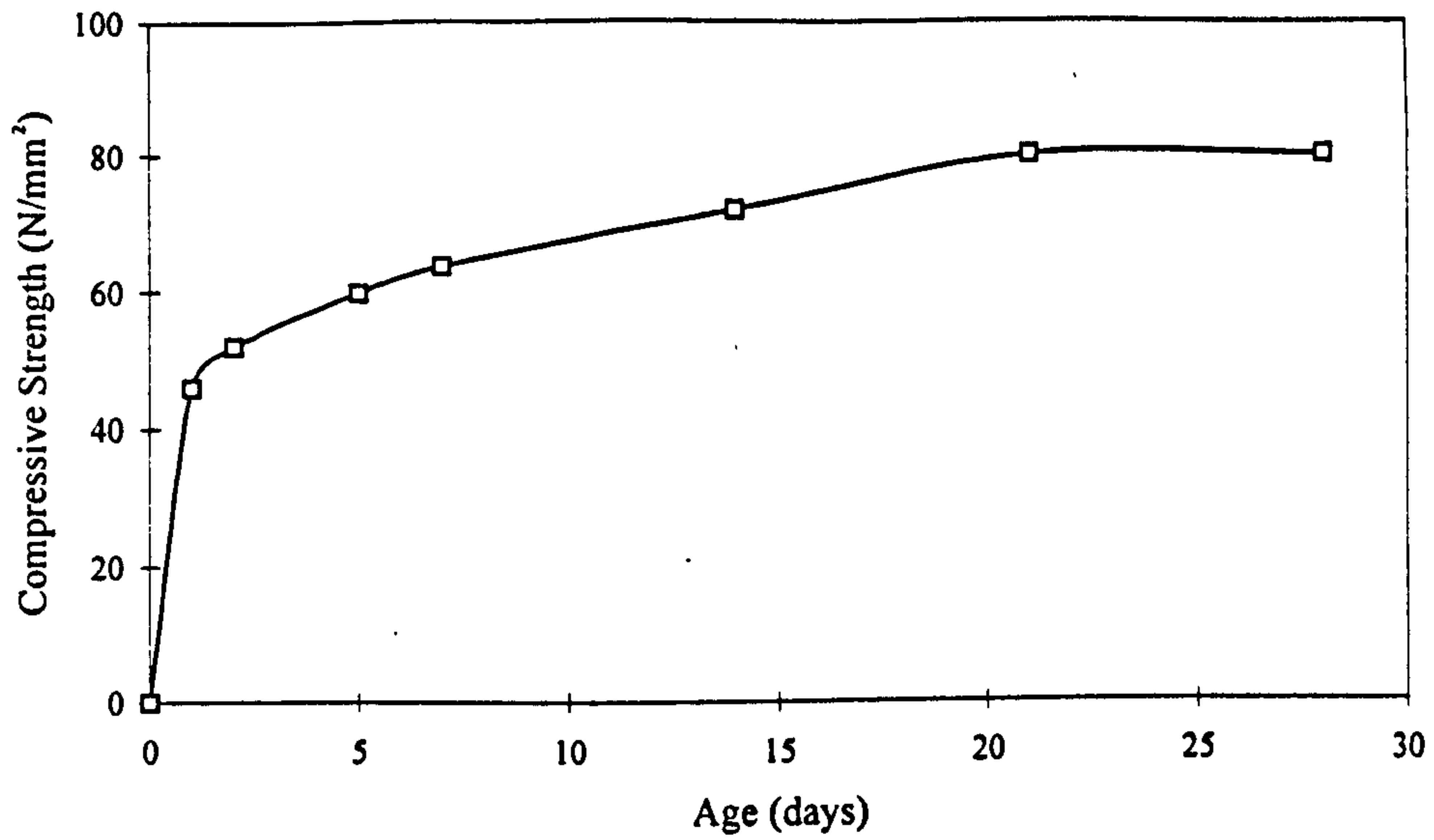


Figure 4-5 Compressive strength gain with age (PB5)

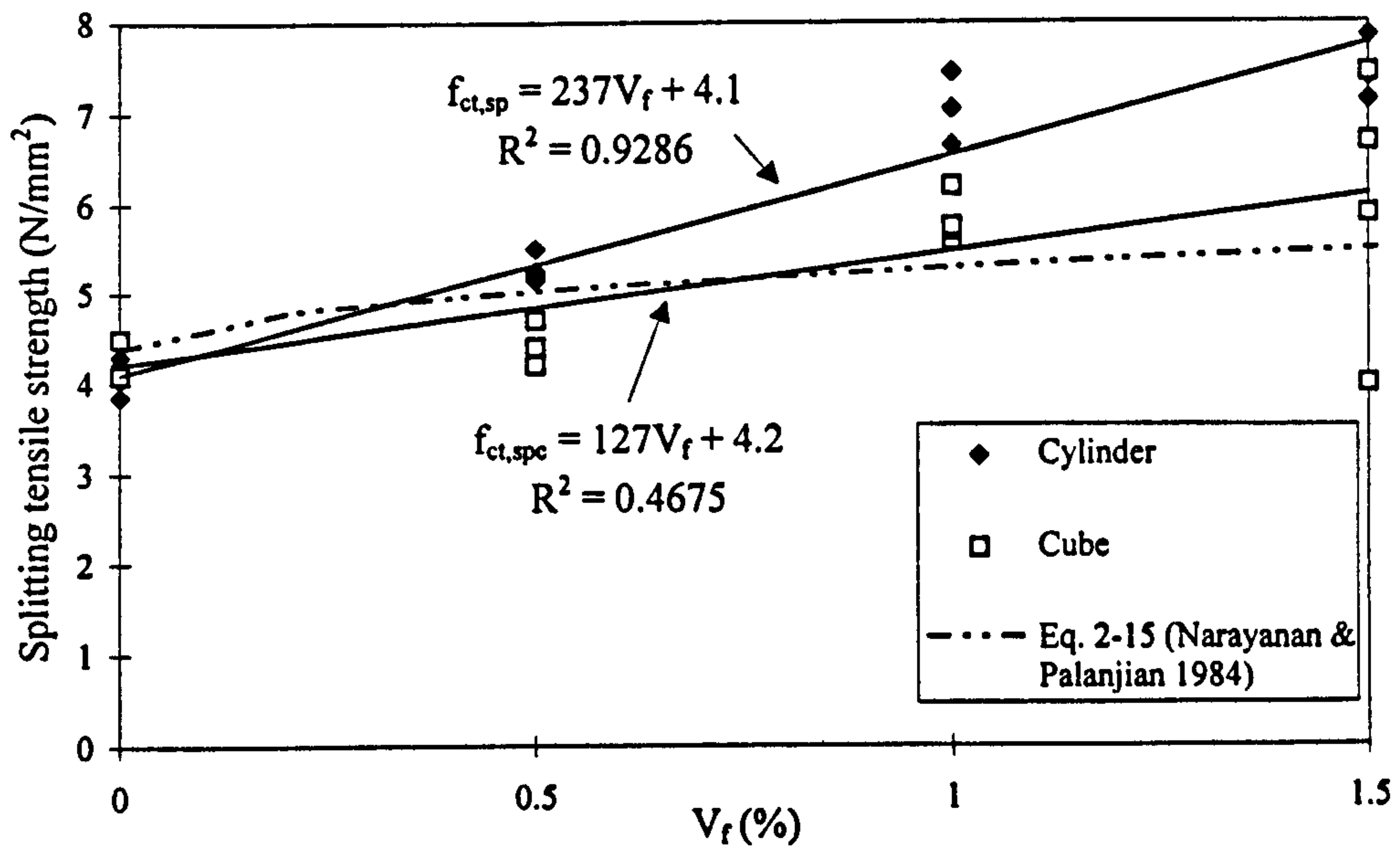


Figure 4-6 Splitting cube and cylinder tensile strength v fibre volume fraction (HS fibres)

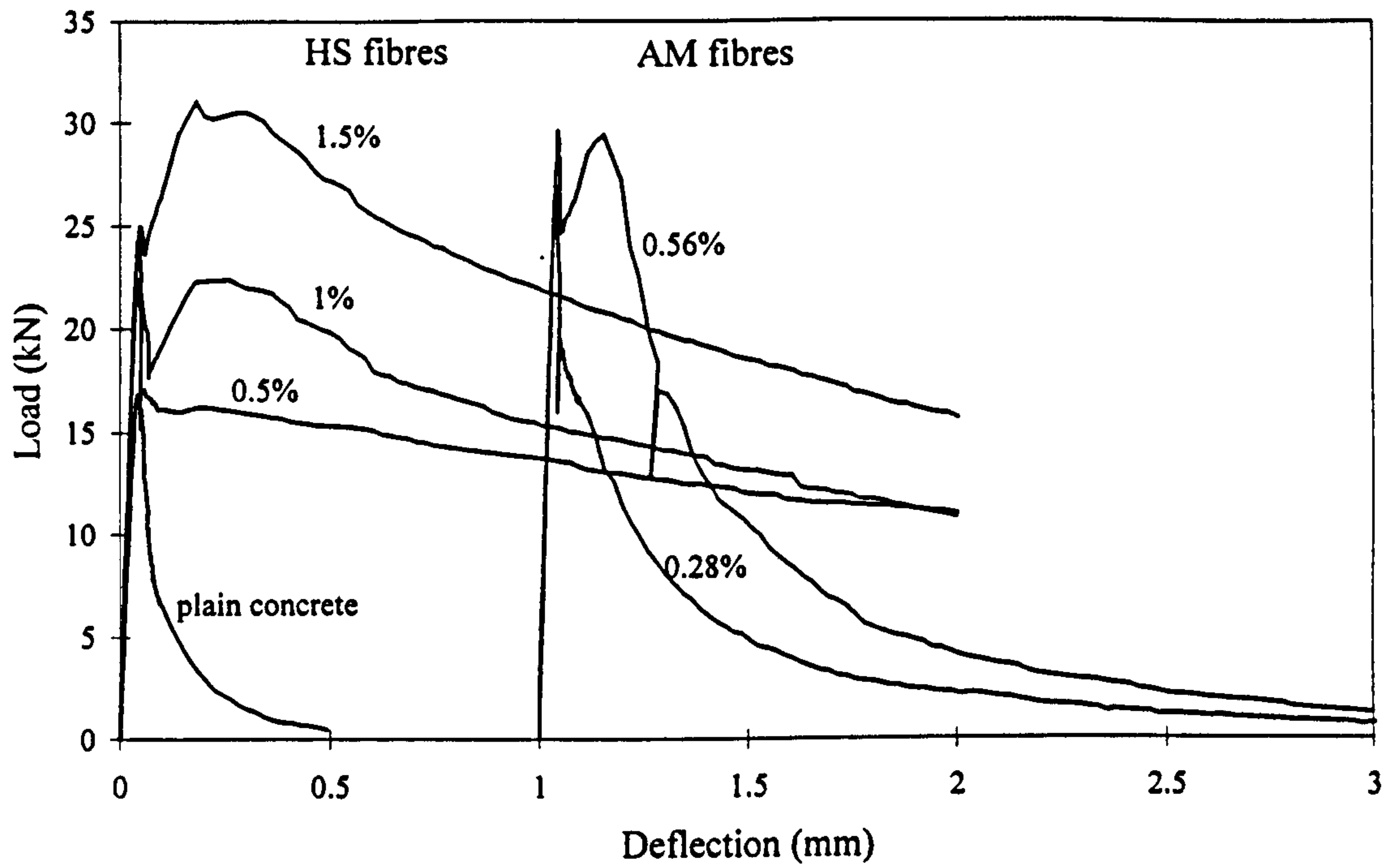


Figure 4-7 Typical load v deflection curves for both fibre types and each fibre volume fraction in flexure

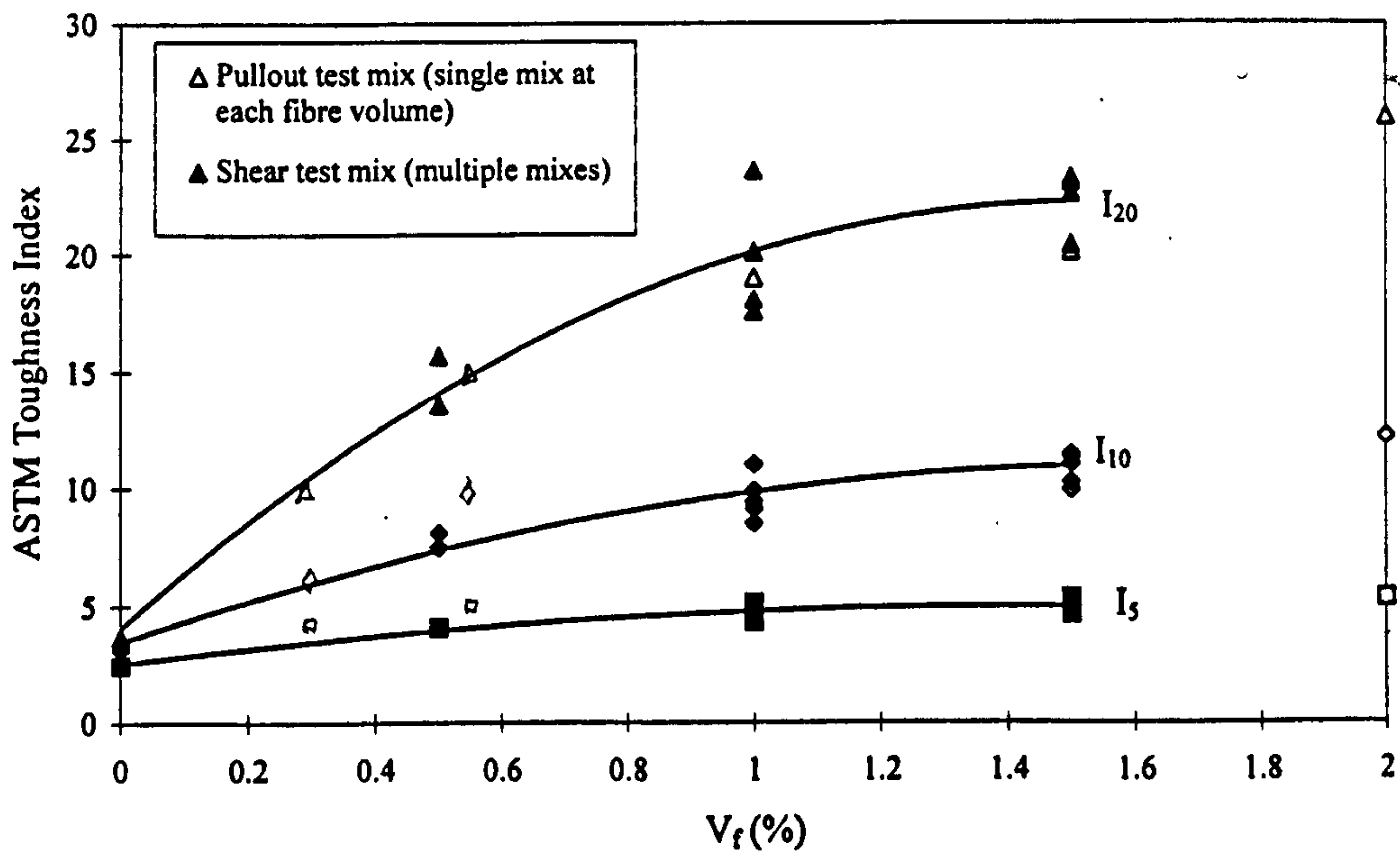
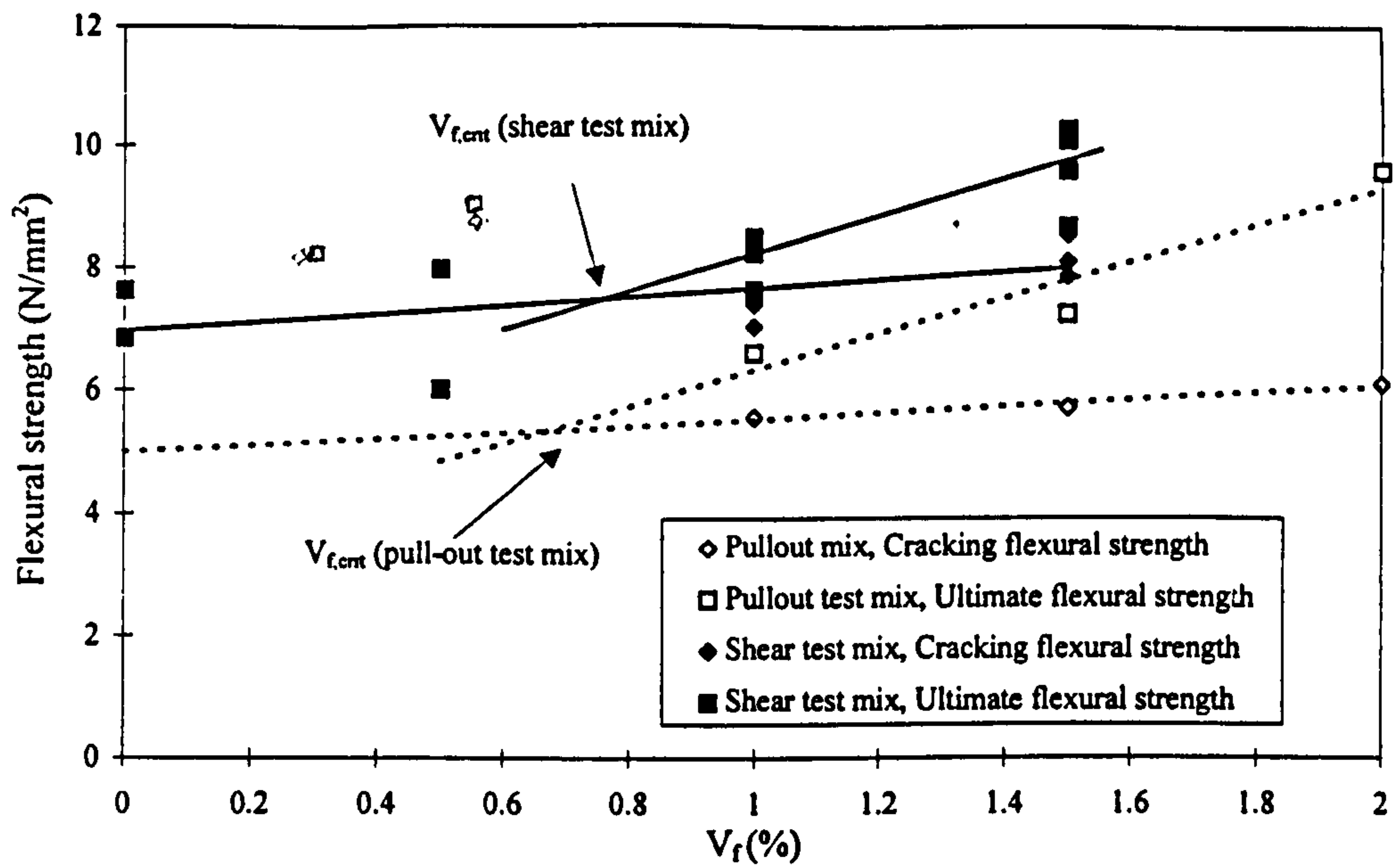


Figure 4-8 Relationship between ASTM toughness indices and fibre volume fraction



Indicates  
flex  
test  
CHS  
only  
And then

Figure 4-9 Increase in average flexural cracking strength and average ultimate flexural strength with fibre volume fraction

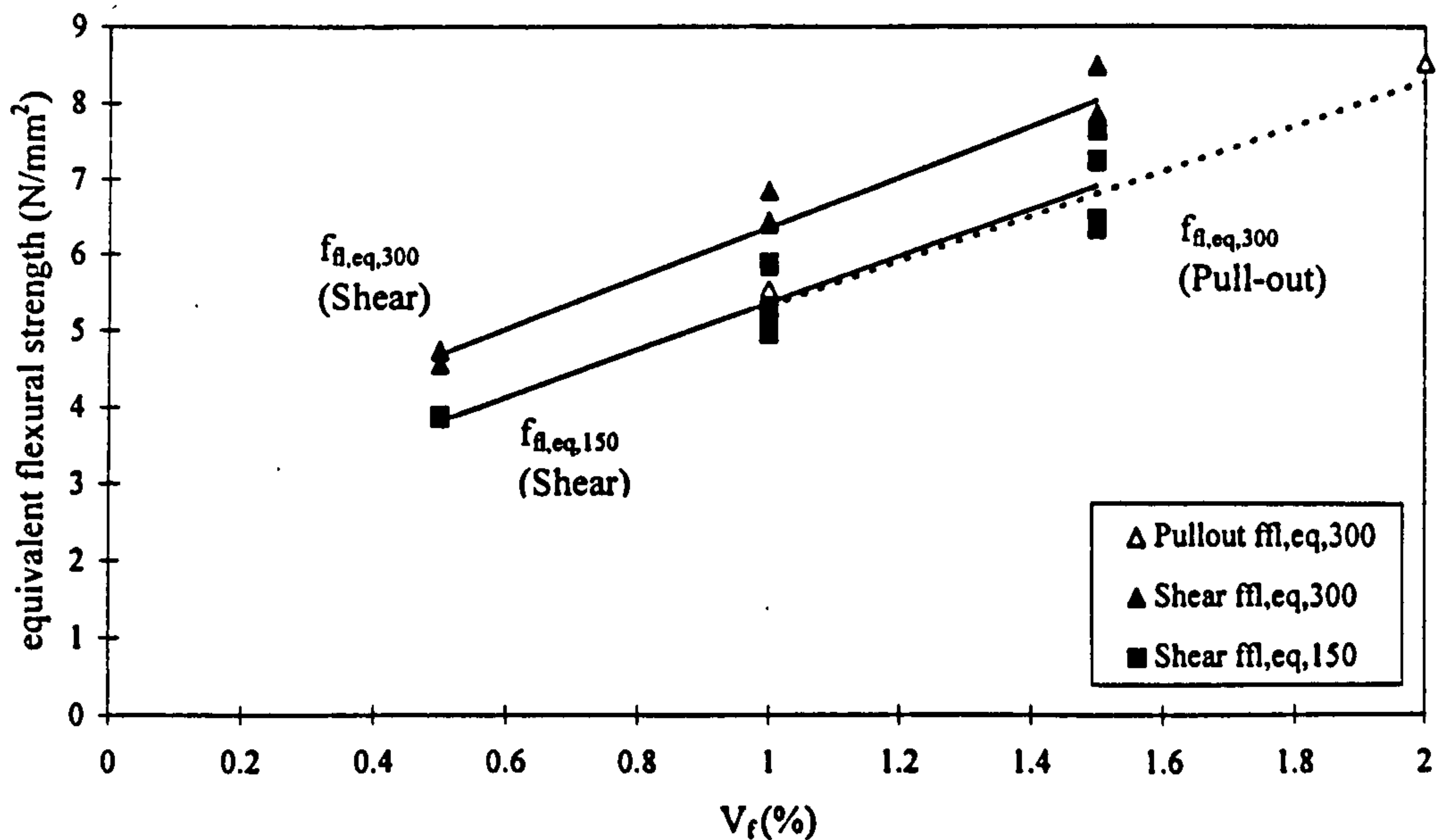
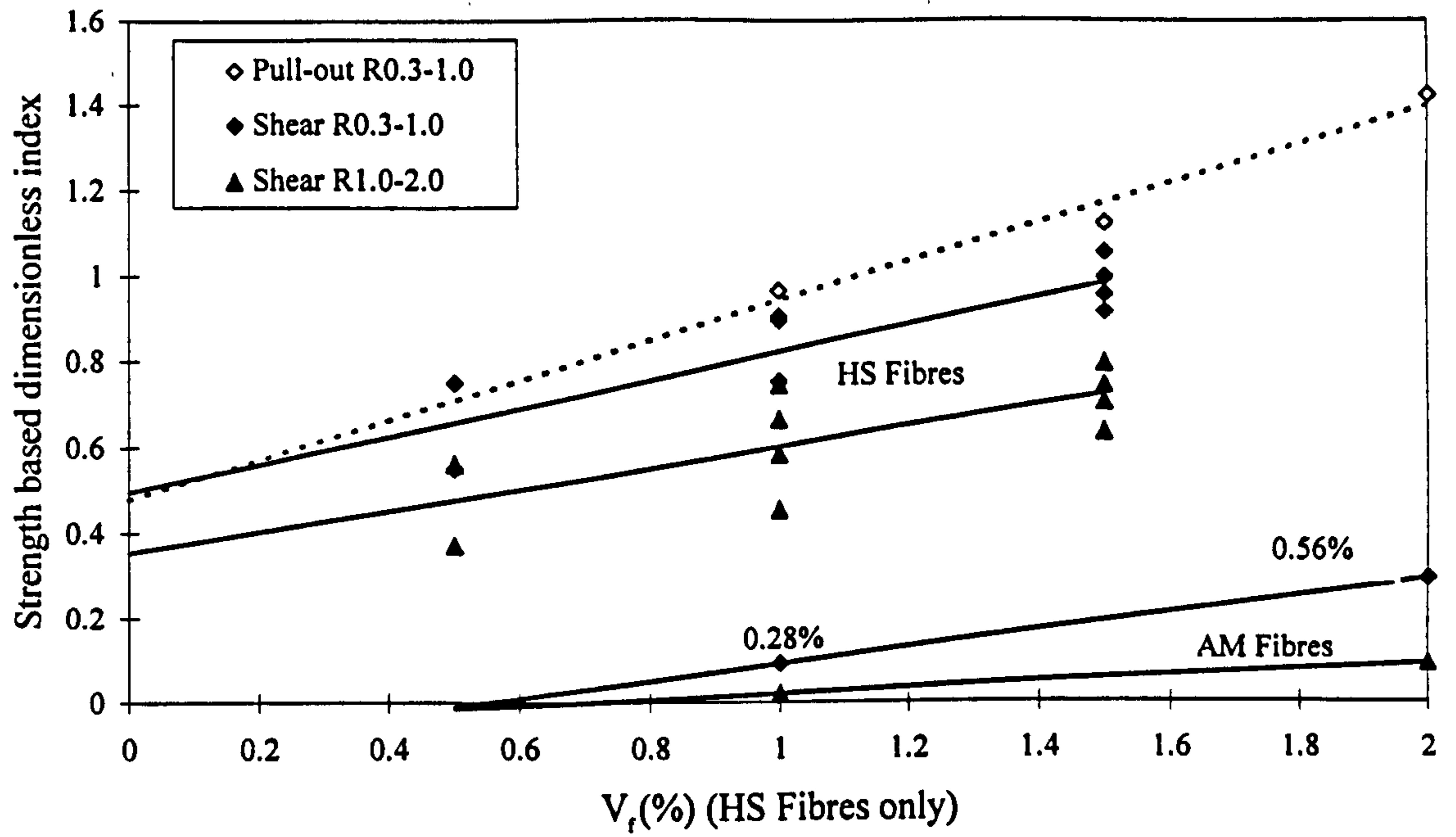
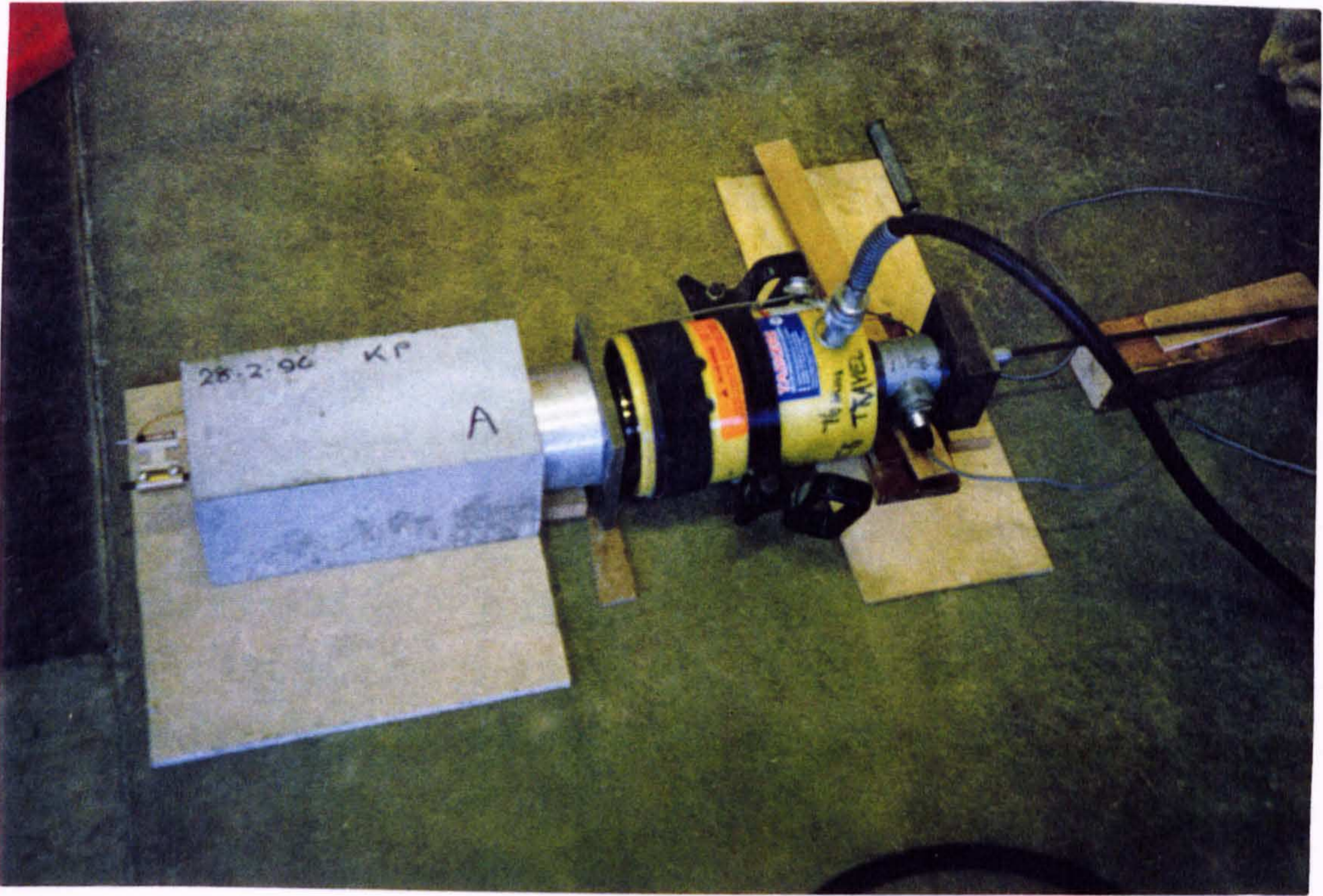


Figure 4-10 Increase in average equivalent flexural strength with fibre volume fraction



**Figure 4-11 Relationship between strength based dimensionless indices and fibre volume fraction for both fibre types**



**Plate 4-1 Small scale pull-out test arrangement**

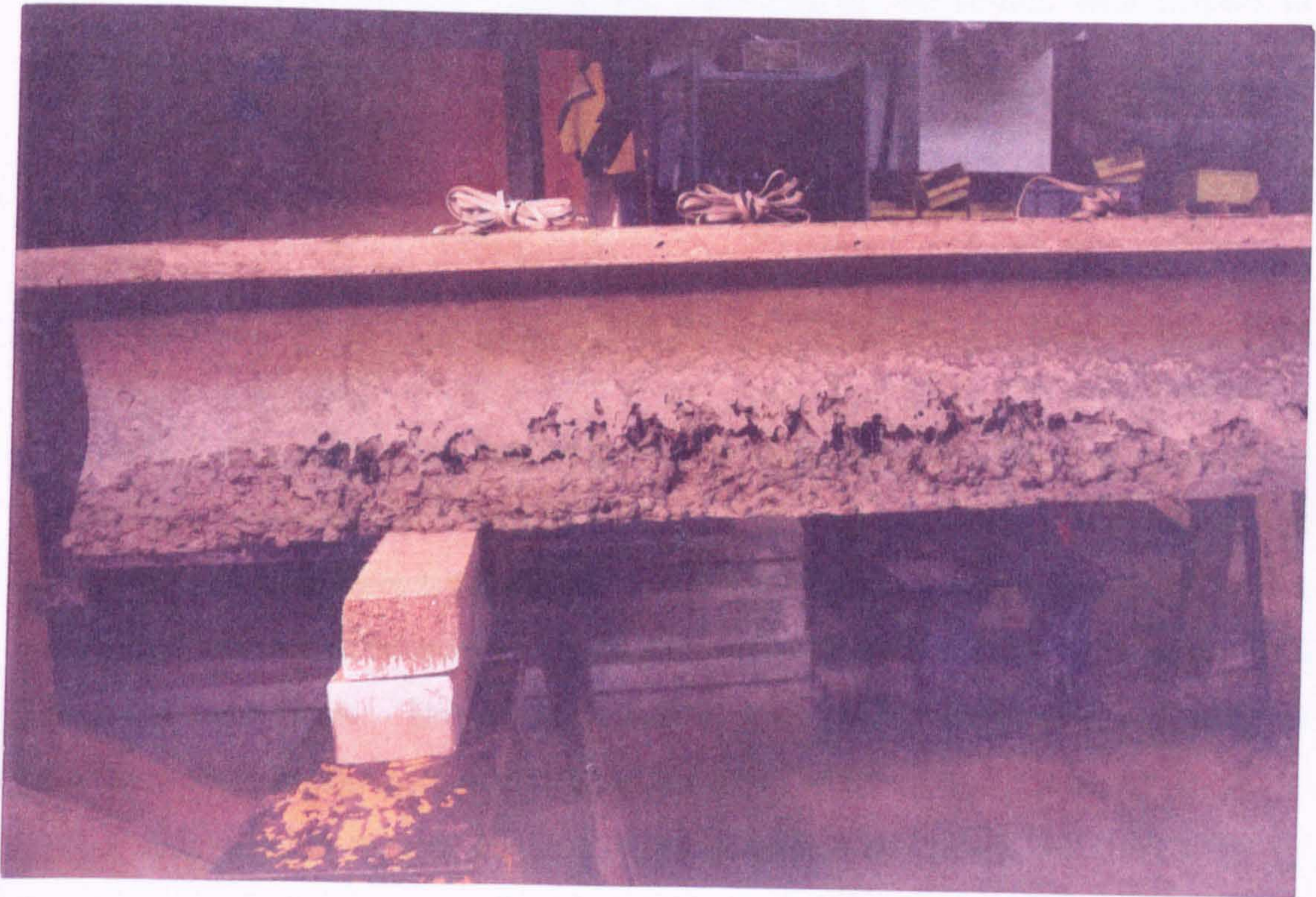


**Plate 4-2 Poor compaction of concrete in specimen PB13**



## **CHAPTER 5**

### **BOND AND SHEAR TESTS ON PFRC**

#### **5.1 Introduction**

The literature review in Chapter 3 showed that two of the most promising attributes of FRC were the bond and shear performance. However, it was reported that there is very little knowledge on the behaviour of fibres in prestressed concrete. This chapter describes two series of tests performed on concrete containing prestressing reinforcement to assess the effects of adding fibres on the bond and shear performance. The chapter presents the results of both the studies, and discusses the trends and inter-relationships involved. Analysis of the results with respect to theoretical and empirical relationships are covered in Chapter 8.

#### **5.2 Pull-Out Bond Tests**

##### **5.2.1 General**

The only previous known study of the bond between FRC and prestressing strand were carried out by Lorentsen (1985). This very brief study compared average bond stress (over a short bond length of 200 mm) against strand slip, and showed a very slight increase in the post-slip bond strength when adding 1.5% by volume of HS (40 x 0.4 mm) fibres. This study, however, gave no information on whether this improvement in bond would give rise to advantageous reductions in transfer length.

This section reports on tests using a longer specimen than that used by Lorentsen, with strain gauges placed on the strand at intervals of 200 mm along the length. With this test set-up it was hoped that the pull-out bond tests would show the

effect of differing fibre contents on the transfer length of seven-wire helical strand in concrete. An unstressed strand was used, and the method practised assumed that the distribution of the pull-out stresses during the test would be the same as that obtained at release of prestress.

Six tests were performed: two on plain concrete (notated as B-0.0A and B-0.0B) and one test each at a fibre volume fraction of 0.5%, 1%, 1.5% and 2% (notated as B-0.5, B-1.0, B-1.5 and B-2.0, respectively). 12.5 mm diameter helical strand conforming to BS 5986 (1981) was used in all the tests. The strand was of low relaxation type and had a Young's Modulus ( $E_s$ ) of 200 kN/mm<sup>2</sup>.

### 5.2.2 Test set-up

The shape and dimensions of the test specimen are shown in Figure 5-1. It was similar to the test specimen used by Lorentsen (1985) but had a much longer embedment length (1 m compared with 200 mm) so that measurements of steel strain could be made along a length of strand greater than the expected transfer length.

The test set-up is shown in Figure 5-2. Load was applied by a hydraulic jack attached to a manual pump and measured with a 250 kN load cell. Load was applied in increments of 10 kN (or smaller) up to 150 kN, beyond which increments of strand movement were used.

Strand movement between the concrete and prestressing strand was measured using linear potentiometers (LP). A pair of LPs were attached to the strand at both the loaded end and the free end (Figure 5-2).

Strains on the strand within the concrete were measured using strain gauges of 3 mm gauge length. These were attached to the strand and covered with araldite to protect from ingress of water and abrasion. Four strain gauges were used on each strand and placed at 200 mm intervals from the loaded end (as shown in Figure 5-2). Only one strain gauge was used at each point since it had previously been shown by Omar (1990) that load is distributed evenly among the strand wires when an axial load is applied. Using only four strain gauges also minimised the effect of debonding along the length of the strand due to the presence of the gauges.

Prior to casting, the strands were cleaned using cleaning agents - because rust, dirt and grease are known to affect the bond properties. This use of clean strand more readily simulated real bond conditions, since strand is used at such a rate in hollow core slab production that it is usually bright and clean prior to tensioning.

The load cell, LPs and strain gauges were attached to an Orion Delta 3350 data logger. Live plots of load versus the loaded end strand movement and the strains at 200 mm and 400 mm from the loaded face were monitored throughout the test.

## **5.3 Results of Pull-Out Bond Tests**

### **5.3.1 Axial steel strains**

Figure 5-3 shows the changes in steel strain with increasing axial stress in the strand for each of the strain gauges on specimen B-0.0A. In the early stages of loading there is effectively no increase in the measured strain in the strain gauges as the stress increases. However, at  $318 \text{ N/mm}^2$  there is a sudden change in the level of measured strain in the gauge situated at a distance of 200 mm from the loaded face. All the other strain gauges are unaffected. At  $747 \text{ N/mm}^2$  the 400 mm strain gauge records a sudden change in strain, and at 600 mm and 800 mm changes in strain are recorded at  $1183 \text{ N/mm}^2$  and  $1700 \text{ N/mm}^2$ , respectively. These sudden changes in strain are due to debonding of the strand, and can be used as an indication of the point of transfer.

Axial stress versus strain curves for each test are shown in Figure 5-4 to Figure 5-7 for each strain gauge location. At the 200 mm position (Figure 5-4) there is little difference in the stress at transfer with the change in strain being measured at about  $400 \text{ N/mm}^2$  in all but specimen B-2.0 which transferred at only  $200 \text{ N/mm}^2$ .

More noticeable differences occurred at 400 mm, where the plain specimen (B-0.0A) transfers at  $747 \text{ N/mm}^2$  whilst the FRC specimens transfer at only  $650 \text{ N/mm}^2$ . In specimen B-2.0 the strain gauge was damaged and gave no reading. Comparison with the other strain gauges on this specimen, however, suggests that it would probably have given the lowest reading. This is because at both 600 and 800

mm the plain specimen is notably the most efficient transferrer of stress, with the FRC specimens producing consistently poorer results and B-2.0 being the worse of these.

The relationship between stress and strain after transfer is linear and has a slope of between  $194 \text{ kN/mm}^2$  and  $214 \text{ kN/mm}^2$ . This is consistent with Young's Modulus of elasticity for steel in tension and suggests that after transfer and with continuing increase in load the strand is simply stretched in tension between the load point and the fully-bonded part of the strand. Any effects of friction between the strand and concrete after transfer appear to be negligible since  $E_s$  can be accurately defined from the curves.

### 5.3.2 Loaded-end strand movement

Figure 5-8 shows axial stress against strand movement at the loaded end of each test. The strand movement is not linear since it is a combination of extension and slip. It can be seen that there is little difference in behaviour between each of the tests.

At an axial stress of  $1328 \text{ N/mm}^2$ , i.e., at 75% of the characteristic tensile strength of the strand ( $f_{puk}$ ) and therefore equivalent to a probable level of prestress in typical UK production, there is no significant difference in strand movement; although the plain specimens show slightly less slip. At around  $1600 \text{ N/mm}^2$  slip appears to become the dominant form of strand movement as the displacements measured increase rapidly with little change in axial stress, although the stress carried by the specimen does increase slightly.

Only test specimens B-2.0 and B-0.0B were tested up to ultimate failure. Figure 5-9 shows stress versus loaded-end strand movement for these two tests. Cracking occurred in both specimens during the first cycle at  $500 \text{ N/mm}^2$  around the strand on the loaded face. With increasing load the cracks propagated radially out from the strand and along the length of the specimen. The nature of the cracking was the same in the plain concrete and FRC specimens, but in the latter specimens the propagation of the cracks was much slower.

Failure of specimen B-0.0B occurred in a brittle and explosive manner after a loaded-end strand movement of 9.8 mm, with the specimen splitting along the entire length. The FRC specimen was taken to a strand movement of 12.5 mm without complete failure, at which point the test was stopped for safety reasons since the axial stress was now greater than the characteristic tensile strength of the strand.

The measured movement at  $0.75 f_{puk}$  is about 2.5 mm for each of the specimens, which is greater than the pull-in values measured in hollow core slabs. However, this value of 2.5 mm resembles the expected initial end slip of a 12.5 mm strand when using Equation 3.15.

### 5.3.3 Remote-end strand movement

Axial stress against the remote-end strand movement for tests B-2.0 and B-0.0B are shown in Figure 5-10 since these were the only tests taken to sufficient levels of stress to obtain reasonable readings. Up to a stress of about  $850 \text{ N/mm}^2$  there is no strand movement. Beyond this stress there was a nominal linear strand movement until  $1700 \text{ N/mm}^2$  when debonding occurred and strand slip took place.

### 5.3.4 Transfer Length

Using the above strain gauge results there are two possible methods of calculating the transfer length. The first method is to take the axial stress at the point of the sudden change in strain or “transfer” for each of the embedment lengths, and from these values interpolate the strand length at which a stress of  $1328 \text{ N/mm}^2$  (i.e.  $0.75 f_{puk}$ ) would produce “transfer”. Figure 5-11 shows axial stress at “transfer” against embedment length for each test. It can be seen that the plain specimens produce shorter transfer lengths than the FRC specimens, and that an increase in fibre volume fraction produces an increase in transfer length. The calculated transfer lengths are shown in Table 5-1, and Figure 5-12 shows the increase in transfer length

with fibre volume fraction with a second order polynomial line of best fit drawn through the data points.

Additionally on Figure 5-11 the relationship between prestress ( $\sigma_p$ ) and transfer length as suggested by the FIP Recommendations (1992) for hollow core slabs has been drawn. Taking into account that this is a conservative design tool it produces a good approximation to the test results. The expected transfer length using the FIP equation is 790 mm and only the plain specimen and 0.5% specimen fall below this value.

The second method of calculating transfer length is to compare the measured strains at a stress of  $1328 \text{ N/mm}^2$  and define the transfer length as the embedment length where zero strain is first recorded. Figure 5-13 compares strain versus embedment length at  $1328 \text{ N/mm}^2$  for each test. It has been assumed that at the loaded-end, i.e. embedment = 0 mm the strain in the curve is equal to  $\sigma/E_s$  since there is no effective bond with the concrete at this point. The transfer length in each test has been calculated by fitting a best-fit linear plot through each data point. The results are shown in Table 5-1 and Figure 5-12 for comparison with Method 1.

The second method produces similar transfer lengths for the average of the two plain specimens as the first method; 673 mm compared with 693 mm. However, rather than suggesting a gradual increase in transfer length with increasing fibre volume fraction this second method suggests that all the FRC specimens have about the same transfer length; the average being 808 mm.

It can be concluded from the test results therefore that the addition of fibres increases the transfer length. The probable reason for this is that as the fibre content increases the workability and placeability of the concrete diminishes. This has the effect of reducing the level of concrete compaction that can be achieved around the strands leading to a higher concentration of air voids and therefore a less efficient bond with the concrete.

There is little to choose between the two methods of obtaining transfer length. The first method probably gives the most accurate answer since it more directly measures the transfer of stress. However, neither method gives the true transfer length because of inherent problems in the test set-up which makes this simulation of

prestress transfer inaccurate. The main difficulty with an un-tensioned direct pull-out test is that it fails to reproduce the so called Hoyer Effect. This is the wedging action that occurs when a tensioned strand expands laterally against the surrounding concrete as the stress is released. This contributes to the normal forces and strengthens the bond. In fact in these pull-out tests, the opposite occurs because as the stress increase the diameter of the strand reduces and so does the level of frictional bond. As such the prestress transfer lengths estimated from this approach are likely to be greater than actual transfer lengths and act as a upper-bound limit.

## **5.4 Shear Tests**

### **5.4.1 General**

The aim of this series of testing was to provide basic knowledge on the use of steel fibres as shear reinforcement in prestressed concrete, with the goal of assessing their suitability for use in prestressed hollow core slabs. Although there have been hundreds of tests on RFRC and PFRC in shear, the tests by this author were significant because:-

(a) Unlike previous tests on PFRC (Balaguru and Ezeldin 1985, Narayanan and Darwish 1987a, Tan *et al.* 1995) the beams tested in this study were fully prestressed and contained no non-prestressed longitudinal reinforcement. The previous studies had used partially prestressed concrete beams in order to prevent flexural failures and force shear to occur. However, since hollow core slabs contain no non-prestressed reinforcement and the aim of this study was to investigate the feasibility of using fibres in these slabs, it was felt that fully prestressed beams were most appropriate.

(b) Previous shear tests - on both RFRC and PFRC - had concentrated on the behaviour of beams with rectangular cross-section or I-beams. For the study presented here an x-shaped section was chosen (see Figure 5-14) because it closely simulates the rounded webs of an extruded hollow core slab. However, more

significantly, this section was also chosen for its symmetry so that the position of the critical shear crack would almost certainly occur at the neutral axis where the web is thinnest and the maximum shear stress occurs. This prevented any differences in location of the crack occurring because of variations in the strength of the matrix throughout the depth of the beam. Since the failure position could be anticipated it also enabled the growth of the crack to be monitored more carefully.

A total of 42 tests were carried out over two  $a/d$  ratios: 2.0 and 2.8. Both were expected to give web shear failures, but with the tests over the smaller  $a/d$  ratio more affected by compressive strut action. The two failure modes were therefore expected to vary slightly. Both fibre types were used, with HS fibres tested at fibre volume fractions of 0.5%, 1% and 1.5% at both  $a/d$  ratios, whilst AM fibres were only tested at  $a/d = 2.8$ ; at fibre volume fractions of 0.28% and 0.56%.

#### **5.4.2 Prestressing**

A three metre long prestressing bed was used to cast the two metre long test beams. Prestress was applied using a Pilcon Super 7 stressing jack operated by a manual hydraulic pump. The configuration of the prestressing wires is shown in Figure 5-14(a) for beams PB1-PB4 and Figure 5-14(b) for beams PB5-PB22. Throughout the tests, two types of prestressing wires both of nominal 7 mm diameter and conforming to BS 5896 (1981) were used. Table 5-2 summarises the prestressing used in each beam. In beams PB1-PB4 one single plain prestressing wire was used. For beams PB5-PB16 three wires were used, two bottom wires indented with “Belgian indentations” and a top wire kept plain to enable easy fixing of strain gauges. In later beams (PB17-PB22) all three wires were indented and where strain gauges were required the indents ground down. The implications of using three indented wires as opposed to two plus a plain wire is discussed in Section 5.5.1. Each of the 7 mm wires was stressed to 45 kN (which approximates to  $0.75 f_{puk}$ ).

Prior to stressing, three electrical resistance strain gauges were placed on the plain wire to: check the stress in the wires; calculate prestress losses; and to compute



the transfer length at release. The wires were placed at distances of 250 mm, 500 mm and 750 mm from one end of the beam. As protection against ingress of water and abrasion at release of the prestress the strain gauges were coated with two or more layers of epoxy resin.

The prestressing force was released 24 hours after casting. The release of stress was by the slow method of gradually reducing the distance between the prestressing blocks. Compared with the rapid release of stress usually practised on hollow core slabs, this was expected to lead to shorter transfer lengths.

### 5.4.3 Testing

Beams were tested at approximately 15 days after casting. Shear tests were performed at the same  $a/d$  ratio on both ends of the beam, and the two tests referred to as the A Test and B Test. The beams were simply supported over effective spans of 1900 mm and 1350 mm for the A and B tests respectively, whilst a bearing of 100 mm was used on both ends of the beam to imitate typical hollow core slab applications. The set-up for both tests is shown in Figure 5-15 and Figure 5-16.

LPs were placed under the beam to measure deflections at the mid-point (Test A only), load-point and a position close to support. Two LPs were used at each location to provide an average reading and to compensate for any twisting. The LPs close to the support were used to check for deformation due to settlement rather than deflection. In later tests LPs were also placed on top of the beam immediately above the centre point of the bearing.

Principal strains were measured by three strain gauges in the form of a 45° (rectangular) strain gauge rosette attached to the concrete surface. This rosette was positioned at mid-height of the web and at the mid-point between the load and support (see Figure 5-15).

Load was applied by a hydraulic jack attached to a manual pump and controlled with a 200 kN load cell. Fibreboard was used between the load plate and beam to compensate for the uneven surface and provide a level loading platform.

The load was applied in increments of 5 kN (or smaller) up to the first crack, with increments of deflection used after cracking. The load, deflections and strains were automatically recorded by a data logger connected to a personal computer. Live plots of load versus deflection were monitored throughout the tests.

During each of the tests, wire slip (or draw-in) was measured using a depth gauge (of accuracy 0.01 mm) to the nearest tenth of a millimetre. Small crack widths were measured using a hand-held microscope and larger crack widths using a steel tape measure.

## **5.5 Results**

### **5.5.1 Prestress and Transfer Length**

Due to the problems which resulted in the poor performance of beams PB1-PB4, some of which were attributable to the bonding of the wire, attention was paid to the prestress losses and build-up of stress in the wire and concrete (transfer length). The transfer length was particularly important since the critical zone for shear in the tests was almost certain to form in the area where full prestress had not been attained.

Each wire in the beams was initially stressed to  $0.75 f_{puk}$ , but immediately after releasing the jack there was relaxation of the grips resulting in a loss of stress to about  $0.6 f_{puk}$ .

In the 24 hour period before stripping and detensioning relaxation of the grips and wires resulted on average in a further 3% loss of stress. At detensioning, the wires were released by a slow method and assuming that the strain gauge at 750 mm from the end of the specimen was reading maximum strain, a further average loss of 6% was measured. Total stress in each wire after prestressing was therefore about  $0.55 f_{puk}$ .

Stresses for each beam at the three strain gauge locations (as a percentage of the stress at the 750 mm gauge) are shown in Figure 5-17 and Figure 5-18 for the beams with strain gauges on plain wire and indented wire, respectively. The average stress build-up curve for each fibre volume fraction has also been drawn using a

second-order polynomial line of best fit. The values for beams PB8, PB10 and PB11 have not been included since the strain gauges were damaged during casting and detensioning, due to either water ingress or abrasion. In beams PB12 and PB13 the concrete was too poorly compacted to produce sensible readings (as discussed earlier) and strain gauges were not placed on PB17. All other results have been included.

The results show that the addition of fibres significantly reduces the build-up of prestress and thereby increases the transfer length. At the theoretical critical location for shear, 207.5 mm from the end of the beam - a distance equal to half the height of the beam from the edge of the bearing (Girhammar 1992) - the prestress in the plain beams is about 70% of the full available prestress. At a fibre volume fraction of 0.5% the prestress is slightly lower at about 65%, and at 1% and 1.5% fibre volume fractions the values are as low as 45% and 25%, respectively.

Both the plain beams and 0.5% HS fibre beams produce similar transfer lengths of about 510 mm. The transfer length for the 1% fibre beams is higher (about 650 mm), whilst it is actually unclear whether the maximum prestress for the 1.5% beams has been achieved by 750 mm, as assumed. Figure 5-19 shows the actual stress achieved at 750 mm for each fibre volume fraction. The trend shown suggests that higher fibre volume fractions give lower prestress values. However, this figure should not be taken as conclusive since the values are also strongly dependant on differences in: initial stress; initial losses after removing the jack; and elastic losses before detensioning, all of which varied throughout the test programme and are independent of the type and quality of concrete used. What this figure does show is that the poor quality of transfer because of fibres is not offset by the ability of FRCs to hold greater levels of stress in the wires; and that in fact the opposite may be true.

The implication as with the pull-out bond tests is that fibres are reducing the effectiveness of the prestress which will have an effect on the shear strength, bearing strength and flexural strength (over small spans). In order to provide improved performance in shear of prestressed concrete beams - the essence of these tests - it is apparent that the fibres first have to overcome additional deficiencies created by their own addition to the mix. These lower prestress values for the FRC specimens

outlined above, reduce the theoretical shear strengths when compared with plain concrete specimens.

Figure 5-20 compares the prestress distributions given in the plain beams using plain wires and indented wires with the theoretical prestress transfer curves given by BS 8110 and Eurocode 2.

It can be seen that there is only a marginal difference in the build-up of prestress using indented wires rather than plain wires. However, in general, the maximum prestress given by the indented wires is greater than the plain wires by about 10%. For tests PB16-PB20 the overall prestress is therefore slightly greater than PB5-PB15 since all three wires were indented. But since this difference is due to just one of the three wires the prestress in PB16-PB20 is only greater by about 3%, and it can therefore be assumed that there is no significant difference between the tests. Both BS 8110 and Eurocode 2 give conservative transfer curves as expected. However, the theoretical transfer length of 546 mm given by Eurocode 2 does correspond well with the test results.

### **5.5.2 General Behaviour of Test Beams**

The failure of the beams PB5-PB22 was by web shear tension in all cases, whilst for beams PB1-PB4 flexural anchorage failure occurred. Although web shear is of most interest, the failure of the first four beams is also described.

#### **PB1-PB4**

Plate 5-1 shows a typical failure for beams PB1-PB4, and it can be seen that the failure is predominately a single crack. This single crack either occurred at a distance of about 410 mm from the edge of the bearing and propagated diagonally towards the load point (at an angle of 70°) or occurred directly under the load point and grew vertically. The two types of failure, similar in nature, were independent of the inclusion of fibres. The crack occurred initially due to flexure at a bending moment of 6.4 kNm and propagated rapidly into the compression flange. In the case of the plain beams the crack width immediately measured about 1 mm, suggesting that

the high shear stresses in the web are significant to the failure mode. Notably no other cracks form and failure is due purely to the propagation and widening of this crack. In the PFRC beams, when the crack reaches the compressive zone it diverges into many small fine cracks. Typical shear load versus gross central deflection curves are shown in Figure 5-21.

### PB5-PB22

Failure of the beams containing three prestressing wires (PB5-PB22) was by web shear tension. Plates 5-2 and 5-3 show typical plain concrete failures, and shear load versus gross deflection curves are shown in Figure 5-22 and Figure 5-23 for  $a/d = 2.0$  and  $a/d = 2.8$ , respectively, where the deflection was recorded directly under the load.

At  $a/d = 2.0$  the critical crack formed at about 100 - 120 mm from the edge of the bearing ( $h/2$ ) in the centre of the web and at its thinnest point. The crack propagated at  $40^\circ$  to  $45^\circ$  to the horizontal towards both the edge of the bearing and the load point. At  $a/d = 2.8$  the critical crack occurred at a distance of 150 mm from the edge of the bearing and propagated at an inclination of about  $30^\circ$  towards the edge of the bearing and load point. After cracking the load carrying capacity of the plain concrete beams reduces considerably which leads to an almost instantaneous failure.

PFRC beams, however, are able to resist the cracking load due to the ability of fibres to cross the shear crack and resist crack propagation and widening. A typical PFRC beam failure is shown in Plate 5-4. Shear load - deflection curves for each of the PFRC beam tests are shown in Figure 5-24 to Figure 5-31. The fibres enable the beams to carry greater loads beyond the initial cracking value, and with increasingly higher fibre volume fractions the post-cracking capacity increases in terms of both capacity and ductility. For the PFRC beams tested over  $a/d = 2.0$ , there is a further increase in the post-crack capacity at large gross deflections of about 17 mm (see Figure 5-24 to Figure 5-26). This can be attributed to dowel action.

All PFRC beams failed due to the propagation and widening of the main shear crack due to fibre pull-out and fibre breaking, in addition to some degree of crushing within the compressive zone.

In almost all the beams a further crack developed after the formation of the initial diagonal web shear crack. This crack, akin to a flexural crack (Plate 5-5), appeared across the soffit at a distance of approximately  $d$  from the edge of the bearing. The crack then grew vertically to intersect the diagonal crack. The ultimate load of each beam tended to correspond with the occurrence of this vertical crack. For the plain beams the vertical crack appeared simultaneously with the diagonal web shear crack.

In all the PFRC tests at  $a/d = 2.8$ , the extra capacity after cracking lead to the formation of flexural cracks in the areas of highest bending moment. The flexural cracks appeared at roughly the same bending moment (23 kNm) in all the beams showing that the flexural strength of prestressed concrete is little affected by the presence of fibres. No flexural cracks formed in any of the tests at the lower  $a/d$ .

### 5.5.3 Shear Capacity

The results of each test are given in Table 5-3 and Table 5-4. Two shear capacities have been defined. The first crack shear capacity ( $V_{cr}$ ) indicates the load at which diagonal cracking first occurred, and the ultimate shear capacity ( $V_{ult}$ ) refers to the highest value of shear the beam withstood.

For each of the plain prestressed beams  $V_{cr} = V_{ult}$ , as can be seen clearly in Figure 5-22 and Figure 5-23. The average shear capacity at  $a/d = 2.0$  is  $V_{cr} = 43$  kN, and at  $a/d = 2.8$  is  $V_{cr} = 34$  kN; an increase of about 25% at the lower  $a/d$ .

Figure 5-32 and Figure 5-33 compare  $V_{cr}$  with increasing fibre volume fraction for the HS fibres and AM fibres, respectively. It is clear that fibres have little effect on the cracking capacity. This is because: the direct tensile strength of concrete is little affected by such a low volume of fibres - a  $V_f$  of 1% increases the theoretical tensile strength by as little as 5% even when the fibres are perfectly aligned in the direction of the stress; and as shown in Section 5.5.1 the presence of fibres increases the transfer length, and may have a negative effect on  $V_{cr}$ .

The result of increasing  $V_f$  on ultimate shear capacity for the two fibre types is shown in Figure 5-34 and Figure 5-35. At  $V_f = 1\%$  (HS fibres) the increase in  $V_{ult}$

with respect to plain beams is 37% at  $a/d = 2.0$ , and 41% at  $a/d = 2.8$ . The increase at 0.56% (AM fibres) at  $a/d = 2.8$  is 23%.

With both fibre types at  $a/d = 2.8$  there is a tendency for the fibre influence to level off at increasing fibre volume fractions. For the HS fibres the difference between the capacities at  $a/d = 2.0$  and  $a/d = 2.8$  at both cracking and ultimate, remains effectively constant at between 25 - 30% independent of  $V_f$  (especially up to 1%). This suggests that the fibre reinforcement mechanism is essentially the same at both  $a/d$  ratios and that enhanced shear capacity at lower  $a/d$  ratios is independent of fibre addition.

The reason for the higher shear capacity at  $a/d = 2.0$  is because of the increasing effect of compressive strut action closer to the support, and the favourable effect of the support pressure occurring above the  $45^\circ$  line (Girhammar 1992).

#### 5.5.4 Ductility

In comparing the ductility of the PFRC beams with the plain beams, a relative measure based on load-based dimensionless indices has been used.

The load-based index  $V_{lim}/V_{cr}$  (see Figure 5-36) is defined as the shear load being sustained at a certain deflection in relation to the first crack shear capacity. The limiting deflections ( $\delta_{lim}$ ) chosen for this study were all arbitrarily related to the span ( $l$ ) as:  $l/150$ ;  $l/250$  and  $l/500$ .  $l/250$  is of particular interest since it relates to the limiting deflection in BS 8110 (1985) before the construction of finishes and partitions.

Figure 5-37 and Figure 5-38 show the average value of the index  $V_{lim}/V_{cr}$  against the fibre volume fraction of HS fibres for  $a/d = 2.0$  and  $a/d = 2.8$ , respectively. At  $a/d = 2.0$  it is apparent that as  $V_f$  increases the ability of the beams to carry higher loads at equal deformations increases. There is a large improvement in performance between  $V_f = 0\%$  and  $0.5\%$ , where after the improvement in ductility is less noticeable. Because of safety reasons during testing, there is no result at  $l/150$  for the plain beam tests due to the severe loss of strength and stability at large deflections. At  $a/d = 2.8$  there is a large increase in ductility for the  $V_f = 0.5\%$  beams compared with

the plain beams, but all the PFRC beams appear to have the same level of ductility. In fact at  $l/250$  the result at  $V_f = 1.5\%$  is lower than at  $1\%$ . The fact that the index  $V_{lim}/V_{cr}$  is little different for all fibre volumes shows that the continuing failure of the PFRC beams is essentially by the same mechanism and must be independent of fibres, i.e., fibre pullout at these deflections (which are large) is no longer an issue and failure is due to concrete crushing in the compressive zone and loss of bond around the strand.

By noting the points at which the curves intersect the line  $V_{lim}/V_{cr} = 1$  it can be seen that to maintain the cracking load after cracking has occurred, i.e., prevent loss of strength, it is necessary to add at least the following fibre contents: at  $a/d = 2.0$  up to a deflection of  $l/500$  and  $l/250$ , a fibre volume fraction of  $0.35\%$  and  $0.55\%$  respectively; and at  $a/d = 2.8$  fibre volume fractions of  $0.25\%$  and  $0.37\%$  for the same deflections, respectively. This suggests that a fibre volume fraction of  $0.5\%$  is particularly suitable for increasing the ductility of prestressed concrete beams. It is noticeable from these numbers that the loss of strength at  $a/d = 2.8$  is slower than at  $a/d = 2.0$  (see Section 5.5.6).

### 5.5.5 Steel Strains

Figure 5-39 to Figure 5-42 show typical shear force v steel strains for each  $V_f$ . Strains are measured using the same gauges used to assess transfer length. The shear cracks in beams tested at  $a/d = 2.0$  crossed the wire at about  $160 - 190$  mm from the end of the beam (i.e.  $60 - 90$  mm from the position of the  $250$  mm strain gauge), whilst the cracks crossed straight through the  $250$  mm strain gauge position for tests with  $a/d = 2.8$ . The  $250$  mm strain gauge was invariably damaged in the  $a/d = 2.8$  tests and was unable to produce readings after cracking. Since it is the post-crack changes in strain that are of interest, only the shear - steel strain curves for the tests at  $a/d = 2.0$  are shown. No strain gauges were placed on beam PB17 and no test was performed on the side of PB13 that contained strain gauges.

In each test there is a linear relationship between shear force and strain as the beam was loaded in the initial elastic region. At cracking there was a sudden loss of



strain as the stress in the wire was released. On each curve, the cracking shear force (as identified by the shear force-deflection curves, as well as by visual inspection) is shown. It is noticeable that in each test there was a loss in strain just prior to cracking. This shows that there is a slight debonding around the wires just prior to the shear cracks forming. It is likely that micro-shear cracks too small to make any noticeable differences to the load-deflection curve, and certainly too small to notice visually, propagated into the cement paste around the wires causing this loss in bond. It is interesting that this occurrence took place in both plain beams where it has been previously acknowledged that failure is immediate and complete once cracks form.

In the FRC beams there is a rapid but not immediate reduction in steel strain in the 250 mm strain gauge after cracking. After only a small increase in deformation to a crack width of about 0.3 mm the steel strain in most beams reduced by around 300 - 500  $\mu\epsilon$  and then remained at approximately this value whilst the shear force increased to the ultimate value. These losses equate to a loss in axial steel stress of about 60 to 100  $\text{N/mm}^2$ , which corresponds to about 33% of the probable prestress in the beams at this point prior to cracking. Since the crack is about 60 - 90 mm away from the strain gauge, and the transfer curves in Figure 5-17 suggest only a 10% increase in stress over such a length, it is clear that at the location of the crack there is not a complete loss in prestress. This is confirmed by the strain gauges at 500 mm from the end of the beam, since in every case (except PB15) the shear force - strain curve is linear showing that losses in stress due to cracking are not affecting the stress in the wires at this point. Since these strain gauges are about 310 - 340 mm from the crack (and even optimistic lower-bound estimates of the transfer lengths are about 600 mm) this shows that there cannot be complete loss of prestress at the crack.

The fact the steel strain remains relatively constant after the initial losses up to ultimate load does not necessarily mean that there is no dowel action taking place, because the strain gauge is not located where the crack crosses the prestressing wire. However, the load versus deflection curves suggest that dowel action does not take place until gross deflections of about 17 mm (towards the end of the tests, when crack widths are very large).

### 5.5.6 Crack Widths

Figure 5-43 and Figure 5-44 show shear load against maximum diagonal shear crack width for beams tested over  $a/d = 2.0$  and  $a/d = 2.8$ , respectively. It can be seen that in all cases the maximum load is achieved whilst the crack widths are still fairly small. With increasing  $V_f$  the crack width at maximum load increases slightly, but not significantly - being about 2 mm at  $V_f = 1.5\%$  and 1 mm at  $V_f = 0.5\%$ . This shows that the ability of fibres to provide additional post-cracking capacity occurs during the early stages of failure when crack widths are small. Therefore, whilst deflections may be large at ultimate load (see Figure 5-24 to Figure 5-29), fibres significantly prevent crack growth.

As previously mentioned when the plain beams first crack there is an immediate loss of load (about 50% of  $V_{cr}$ ) simultaneous with a large crack opening (about 1 mm for PB20). At a crack width of 4 mm for  $a/d = 2.8$  the capacity in the plain beams is about  $0.25 V_{cr}$  whereas in the FRC beams at  $V_f = 1.5\%$  the equivalent capacity is  $1.4 V_{cr}$ , and at  $V_f = 0.5\%$  about  $0.95 V_{cr}$ .

At a shear crack width of 0.3 mm (the serviceability limit for crack width in BS 8110, 1985) which occurs in all FRC beams prior to ultimate load, the shear capacity of the beams lies between  $V_{cr}$  and  $V_{ult}$ . At  $a/d = 2.8$ , independent of  $V_f$  (for FRC beams), the capacity is about  $0.90-0.95 V_{ult}$ , and at  $a/d = 2.0$  the capacity is between  $0.85-0.90 V_{ult}$ . This shows that even within the serviceability limits for crack width much of the additional capacity due to fibres can be utilised. The cracks probably open up more quickly at  $a/d = 2.0$  due to more explosive failures occurring as the result of the higher shear stresses involved at cracking.

### 5.5.7 Wire slip

The steel strain measurements (Section 5.5.5) show that there is a debonding of the wires just prior to the formation of the shear crack, and this corresponds with the onset of wire slip which can be measured at the end of the beam. As deformation increases the wire slip also increases. Figure 5-45 shows typical wire slip - deflection

(c- $\delta$ ) plots, showing a linear relationship between the slip and deflection. The gradient of this relationship can be taken as a measure of the bond between the concrete matrix and the wire and can be used to indicate the influence of fibres on the bonding mechanism. The lower the c- $\delta$  gradient the better the bond.

Figure 5-46 to Figure 5-49 show the relationship between the c- $\delta$  gradient and  $V_f$  for the four different load cases - combination of two a/d ratios and two spans. The results are also presented in tabular form in each of the figures, with additionally the average c- $\delta$  gradient of all the beams and the average c- $\delta$  of just the FRC beams calculated.

In eleven of the twelve cases the average c- $\delta$  gradient of the FRC beams is higher than that when the plain beam is also included. This suggests that there is a reduction in the bond quality when adding fibres and is most aptly demonstrated in Figure 5-47 (a/d = 2.0, B test) where the c- $\delta$  gradient of the wires in the FRC specimens are similar and consistently greater than that of the wires in the plain beam. In other cases, however, the higher average value of the FRC specimens is due to peculiarly high values at one individual fibre volume fraction. For the B tests over a/d = 2.8 (Figure 5-49) both 0.5% specimens have higher c- $\delta$  gradients, and for the A tests at a/d = 2.0 (Figure 5-46) the anomalous fibre volume fraction is 1% - significantly in both cases the same behaviour is shown by the two specimens tested.

The reason for higher c- $\delta$  gradients in the FRC beams is probably because of poorer compaction due to the presence of fibres as discussed in Section 5.4.2. It cannot be explained why differences which occur in both specimens in the A test, for example, should not appear in the B test. The inference is that the c- $\delta$  relationship is not purely a measure of the bond quality but is also partly affected by differences in the failure mechanism of different test set-ups. It would appear that that fibres do have a slightly detrimental effect on the bond between the prestressing wires and concrete.

**Table 5-1 Calculated transfer lengths from pull-out tests**

Specimen No.	$V_f$ (%)	Method 1	Method 2
B-0.0A	0	665 mm	652 mm
B-0.0B	0	720 mm	694 mm
B-0.5	0.5	770 mm	822 mm
B-1.0	1	820 mm	805 mm
B-1.5	1.5	820 mm	814 mm
B-2.0	2	845 mm	792 mm

**Table 5-2 Schedule of prestressed beam tests**

Beams	Fibre type	$V_f$ (%)	a/d	prestress
PB1 & PB2	-	0	3.0	P
PB3 & PB4	HS	0.5	3.0	P
PB5 & PB7	-	0	2.8	P+2C
PB6 & PB8	HS	0.5	2.8	P+2C
PB9 & PB11	HS	1	2.8	P+2C
PB10 & PB12	HS	1.5	2.8	P+2C
PB13 & PB15	HS	1.5	2.0	P+2C
PB14 & PB16	HS	1	2.0	P+2C
PB17 & PB19	HS	0.5	2.0	3C
PB18 & PB20	-	0	2.0	3C
PB21	AM	0.28	2.8	3C
PB22	AM	0.56	2.8	3C

P = 7 mm plain wire, C = 7 mm indented wire

Table 5-3 Shear Test Results  $a/d = 2.8$

$V_r$ (%)	Fibre type	Beam	$\sigma_{cp}$ (N/mm <sup>2</sup> )	$V_{cr}$ (kN)	Average $V_{cr}$ (kN)	$V_{ult}$ (kN)	Average $V_{ult}$ (kN)	$V_{ult}$ (N/mm <sup>2</sup> )
0		PB5A	4.3	31.3	33.6	31.3	33.6	5.2
		PB5B	4.3	35.4		35.4		5.8
		PB7A	5.7	33.5		33.5		5.5
		PB7B	5.7	34.3		34.3		5.6
0.5	HS	PB6A	6.1	34.0	33.9	46.3	42.4	7.6
		PB6B	6.1	34.0		45.5		7.5
		PB8A	4.9	36.0		42.3		7.0
		PB8B	4.9	31.5		35.5		5.8
1	HS	PB9A	5.8	36.0	35.0	57.7	47.3	9.5
		PB9B	5.8	35.0		48.3		7.9
		PB11A	5.0	34.0		39.6		6.5
		PB11B	5.0	35.0		43.7		7.2
1.5	HS	PB10A	5.0	32.5	33.5	44.5	48.1	7.3
		PB10B	5.0	34.5		51.7		8.5
		PB12B	5.4					
0.28	AM	PB21A	5.4	33.0	35.0	38.4	39.7	6.3
		PB21B	5.4	37.0		41.0		6.7
0.56	AM	PB22A	5.4	39.0	34.8	43.3	41.2	7.1
		PB22B	5.4	30.5		39.1		6.4

For calculation of  $v_{ult}$ ,  $I_b/A_y$  taken as 6082 mm<sup>2</sup>

Table 5-4 Shear Test Results  $a/d = 2$

$V_f$ (%)	Fibre type	Beam	$\sigma_{cp}$ (N/mm <sup>2</sup> )	$V_{cr}$ (kN)	Average $V_{cr}$ (kN)	$V_{ult}$ (kN)	Average $V_{ult}$ (kN)	$V_{ult}$ (N/mm <sup>2</sup> )
0		PB18A	5.7	40.7	42.7	40.7	42.7	6.7
		PB18B	5.7	39.0		39.0		6.4
		PB20A	5.3	48.5		48.5		8.0
		PB20B	5.3	42.7		42.7		7.8
0.5	HS	PB17A	5.4	40.5	42.5	57.7	53.1	6.7
		PB17B	5.4	41.5		50.6		6.7
		PB19A	5.4	44.5		56.0		6.6
		PB19B	5.4	43.5		48.0		6.6
1	HS	PB14A	5.1	43.5	45.0	55.9	58.4	8.3
		PB14B	5.1	48.5		61.1		8.3
		PB16A	5.0	42.0		54.5		7.8
		PB16B	5.0	46.0		62.1		7.8
1.5	HS	PB13A	5.2	44.5	48.8	61.9	65.1	9.1
		PB15A	5.1	51.0		66.2		8.6
		PB15B	5.1	51.0		67.3		8.6

For calculation of  $v_{ult}$ ,  $I_b/A_y$  taken as 6082 mm<sup>2</sup>

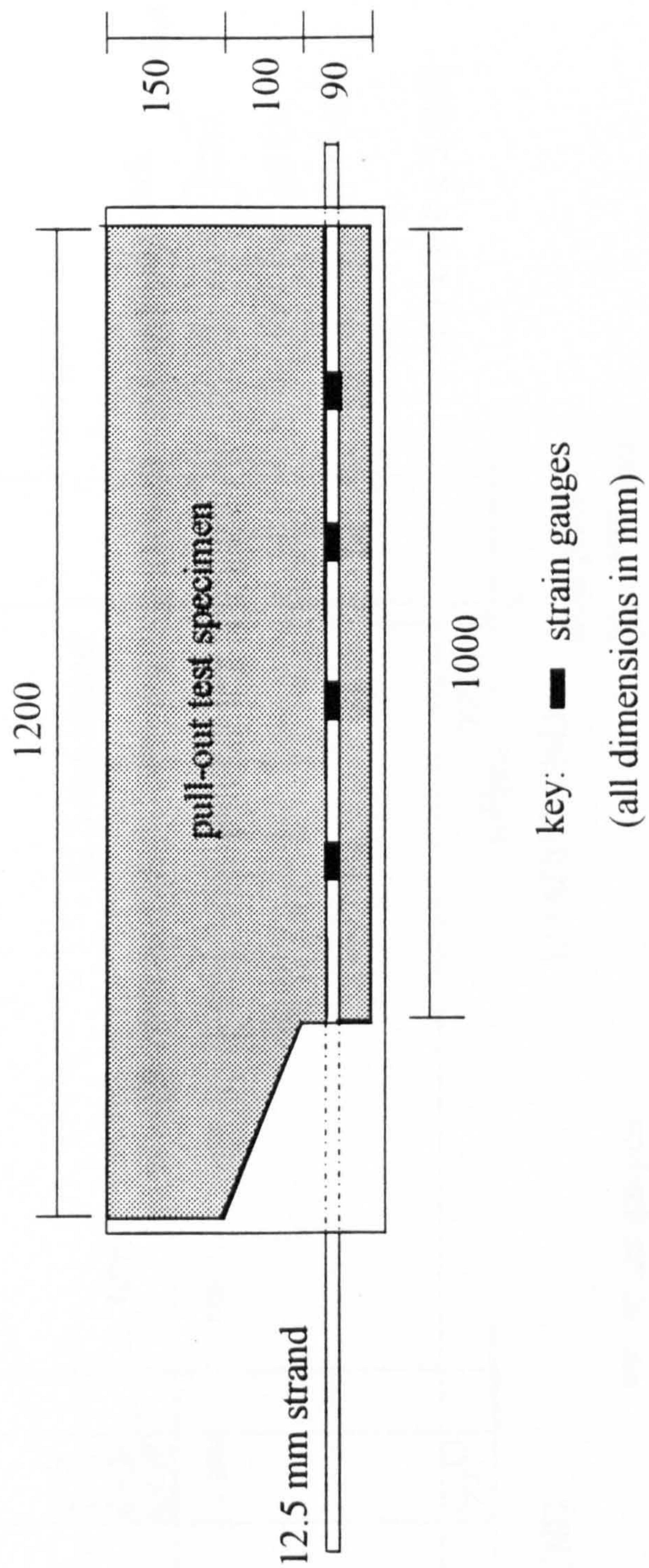


**Figure 5-1 Test specimen for Pull-out tests**

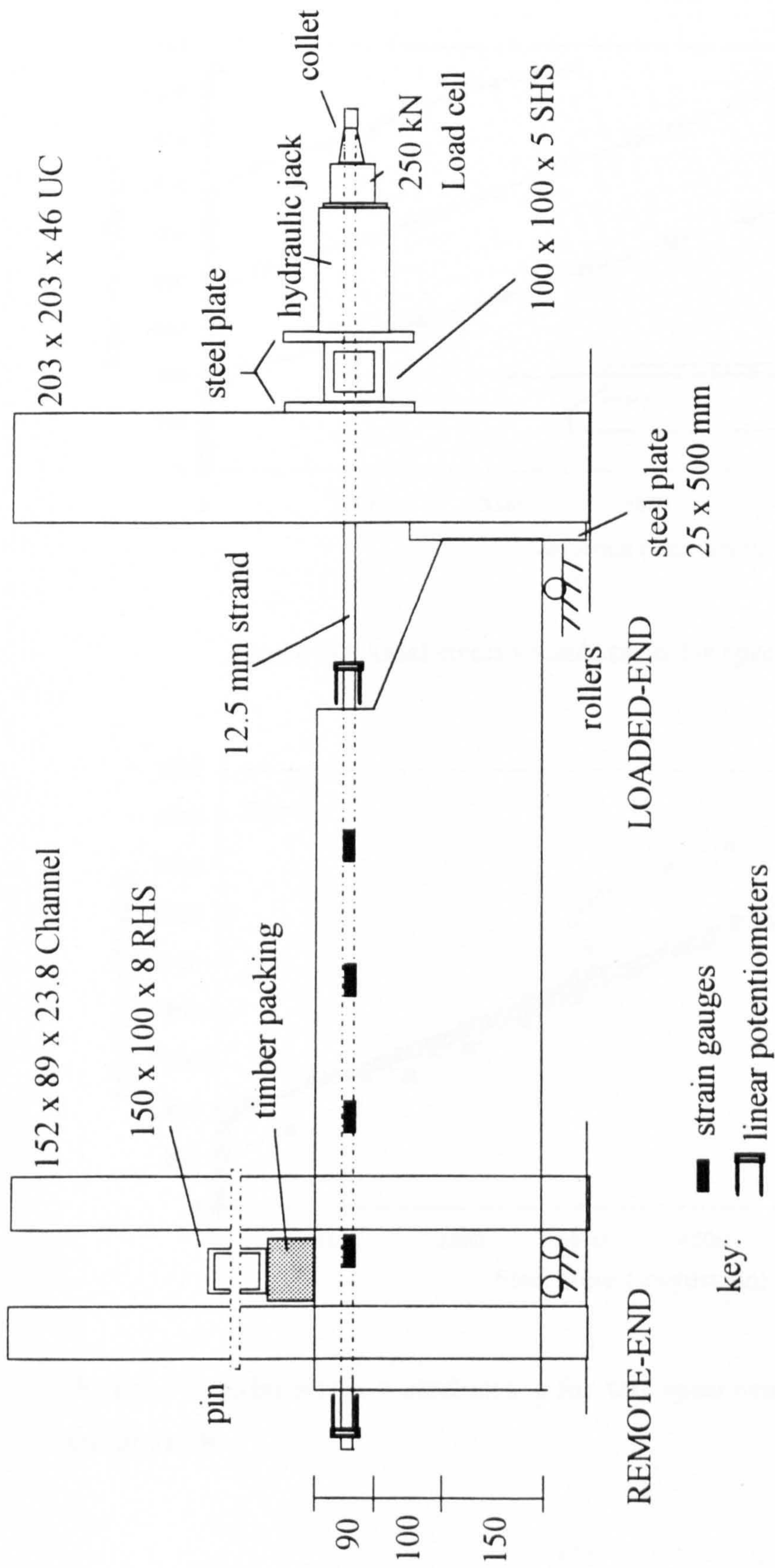


Figure 5-2 Pull-out test arrangement



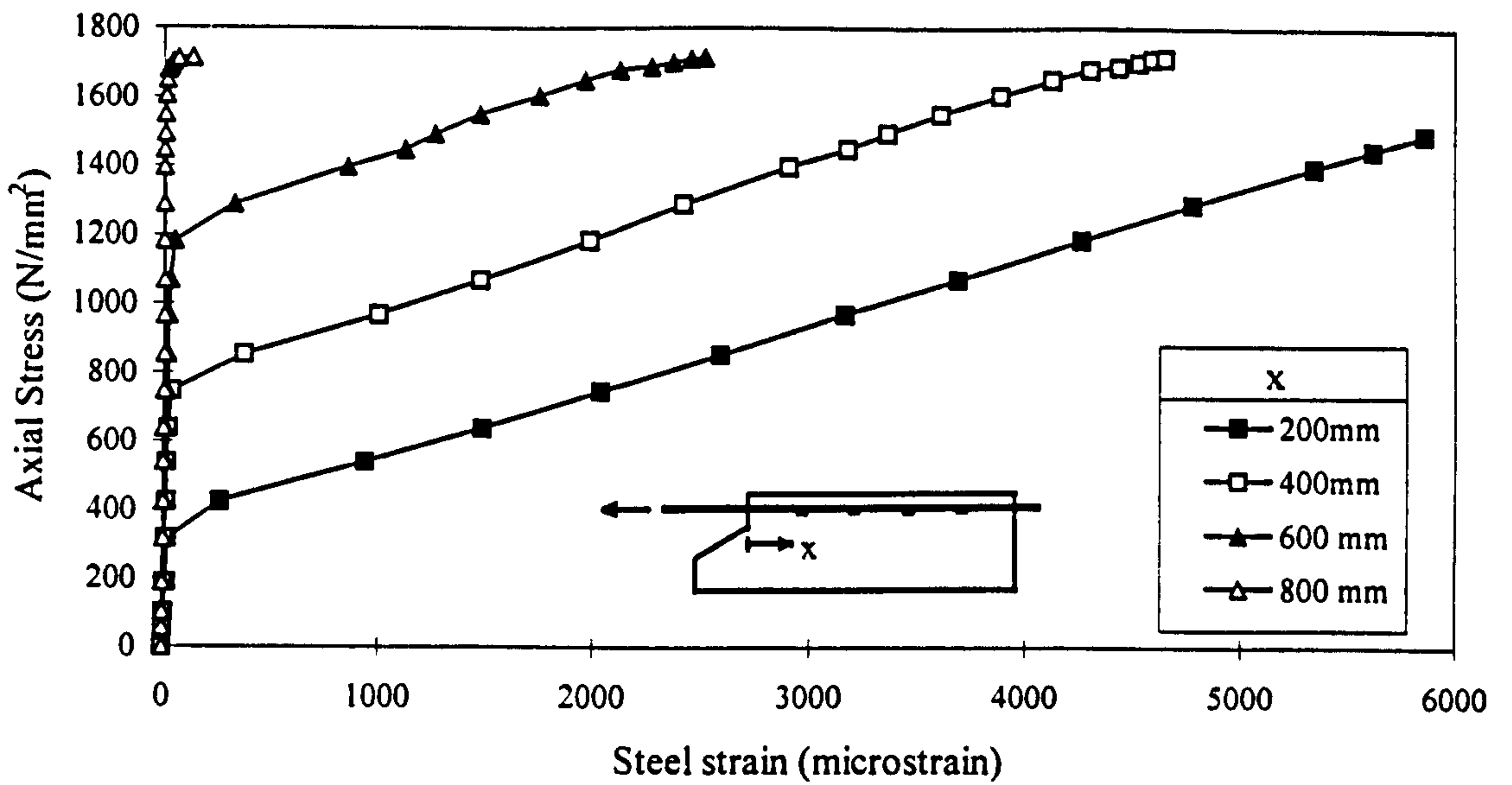


Figure 5-3 Axial stress v steel strain for specimen B-0.0A

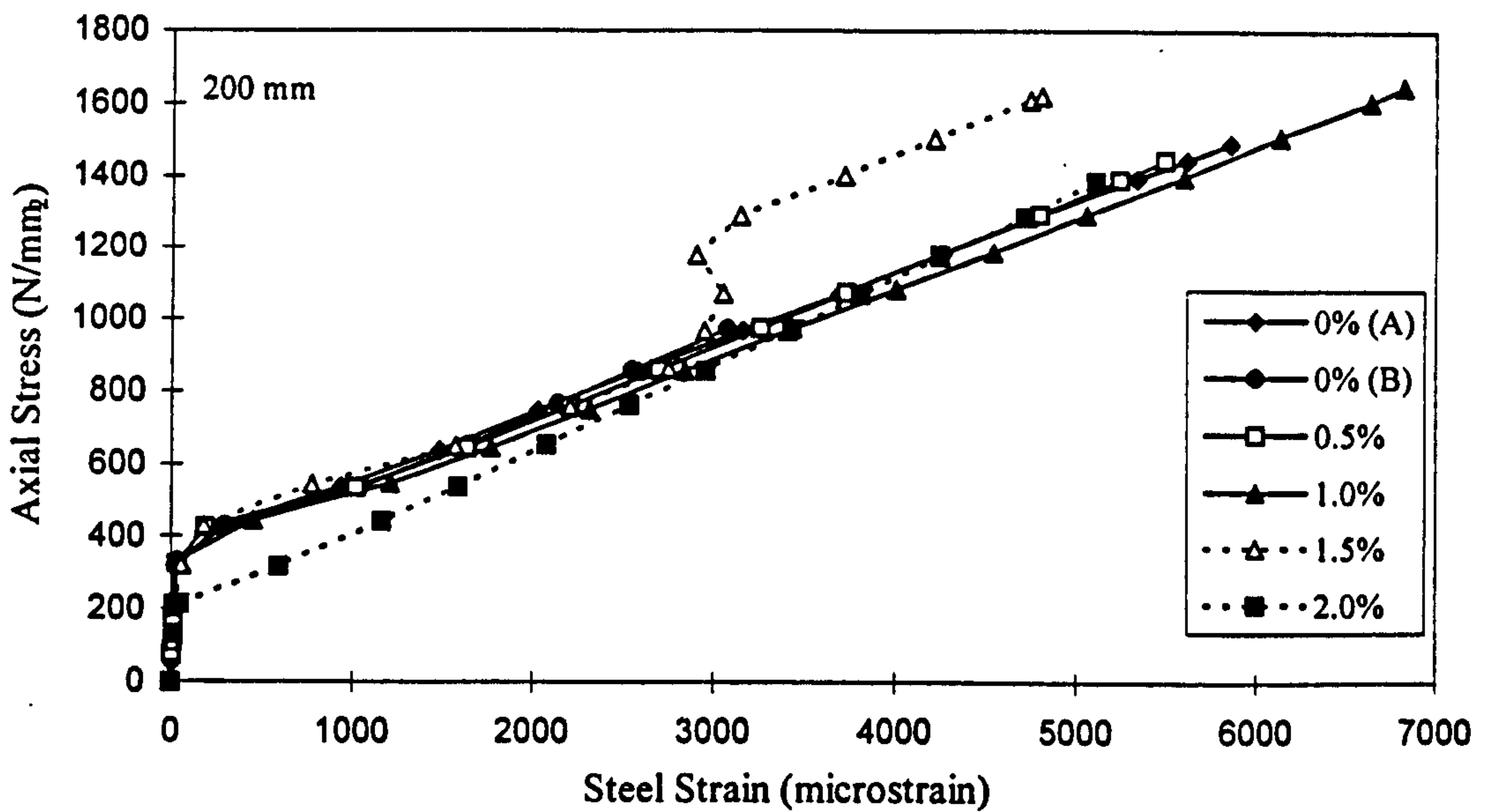


Figure 5-4 Axial stress v steel strain for test specimens at 200 mm embedded strain gauge

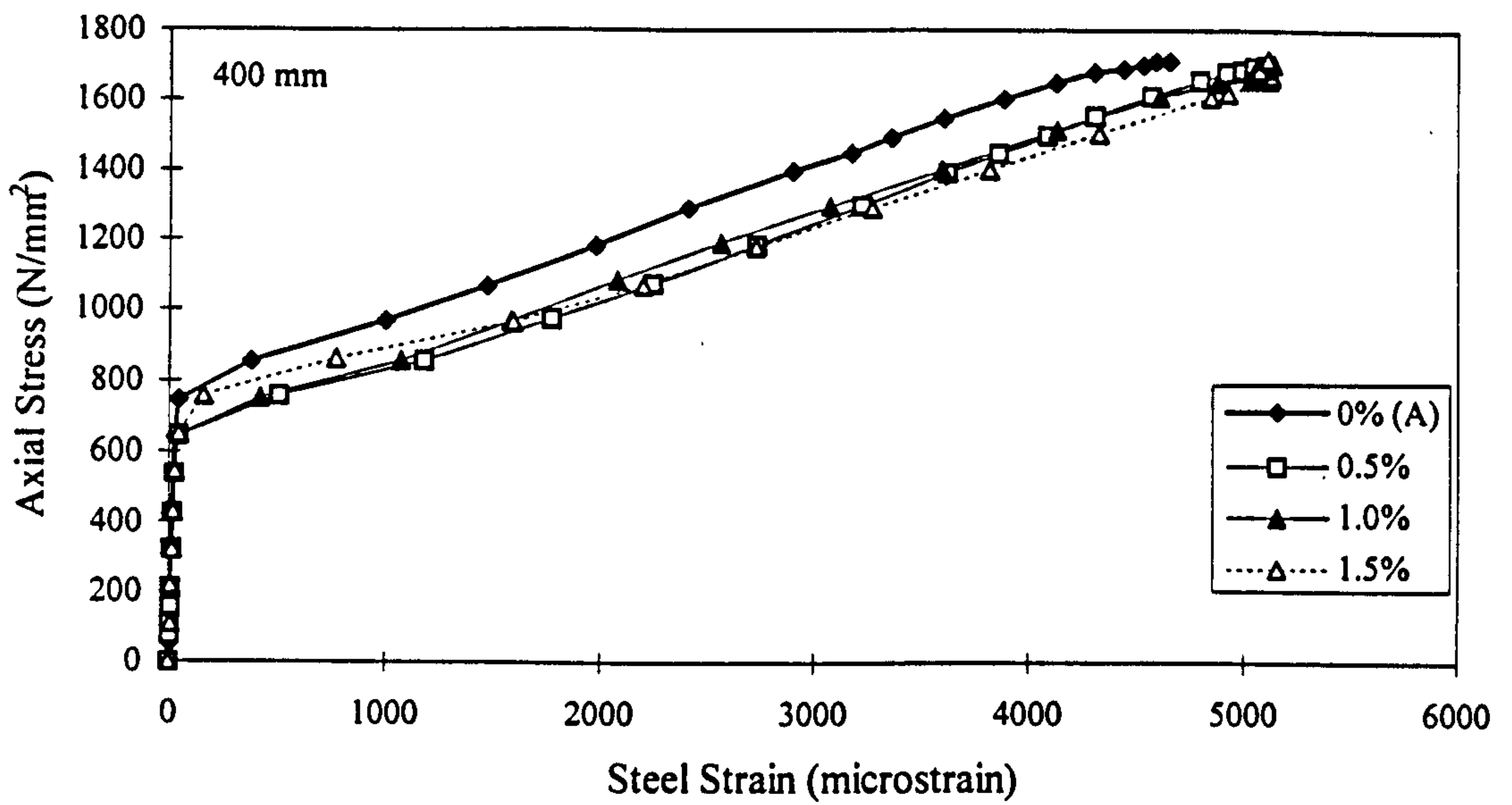


Figure 5-5 Axial stress v steel strain for test specimens at 400 mm embedded strain gauge

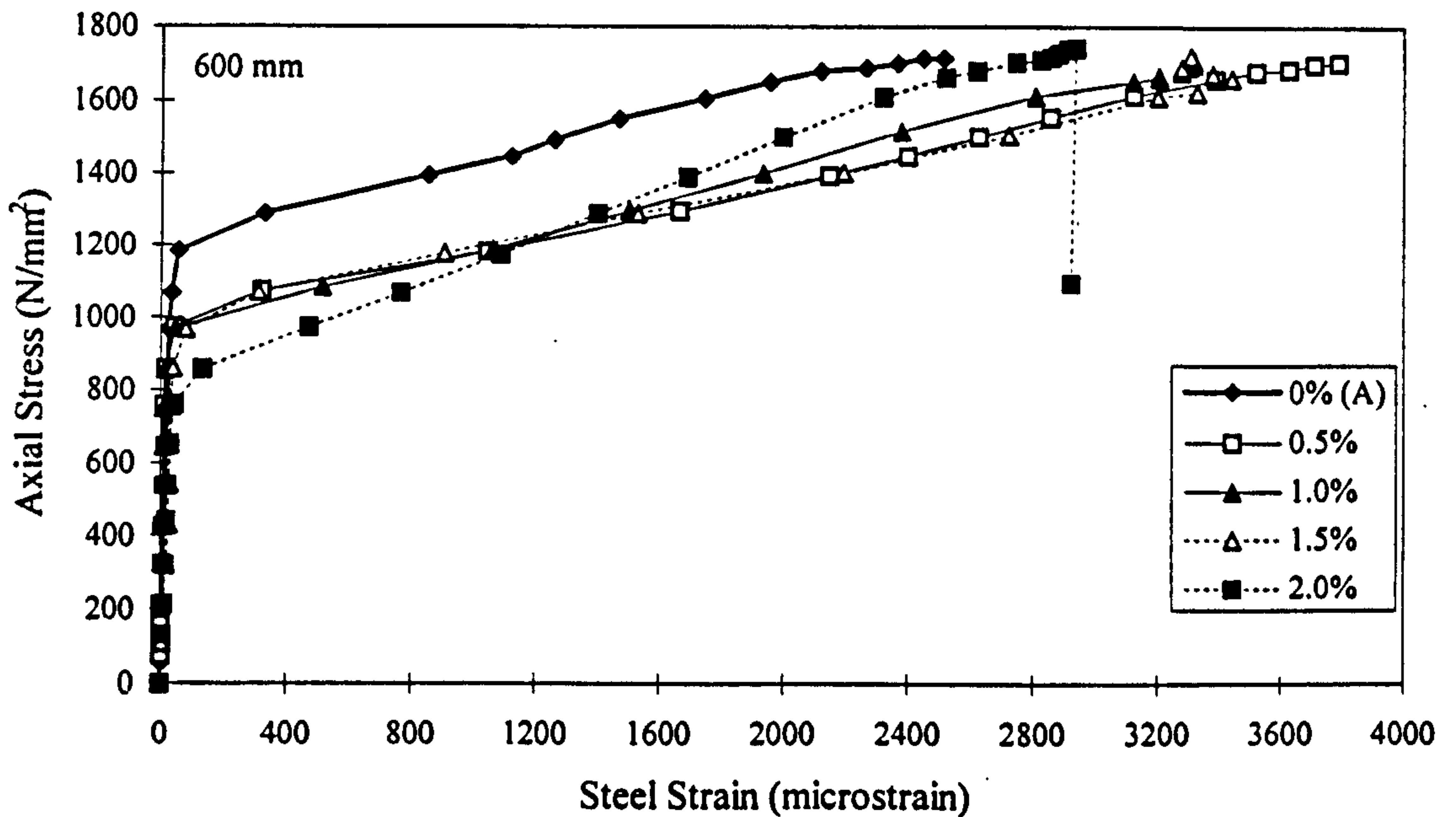


Figure 5-6 Axial stress v steel strain for test specimens at 600 mm embedded strain gauge

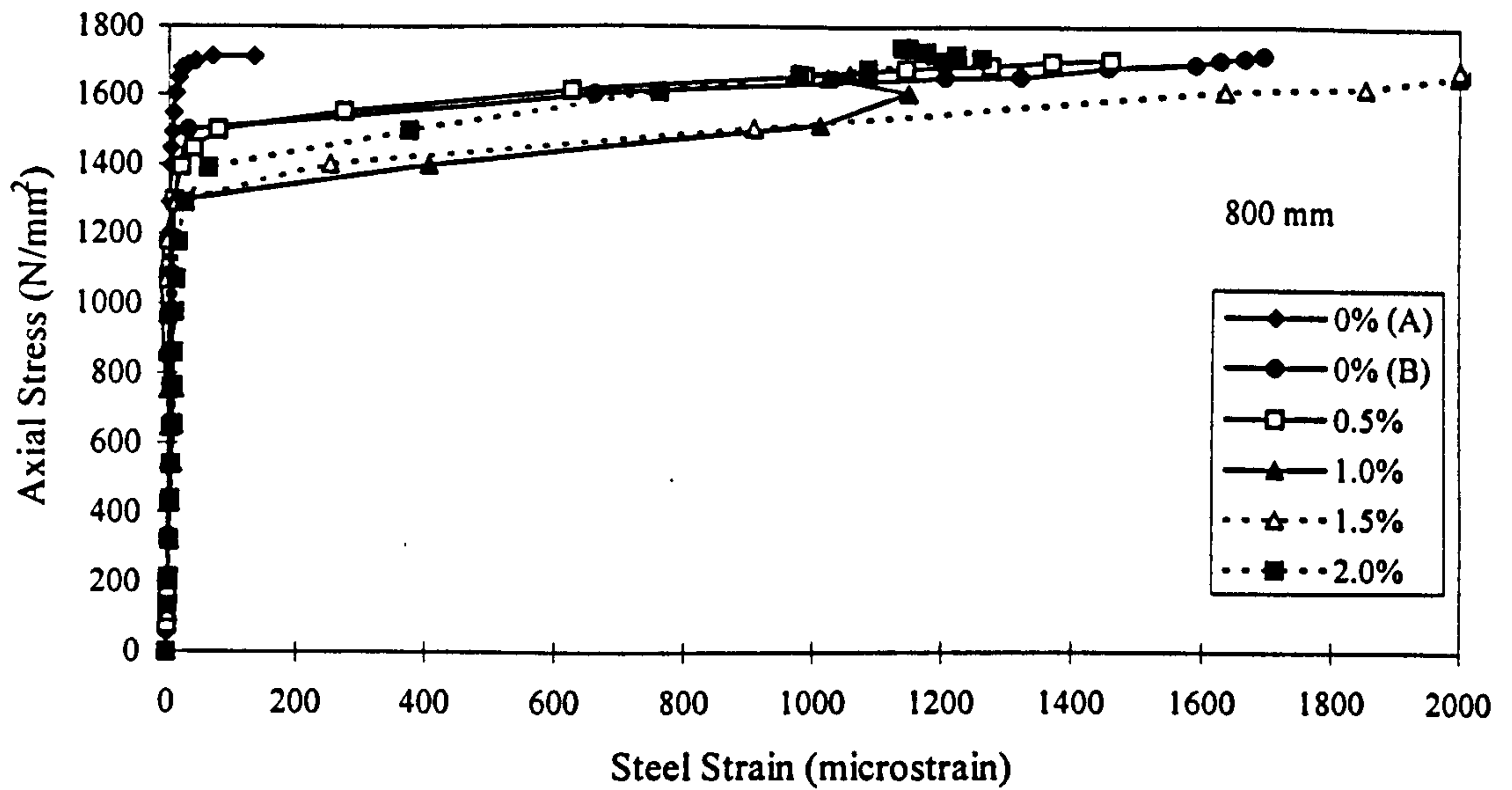


Figure 5-7 Axial stress v steel strain for test specimens at 800 mm embedded strain gauge

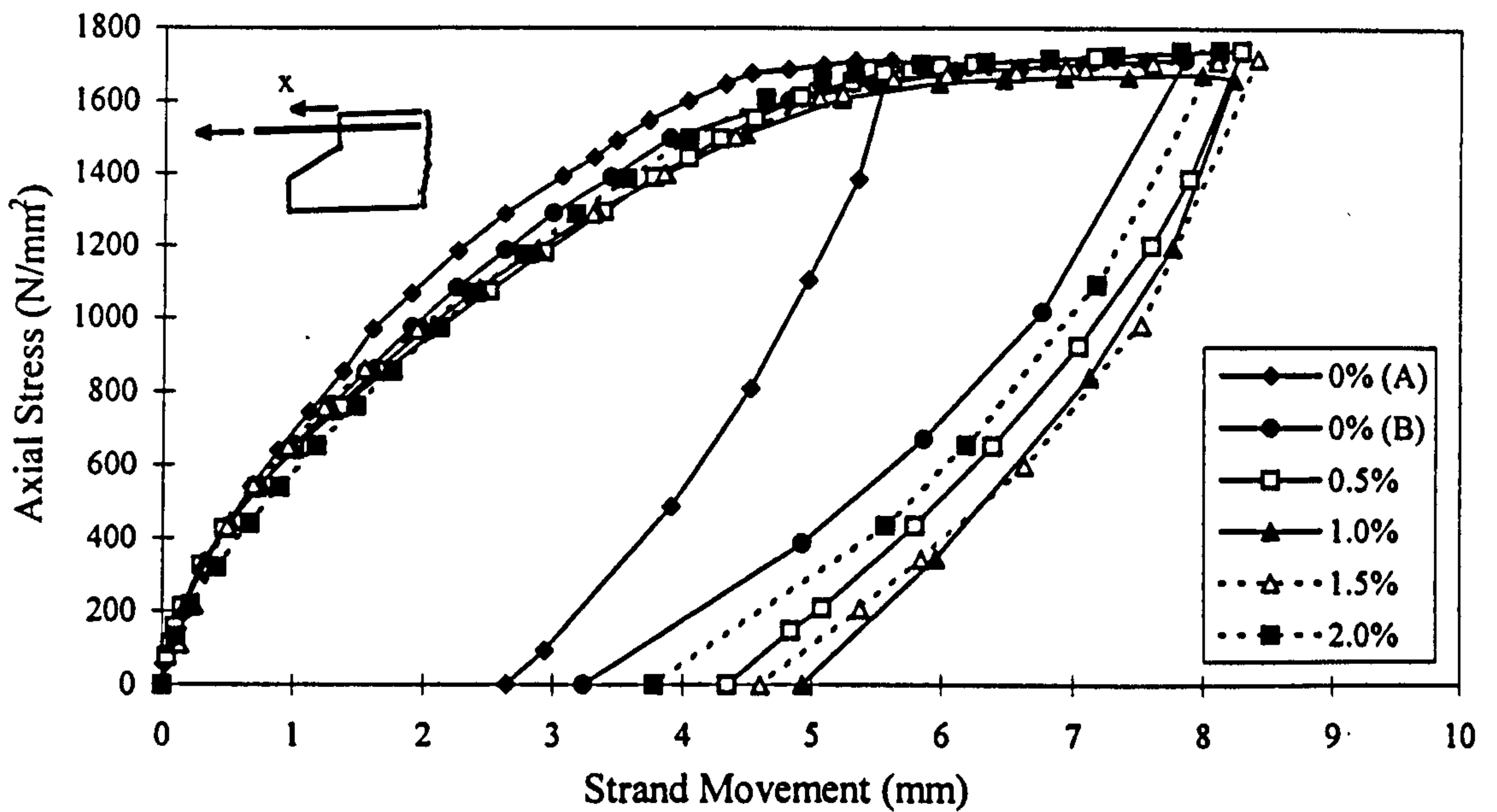


Figure 5-8 Axial stress v loaded-end strand movement

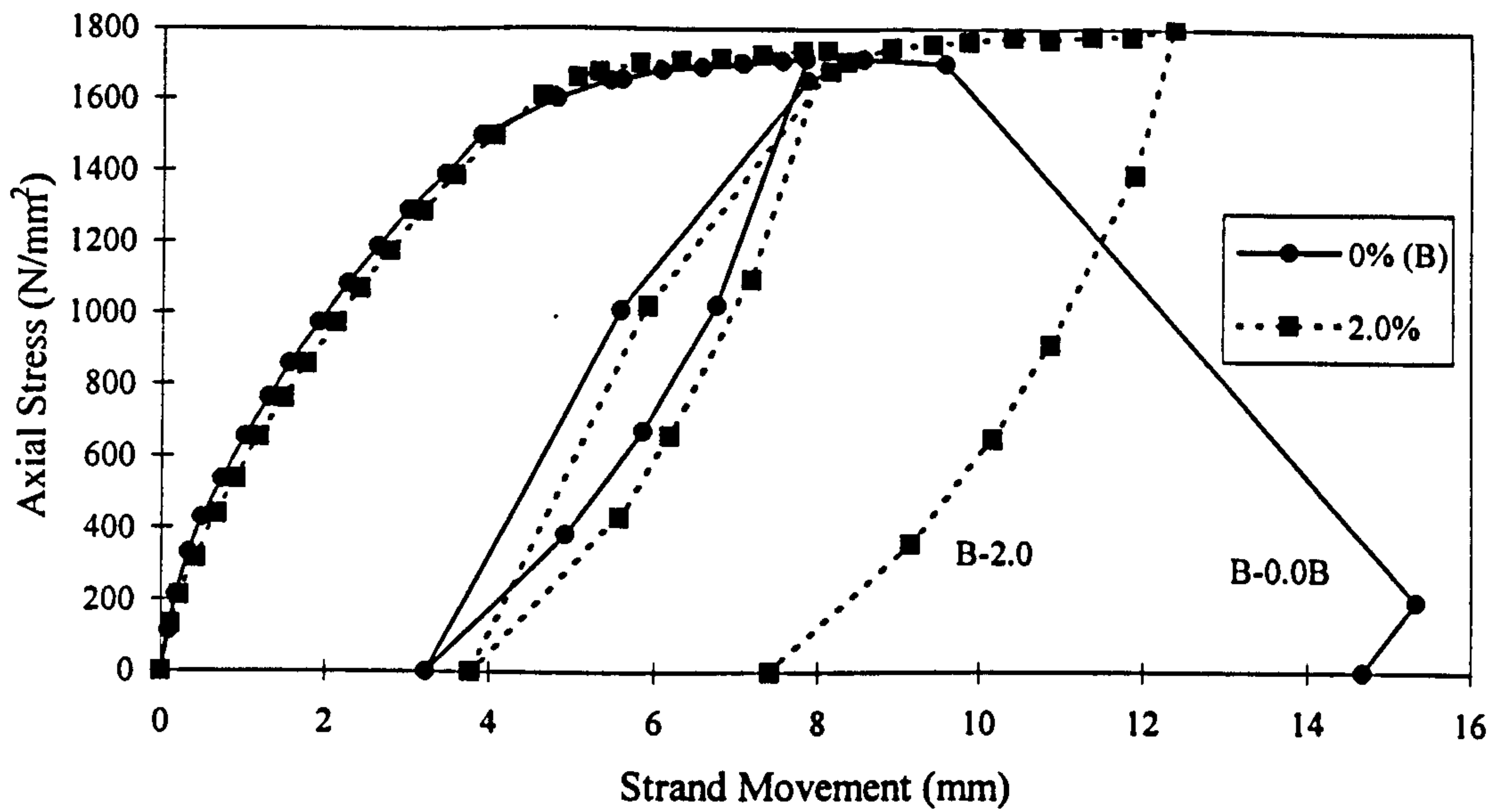


Figure 5-9 Axial stress v loaded-end strand movement for specimens B-2.0 and B-0.0B up to ultimate

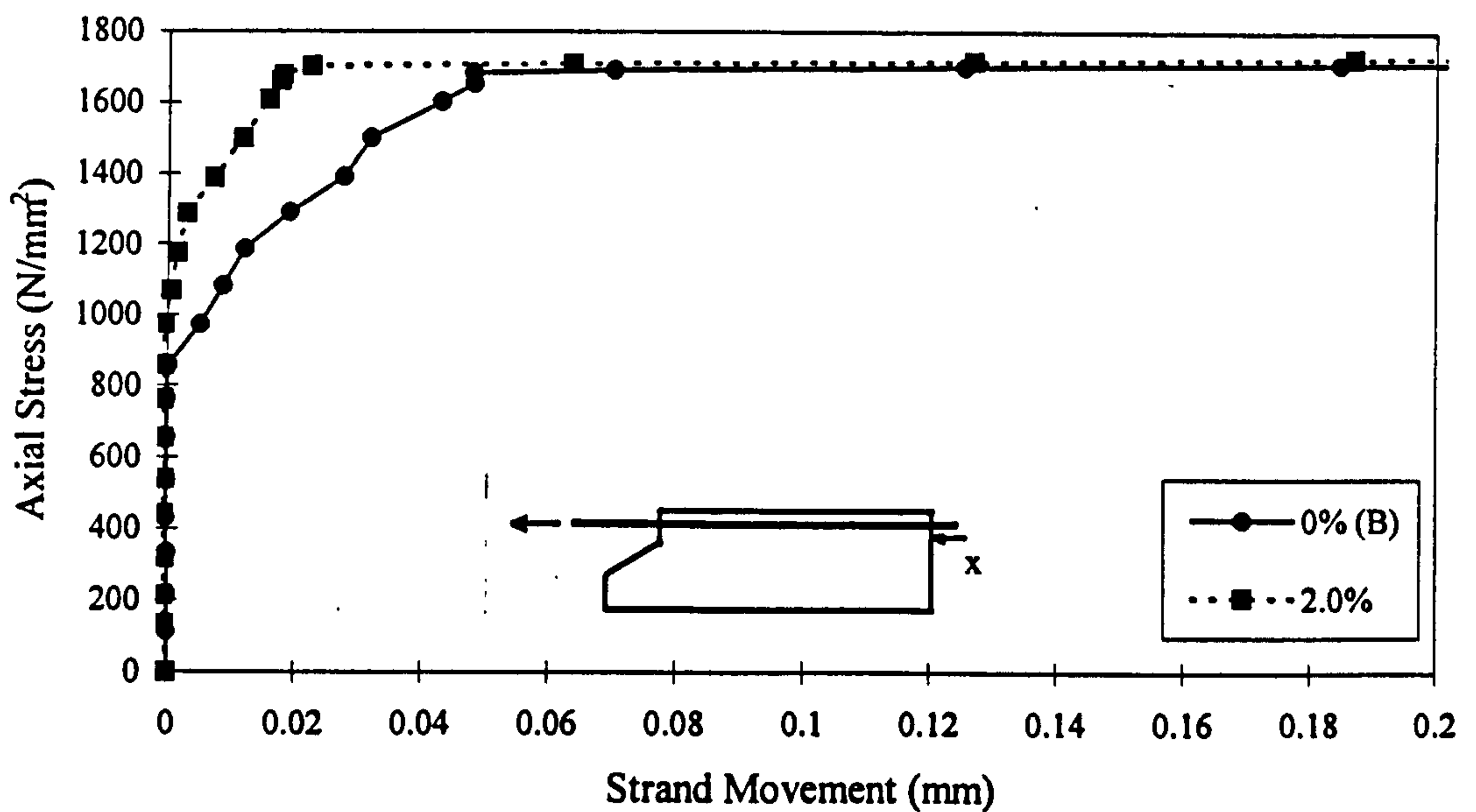


Figure 5-10 Axial stress v remote-end strand movement for specimens B-2.0 and B-0.0B

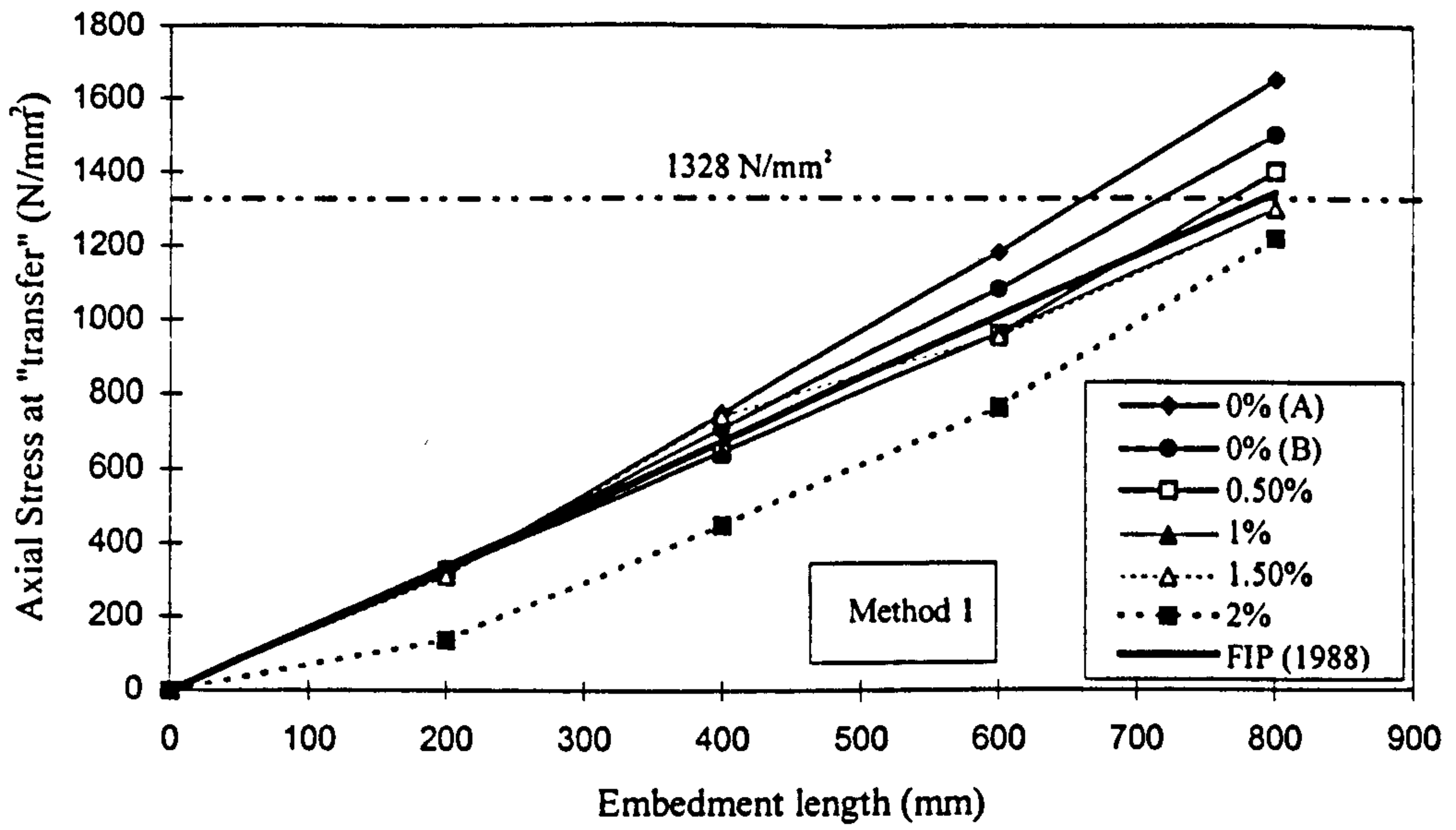


Figure 5-11 Axial stress at "transfer" of stress v embedment length of strain gauge

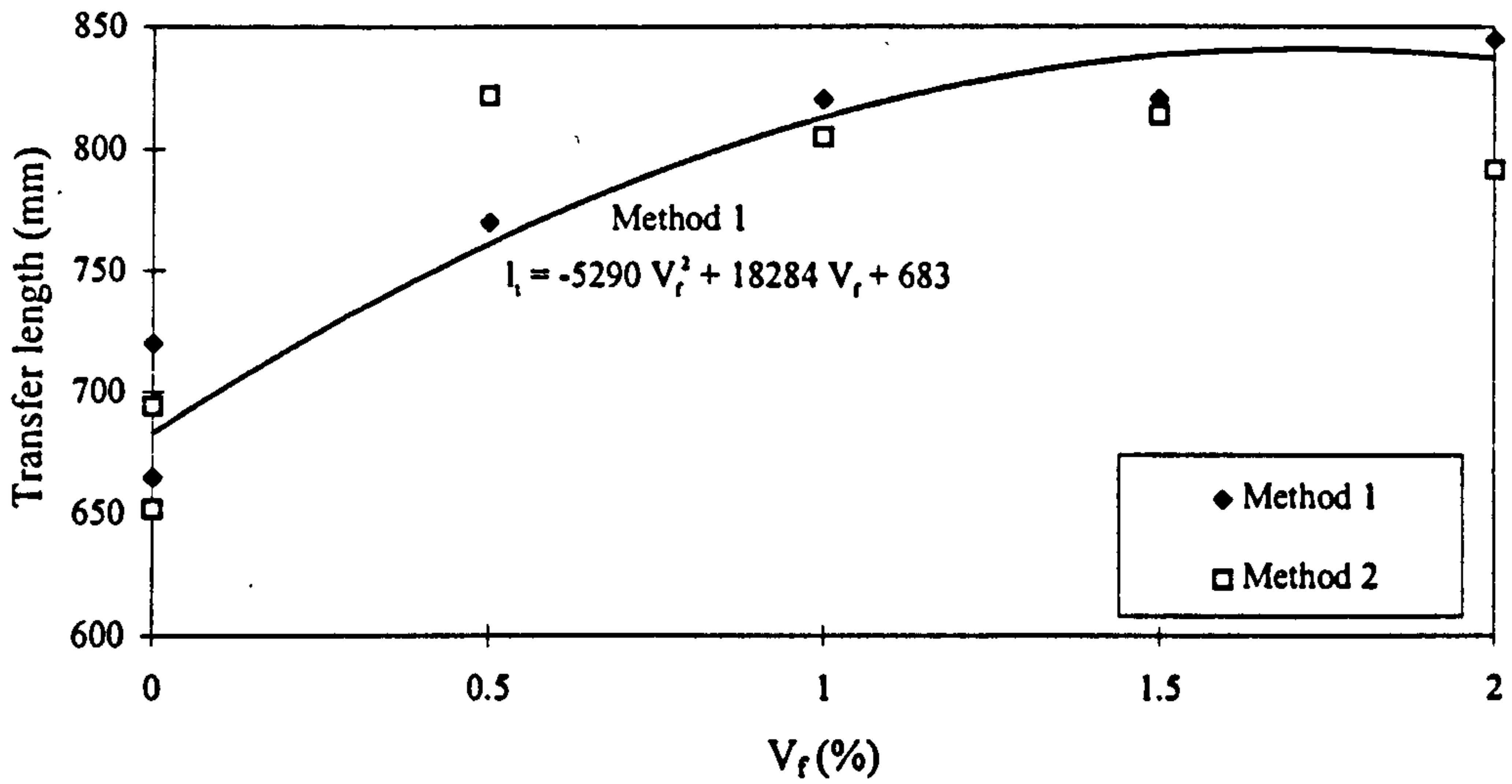


Figure 5-12 Effect of fibre volume fraction on calculated transfer length

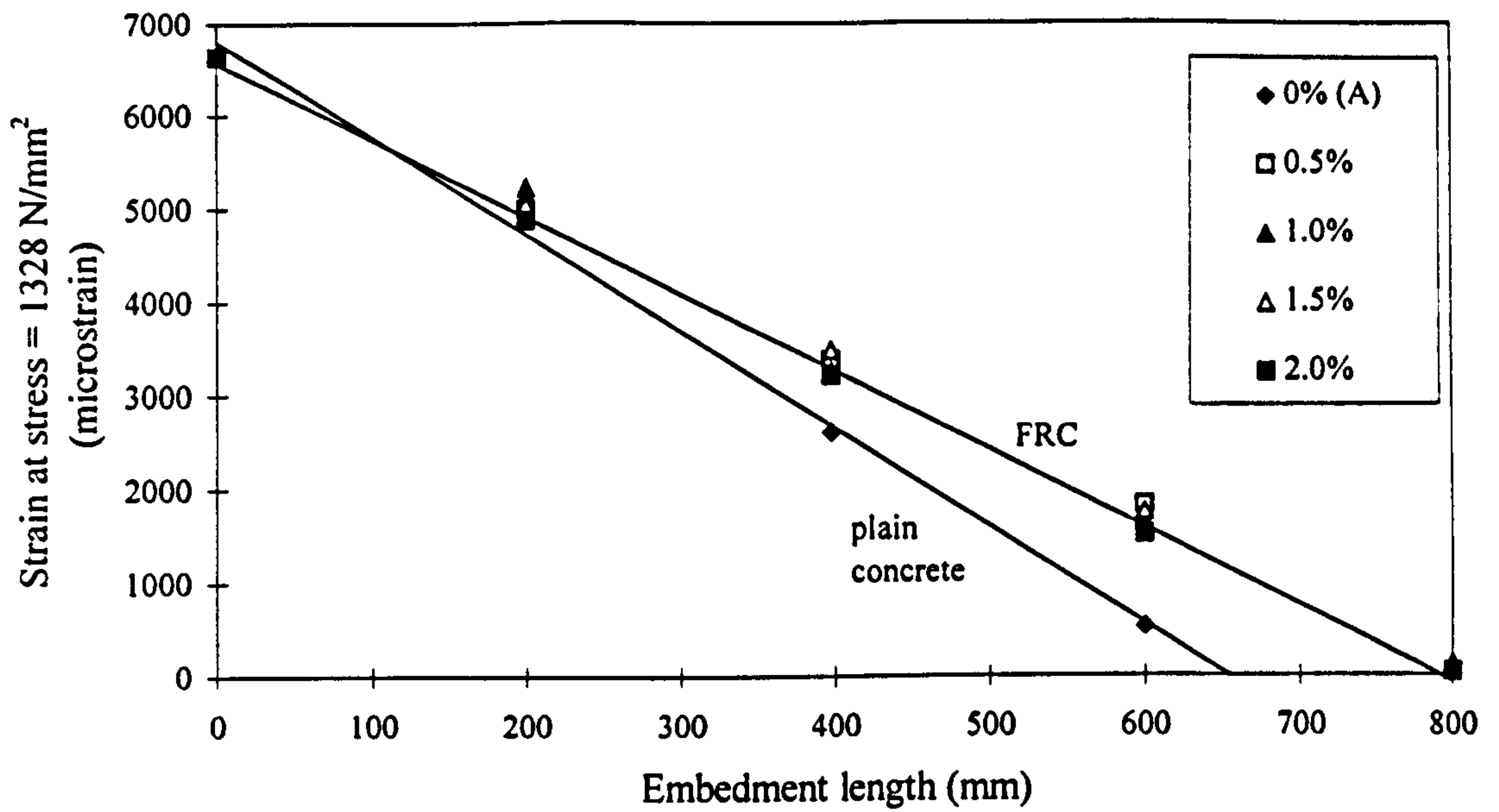


Figure 5-13 Strain at 1328 N/mm<sup>2</sup> v embedment length of strain gauge

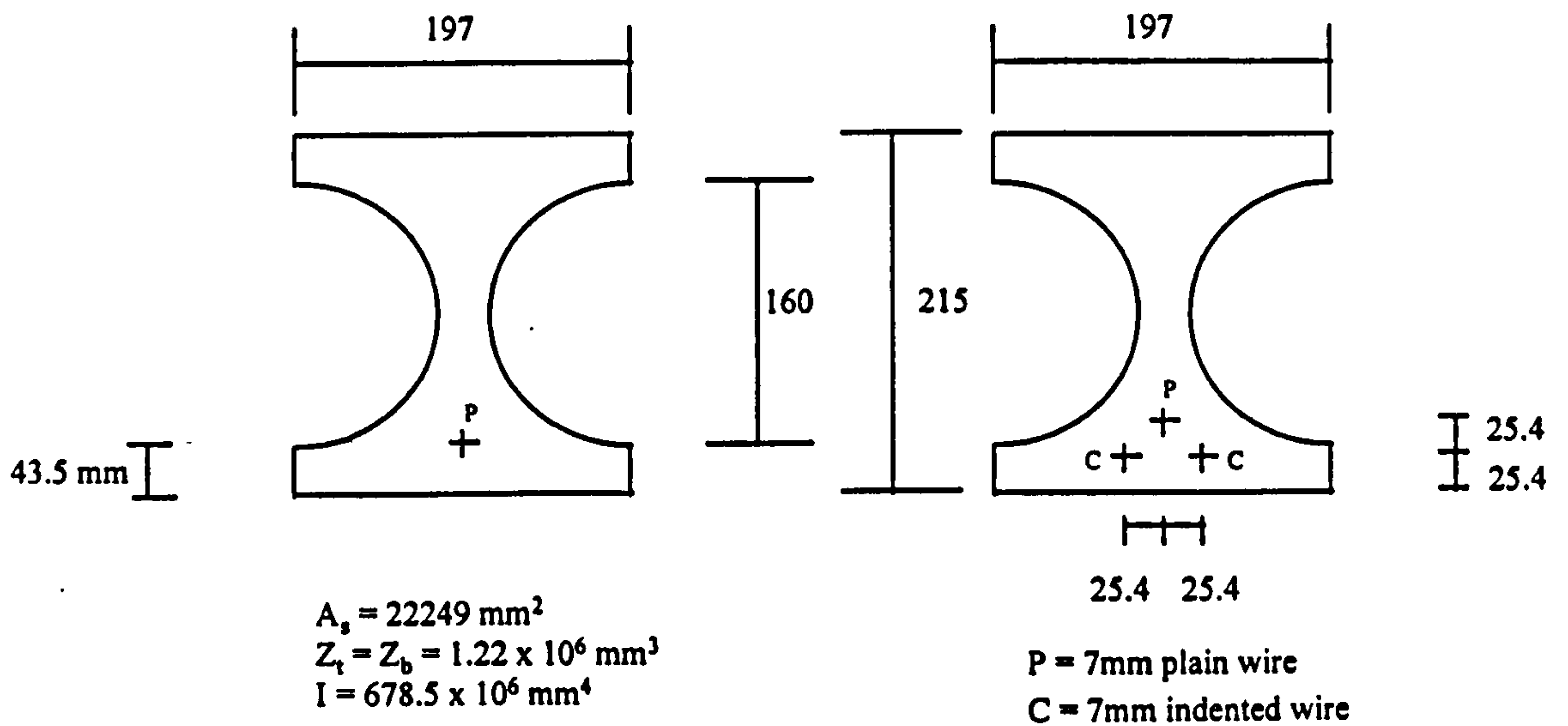


Figure 5-14 X-beam test specimen, (a) PB1-PB4, (b) PB5-PB22

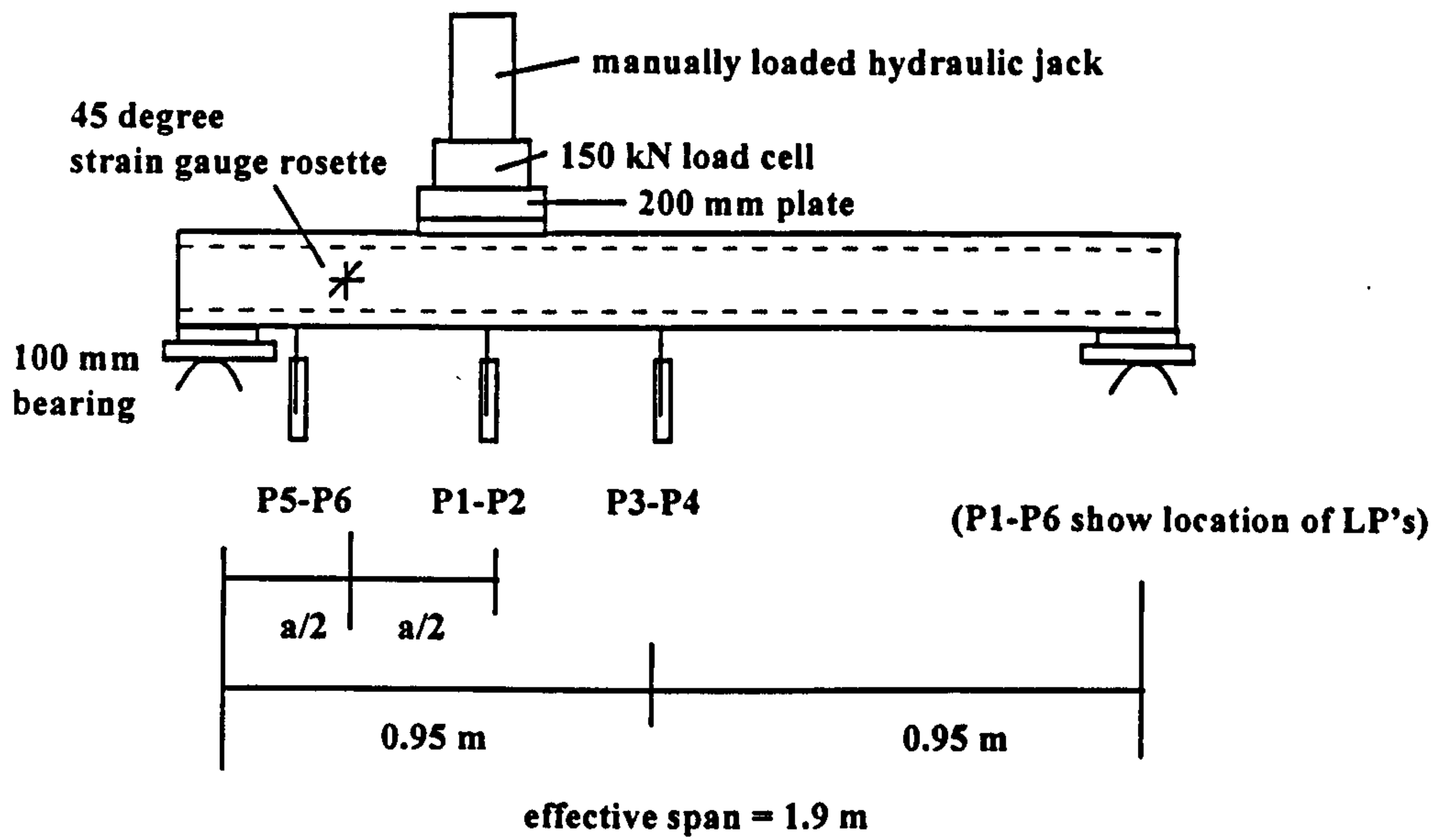


Figure 5-15 Test set-up for X-beam tests (A Test)

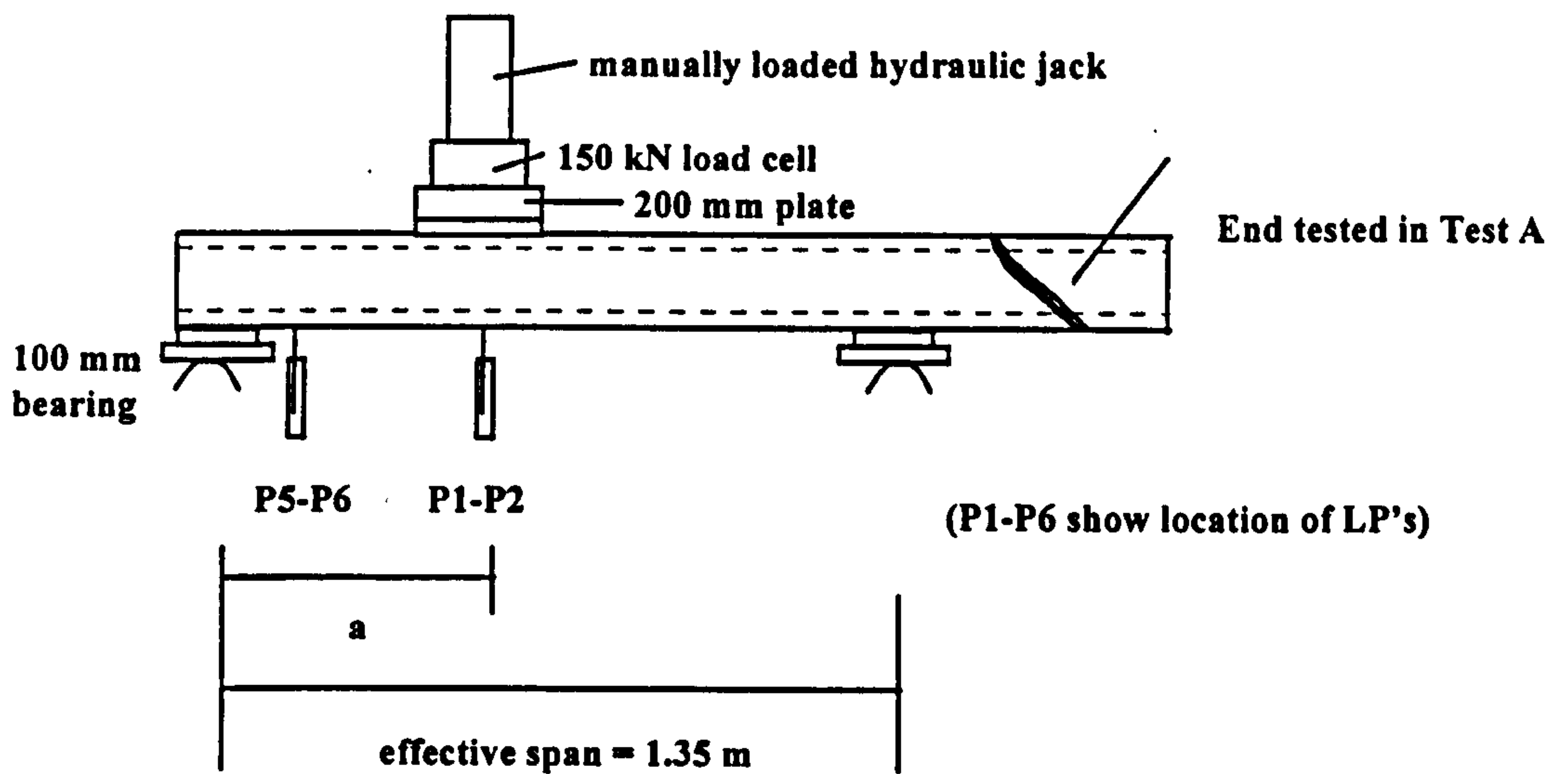


Figure 5-16 Test set-up for X-beam tests (B Test)

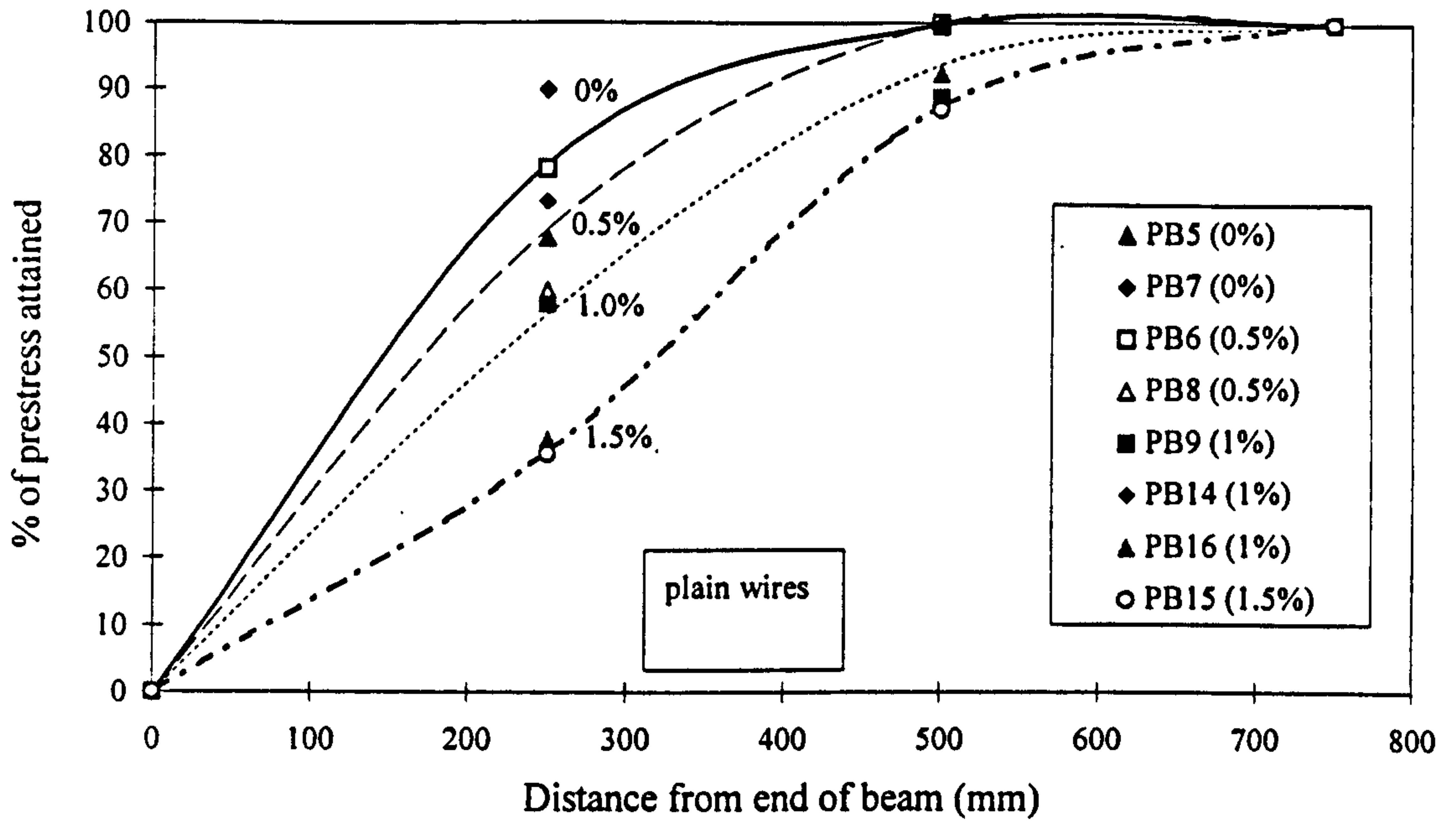


Figure 5-17 Experimentally measured prestress transfer curve for plain wires

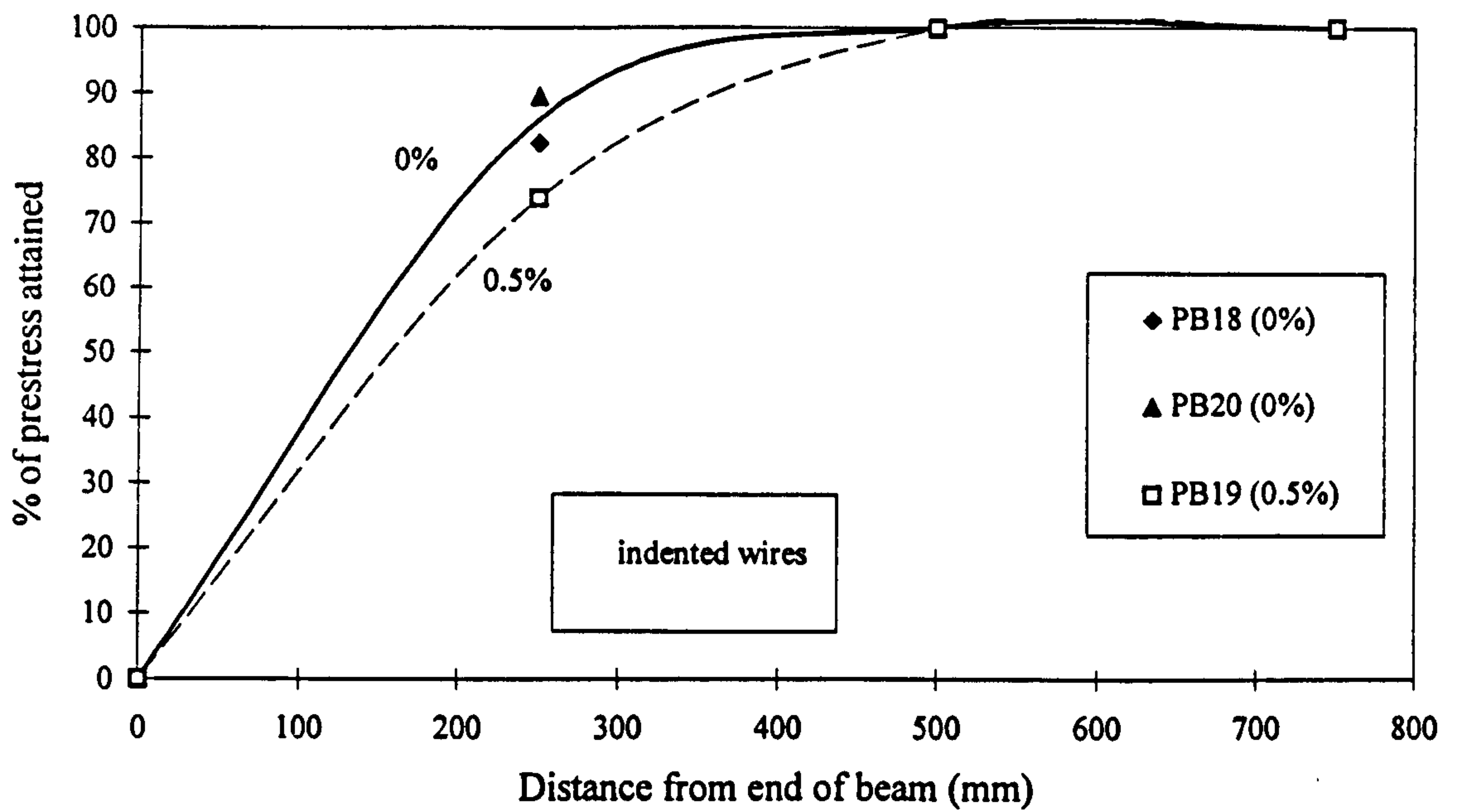


Figure 5-18 Experimentally measured prestress transfer curve for indented wires



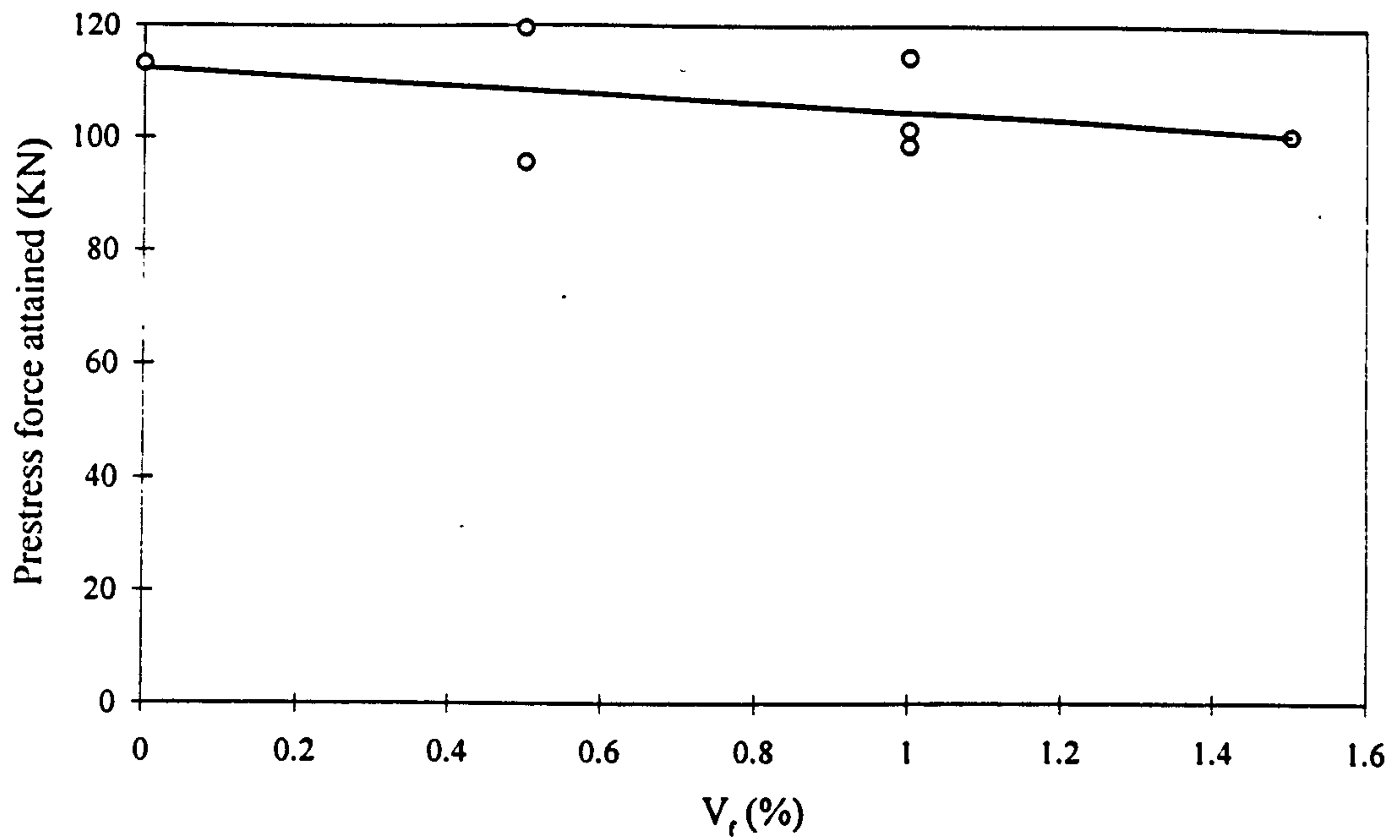


Figure 5-19 Prestress attained at 750 mm from end of beam v fibre volume fraction

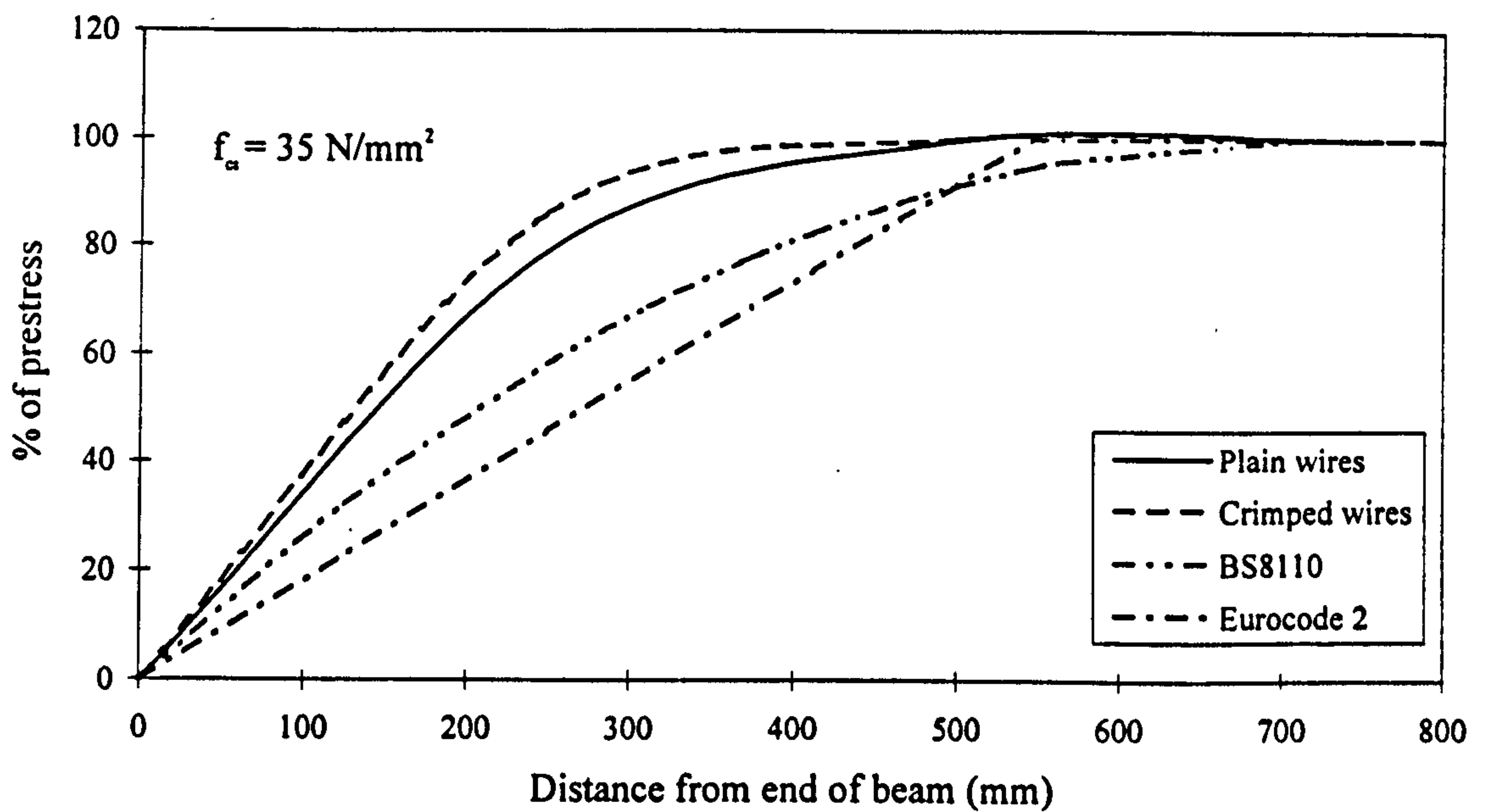


Figure 5-20 Comparison of experimental transfer curves with BS 8110 and Eurocode 2

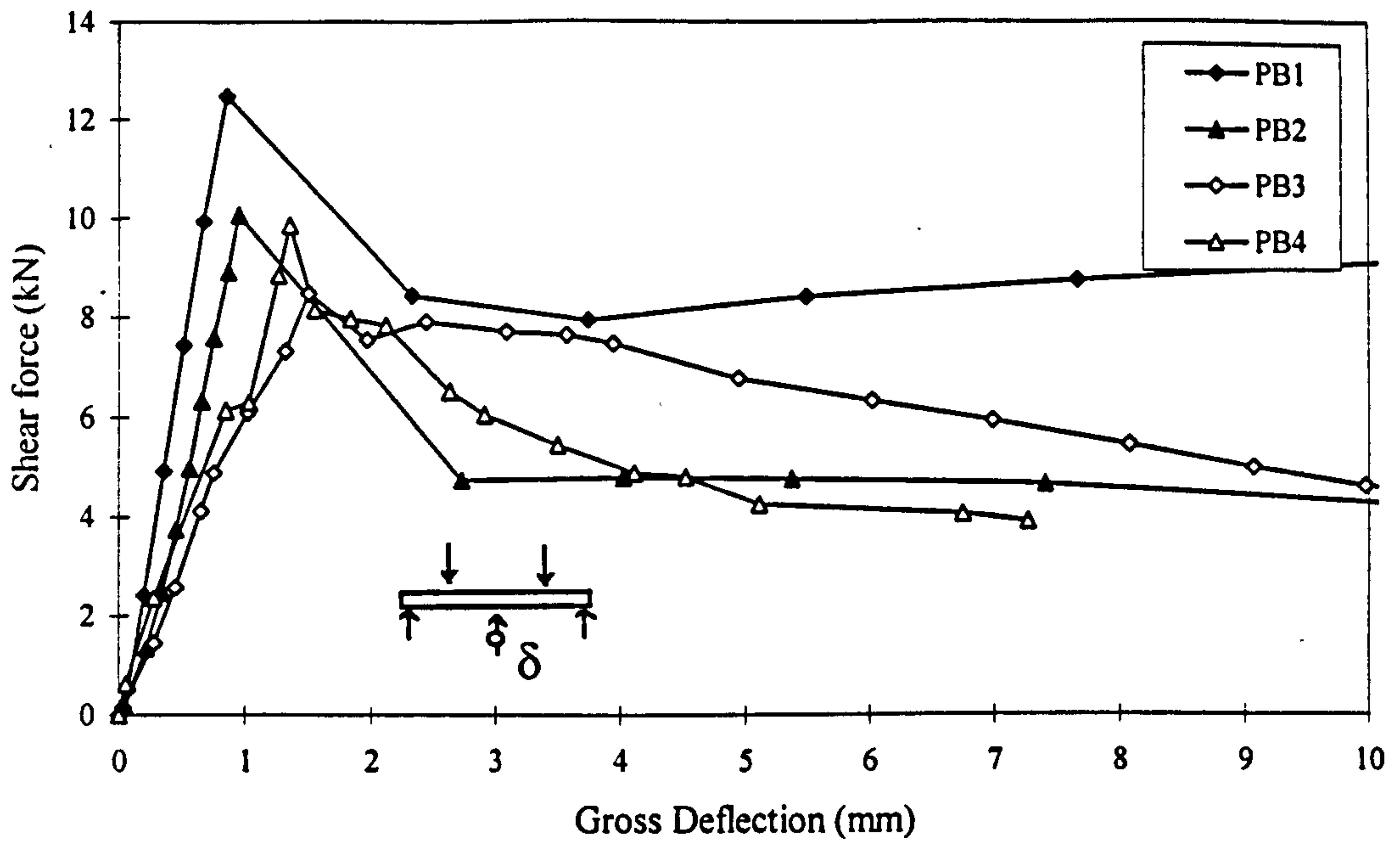


Figure 5-21 Shear force v deflection for PB1 - PB4

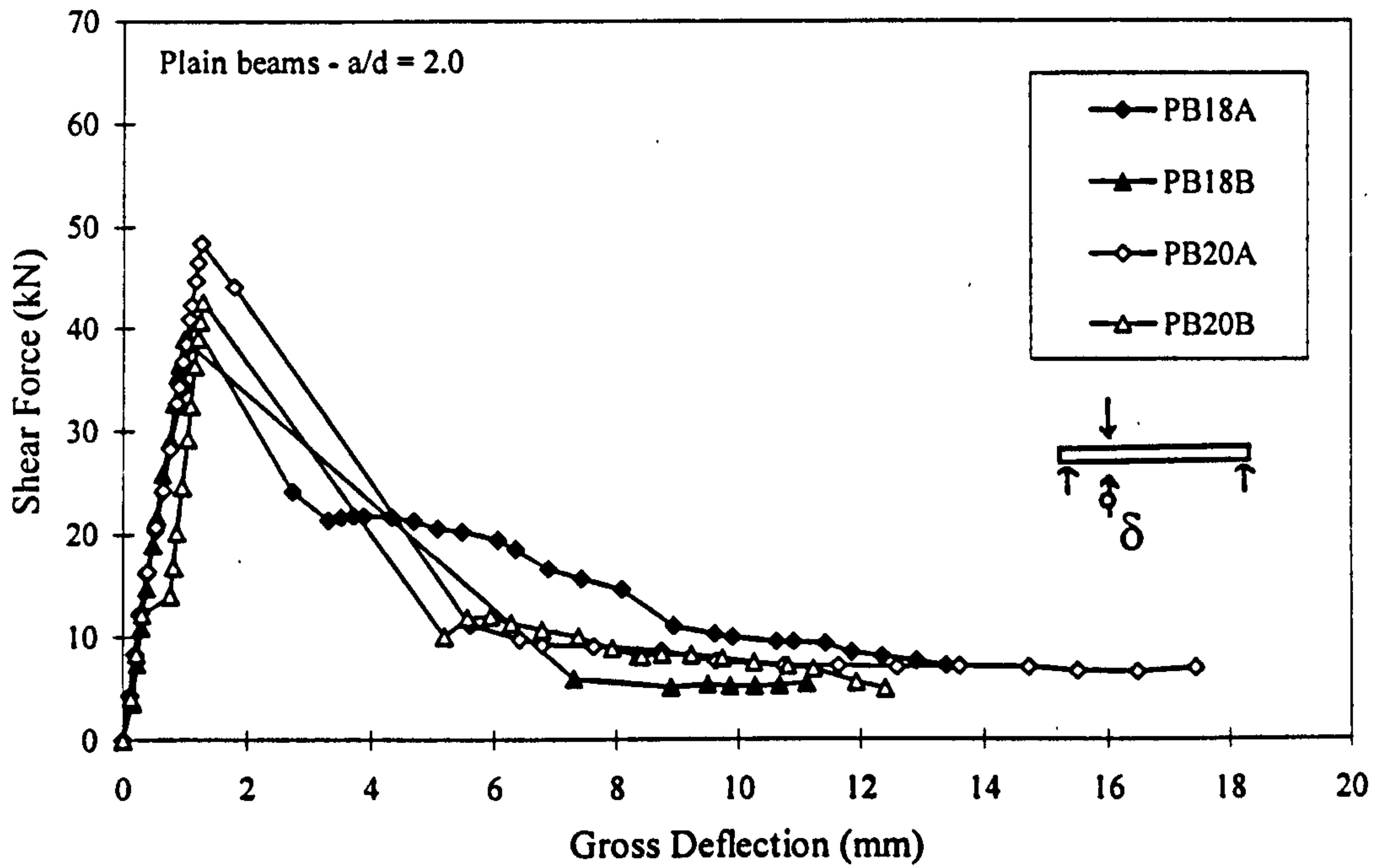


Figure 5-22 Shear force v deflection for  $V_f = 0\%$  at  $a/d = 2.0$

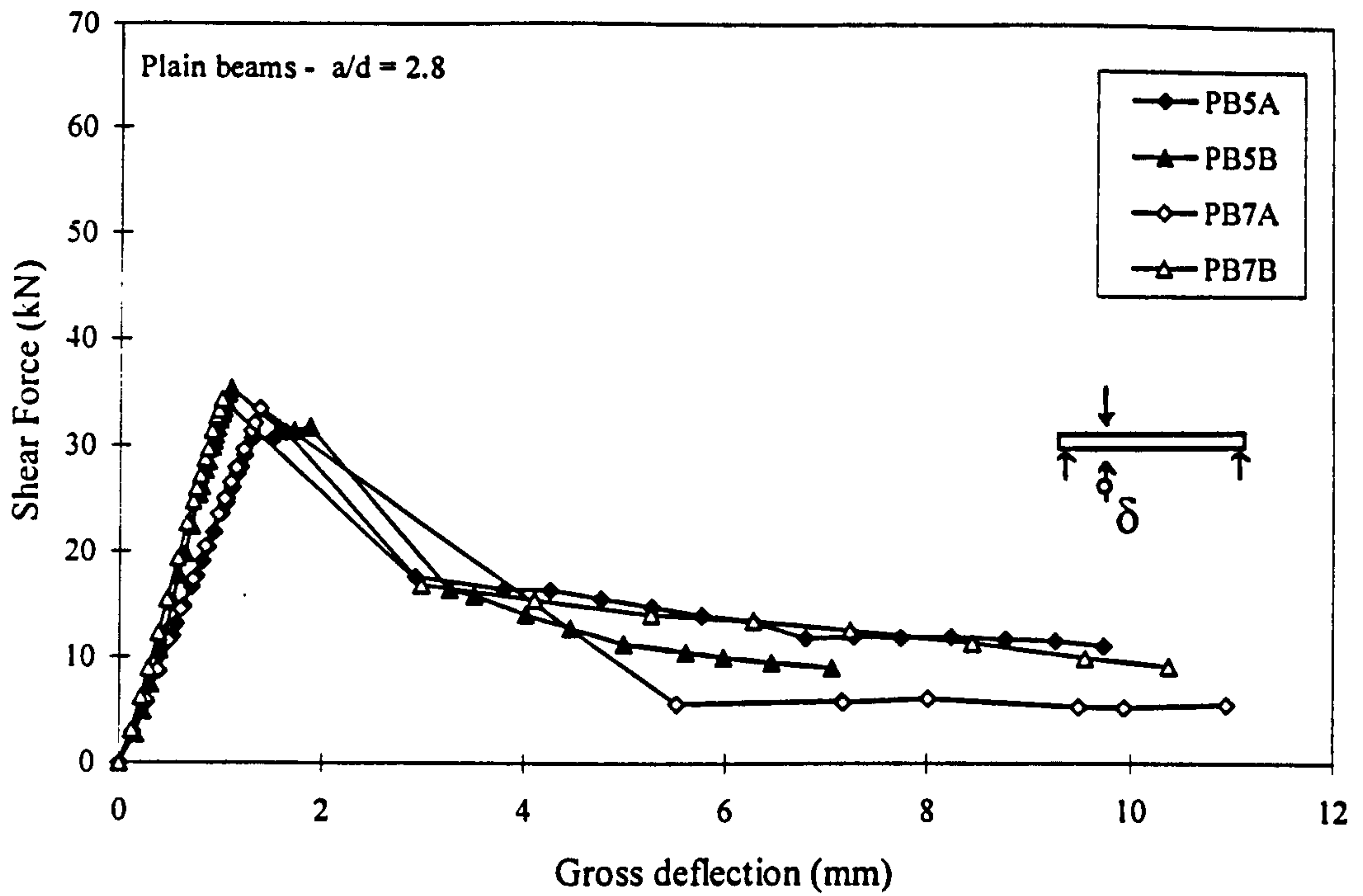


Figure 5-23 Shear force v deflection for  $V_f = 0\%$  at  $a/d = 2.8$

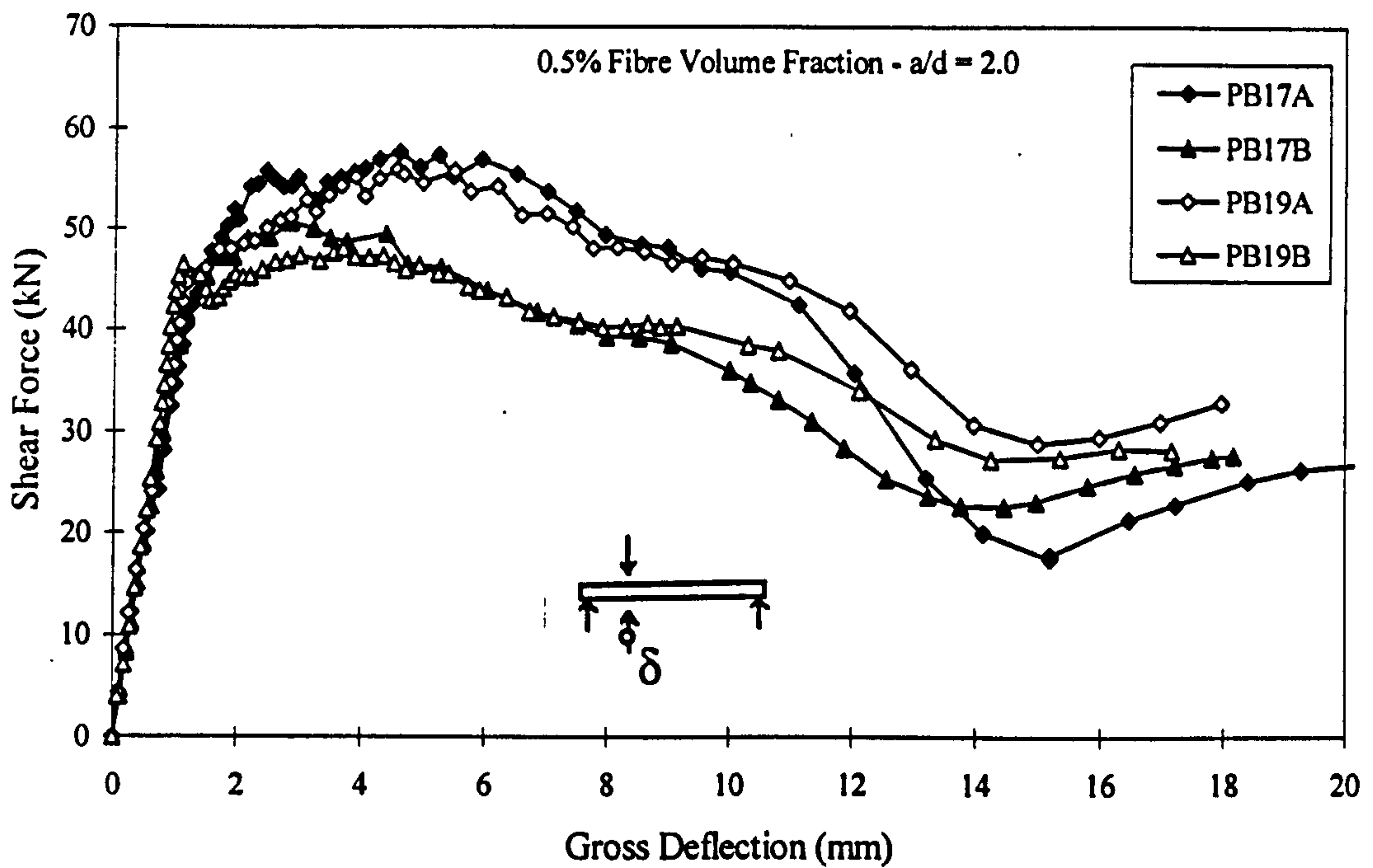


Figure 5-24 Shear force v deflection for  $V_f = 0.5\%$  (HS) at  $a/d = 2.0$

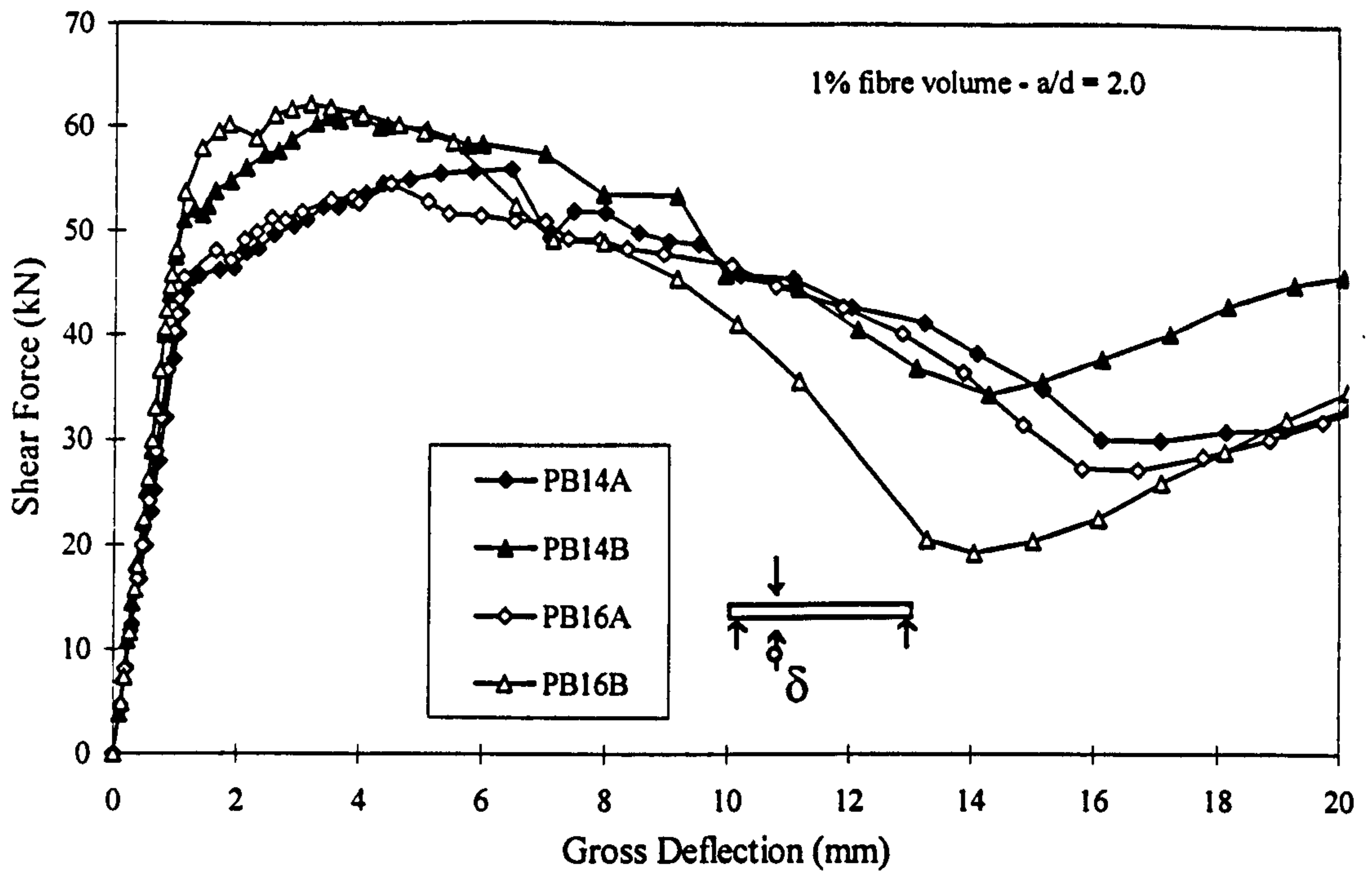


Figure 5-25 Shear force v deflection for  $V_f = 1\%$  (HS) at  $a/d = 2.0$

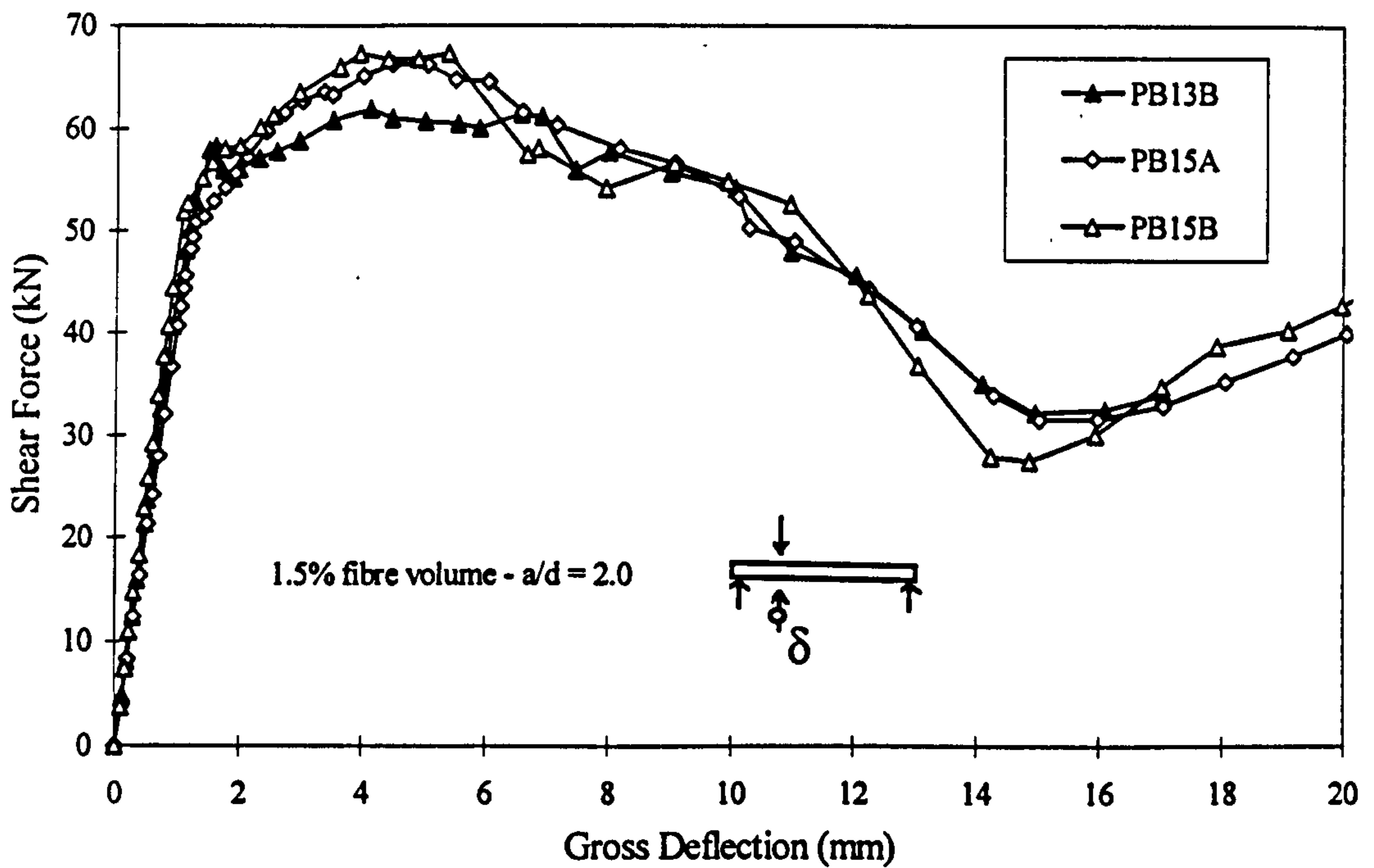


Figure 5-26 Shear force v deflection for  $V_f = 1.5\%$  (HS) at  $a/d = 2.0$

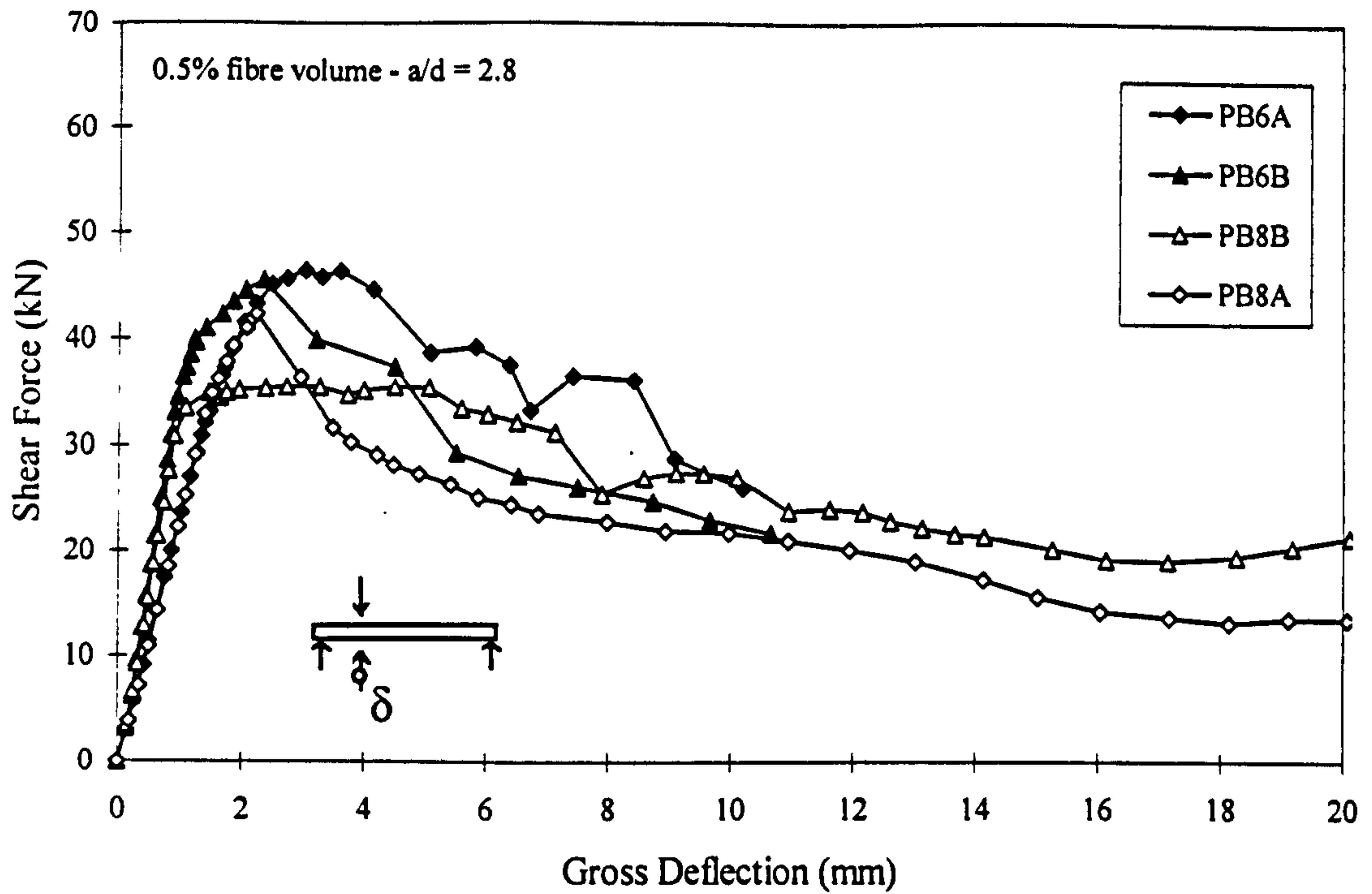


Figure 5-27 Shear force v deflection for  $V_f = 0.5\%$  (HS) at  $a/d = 2.8$

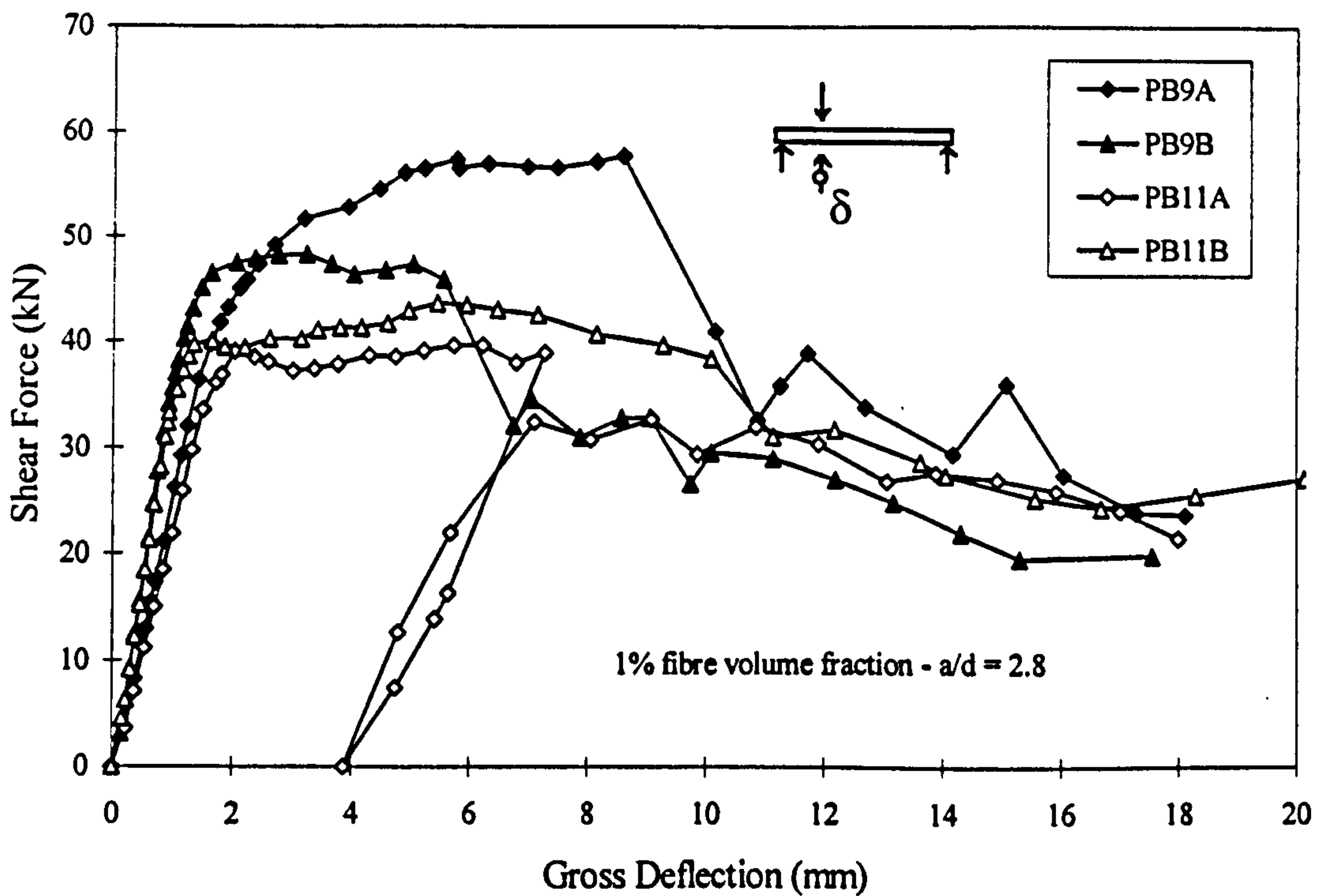


Figure 5-28 Shear force v deflection for  $V_f = 1\%$  (HS) at  $a/d = 2.8$

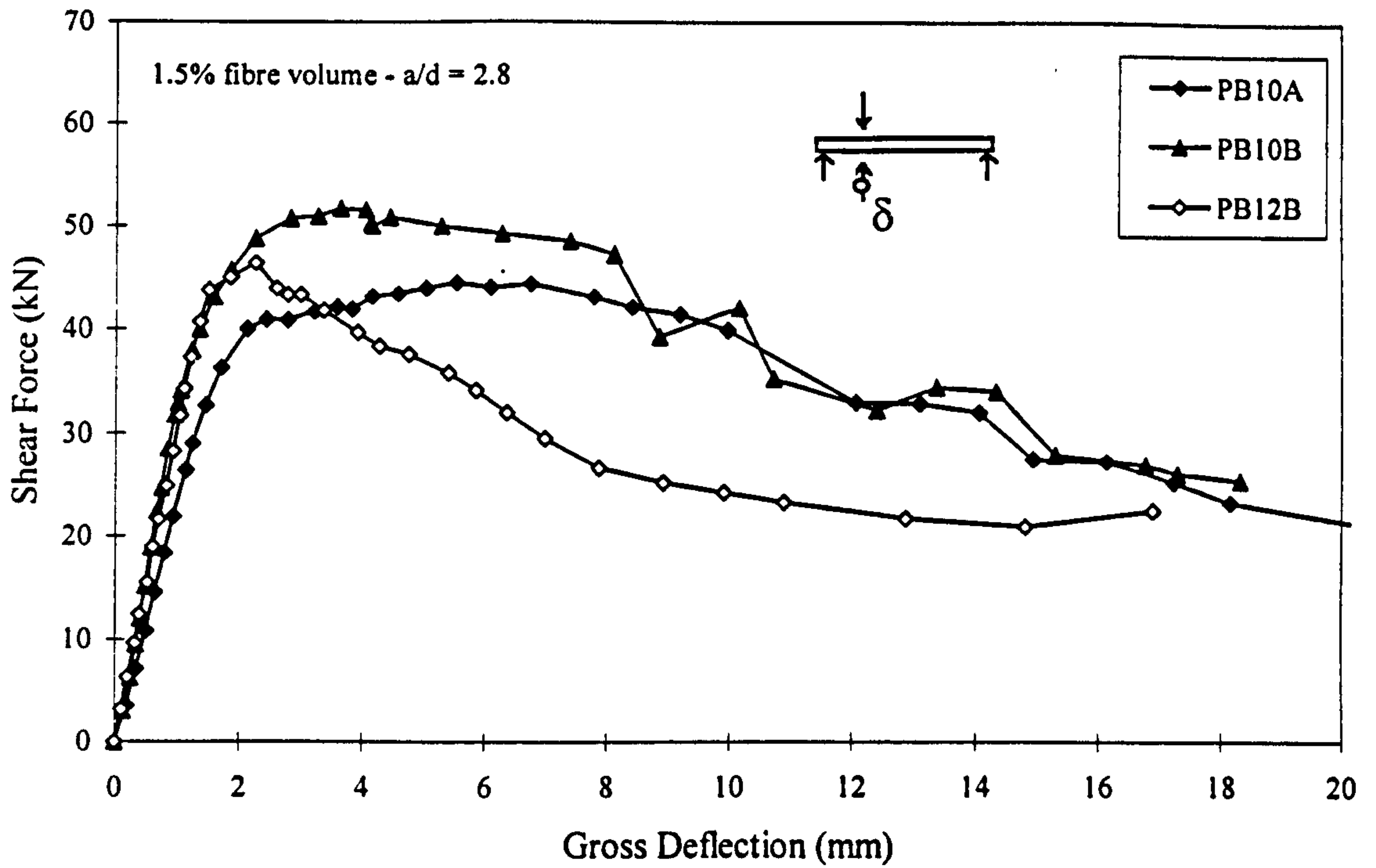


Figure 5-29 Shear force v deflection for  $V_f = 1.5\%$  (HS) at  $a/d = 2.8$

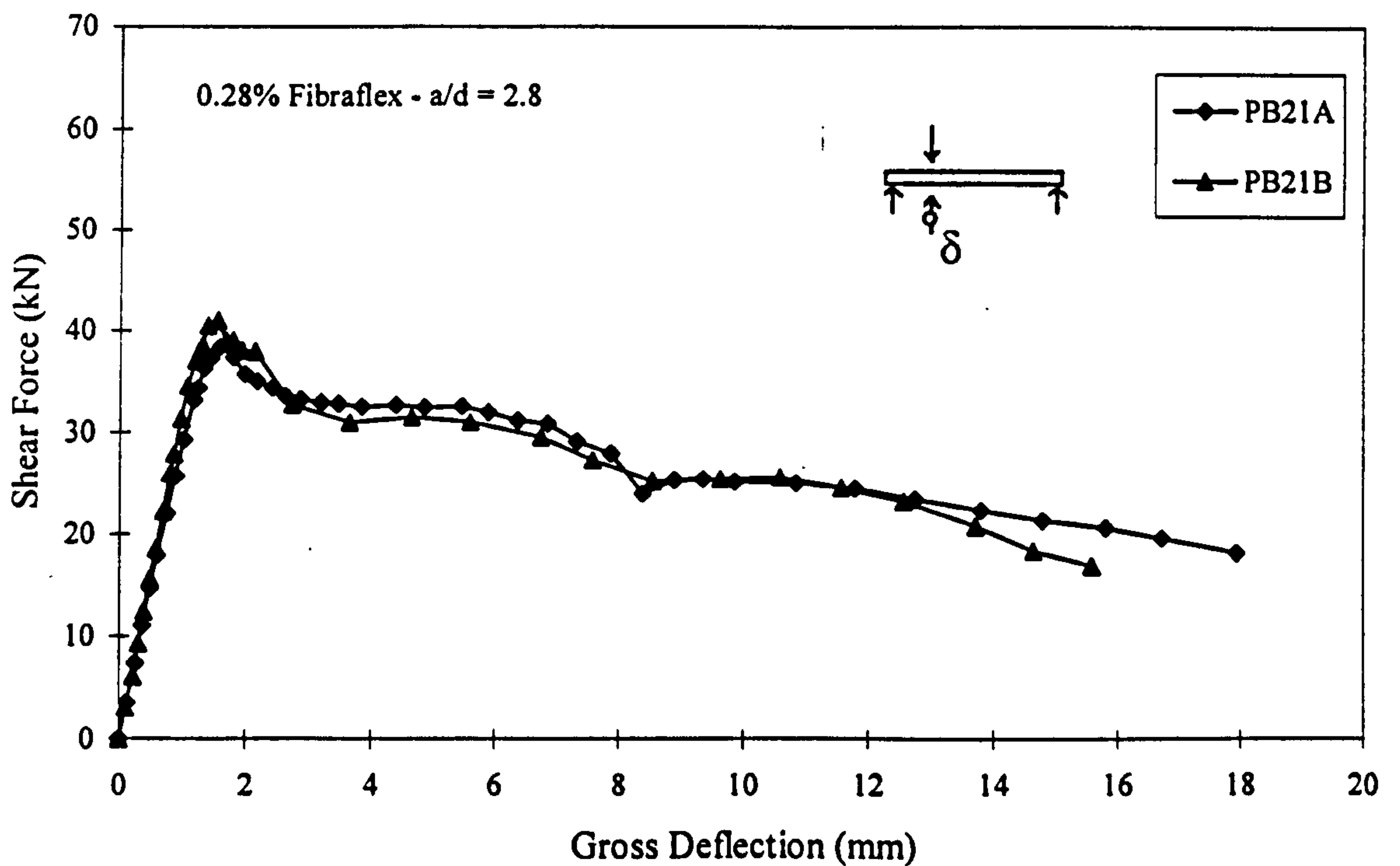


Figure 5-30 Shear force v deflection for  $V_f = 0.28\%$  (AM) at  $a/d = 2.8$

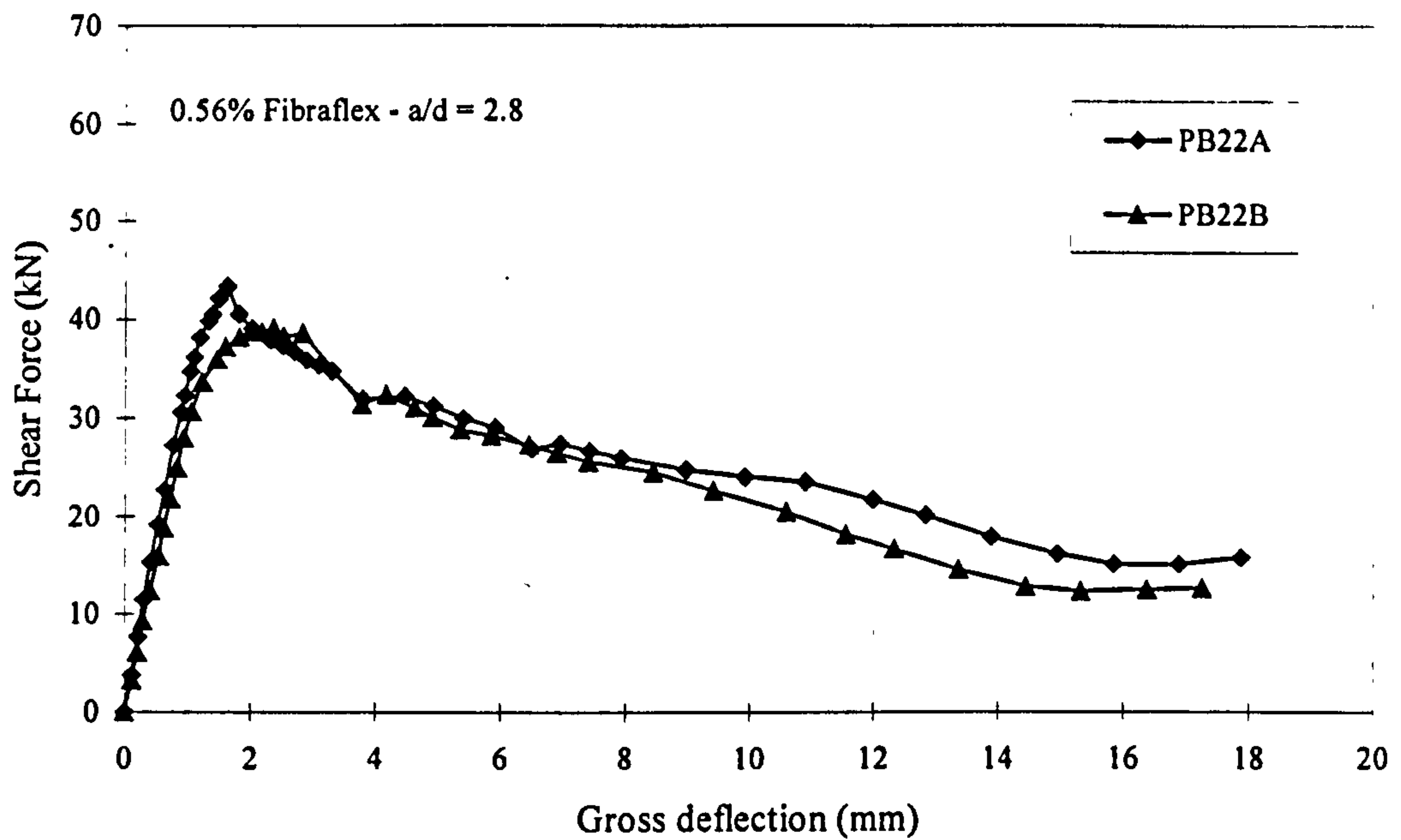


Figure 5-31 Shear force v deflection for  $V_f = 0.56\%$  (AM) at  $a/d = 2.8$

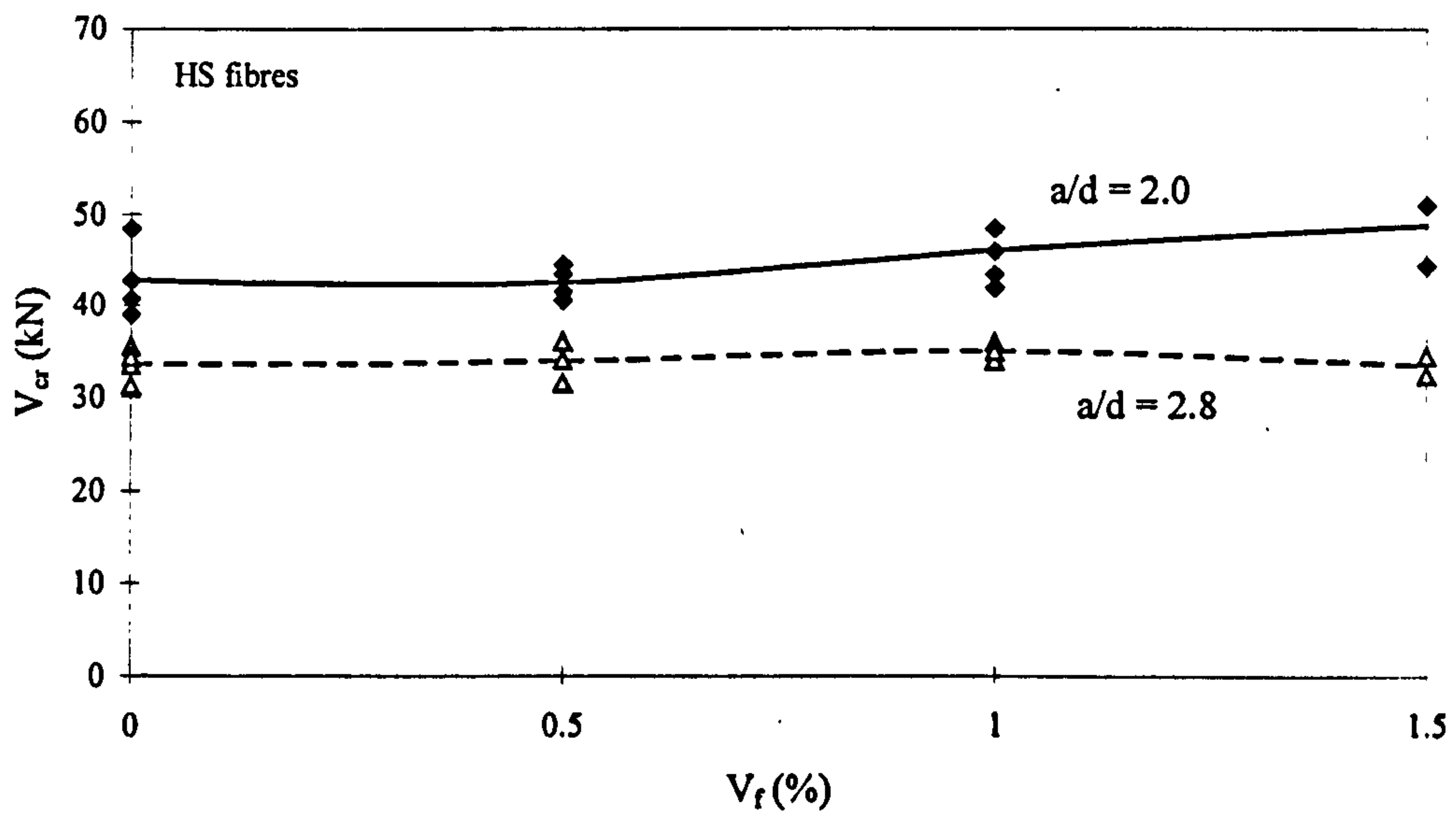


Figure 5-32 Cracking shear capacity v fibre volume fraction (HS fibres)

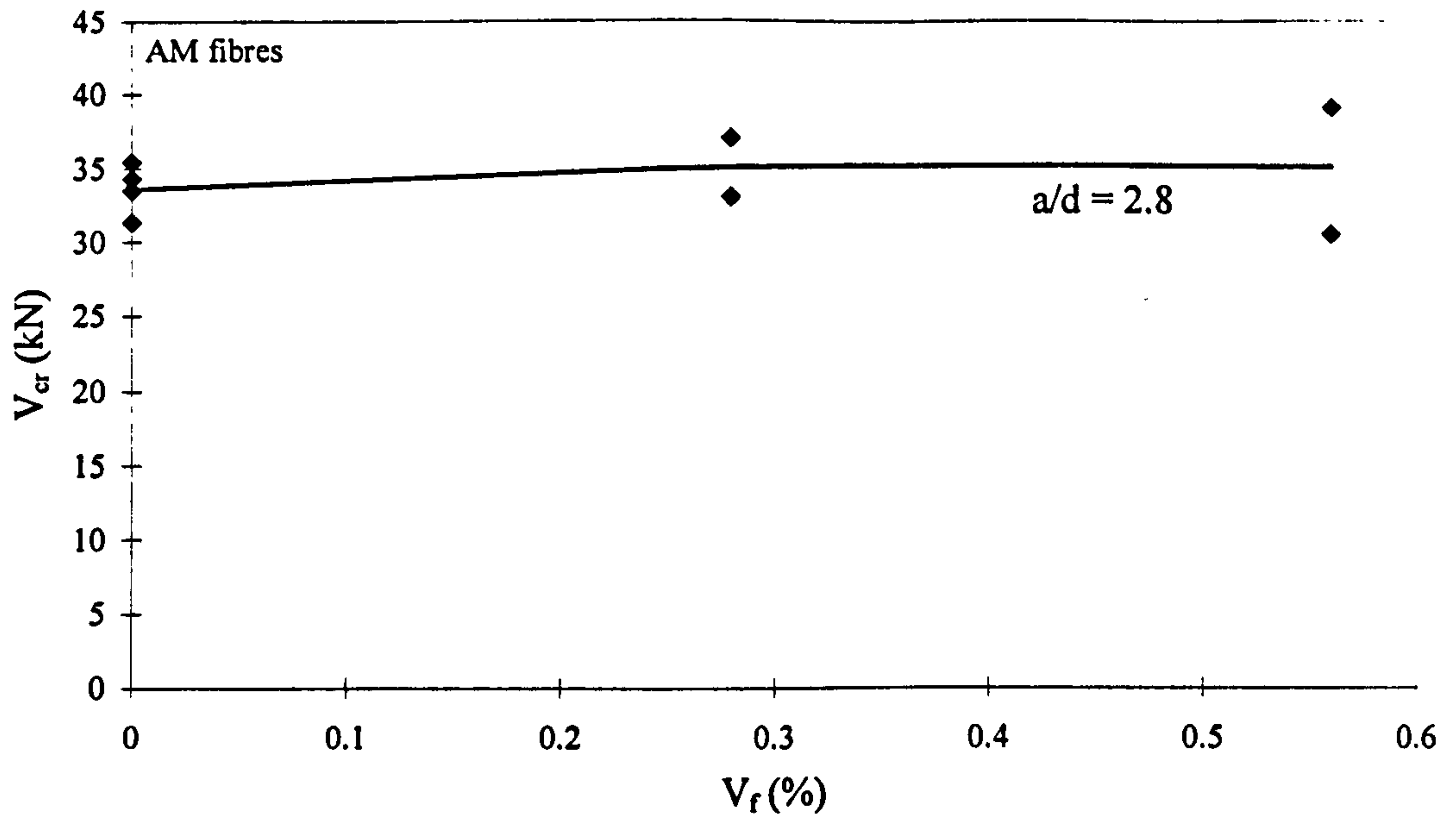


Figure 5-33 Cracking shear capacity v fibre volume fraction (AM fibres)

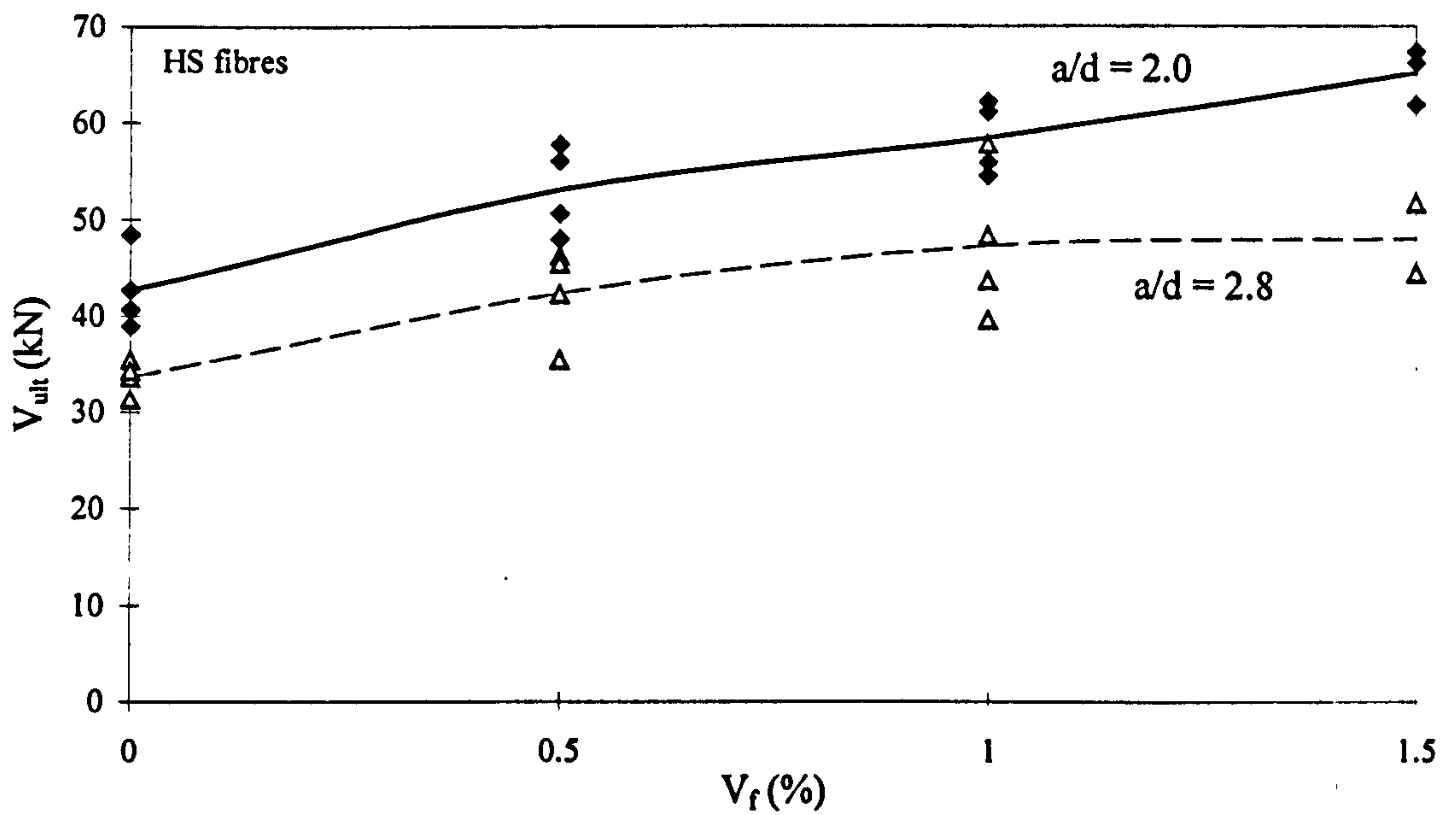
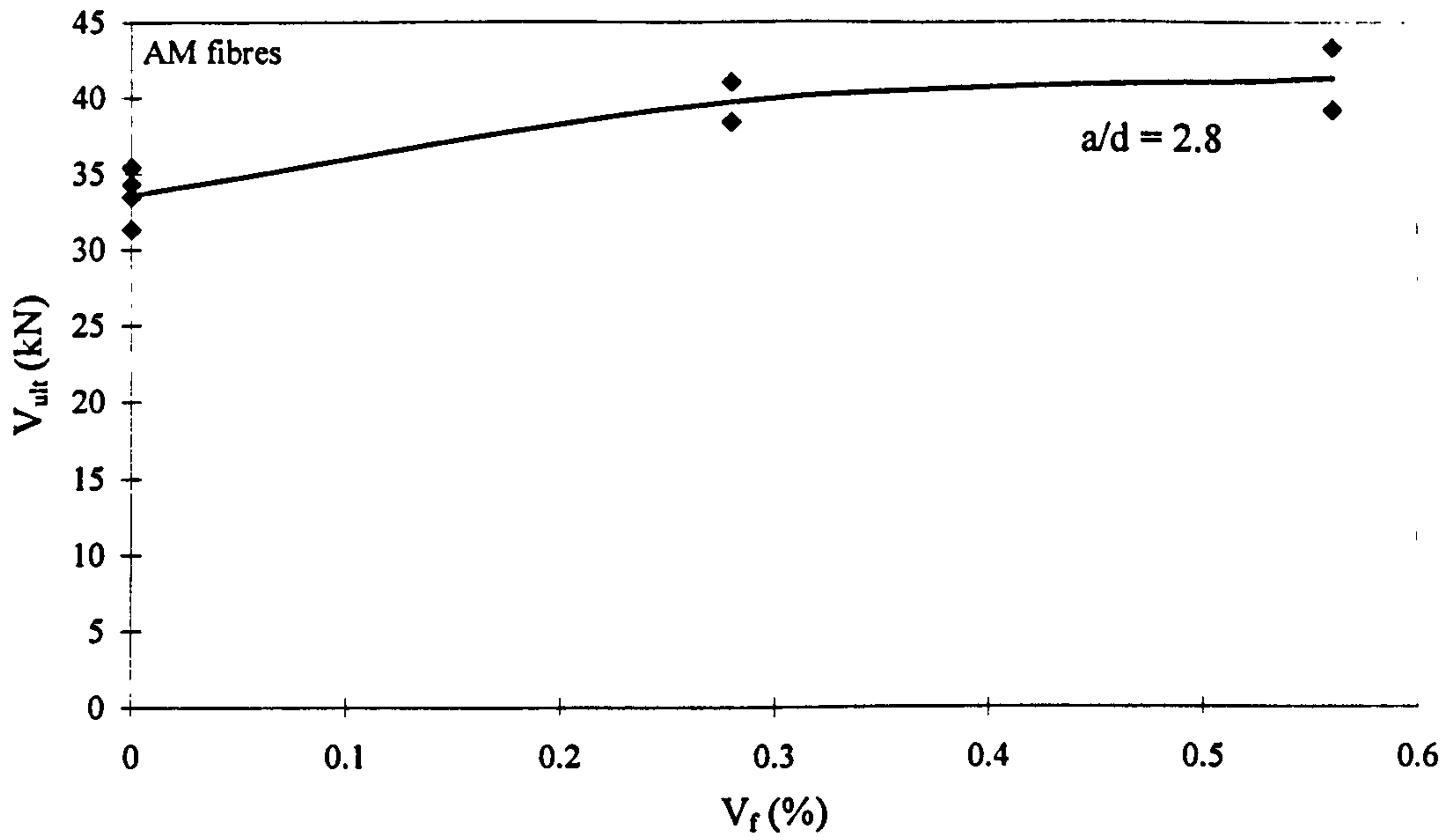
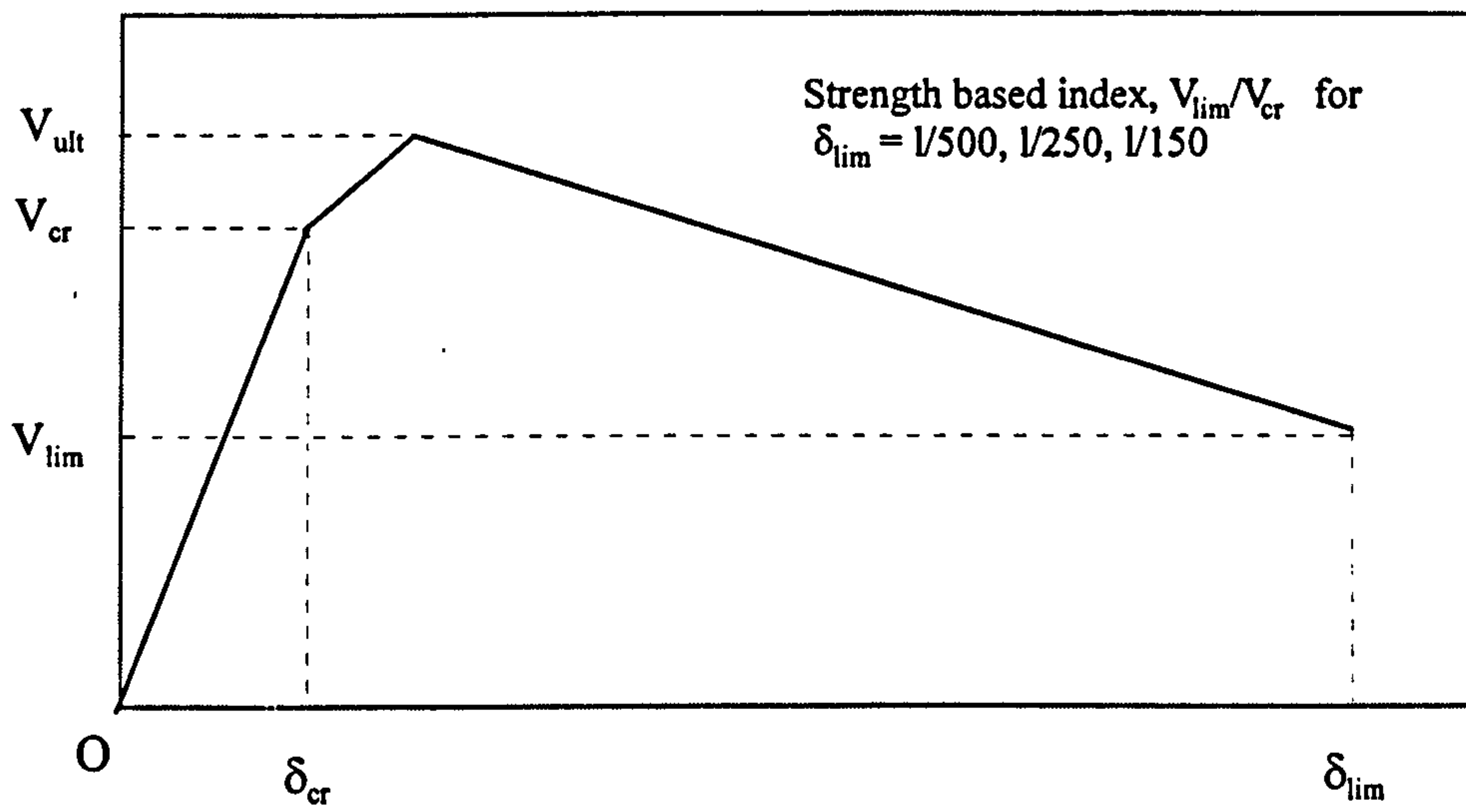


Figure 5-34 Ultimate shear capacity v fibre volume fraction (HS fibres)





**Figure 5-35 Ultimate shear capacity v fibre volume fraction (AM fibres)**



**Figure 5-36 Definition of ductility term  $V_{lim}/V_{cr}$**

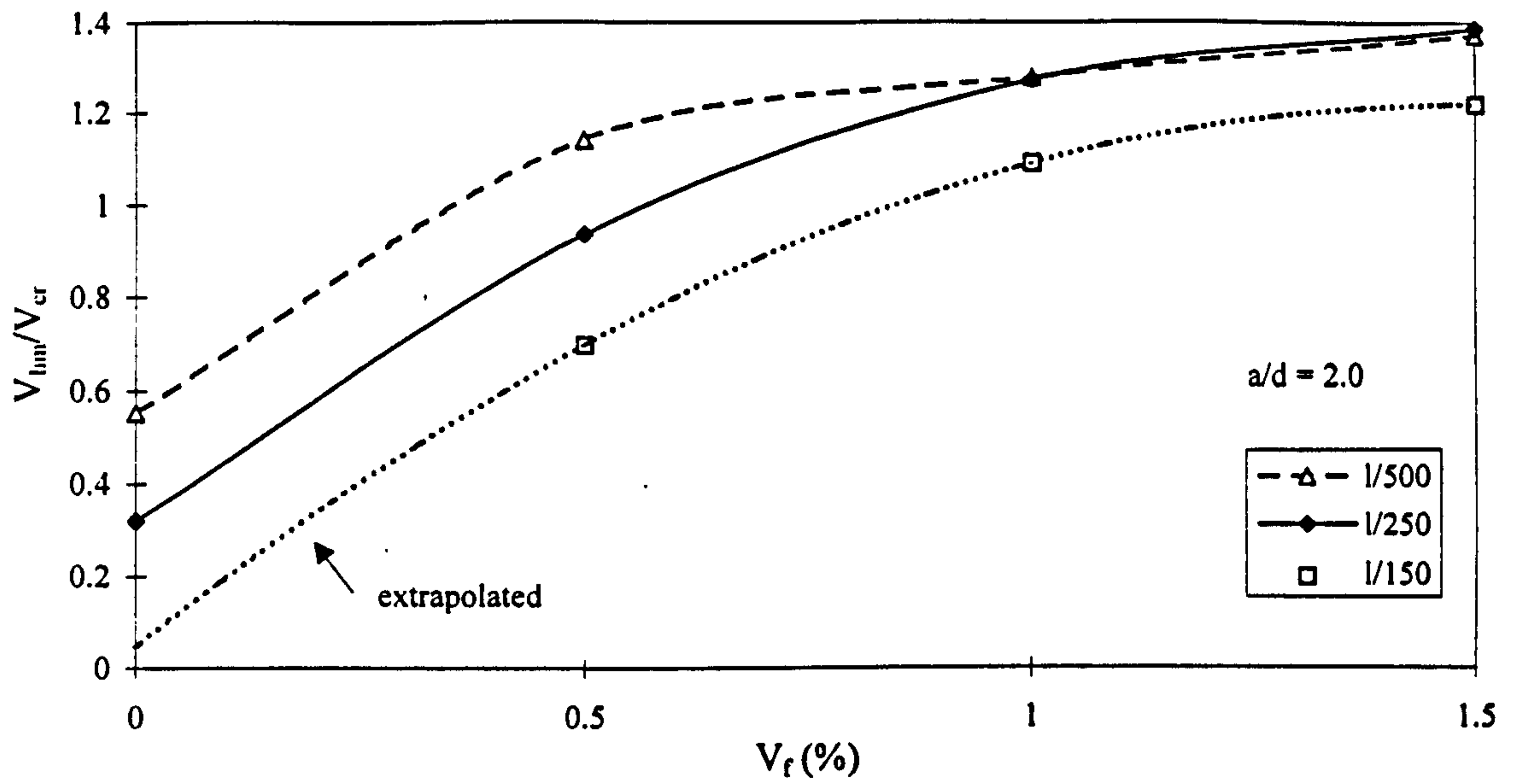


Figure 5-37  $V_{lim}/V_{cr}$  v fibre volume fraction (HS fibres) at  $a/d = 2.0$

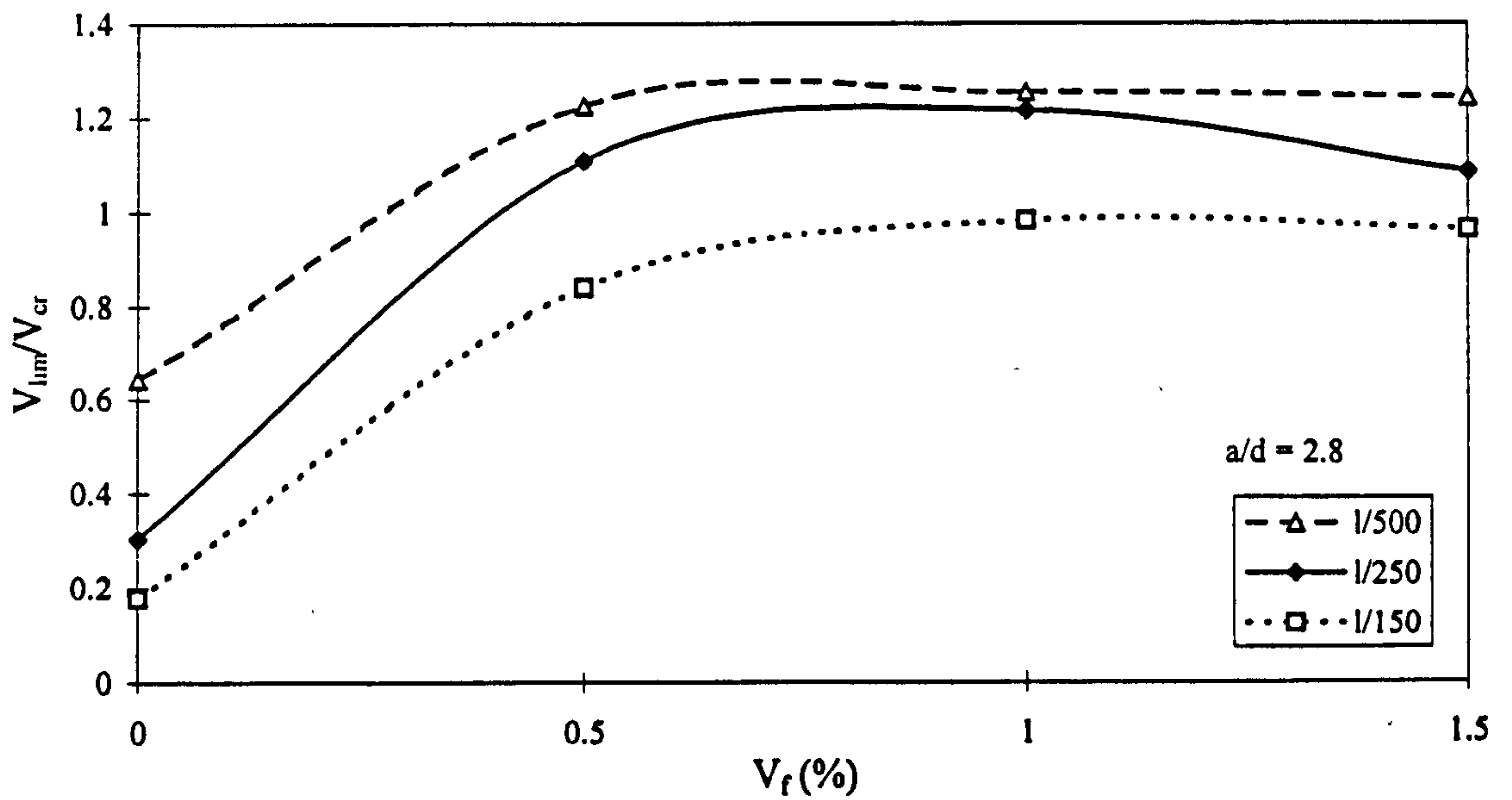


Figure 5-38  $V_{lim}/V_{cr}$  v fibre volume fraction (HS fibres) at  $a/d = 2.8$

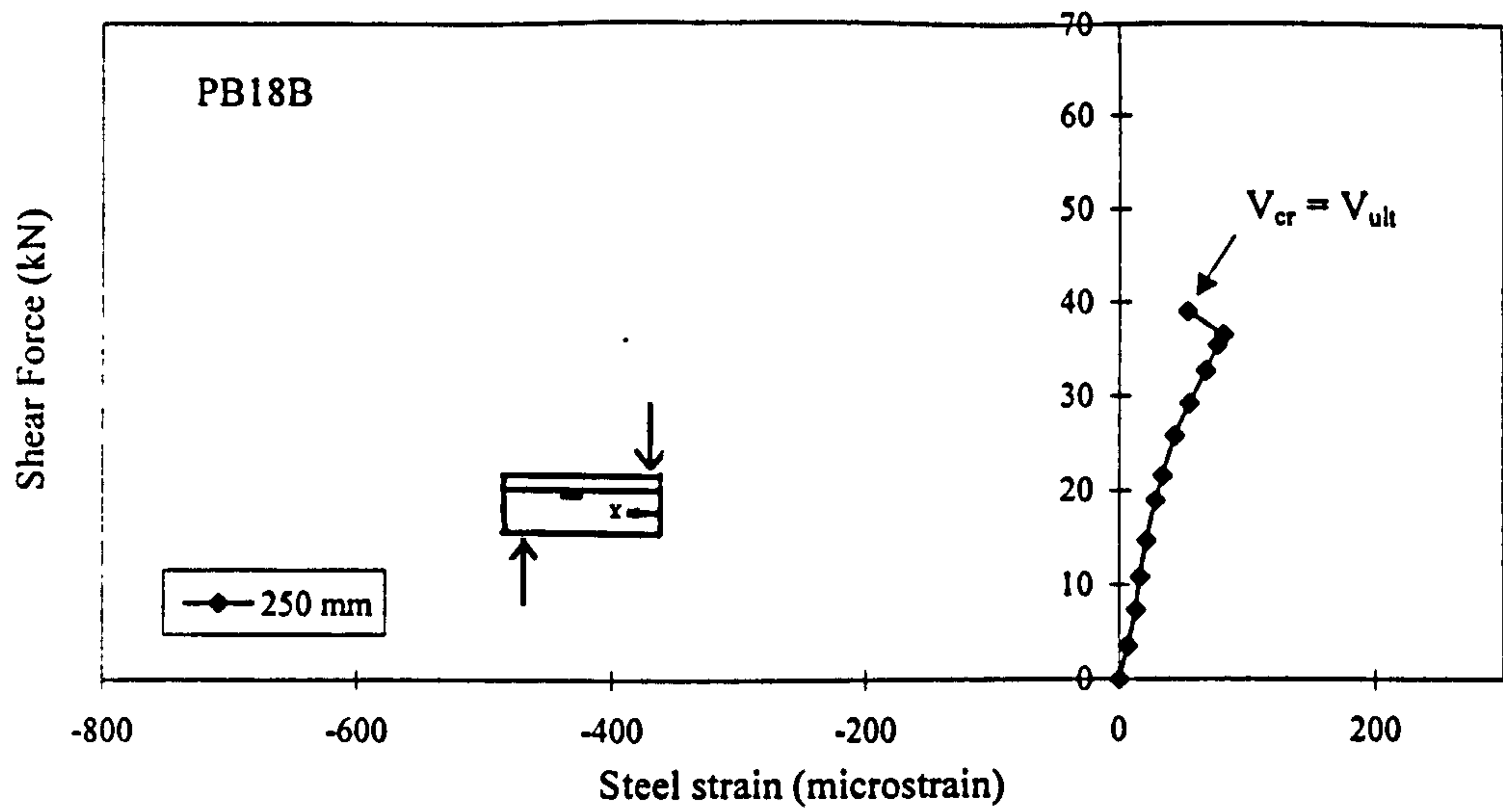


Figure 5-39 Shear load v steel strain for  $V_f = 0\%$  (PB18B)

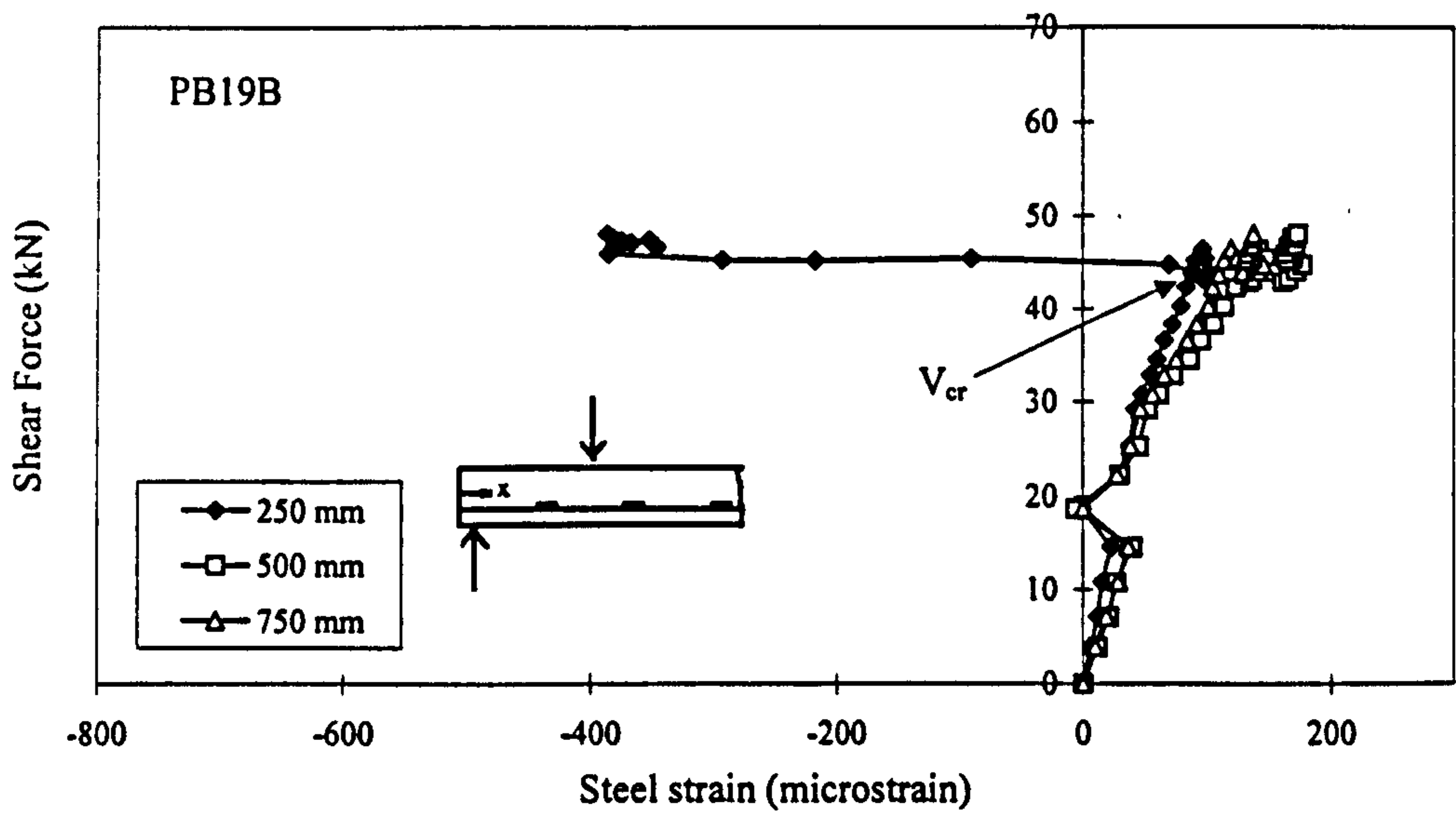


Figure 5-40 Shear load v steel strain for  $V_f = 0.5\%$  (PB19B)

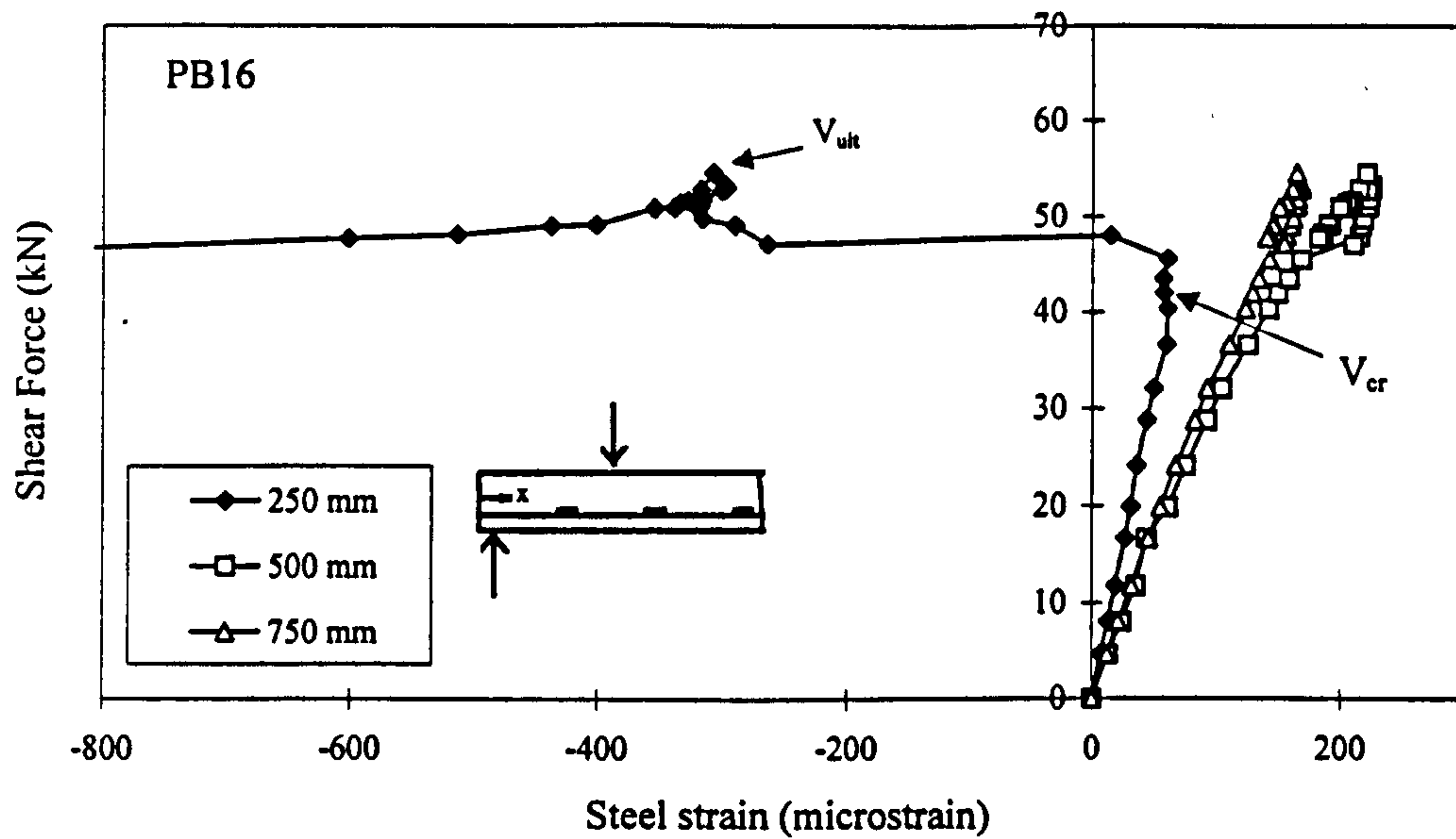


Figure 5-41 Shear load v steel strain for  $V_f = 1.0\%$  (PB16)

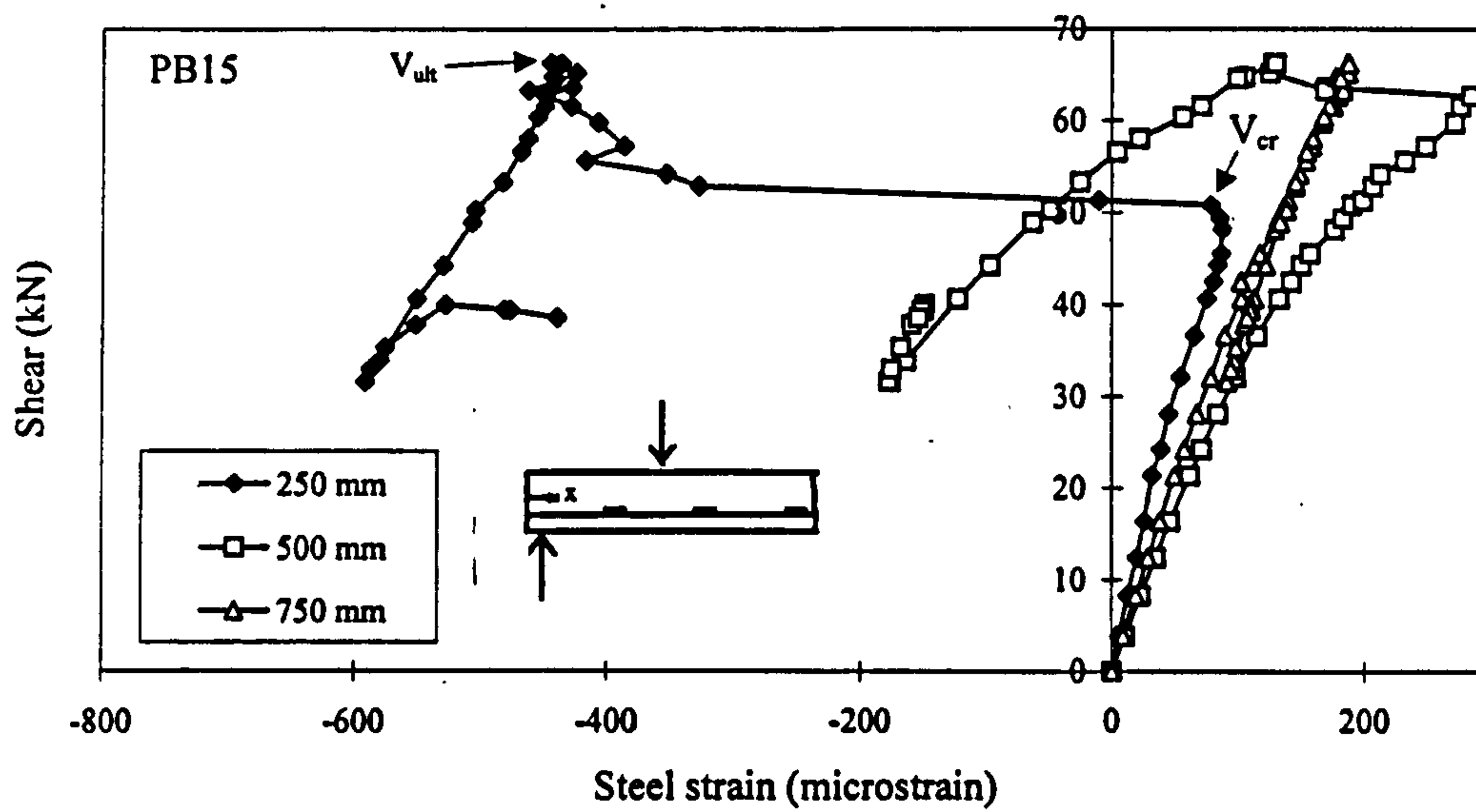
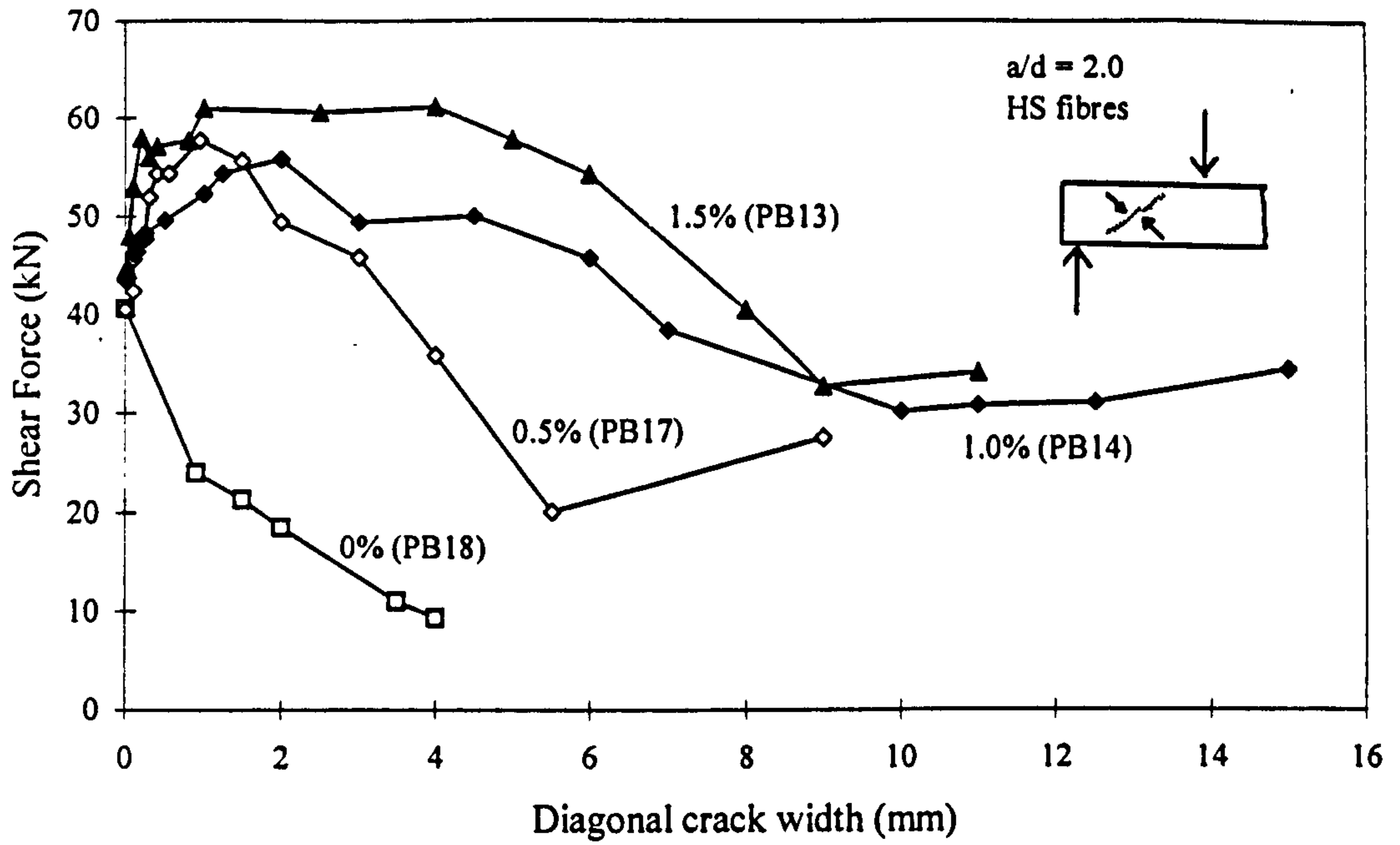
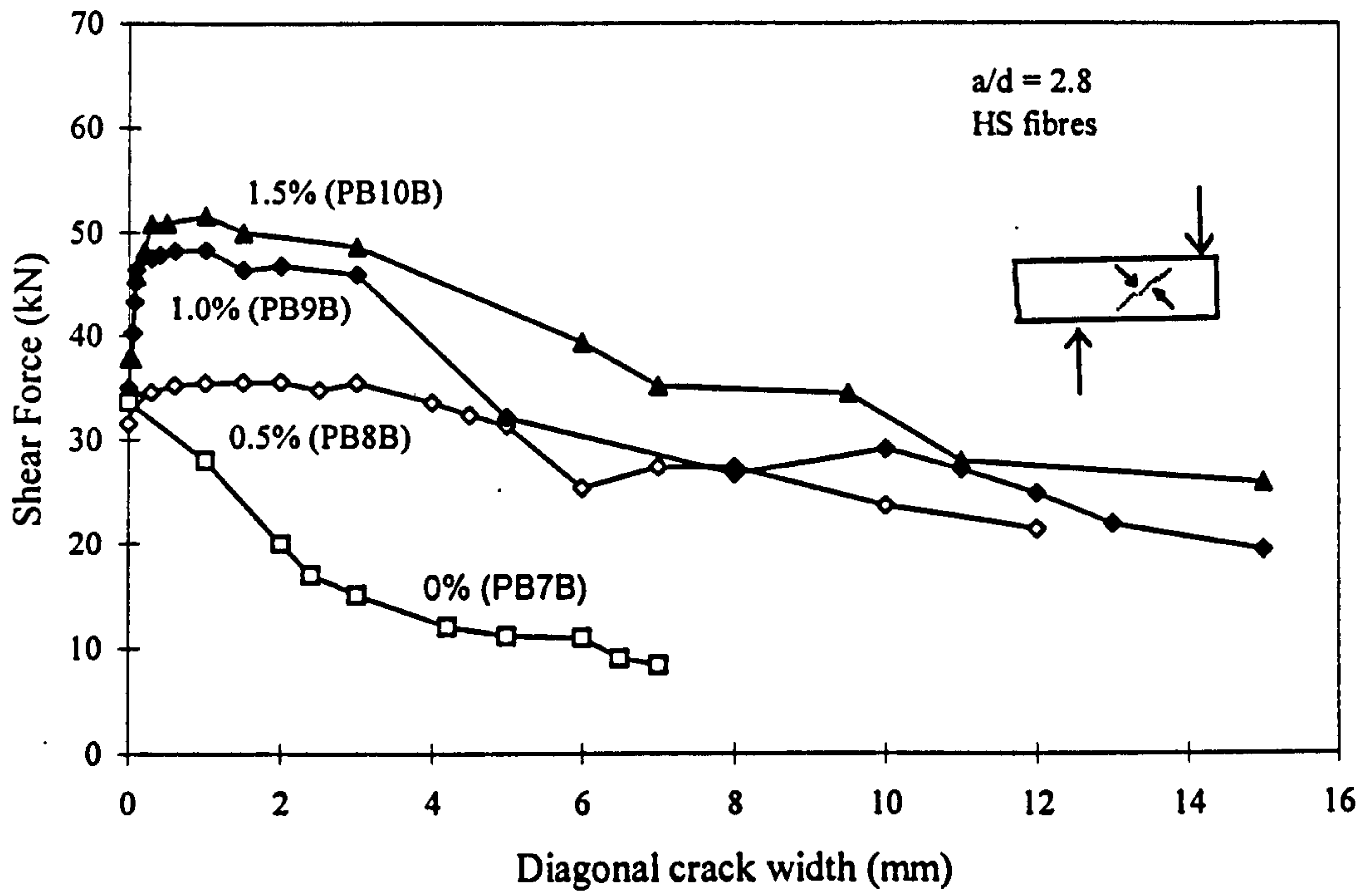


Figure 5-42 Shear load v steel strain for  $V_f = 1.5\%$  (PB15)



**Figure 5-43 Shear load v diagonal shear crack width ( $a/d = 2.0$ )**



**Figure 5-44 Shear load v diagonal shear crack width ( $a/d = 2.8$ )**

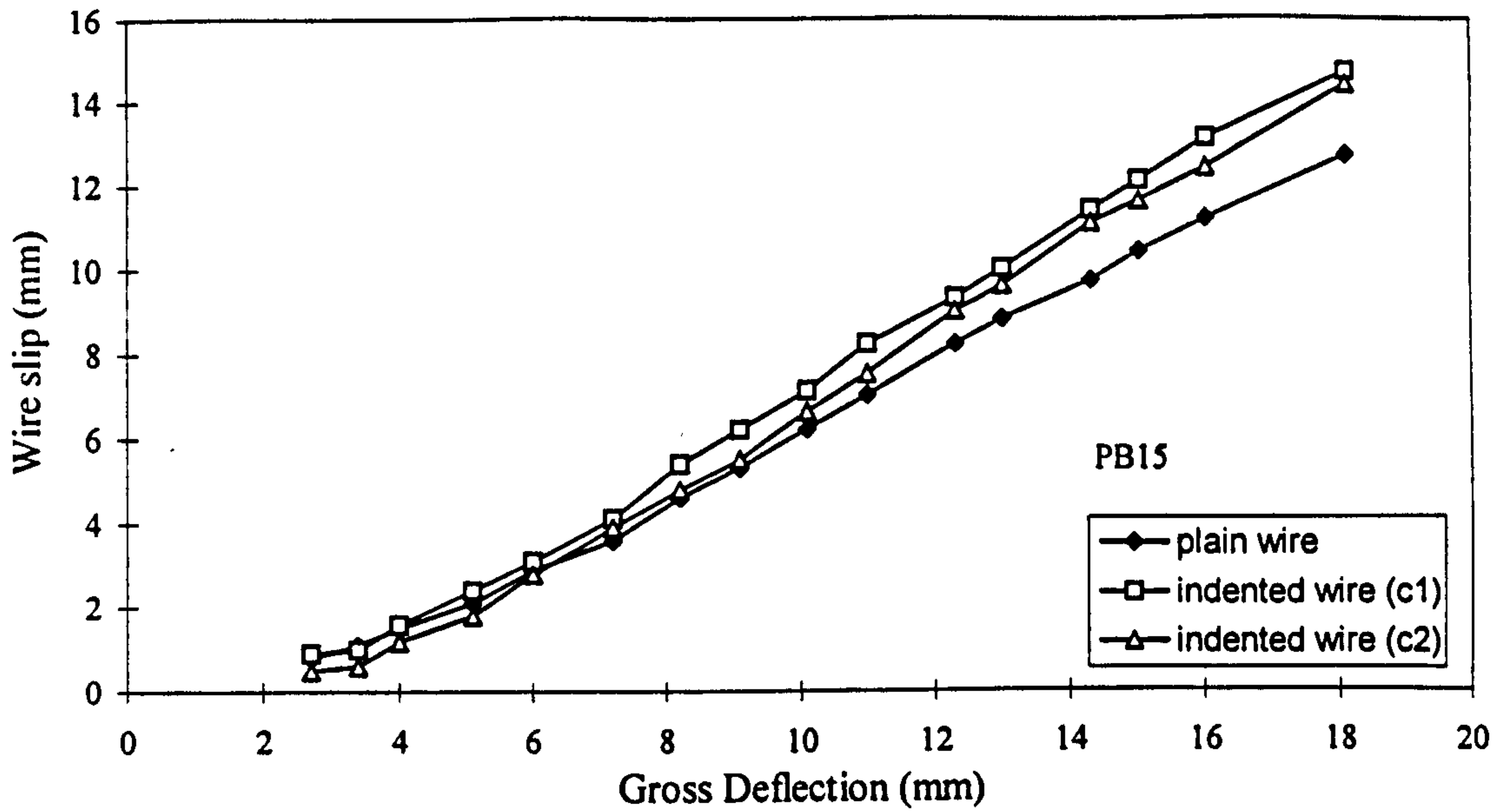


Figure 5-45 Typical wire slip v deflection curves

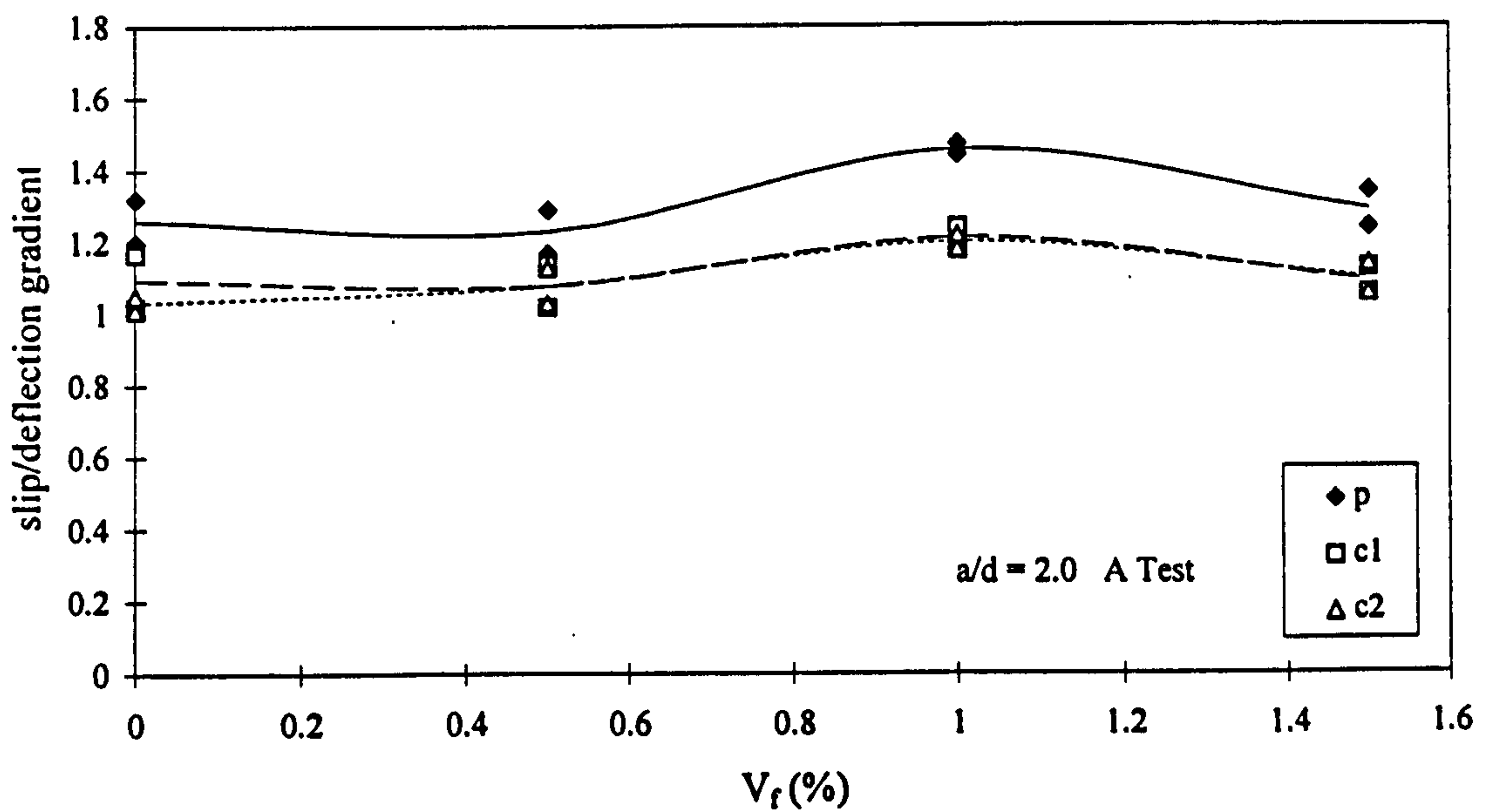


Figure 5-46 Wire slip/deflection gradient for  $a/d = 2.0$  and span = 1900 mm

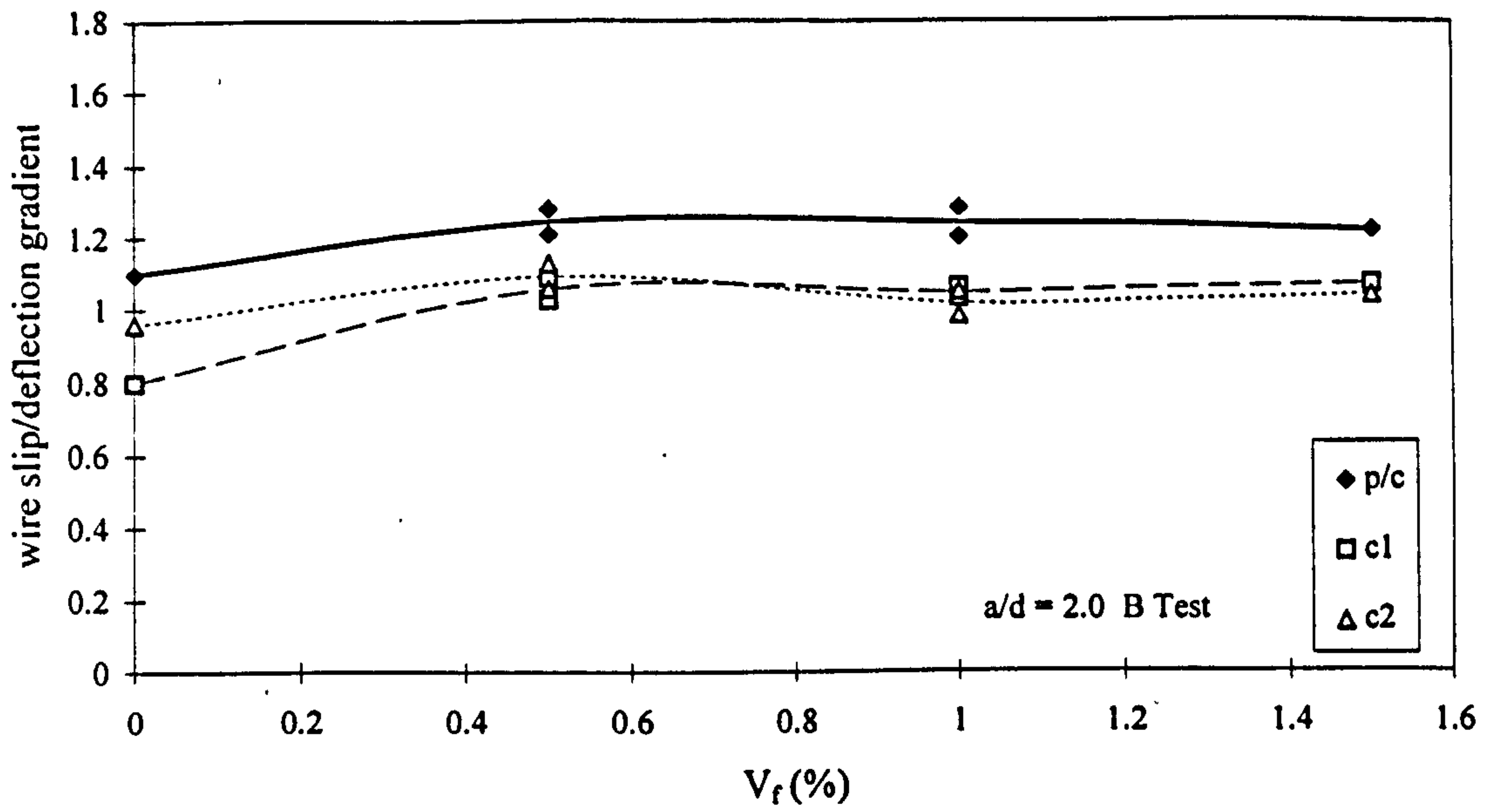


Figure 5-47 Wire slip/deflection gradient for  $a/d = 2.0$  and span = 1350 mm

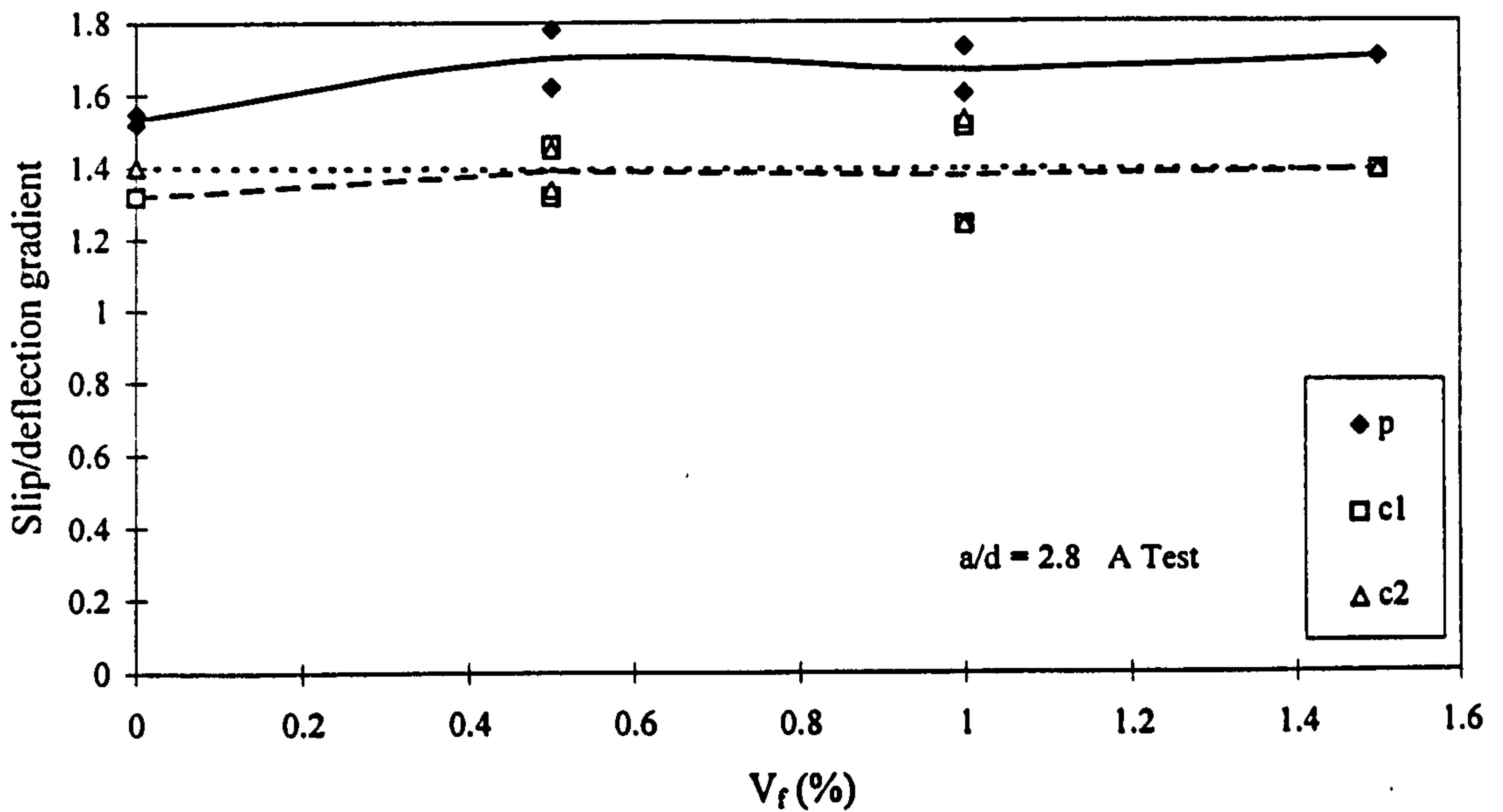


Figure 5-48 Wire slip/deflection gradient for  $a/d = 2.8$  and span = 1900 mm

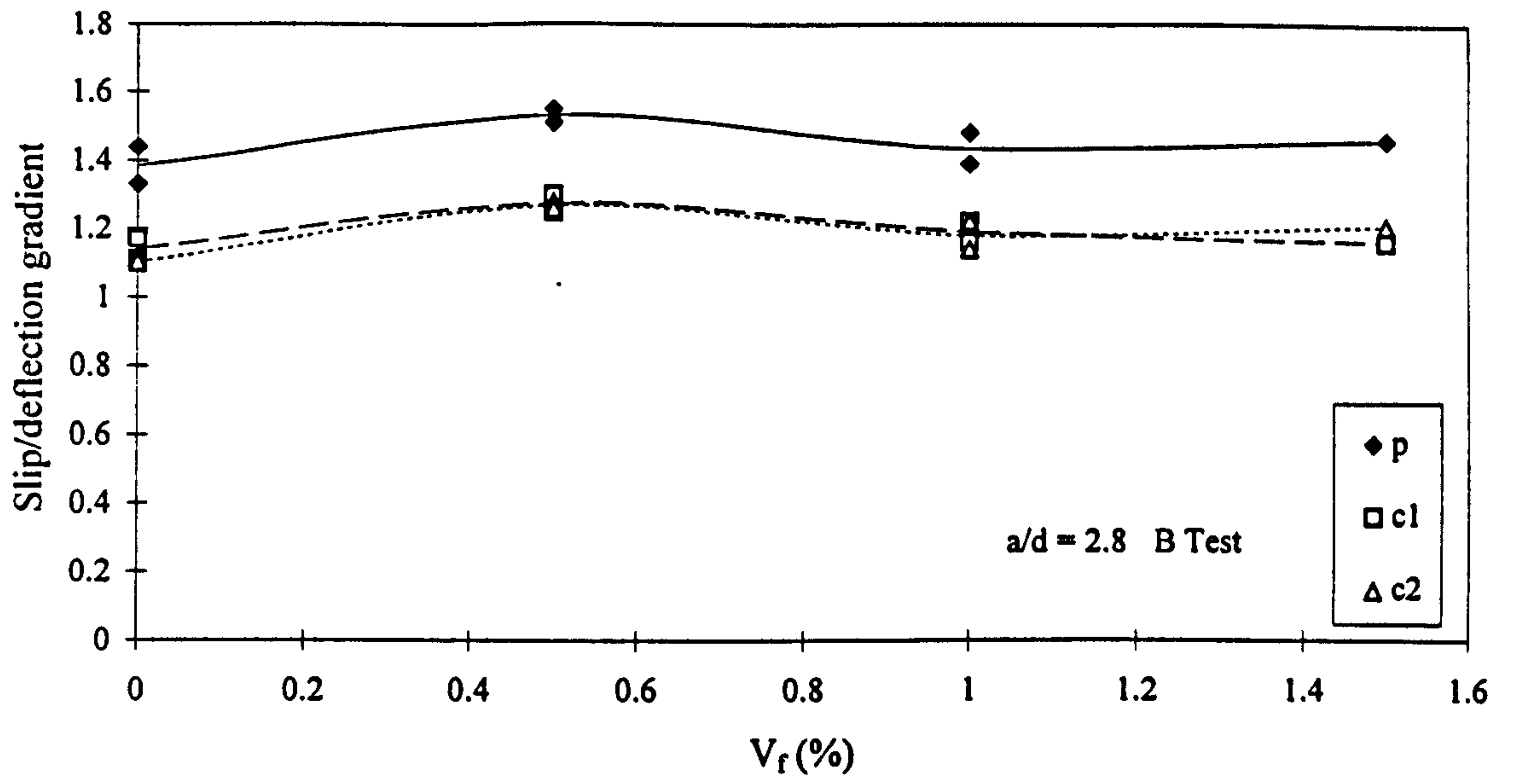
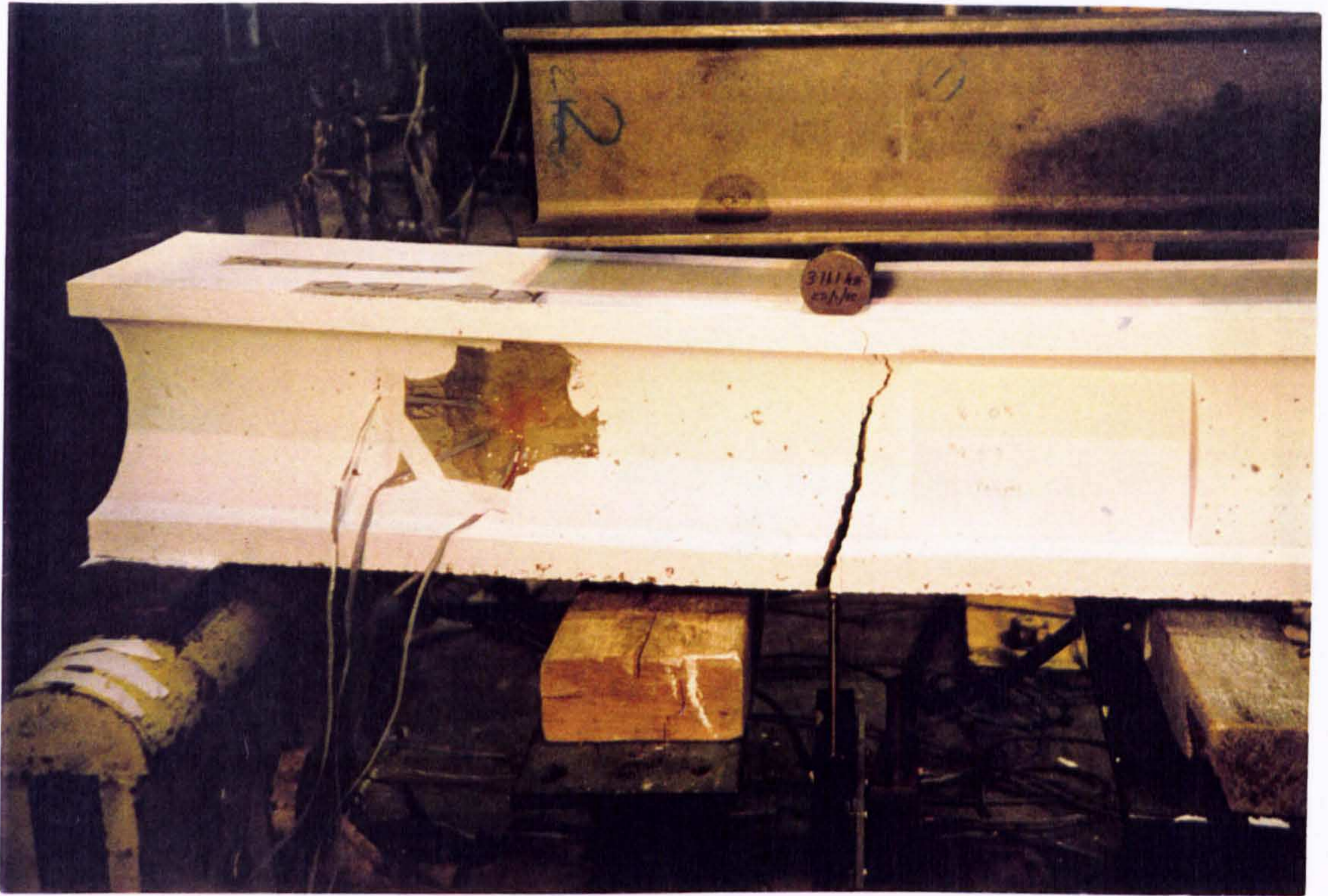
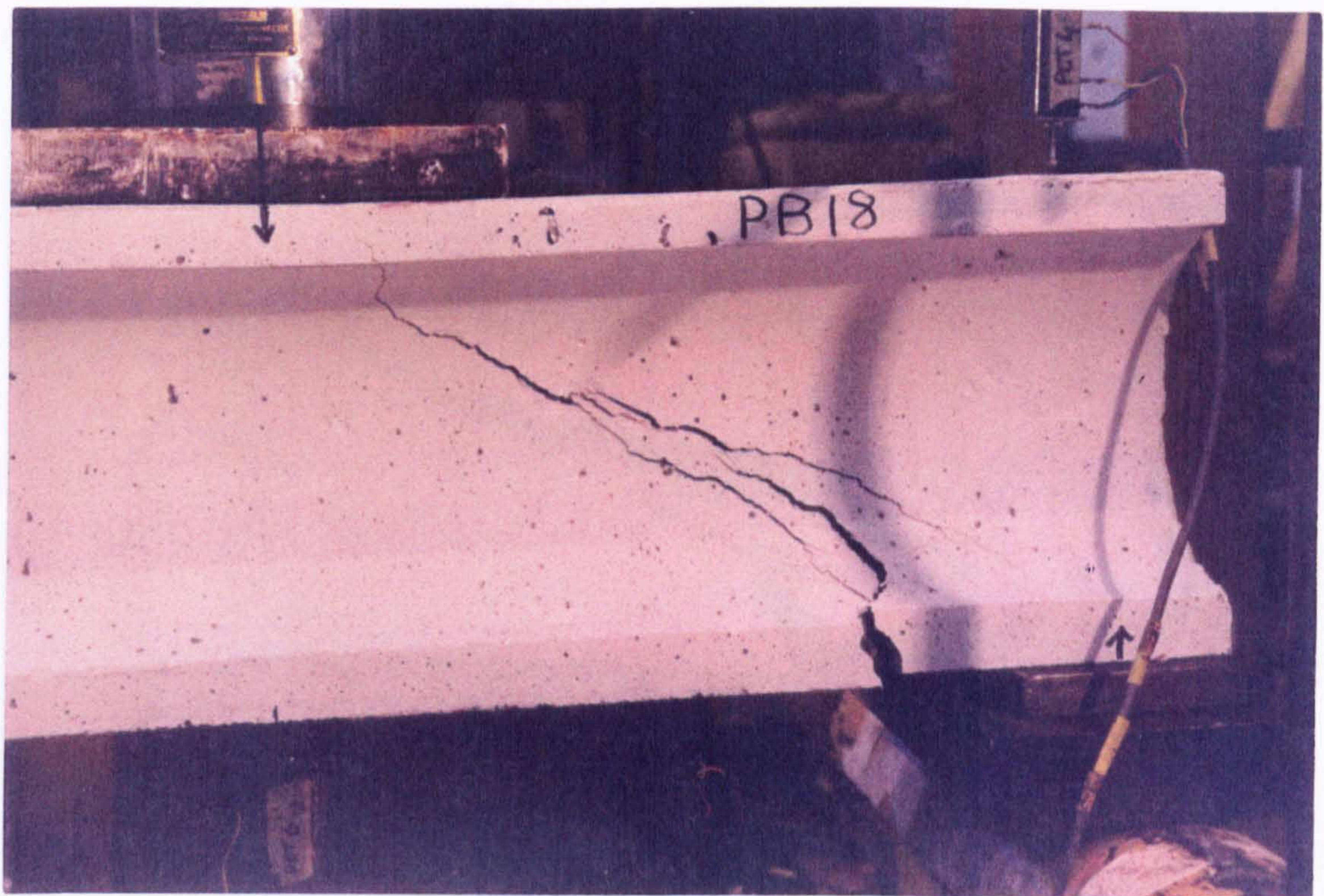


Figure 5-49 Wire slip/deflection gradient for  $a/d = 2.8$  and span = 1350 mm





**Plate 5-1 Failure of specimen PB2**



**Plate 5-2 Failure pattern for plain beam at  $a/d = 2.0$**

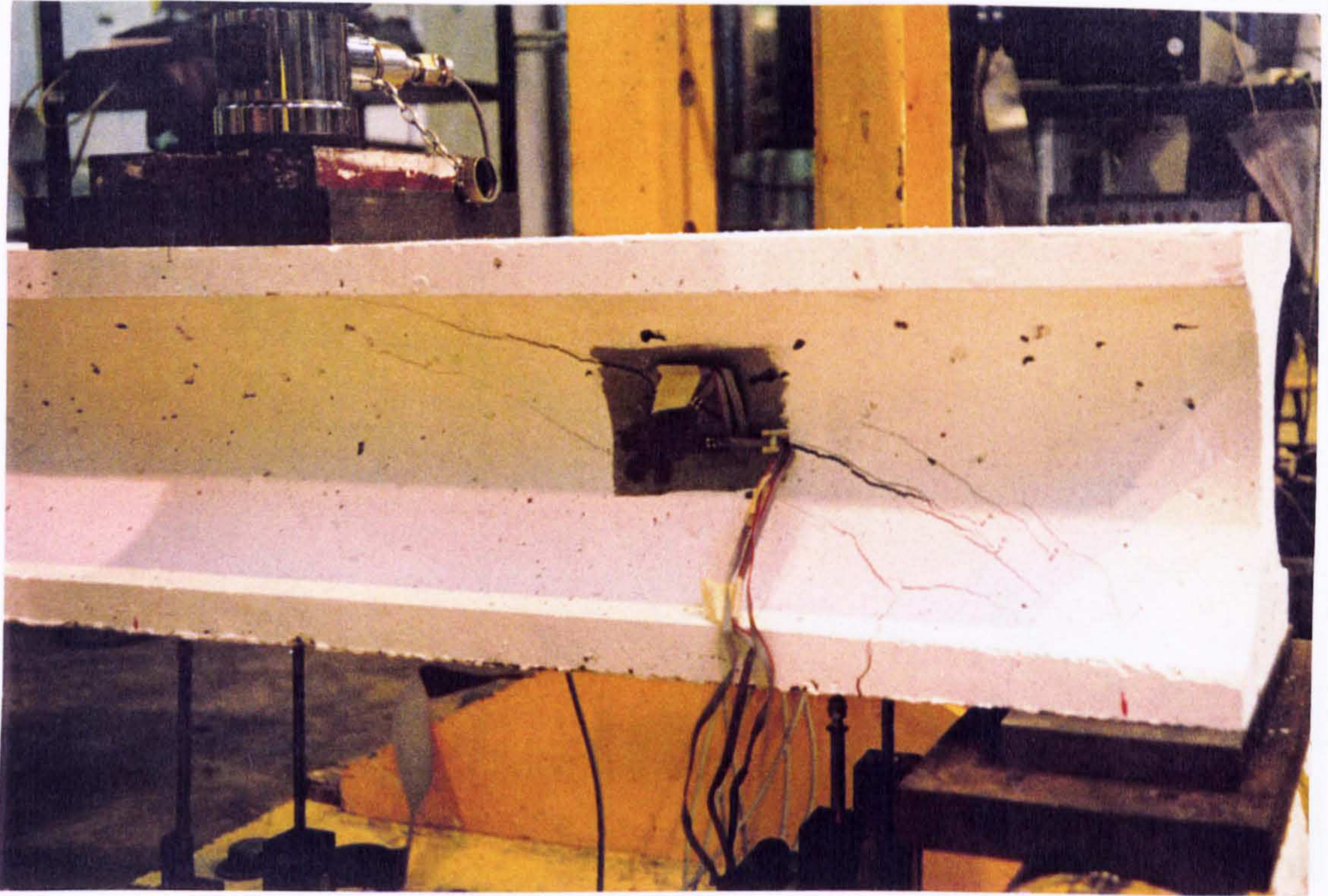


**Plate 5-3 Failure pattern for plain beam at  $a/d = 2.8$**

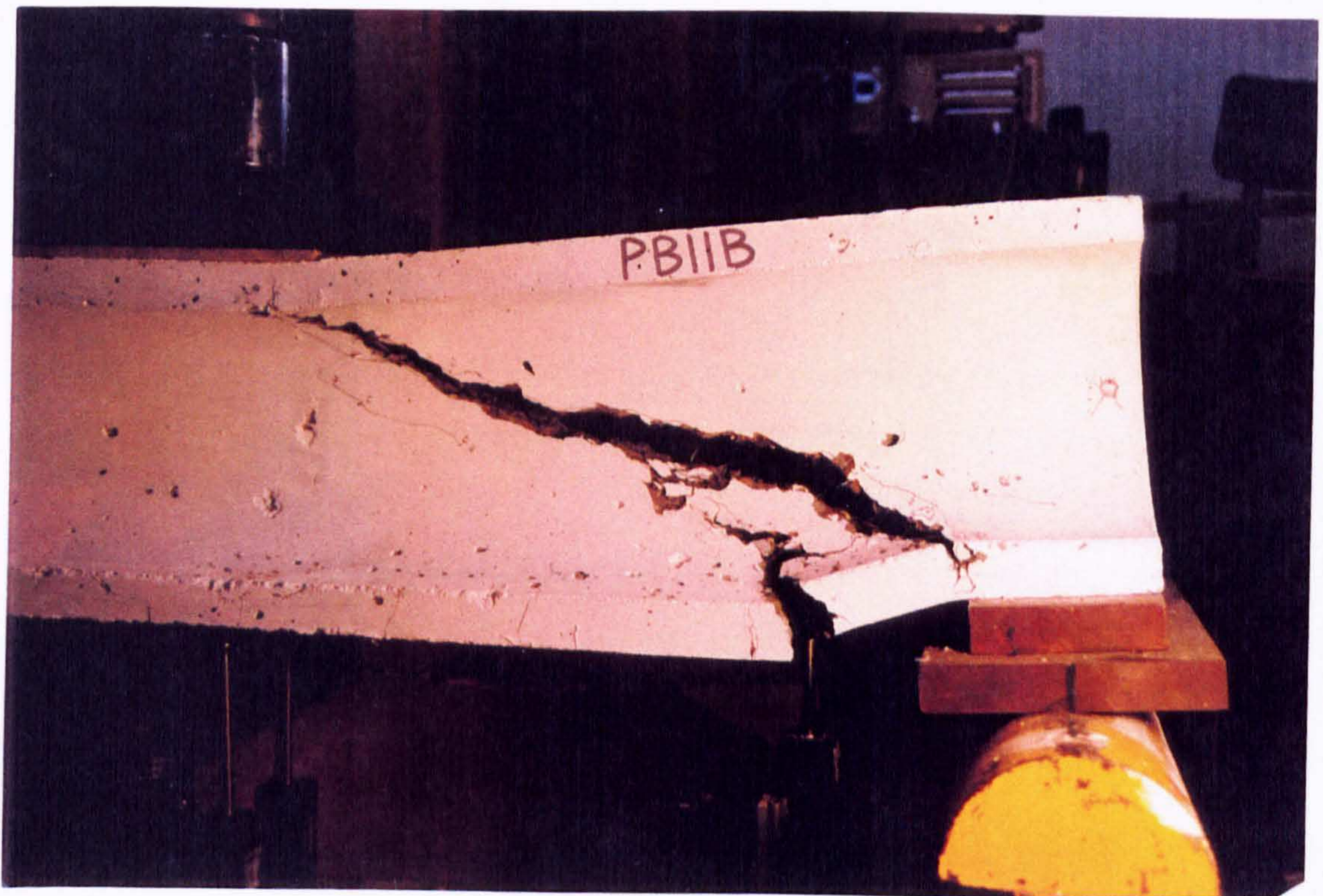


**Plate 5-4 Typical failure of PFRC beam at end of test (PB11B)**



**Plate 5-5 "Soffit crack" in beam PB10B**

# CHAPTER 6

## MANUFACTURE OF FIBRE REINFORCED HOLLOW CORE SLAB

### 6.1 Introduction

This chapter reports the trial manufacture of extruded fibre reinforced hollow core slabs which took place in a total of four trials at the premises of Richard Lees Ltd. near Derby.

Mixes used in hollow core slabs are dry and harsh, and have zero slump. For this reason prior to manufacturing any fibre reinforced slabs, a laboratory investigation was carried out to identify any specific problems with adding fibres to such mixes. This investigation is reported in this chapter and was mainly concerned with obtaining a suitable mixing procedure. Changes to the mix although considered were never implemented.

Following the laboratory investigation, the next stage was to examine how FRC would behave in the extrusion process and whether adequate compaction could be achieved. This preliminary trial production was successful, given a slight addition to the quantity of the mix water and was followed by three main trials from which the test specimens were produced.

As well as reporting on mixing and compaction of FRC hollow core slabs, this chapter also reports on the effects of extrusion on the distribution and orientation of fibres within the slabs. This was because it was expected that these factors may be affected by the flow of concrete around the augers, and the localised interruption to concrete flow due to the presence of the prestressing strand on the centre line of the web. Samples were taken from each of the four trials and from each of the tested FRC slabs to investigate these effects.

## **6.2 Laboratory Investigation**

### **6.2.1 Plain Mix**

A preliminary study was made on a typical hollow core mix in order to observe properties of the mix with regard to workability and texture. The mix used is given in Table 6-1, and was based on the mix used by the hollow core manufacturer Richard Lees Ltd., who supplied the sand and coarse aggregate used in this study. The water/cementitious material ratio of the mix was 0.3, and the aggregate/cementitious material ratio was 4.93. The percentage of coarse aggregate to total combined aggregate by volume was 62%.

The nature of the material was found to be very harsh and it was not possible to perform conventional workability tests. The concrete had zero slump and failed to compact under the small compactive effort of a Vebe Consistometer. In order to compact the concrete for conventional cube and beam tests it was found necessary to use a vibrating mechanical hammer (Kango hammer); as permitted by BS 1881 (1983). It was therefore impractical to make large specimens with this mix in the laboratory.

### **6.2.2 FRC Mix**

Considering the unworkable nature of the plain mix it was felt that there could be a need to use a water-reducing admixture, such as a plasticizer or super-plasticizer, to improve workability; since ACI Committee 544 (1993) has reported that there is a high likelihood of fibre balls occurring when fibres are added too quickly to an unworkable mix. In this report an unworkable mix is described as having a ratio of coarse aggregate to total combined aggregate by volume greater than 0.55. Since the ratio for this mix is 0.62, consideration was also given to increasing the amount of fine aggregate in proportion to the coarse aggregate.

However, as a first trial, the fibres were simply added to the plain mix. Mix proportions are shown in Table 6-1. As with the plain mix the water/cement ratio was 0.3. HS fibres (30 mm x 0.5 mm) were added at a fibre volume fraction of 0.5%.

Both ACI Committee 544 (1993) and JCI SF1 (1983a) recommend that fibres should be added to the concrete mix as the final ingredient after all other mixing has been completed, and therefore the following mixing procedure was adopted:-

1. Mix coarse aggregate and sand for 30 seconds
2. Add the cement and pulverised fuel ash (PFA) and mix for a further 30 seconds.
3. Add water whilst mixing and continue for a further 2 minutes.
4. Add steel fibres and mix for 1 minute.

Using this mixing procedure it was observed that the majority of fibres failed to separate and remained in the collated form. This suggested that the water was being absorbed by the aggregates and leaving too little free water to separate the fibres.

However the fibres that did separate were well distributed and did not form into balls. It was possible that this separation of fibres was due to the scouring action of the coarse aggregate on the fibres and not due to the dissolving effect of the water. An alternative mixing procedure was therefore developed after consultation with the fibre manufacturers (Greenhalgh 1995). No changes were made to the mix design since no problems had occurred with regard to the aggregates, and any suggestion of increasing the water content was resisted since it would have an adverse effect on the concrete strength. The revised mixing procedure was:-

1. Mix coarse aggregate, sand, cement, PFA and steel fibres for 1 minute.
2. Add water and mix for a further 2 minutes.

The mix water, suitably adjusted to account for the 4% moisture content in the sand, was added last so that all free water was available to disperse the fibres. The revised procedure was also consistent with the method of mixing at Richard Lees,

where all dry materials are added together before mixing. It was observed after this first stage of the modified procedure that some of the fibres had separated, thus confirming that the scouring action of aggregates on the fibres was responsible for the fibre separation observed when using the initial mixing procedure.

After addition of the water, the further mixing dispersed all of the fibres without any fibre balls occurring. This confirmed the original finding that no changes to the mix were required in order to obtain adequate distribution of the fibres. The revised mixing procedure was therefore felt to be sufficient for use in manufacturing extruded hollow core slabs.

## **6.3 Trial Production of FRC Hollow Core Slabs**

### **6.3.1 General**

The next stage of the study, was to investigate adding fibres in to the extrusion process. It was particularly important to investigate whether fibres would pass through the extrusion machine and what levels of compaction could be achieved. A trial production was carried out in the factory at Richard Lees Ltd. A 15 m length of 200 mm deep x 1200 mm wide slab was made. This size of slab was chosen since it is the most common type produced world-wide. Nominal section properties are given in Table 6-2. The slab was reinforced with seven 11 mm diameter helical prestressing strands prestressed to 70% of their characteristic tensile strength.

The mix used in this trial is given in Table 6-3 (which differs slightly from that in Table 6-1) and the fibre volume fraction used was 0.6%.

### **6.3.2 Mixing Procedure**

The mixing procedure recommended in Section 6.2.2 from the preliminary laboratory trials was used. The mixer was a pan type and had a capacity of 0.65m<sup>3</sup>. However because the lid of the mixer could not be raised, the fibres had to be added by hand through the observation port in the mixer. This took between 3 and 4 minutes

to complete, making the time for dry mixing longer than normal. However this did further reduce the chances of fibre balling. After the addition of water the concrete was discharged into a skip for delivery to the extruder. Visual inspection of the material in the skip showed the fibres to be well separated and distributed.

### 6.3.3 Extrusion

The slabs were produced using the 'Spiroll' extrusion technique in which the zero slump, dry mix concrete, which is self-supporting over the voids, is compacted by rotating augers to produce the required cross-section. Three batches of material were made, each producing a five metre length of slab. For the first batch the fibres were added to the traditional plain mix. Although the resulting fibre reinforced material passed through the rotating augers with no apparent difficulties, it was clear that there was poor compaction as the top surface had a very obvious honeycombed texture. This poor compaction led to the unusual circumstance of a worker accidentally stepping through the top surface of the slab into a central core.

For the second batch, an additional  $5 \text{ kg/m}^3$  of water was added to the mix shown in Table 6-3 (increasing the water/cementitious material ratio from 0.32 to 0.33) to increase the workability. This gave better compaction except over the central web, where a core taken at a later date showed the density to be only  $2350 \text{ kg/m}^3$  compared with  $2450 \text{ kg/m}^3$  for plain slabs. For the third batch, a further  $3 \text{ kg/m}^3$  of water was added, resulting in a well compacted FRC slab, which visually compared well with the plain concrete mix slabs produced immediately prior to the FRC slabs on the same bed. Plate 6-1 clearly shows the differences in compaction among the three batches.

During slab production three 100 mm cubes were made from batch three FRC for testing the compressive strength. Since the mix is too dry for normal gravity vibration compaction methods, a mechanical hammer with a footprint of 100 mm square was used. The higher water content used in Batch 3 lead to a slight reduction in the compressive strength compared with the plain mix (Table 6-4). It is possible that a superplasticizer may improve the ease of compaction of concrete and maintain



the compressive strength. However, at present it is unclear which superplasticizers are suitable for use in zero slump extruded concrete (Juvas 1996). It should be noted that the operation of the machine was not adjusted to allow for the presence of fibres, and nor was the portal above the augers opened wider to allow an easier passage of material. After detensioning, the slabs were cut to the lengths required for testing and stored in an open air stockyard prior to transporting to the University of Nottingham for testing.

## 6.4 Production of FRC Hollow Core Slabs

Following the successful trial production it was possible to produce the main FRC hollow core slabs for use in the tests described in Chapter 7. Slabs were made using both types of 30 mm long fibre previously used; the HS fibre and AM fibre.

Table 6-5 summarises the type of slab produced at each of the three main trials. Values of  $f_t$ ,  $f_b$  and  $\sigma_{cp}$  have been calculated from the known value of  $P$  and the nominal values of  $A$ ,  $Z_t$  and  $Z_b$  given in Table 6-2. The value of the eccentricity,  $e$ , has been estimated as the distance from the centroid of the prestressing tendons to the mid-height of the slab. Most of the hollow core slabs produced were cut into two metre lengths for shear and concentrated load testing, but additionally from the first trial, four sections of length 200 mm, 300 mm, 500 mm and 1 m were cut for transverse flexural testing and two metre long x-section beams were cut from the Trial 3 slab for testing individual webs in shear.

1200 mm wide by 200 mm deep slabs were produced in all the trials. In trials 1 and 2, the slabs were reinforced with seven helical strands of nominal diameter 12.5 mm. In trial 3, the reinforcement was a combination of four 7 mm diameter "Belgian crimped" wires and three 9.3 mm nominal diameter helical strands. Strands and wires were of relaxation class 2 (BS 5896, 1980) and initially prestressed to 70% of their characteristic tensile strength (i.e., 1239 N/mm<sup>2</sup>). For comparison a number of nominally identical plain slabs and x-section beams were taken from the Richard Lees stockyard for testing. The geometrical properties and prestressing details for the plain slabs are shown in Table 6-6.

Since some adjustments in the mix quantities occur on a day-to-day basis at the factory to account for small variations in aggregate quality, ambient weather conditions and individual machines, the exact increase in water content required to improve the workability of the FRC slabs was unknown. But the knowledge attained from the preliminary trial and the experience of the Richard Lees work force enabled good compaction in all slabs to be achieved - except for a slight problem in part of the 1% HS fibre slab. The exact batch quantities for each mix are given in Appendix C. The average 28 day cube results from two cubes produced from each mix are shown in Table 6-7.

## **6.5 Fibre distribution**

### **6.5.1 Wash-Out Tests**

Fibre distribution within the cross-section was investigated by simple wash-out tests on wet samples taken immediately after casting. Samples were taken from the end unit of each trial; i.e. Batch 3 from the preliminary trial (0.6% HS), 0.5% HS from Trial 1, 1% HS from Trial 2 and the AM specimen from Trial 3. The samples were weighed and then washed through a 300  $\mu\text{m}$  sieve until the retained material was free of cement and a magnet then used to extract the fibres. The weights of the sample and the extracted fibres are converted into their respective volumes, and the fibre volume fraction calculated. Collection of a representative sample is difficult because the concrete is dry and well compacted, with samples around the strand being especially difficult to collect.

The results of each of the tests are shown in Figure 6-2 at the location of each sample. The wash-out test at the preliminary trial was the most extensive of any of the trials and shows that fibres appear to be evenly distributed throughout the cross-section. Since the mean fibre volume fraction from the seven samples is 0.6%, this suggests that a negligible amount of fibres are lost in production.

The results from Trial 1 gave fibre volume fractions that were greater than expected but show good distribution. The four results from Trial 2 are widely spread

although the average value equates to the 1% fibre volume fraction added and in Trial 3 the values were as expected (0.28%) in all but one of the webs which gave a high value of 0.54%.

It can be tentatively concluded that there are only small variations in the concentration of fibres throughout the cross-section, and that the fibres are well distributed. The wash-out tests give a qualitative indication of this distribution, but are rather variable due to their nature.

### 6.5.2 Crushed Cores

To check the distribution of fibres within the length of the slab, and confirm the fibre volume fractions added, a 70 mm core bit was used to cut specimens at random locations vertically through the webs of each slab from trials 1 to 3. The possibility of choosing a light or heavily fibre reinforced region was equal for each of the slabs. Each of the cores were taken from the surface to a depth just above that of the strand or wire. A similar method to that used in the wash-out tests was then adopted. The volume of the resulting non-cylindrical cores was obtained by hydrostatic weighing and the cores then crushed to enable the fibres to be extracted by magnet. The average fibre volume fraction found in each slab is recorded in Table 6-7.

It can be seen that in the majority of slabs the measured fibre volume fractions are within 10% of the intended value. Given the method of calculating these values this would appear to be a perfectly reasonable tolerance. Slab F7 is one of only two slabs which give an average value outside this arbitrary 10% tolerance; the average fibre volume fraction value being 0.6% which is higher than that intended. This may imply that part of this slab was cut from the  $V_f = 1\%$  slab section. This is possible since the exact boundary between separate batches is not clear and the high average value of F7 is due to the peculiarly high  $V_f$  in just one core.

Of concern are the low values measured for the  $V_f = 1\%$  slab specimens. In none of the crushed cores was a fibre volume fraction greater than 1% measured and in some cores  $V_f$  was as low as 0.55%. A possible reason for the low  $V_f$ 's are that

such a high fibre content caused balling of fibres which became stuck in the mixer, hopper or extruder. However, no evidence of this was noticed at the time and Richard Lees reported no change in the level of “fibre waste” found after this trial compared with the other three trials.

A possible problem of fibre contamination had been envisaged prior to performing Trial 3 since it was not possible to clean the mixer and extruder between using the HS fibres and AM fibres. A number of HS fibres were therefore expected to be present in the AM fibre slabs. However, it was found from the crushed cores that the average  $V_f$  of HS fibres present in the AM fibre slabs was only 0.02%, with the highest  $V_f$  found to be 0.03%. Any effects of the HS fibres on AM fibre slab behaviour can therefore be assumed to be negligible.

It may be concluded that the distribution of fibres throughout the slabs was good, and that the intended levels of fibre content were reached. These cores and measured fibre volume fractions were also used to compare the density of the plain concrete within each slab - as a check on the levels of compaction achieved (see Section 6.7).

## **6.6 Fibre orientation**

### **6.6.1 Method**

A random three dimensional fibre orientation within the slab was considered unlikely due to the narrow thickness of the flanges and webs, and to the polarisation of the compaction of concrete as the extrusion machine travels along the bed.

The method used to evaluate changes in the fibre orientation through the depth of the slabs was to saw the web into a number of roughly 40 mm cubic sections so that the fibres in each of the orthogonal directions were exposed. The number of fibres intercepting each of the six faces were visually counted and an orientation factor, the average ratio of the projected fibre length in each direction to the actual fibre length, calculated from the following relationship (Armelin and Helene 1996)

$$\eta_{\theta} = \frac{N.V}{\Sigma L_f}$$

where  $N$  is the number of fibres per unit area;  $V$  is the sample volume found by hydrostatic weighing of the specimen; and the total length ( $\Sigma L_f$ ) of all the fibres in the specimen is obtained by crushing the specimen and collecting the fibres. For a 3-dimensional random distribution where the fibres have an equal probability of orienting in any direction, a theoretical orientation factor of 0.41 exists (Romualdi and Mandel 1964) as previously explained in Section 2.1.1.

This type of method had previously been successfully employed on flexural test specimens (Soroushian and Lee 1991) and sprayed concrete panels (Armelin and Helene 1996). In these previous examinations the specimens had been fractured such that fibres were projecting from a cracked surface. Both these examinations were interested in the fibre orientation across one specific plane.

For this study of orientation in hollow core slabs, all three orthogonal directions were of interest. Specimens were therefore sawn from the slab, which left flat smooth surfaces from which fibres are less clear. This was not a problem with the HS fibre, but made AM fibres very difficult to pick out due to their small thickness. Each of the sections cut from AM fibre slabs were therefore submerged in 10% dilute hydrochloric acid for four days to remove a thin coat of concrete on each side.

Four sections were cut from the 0.6% HS slabs (preliminary trial - batch 3) which were: two vertical sections; one section aligned at an angle of  $35^\circ$  to the longitudinal; and a section aligned at an angle of  $45^\circ$  to the longitudinal. Additionally two vertical sections were cut from the AM fibre slab.

Each of the sections were cut from undamaged parts of the slab after shear testing (Chapter 7). The chosen angles of  $35^\circ$  and  $45^\circ$  to the longitudinal for the HS slabs correspond with the shear failure planes formed at  $a/d = 2.8$  and  $a/d = 2.0$ , respectively, found in these shear tests and in the tests on PFRC x-beams (Chapter 5).

## 6.6.2 Results and Discussion

Figure 6-3 shows the average results from the two HS fibre slab vertical sections. At the top of the web, fibre orientation is shown to be more pronounced in the longitudinal direction (the direction that the slab is produced). This is probably due to the drag of the machine moving over the top surface reorienting many vertically aligned fibres; such fibres may provide resistance to cracks caused by tensile stresses at the release of prestress.

There appears to be no favourable orientation at the bottom of the slabs with the values close to that expected for a random distribution. However, because of the location of the prestressing strand the prism cut from the bottom of the slab was about 60 mm high and the orientation effects that might have been expected in the vicinity of the boundary may have been masked. An alignment in the horizontal plane might have been anticipated and this would increase strength and ductility in the transverse direction. In the web the situation is significantly different. The rotating augers appear to cause fibres to orient vertically, at the expense of the longitudinally and transversely aligned fibres. It would be expected that this could provide beneficial shear reinforcement.

Figure 6-4 shows results from the two diagonally cut HS fibre specimens showing fibre orientation perpendicular to the equivalent of a 45° inclined shear crack and a 35° inclined shear crack, respectively.

For the 45° specimens, two pairs of faces are inclined at 45° to the longitudinal, and it would be expected that they would give identical results if the orienting of fibres was in a straightforward vertical sense due to the rotation of the augers. However, Figure 6-4 clearly shows that there is a further mechanism affecting the fibres. Fibre alignment is strong in the x direction at the top of the slab (i.e. greater than 0.41) but weak at the bottom, and vice versa for the z direction. The two 45° sections are therefore effectively mirror images of each other, and interestingly the cross-over point is in the centre of the slab at a depth of about 100 mm. The direction in which the slab is formed has an effect on the orientation but the effect is different at the bottom and the top. The section cut at 35° is similar to the z section at

45°, with a weaker alignment at the top and a stronger alignment at the bottom. For both 35° and 45° planes, however, the average orientation factor is equal to the random distribution factor of 0.41. Therefore despite the effects of the augers and manufacturing method, it can be supposed that the orientation factor for fibres acting as shear reinforcement can be taken as 0.41. This value is therefore used for HS fibres in the theoretical section of this thesis (Chapter 8). For other types of failure, alternative orientation factors may be appropriate.

The average result for each orthogonal direction from the two AM fibre slab specimens (i.e. four faces) are shown in Figure 6-5. The average fibre orientation factor of 0.61 is significantly higher than the value of 0.41 found for HS fibres. This suggests that the theory which works for rounded fibres may be inappropriate for thin ribbon-like fibres which have a much greater width to thickness ratio.

The AM fibres in the centre of the web tend to be aligned in the vertical direction (like the HS fibres) at the expense of transverse and longitudinal directions. Towards the soffit the orientation factor in all orthogonal directions is similar and equal to that of the average value - suggesting no favourable orientation. The general features of the effect of extrusion orientation therefore appear to be consistent with both fibre types. However, the high orientation factors found towards the top of the slab cannot be explained.

For comparative purposes Figure 6-6 and Figure 6-7 show the orientation factor through the depth of three laboratory-cast prestressed x-beams used in the testing described in Chapter 5. The beams PB5, PB16 and PB15 represent 0.5%, 1.0% and 1.5% HS fibre volume fractions, respectively, and the figures refer to vertical sections and sections cut at 45° to the horizontal. In each case there are no obvious patterns to the variation in orientation factor through the depth of the slabs and it can be inferred that laboratory casting of these x-beams has no apparent effect on the orientation of the fibres. The average fibre orientation factor calculated from all the orthogonal directions and depths is given in each figure, and can be seen to vary between 0.38 and 0.45. This shows that the orientation factor of 0.41 is equally suitable for use in these beams. The different manufacturing method adopted for the

laboratory cast x-beams and the factory cast x-beams and slabs should not therefore cause any differences in the amount and provision of fibre reinforcement.

## 6.7 Concrete Density of Slabs

Each of the cores used for calculating the distribution of the fibres were additionally used for checking the density of the plain and fibre reinforced concrete. Measurement of the density of the FRC ( $\rho_{FRC}$ ) was simply achieved by hydrostatic weighing of the specimens, and the density of the plain concrete, or matrix ( $\rho_{conc}$ ) was then estimated as

$$\rho_{conc} = \frac{\rho_{FRC} - V_f \rho_f}{(1 - V_f)}$$

... 6-2

where  $\rho_f$  is the density of the fibres used.

The average results for each slab are shown in Table 6-8. The most interesting densities are those of the matrix since this can be used to compare the degree of compaction achieved in each of the slabs. This is because given identical mix proportions, the density is directly related to the degree of compaction. With slight excesses in any of the mix proportions, the density can easily vary by as much as 20 kg/m<sup>3</sup>. Since the only intended variation in the matrix of the fibre mixes was a slight adjustment in the water content, the ingredient with the lowest specific gravity, it would be expected that the matrix density in the FRC slabs would be within this 20 kg/m<sup>3</sup> of the density of plain concrete slabs.

For comparison, the density of some plain hollow core sections were measured as: 2438 kg/m<sup>3</sup> (slab P15), 2451 kg/m<sup>3</sup> (slab P16) and 2441 kg/m<sup>3</sup> (transverse section P500) which gives an average value of 2444 kg/m<sup>3</sup> at a standard deviation of 12 kg/m<sup>3</sup> for the nine cores tested.

It can be seen that the density of the concrete matrices achieved in the FRC slabs are very similar to that in the plain slabs. The slabs from the first trial, however,



give lower than expected densities, but this was to some extent expected because compaction had been difficult due to the quantities of water used being on the low side of that used in the preliminary trial. The poor compaction of the 1% fibre volume fraction slabs (as previously noted) are shown in the result of slab F8, although slab F9 appears to have been as well compacted as the plain slabs. The low density of F8 along with the apparently low fibre volume fraction (see Section 6.5.2) suggests that this slab may not be a representative test specimen.

Interestingly the highest matrix densities were for the slabs made with AM fibres, suggesting that flexible fibres are less troublesome to the extrusion process than the more rigid HS fibres. (This was also acknowledged by the factory workers who commented that the AM fibres were by far the easier to use.)

In general the density of the concrete matrix achieved in the plain and fibre reinforced concretes are very similar and it can be concluded that the extruded fibre reinforced slabs are as well compacted as their plain counterparts.

**Table 6-1 Mix Proportions used in Preliminary Trials (kg/m<sup>3</sup>)**

	Plain	FRC
Sand <sup>1</sup>	732	728
10 mm Aggregate	678	674
14 mm Aggregate	523	520
RHPC <sup>2</sup>	323	321
PFA <sup>3</sup>	69	68
Water	118	118
HS Fibres	-	39

<sup>1</sup>Medium zone sand, complying with BS 882 (1992), <sup>2</sup>Rapid hardening Portland cement, complying with BS 12 (1991), <sup>3</sup> Pulverised fuel ash, complying with BS 3892: Part 1 (1993)

**Table 6-2 Section properties based on nominal properties of hollow core slab**

slab thickness	203 mm	nominal slab width	1200 mm
Cross-sectional area, A	135 x 103 mm <sup>2</sup>	height to neutral axis	102 mm
Second moment of area, I	678.5 x 106 mm <sup>4</sup>	effective depth, d	160 mm
Section modulus (bottom), Z <sub>b</sub>	6.65 x 106 mm <sup>3</sup>	self - weight	2.67 kN/m <sup>2</sup>
Section modulus (top), Z <sub>t</sub>	6.72 x 106 mm <sup>3</sup>		

**Table 6-3 Concrete Mix used in Trial Production of Hollow Core Slab**

	Plain Mix	FRC Mix (Batch 1)	
	(kg/m <sup>3</sup> )	Batch Weight (kg)	(kg/m <sup>3</sup> )
Sand <sup>1</sup>	757	515	754
10 mm Aggregate	669	455	666
14 mm Aggregate	515	350	512
RHPC <sup>2</sup>	319	217	318
PFA <sup>3</sup>	68	46	67
Water	124	84	123
HS Fibres	-	33	48

<sup>1</sup>Medium zone sand, complying with BS 882 (1992), <sup>2</sup>Rapid hardening Portland cement, complying with BS 12 (1991), <sup>3</sup> Pulverised fuel ash, complying with BS 3892: Part 1 (1993)

**Table 6-4 Result of cube compression tests on preliminary trial slab mix**

	Compressive strength (N/mm <sup>2</sup> )	Mean compressive strength (N/mm <sup>2</sup> )
Plain Mix	93	94
	92	
	97.5	
FRC Mix (Batch 3)	93	90.5
	90	
	89	

Table 6-5 Specimens produced at each of the main FRC trials

Trial	Slab No.	Fibre Type	$V_f$ (%)	Wires and Strands	P (kN)	b (mm)	h (mm)	e (mm)	$f_t$ (N/mm <sup>2</sup> )	$f_b$ (N/mm <sup>2</sup> )	$\sigma_{cp}$ (N/mm <sup>2</sup> )
1	F1	HS	0.5	7x12s	806	271	198	45	0.6	11.4	6
	F2					269	198	46	0.5	11.5	6
	F3					293	198	44	0.7	11.3	6
	TS										
2a	F4	HS	0.5	7x12s	806	252	199	52	-0.2	12.2	6
	F5					250	199	50	0	12	6
	F6					253	198	51	-0.1	12.2	6
	F7										
2b	F8	HS	1	7x12s	806						
	F9					272	196	47	0.3	11.7	6
3a	F10	AM	0.28	3x9s + 4x7w	518	298	210	56	-0.6	8.3	3.9
	F11					245	210	56	-0.6	8.3	3.9
3b	F12	HS	0.5	3x9s + 4x7w	518	241	208	60	0.7	8.5	3.9
	x-beams										

TS = transverse specimens (F100, F200, F500 and F1000)

12s = 12.5 mm helical strand, 9s = 9.3 mm helical strand, 7w = 7 mm indented wire

**Table 6-6 Geometrical properties and reinforcement details for plain concrete slabs**

Slab No.	Wires and Strands	P (kN)	b (mm)	h (mm)	e (mm)	$f_t$ (N/mm <sup>2</sup> )	$f_b$ (N/mm <sup>2</sup> )	$\sigma_{cp}$ (N/mm <sup>2</sup> )
P13	7x12s	806	260	200	55	-0.6	12.6	6
P14			287	199	50	0	12	6
P15			288	201	55	-0.6	12.6	6
P16								
P17			288	202	62	-1.5	13.5	6
P18			264	203	61	-1.3	13.4	6
P19	3x9s + 4x7w	518	296	202	58	-0.6	8.3	3.9
P20			312	200	56	-0.5	8.2	3.9

12s = 12.5 mm helical strand

9s = 9.3 mm helical strand

7w = 7 mm indented wire

**Table 6-7 Compressive strength and measured *in situ* fibre volume fraction**

Trial	Slab No.	Fibres	$f_{cu}^a$ (N/mm <sup>2</sup> )	Intended $V_f$ (%)	Measured $V_f$ (%) <sup>b</sup>	standard deviation (%)
1	F1	HS	86.5	0.5	0.46	0.04
	F2	HS		0.5	0.54	0.06
	F3	HS		0.5	0.49	0.06
2	F4	HS	79.5	0.5	0.51	0.08
	F5	HS		0.5	0.54	0.05
	F6	HS		0.5	0.53	0.02
	F7	HS		0.5	0.6	0.11
	F8	HS	91.2	1	0.71	0.24
	F9	HS		1	0.91	0.03
3	F10	AM	89	0.28	0.29	0.13
	F11	AM		0.28	0.25	0.02
	F12	HS	81.5	0.5	0.5	0.05

*plum rouge*

<sup>a</sup> mean of 2 results

<sup>b</sup> mean of 3 results

**Table 6-8 Density of FRC slabs and calculated density of the matrix**

Trial No.	Slab No.	Fibre type	Density of FRC (kg/m <sup>3</sup> )	Density of matrix (kg/m <sup>3</sup> )
1	F1	HS	2432	2408
	F2	HS	2434	2418
	F3	HS	2436	2409
2	F4	HS	2467	2444
	F5	HS	2466	2440
	F6	HS	2464	2430
	F7	HS	2468	2439
	F8	HS	2463	2419
	F9	HS	2483	2435
3	F10	AM	2476	2463
	F11	AM	2453	2449
	F12	HS	2464	2437

<sup>a</sup> mean of 3 results

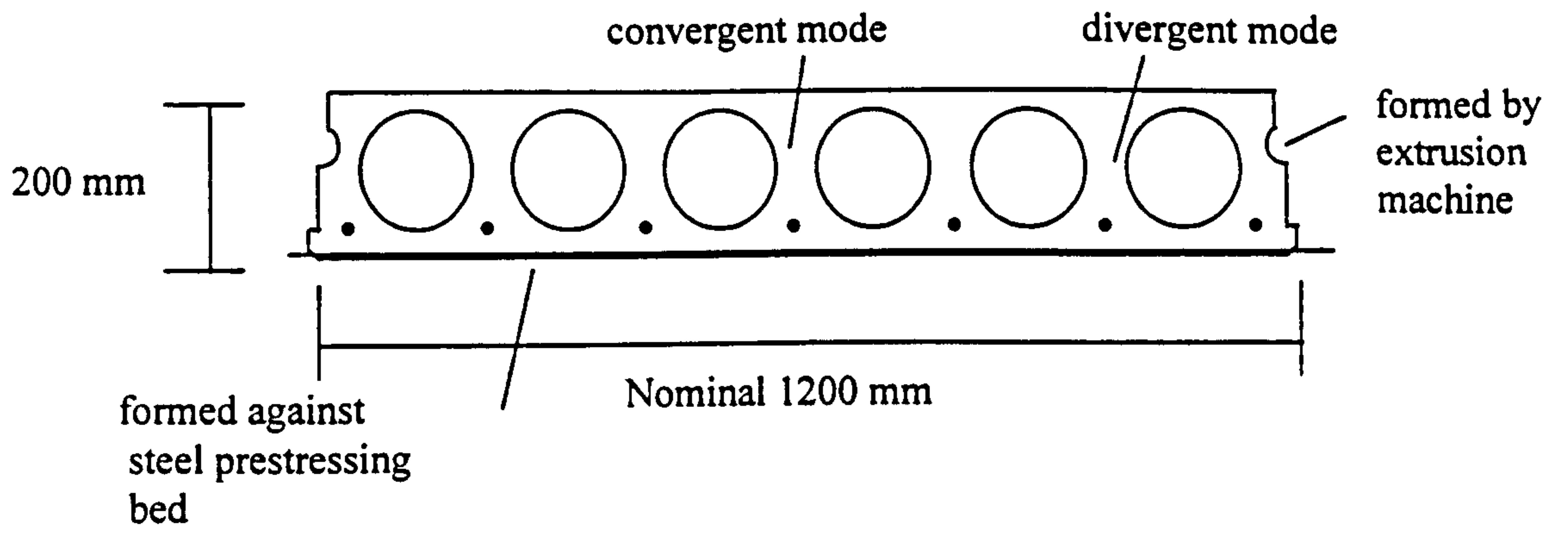
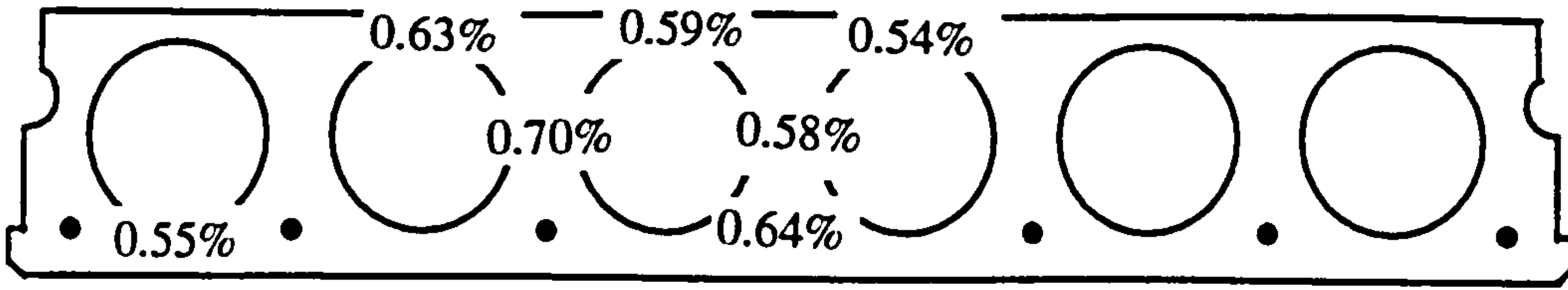
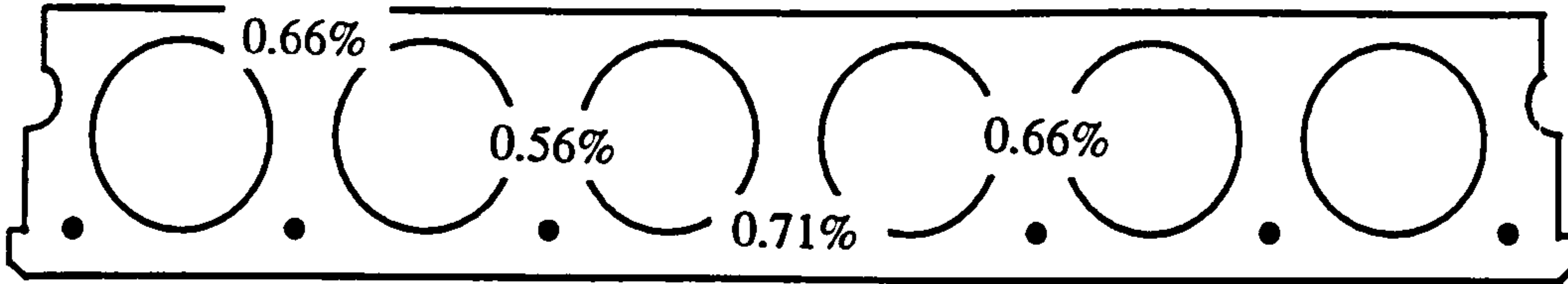


**Figure 6-1 Rotation of augers in 'Spiroll' extrusion**

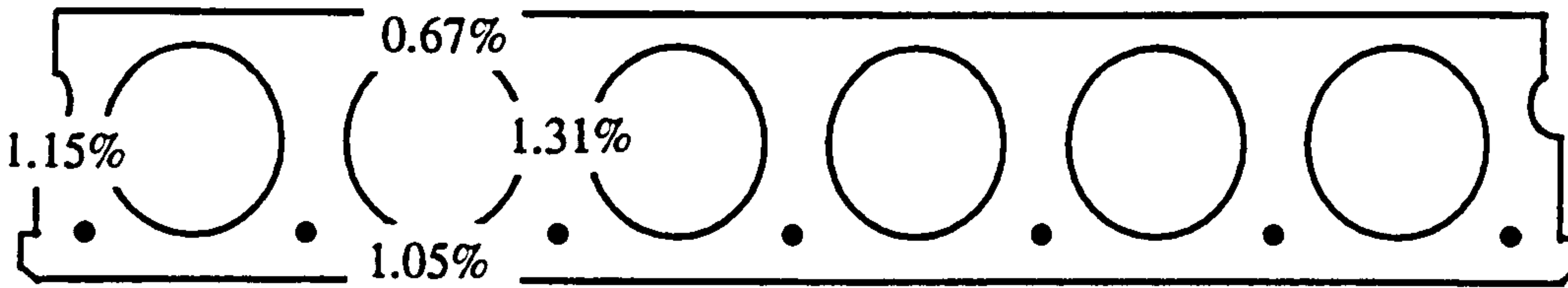




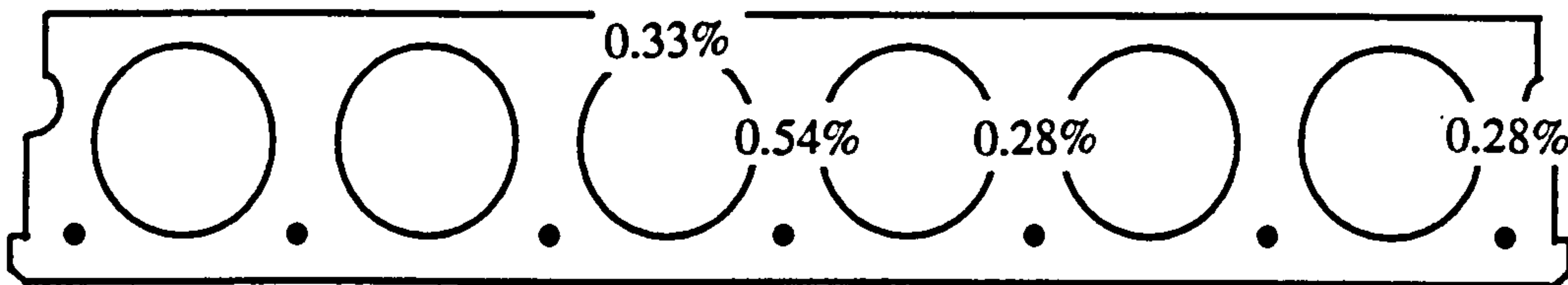
a) Preliminary trial - 0.6% HS



b) Trial 1 - 0.5% HS



c) Trial 2 - 1% HS



d) Trial 3 - 0.28% AM

**Figure 6-2 Wash-Out test results: a) Preliminary trial (0.6% HS), b) Trial 1 (0.5% HS), c) Trial 2 (1% HS), d) Trial 3 (0.28% AM)**

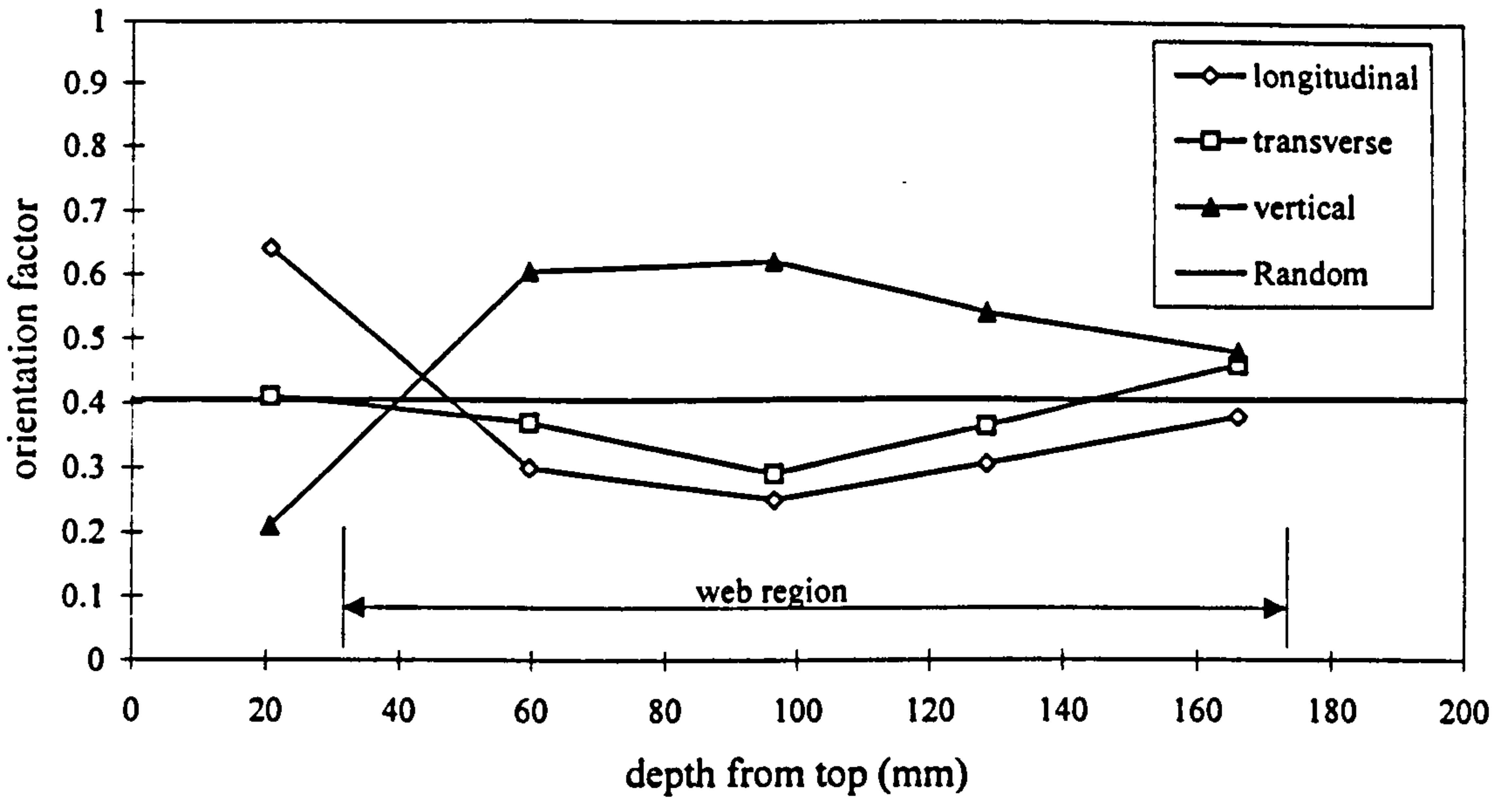


Figure 6-3 Orientation factor for the three orthogonal directions throughout depth of slab (HS fibre slabs)

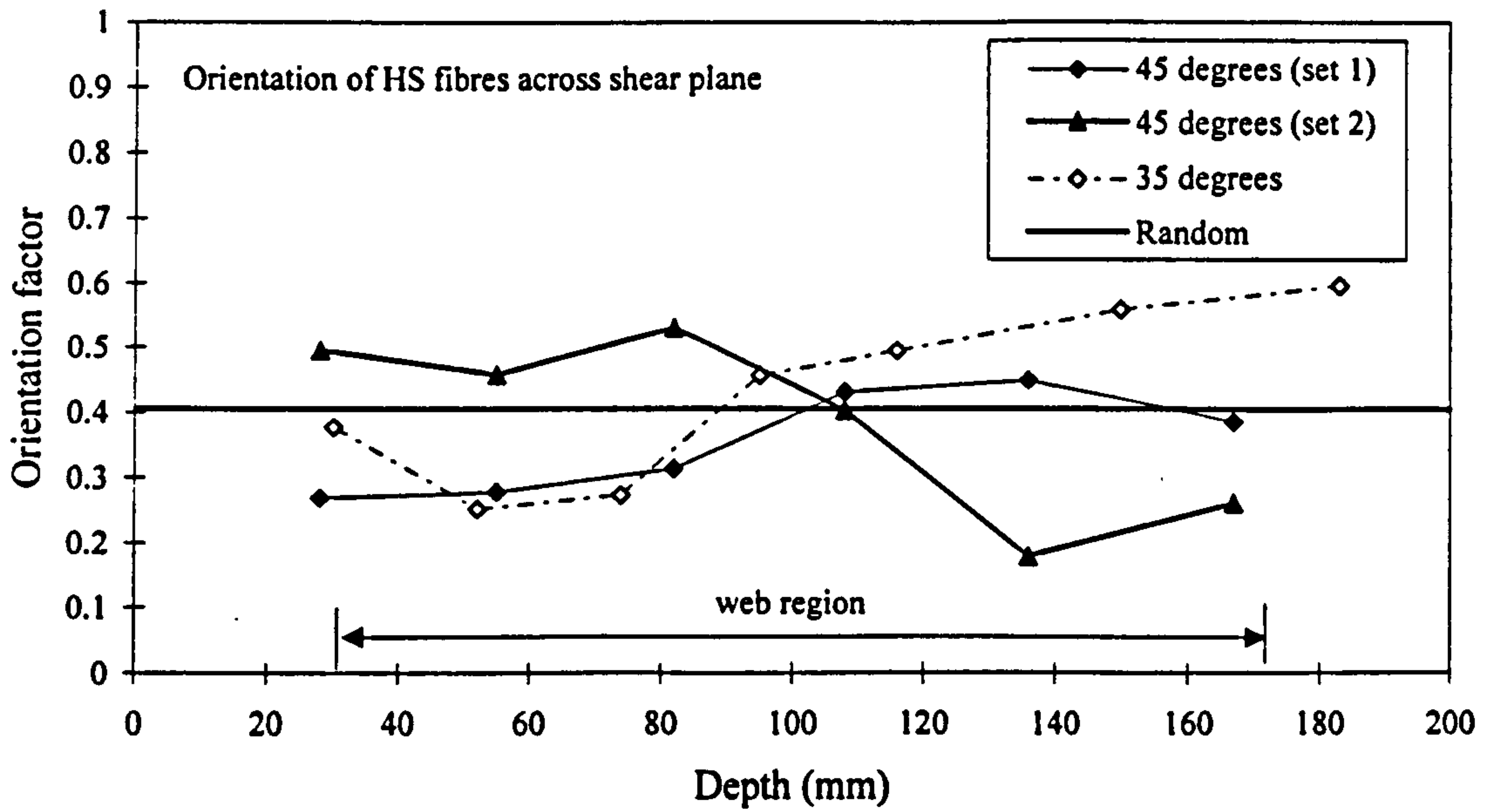
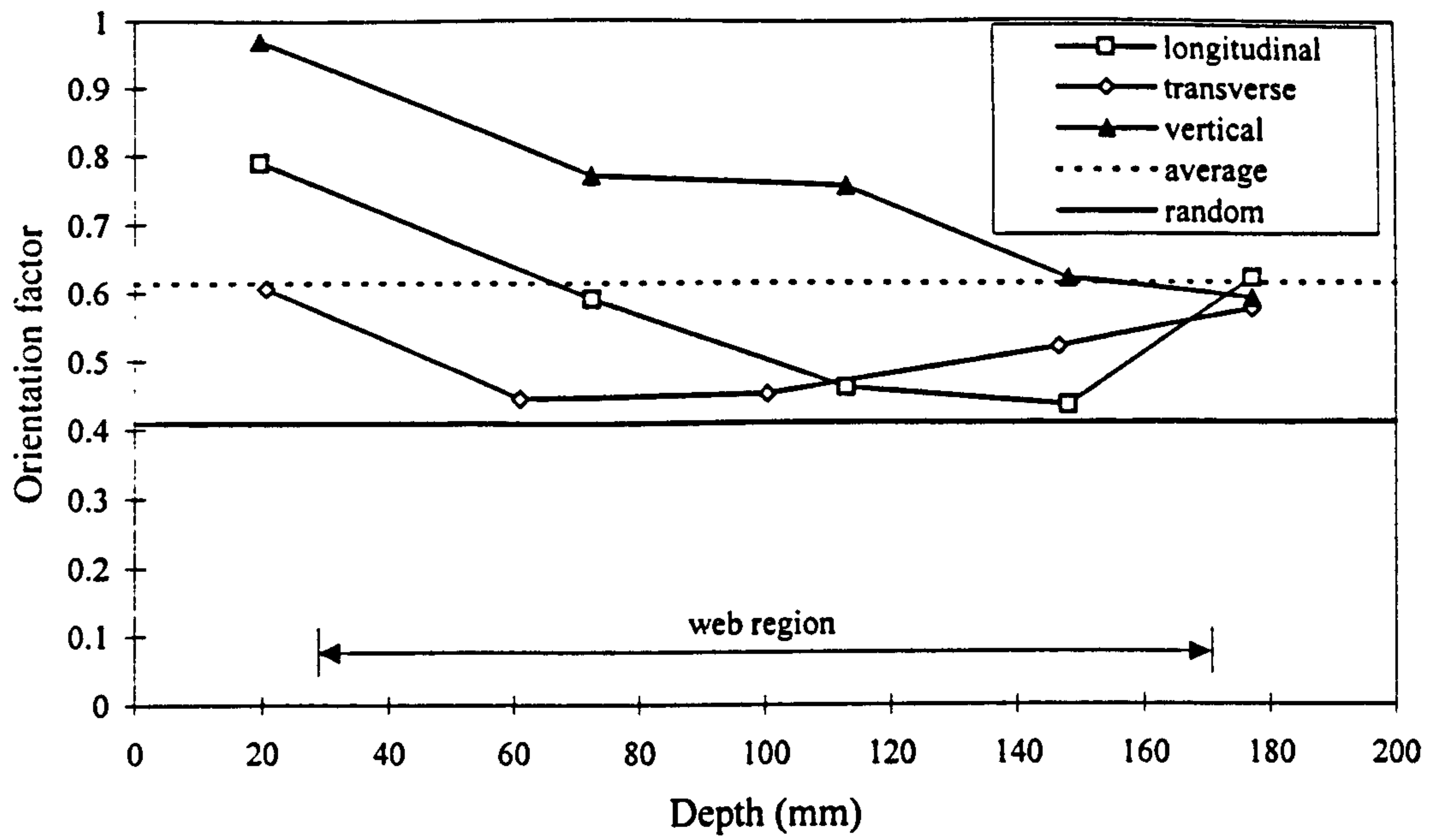


Figure 6-4 Orientation factor for fibres crossing shear planes angled at 45° and 35° to the longitudinal.



**Figure 6-5 Orientation factor for the three orthogonal directions throughout depth of slab (AM fibre slabs)**

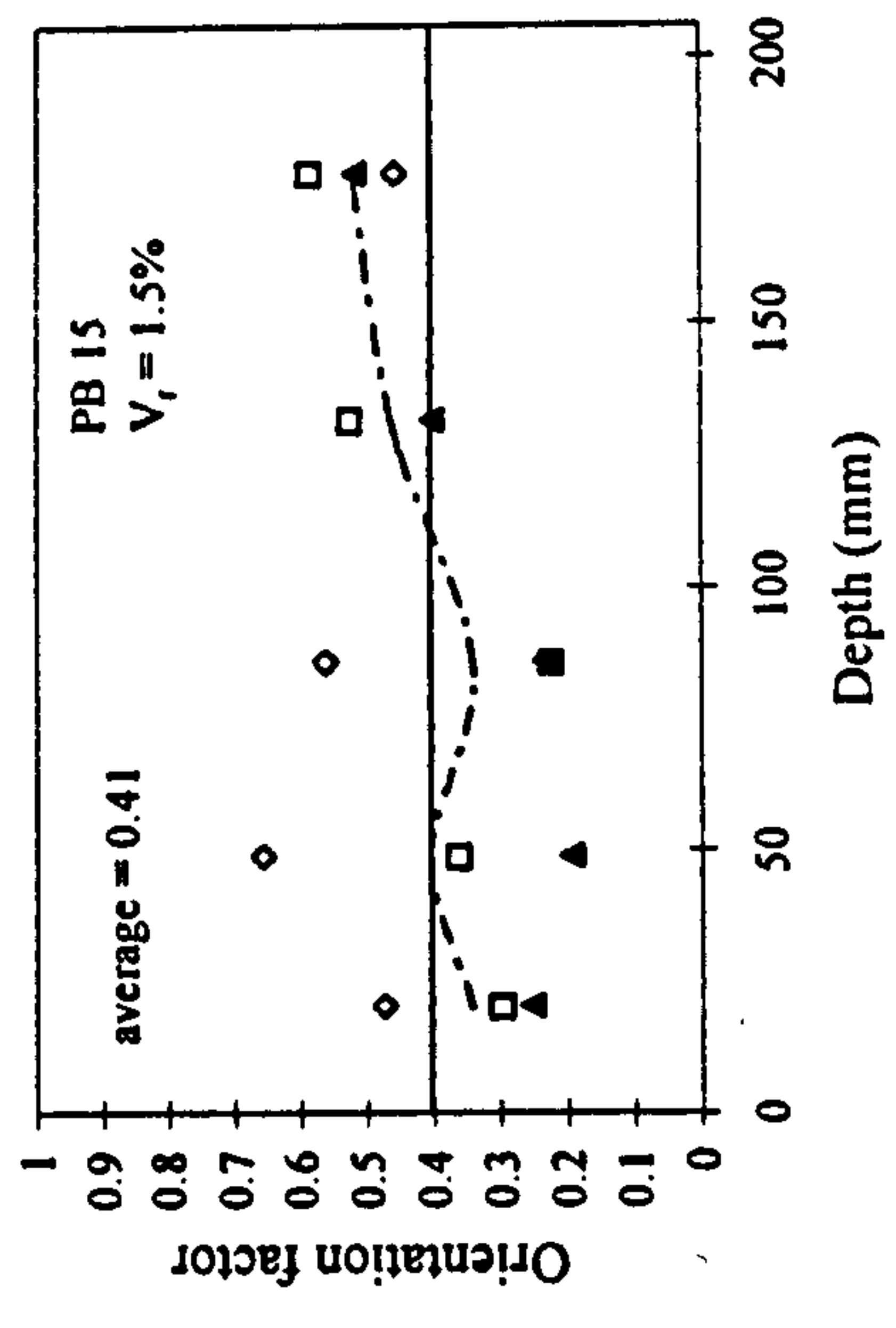
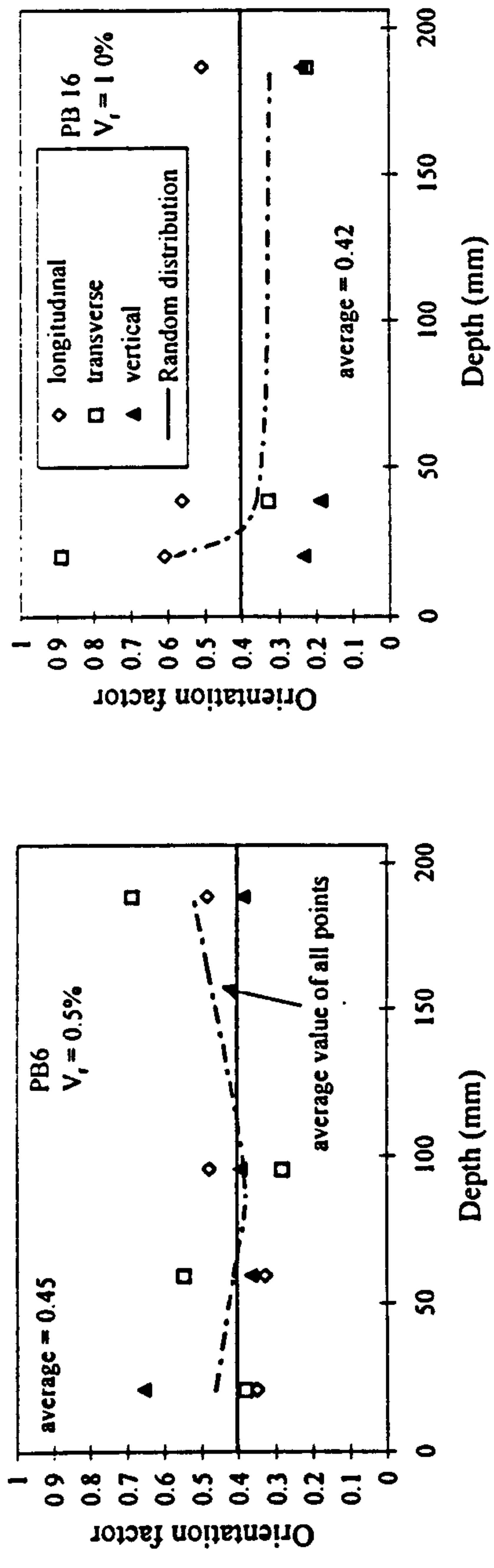


Figure 6-6 Orientation factor through vertical depth of slab for laboratory cast specimens PB5, PB16 and PB15.

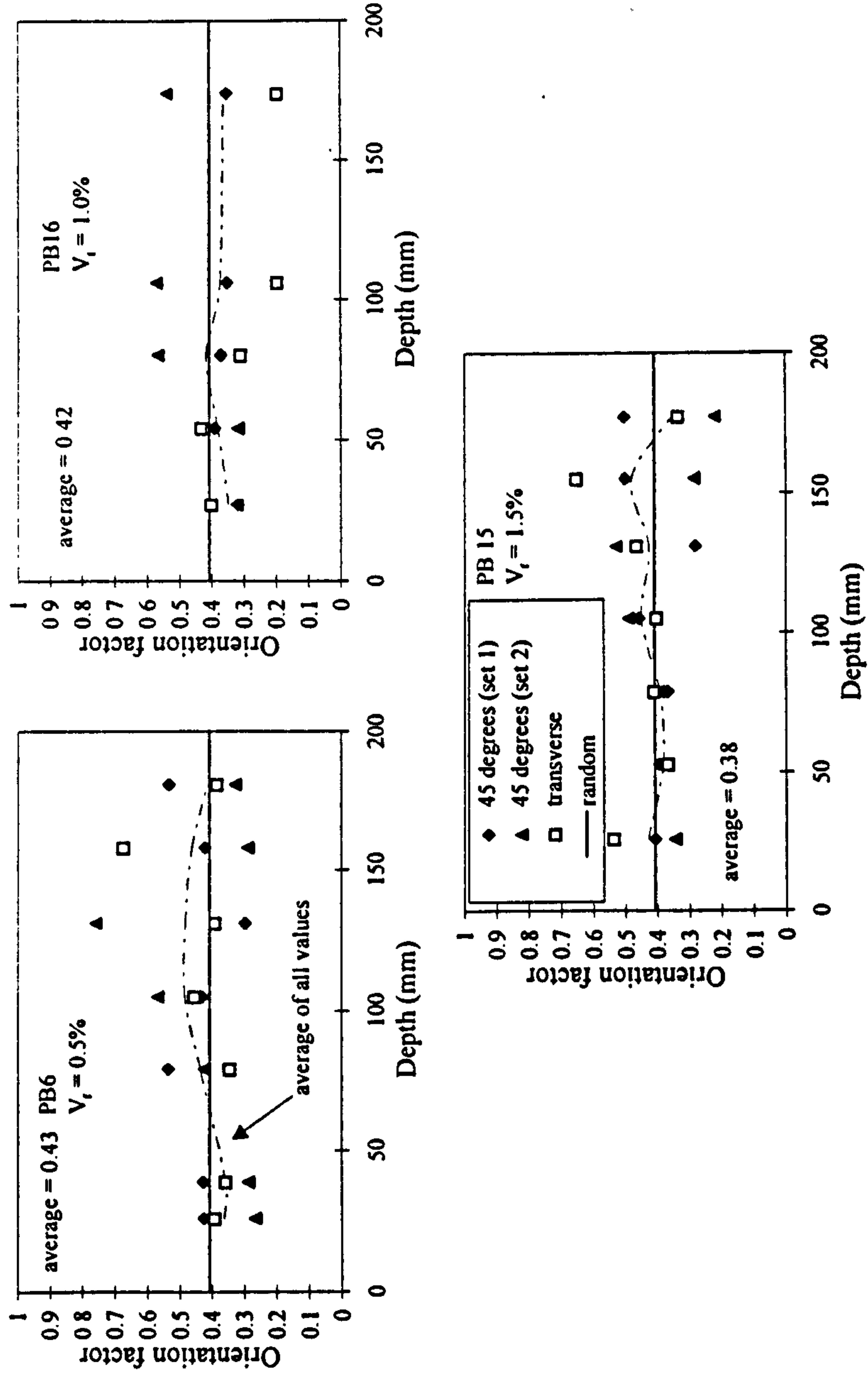


Figure 6-7 Orientation factor through across 45° shear plane for laboratory cast specimens PB5, PB16 and PB15.



**Plate 6-1 Compaction of the three batches at the preliminary trial**

## CHAPTER 7

# TESTING OF FIBRE REINFORCED HOLLOW CORE SLABS

### 7.1 Introduction

The benefit of fibre addition to prestressed hollow core slabs was examined directly by a variety of tests. These comprised of shear, transverse bending and concentrated load tests (Table 7-1).

The majority of slabs were cut to 2 m length and tested in conventional shear under a line load across the full width of the slab. A total of nine FRC slabs were tested in shear, making a total of 18 tests, comprising: two different prestressing configurations; two fibre types; different  $V_f$ 's; and two a/d ratios. Additionally, one of the  $P = 518$  kN HS fibre reinforced slabs (see Table 6-5) was cut into four longitudinal x-shaped strips and each tested in shear to investigate cracking in individual webs and for comparison with the laboratory cast x-beam tests described in Chapter 5.

The transverse bending tests were conducted with the slabs simply supported on their longitudinal edges so that no benefit could be gained from the prestressing reinforcement. The length of the slabs was less than 1 m, so there was insufficient length for the prestress to build-up and cause any biaxial effects on the transverse strength. The main objective of these tests was to obtain a measure of the transverse bending strength of hollow core slabs. These tests were also planned, however, to investigate the extent to which increasing the longitudinal length of the slab would increase the transverse moment carrying capacity of the slab under a concentrated load. It was felt that there was likely to be a maximum length beyond which any further increase in length would provide no further strength benefit.

Along similar lines to the transverse tests, a number of concentrated load tests were performed on longitudinally spanning slabs. Nine load tests were performed over a span of 1m on the undamaged central part of slabs that had previously been

used for the conventional shear tests. The likelihood was that the slabs would fail due to transverse bending and the objective was to measure the increase in strength with increasing  $V_f$ .

Three FRC slabs and one plain slab were also tested in a similar fashion to the conventional shear tests at  $a/d = 2.8$  but under a concentrated point load, placed eccentric to the centre line of the slab. These tests were for comparison with the conventional shear tests over the same  $a/d$  ratio, and to investigate to what extent such a load produces a non-uniform distribution of deflections and strain.

## **7.2 Shear Tests on Full Width Hollow Core Slabs**

### **7.2.1 Test set-up**

Shear tests were carried out on each end of 2m long slabs subjected to a line load over their full 1200 mm width. The tests were referred to as the A Test and B Test, and the slabs were simply supported over effective spans of 1900 mm and 1470 mm for the two tests, respectively. A bearing length of 100 mm was used at both ends of the slab as is common in typical hollow core slab applications. The general arrangement for the tests is shown in Figure 7-1 and details of the full test programme are given in Table 7-2. The test variables were fibre volume fraction,  $a/d$  and prestress. At least two nominally identical tests were conducted for each combination of variables.

Linear voltage potentiometers (LPs) were placed under the slabs to measure deflections at the load-point and at positions close to the supports. Two LPs were used at each location, one on either side of the centre line of the slab, to provide an average reading and to compensate for any twisting. In later tests, a deflection bar was used to suspend the LPs from the slab so that net deflections free of extraneous deformations could be obtained (see Appendix E).

Load was applied with a hydraulic jack attached to a manual pump and measured with a 500 kN load cell. The load was applied in increments of up to 10 kN until first crack, after which increments of deflection were used. Tests were stopped when the average shear crack width equalled 15 mm (equal to half the length of a fibre).



Changes were made to the loading arrangement throughout the series of tests to try and improve the distribution of the load across the width of the slab. In the first tests (Slabs F1 and F2) the load was applied through one rigid transverse steel spreader beam (150 x 250 mm RHS) set atop of a layer of fibreboard. After what appeared to be uneven loading in each of these tests, a layer of plaster was cast on top of all the other slabs to provide a level surface on which the fibreboard and spreader could be placed. Additionally, a smaller spreader beam was placed on top of the full width spreader beam as an attempt to distribute more of the load to the edge of the slab (see Plate 7-1).

As with the x-beams, strand or wire slip (or draw-in) was measured using a depth gauge. Edge cracks (both shear and flexural) were measured using a microscope or steel tape measure depending on the width of the crack.

## **7.2.2 General Behaviour of Test Specimens**

In most of the tests the failure was by web shear tension, although in some cases failure occurred as a result of anchorage failure induced by flexural shear cracking. Table 7-3 to Table 7-5 which present the test results denote the actual failure type of each test. Shear failures and flexural failures are denoted by S and F, respectively. In slabs where some webs failed in shear and others in flexure the failure is denoted as S & F. Where flexural cracking occurred and was followed at further loading by a shear crack the notation is F/S. Load versus gross deflection curves for the tests are shown in Figure 7-2 to Figure 7-7.

Typical web shear tension failures in hollow core slabs at  $a/d = 2.0$  and  $a/d = 2.8$  are shown in Plate 7-2 and Plate 7-3, respectively. A typical anchorage type failure is shown in Plate 7-4.

The general behaviour of the web shear tension failures was very similar to those failures occurring in the prestressed x-beams PB5 - PB22 described in Chapter 5. At  $a/d = 2.0$ , the critical crack occurred at roughly  $h/2$  from the edge of the bearing and ran at approximately  $45^\circ$  to the direction of the slab. At  $a/d = 2.8$ , the critical cracks occurred at about  $0.8h - 1.0h$  from the edge of the bearing and subtended an angle of  $35^\circ$  to the horizontal.

The general differences in behaviour between the shear failures in the plain concrete slabs and FRC slabs were identical to those found in the x-beams (Chapter 5). However, due to: the larger width of the hollow core slabs; the variation in the width of the webs; and the problem of obtaining a truly even distribution of the load across the width of the slab, a distinct cracking behaviour occurred. This behaviour is explained below.

Since the load was generally greatest in the centre of the slabs, initial cracking tended to occur in the central webs before the edge webs, and due to variations in the width of the webs cracking predominately occurred in the thinnest central web first. In plain slabs this phenomenon had little effect on the overall behaviour, because cracking in a web substantially reduced its load-bearing capacity leading to overloading of adjacent webs causing almost immediate failure. However, in the FRC slabs the webs are still able to carry a substantial load after cracking (see tests on x-beams in Chapter 5). Therefore an intermediate phase occurs between pre-cracking and post-cracking in which some webs are cracked and less stiff than others. During this phase the FRC slabs behave in a three-dimensional manner and transverse cracks as well as torsional cracks occur. Although these cracks can occur to some extent in plain slabs they are far less severe. Difficulties therefore exist with identifying and defining the first crack.

Flexural failures occurred mainly in the  $P = 518$  kN slabs where the prestress levels were insufficient to prevent flexural cracking. The cracks formed at the point of greatest bending moment and grew vertically to the load point. Since these failures are less destructive than web shear tension, a considerable amount of load could be carried after cracking. In the case of Test F10B the extra capacity enabled enough stress to build up in the web that a shear tension failure occurred. However, in most of the tests final failure would have been through rupture of the strand. An eventual failure of this type was never implemented, although in Test P19B three of the four 7 mm wires did rupture.

### 7.2.3 Shear Capacity

Table 7-3 to Table 7-5 show  $V_{cr}$  and  $V_{ult}$  for each of the tests. The geometrical dimensions of each slab as measured in accordance with European standard prEN 1168 (1995) are shown in Table 6.5 and partly explain the variation between nominally identical tests.

For the plain concrete slabs that failed in shear it can be seen that  $V_{cr} = V_{ult}$  (except Test P17B). At  $a/d = 2.0$  and  $a/d = 2.8$ , for the slabs with the  $P = 806$  kN prestressing, the average cracking capacities were 153 kN and 132 kN, respectively. These correspond to average cracking capacities of 21 kN and 19 kN per web, assuming each web to take an equal share of the load.

For the slabs where  $P = 518$  kN, the average cracking capacity of the slabs, ignoring the unexpectedly low capacity of P19A, were 160 kN and 138 kN for  $a/d = 2.0$  and  $a/d = 2.8$ , respectively. These values are higher than those of the more highly prestressed slabs and show the relatively small effect of prestressing on shear capacity. It can be seen from Table 6-5 that the  $P = 518$  kN slabs are on average about 10 mm deeper than the  $P = 806$  kN slabs and this partly explains the reason for this higher capacity.

The effect of adding HS fibres on  $V_{cr}$  and  $V_{ult}$  are shown in Figure 7-8 and Figure 7-9. As with the laboratory-cast x-beams, the capacity at  $a/d = 2.0$  is greater than at  $a/d = 2.8$  for the same fibre volume fraction, but the difference in capacity is only about 10 to 15% compared with an increase of 25 to 30% measured for the laboratory-cast x-beams.

Unlike the behaviour in these x-beams, the fibres have a favourable effect on both the cracking capacity and ultimate capacity at both  $a/d$  ratios. The observation for the x-beams being that the fibres had negligible effect on the cracking capacity. In fact at  $a/d = 2.0$ ,  $V_{cr}$  and  $V_{ult}$  occur simultaneously in most of the slabs. At  $a/d = 2.8$  there is an observed increase of 9% in  $V_{ult}$  (average 172 kN) over  $V_{cr}$  (average 158 kN).

Differences in shear capacity when adding fibres to the  $P = 518$  kN slabs are masked by the fact that many of the failures initiated by flexurally induced anchorage loss or failed in this manner after initial shear cracking. However, it can be deduced that addition of AM fibres at  $V_f = 0.28\%$  has no effect on  $V_{cr}$  or  $V_{ult}$  at either  $a/d$  ratio,

and that they are less effective as shear reinforcement in hollow core slabs than HS fibres.

A theoretical comparison between each of the fibre types and fibre volume fractions is made in Chapter 9, where the results are additionally compared with those from the factory and laboratory cast x-beam tests.

#### 7.2.4 Ductility

Figure 7-10 shows the average value of  $V_{lim}/V_{cr}$  against  $V_f$  for the plain and HS fibre slab tests, calculated in the same manner as Section 5.5.4. It is apparent that after cracking, all of the FRC slabs are able to carry higher loads than the plain slabs. It is possible that a maximum value for  $V_{lim}/V_{cr}$  exists at a  $V_f$  of about 0.75% (see also Paine *et al.* 1997), suggesting an optimum fibre volume fraction for improving the ductility of hollow core slabs. A reason for higher fibre volume fractions being less effective is possibly related to the difficulties found in compacting higher volume fractions in the extrusion machine.

There is little difference in the reduction of the index  $V_{lim}/V_{cr}$  with increasing deflection for the plain and FRC slabs (i.e., the distance between the lines in Figure 7-10 are similar at each  $V_f$ ). This seems to suggest that at the deflections chosen (which are much greater than the initial cracking deflection) the deterioration of both the plain and fibre reinforced concrete is by the same action i.e., concrete crushing in the compression zone and loss of bond around the strand. Therefore the loss of capacity due to fibres pulling out or breaking is relatively small.

#### 7.2.5 Crack Widths

Crack widths were measured at the edge of each of the slabs. However, because of the non-uniform distribution of load the occurrence of the edge crack did not coincide with cracking in the central webs which occurred earlier. The edge shear crack width is therefore not representative of the average shear crack across the slab.

Direct comparison between the edge shear crack width for the plain concrete and FRC slabs is meaningless because the central FRC webs are able to carry

significant post-cracking stresses at large crack widths before transferring the load to adjacent webs. The difference between the average crack width and edge crack width in the FRC slabs, is therefore greater than in the plain slabs. This could be observed visually during the tests.

### **7.2.6 Wire slip**

Wire slip v deflection ( $c-\delta$ ) ratios for each of the shear tests are given in Table 7-3 to Table 7-5 (no ratio is given for Test P18A because the failure was so brittle that only two post-cracking values could be measured and therefore a meaningful  $c-\delta$  ratio could not be calculated). The two ratios shown for the  $P = 518$  kN reinforced slabs are for the strands and wires, respectively. In each case the values are almost identical showing that there is no difference between the active slip of a strand and a wire in a shear failure.

At  $a/d = 2.8$  for each span there is no significant difference between the values as  $V_f$  increases. At  $a/d = 2.0$  the values for the FRC beams are very similar. However, three of the four plain beams have significantly higher  $c-\delta$  ratios. It is probable that in each of these cases the shear failures were more explosive, leading to a wider initial shear crack at the strand level. This would result in a longer de-bonded length of strand and therefore greater pull-in.

From these limited results there is no reason to suspect there are any differences in the bond between wires (or strands) in concrete reinforced using HS fibres or AM fibres.

## **7.3 Factory Produced X-Beam Tests**

### **7.3.1 Test set-up**

In addition to the tests on full width slabs, three slabs were cut longitudinally to form ten factory-produced x-beams of varying prestress reinforcement and fibre volume fraction according to the schedule in Table 7-6. These were tested over two spans and a number of different  $a/d$  ratios to make a total of 19 tests. The test notation

refers to whether the beam was plain (P) or fibre reinforced (F), the diameter of the tendon (7 = 7mm wire, 9 = 9.3 mm strand and 12 = 12.5 mm strand), the a/d ratio and the span of the test (A= 1900 mm and B= 1350 mm).

The one FRC slab cut up for these tests contained HS fibres at  $V_f = 0.5\%$ , and contained both 7 mm wire and 9.3 mm strand. Two webs of each type of prestressing reinforcement were tested at both ends to produce two test results at a/d of 2.0 and 2.8. A plain slab of similar prestressing reinforcement had only two webs cut and the two ends were tested at different a/d ratios to produce a comparison for each of the FRC beams. The third slab was plain concrete and contained 12.5 mm strand. This was cut into four beams, and tested with the load in the centre of the span (a/d = 5.2), and a/d = 3.5, 2.8 and 2.0. For the latter three a/d ratio's both ends were tested but the position of the crack in test P12-35 meant that the other end was only suitable for a third test over a span of 1350 mm with a/d = 2.0. (denoted as P12-2C). The test set-up was identical to that used in the laboratory cast x-beams (Chapter 5), except that no strain gauges were attached to the beams or reinforcement. Because the beams were cut from hollow core slabs, which have a non-uniform cross-section, each beam had a slightly different geometry, which in some cases varied significantly along the length. In addition, because of the way the beams were cast and cut, individual beams had a degree of non-symmetry to their cross-section (Plate 7-5).

### 7.3.2 General Behaviour of Test Beams

In contrast to the full-width slab tests, all but one of these factory-produced x-beams initially cracked due to flexurally induced anchorage failure, and in only seven of the 19 tests could the load be increased sufficiently to produce a web shear crack. Test P12-2B failed in web shear before the occurrence of flexural cracking. Pure flexural failure was not expected in any of the tests because the beams were too short to attain the necessary critical anchorage length. Equation 3-17 gives the critical anchorage length for the 12.5 mm strand beams as 1230 mm, which compares with the length of 1000 mm available in the beams.

The anchorage failures were similar to that shown in Plate 5-2 which occurred in the laboratory cast x-beams PB1-PB4. Moment - gross deflection curves for the

tests are shown in Figure 7-11 to Figure 7-13. The seven specimens to fail in shear came from the beams with greatest prestress tested over the lowest  $a/d$  ratios, and were namely: FRC beams with 9.3 mm strand at  $a/d = 2.0$ ; and the plain 12.5 mm strand beams at  $a/d = 2.0$  and 2.8. In each case the failures were typical of web shear tension and failed in an identical manner to the laboratory cast x-beams.

Where shear failures occurred the tests were terminated at a maximum crack width of about 15 mm. Alternatively where it was felt that shear failure was unlikely the tests were terminated when sufficient information on the failure had been obtained. Test F7-2A, in which anchorage failure occurred, was continued up to total failure of the specimen. The failure was extremely brittle since the wire ruptured in tension causing total destruction of the specimen. Since the crack was directly under the load there was still sufficient length of beam for test F7-2B.

### 7.3.3 Flexural Capacity

The result of each of the tests is given in Table 7-7. The geometrical properties shown were calculated from actual measurements made on each of the beams, with the eccentricity  $e$  estimated as the distance from the centroid of the prestressing tendon to the mid-height of the beam. The cracking moment ( $M_{cr}$ ) is defined as the maximum bending moment at initiation of the flexural failure (i.e., at the load-point).  $M_{ult}$  the ultimate bending moment was attained in test F7-2A only, as explained in Section 7.3.2.

It can be seen that there is little effect of the fibre volume fraction on  $M_{cr}$ . The 9.3 mm strand beams at  $a/d = 2.0$  are an exception, but this is because the plain beam failed at a very low load and was in fact weaker than that of the lighter reinforced 7 mm wire plain beam. All of the 7 mm wire beams gave roughly the same flexural cracking capacity. However, the  $a/d$  over which the beams reinforced with strand were tested appears to have a strong influence on the flexural cracking capacity. Figure 7-14 shows the effect of increasing  $a/d$  on the  $M_{cr}$  for the plain 12.5 mm strand beams tested over  $a/d$  ratios of 2.0, 2.8, 3.5 and 5.2. The reason for the higher cracking moments at increasing  $a/d$  is due to the changing location of the initiation of the flexural crack. This occurs approximately under the load at the point of highest bending moment. Therefore with increasing  $a/d$  ratio the cracking is induced at a

point where the development of prestress is greater. Beyond the transfer length, it would be expected that there is a constant maximum value of  $M_{cr}$ . The value of 18.0 kNm for Test P12-52, which failed in flexure, with the crack occurring at a distance of 850 mm from the end of the beam is likely to equal the maximum value of  $M_{cr}$ , given that the transfer length of a 12.5 mm strand in a hollow core slab is conservatively estimated to be between 738 mm (FIP 1992) and 813 mm (European pre-standard prEN 1168, 1995) for a strand released in a concrete at a compressive cube strength of 35 N/mm<sup>2</sup>. (The pull-out bond tests in Chapter 5 suggested a transfer length of 700 mm for concrete at 40 N/mm<sup>2</sup>.) A bi-linear curve has therefore been drawn, with the result over  $a/d = 5.2$  assumed to give the maximum value possible of  $M_{cr}$ , whilst a best-fit linear curve has been fitted through the other four datum points. The intersection of the two lines at  $a/d = 4.2$  indicates a transfer length of approximately 680mm.

The relationship between the "pre-compression"  $f_b$  at the soffit and  $M_{cr}$  is shown in Figure 7-15. In producing the curves in this figure the low result of Test P9-2B has been omitted. From the two curves the cracking moment of an un-prestressed beam can be estimated as approximately 11 kNm which corresponds with a very high modulus of rupture of about 9 N/mm<sup>2</sup>.

#### **7.3.4 Shear Capacity**

The shear capacity of each test failing by web shear tension is given in Table 7-8. In each of these beams the initial shear crack led to an immediate failure and therefore  $V_{cr} = V_{ult}$ . Also shown in Table 7-8 is a x-beam containing 0.6% HS fibres cut from one of the preliminary trial slabs and tested in four-point bending at an  $a/d$  ratio of 2.0 (Paine 1996). As in Table 7-7, the geometrical properties shown were calculated from measurements made on each of the beams.

The shear capacity of the 12.5 mm strand beams was in the order of 45 to 51 kN, with those tested at  $a/d = 2.0$  having slightly greater capacity than those at  $a/d = 2.8$  as would be expected. The reason for the low capacity of test P12-2B, that failed even before flexural cracking initiated is not clear.



Although tests F9-2A and F9-2B gave two widely varying shear capacities, their average shear capacity was similar to the 12.5 mm strand plain beams, and the 10.9 mm beam containing 0.6% HS fibres. The influence of the prestressing and  $V_f$  from these tests is therefore inconclusive.

However, these results show that the average shear capacity of an individual web of a hollow core slab tested at  $a/d = 2.0$  is around 45 to 50 kN. This is much greater than the shear capacity of 21 kN determined from the full scale tests (Section 7.2.3). This seems to imply that at cracking, the central webs in the slab tests may be bearing greater load than the outer webs. This may in part explain the variation in shear capacity observed in the slab tests.

### 7.3.5 Strand slip

Figure 7-16 and Figure 7-17 show strand slip-deflection curves for comparable tests on the 9.3 mm and 12.5 mm strand reinforced beams. In each case the initial strand slip was induced by a flexural anchorage failure. For the smaller  $a/d$  ratio the amount of strand slip with increasing deflection is much greater and is probably associated with the greater beam rotation. Interestingly the strand in the FRC beam at  $a/d = 2.0$  has a greater slip gradient than that of the strand in the plain beam.

The sudden increase in slip - deflection curve for the tests at  $a/d = 2.8$  in Figure 7-17, coincides with the occurrence of web shear tension failure. This shows that damage to the concrete-to-strand bond inflicted by shear failures is greater than that caused by anchorage failures.

Although the failure in each of the 7 mm wire reinforced beams was also by anchorage failure, there was no significant wire slip measured in any of the tests.

## **7.4 Transverse Flexural Tests**

### **7.4.1 Test set-up**

Transverse tests were performed on sections of hollow core slab cut transversely into longitudinal specimen widths of 200 mm, 300 mm, 500 mm and 1000 mm. Tests on both plain slabs and 0.5% HS fibre slabs were carried out. Each test was labelled by its width in mm and prefixed by either P or F according to type as before. The test set-up is shown in Figure 7-18. The load was eccentrically placed over one of the central voids, and the slab tested over a span of 1100 mm. To compensate for the uneven surface of the slabs, an intermediate layer of plaster was cast between the loading plate and the surface of the beam. Since a 200 mm square plate was used for loading, the tests on the 200 mm wide specimens were effectively simple bending tests. Each of the other tests gives an indication of the ability of fibres to restrain transverse flexural cracks as they propagate in the longitudinal direction away from the load point.

The plain and FRC slabs were taken from separate productions, and therefore the dimensions of the slabs varied. The average dimensions of the plain and FRC slabs are shown in Table 7-9. The values fall within the required slab tolerances given by European standard prEN 1168 (1995).

### **7.4.2 Behaviour of Transverse Tests**

Load versus deflection curves are shown for each of the eight tests in Figure 7-19 and Figure 7-20. At cracking each test suffered a large loss in strength. For the plain slabs and specimen F200, this led to immediate destruction of the specimen with the flexural crack propagating through the full depth of the section. The other three FRC beams had some post-cracking capacity after failure, but were only able to sustain a load of about 3% of the cracking load. However, F500 and F1000 were able to sustain this load over large deflections (approximately  $l/150$ ), and in each case this was due to the toughness and cracking resistance of the FRC in the compressive zone in the top flange. The influence of the fibres in the tensile region (i.e., the bottom flange) was negligible. Since the crack occurred beneath a core, the effective section

of resistance was comprised of the top and bottom flanges only. Plate 7-6 shows a typical failure.

### **7.4.3 Transverse Flexural Capacity**

Table 7-10 shows the ultimate load attained in each test. For each equivalent test the capacity of the plain slabs is greater than that of the FRC slabs. However, these differences in capacity can be explained by the differences in flange thickness, height and length given in Table 7-9. Using these values it can be calculated by simple elastic analysis that the plain slabs should have been theoretically 10% stronger than the FRC slabs, as was observed.

The results show that the transverse flexural cracking capacity of the plain slabs and FRC slabs was effectively identical and that fibres have no beneficial or disruptive influence. Figure 7-21 shows a nearly linear relationship between the width of the specimens and the cracking load. From these tests there is no evidence to suggest that a critical slab width and maximum load exist. The stiffness of the slabs is therefore sufficiently great that the load can be distributed across the entire longitudinal length up to 400 mm either side of the load.

The transverse bending capacity of a hollow core slab loaded over its full width, calculated from the 200 mm specimens, is between 3.0 and 3.5 kNm. This approximates to a cracking strength of about 3.5 N/mm<sup>2</sup>. Because of the close proximity of the cores which prevents plastification, this value is not equal to the flexural cracking strength that would be calculated from solid prisms. However, it is likely to very closely approximate the axial tensile strength of the concrete.

### **7.4.4 Ductility**

As previously mentioned, the plain specimens failed in a brittle manner, whilst the FRC specimens appeared to behave only slightly more ductile. The ductility of the specimens appears therefore to be insignificant, although the results are to some extent questionable because of the lack of displacement control. In the flexural toughness tests on FRC described in Chapter 4 the prisms showed significant post-

cracking toughness. This difference in behaviour is attributable to the small thickness of the lower flange in the hollow core specimens. In flexural prism tests the increase in toughness is provided by fibres controlling cracking in the centre of the beam and therefore restricting migration of the neutral axis towards the top of the beam. In these tests the lower flange depth is almost entirely composed of the traction free zone in which fibres have completely pulled out of the matrix (Robins *et al.* 1996) which forms quickly on initial cracking. The other three areas highlighted by Robins *et al.* (1996) in which the aggregate and fibres are effective in resisting flexural tensile stresses are all within the part of the tensile region made up entirely of the void, and are therefore non-existent. There is therefore little post-cracking ductility for FRC hollow core slabs failing in transverse flexure.

## **7.5 Concentrated Load Tests**

### **7.5.1 Test set-up**

#### ***Centric load tests***

A number of the previously tested 2m long slabs were tested a third time under a centrally located concentrated load, over a span of 1m. The test set-up is shown in Figure 7-22 and Plate 7-7.

The load was applied through a 200 mm square plate positioned directly in the centre of the slab so that it was nominally over the central web. Deflections were measured at the centre of the span, directly under the load and offset at 400 mm on either side. The  $a/d$  ratio for these tests was approximately 5.5.

#### ***Eccentric load tests***

The test set-up for the eccentric concentrated load tests was almost identical to that of the conventional shear tests. However instead of the load being applied across the full width of the slab it was concentrated through a 200 mm square plate situated

at a shear span of  $a/d = 2.8$  offset at 84 mm from the centre of the slab directly over one of the two central cores; shown as core CD in Figure 7-23.

Deflections were measured at positions directly under the load and beneath three other cores (see Figure 7-23) to enable measurement of the transverse bending of the slabs. Two other LPs were attached to deflection bars and located at a distance of 280 mm from either side of the centre line at a distance of  $a/d = 2.8$  longitudinally.

Strain gauges were placed on the soffit of the slab in the positions shown in Figure 7-23

### 7.5.2 Results of centric concentrated load tests

The slabs failed initially as a result of flexural cracking in the longitudinal direction. Two flexural cracks occurred in all of the tests at a distance of 50 - 70 mm either side of the centre line of the slab. This was due to a combination of the prestressing strand located directly beneath the load position on the centre line of the slab, and the flanges being more susceptible to cracking than the web.

The cracking load ( $W_{cr}$ ) is given in Table 7-11, together with the estimated transverse cracking moment ( $M_{t,cr}$ ) as calculated from  $W_{cr}$  using grillage analysis on a commercially available analytical computer package (Appendix D). Given that the capacity of the 0.5% HS slabs varied between  $W_{cr} = 141$  kN and 232 kN and the capacity of the plain slabs was between this range, it can be assumed that fibres have no effect on  $W_{cr}$ . Additionally, since the slab containing 0.28% AM fibres, which had the lowest prestress, had similar  $W_{cr}$  to the other tests, it can be deduced that the level of the longitudinal prestress has no effect on the cracking capacity.  $W_{cr}$  is therefore a function of the flexural cracking capacity of the concrete only.

After cracking both of the plain concrete slabs failed immediately with the longitudinal flexural cracks propagating to the surface and along the length of the slab. Each of the FRC slabs was able to provide extra capacity after cracking by preventing the propagation of the cracks. The ultimate load ( $W_{ult}$ ) and the ratio  $W_{ult}/W_{cr}$  for each of the tests is given in Table 7-11. It can be seen that for the HS slabs  $W_{ult}/W_{cr}$  lies between 1.15 - 1.20, whilst the AM fibre slab that was tested gave

a slightly lesser value of  $W_{ult}/W_{cr} = 1.08$ . Typical load - deflections for each fibre type and fibre volume fraction are presented in Figure 7-24.

The cracking pattern from each of the tests was essentially the same with the flexural cracks emerging on the top surface at a distance of about 120 mm from the centre line (i.e. 20 mm from the loading platen). Figure 7-25 demonstrates the wedge shaped cracking that emerged and which is probably due to the load plate being punched between the two flexural cracks. Note that the wedge is the opposite shape to that associated with punching shear. Crack pattern and spacing was identical along the length of the specimen until disturbed very close to the supports. Plate 7-8 shows the failure of Test 10P.

### **7.5.3 Result of eccentrically loaded tests over span of 1900 mm**

In these tests there were two forms of cracking, web shear tension occurring within the longitudinal shear span and transverse flexural cracking along the entire longitudinal length of the slab, as shown in Figure 7-26.

The cracking load ( $W_{cr}$ ) calculated as the point of first non-linearity on the load-deflection curves shown in Figure 7-27, and the ultimate load ( $W_{ult}$ ) for each of the tests is shown in Table 7-12. The total support reactions at cracking ( $V_{cr}$ ) and at ultimate ( $V_{ult}$ ) are also shown.

The values of  $V_{cr}$  and  $V_{ult}$  are between 82% - 90% of the equivalent capacities observed in the conventional full width shear tests (Table 7-4), and suggests that the slabs had sufficient torsional stiffness to distribute the point load to almost all the webs across the section. Similar comparative values between full line loads and concentrated loads were found for plain slabs failing in flexure by Walraven and Mercx (1983). Figure 7-28 shows the load - deflections across the width of Test 6P and it can be seen that up to  $W_{cr}$  the deflections are almost identical; although the deflection furthest from the load (LP1) is least. Similarly, up to  $W_{cr}$  there is no measured change in strain across the width of the slab (Figure 7-29). At loads greater than  $W_{cr}$ , the tensile strain beneath the load (SG2) increases considerably leading to longitudinal cracking.

From test observation and the measured strand slip it is likely that  $W_{cr}$  corresponds with the first shear crack in the two webs closest to the load, denoted D and E in Figure 7-23. The critical crack position in each of these webs was 280 mm from the bearing ( $1.4 h$ ), which is greater than that observed in the conventional shear tests over the same  $a/d$  ratio.

For this critical crack position, grillage analysis of an elastic slab estimates a shear force of  $0.2W$  in these two webs, which in the case of the 0.5% HS slabs corresponds to a shear cracking load of  $V_{cr} = 38$  kN. This is less than the capacity of 45 kN observed from the tests on the x-beams cut from slabs and tested with the same  $a/d$  ratio, and almost twice that estimated from the conventional shear tests. This adds to the suspicion that the load in the conventional shear tests was not evenly distributed across the width of the slab, but contrasts with the observation of little transverse behaviour prior to cracking.

After cracking, the load bearing capacity in the two webs D and E is reduced which induces greater loads to be carried by the webs either side. Eventually the shear forces in these webs reach  $V_{cr}$  and the webs fail, transferring their load to their adjacent webs. The critical crack position for each of the webs gets progressively closer to the bearing point with transverse distance from the load; distances of  $0.75 h - 0.85 h$  being measured for webs C and F, and about  $h/2$  for webs B and G. This is as a result of the shear forces across the width of the slab becoming more evenly distributed with distance from the load.

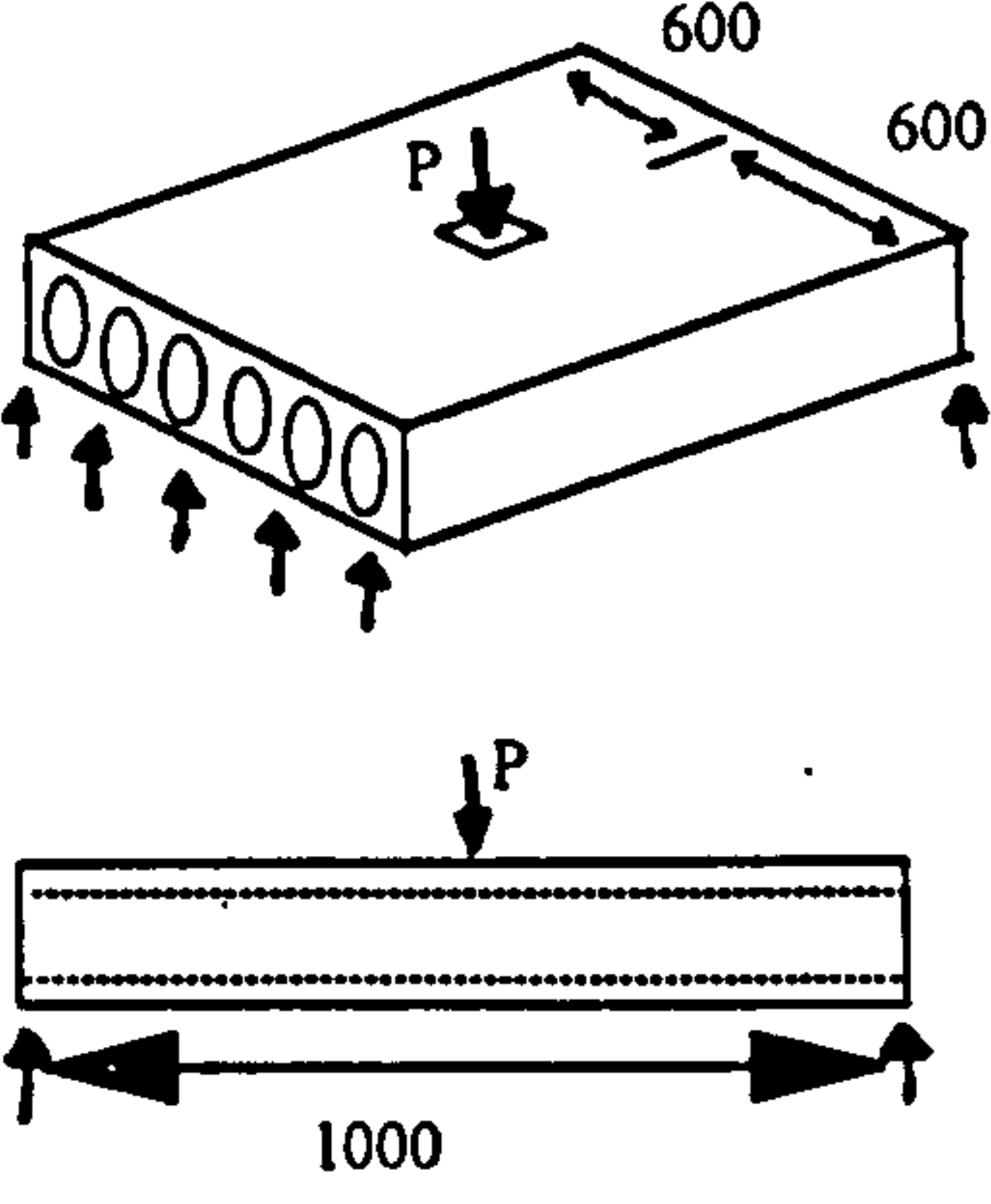
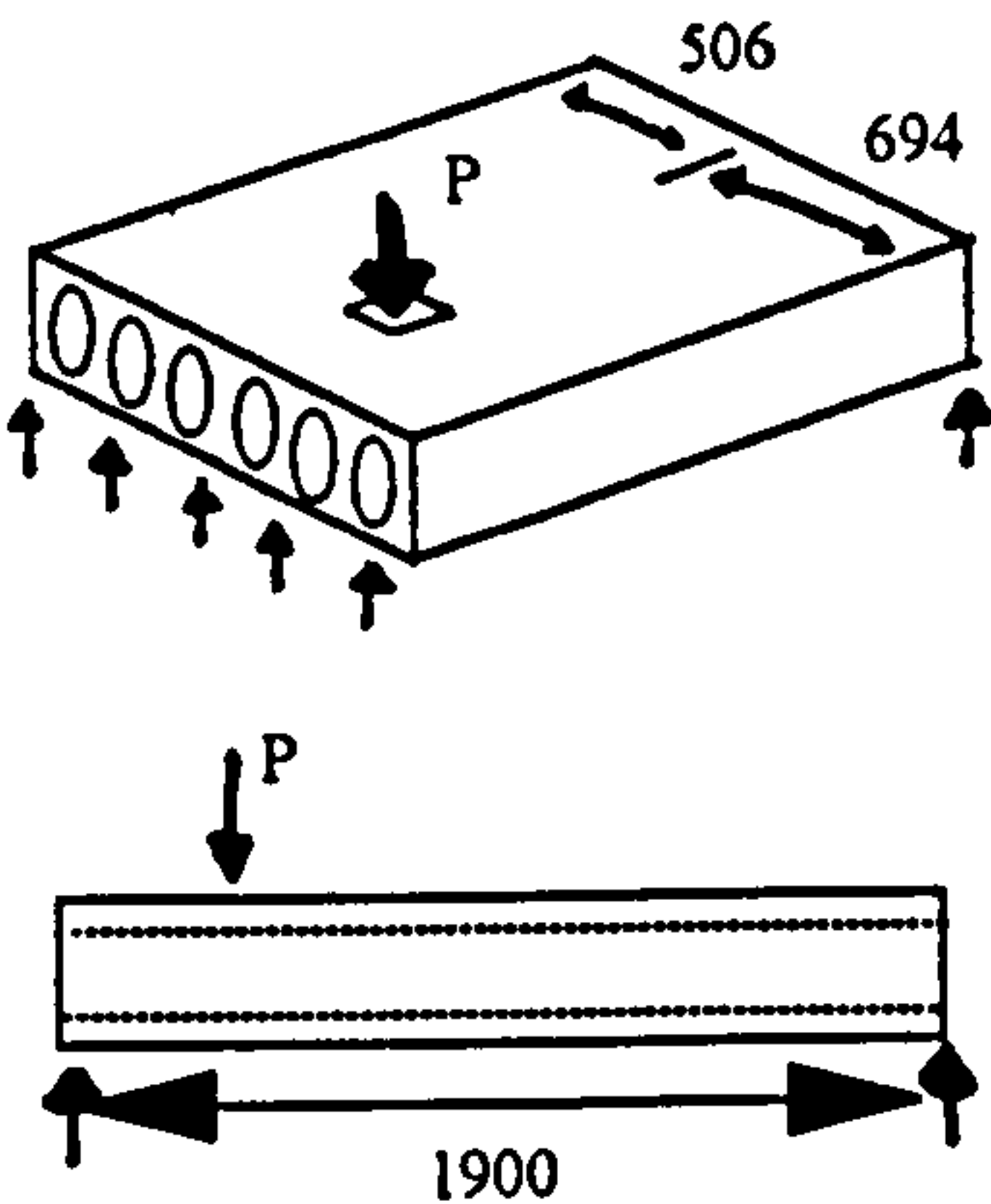
Measurement of the strand slip in each of the webs confirmed that webs D and E failed in shear first, followed by the adjacent webs. Strand slip - deflection curves for each web are shown in Figure 7-30. In the plain slab the initial strand slip for all the webs took place at a deflection of about 0.75 mm, while in the 1% HS slab initial strand slip occurred in web D at a deflection of 0.85 mm, but did not take place in webs B and G until a deflection of about 3.5 mm. This suggests that initial losses in load-carrying capacity in the fibre reinforced webs are less than those in the plain webs, and that the smaller loads which are transferred to adjacent webs are not enough to cause the webs to fail immediately. Each of the FRC slabs can therefore withstand a greater load after cracking, as shown in Table 7-12. The strand slip - deflection data shows that ultimate load corresponds with the failure of the last of the webs to fail in shear. Therefore in all four tests the principal failure mechanism is shear.

The secondary failure mode of longitudinal cracking along the length of the slab which occurs in each of the tests initiates after the occurrence of shear cracking as explained above. Grillage analysis of an elastic slab gives a maximum transverse moment of 4.2 kNm at ultimate for the 1% HS slab. Compared with the higher cracking moments found from the centrically loaded tests (Section 7.5.2), it is apparent that transverse cracking does not initiate independently of the shear failures.



**Table 7-1 Programme for factory cast slabs and x-beams**

Sect.	Title	Description	a/d	Vf (%) and fibre type	Prestress
7.2	Shear tests on hollow core slabs  (32 tests)		2.0	0 0.28 AM 0.5 HS 1.0 HS	7x12.5φ 3x9.3φ + 4x7φ
			2.8	0 0.28 AM 0.5 HS	7x12.5φ 3x9.3φ + 4x7φ
			3.5	0	7x12.5φ
7.3	Factory-cut x-beams  (19 tests)		2.0 2.8 3.5 5.2	0	1x7φ 1x9.3φ 1x12.5φ
			2.0 2.8	0.5 HS	1x7φ 1x9.3φ
7.4	Transverse flexure on hollow core slabs  (8 tests)		n/a	0 0.5 HS	7x12.5φ  note: prestress perpendicular to span

7.5	<p>Centric concentrated point load on hollow core slabs</p> <p>(9 tests)</p>		5.5	<p>0 0.28 AM 0.5 HS 1.0 HS</p>	<p>7x12.5φ 3x9.3φ + 4x7φ</p>
7.5	<p>Eccentric concentrated point load on hollow core slabs</p> <p>(4 tests)</p>		2.8	<p>0 0.5 HS 1.0 HS</p>	<p>7x12.5φ</p>

**Table 7-2 Test programme for shear tests on hollow core slabs**

a/d	P <sub>i</sub> (kN)	fibre type	V <sub>f</sub> (%)	Slab Nos.	No. of tests
2.0	806	-	0	P13 & P17	4
2.0	806	HS	0.5	F1B, F2 & F5	5
2.0	806	HS	1.0	F9	2
2.0	518	-	0	P19	2
2.0	518	AM	0.28	F11	2
2.0	518	HS	0.5	F12	2
2.8	806	-	0	P14 & P18	4
2.8	806	HS	0.5	F1A, F4 & F6	5
2.8	518	-	0	P20	2
2.8	518	AM	0.28	F10	2
3.5	806	-	0	P15	2

Table 7-3 Shear Tests over  $a/d = 2.0$

Test No.	P (kN)	Fibre type	$V_f$ (%)	Span (mm)	$V_{cr}$ (kN)	average $V_{cr}$ (kN)	$V_{ult}$ (kN)	average $V_{ult}$ (kN)	$v_{ult}$ (N/mm <sup>2</sup> )	c- $\delta$ ratio	Failure type
P13A	806	-	0	1900	113	153	113	166	3.2	1.03	S
P13B	806	-	0	1470	169		169		4.9	1.06	S
P17A	806	-	0	1900	214		214		5.5	0.67	S & F
P17B	806	-	0	1470	117		168		3.0	1.14	S
F1B	806	HS	0.5	1470	200	185	200	188	5.6	0.58	S
F2A	806	HS	0.5	1900	219		219		6.1	0.58	S
F2B	806	HS	0.5	1470	194		194		5.4	0.62	S
F5A	806	HS	0.5	1900	159		159		4.8	0.7	S
F5B	806	HS	0.5	1470	151		170		5.1	0.77	S
F9A	806	HS	1.0	1900	220	208	232	217	6.5	0.65	S
F9B	806	HS	1.0	1470	195		202		5.7	0.72	S
P19A	518	-	0	1900	107	134	108	134	2.7	0.73/0.77	S
P19B	518	-	0	1470	160		160		4.0	0.59/0.68	F/S
F11A	518	AM	0.28	1550	166	185	166	185	4.8	0.70/0.65	S
F11B	518	AM	0.28	100	204		204		5.9	0.80/0.89	S & F
F12A	518	HS	0.5	1400	229	290	261	306	7.7	0.56/0.34	F/S
F12B	518	HS	0.5	1000	350		350		10.4	0.93/0.99	S

For calculation of  $v_{ult}$ ,  $I_b/A_y$  approximated as  $0.67bh$

Table 7-4 Shear Tests over  $a/d = 2.8$

Test No.	P (kN)	Fibre type	V <sub>f</sub> (%)	Span (mm)	V <sub>cr</sub> (kN)	average V <sub>cr</sub> (kN)	V <sub>ult</sub> (kN)	average V <sub>ult</sub> (kN)	V <sub>ult</sub> (N/mm <sup>2</sup> )	c-δ ratio	Failure type
P14A	806	-	0	1900	147	132	147	145	3.8	0.47	S
P14B	806	-	0	1470	157		157		4.1	0.54	S
P18A	806	-	0	1900	82		98		2.3	-	S
P18B	806	-	0	1470	140		177		3.9	0.46	F
F1A	806	HS	0.5	1900	165	158	180	172	5.0	0.36	S
F4A	806	HS	0.5	1900	164		164		4.9	0.49	S
F4B	806	HS	0.5	1470	160		161		4.8	0.64	S
F6A	806	HS	0.5	1900	159		183		5.6	0.58	S
F6B	806	HS	0.5	1470	141		174		5.2	0.57	S
P20A	518	-	0	1900	131	138	134	146	3.2	1.00/1.00	S
P20B	518	-	0	1470	144		158		3.8	0.54/0.57	S & F
F10A	518	AM	0.28	1900	132	140	132	171	3.2	0.52/0.51	S
F10B	518	AM	0.28	1470	148		210		5.0	0.65/0.61	F/S

For calculation of  $v_{ult}$ ,  $I_b/A_y$  approximated as  $0.67bh$

Table 7-5 Shear Tests over  $a/d = 3.5$

Test No.	P (kN)	Fibre type	$V_f$ (%)	Span (mm)	$V_{cr}$ (kN)	average $V_{cr}$ (kN)	$V_{ult}$ (kN)	average $V_{ult}$ (kN)	$V_{ult}$ (N/mm <sup>2</sup> )	c- $\delta$ ratio	Failure type
P15A	806	-	0	1900	114	147	115	151	3.0	0.99	S
P15B	806	-	0	1470	179		186		4.8		S

Table 7-6 Test programme for factory-produced x-beams

Reinforcement diameter (mm)	P (kN)	Plain concrete beams $V_f = 0\%$		FRC beams $V_f = 0.5\%$	
		a/d ratio		a/d ratio	
7	42	2.0	P7-2B	5.2	F7-2A
		2.8	P7-28A	2.0	F7-28A
9.3	64	3.5	-	-	F7-28B
		2.8	P9-28A	-	F9-28A
12.5	115	3.5	-	-	F9-28B
		2.8	P12-28A	P12-52	-
		2.8	P12-28B	-	-
			P12-2C		

Table 7-7 Flexural test results of factory-produced x-beams

Test No.	a/d	V <sub>f</sub> (%)	span (mm)	A <sub>c</sub> (mm <sup>2</sup> x 10 <sup>3</sup> )	Z <sub>b</sub> (mm <sup>3</sup> x 10 <sup>6</sup> )	e (mm)	M <sub>cr</sub> (kNm)	M <sub>ult</sub> (kNm)
P7-2B	2.0	0	1350	30.2	1.28	57	11.8	
F7-2A	2.0	0.5	1900	31.2	1.40	60	11.1	16.5
F7-2B	2.0	0.5	1350	30.9	1.41	60	13.3	
P7-28A	2.8	0	1900	28.4	1.16	60	10.9	
F7-28A	2.8	0.5	1900	31.5	1.32	55	11.2	
F7-28B	2.8	0.5	1350	31.2	1.37	57	12.2	
P9-2B	2.0	0	1350	29.6	1.20	61	8.8	
F9-2A	2.0	0.5	1900	30.7	1.39	66	11.4	
F9-2B	2.0	0.5	1350	30.7	1.39	66	11.9	
P9-28A	2.8	0	1900	30.0	1.19	57	13.6	
F9-28A	2.8	0.5	1900	32.6	1.41	59	13.1	
F9-28B	2.8	0.5	1350	33.1	1.41	58	14.1	
P12-2A	2.0	0	1900	30.6	1.24	54	14.0	
P12-2B	2.0	0	1350	31.0	1.30	49	10.9*	
P12-2C	2.0	0	1350	30.7	1.29	56	13.3	
P12-28A	2.8	0	1900	30.7	1.23	41	14.6	
P12-28B	2.8	0	1350	30.6	1.27	46	11.0	
P12-35	3.5	0	1900	31.0	1.26	52	17.0	
P12-52	5.2	0	1900	31.4	1.22	57	18.0	

\* this beam failed in web shear tension prior to formation of flexural cracking



Table 7-8 Results of factory-produced x-beams failing in shear

Test No.	a/d	V <sub>f</sub> (%)	span	σ <sub>cp</sub> (N/mm <sup>2</sup> )	I (mm <sup>4</sup> x 10 <sup>6</sup> )	b (mm)	A <sub>y</sub> (mm <sup>2</sup> x 10 <sup>3</sup> )	V <sub>cr</sub> = V <sub>ult</sub> (kN)	V <sub>ult</sub> (N/mm <sup>2</sup> )
F9-2A	2.0	0.5	1900	2.05	143	37	736	38.1	5.3
F9-2B	2.0	0.5	1350	2.05	143	37	736	53.0	8.1
<sup>A</sup> -	2.0	0.6	1900	-	-	-	-	52.3	-
P12-2A	2.0	0	1900	3.72	126	41	625	51.0	6.2
P12-2B	2.0	0	1350	3.72	126	41	625	30.1	3.6
P12-2C	2.0	0	1350	3.75	130	38	617	48.1	6.0
P12-28A	2.8	0	1900	3.75	125	42	668	45.3	5.7
P12-28B	2.8	0	1350	3.75	125	42	668	45.3	5.7

<sup>A</sup> x-beam cut from a slab produced in the preliminary trial

**Table 7-9 Average dimensions of transverse test specimens**

	slab depth (mm)	upper flange thickness (mm)	lower flange thickness (mm)
Plain slabs	200	29	31
FRC slabs	196	22	34

**Table 7-10 Ultimate strength of transverse bending tests**

Plain concrete beams			FRC beams	
Nominal length of beam (mm)	actual length (mm)	Ultimate load (kN)	actual length (mm)	Ultimate load (kN)
200	200	13.2	202	11.0
300	290	23.1	291	20.8
500	521	37.8	499	35.2
1000	990	73.1	980	65.2

**Table 7-11 Results of Centric Concentrated Load Tests**

$V_f$ (%)	Fibre type	Test No.	$W_{cr}$ (kN)	$M_{t,cr}$ (kNmm)	$W_{ult}$ (kN)	$W_{ult}/W_{cr}$
0	-	P13P	180	4.50	180	1.00
0	-	P14P	200	5.00	200	1.00
0.5	HS	F1P	141	3.50	170	1.21
0.5	HS	F2P	158	3.95	185	1.17
0.5	HS	F4P	227	5.68	251	1.10
0.5	HS	F5P	232	5.80	269	1.16
0.5	HS	F6P	220	5.50	260	1.18
1	HS	F9P	193	4.83	229	1.19
0.28	AM	F10P	170	4.25	184	1.08

**Table 7-12 Results of Eccentric Concentrated Load Tests**

$V_f$ (%)	Fibre type	Slab No.	$W_{cr}$ (kN)	$W_{ult}$ (kN)	$V_{cr}$ (kN)	$V_{ult}$ (kN)
0	-	P16	162	162	123	123
0.5	HS	F3	187	187	142	142
0.5	HS	F7	190	205	144	156
1	HS	F8	221	224	168	170

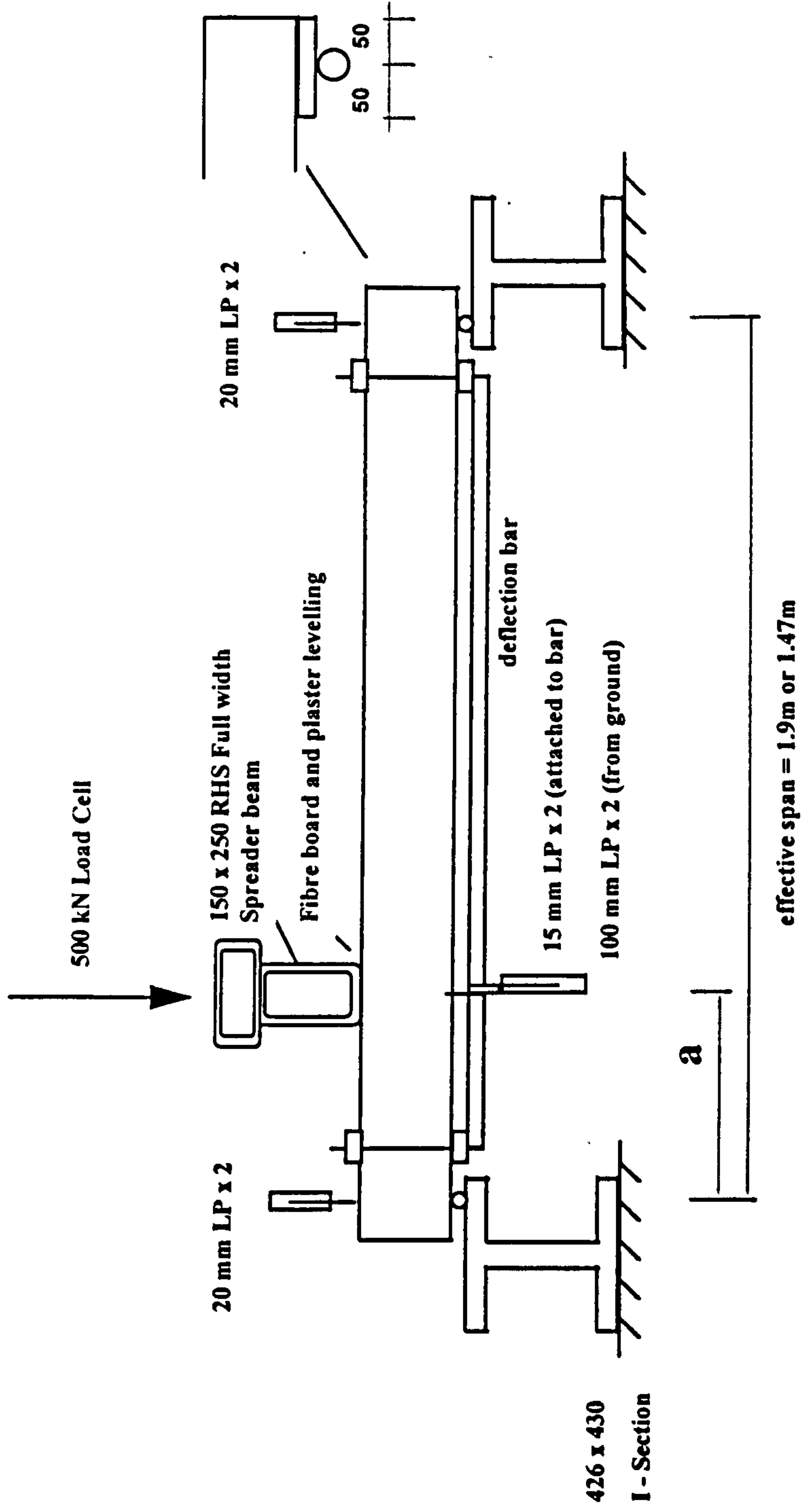
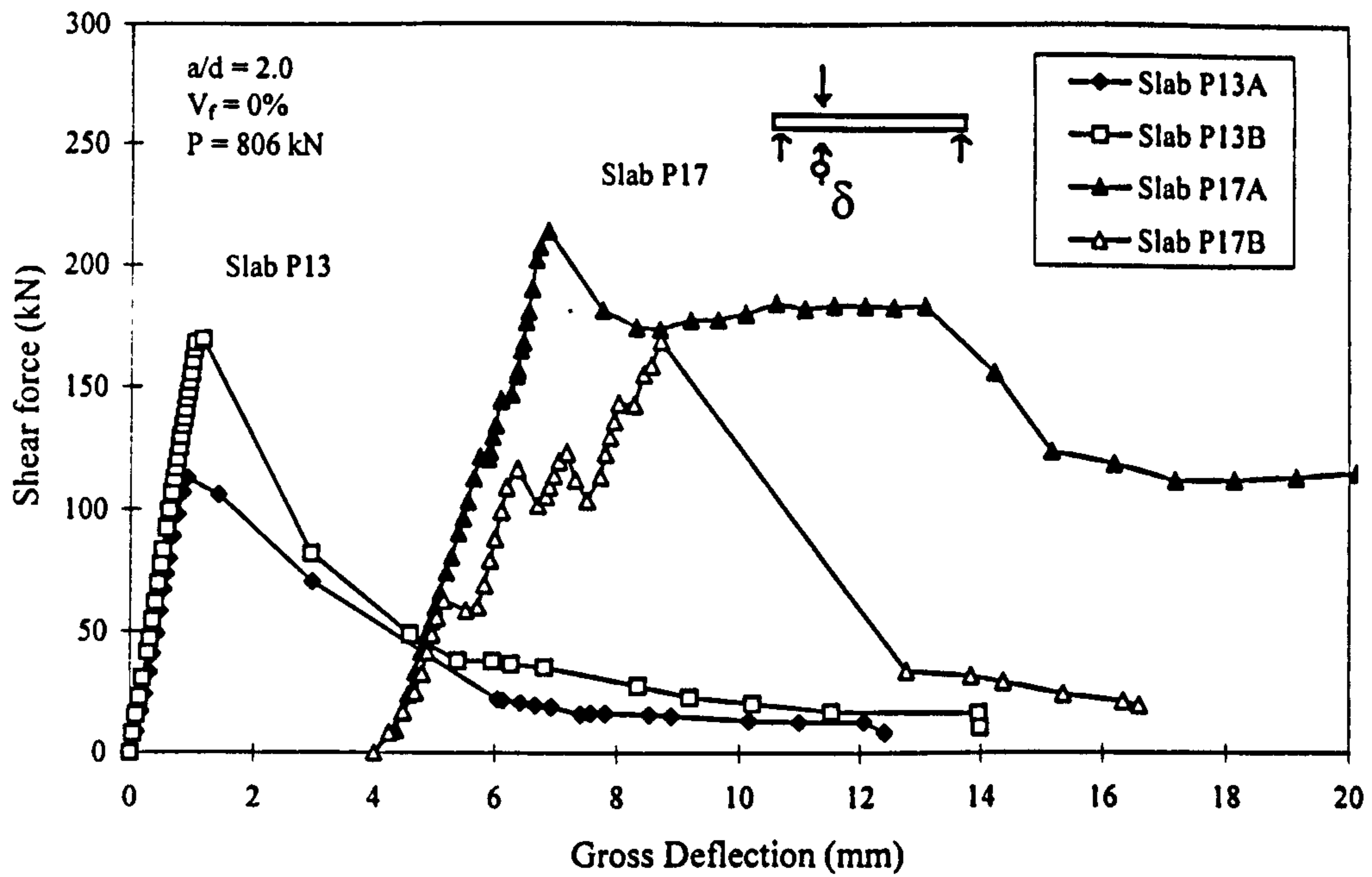
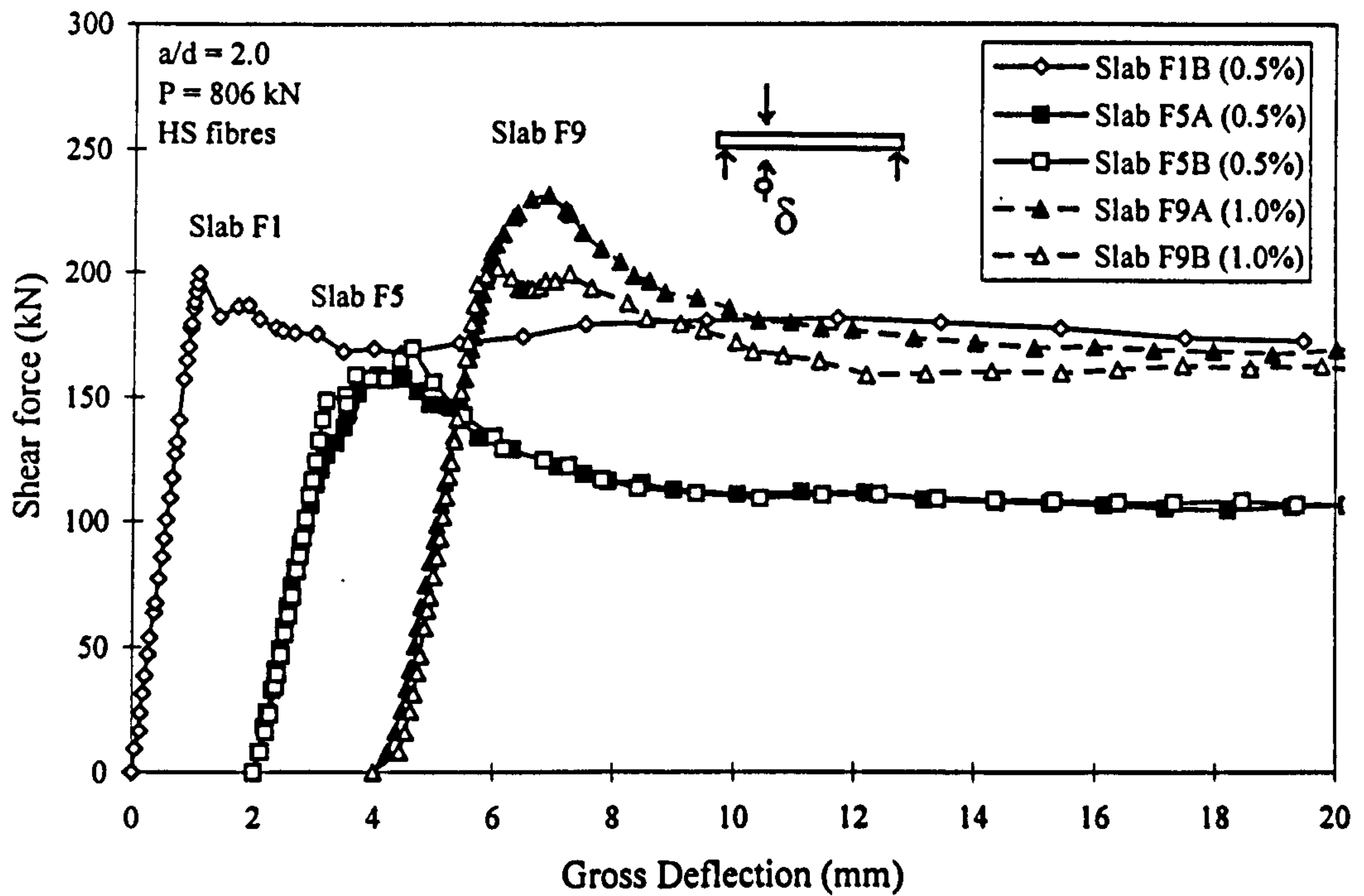


Figure 7-1 General arrangement of shear test set-up on full width slabs



**Figure 7-2 Shear load v deflection curves for plain P= 806 kN reinforced slabs at  $a/d = 2.0$**



**Figure 7-3 Shear load v deflection curves for FRC P= 806 kN reinforced slabs at  $a/d = 2.0$**

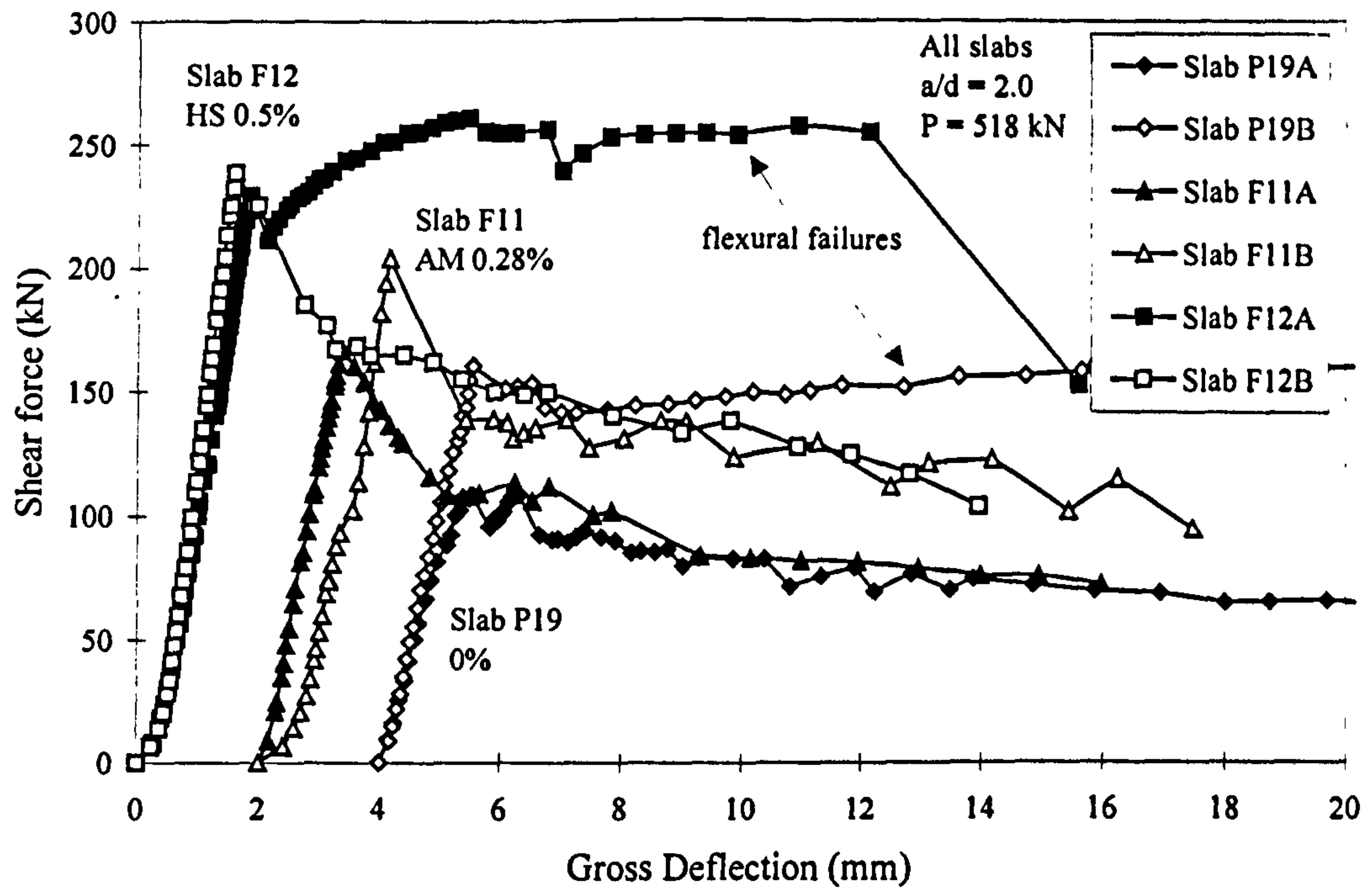


Figure 7-4 Shear load v deflection curves for  $P = 518$  kN reinforced slabs at  $a/d = 2.0$

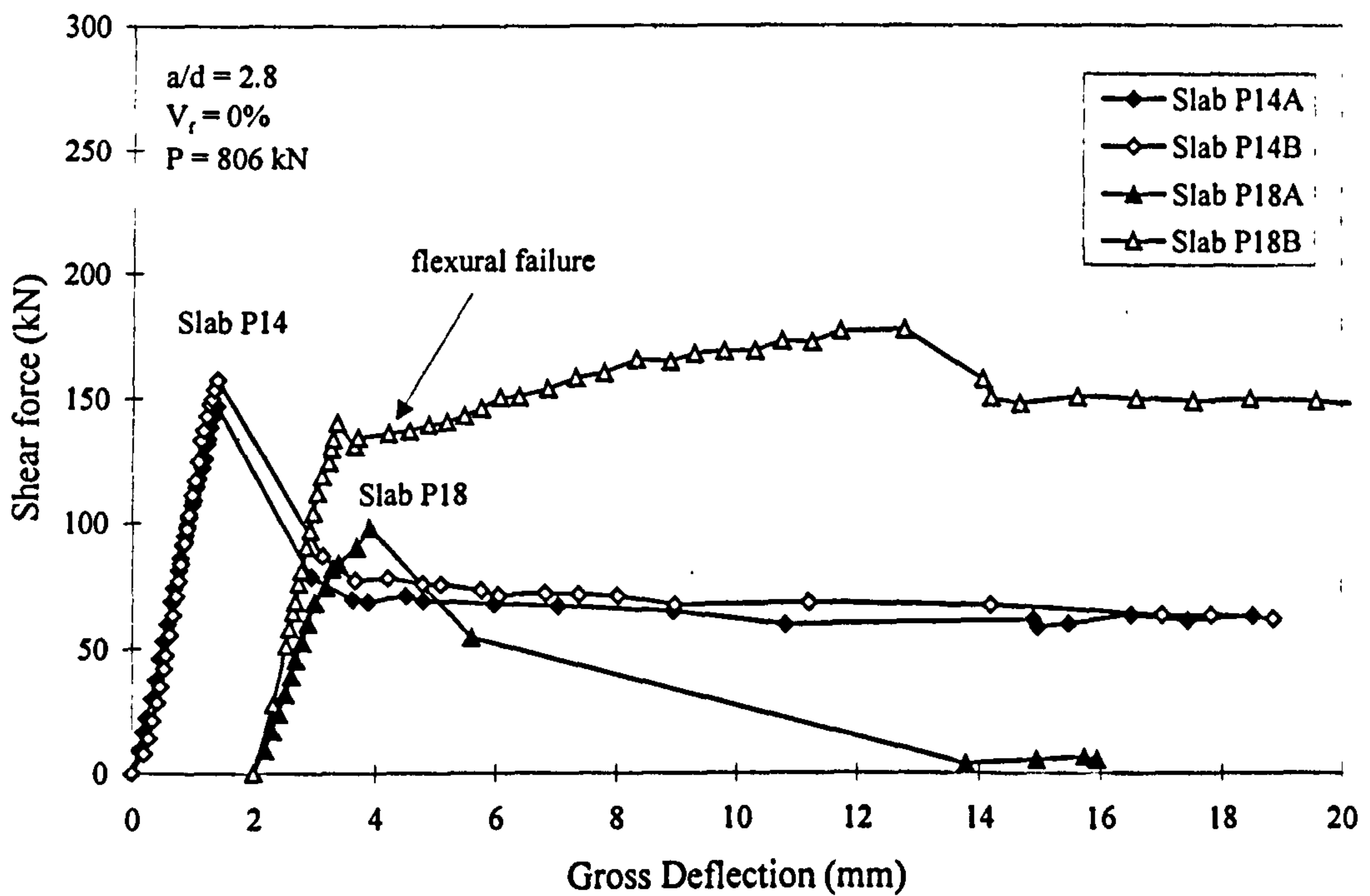


Figure 7-5 Shear load v deflection curves for plain  $P = 806$  kN reinforced slabs at  $a/d = 2.8$

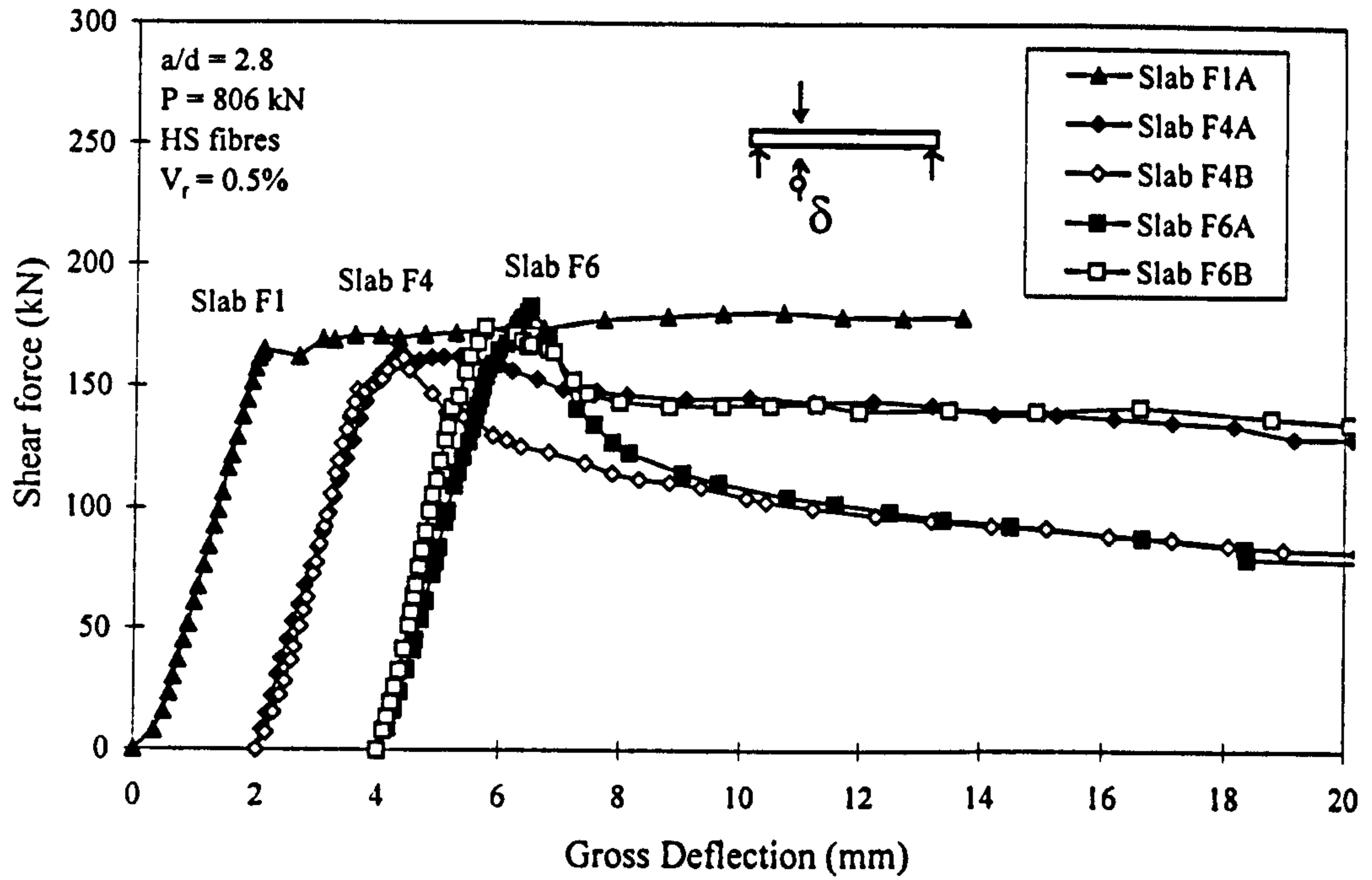


Figure 7-6 Shear load v deflection curves for  $P = 806$  kN reinforced slabs at  $a/d = 2.8$

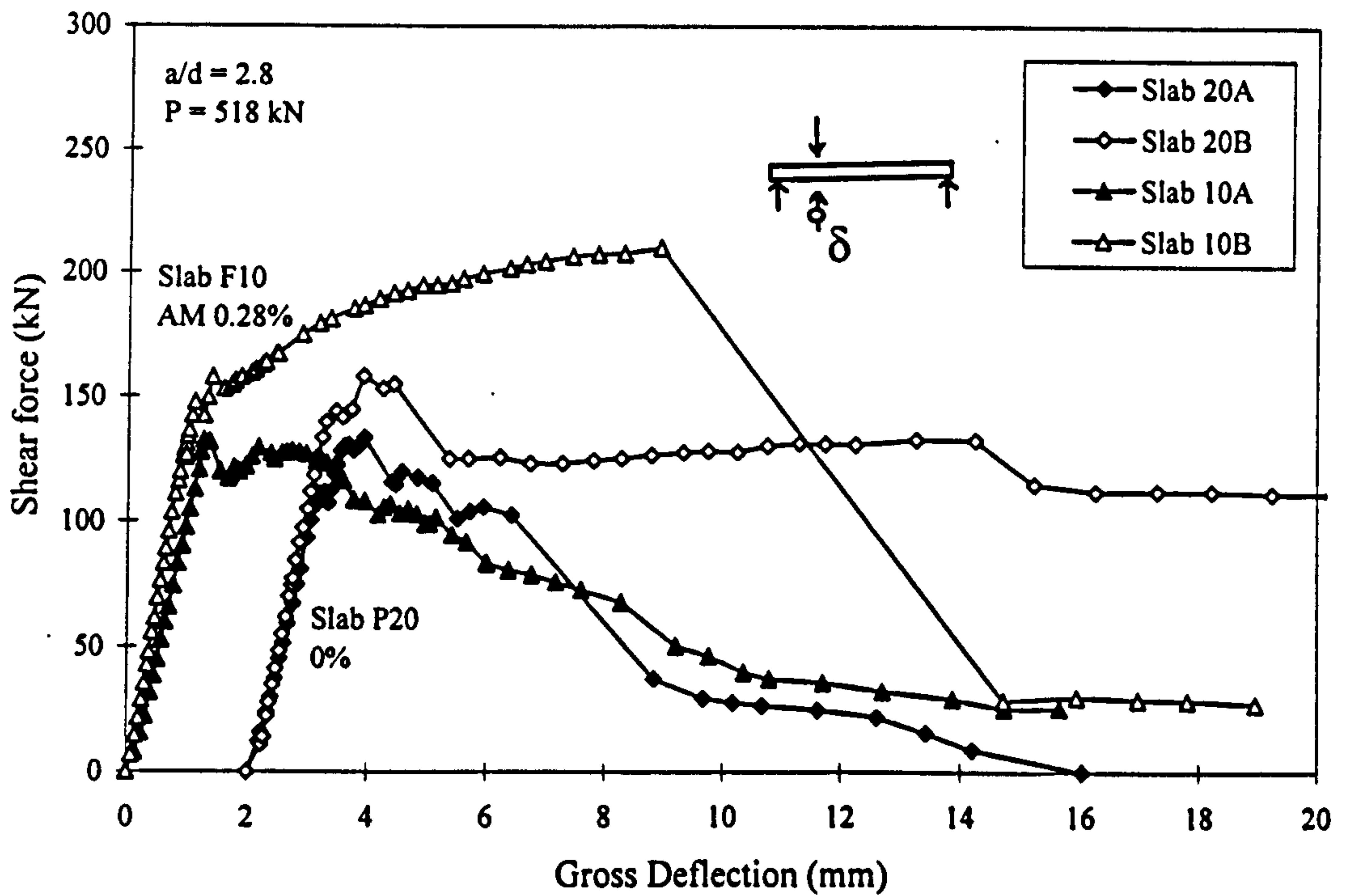


Figure 7-7 Shear load v deflection curves for  $P = 518$  kN reinforced slabs at  $a/d = 2.8$

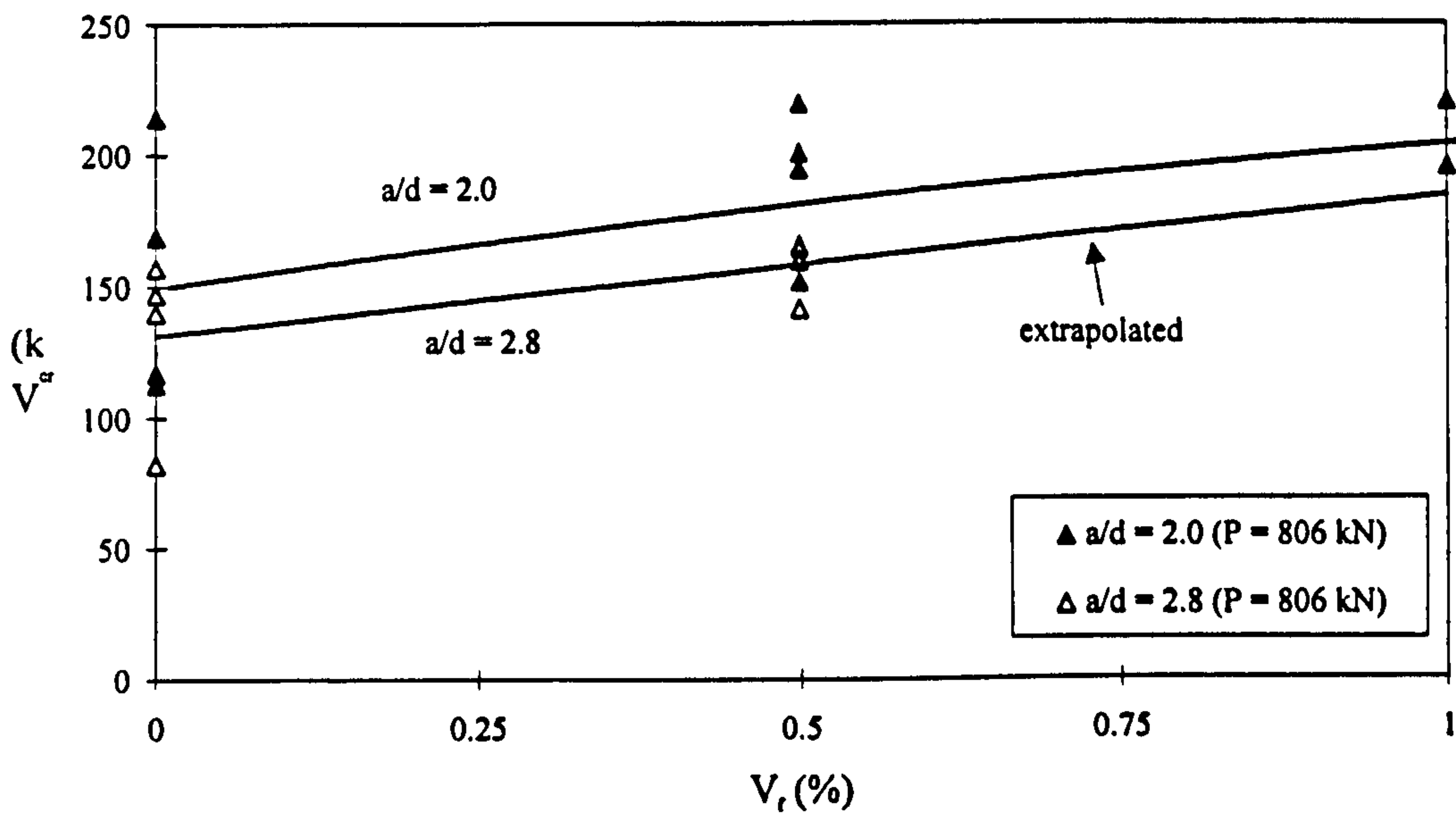


Figure 7-8 Effect of fibre volume fraction on  $V_{cr}$

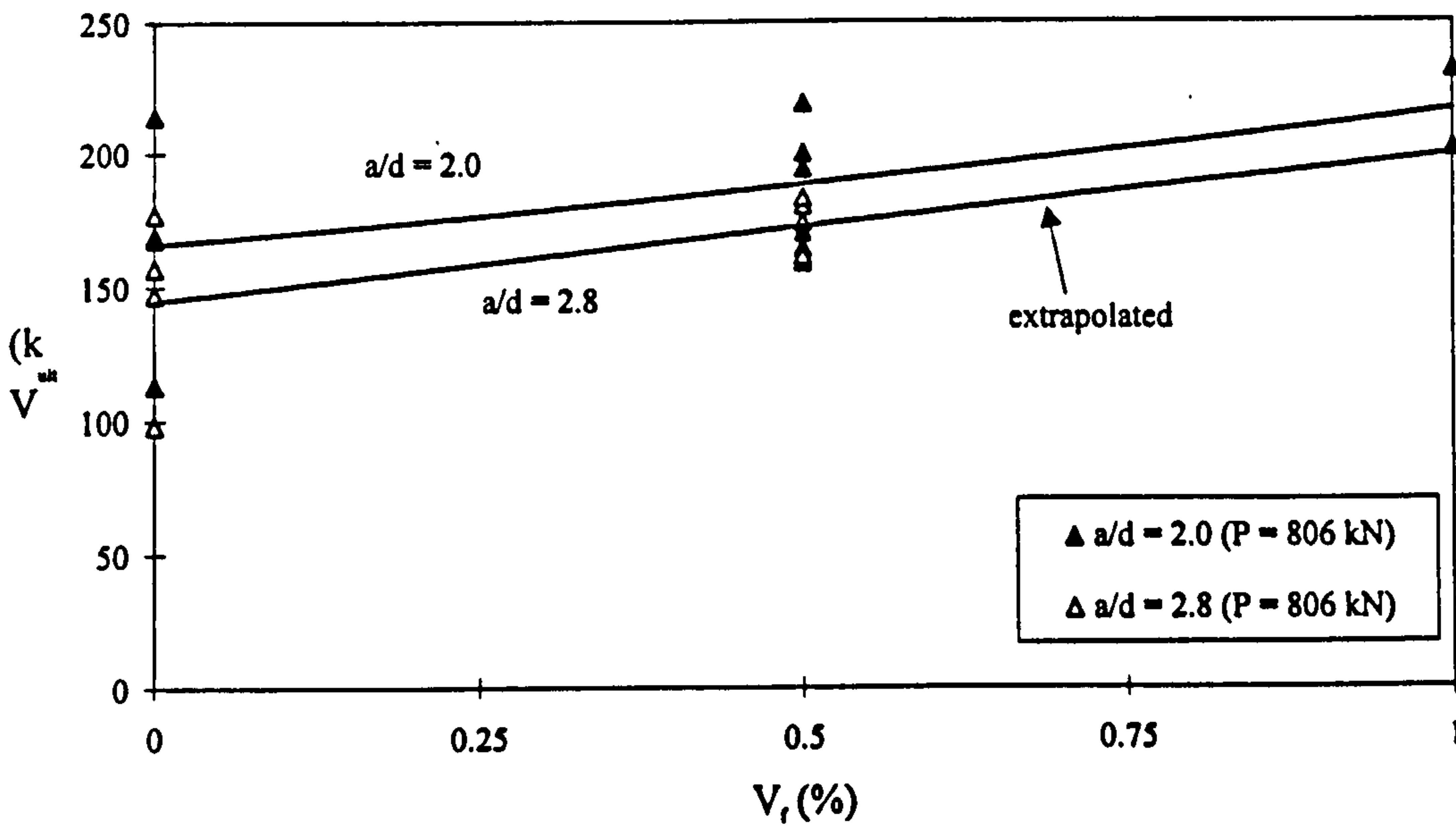


Figure 7-9 Effect of fibre volume fraction on  $V_{ult}$



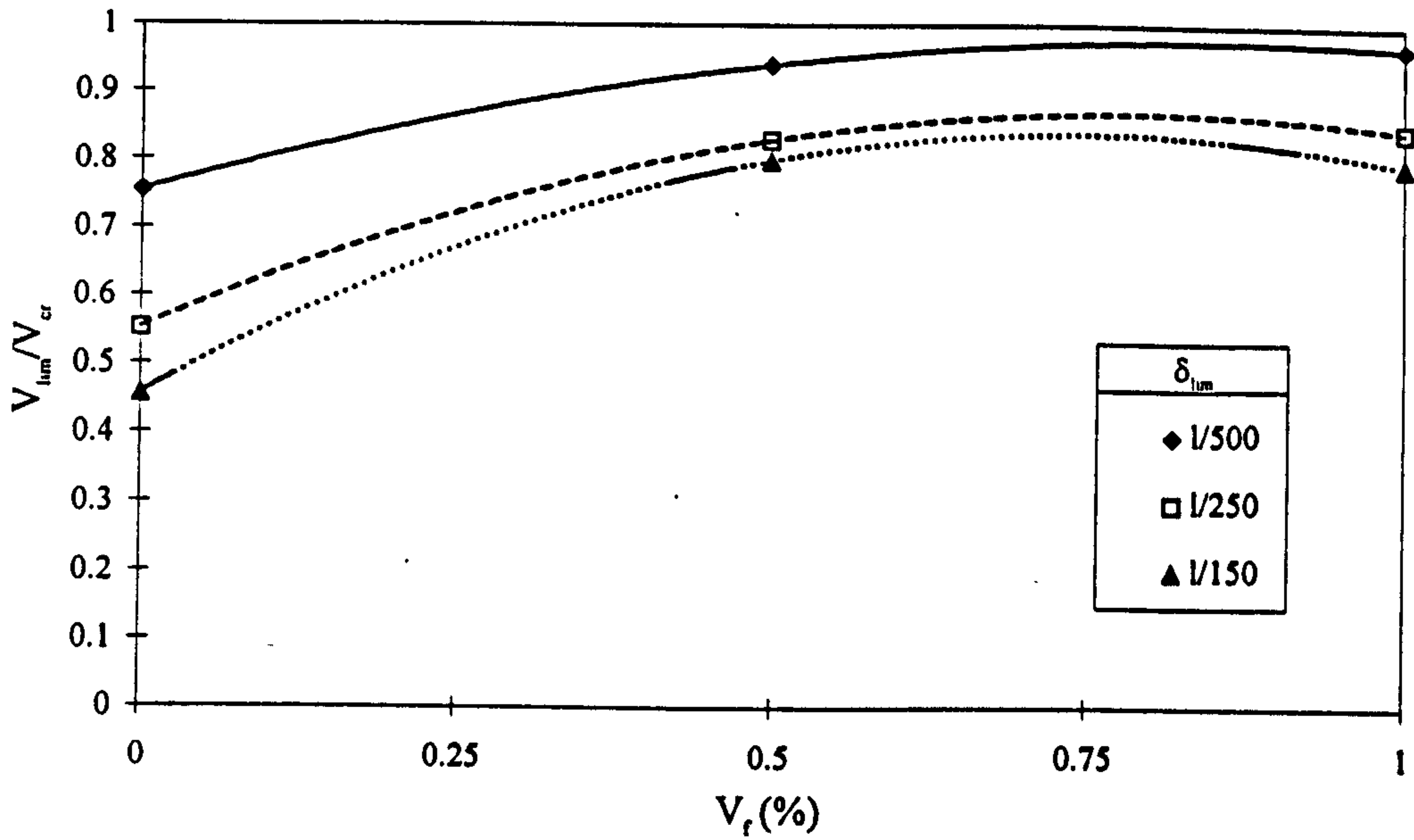


Figure 7-10  $V_{lim}/V_{cr}$  v  $V_r$  for HS fibre slabs

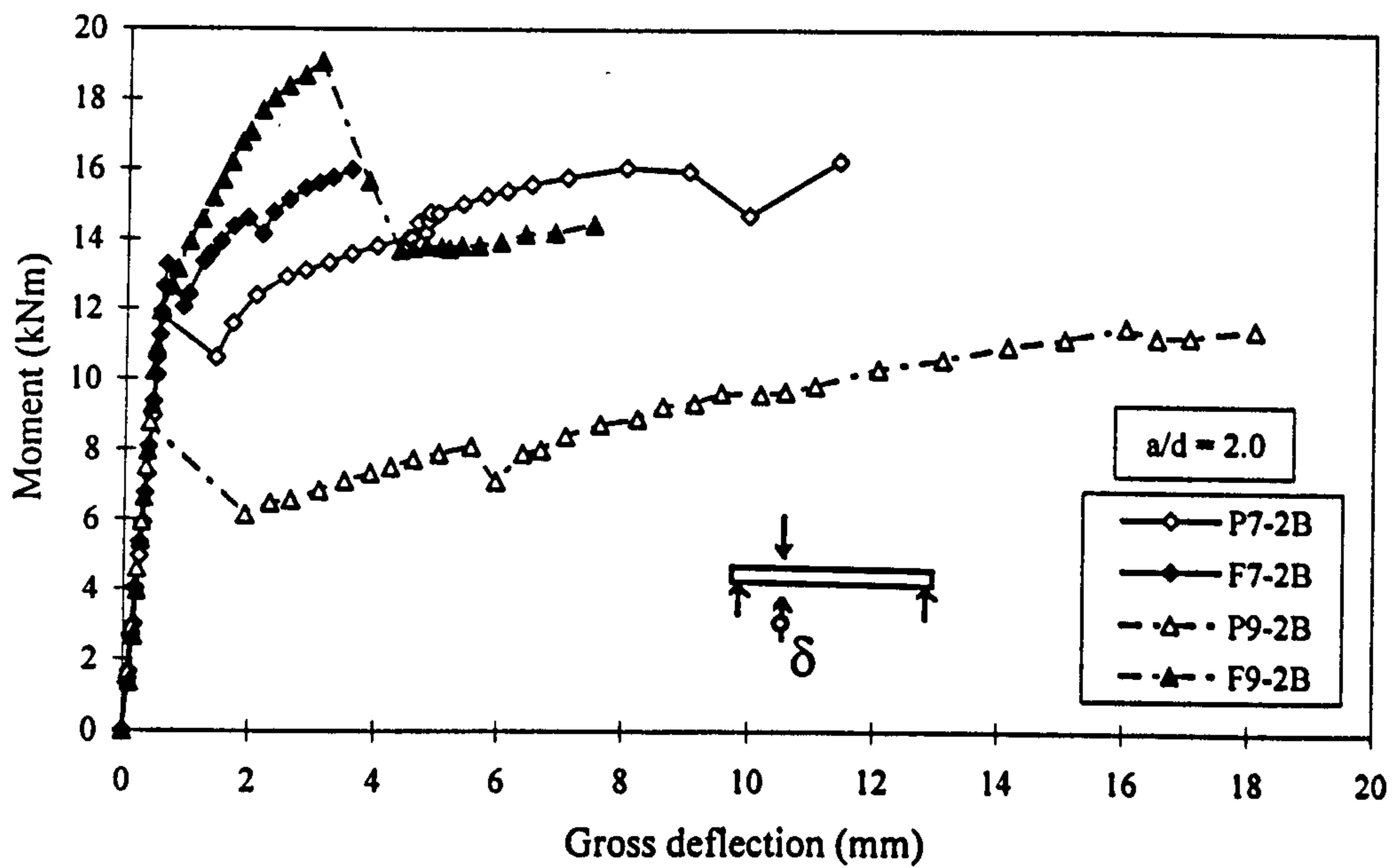


Figure 7-11 Moment v deflection curves for x-beams reinforced with 7 mm wire and 9.3 mm strand at  $a/d = 2.0$

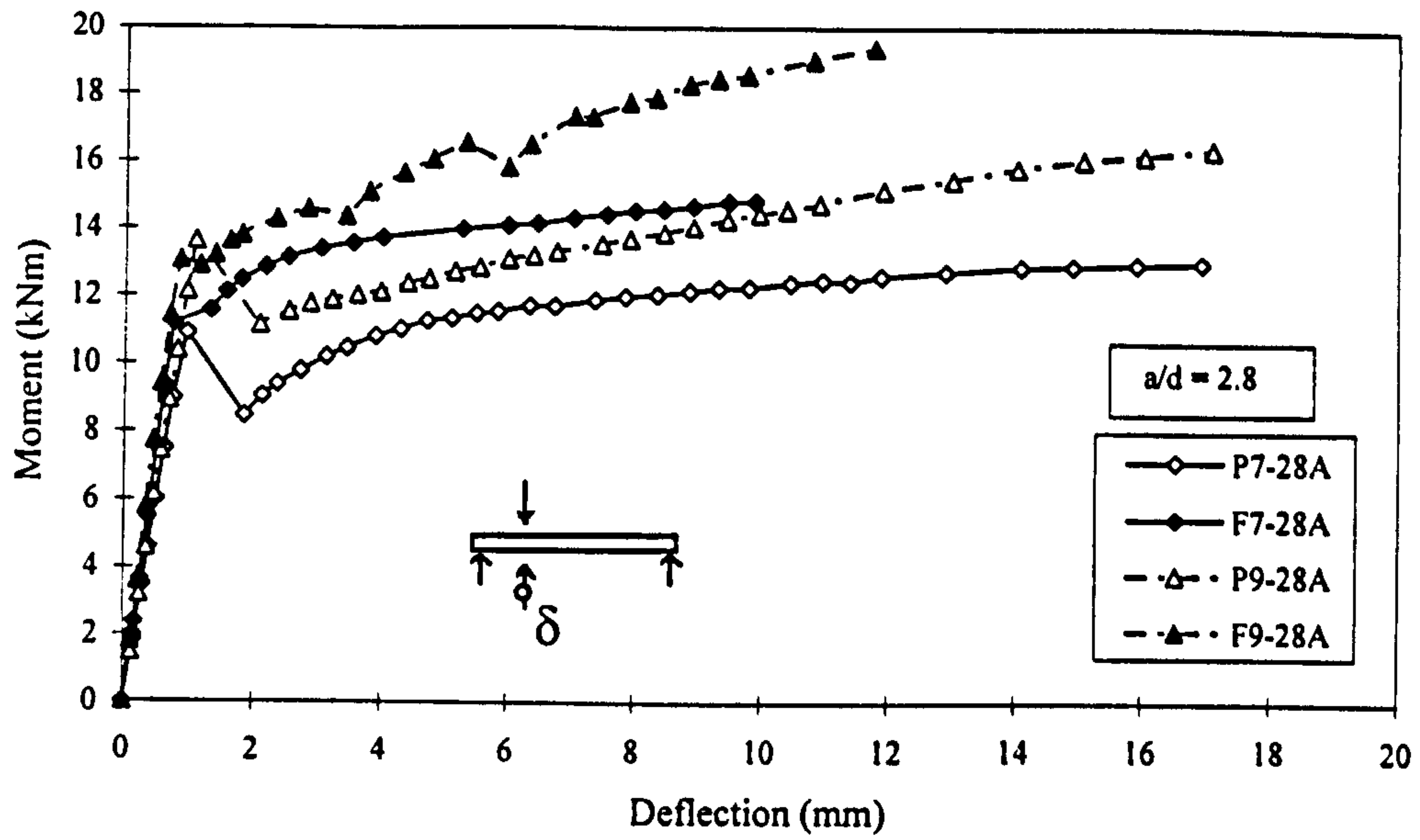


Figure 7-12 Moment v deflection curves for x-beams reinforced with 7 mm wire and 9.3 mm strand at  $a/d = 2.8$

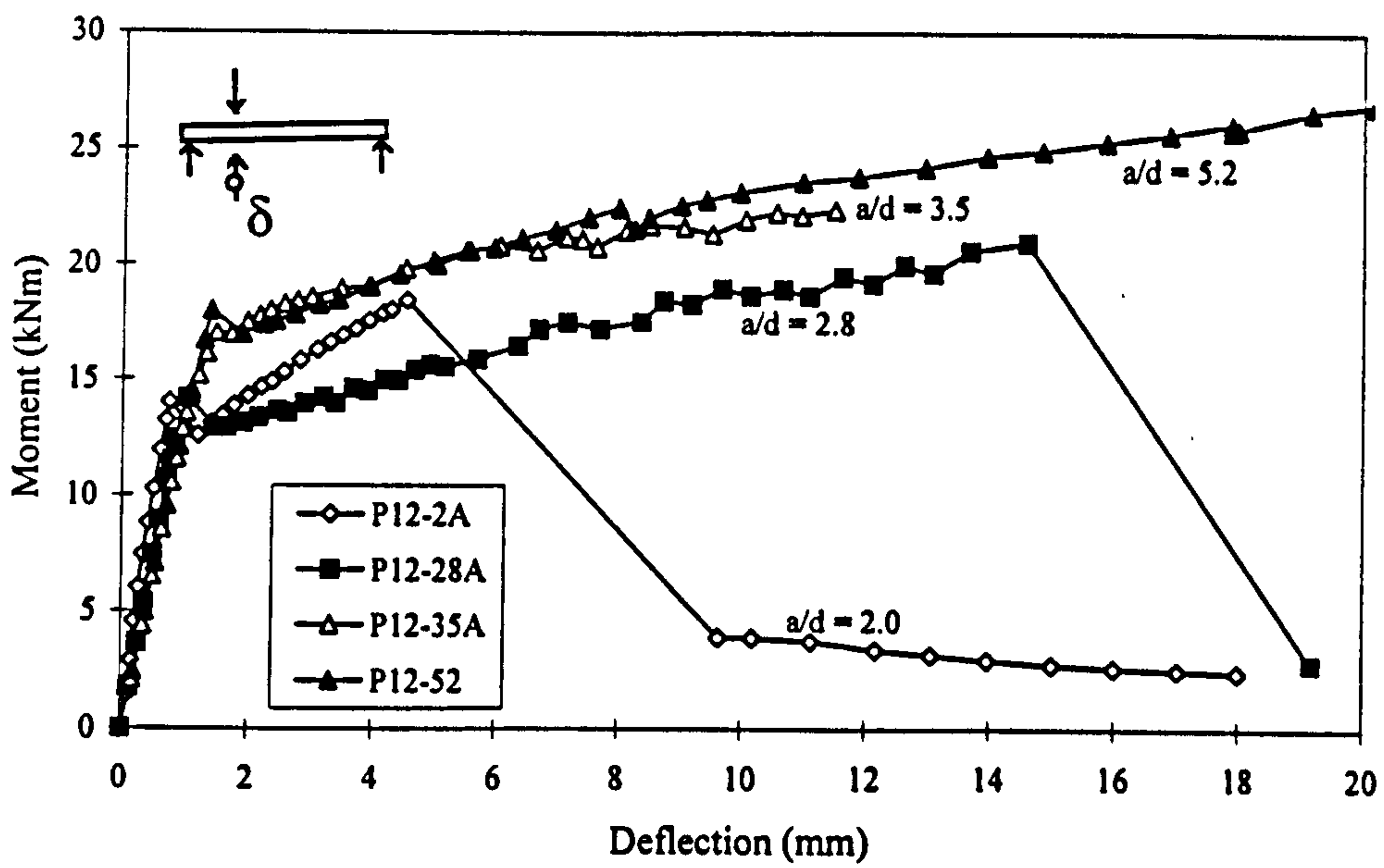


Figure 7-13 Moment v deflection curves for x-beams reinforced with 12.5 mm strand at different  $a/d$

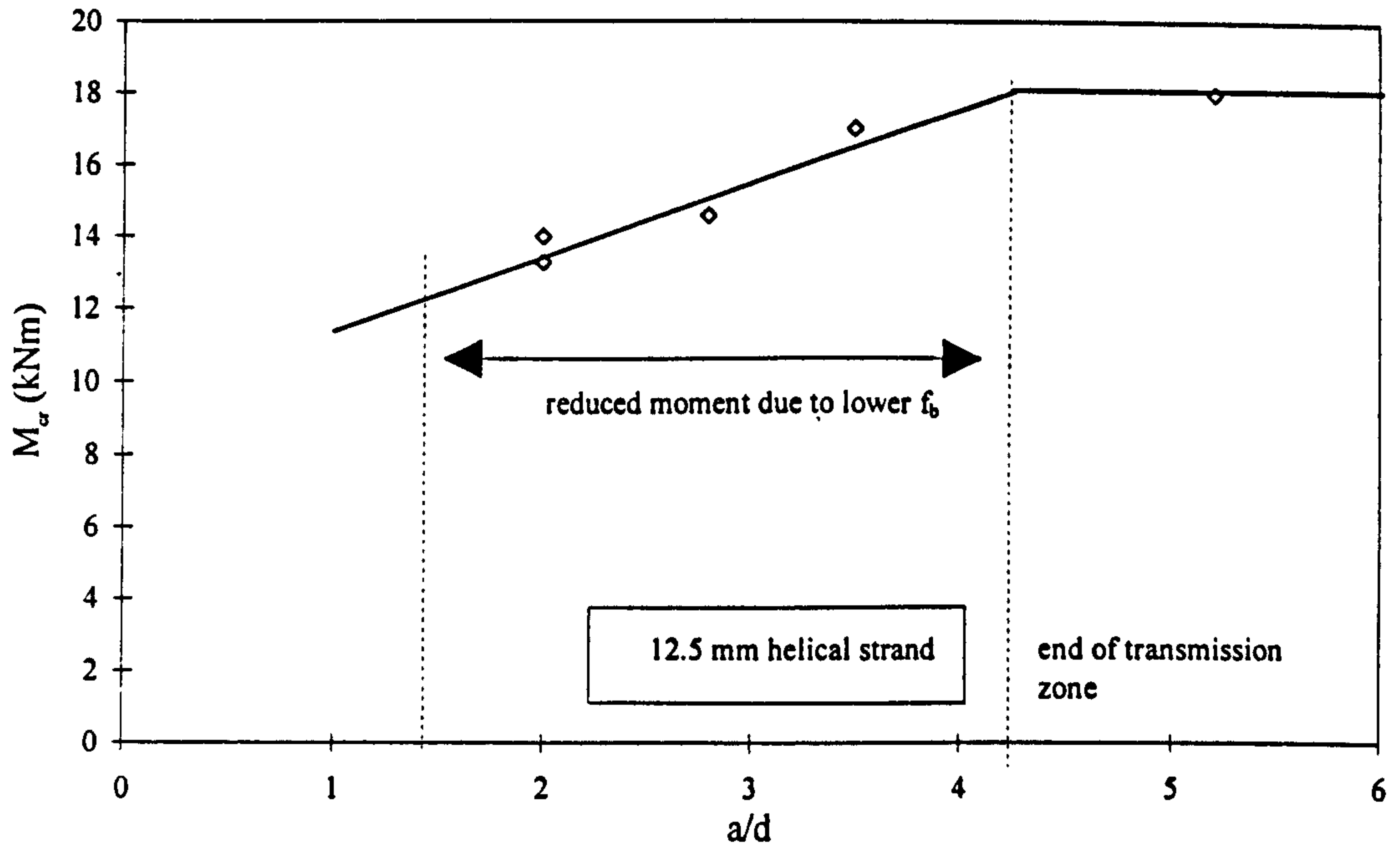


Figure 7-14 Effect of  $a/d$  on  $M_{cr}$

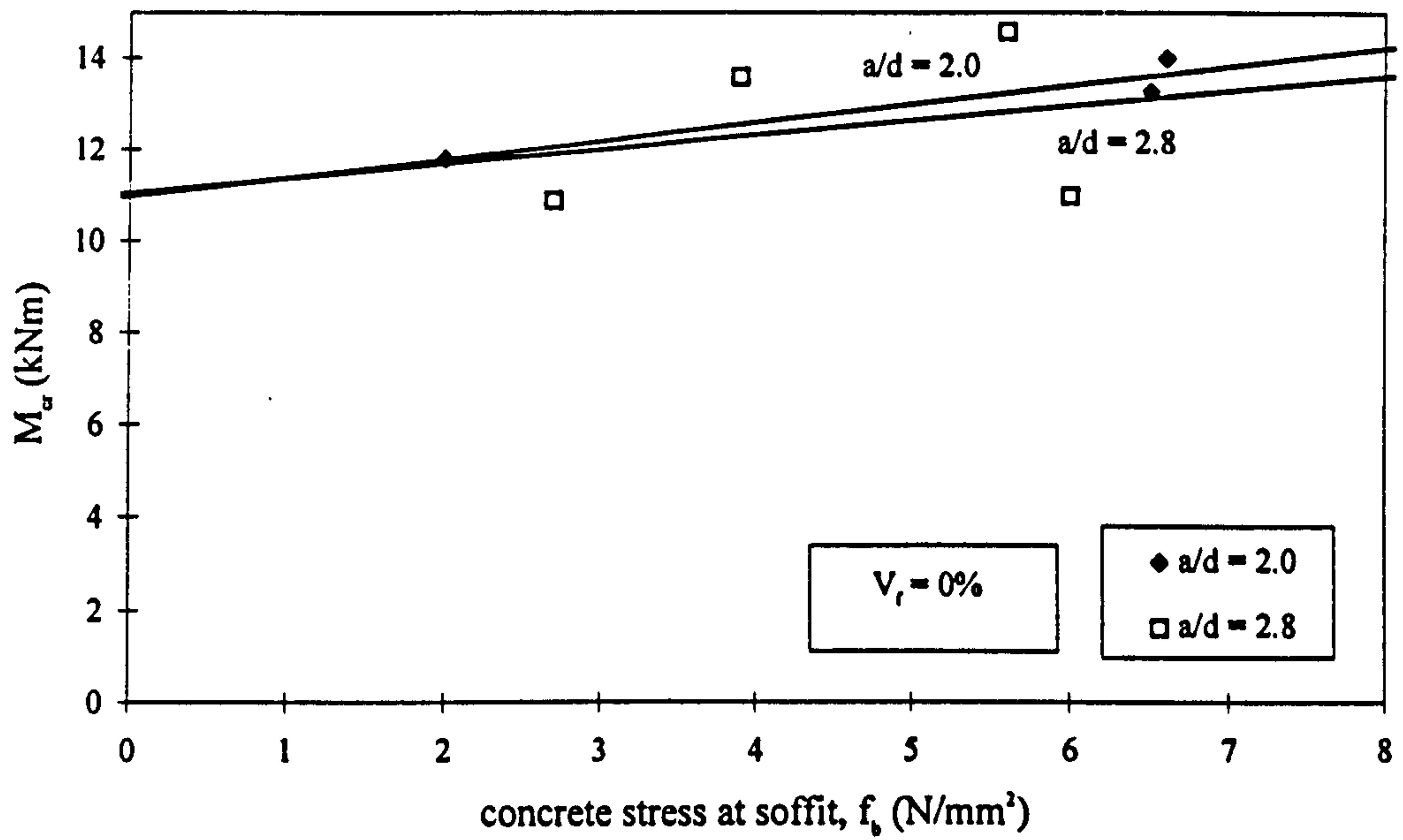


Figure 7-15 Effect of precompression in soffit on  $M_{cr}$

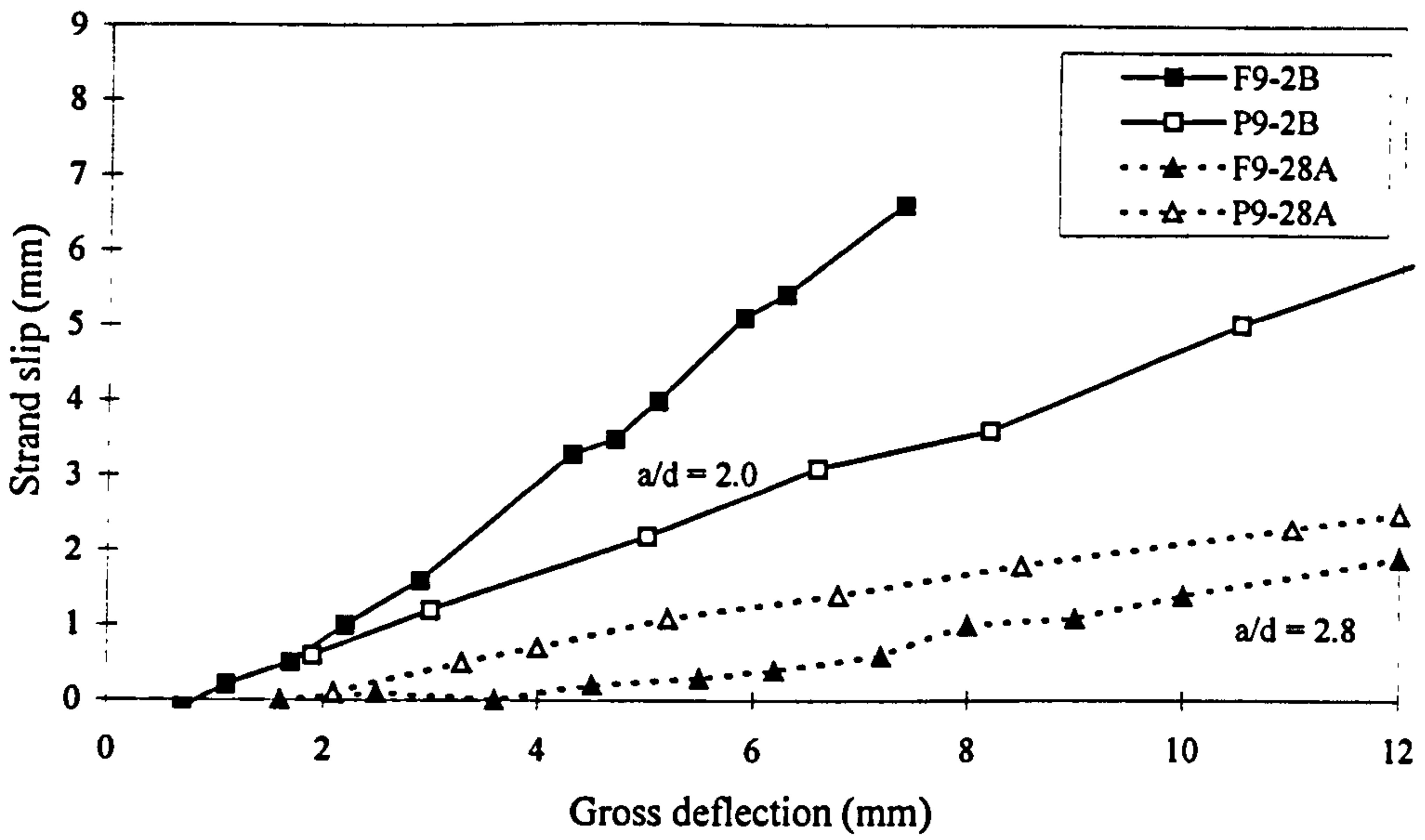


Figure 7-16 Strand slip v deflection for 9.3 mm strands in plain concrete and FRC

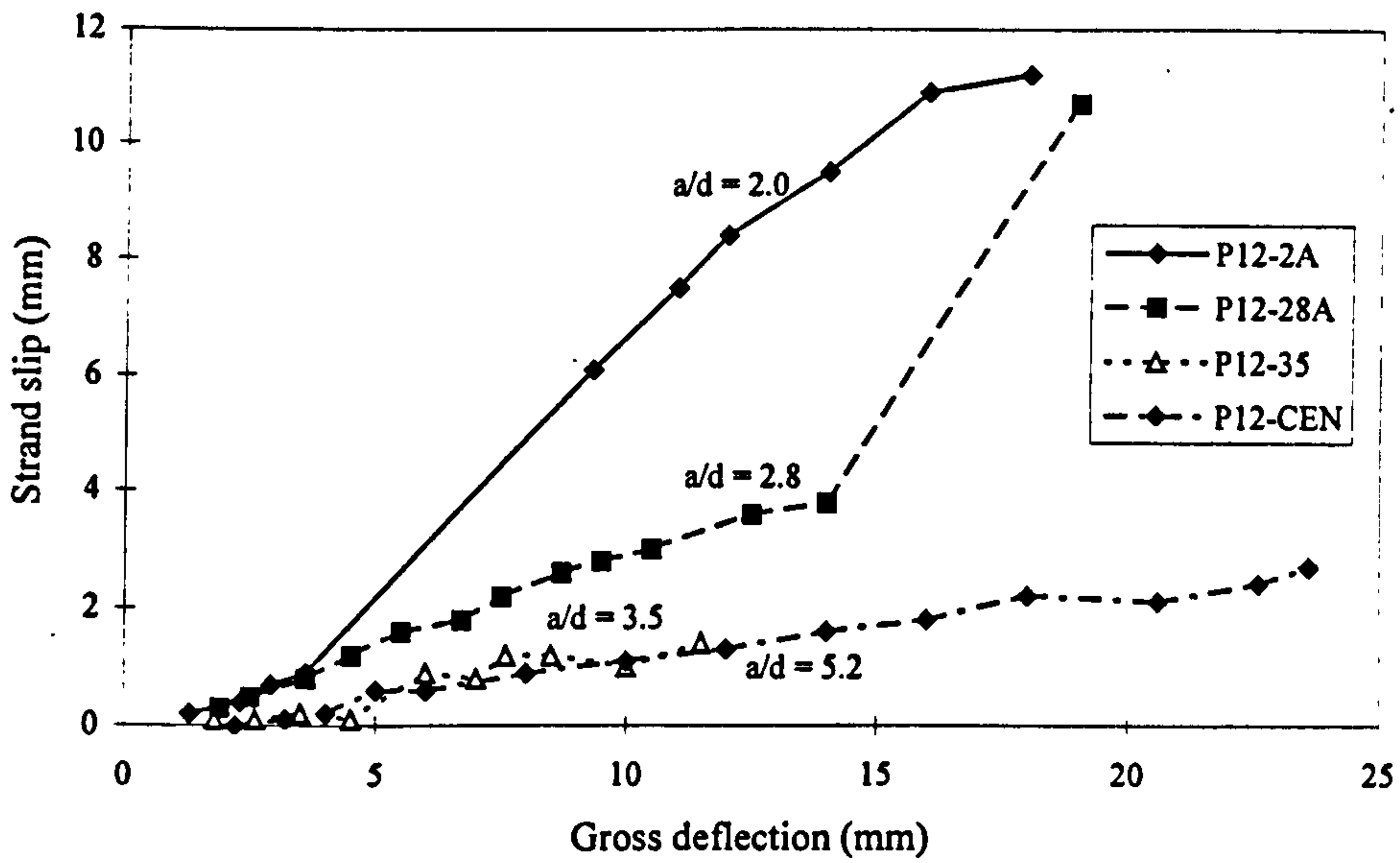
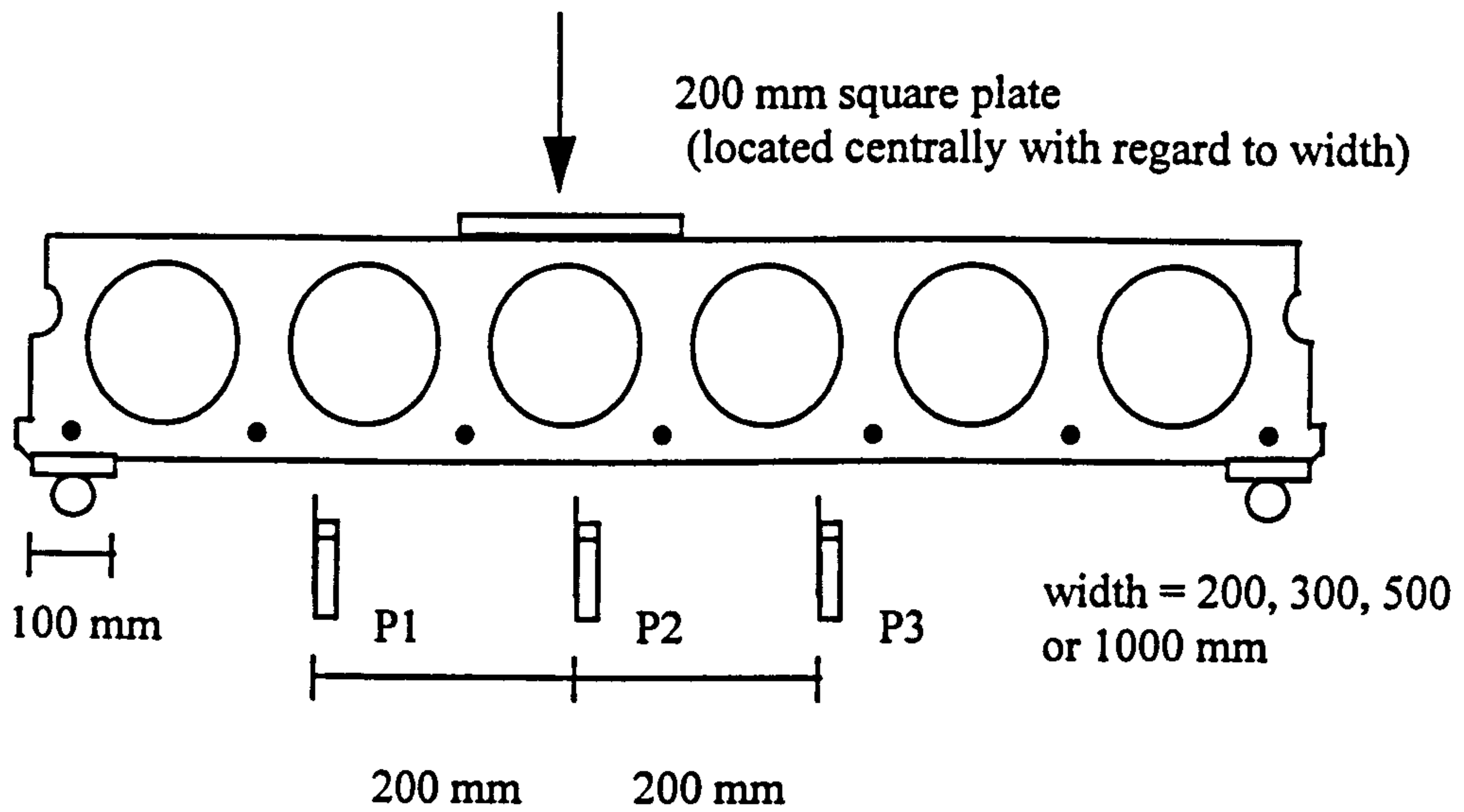
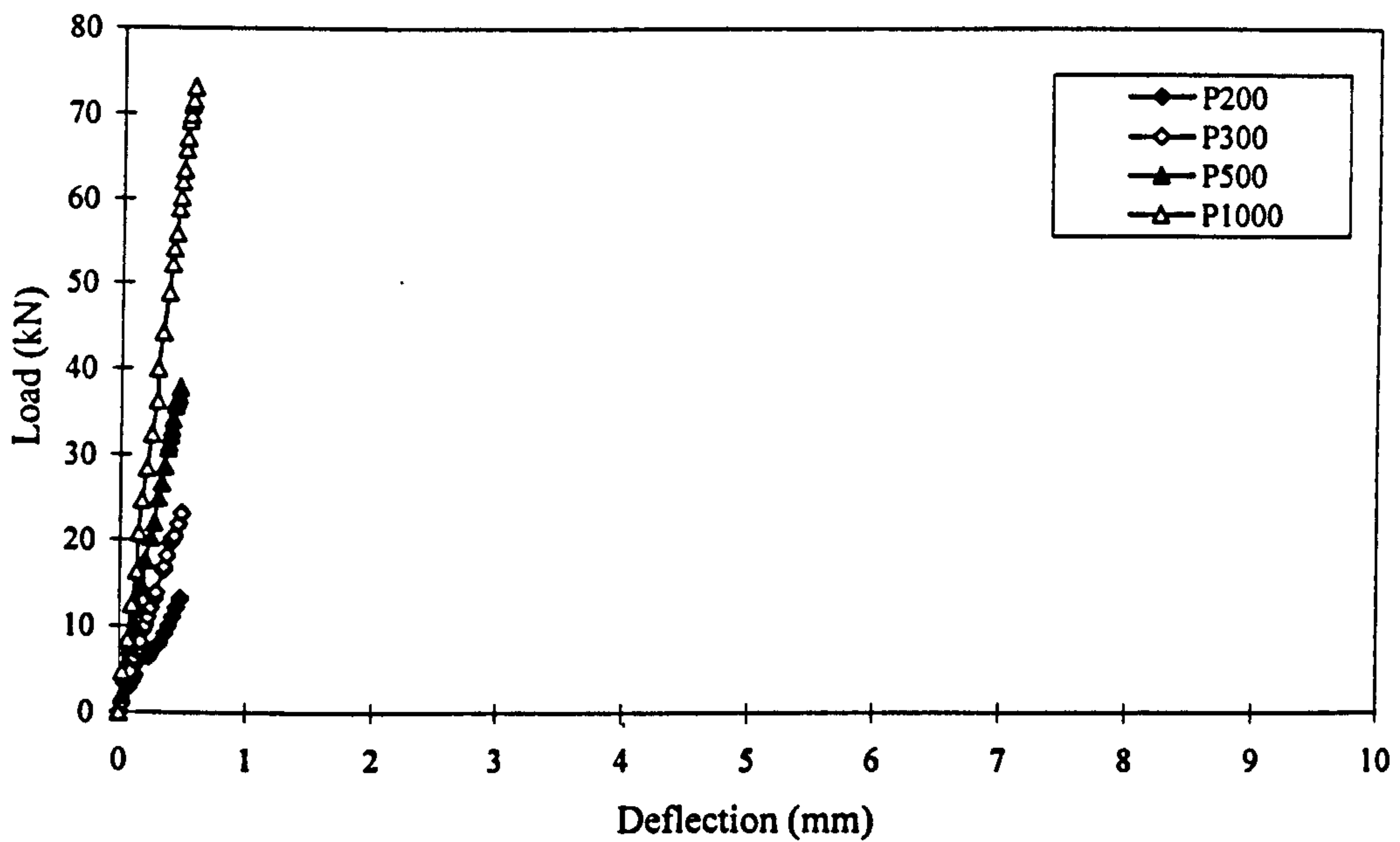


Figure 7-17 Strand slip v deflection for 12.5 mm strands



**Figure 7-18 Test set-up for transverse bending tests**



**Figure 7-19 Load v deflection curves for plain concrete transverse bending tests**

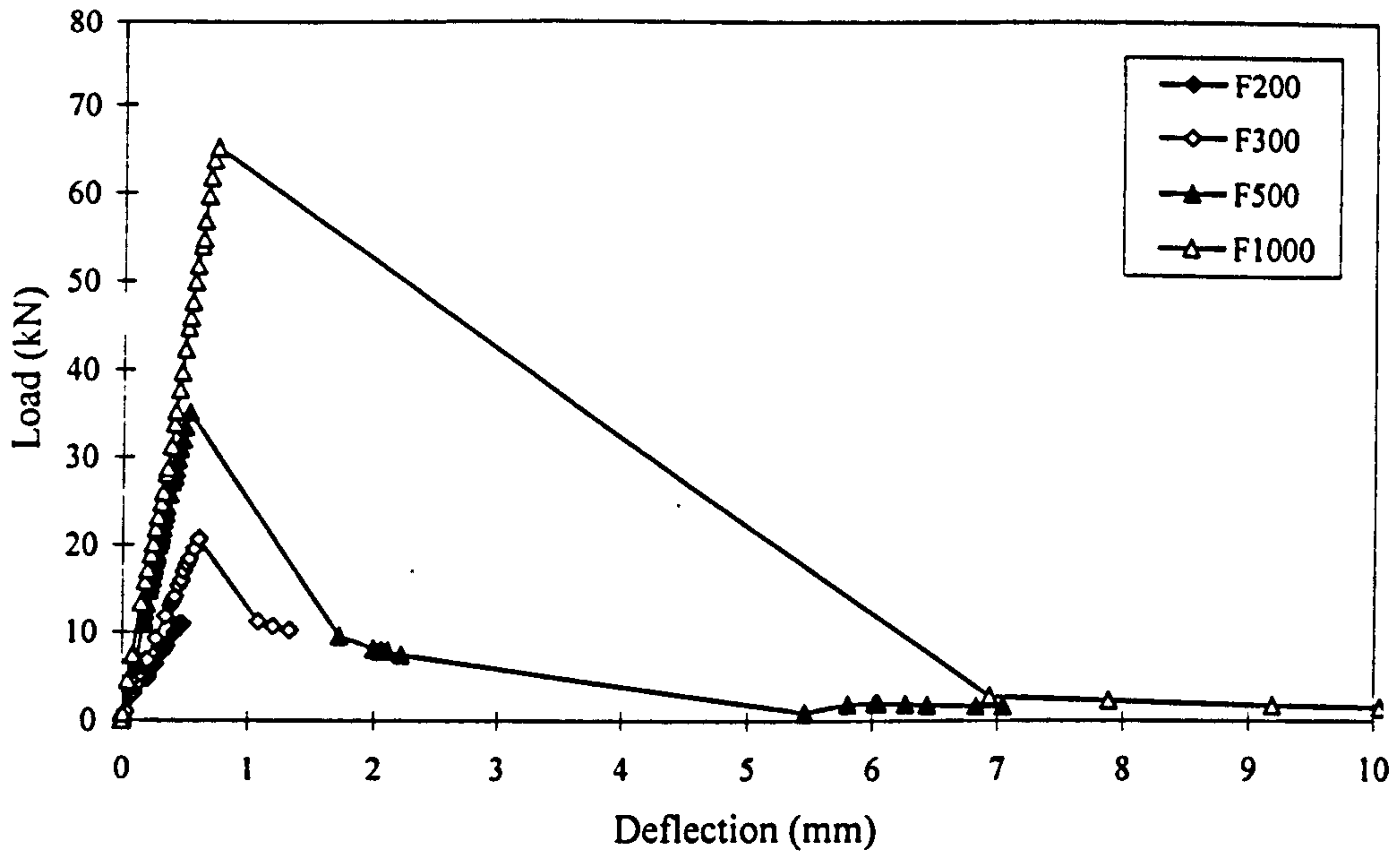


Figure 7-20 Load v deflection curves for FRC transverse bending tests

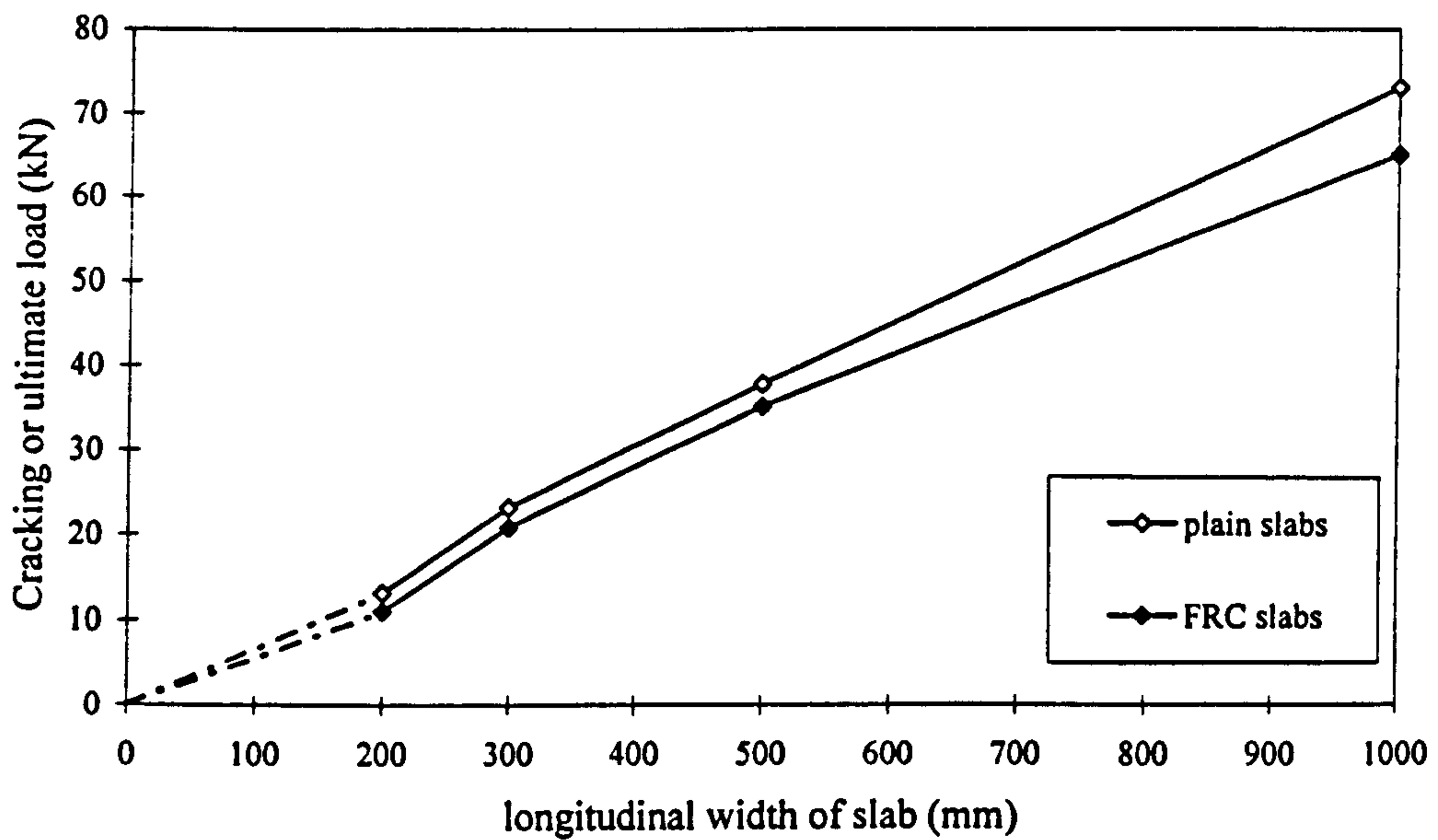
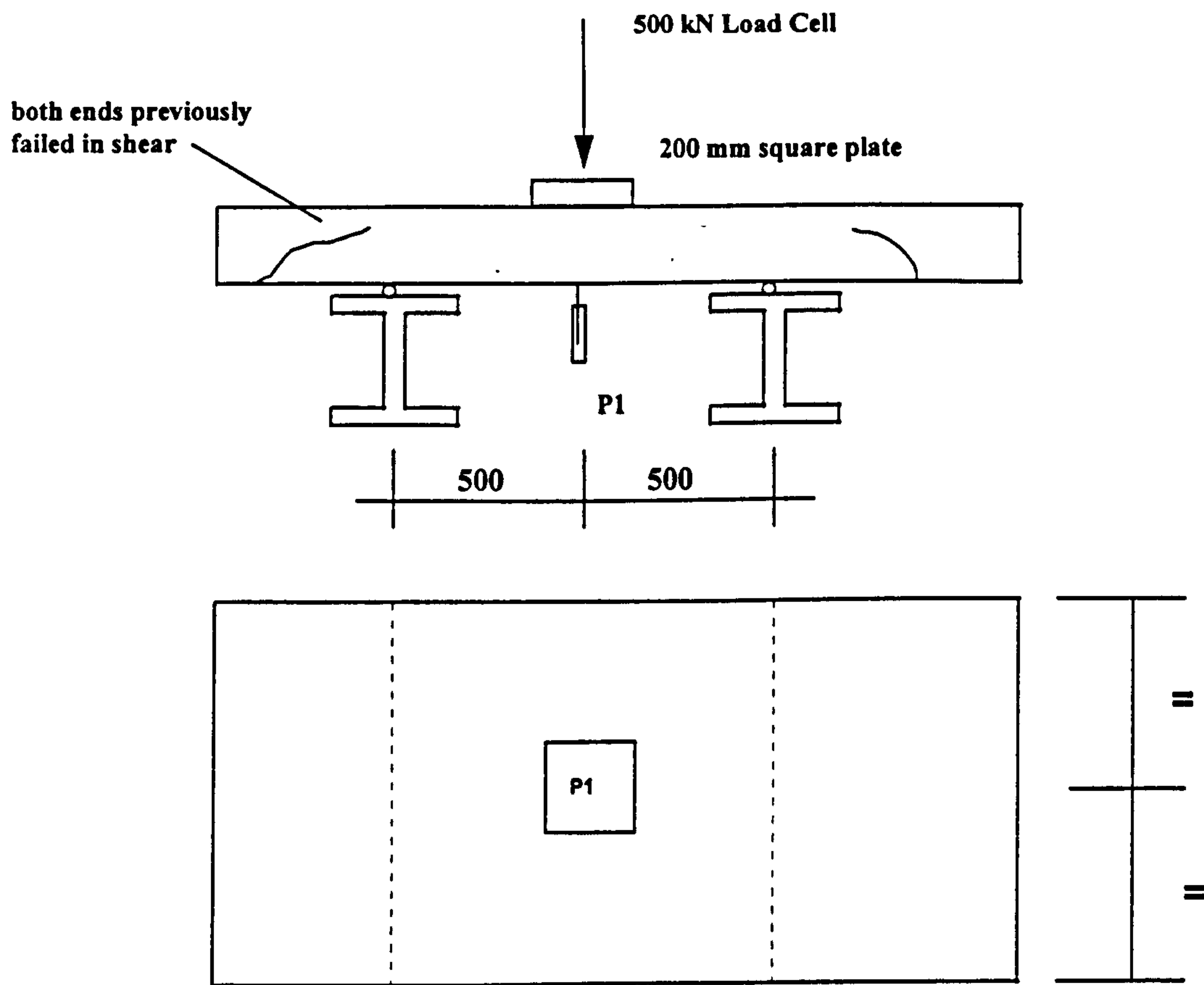


Figure 7-21 Relationship between longitudinal width of slab and transverse cracking load



**Figure 7-22 Test set-up for centric concentrated load test**

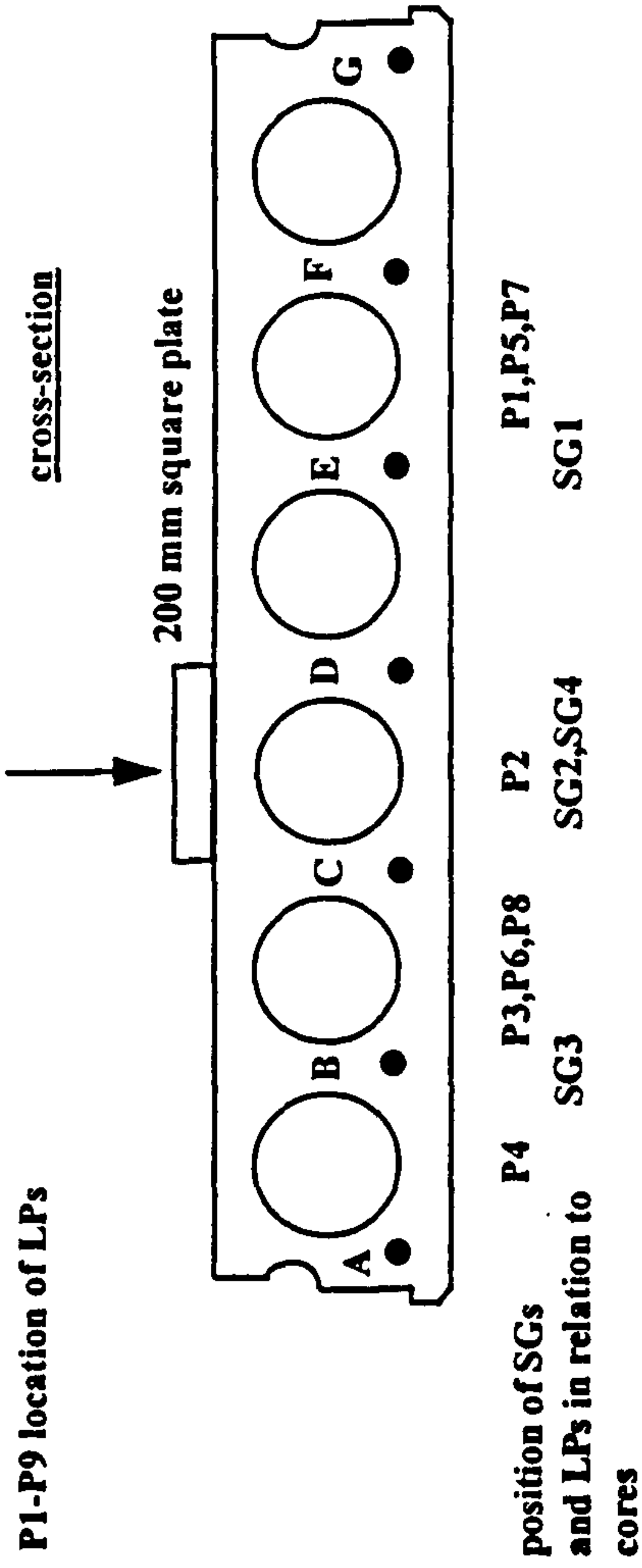
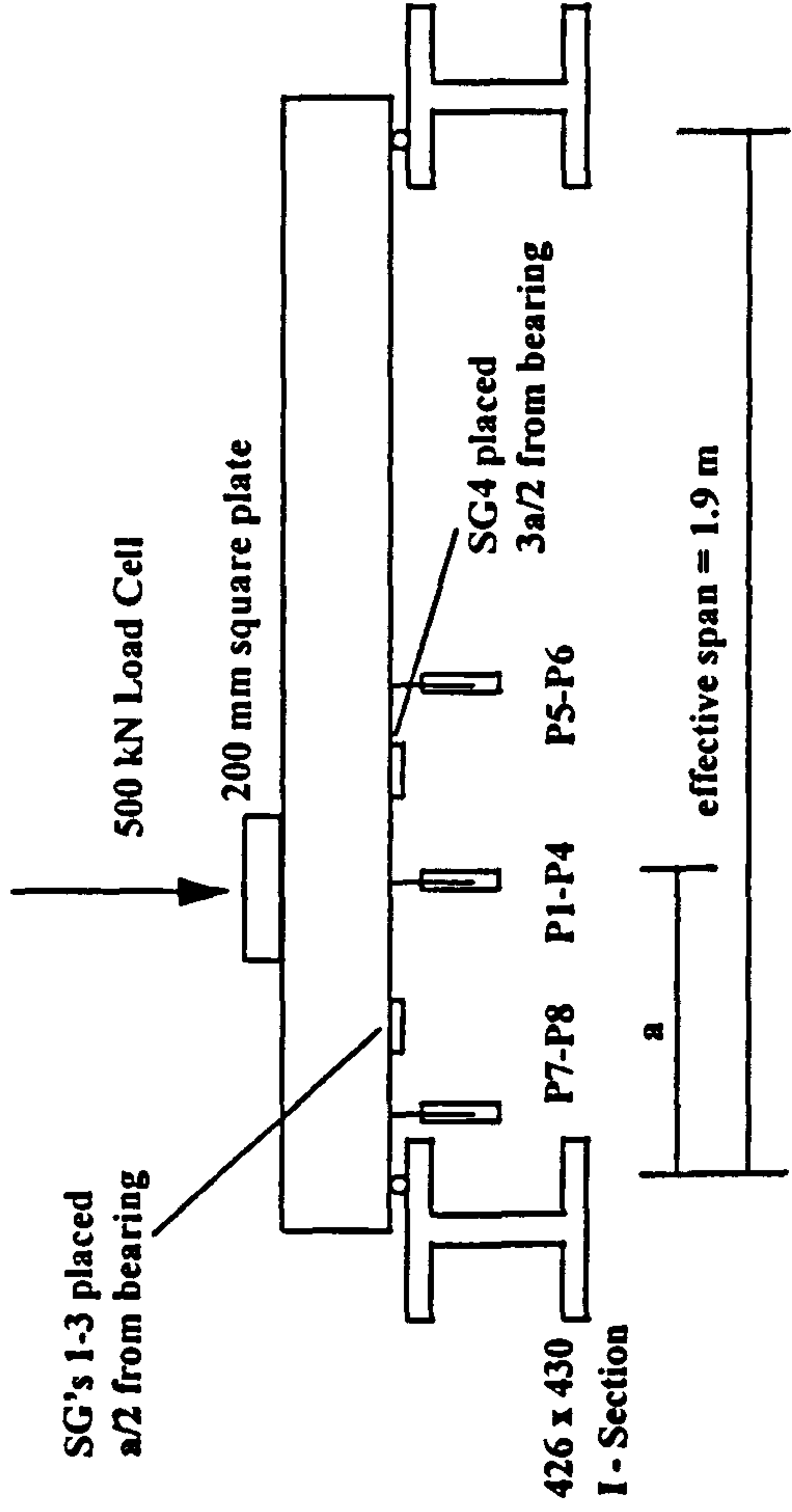
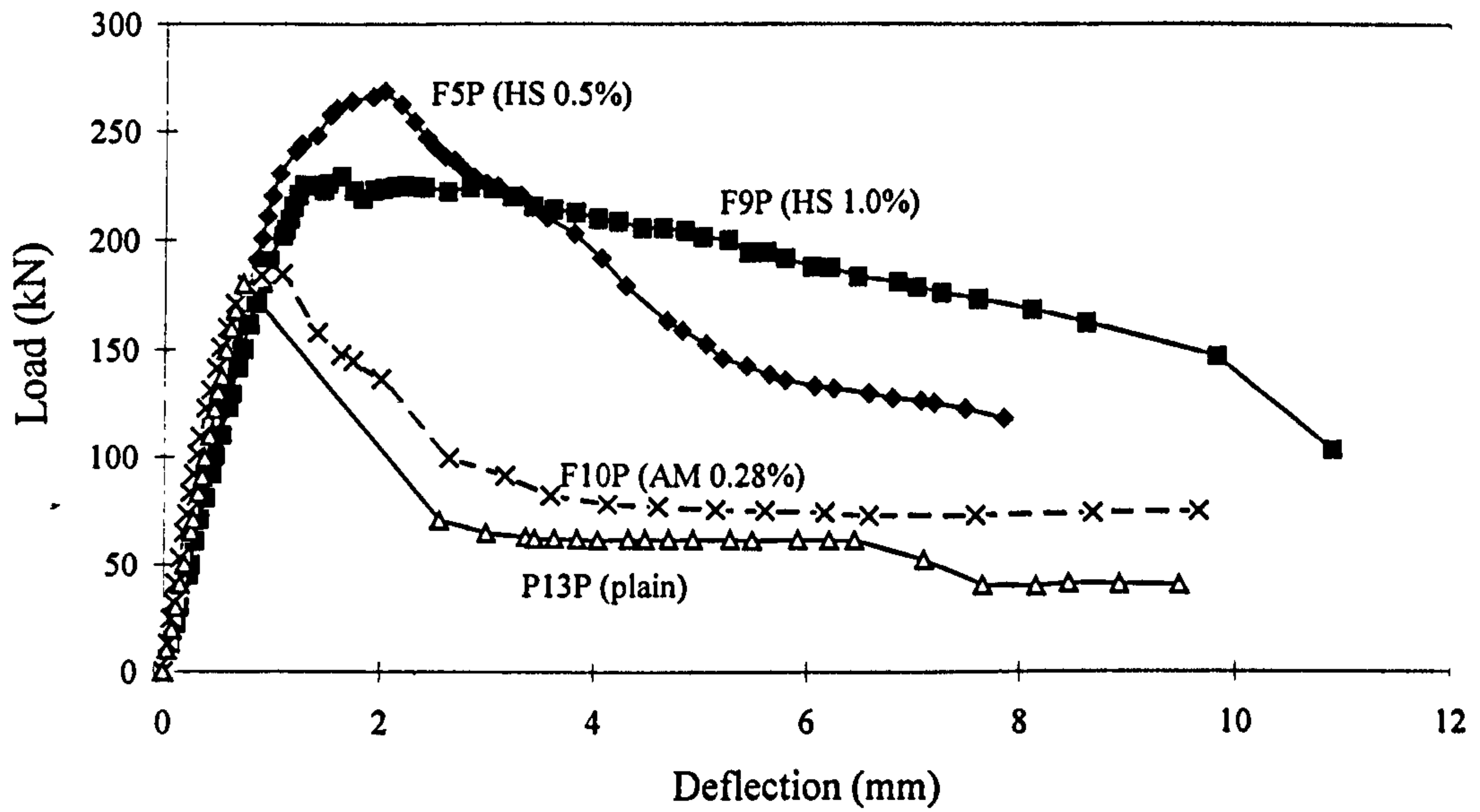
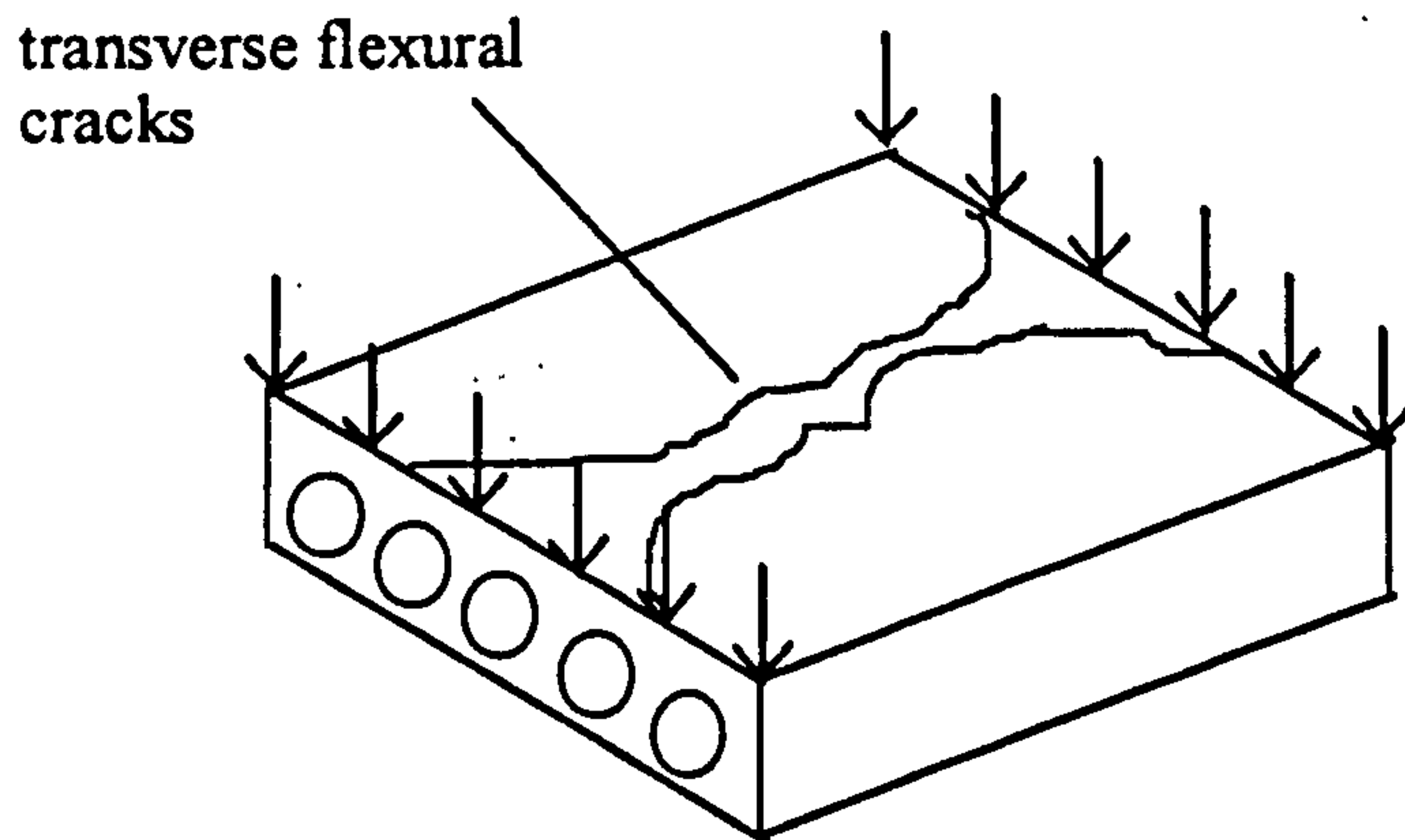


Figure 7-23 Test set-up for eccentric concentrated load test





**Figure 7-24 Typical load v deflection curves from centrally loaded tests**



**Figure 7-25 Typical wedge shaped cracking from centrally loaded tests**

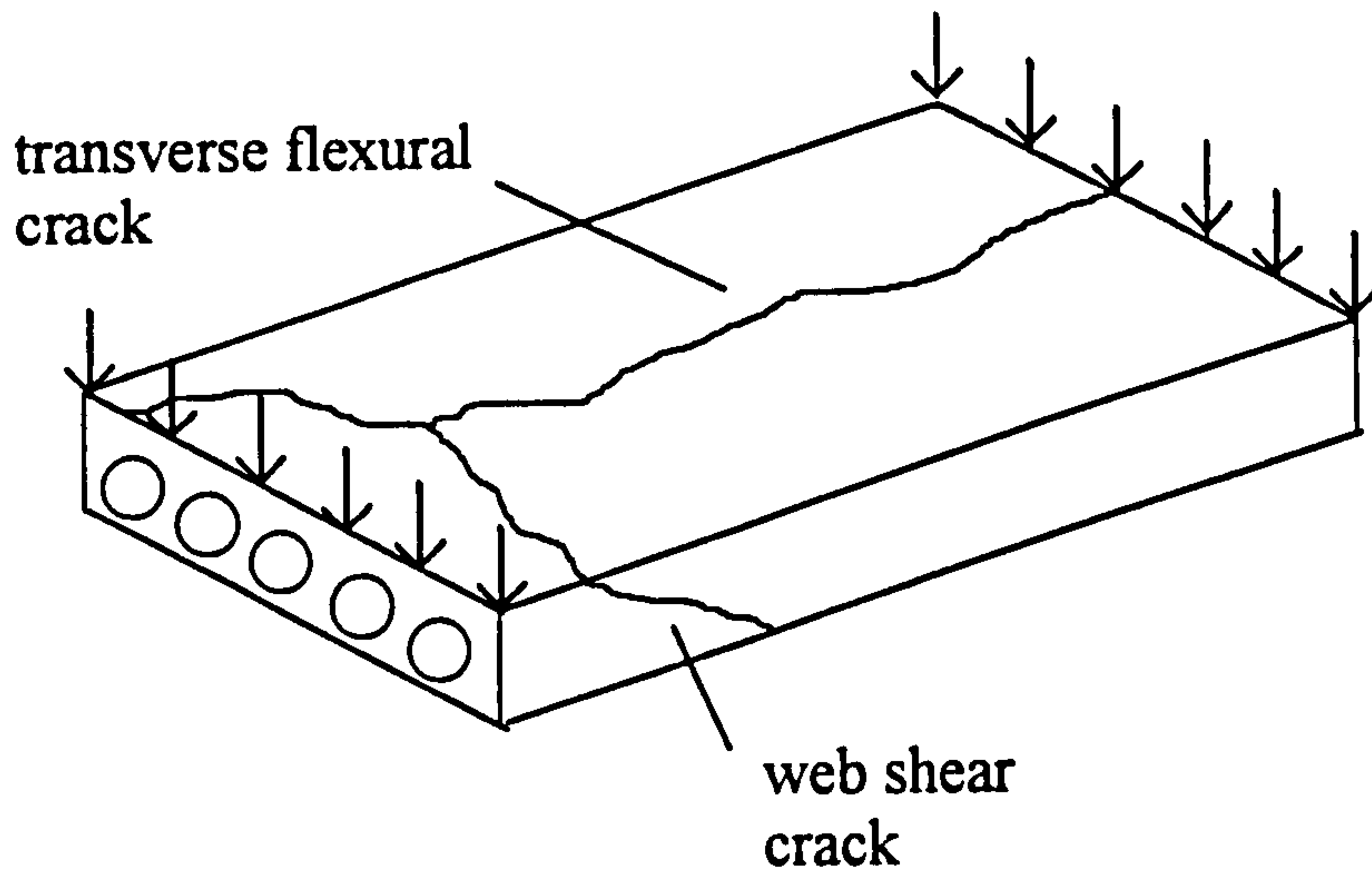


**Figure 7-26 Failure pattern in eccentric load tests**

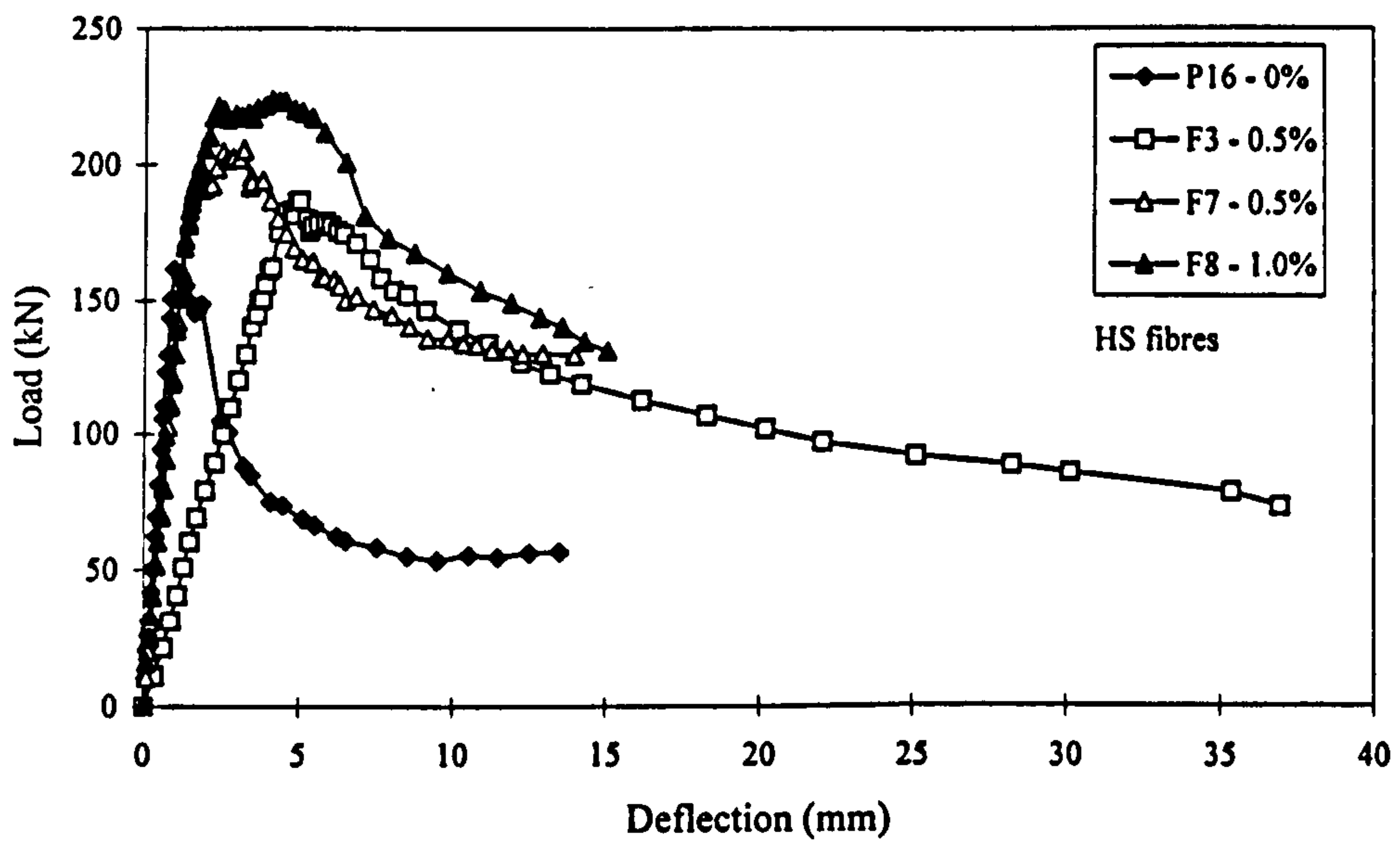


**Figure 7-27 Load v deflection curves for eccentric load tests**

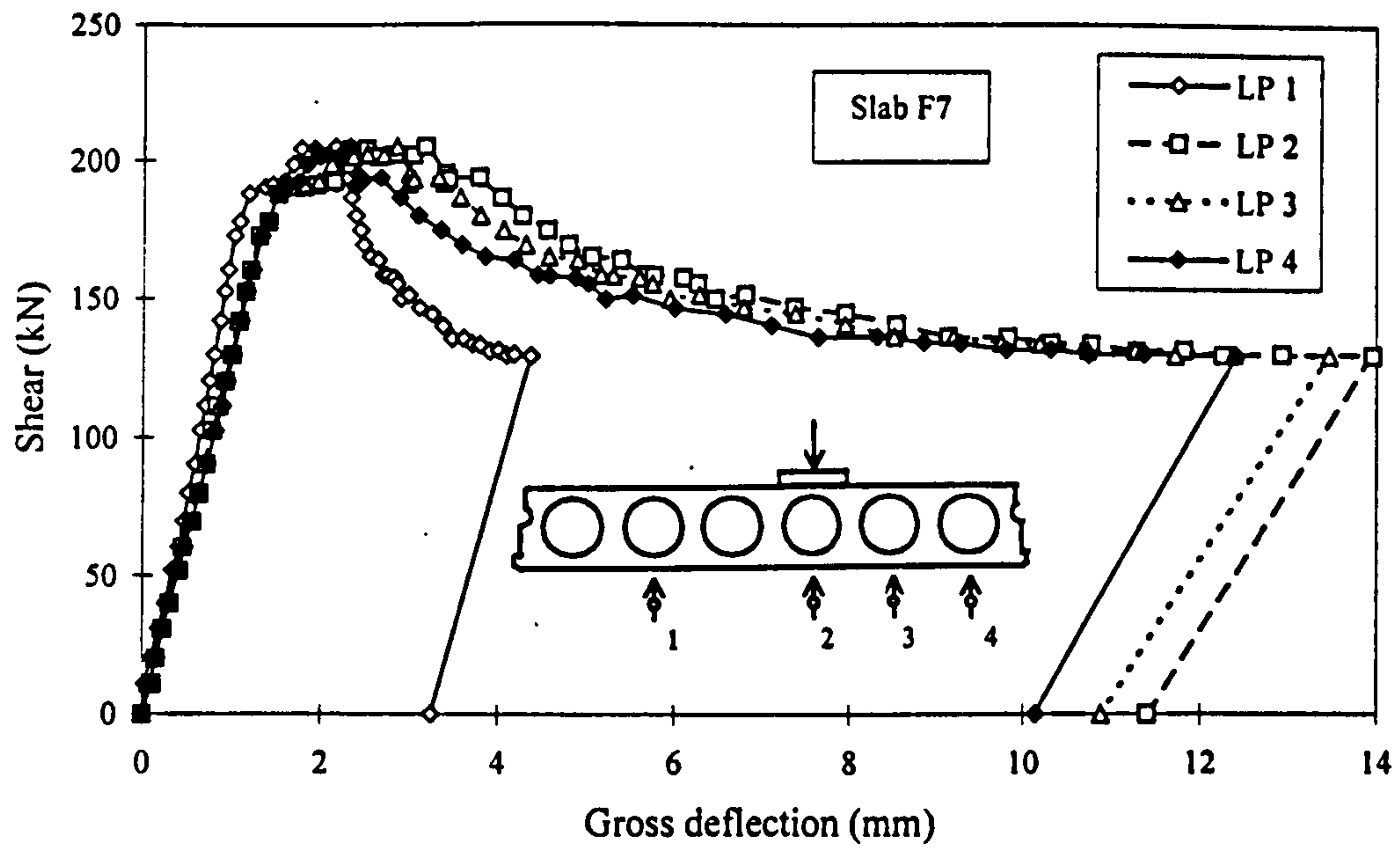


Figure 7-28 Load v deflection curves for the four LPs across the width of Test F7

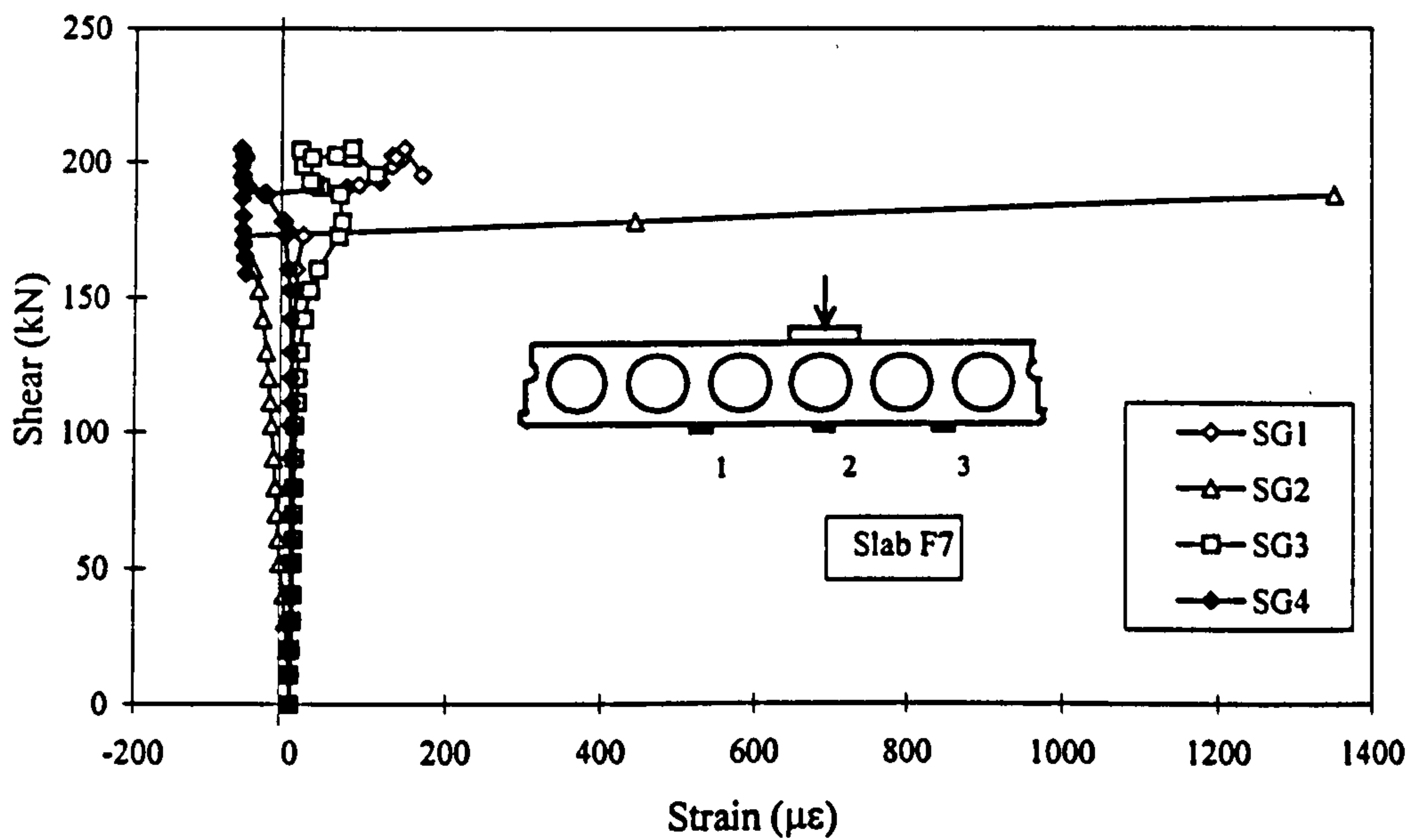


Figure 7-29 Load v strain on the soffit for Test F7

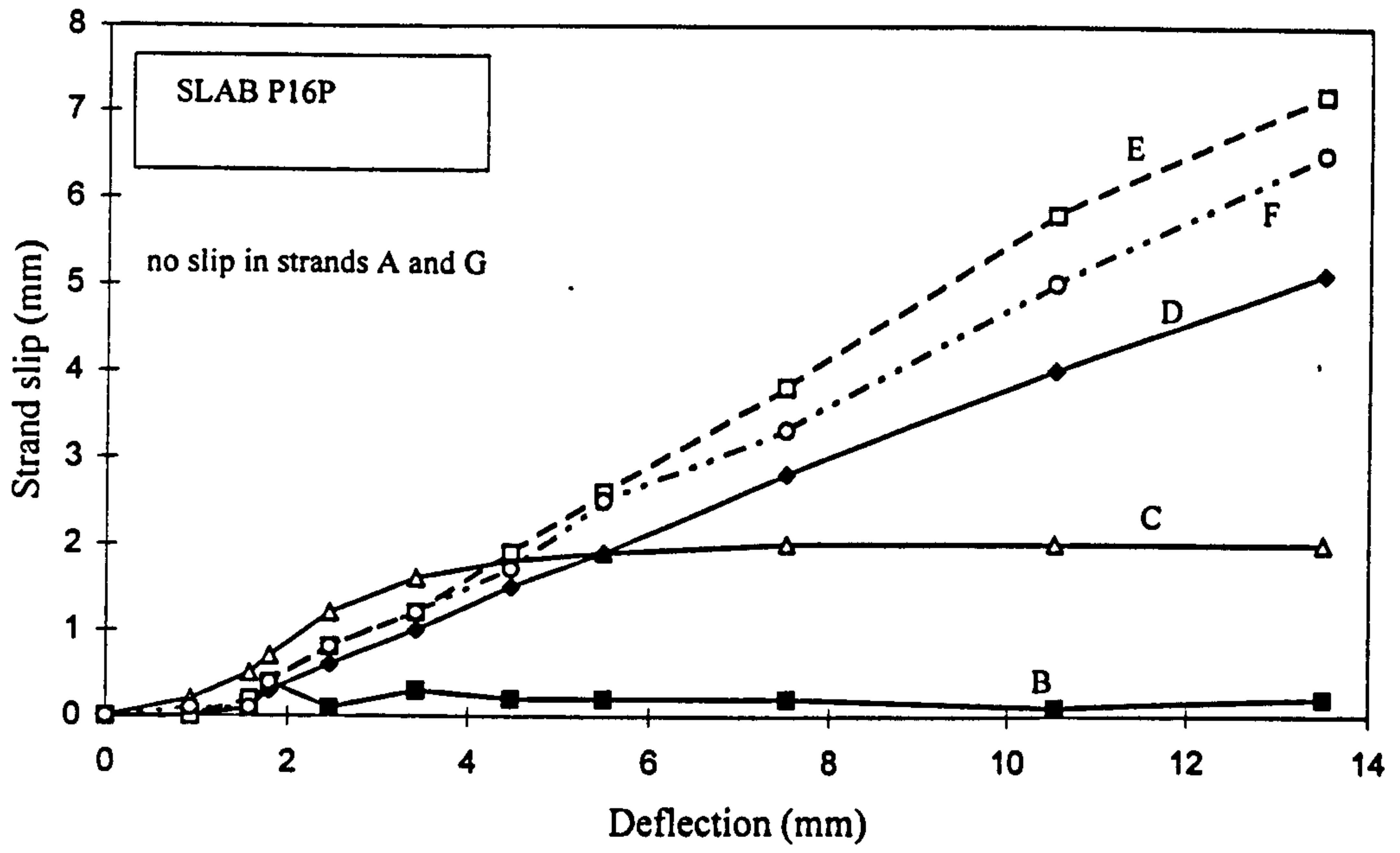
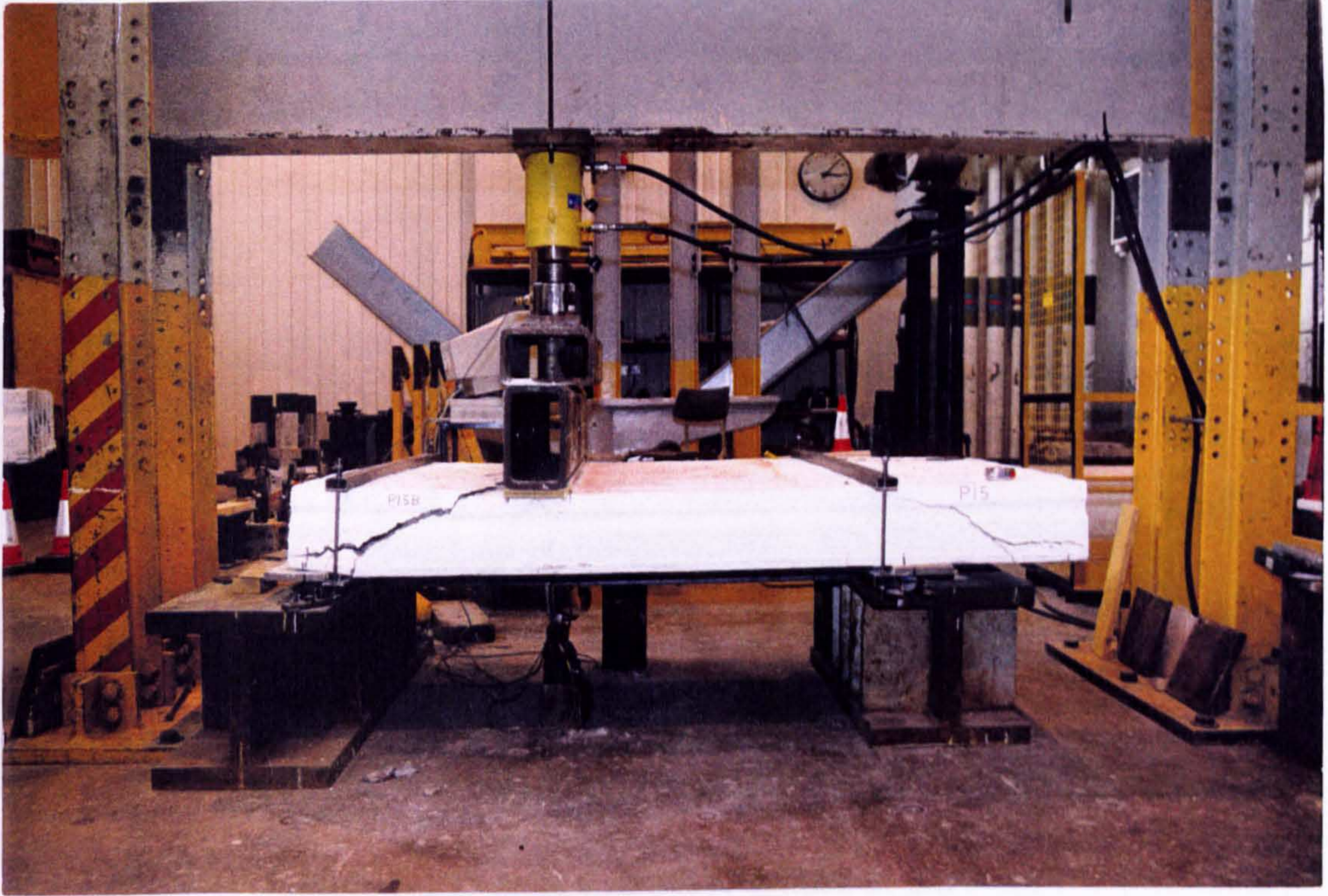
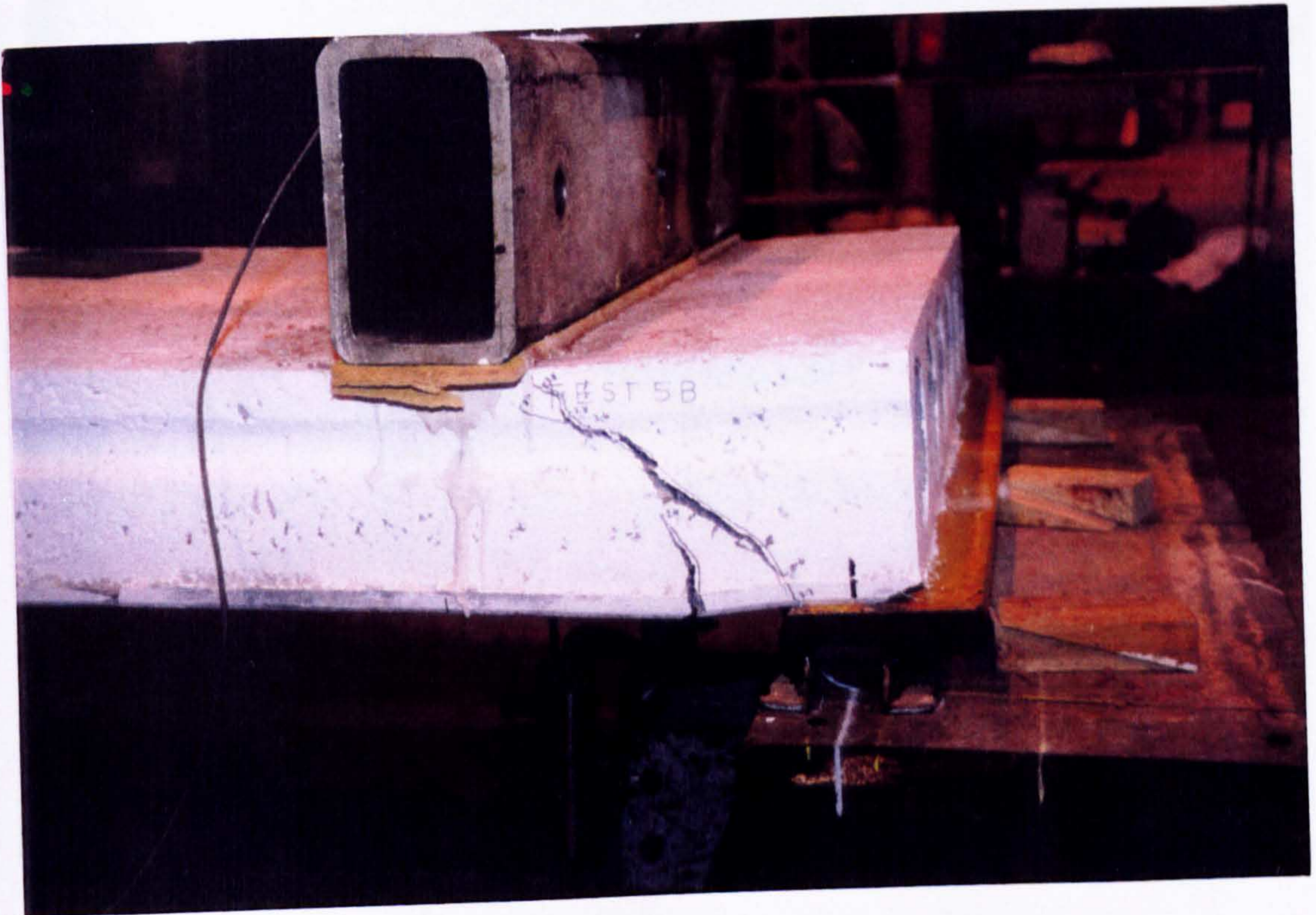


Figure 7-30 Strand slip v deflection curve for all strands in eccentric load Test P16



**Plate 7-1 Shear test set-up for tests with two spreader beams**



**Plate 7-2 Typical web shear failure at  $a/d = 2.0$**

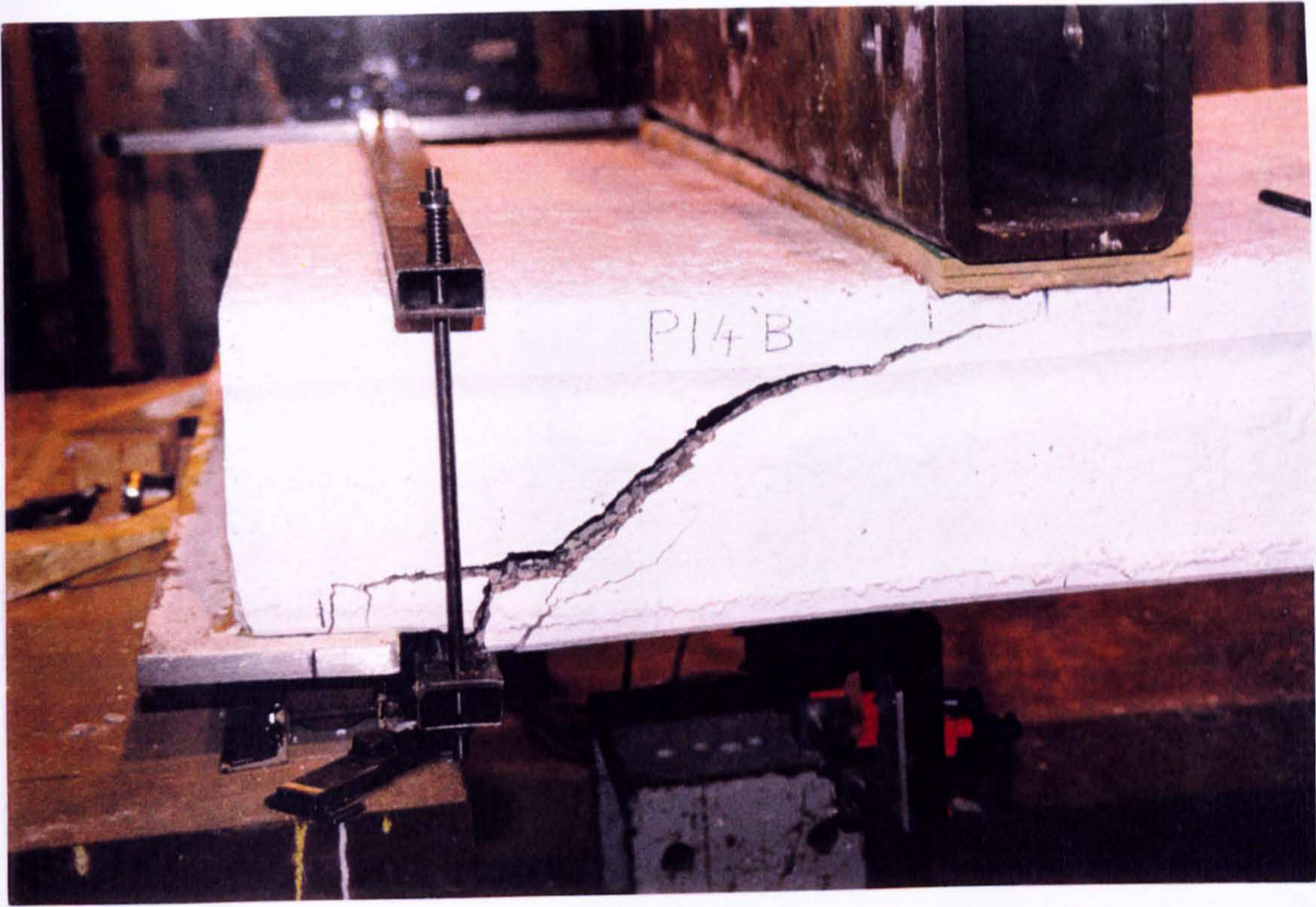


**Plate 7-3 Typical web shear failure at  $a/d = 2.8$**

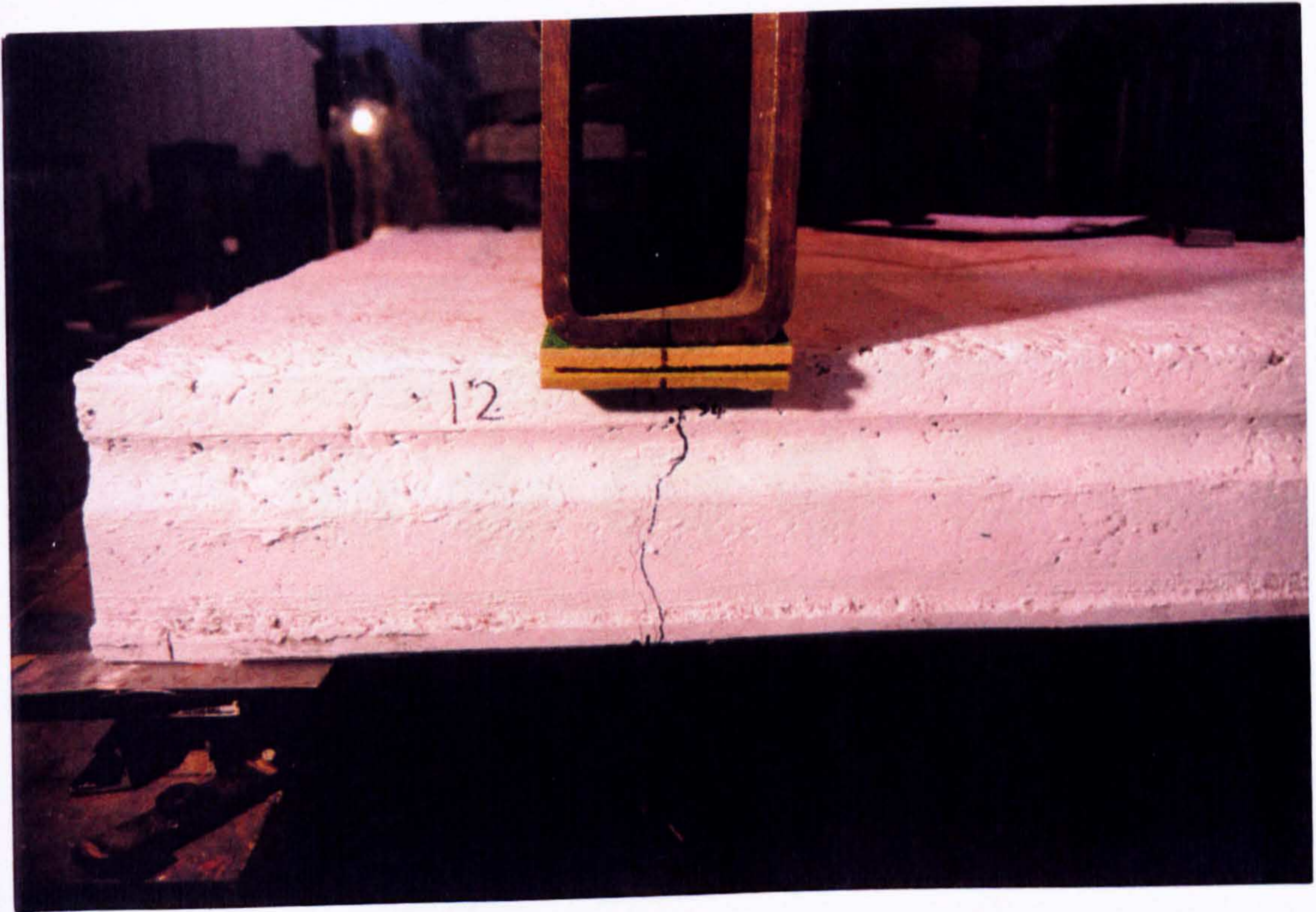


**Plate 7-4 Typical anchorage failure (Test F12A)**

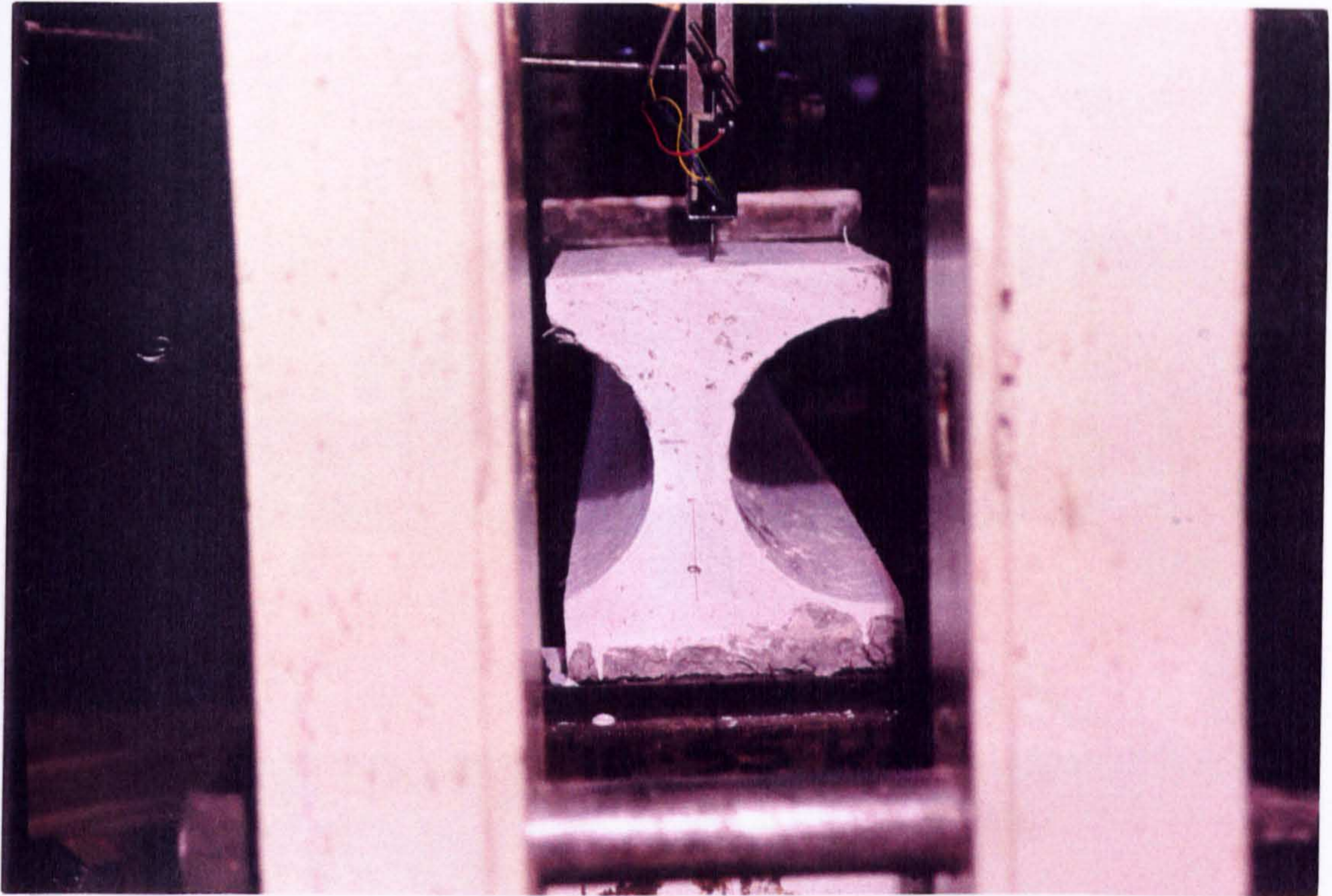


**Plate 7-5 Non-Symmetry of the factory-produced x-beams (Beam F9/2)**

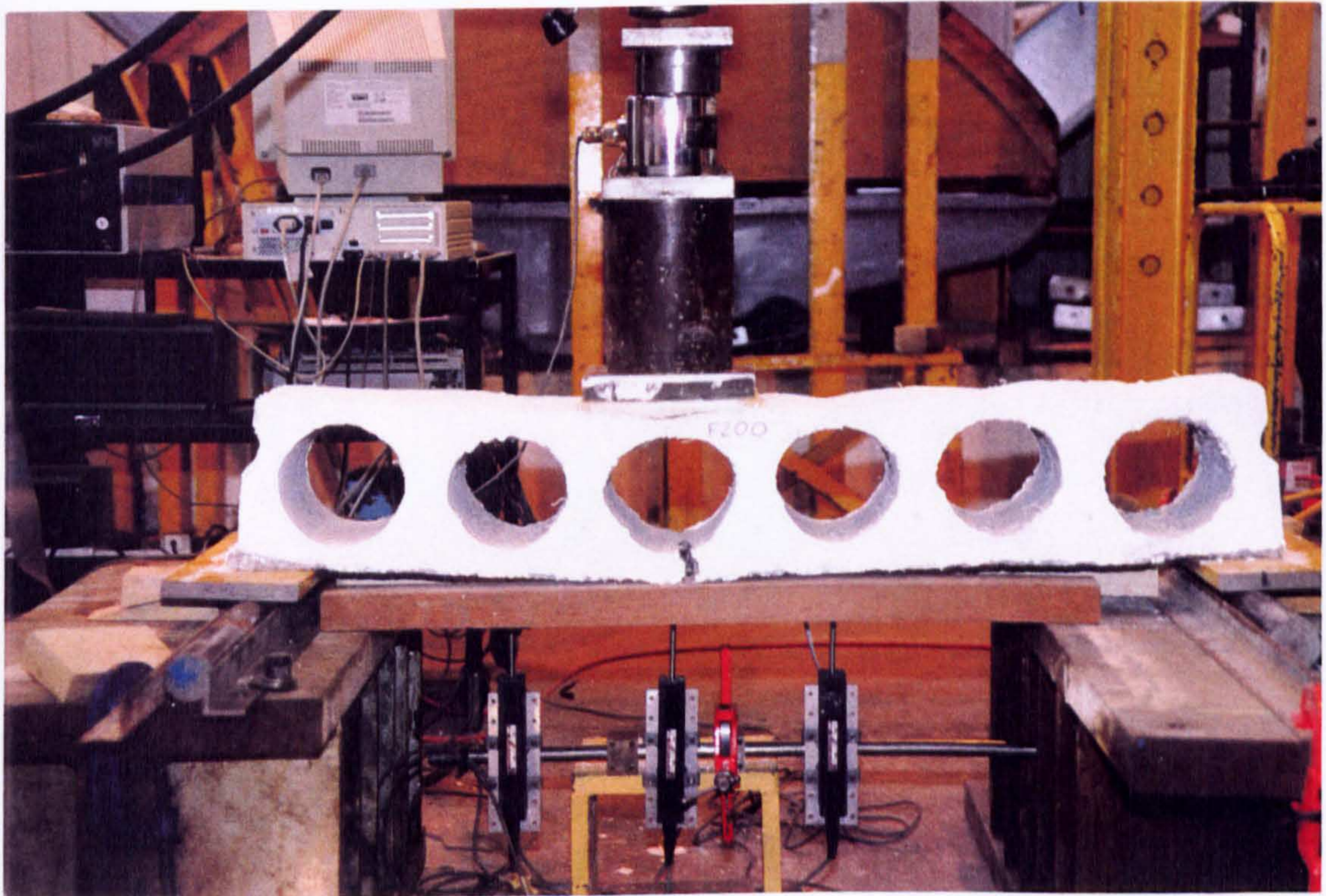


**Plate 7-6 Transverse flexural failure from test F200**

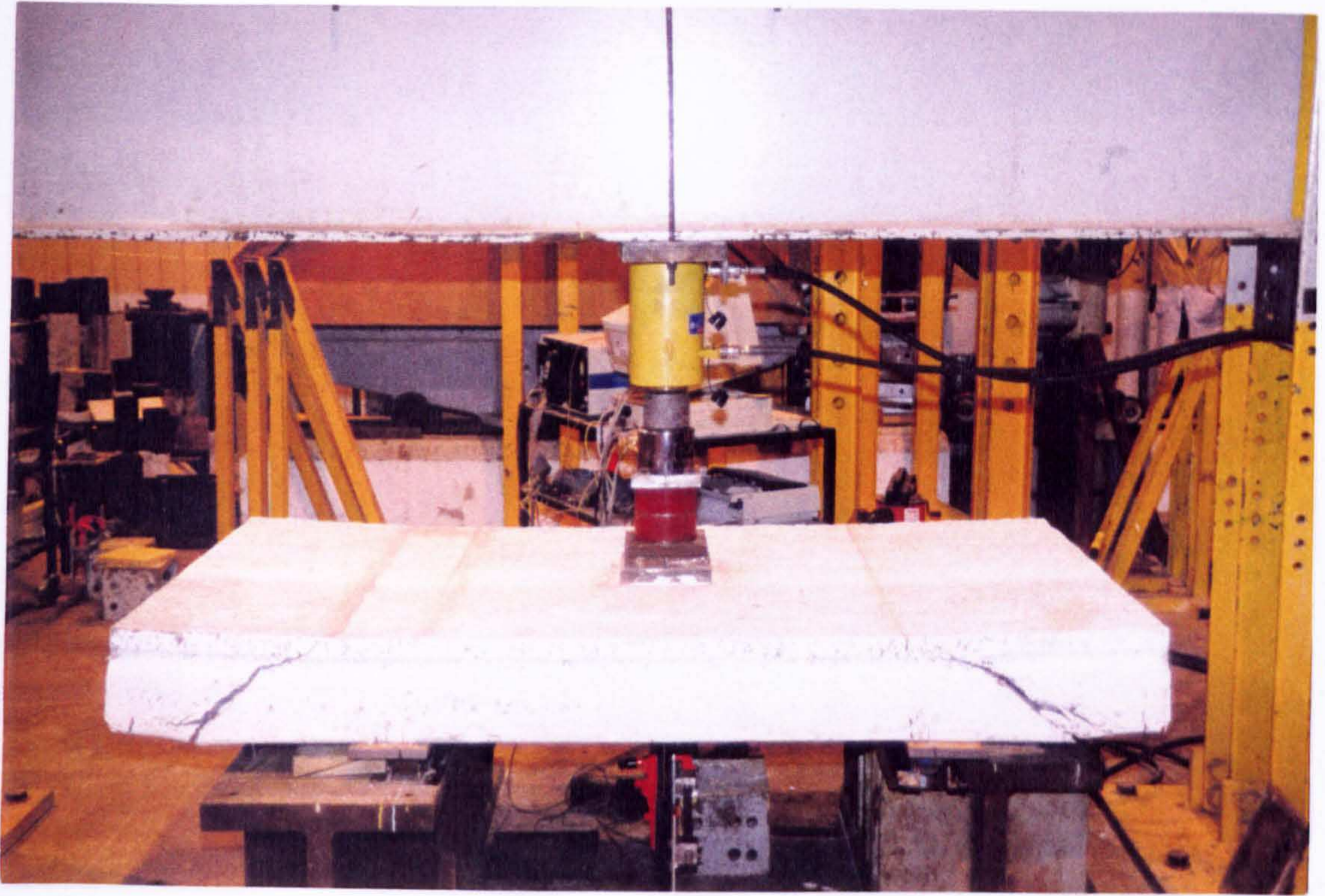


**Plate 7-7 Test set-up for centric concentrated load test**

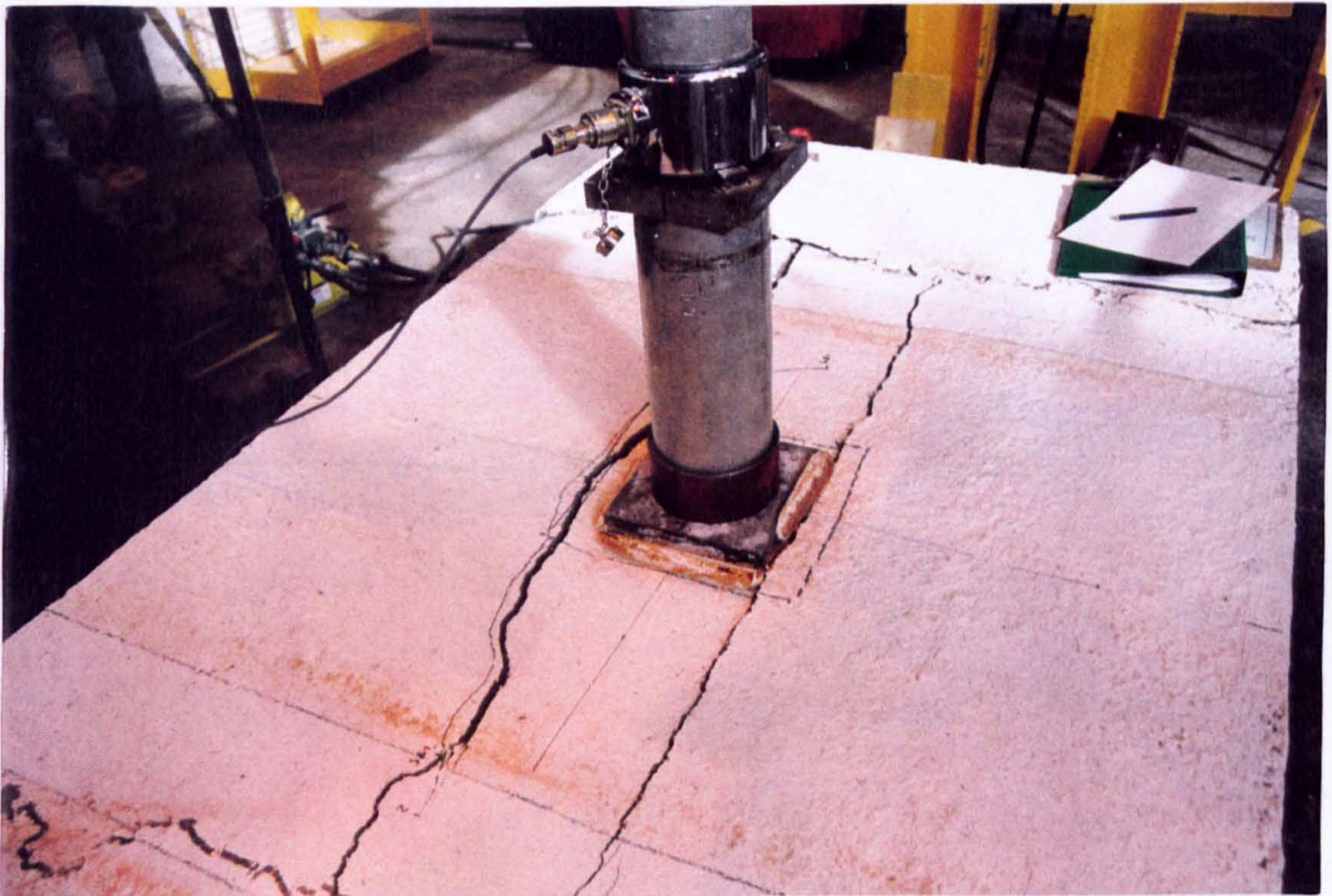


**Plate 7-8 Typical failure in centric concentrated load test (Slab 10)**



## CHAPTER 8

# THEORETICAL ANALYSIS OF PFRC IN SHEAR

### 8.1 Introduction

The tests on fibre reinforced slabs and beams described in Chapters 5 and 7 show that the inclusion of fibres significantly increases the capacity and ductility of prestressed concrete failing in shear. This chapter discusses the post-cracking shear behaviour of the prestressed fibre reinforced x-beams and the separate contributions to strength and ductility provided by the dowel action, aggregate interlock, fibre bridging and compressive resistance.

The latter part of this chapter develops a semi-empirical equation for predicting the shear strength based on these effects. Additionally, the equation is given in two forms. Firstly, a form which is compatible with existing formulae for predicting the shear strength of prestressed concrete as found in BS 8110, Eurocode 2 and the FIP Recommendations for hollow core slabs (1988), and a second form which is similar to that given by the PCI (1991) for the design of hollow core slabs. This second form is also consistent with the present approaches for designing FRC in structural elements advocated by RILEM TC 162 (1997) and the Dramix Guidelines (1995).

## 8.2 Contributions to shear strength

### 8.2.1 Plain concrete contribution

The failure of plain prestressed concrete beams in web shear tension is explosive and destructive, and there is complete loss of prestress in the strand immediately on cracking. This results in no effective compressive stress across the crack. The subsequent large crack width means that aggregate interlock is ineffective, since aggregate interlock is only effective in tension up to crack widths of about 0.3 mm (Stang and Aarre 1992). The post-cracking resistance is therefore provided by dowel action and the compressive contribution at the top of the beam. With increasing deflection this compressive contribution diminishes as the shear crack propagates into this zone, until at a large deflection the shear is carried entirely by the dowel forces.

Equation 8-1 based on the tension softening curve of concrete (Equation 2-10) can be used to describe the loss in the plain prestressed concrete shear capacity with increasing crack width:

$$V(w) = \frac{V_{cr}}{1 + (w / w_o)^p}$$

.. 8-1

where  $w_o$  is the maximum crack width at the neutral axis at  $V=V_{cr}/2$ , and  $p$  describes the shape of the curve. For the laboratory-cast x-beams at  $a/d = 2.0$  and  $2.8$ , the following values have been found to approximate to the average shear force-crack width curves with coefficients of determination ( $R^2$ ) of 0.99 (see Figure 8-1):

x-beams	$a/d = 2.0$	$w_o = 1.3 \text{ mm}, p = 1.2$
x-beams	$a/d = 2.8$	$w_o = 2.7 \text{ mm}, p = 1.2$

The parameter  $p$  is notably the same at both  $a/d$  ratios. Incidentally, the post-cracking curves of the plain hollow core slabs can be described by the following two

curves which also have the same value for  $p$ . This shows that the shear failure mode is essentially the same in all of the tests.

hollow core slabs	$a/d = 2.0$	$w_0 = 1.6 \text{ mm}, p = 1.2$
hollow core slabs	$a/d = 2.8$	$w_0 = 3.3 \text{ mm}, p = 1.2$

The different values for  $w_0$  show that the failures at the higher  $a/d$  ratio are less brittle than those at lower  $a/d$  ratios.

Also shown in Figure 8-1 is the aggregate contribution to shear strength by tensile bridging across the crack as derived from Li *et al.* (1993). It can be seen that this contribution to shear strength is effectively negligible. At large crack widths,  $w > 4 \text{ mm}$ , the shear stress at both  $a/d$  ratios is equal to the estimated value of the dowel contribution given by Equation 3-19. This shows that at large crack widths the crack has extended through the compressive zone and that the only resistance to the load is that due to yielding of the reinforcement. This can be clearly seen in Plate 8-1.

### 8.2.2 Fibre bridging component

It is widely acknowledged that the contribution of fibres to shear strength is provided by the fibres bridging across the crack. Since the crack is formed by principal tensile stresses, the fibre bridging is essentially the same as that in direct tension. The relationship between fibre bridging stress and crack width can therefore be described by the equations derived by Li *et al.* (1993) - Section 2.2.2. Additionally, the fibre prestress contribution to shear strength due to fibre-matrix load sharing prior to cracking is also relevant. Figure 8-2 shows the shear force - crack width ( $V$ - $w$ ) relationships for  $V_f = 1\%$  formed from the combination of the plain concrete contribution (Equation 8-1), fibre bridging (Equation 2-12) and fibre prestress (Equation 2-11), and compares it with actual  $V$ - $w$  relationships recorded in the tests.

It can be seen that the increased ductility of the PFRC beams cannot be explained by the fibre bridging mechanism, although the ultimate strength of the theoretical  $V$ - $w$  curve is similar to that observed in the tests. Therefore, although the

fibres may provide the increase in shear strength, there is a further action provided by the addition of fibres resulting in the ability of the beams to carry shear forces over large deflections and at large diagonal crack widths.

The reason for the theoretical small increase in  $V$  at small crack widths which was not observed in the tests is due to the simplified assumption that the shear crack develops through the complete depth of the beam immediately. In reality, however, the crack gradually propagates through the depth such that the fibre volume fraction actively resisting tension increases with crack width.

In PFRC beams, the shear crack never fully develops through the depth as there is a crack arrest mechanism, due to fibre pinching forces at the crack tip, which prevents the crack from propagating into the compressive zone. The compressive resistance of the fibre reinforced beams is therefore retained at significantly greater deformations than in the plain concrete beams. It is this ability of the fibres to arrest the shear crack, and maintain a compressive resistance that provides the PFRC beams with a significantly improved ductility. Calculation of this compressive resistance is described in Section 8.2.3.

It is possible that the fibres also improve the dowel resistance to shear after cracking, as shown by Swamy and Bahia (1979). However, Equation 3-19 which was derived for use with ribbed reinforcing bars, gives an improvement of only  $V = 5$  kN at ultimate with  $V_f = 1\%$ . The improvement in dowel resistance with increasing fibre volume using this equation and the flexural test results from Chapter 4 are shown in Figure 8-3. This shows the improvement in strength to be almost negligible when compared with the shear force that must be carried by the compression zone. Further, the tests on the x-beams showed no improvement in the quality of the bond between the concrete and wires when fibres were added. The necessary improvement in the stiffness of the concrete-dowel interface, observed by Swamy and Bahia, is therefore difficult to justify with regard to these tests.

In conclusion, the improved strength and ductility in shear of these PFRC beams will therefore be regarded as the result of the combined effects of fibre bridging across the crack, and fibre crack arrest in the compressive region.

### 8.2.3 Calculation of compressive resistance

The additional forces carried by the compression zone in the x-beams due to fibre crack arrest varies from zero at cracking to a maximum value at a crack width of about 5 mm where many of the fibres have pulled out and the only other resistance to shear is due to dowel action. The average additional shear force carried by the compressive region after cracking can be calculated from the shear load - deflection curves. For the purposes of this calculation (which is described below), net deflections as opposed to gross deflections were used.

Firstly, the entire contribution attributable to fibre addition (fibre bridging and compression) was determined by subtracting the total area under the shear load - deflection curve of a plain prestressed concrete beam from that of a PFRC beam, for specified deflections (see Figure 8-4). This area was then divided by the deflection to give the average additional shear force due to fibres. Four deflections were used;  $l/200$ ,  $l/300$ ,  $l/400$  and  $l/500$ , where  $l$  is the span.

The average additional shear force carried in the compression zone ( $V_{cf}$ ) was then computed by subtracting the average fibre bridging contribution (Equation 3-20) from the above. To simplify this computation the constant tensile bridging stress proposed by Lim *et al.* (1987a) - Equation 2-9 - was used.

At large deflections the beam tends to hinge about the compression zone. The compressive resistance is therefore perhaps best analysed by considering the shear load in terms of a bending moment and the compressive resistance in terms of a moment of resistance. In Figure 8-5, a triangular stress distribution has been assumed in the compressive zone because the compressive forces carried are much less than the compressive strength of the concrete. The value of  $0.1h$  for the height of the compression block is consistent with that observed in the x-beam tests, and with that observed in RFRC beam tests by Swamy *et al.* (1993) and Casanova *et al.* (1997).

In considering the compressive stress, it is necessary to consider a complementary tensile stress acting across the crack to provide equilibrium. For the purposes of this calculation this has been assumed constant through the depth of the tensile region. In this way, the additional shear forces carried by the compression block can be considered in terms of a tensile stress acting across the crack. This leads to the fibre contribution to shear being described by the combination of two different

tensile stress components, viz. fibre bridging and the reactive tensile stress described above.

The values of the maximum compressive and tensile stresses,  $f_{c,M}$  and  $f_{t,M}$ , can be calculated as

$$f_{c,M} = \frac{V_{cf}a}{0.026h^2b_f} \quad .. 8-2$$

where  $b_f$  is the width of the flange; and

$$f_{t,M} = \frac{V_{cf}a}{0.468h^2b_d} \quad .. 8-3$$

where  $b_d$  is the average width of the beam in the tension zone.

The values of  $f_{c,M}$  and  $f_{t,M}$  are shown in Table 8-1. It can be seen that all the values of  $f_{c,M}$  are less than  $50 \text{ N/mm}^2$  ( $< 0.7f_{cu}$ ) which suggests that the assumption of a triangular stress block is satisfactory.

The deflection at which ultimate load occurs varies from test to test, but is in general approximately equal to  $1/350$  for the tests where  $a/d = 2.0$  and  $1/450$  for the tests where  $a/d = 2.8$ . Average values of  $f_{c,M}$  and  $f_{t,M}$  calculated at deflections of  $1/175$  ( $=21/350$ ) and  $1/225$ , are therefore likely to approximate to the values of  $f_{c,M}$  and  $f_{t,M}$  at ultimate. Figure 8-6 shows that  $f_{t,M}$  reaches a maximum value at a deflection of approximately  $1/200$ , although this cannot be confirmed because all the plain beam tests were terminated at such a large deflection. This observation is probably correct because the force carried by the compression zone is, to a large extent, that shear load shedded by the plain concrete as its ability to carry shear reduces with increasing crack width.

Using the deflections  $1/175$  and  $1/225$ , the tensile stress across the crack can be calculated as  $f_{t,M} = 4.66 \text{ N/mm}^2$  and  $f_{t,M} = 3.97 \text{ N/mm}^2$  at  $a/d = 2.0$  and  $a/d = 2.8$ , respectively, which approximate to values of  $0.55\sqrt{f_{cu}}$  and  $0.47\sqrt{f_{cu}}$ . Assuming a shear crack angle of  $45^\circ$ , these values can be directly described as the additional tensile

stress carried across the crack as a consequence of the fibres preventing propagation of the crack into the compressive zone. The tensile stress across the crack is therefore a combination of this stress and the fibre bridging stress.

The values of  $f_{t,M} = 0.55\sqrt{f_{cu}}$  and  $0.47\sqrt{f_{cu}}$  are approximately equal to the cracking tensile stress observed in the splitting tensile tests, described in Section 4.3.2 and Section 4.5.3. The following section discusses the fibre contribution to the splitting tensile strength and a basis on which the fibre reinforcing mechanism in splitting may be utilised in the design of PFRC beams in shear.

### 8.3 Theoretical equation

#### 8.3.1 Splitting tensile strength

Each of the equations for the splitting tensile strength of FRC comprising HS fibres given in Sections 4.3.2 and 4.5.3 can be rewritten as

$$f_{ct,sp} = 0.5\sqrt{f_{cu}} + AV_f \quad .. 8-4$$

where  $0.5\sqrt{f_{cu}}$  is the splitting tensile strength of the matrix, and A is related to the effect of the fibres and increases in relation to  $f_{cu}$ .

If it is considered that the increase in splitting strength is due to fibre bridging, then the  $AV_f$  term can be related to the average bridging stress (Equation 2.9) to give

$$A = \eta_\theta \cdot \lambda_f \cdot \tau_f \quad .. 8-5$$

This implies that the matrix contribution to post-cracking strength is constant. This is possible because unlike in plain splitting tensile tests the crack does not propagate through the entire diameter of the cylinder immediately on forming. In fact observation of the crack in tests performed at the University of Nottingham

(Thompson, 1998) show that the crack is prevented from propagating by both compressive zones (Figure 2-9) over large crack widths. It is therefore reasonable to assume that the load previously carried by the plain concrete is transferred to these compressive regions and that all additional load is carried by fibre bridging.

Since  $\eta_\theta$  and  $\lambda_f$  are constants for any fibre, a relationship between  $f_{cu}$  and  $\tau_f$  can be produced from Equation 8-4 using the relationships given in Chapter 4. This is shown in Figure 8-7. Two additional data points are shown in this figure which relate to the splitting tensile tests on FRC containing identical fibres performed by Mansur *et al.* (1986) and Fattuhi (1994).

This relationship between  $AV_f$  and the fibre bridging stress is substantiated by the splitting tests performed on the AM fibres in which the fibres ruptured at ultimate as opposed to pulling out. The value of  $\tau_f$  at ultimate for AM fibres is therefore related to the ultimate tensile strength of the fibre rather than the strength of the matrix. The value of A can therefore be given as

$$A = \eta_\theta \cdot \lambda_f \cdot \left( \frac{2r \cdot f_{fu}}{l_f} \right) \quad \dots 8-6$$

where  $2r \cdot f_{fu} / l_f$  is the critical fibre matrix-interfacial bond strength equal to the value of  $\tau_f$  at rupture of the fibres. This equals  $2.5 \text{ N/mm}^2$ , assuming that  $f_{fu} = 1900 \text{ N/mm}^2$  as given by the fibre manufacturers (Boucharet 1997). This equates to a value of  $A = 321$  taking  $\eta_\theta = 0.41$ . The value of A obtained experimentally from the splitting tests equals 336 - which shows a good correlation, and shows that A is a measure of the fibre bridging component.

The critical fibre-matrix interfacial bond strength can be calculated in a similar manner for the HS fibres, and equals  $9.2 \text{ N/mm}^2$  when  $f_{fu}$  is taken as the minimum strength of  $1100 \text{ N/mm}^2$ . This value is shown in Figure 8-7, and suggests that fibres in concretes with a compressive cube strength greater than  $70 \text{ N/mm}^2$  will fail by rupture rather than by pulling-out of the matrix. The observation in the shear tests for such high strength concrete was that whilst occasional fibres did rupture, the overall fibre mechanism was pull-out. This slight inconsistency is because Equation 8.5 is



only an approximation, and because the average value of  $f_{fu}$  is greater than 1100 N/mm<sup>2</sup>.

Therefore from Equations 8-4 and 8-5, the splitting tensile strength can be written as

$$f_{ct,sp} = 0.5\sqrt{f_{cu}} + \eta_{\theta} \cdot \lambda_f \cdot \tau_f \cdot V_f \quad \text{.. 8-7}$$

where

$$\tau_f = f(f_{cu}) \approx 1.7e^{0.024f_{cu}} \quad \text{.. 8-8}$$

According to the Dramix Guidelines (1995) the maximum fibre bridging stress in tension may be approximated as  $0.37 f_{fl,eq,300}$ ; a value which is intrinsically related to the matrix strength. Equation 8.7 may therefore be re-written as

$$f_{ct,sp} = 0.5\sqrt{f_{cu}} + 0.37f_{fl,eq,300} \quad \text{.. 8-9}$$

Equation 8.9 is compared with the experimental data (Chapter 4) obtained for  $f_{ct,sp}$ ,  $f_{fl,eq,300}$  and  $f_{cu}$  in Figure 8-8. It can be seen that there is a very good correlation between the test data and the equation, suggesting that  $f_{fl,eq,300}$  is a good measure of the fibre bridging stress. This equation could be further refined in Equation 8-10, because the splitting tensile strength of plain concrete can also be estimated from the flexural cracking strength of plain concrete prisms as  $0.6 f_{fl}$  (Dramix Guidelines 1995).

$$f_{ct,sp} = 0.6f_{fl} + 0.37f_{fl,eq,300} \quad \text{.. 8-10}$$

This gives the ultimate splitting tensile strength purely in terms of flexural properties. Note that Pisanty (1992) suggested a value of  $0.55 f_{fl}$  from prisms extracted from

hollow core slabs, and the results of the splitting and flexural tests described in Chapter 4 suggest a value of  $f_{ct,sp} = 0.53 f_{fl}$  for plain concrete.

However, Equation 8-9 is of most interest since it shows the ultimate tensile strength as the sum of a constant stress related to the matrix cube strength plus a stress related to the fibre bridging mechanism. These values are approximately the same as those relating to the compressive resistance component and fibre bridging component in the shear tests.

### 8.3.2 Development of semi-empirical equation

In BS 8110 and most European codes of practice the method of calculating the shear resistance of a prestressed concrete beam is to restrict the maximum principal tensile stress at the geometric axis of the section to the tensile strength of the concrete. For PFRC beams, a similar approach can be used but for these beams the maximum tensile stress that can be carried across the shear crack at the geometric axis is equal to the sum of the fibre bridging stress and the reactive tensile stress due to compressive forces at the top of the beam. The maximum principal tensile stress may therefore be equated to  $f_{ct,sp}$  (Equation 8-9) to give the ultimate shear strength of PFRC beams ( $v_{cou}$ ) as

$$v_{cou} = \sqrt{f_{ct,sp}^2 + f_{ct,sp} \sigma_{cpx}} \quad .. 8-11$$

where  $f_{ct,sp}$  is given as  $0.5\sqrt{f_{cu}} + 0.37 f_{fl,eq,300}$ , and where flexural properties are not known  $f_{fl,eq,300}$  is taken as  $\eta_{\theta} \cdot \lambda_f \cdot \tau_f \cdot V_f$ .

This equation needs further adjusting, however, to account for the experimentally observed losses in prestress after cracking of the PFRC beams. The value of  $\sigma_{cpx}$  at ultimate was found to be approximately 67% of that at cracking, independent of fibre volume fraction.  $v_{cou}$  can therefore be given as:

$$v_{cou} = \sqrt{f_{ct,sp}^2 + 0.67 f_{ct,sp} \sigma_{cpx}} \quad .. 8-12$$

This equation could also be rewritten in the form recommended by Girhammar (1992) and used by PCI to give:

$$v_{cou} = 0.5\sqrt{f_{cu}} + 0.37f_{fl,eq,300} + 0.3(0.67\sigma_{cpx}) \quad .. 8-13$$

with the shear strength of plain prestressed concrete expressed as

$$v_{co} = 0.5\sqrt{f_{cu}} + 0.3\sigma_{cpx} \quad .. 8-14$$

If  $f_{ct} = 0.5\sqrt{f_{cu}}$  as suggested by the splitting tensile tests, then the shear supplement due to adding fibres ( $v_b$ ) can be calculated as:

$$v_b = v_{cou} - v_{co} = 0.37f_{fl,eq,300} - 0.1\sigma_{cpx} \approx \eta_\theta \cdot \lambda_f \cdot \tau_f \cdot V_f - 0.1\sigma_{cpx} \quad .. 8-15$$

For non-prestressed beams ( $\sigma_{cpx} = 0$ ) this is consistent with Equation 3.19 for RFRC beams suggested by Mansur *et al.* (1986) and is four times greater than that proposed by RILEM TC-162 (1997) which is known to be too conservative for non-rectangular beams.

The shear strength of PFRC beams can therefore be given by two equations. One consistent with the design of prestressed beams and hollow core slabs in the European codes, and a second equation which is consistent with the approaches currently advocated for design of RFRC beams in shear.

**Table 8-1 Average results from analysis of compressive resistance**

Deflection:		1/500	1/400	1/300	1/200				
		tensile and compressive stresses (N/mm <sup>2</sup> )							
$V_f$ (%)	a/d	$f_{c,M}$	$f_{t,M}$	$f_{c,M}$	$f_{t,M}$	$f_{c,M}$	$f_{t,M}$	$f_{c,M}$	$f_{t,M}$
0.5	2.0	17.13	2.68	20.81	3.26	25.17	3.94	30.6	4.79
1.0	2.0	11.95	1.87	19.14	3.10	25.75	4.03	29.6	4.64
1.5	2.0	10.25	1.61	19.57	3.07	22.75	3.56	30.51	4.78
<i>average</i>		<i>13.37</i>	<i>2.09</i>	<i>19.87</i>	<i>3.11</i>	<i>24.72</i>	<i>3.87</i>	<i>30.21</i>	<i>4.73</i>
0.5	2.8	17.42	2.74	18.43	2.90	24.74	3.89	24.60	3.87
1.0	2.8	11.77	1.85	20.23	3.18	25.64	4.03	31.76	4.99
1.5	2.8	2.75	0.43	13.53	1.34	18.21	2.86	25.10	3.94
<i>average</i>		<i>12.22</i>	<i>1.92</i>	<i>17.17</i>	<i>2.70</i>	<i>23.79</i>	<i>3.74</i>	<i>27.56</i>	<i>4.33</i>

N.B. Each value is average of four results

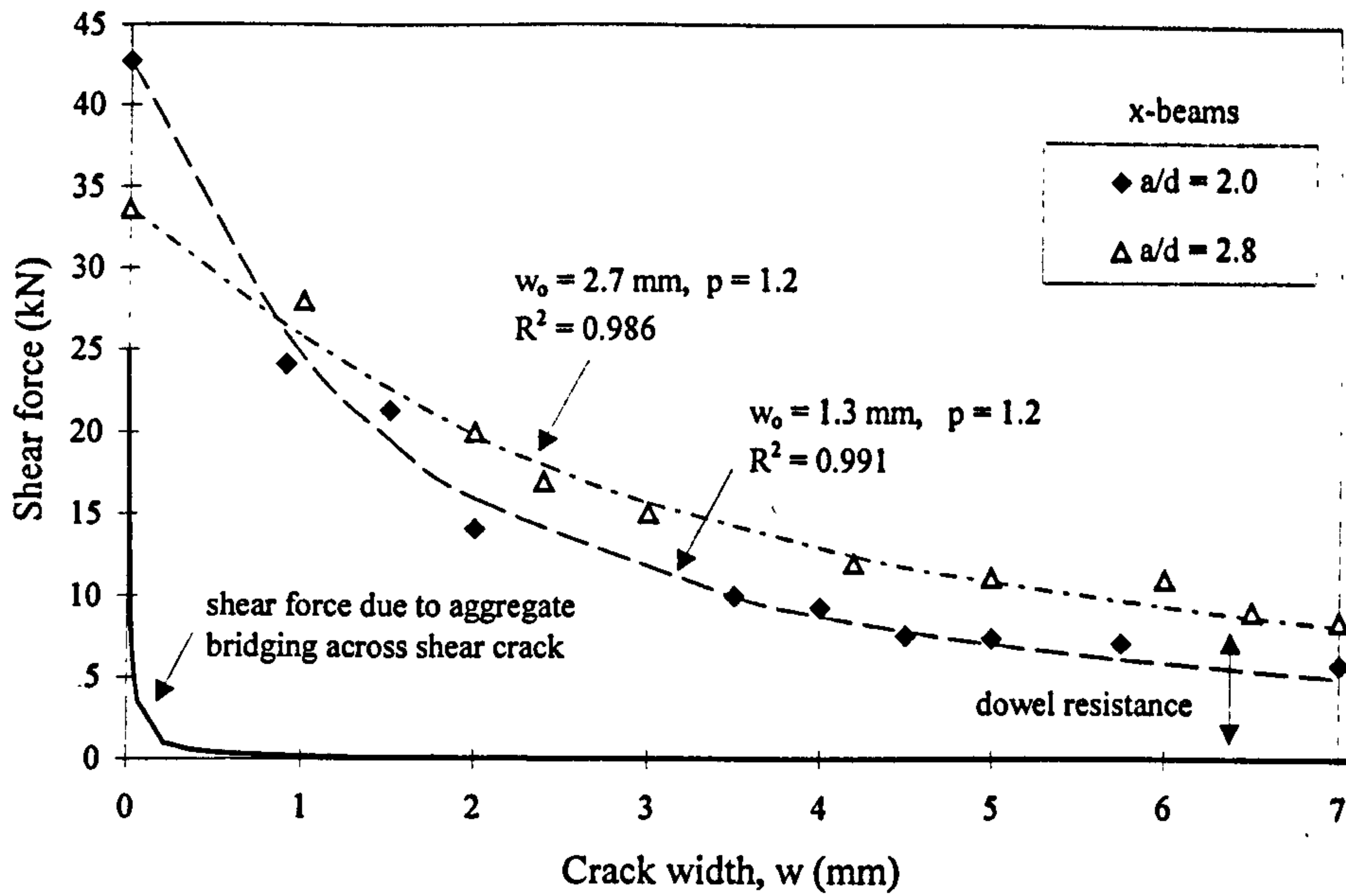


**Figure 8-1 Shear carrying capacity of plain prestressed concrete with increasing crack width**

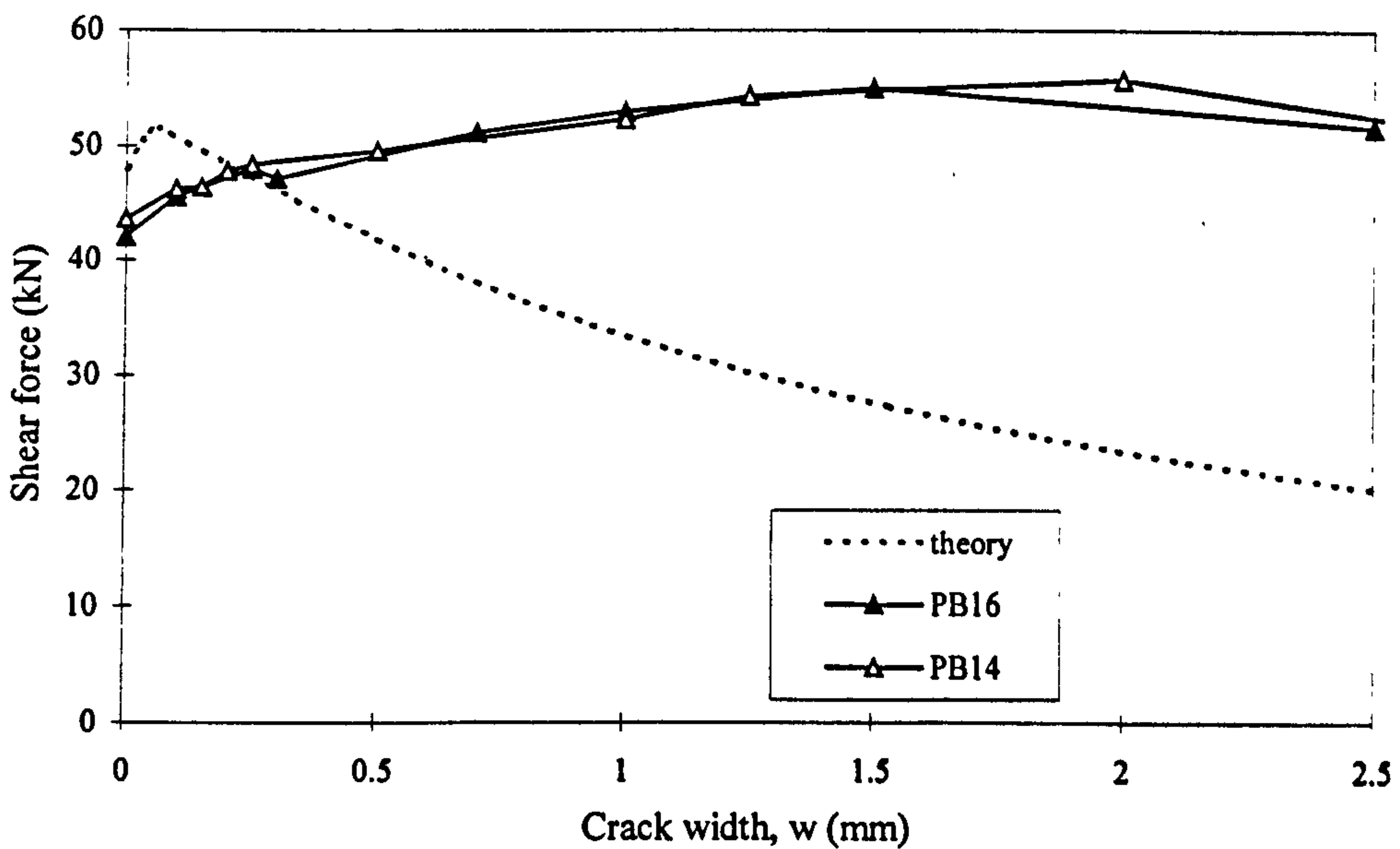


**Figure 8-2 Theoretical V-w relationship for FRC ( $V_f = 1.0\%$ ) formed from combination of fibre bridging, fibre prestress and plain concrete contribution in comparison with actual V-w relationships.**

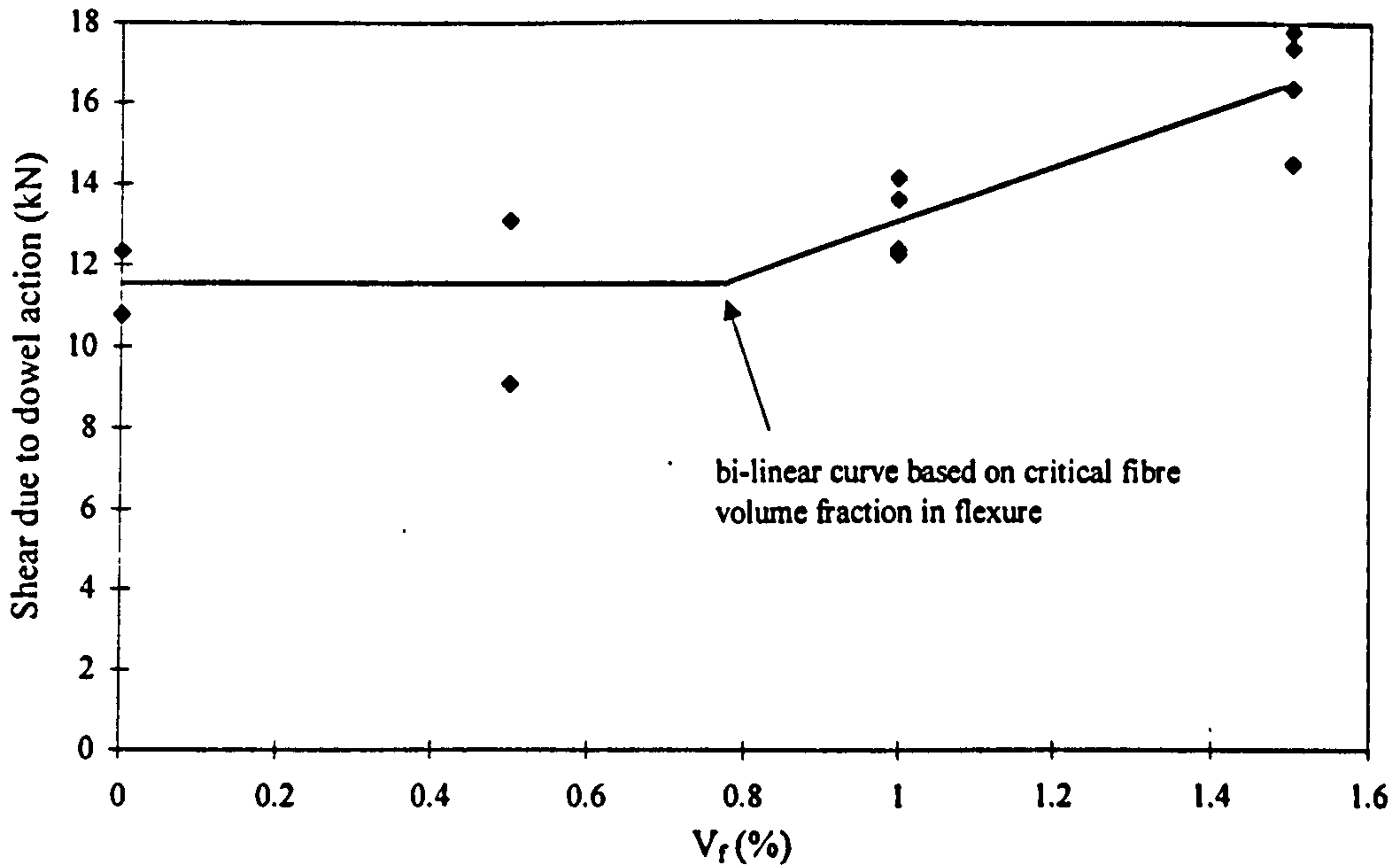


Figure 8-3 Improvement in dowel contribution to shear resistance with increasing fibre volume fraction in prestressed x-beams according to Equation 3-19.

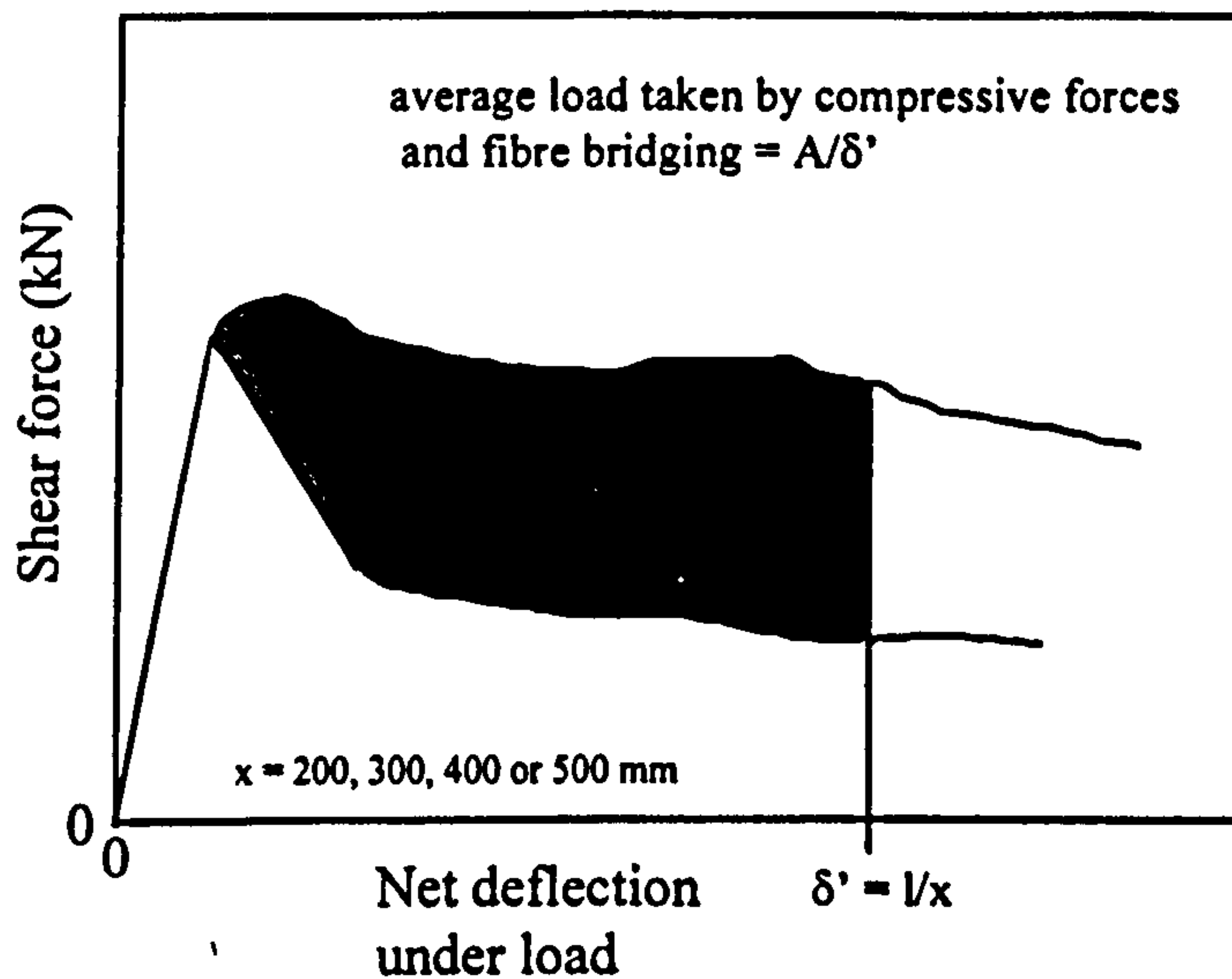


Figure 8-4 Computation of average additional shear force carried by compressive zone due to fibre crack arrest

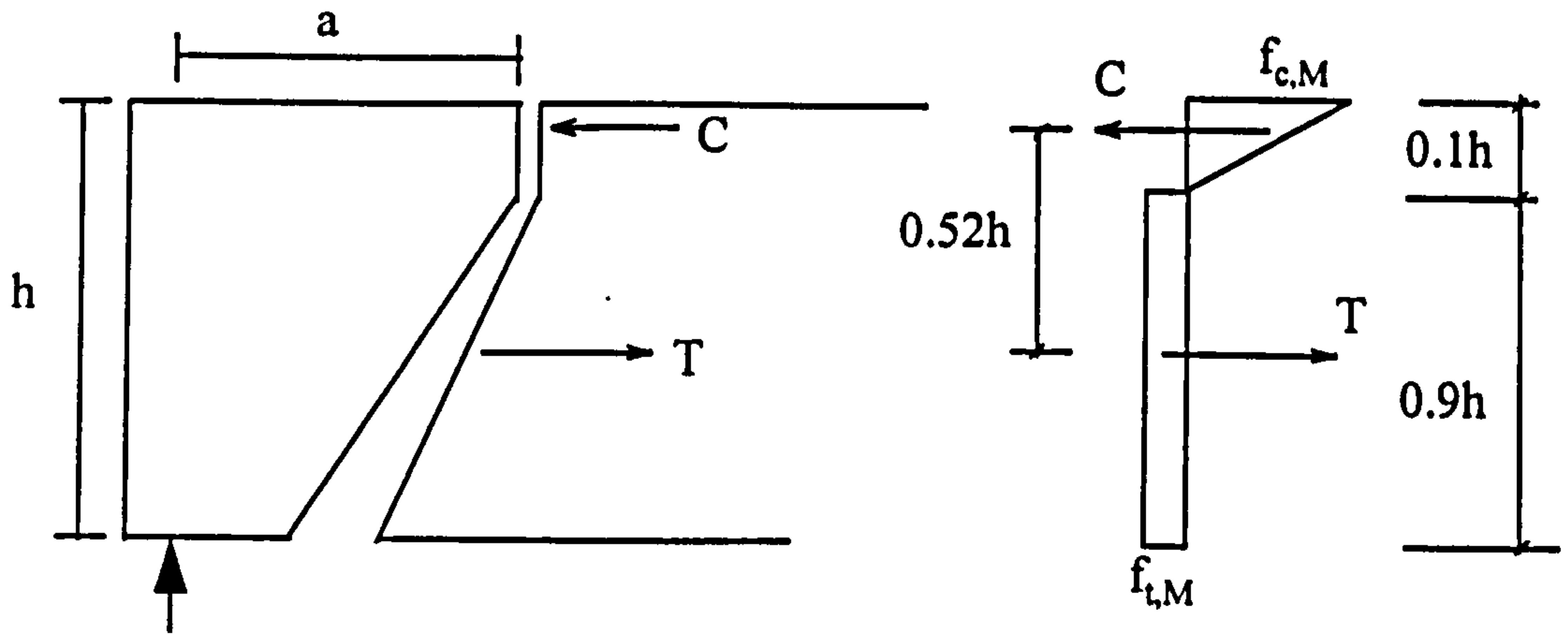


Figure 8-5 Proposed stress block for analysis of compressive resistance

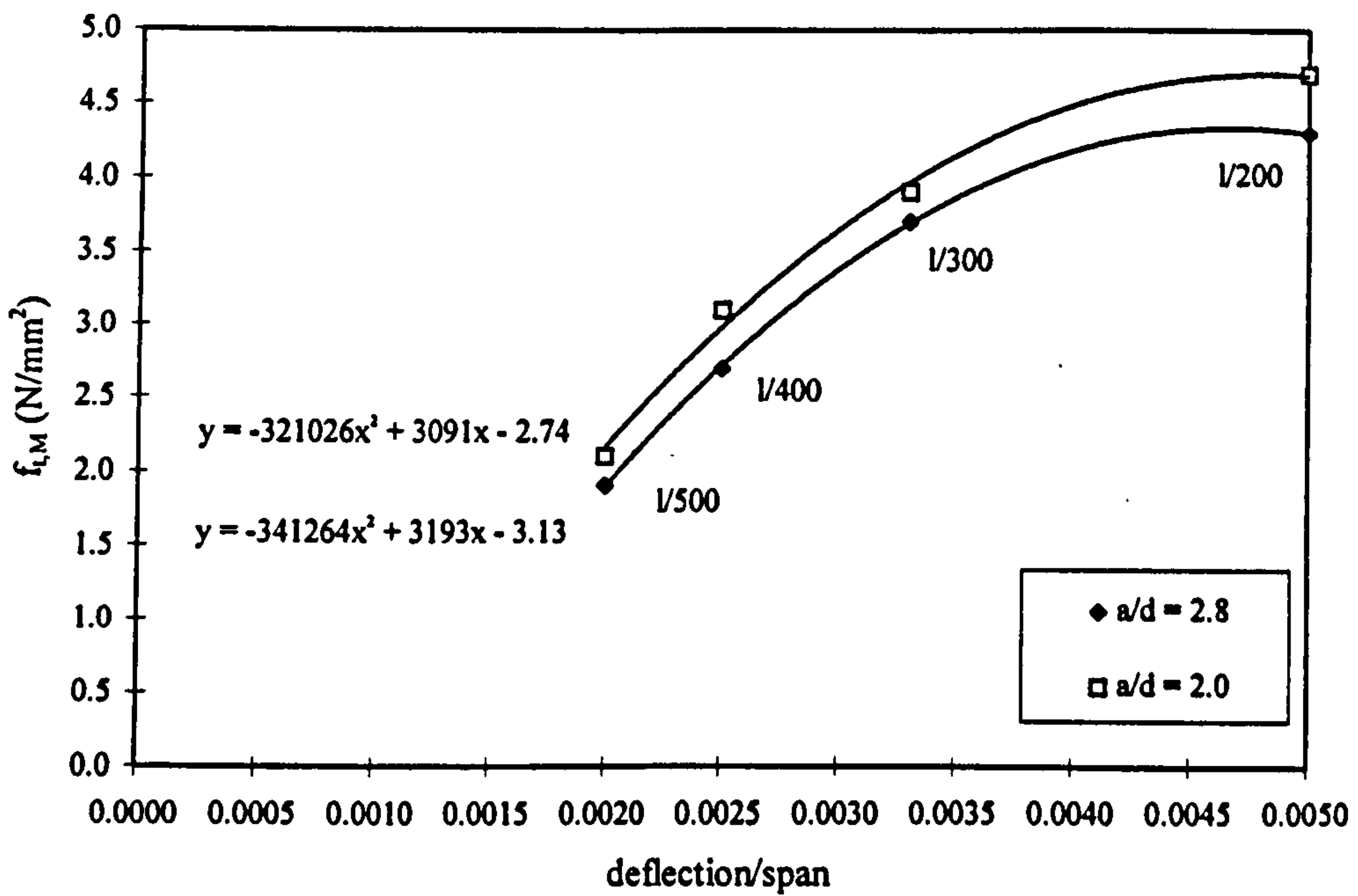


Figure 8-6 Variation of average tensile stress component ( $f_{t,M}$ ) with deflection

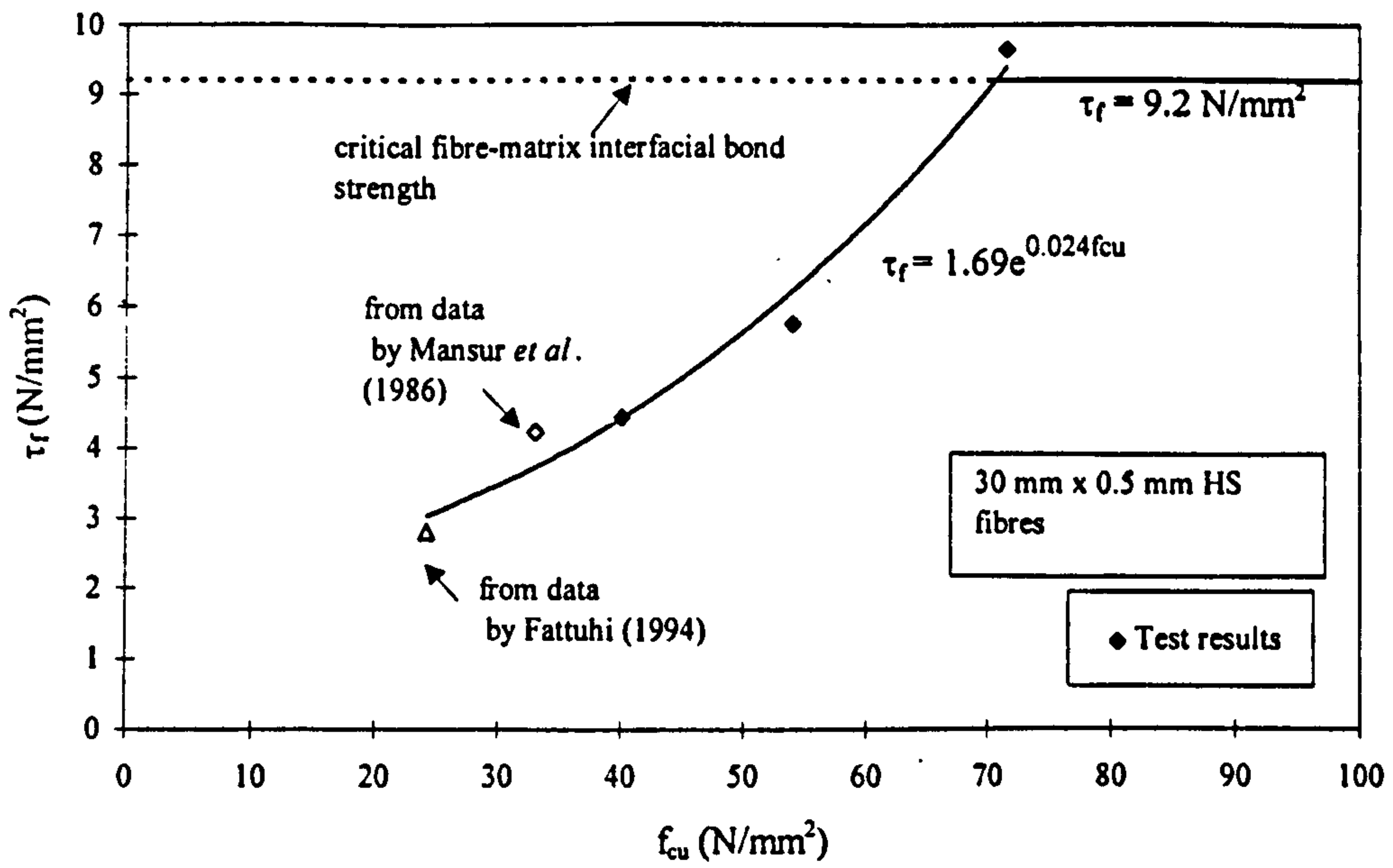


Figure 8-7 Relationship between  $\tau_f$  and  $f_{cu}$  as calculated from splitting tensile tests

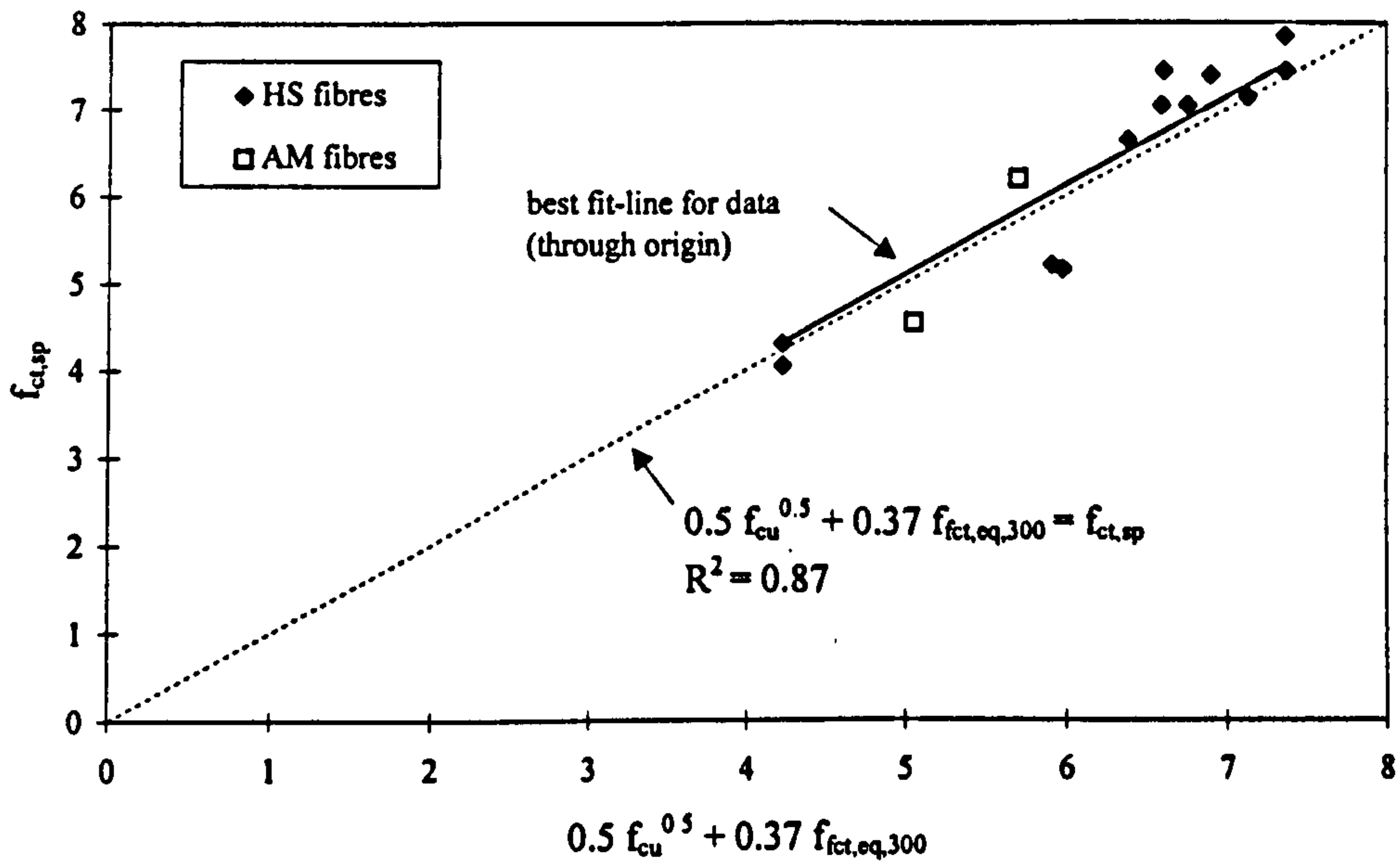


Figure 8-8 Comparison of  $f_{ct,sp}$  with Equation 8-9





**Plate 8-1 Dowel action in plain concrete at large deflections**

## **CHAPTER 9**

### **ANALYSIS AND DISCUSSION OF RESULTS**

#### **9.1 Introduction**

The main series of tests are analysed and discussed in this chapter; namely the bond tests to assess the effect of steel fibres on prestress transfer lengths, shear tests and transverse flexural tests. Also discussed are the results of the beams which failed in flexure due to loss of anchorage.

In the latter part of the chapter the implications of the results of all the tests for the use of steel fibres in hollow core slabs, implications to the design of FRC hollow core slabs and situations in which fibres may best be utilised within this field are discussed.

#### **9.2 Prestress transfer**

##### **9.2.1 Introduction**

The transfer length of prestressing tendons was measured by two techniques as described in Chapter 5: first the direct pull-out of 12.5 mm diameter seven-wire strand from a block of concrete; and second the direct measurement of strains on a pretensioned 7 mm wire at detensioning. Both investigations compared the transfer length in plain concrete with those in FRC, and found that the inclusion of fibres tended to lengthen the prestress transfer zone. This was attributed in both cases to a reduction in the workability of the concrete, and associated difficulties in compacting the concrete around the tendons. An analysis and comparison of the results with the predictive design equations reviewed in Chapter 3 follows.

### 9.2.2 Transfer length in plain concrete

Two methods, Methods 1 and 2 (see Section 5.3.4), were used to calculate the transfer lengths from the two pull-out bond tests (B-0.0A and B-0.0B) performed on 12.5 mm strand in plain concrete. Different lengths were observed in each of the tests and this was probably attributable to the different concrete strength of the two specimens at the test age. The respective strengths were 42 N/mm<sup>2</sup> and 36 N/mm<sup>2</sup> for Tests B-0.0A and B-0.0B. The shorter transfer lengths were measured in the stronger concrete by both methods of calculation.

The results of the pull-out tests are compared with predictive equations in Table 9-1, where for comparative purposes the transfer length of each test has been taken as the average of the transfer length calculated by both Methods 1 and 2. These transfer lengths of 659 mm and 707 mm correspond to lengths of 53 $\phi$  and 57 $\phi$ , respectively, and are consistent with the prediction of  $l_t = 55\phi$  for slow release of strands proposed by Lin Yang (1995).

A possible problem with the pull-out test method adopted for these tests was that they did not simulate the exact bond mechanism in prestressed concrete; in particular they did not include the Hoyer effect. However, the results of the flexural strength tests on factory-produced x-beams containing 12.5 mm strand in Section 7.3, concluded that the transfer length was approximately 680 mm (see Figure 7-14). This is consistent with the transfer lengths measured by the pull-out bond tests and suggests that the slightly different bond mechanism is not significant.

Comparison of the calculated transfer lengths with the predictive equations in Table 9-1 shows that the FIP/PCI and EC2 methods over-predict the transfer length, whilst the other three methods predict shorter transfer lengths. However, interestingly, the methods employed by BS 8110 and by Olesniewicz which are dependant on  $f_{ci}$ , both predict the transfer length in Test B-0.0B to be 8% greater than that in B-0.0A. This is similar to the actual increase in transfer length of 7%, and further suggests that the different transfer lengths in the two bond tests is related to this difference in concrete strength.

The FIP/PCI equation, which does not involve concrete strength, is solely based on  $\sigma_p$  and thus predicts the same transfer length for both specimens. This value of 780 mm is approximately 1.15 times greater than the test results. The lengths given by EC2 are approximately 1.3 times greater than those measured. Based on the evidence of the two tests carried out here, the FIP/PCI recommendation therefore appears to be the most appropriate equation for predicting the transfer length of helical strands.

The transfer length of the 7 mm wires used in the laboratory-cast x-beams was less easy to identify, but is approximately 510 mm (Section 5.5.1), which corresponds to  $73\phi$ . Both indented and plain wires were investigated, and although the indented wires had better bond than the plain wires the observed differences were too small to justify a different value for the transfer length. The above value of  $l_t = 510$  mm is compared with the predictive equations in Table 9-1.

It can be seen that the prediction of BS 8110 over-predicts the transfer length by 30%, whilst both EC2 and the CEB-FIP model give good approximations to the results. Although included in Table 9-1 for completeness, neither the method of Olesniewicz or FIP/PCI are intended for wires, and thus give poor results.

It is proposed therefore that for the analysis of the tests in this thesis, that the EC2 equations for predicting transfer length are used for wires and the FIP/PCI equation for strands. However, since both methods predict a linear distribution of stress into the concrete, which is unlikely, it is proposed to use Equation 3-7 to describe the distribution of prestress.

### 9.2.3 Transfer length in FRC

The test evidence suggests that the inclusion of fibres in prestressed concrete increases the transfer length. Method 1 used for the pull-out bond tests suggests that the transfer length (in mm) of 12.5 mm strand can be estimated as (see Figure 5-12):

$$l_t = 683 + 182V_f - 53V_f^2$$

.. 9-1

where  $V_f$  is given as a percentage. This shows that the inclusion of  $V_f = 1.5\%$  increases the transfer length by 18%. However, the observations from the direct measurement of the x-beams gives an increase in transfer length of 47% for  $V_f = 1.5\%$ . This anomaly is to be expected, since the influence of the fibres is to reduce the compactability, and is therefore strongly affected by the shape of the mould and the workability of the matrix. The observation made during the placing of concrete was that compaction of FRC in the x-beams at a fibre volume fraction of 1.5% was more difficult than in the pull-out bond specimens.

An equation relating transfer length to fibre volume fraction is therefore not feasible, and in order to account for fibres in prestressed concrete it is necessary to implement additional safety factors on existing equations.

This increased transfer length due to adding fibres has the effect of reducing the effective prestress at the critical location for shear resistance. The observed increases in  $l_t$  from 510 mm for  $V_f = 0\%$  to  $l_t = 750$  mm for  $V_f = 1.5\%$  for the x-beams, reduces the effective prestress from  $0.63 \sigma_{cpX}$  to  $0.46 \sigma_{cpX}$  using Equation 3.7; a reduction of 27%. However, this corresponds to a reduction in cracking shear strength, using Equation 3.4, of only 4%. Such a small reduction could be overcome by increases in the tensile strength of FRC due to fibre-matrix load sharing in the uncracked condition, which can be as much as 10-15%.

Therefore, although the effect of fibres on transfer length is an important consideration, and the fibres do significantly increase the transfer length, the effect of this increase on cracking shear strength can be regarded as insignificant.

## **9.3 Shear**

### **9.3.1 Introduction**

In the following section the shear test results from the tests on both prestressed hollow core slabs and x-beams are compared with the two theoretical equations derived in Chapter 8. In general, it is found that the equations give a close approximation to the actual results for the x-beams (both laboratory-cast and factory-

produced), but overestimate the strength of the slabs. Reasons for this anomaly are propounded in Section 9.3.4.

### 9.3.2 Shear strength of plain beams and hollow core slabs

The average ultimate shear strength from each series of shear tests on plain prestressed concrete elements are compared with the theoretical Equation 3.4 in Table 9-2. To be consistent with Equation 8-11,  $f_{ct}$  has been taken as  $0.5\sqrt{f_{cu}}$  as suggested from the splitting tensile tests. This is much larger than the recommended value of  $0.3\sqrt{f_{cu}}$  given in BS 8110 (1985). For comparative purposes, the strength has been given by dividing the ultimate shear force by the effective area of resistance against direct shear,  $I_b/A_y$ . For the slabs, the approximate value of  $0.67 bh$  given in BS 8110 (1985) has been used.

In using Equation 3-4 the value of  $\sigma_{cpX}$  has been estimated using the respective equations for wires and strands proposed in Section 9.2.2. The critical section for shear has been conservatively assumed to occur at the intersection of a  $45^\circ$  line from the edge of the bearing and the centroidal axis of the element.

It can be seen in Table 9-2 that the theoretical equation gives good correlation with the test results from the x-beams produced both in the laboratory and at the factory, giving values of  $v_{ult}/v_{co}$  between 1.01 and 1.08. However, the ratio  $v_{ult}/v_{co}$  for the laboratory x-beams at  $a/d = 2.0$  is higher, at about 1.4. The observation that higher strengths were obtained at  $a/d = 2.0$  was mentioned in Chapter 5, and is attributable to a greater compressive strut action through the depth of the beams. Why this behaviour is not observed in the factory-produced x-beams, however, is unclear.

With regard to the slabs, Equation 3-4 significantly over-predicts the ultimate shear strength. On average, the observed shear strength is about 67% of that given by the equation. Since, the equation gives a good estimate of the shear strength of the factory-produced x-beams, it is clear that this poor correlation is not due to an inaccurate value of  $f_{ct}$ , and it should also be noted that a reduction in the slightly higher value of  $\sigma_{cpX}$  assumed for the slabs would not be significant enough to reduce  $v_{co}$  to the observed test strength.

A further point to note is that the value of  $v_{ult}$  is in fact slightly high because of the use of  $0.67 bh$  for the shear area as opposed to the higher value of  $Ib/Ay$ . The values of  $v_{ult}/v_{co}$  should therefore be even lower.

The reasons for the low  $v_{ult}/v_{co}$  ratios found for the plain slabs are discussed in detail in Section 9.3.4, given further evidence from the tests on fibre reinforced slabs and x-beams.

### 9.3.3 Shear strength of FRC beams

A comparison between the average ultimate shear stress and the predicted strength given by Equation 8-12, for the factory-produced and laboratory-cast x-beams at each fibre volume fraction and  $a/d$  ratio, is given in Table 9-3. A comparison of individual results is shown in Figure 9-1. The theoretical equation for shear strength of PFRC beams suggested by Narayanan and Darwish (1987a) - Equation 3-28 - is also compared with the test results in Table 9-3. In calculating the shear strength using Equation 3-28, a value of  $\eta_b = 1.0$  has been chosen for the HS fibres as suggested by Imam *et al.* (1997) and a value of  $\eta_b = 0.5$  for the AM fibres - identical to the value for a straight smooth circular fibre given by Narayanan and Darwish (1987a). As with the plain x-beams,  $v_{ult}$  has been calculated as  $V_{ult}/(Ib/Ay)$ .

It can be seen that the calculated ratios of  $v_{ult}/v_{cou}$  using Equation 8-12 are similar to the ratios of  $v_{ult}/v_{co}$  calculated for the equivalent plain concrete beams. Once again, the ratio is higher for  $a/d = 2.0$  than for  $a/d = 2.8$ .

In general, the Narayanan and Darwish equation gives similar results to Equation 8-12, despite the fact that Equation 2-15, used to estimate  $f_{ct,sp}$ , under-predicts the post-cracking principal tensile strength observed in the splitting tension tests (see Figure 4-6). This is partly because the lower splitting tensile strength is nullified by Narayanan and Darwish's assumption that there is no loss in  $\sigma_{cp,x}$  at ultimate.

### 9.3.4 Shear strength of FRC hollow core slabs

The predictive Equations 8-12 and 3-28 are compared with the test results of the fibre reinforced slabs in Table 9-4. For calculating the fibre bridging component of Equation 8-12 (since the equivalent flexural strength is not known), Equation 8-8 has been used to calculate  $\tau_f$  for HS fibres, up to a maximum value of  $9.2 \text{ N/mm}^2$ . For AM fibres,  $\tau_f$  has been taken as  $2.5 \text{ N/mm}^2$  (see section 8.3.1).

As with the plain slabs the equations over-predict the shear strength of the slabs. The average values of  $v_{ult}/v_{cou}$  are 0.84 and 0.74 for  $a/d = 2.0$  and  $a/d = 2.8$ , respectively. These are higher than for the plain slabs.

It is shown therefore that Equation 8-12 gives a good approximation to the strength of the factory-produced x-beams cut from FRC hollow core slabs and Equation 3-4 gives a good approximation for the plain concrete beams. However, since both equations over-estimate the strength of the slabs, it is apparent that there must be some behavioural effect with the slabs that causes lower strengths than with individual webs.

This behavioural effect is partly attributed to the problems found in obtaining a truly even distribution of load across the full-width of the slabs, which results in the central webs being subjected to a greater stress than the outer webs. Thus, the average stress reported in Table 9-4 is lower than the actual maximum shear stress which causes initial cracking in the centre of the slabs (Appendix F describes a load test performed on the spreader beam used in the shear tests, and shows that the shear stress in the centre of the beams is 1.2 times greater than the average shear stress.)

This alone, however, is not enough to fully explain the lower strength of the slabs. The problem is compounded when the variation in the web thickness across the width is considered. This has been measured to vary by as much as 5 mm from the mean value, which is equivalent to a variation in shear strength of approximately 14 %.

In the author's opinion, the problem of uneven stress distribution across the width is not solely connected with the tests performed in this thesis but is likely to occur in actual applications of hollow core slabs. This is because of uneven bearing of the slabs on the support beams and the unlikelihood of an evenly distributed load



situation. The additional problem of variations in web thickness across the cross-section is a feature of extruded hollow-core slabs, especially those formed by the 'Spiroll' manufacturing method. This problem is therefore certain to exist in the field.

To overcome these phenomena it is perhaps sensible to implement an overall reduction factor in Equation 8-12 for use with hollow core slabs. This is in common with suggestions for overall reduction factors made for different reasons by Walraven and Mercx (1983) and Pisanty (1992). From the tests on the plain concrete hollow core slabs a reduction factor of about 0.6 would appear appropriate.

However, for the FRC slabs a less significant reduction factor is required since  $V_{ult}/V_{cou}$  on average is approximately equal to 0.8. This is because the fibres are able to maintain the post-cracking stresses in the webs as previously discussed in Section 7.2.2. This means that the FRC slabs are able to better distribute the load across the width of the slabs after cracking, making more use of the end webs. Subsequently the strength obtained in the slabs is closer to the theoretical strengths.

The concerns expressed by Sebaratnam and Rangan (1992) about cubes and cylinders compacted in a different manner to the slabs, tending to overestimate the tensile strength, are not shown up in this study, where the value of  $0.5\sqrt{f_{cu}}$  for the principal tensile strength of concrete is suitable for predicting the strength of factory-produced x-beams.

### 9.3.5 Fibre shear supplement

Figure 9-2 shows the variation in the fibre shear supplement with  $V_f$ . This is the arithmetic difference between the measured shear strength of each of the laboratory-cast PFRC beams and the average shear strength of the equivalent plain concrete beams, all other parameters being constant. The shear supplement is compared with the equations proposed for RFRC by Dramix Guidelines (1995), RILEM TC-162 (1997) and Mansur *et al.* (1986) - respectively Equations 3-21, 3-23 and 3-20. Also shown is the shear supplement for PFRC beams given by Equation 8-15.

For low fibre volume fractions it can be seen that both Equation 8-15 and 3-20 give similar results, which correlate well with the test results. For  $V_f = 1.5\%$ ,

Equation 3-20 tends to overestimate the shear strength and falls outside of  $\pm 1$  standard deviation ( $\sigma$ ) of the mean test result, while Equation 8-15 fits well within  $\pm 1\sigma$ . The coefficient of determination between Equation 8-15 and the mean value of  $v_b$  at each fibre volume fraction is  $R^2 = 0.97$ , whilst Equation 3-20 gives  $R^2 = 0.26$ .

The curve produced by Equation 3-21 is similar to that given by Equation 8-15 but is too conservative at large fibre volume fractions, and falls outside of  $\pm 1\sigma$  at  $V_f$ 's greater than 1%. However, for practical levels of fibre volume fraction in hollow core slabs ( $V_f < 1\%$ ), both Equations 3-20 and 3-21 give reasonably good approximations of the fibre shear supplement. This can be seen in Figure 9-3 where the shear supplement for the FRC hollow core slabs is compared with these two equations. Equation 3-20 would better approximate to the results if the loss of prestress at ultimate was considered (as Equation 8-15). Equation 3-23 can be seen to be highly conservative.

## 9.4 Flexure

### 9.4.1 Flexural cracking strength

It was not intended in this thesis to study the effect of fibres on the longitudinal flexural strength of PFRC beams and hollow core slabs. However, given that many of the factory-produced x-beams as well as beams PB1-PB4 failed in anchorage due to flexural cracking, it is perhaps appropriate to briefly study the flexural cracking strength of these beams. Therefore in this section the flexural cracking strength of the factory-produced x-beams and the laboratory-cast x-beams PB1-PB4 are compared with the theoretical flexural strength described in Section 3.3.5. This describes the first crack as occurring when the tensile stress at the soffit due to imposed load equals the sum of the prestress at the soffit and the flexural tensile strength of the concrete. The cracking moment is given by:

$$M_{cr} = (f_b + f_{fl,cr})Z_b$$

.. 9-2

For the factory-produced x-beams, the effective prestress at the soffit ( $f_b$ ) for use in Equation 9-2 has been calculated from the assumed initial prestress force reduced to account for short-term prestress losses between casting and testing. The usual loss of prestress in hollow core slabs is between 19-26% (Elliott 1996) depending on the initial level of prestress, and a conservative value of 25% recommended by Girhammar (1992) has been used since the initial prestress was 70% of ultimate. The prestress value has been further reduced in some beams to account for the fact that the flexural crack occurred within the transfer length where the full prestress force has not developed. The transfer length and necessary reduction have both been calculated using BS 8110, and the location of the crack along the length of the beam is that measured in the tests.

BS 8110 estimates the flexural cracking strength of plain concrete as  $0.6\sqrt{f_{cu}}$ , when a material safety factor of 1.3 omitted. This is twice the value of the tensile strength as predicted by BS 8110, and is consistent with the observation between the flexural tests and splitting tests in Chapter 4 of  $f_{fl}/f_{ct,sp} = 1.9$ . It is known, however, that in hollow core slabs the presence of the core does not allow exploitation of the strain-softening behaviour of concrete (Pajari 1991), and therefore the flexural tensile strength and the direct tensile strength are approximately the same. A value for the flexural cracking strength of  $1.1 f_{ct,sp}$  (Girhammar 1992) is therefore more appropriate, if it is accepted that  $f_{ct,sp}$  is a measure of the direct tensile strength for plain concrete.

To estimate the flexural cracking strength of the beams for use in predictive equations, a value of  $f_{fl,cr} = 1.1 f_{ct,sp}$  has been used, where  $f_{ct,sp}$  is calculated from Equation 8-4. This gives a value of  $0.5\sqrt{f_{cu}}$  consistent with all the splitting tensile tests reported in Chapter 4.

Since the ultimate splitting tensile strength of FRC is not related to the direct tensile strength it cannot be used to estimate the flexural cracking strength. The flexural cracking strength of FRC ( $f_{fl,cr(FRC)}$ ) has therefore been calculated from the following equation, based on the law of composites:

$$f_{fl,cr(FRC)} = 1.1((1 - \eta_{\theta} V_f) f_{ct,sp(plain)} + \sigma_{ps})$$

.. 9-3

where  $\sigma_{ps}$  is given by Equation 2-11 and is the fibre contribution to load-sharing before cracking of the matrix.

For the four laboratory-cut beams which failed in flexure (PB1-PB4), the prestress at the soffit (as explained in Section 4.4.1) is unknown but is likely to be low because of excess slip of the wires at release. A value assuming all of the prestress to be lost ( $f_b = 0$ ) has been used as an approximation.

The theoretical and actual flexural cracking moments of each of the x-beams that failed in flexure are compared in Table 9-5 to Table 9-7. For the factory-produced x-beams it can be seen that there is a good correlation between the two results; the average value of  $M_{cr}/M_{th}$  being 1.07 and 1.15 for the plain and fibre reinforced beams, respectively. The standard deviation of these results being only 0.22 and 0.15.

For the laboratory-cast specimens there is an average value of  $M_{cr}/M_{th} = 0.99$  at a standard deviation of 0.16. The actual cracking strength was only greater than the theoretical cracking moment for one of the beams (PB1) despite the assumption that there was zero prestress.

It is shown, therefore, that the flexural cracking moment of prestressed beams is little improved by the addition of fibres, and can be calculated from Equations 9-2 and 9-3. The above results also support the theory that the flexural cracking strength of concrete in a hollow core slab is only slightly greater than the direct or splitting tensile strength.

#### **9.4.2 Transverse flexural cracking strength**

The results of the transverse flexural strength tests in Section 7.4 showed that the transverse flexural cracking strength of the section beneath one of the hollow cores was approximately  $3.5 \text{ N/mm}^2$ . This is less than the presumed splitting strengths given by Equation 2-15.

The centric concentrated load tests in Section 7.5 also give an indication of the transverse flexural cracking strength. The calculated transverse cracking moments from these tests, however, are scattered. The average transverse flexural cracking moment is about 4.8 kNm. Assuming only the flanged section to be resisting the

bending moment as with the straightforward transverse flexural test above, this produces a transverse flexural cracking strength of  $5.2 \text{ N/mm}^2$ . For plain concrete this corresponds to a value of  $1.1 f_{ct,sp}$ . This is consistent with the observations for longitudinal flexure above.

The lower value for the transverse flexural cracking strength is probably because of the localised compressive stress over the tops of the hollow core. The value of  $3.5 \text{ N/mm}^2$  is therefore probably very close to the direct tensile strength, because there could have been almost no plastification of concrete through the web, and the crack would have penetrated through to the core immediately. This suggests that the splitting strength is not equal to the direct tensile strength, which is perfectly reasonable given the arguments by Hansen (1996) in Section 2.2.4.

## **9.5 Implications for the design of FRC hollow core slabs**

### **9.5.1 Transverse and flexural reinforcement**

The use of steel fibres as transverse reinforcement in hollow core slabs has been shown by the results of experiments to be impractical because of the small depth of the flanges, no significant increases in strength or ductility being observed. Results also suggest that fibres do not prevent the propagation of longitudinal cracks along the length of the slab.

The influence of fibres on the anchorage and flexural cracking capacity of the hollow core slabs is also negligible, while the ability of fibres to provide enhanced ultimate flexural strength was not tested.

### **9.5.2 Shear reinforcement**

To study the increases in shear strength provided by the inclusion of steel fibres, the following example is presented in which the sensitivity of different parameters on the shear strength of a typical plain 200 mm deep hollow core slab as predicted by Equation 8-11 with an overall reduction factor of 0.6 are compared.

For a plain slab, with  $f_{cu} = 60 \text{ N/mm}^2$ ,  $\sigma_{cpk} = 2.7 \text{ N/mm}^2$  (equivalent to seven 12.5 mm strands stressed to  $0.7 f_{pu}$ ), and  $I_b/A_y = 41588 \text{ mm}^2$ , Equation 8-11 predicts a strength of 126 kN. By adding a fibre volume fraction of 1%, the ultimate shear strength (Equation 8-12) can be increased by 36 kN, using the same overall reduction factor of 0.6 which is conservative for FRC. Table 9-8 shows the necessary increases in compressive strength, prestress and geometrical properties necessary to obtain this magnitude of shear supplement in a plain concrete slab.

It can be seen that to realise the same increases in shear strength it is necessary to increase the compressive strength by 85% or the prestress by 156%. The increase in compressive strength is equivalent to a 45% increase in tensile strength, but is impractical because concretes with such a high compressive strength are extremely difficult to obtain and such concrete is unlikely to be feasible for use in hollow core slabs. Additionally, it is unlikely that equations relating  $f_{cu}$  to  $f_{ct}$  are applicable at such high strengths. Likewise, the increase in prestress, in the above example, would require a minimum of an additional eleven 12.5 mm strands. This would lead to very high bursting stresses in the development area, and to excessive tensile stresses and cracking in the top of the slabs. Fibres are therefore far more practical than increasing concrete strength and the level of prestress.

However, the increase in shear strength is small when compared with the small change required in the geometrical slab property,  $I_b/A_y$ . The increase in  $I_b/A_y$  from  $41588 \text{ mm}^2$  to  $51500 \text{ mm}^2$  corresponds to an increase in the depth of the hollow core slab from 200 mm to 230 mm. For the next depth of slab manufactured by Richard Lees Ltd. (260 mm deep hollow core slabs),  $I_b/A_y$  is approximately  $63000 \text{ mm}^2$ .

Additionally, increasing the depth of a hollow core slab has little affect on the cost of manufacture. However, it has been shown that because of increased transportation costs and increased craneage costs at site a 250 mm deep slab is approximately 15% more expensive than a 200 mm deep slab. Thus at present UK prices<sup>1</sup> (1998), a 200 mm deep hollow core slab costs approximately  $\text{£}27/\text{m}^2$  and a 250 mm deep slab costs  $\text{£}31/\text{m}^2$ .

---

<sup>1</sup> based on estimates provided by two UK hollow core slab manufacturers, both of whom wish to remain anonymous

The addition of a fibre volume fraction of 1% of HS fibres ( $W_f = 78 \text{ kg/m}^3$ ) equates to the addition of  $9 \text{ kg/m}^2$ . At current UK prices, HS fibres cost approximately  $\text{£}0.75/\text{kg}$  which equates to an additional cost of adding fibres to hollow core slabs of approximately  $\text{£}7/\text{m}^2$ . The price for a 200 mm deep fibre reinforced hollow core slab is therefore approximately  $\text{£}34/\text{m}^2$ , an increase of about 25%. The use of AM fibres which are roughly five times more expensive than HS fibres would be impractical economically.

Therefore, increasing the depth of hollow core slabs is a far more effective method of improving the shear strength. However, there are further reasons why a designer would choose not to increase the depth which are dependant on particular structures. These include the necessary depth of support beams to support deeper slabs, and the implications of increased weight on the overall structure. For example increasing the depth from 200 mm to 260 mm increases the mass per unit area from  $272 \text{ kg/m}^2$  to  $405 \text{ kg/m}^2$  (Richard Lees Ltd. data), whereas using 1% fibre volume fraction of HS fibres increases the weight to only  $280 \text{ kg/m}^2$  - a huge saving.

Alternative shear strength improving methods, such as filling in the cores with concrete and including shear links, will also give greater increases in shear strength than adding fibres. However, the filling-in of cores and inclusion of shear links are time consuming and expensive activities, which additionally increase the weight of the slabs.

For example, to obtain the necessary increase in strength and maintain symmetry of the system it would be necessary to fill-in a minimum of two cores. Given that  $V_{co}$  is approximately twice the flexural shear cracking capacity for a 200 mm deep hollow core slab then it is necessary to fill-in the cores for a length of approximately  $\text{span}/4$  assuming a uniformly distributed load. For a 4 m spanning slab which is about the shortest length commonly used in practice, and therefore the most susceptible to shear, this equates to an increase in weight of about 7%. The equivalent increase in weight using HS fibres is approximately 3% but would be less if it was not necessary to add fibres throughout the entire length. With modern manufacturing methods it is unlikely that there would be any way of accurately adding fibres to only specific lengths of slab.

However, filling-in of cores is time-consuming and labour intensive, and can quite easily double the cost of slabs. Fibres on the other hand increase costs by only

25%, and their only hindrance to the manufacturing process is a tripling in the mixing time (using the method in Chapter 6).

The use of steel fibres in hollow core slabs as shear reinforcement therefore has to be considered carefully alongside other forms, in terms of both cost and weight. It is important to note that although increasing the depth and filling-in of cores give greater increases in strength, neither method provides similar levels of ductility to that which can be achieved using fibres. It is in this area that the improved performance of FRC hollow core slabs can be best implemented.



**Table 9-1 Comparison of measured transfer lengths for 12.5 mm strand and 7 mm wire in plain concrete with predictive equations**

	Transfer length (mm)					
	Test results	BS 8110 (Eq. 3-9)	EC2 (Eq. 3-10)	FIP/PCI (Eq. 3-11) <sup>†</sup>	Oles'wicz (Eq. 3-12)	CEB-FIP (Eq. 3-14)
<b>12.5 mm strand</b>						
B-0.0A	659	463	830	780	492	416
B-0.0B	707	500	890	780	531	452
<b>7 mm wire</b>						
PB5 & PB7	510	660	473	352	284	491

<sup>†</sup> In using Equation 3-11, initial prestress losses of 1.3% and 4% have been assumed for strands and wires, respectively.

**Table 9-2 Comparison of theoretical equation with average ultimate shear strength of plain slabs and x-beams**

	a/d	$\sigma_{cpx}$ (N/mm <sup>2</sup> )	$V_{ult}$ (N/mm <sup>2</sup> )	$V_{co}$ (N/mm <sup>2</sup> ) Equation 3-4	$V_{ult}/V_{co}$	s.d. of $V_{ult}/V_{co}$
laboratory-cast x-beams	2.0	3.5	7.23	5.27	1.37	0.20
	2.8	3.2	5.53	5.18	1.07	0.10
					<u>1.22</u>	<u>0.21</u>
factory-produced x-beams	2.0	1.8	5.28	5.22	1.01	0.28
	2.8	1.8	5.62	5.22	1.08	0.03
					<u>1.05</u>	<u>0.20</u>
factory-produced slabs	2.0	2.4	3.33	5.50	0.61	0.17
	2.0	2.8	4.15	5.66	0.73	0.22
	2.8	2.4	3.49	5.49	0.64	0.07
	2.8	2.8	3.53	5.66	0.62	0.15
	3.5	2.8	3.88	5.66	0.69	0.23
				<u>0.66</u>	<u>0.16</u>	

$V_{ult}$  calculated from average of all tests.  $V_{co}$  calculated as average theoretical value of all tests

Table 9-3 Comparison of theoretical equations with average ultimate shear strength of FRC x-beams

a/d	fibres	$V_f$ (%)	$V_{ult}$ (N/mm <sup>2</sup> )	$V_{con}$ (N/mm <sup>2</sup> ) (using Equation 8-12)	$V_{ult}/V_{con}$ s.d. of $v_{ult}/v_{con}$	$V_{con}$ (N/mm <sup>2</sup> ) (using Equation 3-28)	$V_{ult}/V_{con}$ s.d. of $v_{ult}/v_{con}$
laboratory-cast							
2.0	HS	0.5	8.73	7.01	1.25	6.21	1.41
2.0	HS	1.0	9.60	7.58	1.27	6.68	1.44
2.0	HS	1.5	10.71	8.40	1.28	7.31	1.47
				<u>1.27</u>	<u>0.09</u>	<u>1.43</u>	<u>0.09</u>
laboratory-cast							
2.8	HS	0.5	6.97	7.01	0.99	6.56	1.06
2.8	HS	1.0	7.78	7.68	1.01	6.95	1.12
2.8	HS	1.5	7.91	8.06	0.98	6.39	1.24
2.8	AM	0.28	6.53	6.10	1.07	6.34	1.03
2.8	AM	0.56	6.77	6.77	1.00	6.71	1.01
				<u>1.01</u>	<u>0.10</u>	<u>1.09</u>	<u>0.12</u>
factory-produced							
2.0	HS	0.5	6.33	5.96	1.06	6.09	1.04

$v_{ult}$  calculated from average of all tests.  $v_{con}$  calculated as average theoretical value of all tests

**Table 9-4 Comparison of theoretical equations with average ultimate shear strength of FRC hollow core slabs**

a/d	fibres	$V_f$ (%)	$V_{ult}$ (N/mm <sup>2</sup> )	$V_{comp}$ (N/mm <sup>2</sup> )	$v_{ult}/v_{comp}$ (using Equation 8-12)	s.d. of $v_{ult}/v_{comp}$	$V_{cou}$ (N/mm <sup>2</sup> )	$v_{ult}/v_{cou}$ (using Equation 3-28)	s.d. of $v_{ult}/v_{cou}$
2.0	HS	0.5	5.40	6.43	0.84	0.08	6.87	0.79	0.06
2.0	HS	1.0	6.08	7.57	0.80	0.08	6.93	0.88	0.09
2.0	AM	0.28	5.37	6.06	0.89	0.13	7.07	0.76	0.11
					<u>0.84</u>	<u>0.08</u>		<u>0.80</u>	<u>0.08</u>
2.8	HS	0.5	5.06	6.43	0.79	0.04	6.97	0.73	0.02
2.8	AM	0.28	4.08	6.06	0.67	0.22	7.07	0.58	0.19
					<u>0.73</u>	<u>0.12</u>		<u>0.68</u>	<u>0.11</u>

$v_{ult}$  calculated from average of all tests.  $v_{cou}$  calculated as average theoretical value of all tests

**Table 9-5 Comparison of observed and theoretical cracking moments for factory-produced plain concrete x-beams**

	$V_f$ (%)	$f_b$ (N/mm <sup>2</sup> )	$f_{t,cr}$ (N/mm <sup>2</sup> ) $\times 10^6$ (mm <sup>4</sup> )	$Z_b$ (mm <sup>4</sup> ) $\times 10^6$ (mm <sup>4</sup> )	$M_{th}$ (kNmm)	$M_{cr}$ (kNmm)	$M_{cr}/M_{th}$
P7/2B	0	2.04	5.36	1.28	8.8	11.8	1.34
P7/28A	0	2.65	5.36	1.17	8.7	10.9	1.25
P9/2B	0	2.69	5.36	1.20	10.7	8.8	0.82
P9/28A	0	2.57	5.36	1.20	10.5	13.6	1.30
P12/2A	0	6.58	5.36	1.24	14.2	14.0	0.99
P12/2B	0	5.77	5.36	1.30	13.9	10.9	0.79
P12/2C	0	6.46	5.36	1.29	14.6	13.3	0.91
P12/28A	0	5.56	5.36	1.23	12.8	14.6	1.14
P12/28B	0	5.96	5.36	1.27	13.8	11.0	0.80
P12/35	0	6.38	5.36	1.26	14.2	17.0	1.20
P12/52	0	6.77	5.36	1.22	14.2	18.0	1.27
						mean =	1.07
						standard deviation =	0.22

**Table 9-6 Comparison of observed and theoretical cracking moments for factory-produced FRC x-beams**

	$V_f$ (%)	$f_b$ (N/mm <sup>2</sup> )	$f_{t,cr}$ (N/mm <sup>2</sup> )	$Z_b$ $\times 10^6$ (mm <sup>4</sup> )	$M_{th}$ (kNmm)	$M_{cr}$ (kNmm)	$M_{cr}/M_{th}$
F7/2A	0.5	2.18	5.55	1.40	9.9	11.1	1.12
F7/2B	0.5	1.94	5.55	1.41	9.6	13.3	1.39
F7/28A	0.5	2.22	5.55	1.32	9.4	11.2	1.20
F7/28B	0.5	2.3	5.55	1.37	9.8	12.2	1.24
F9/2A	0.5	3.88	5.55	1.39	12.2	11.4	0.94
F9/2B	0.5	3.88	5.55	1.39	12.2	11.9	0.98
F9/28A	0.5	3.52	5.55	1.41	11.8	13.1	1.11
F9/28B	0.5	3.44	5.55	1.41	11.7	14.1	1.20
mean =							1.15
standard deviation =							0.15

**Table 9-7 Comparison of observed and theoretical cracking moments for laboratory-cast x-beams**

	$V_f$ (%)	$f_b$ (N/mm <sup>2</sup> )	$f_{t,cr}$ (N/mm <sup>2</sup> )	$Z_b$ $\times 10^6$ (mm <sup>4</sup> )	$M_{th}$ (kNmm)	$M_{cr}$ (kNmm)	$M_{cr}/M_{th}$
PB1	0	0	4.38	1.22	5.4	6.4	1.20
PB2	0	0	4.24	1.22	5.2	5.2	1.00
PB3	0.5	0	4.37	1.22	5.3	4.4	0.82
PB4	0.5	0	4.37	1.22	5.3	5.0	0.94
							mean = 0.99
							standard deviation = 0.16

**Table 9-8 Increases in slab properties to attain same increase in ultimate shear strength as adding a fibre volume fraction of 1.0%**

$V_f$ (%)	$f_{cu}$ (N/mm <sup>2</sup> )	$\sigma_{cpx}$ (N/mm <sup>2</sup> )	Ib/Ay (mm <sup>2</sup> )	$V_{ult}$ (kN)
0	60	2.7	41588	126.0
1.0	60	2.7	41588	161.5
0	111 (+85%)	2.7	41588	161.5
0	70	6.9 (+156%)	41588	161.5
0	70	2.7	53330 (+28%)	161.5



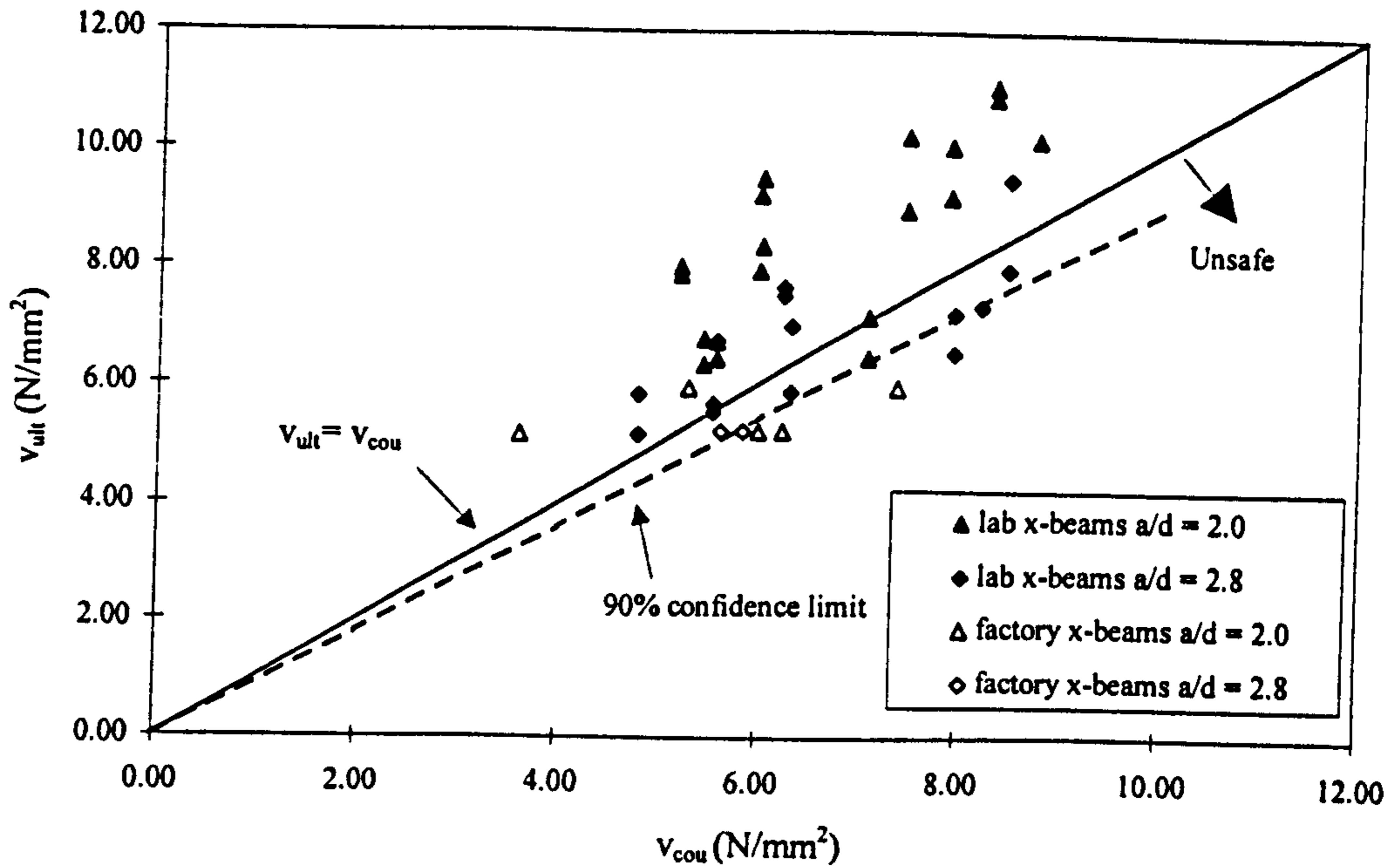


Figure 9-1 Comparison of ultimate shear stress ( $v_{ult}$ ) for FRC x-beams with theoretical equation for  $v_{cou}$

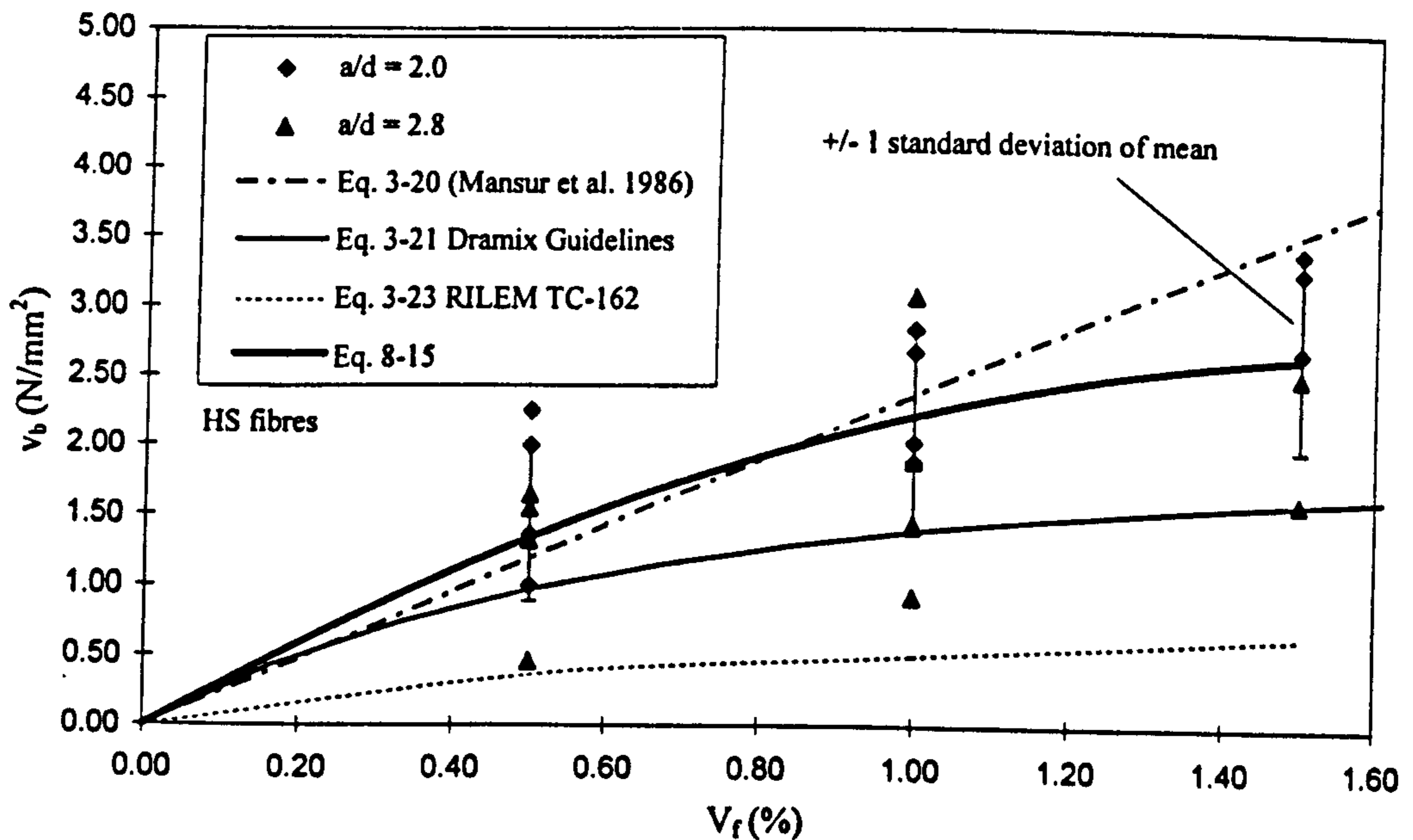
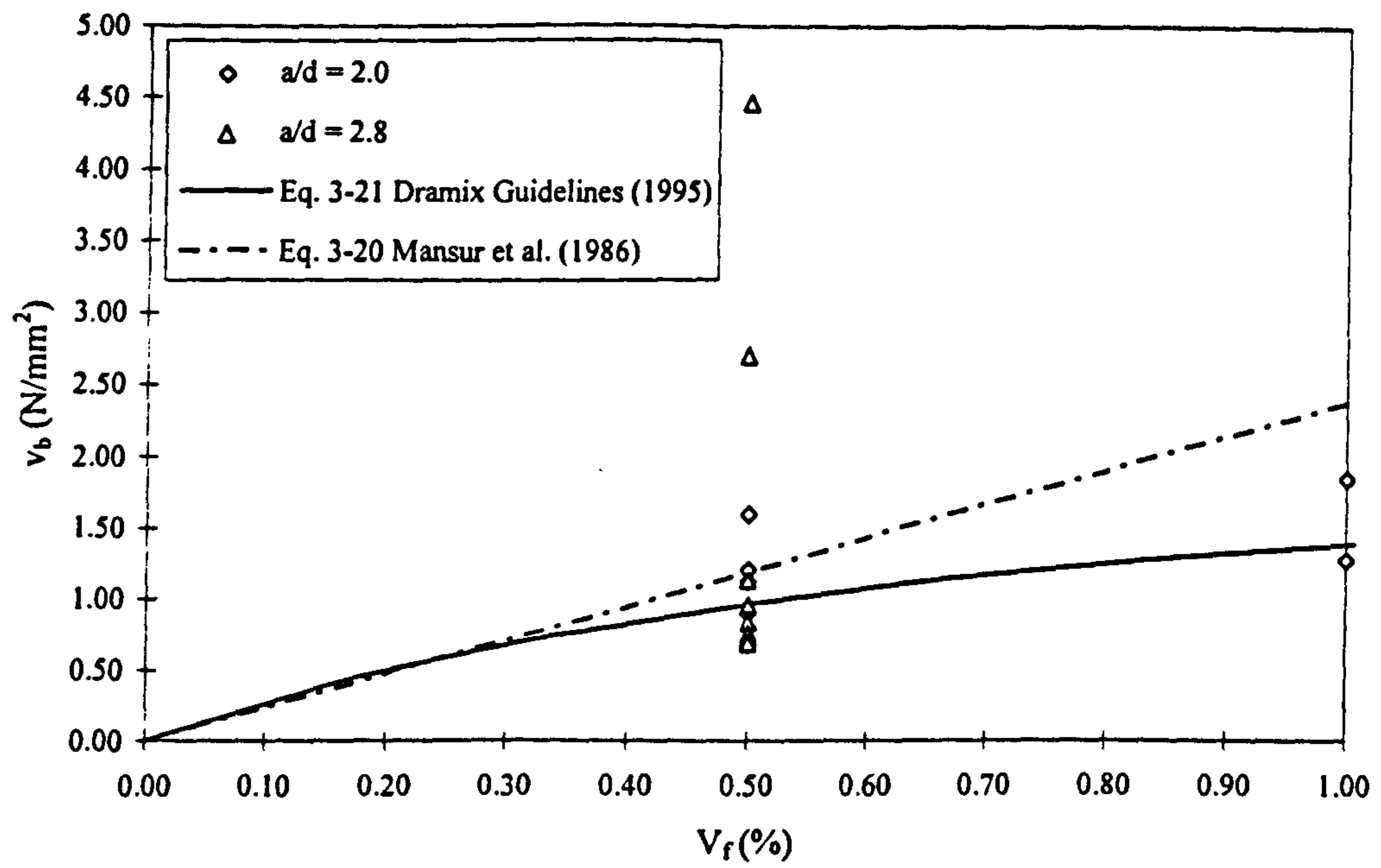


Figure 9-2 Increase in shear strength with fibre volume fraction for laboratory-cast x-beams compared with predictive equations for fibre shear supplement



**Figure 9-3 Increase in shear strength with fibre volume fraction for hollow core slabs compared with predictive equations for fibre shear supplement**

## **CHAPTER 10**

### **CONCLUSIONS AND FUTURE WORK**

#### **10.1 Introduction**

The objectives of the work presented in this thesis were listed in Section 1.4 as:

- (1) To investigate the performance of prestressed concrete in combination with steel fibres in areas of shear, flexure and bond.
- (2) To relate improvements in strength and ductility into design equations in common with current design recommendations for prestressed concrete and fibre reinforced concrete (FRC).
- (3) To study the possibility of using FRC in prestressed hollow core slabs.

Each of these objectives have been met practically on the basis of the following experimental work:

- a) Standard production of FRC hollow core slabs using different fibre types and fibre volume fractions
- b) full-scale testing of precast concrete elements under shear, bending and concentrated loading
- c) investigation of the material properties of fibre reinforced hollow core slabs
- d) laboratory-tests on prestressed beams simulating hollow core slab webs, and bond tests on prestressing strand embedded in FRC
- e) flexural toughness tests on the FRC used in all laboratory tests.

The conclusions of this work are outlined below and concentrate on the manufacture of fibre reinforced hollow core slabs (Objective 3), testing of FRC units (Objectives 1 and 3), and the implementation of a design equation for prestressed fibre reinforced concrete (Objective 2).

Requirements for future work are given in Section 10.5.

## **10.2 Manufacture**

### **10.2.1 Manufacture of extruded FRC slabs**

The research has shown that fibre reinforced prestressed concrete hollow core slabs can be manufactured using the Spiroll extrusion method. Preliminary laboratory trials to assess the mixing methods for FRC showed that because of the low water content used in extruded slabs it is necessary to add collated hooked-end steel (HS) fibres (30 mm long x 0.5 mm diameter) before the addition of any free water to obtain adequate separation. Fibre volume fractions ( $V_f$ ) of 0.5% to 1% were successfully added.

To obtain adequately compacted FRC slabs it was found necessary to slightly increase the water/cementitious material ratio. For the trials in this work changes in water/cementitious material ratios from 0.32 to 0.34 were reported. It was found that there was no need to alter any dry material proportions to account for the steel fibres, and nor was it necessary to use a water-reducing admixture or superplasticizer. The density of the hardened matrix component of well compacted FRC slabs was equal to the density of plain concrete slabs.

It was observed that flexible amorphous metal (AM) fibres (30 mm long) were easier to compact and mix in dry, extrudable concrete than the stiffer HS fibres. In addition, HS fibres tended to project from the top and sides of the slabs and raised safety concerns with the hollow core slab manufacturer.

### **10.2.2 Fibre orientation**

The orientation of HS fibres can be adequately assessed from small prismatic sections cut from the specimens. However, the method proved to be less successful with AM fibres.

For the laboratory-cast beams the orientation of the fibres through the depth was found to vary widely from beam to beam. However, the average orientation factor ( $\eta_\theta$ ) of all the measured prisms for each beam was found to be approximately 0.41. This is equal to the theoretical value for random distribution. The same value of 0.41 was obtained for fibres crossing a 45° inclined shear plane.

In hollow core slabs the fibres do not orient randomly and are strongly affected by the rotation of the augers and the direction of travel of the extrusion machine. In the webs, the fibres tend to align vertically with  $\eta_\theta \cong 0.6$ . At the top of the slabs the fibres tend to align in the longitudinal direction along the length of the slab, while at the bottom random orientation was observed.

Despite, this strong orientation of fibres in the vertical direction within the web, it was found that the orientation of fibres across the shear plane can be assumed to be random. A value of 0.41 for  $\eta_\theta$  is therefore sufficient.

### **10.2.3 Fibre distribution**

Wash-out tests performed immediately after each trial suggested that the fibres are randomly distributed throughout the cross-section. Such tests are rather variable due to their nature and gave only a qualitative indication of the fibre distribution.

Crushing of cores randomly cut from hardened slabs showed that the distribution of fibres throughout the length and width of the slabs is relatively consistent. For  $V_f = 0.5\%$ , actual values varied from the intended quantity by not more than 8%.

## **10.3 Testing**

### **10.3.1 Bond**

Bond of FRC and prestressing strand was studied because the development of prestress within a pretensioned concrete element is important with regard to web shear tension and anchorage failures. Previous tests found in the literature had shown that fibres could improve the bond and lead to reduced prestress transfer lengths.

This work showed that the addition of fibres to concrete tends to disrupt or reduce the bond between matrix and helical strand. In the pull-out tests, larger strand slips were measured in all of the FRC specimens than were measured in the plain concrete specimens. However, on the positive side, fibres prevent explosive bond failures by bridging across bond cracks. This implies that the use of large prestresses is safer in FRC than in plain concrete, if no more practical.

From the shear tests on both beams and slabs, no significant differences were found in the rate of wire slip versus gross deflection (under the load) between wires embedded in plain concrete and FRC. However, the results may suggest that the addition of fibres does have a slightly negative affect on the matrix-strand bond.

In direct pull-out tests the prestress transfer length in FRC is longer than in plain concrete. Depending on how this was measured the transfer lengths either increase with increasing fibre content or are at a consistently longer length for FRC. This was also observed on plain and indented prestressed wires in plain and fibre reinforced concrete beams at release of the prestress.

Although the addition of fibres does appear to have a disruptive influence on the bond, the affects are relatively small. For example the observed increase in transfer length of 47% for  $V_f = 1.5\%$  only reduces the cracking shear capacity by 4%.

### **10.3.2 Shear**

Shear is a major problem in prestressed hollow core slabs because of restrictions in the placement of traditional reinforcement. Hollow core slabs therefore rely on the development of prestress and the tensile strength of the concrete to prevent shear failure. Since steel fibres are known to lead to enhanced shear performance, an investigation was carried out into the performance of prestressed fibre reinforced concrete under shear.

To understand shear failure in prestressed hollow core slabs, tests were performed on both full-width slabs and single webs cut from hollow core slabs. For a fuller picture with regard to the nature of shear failure in prestressed concrete, beams were cast in the laboratory to simulate webs of hollow core slabs.

It was found that steel fibres increase the ultimate shear capacity of prestressed concrete beams, but have minimal effect on the cracking shear capacity of prestressed concrete beams.

Observation of the failures and theoretical analysis, suggest that the increases in capacity are a combination of the ability of the fibres to transfer tensile stresses across the crack by a bridging mechanism, and a crack arrest mechanism which prevents propagation of the shear crack into the compressive zone. The increased capacity of PFRC beams is maintained over wide crack widths and large deflections.

Experimental measurement of strains in the wires suggests that complete loss of prestress occurs at cracking in plain prestressed concrete beams. However, in PFRC beams it was shown that there is a gradual loss of prestress after cracking, and that about 67% of the initial prestress is still present when the ultimate shear capacity is attained.

The above affects are relevant to both prestressed beams and hollow core slabs, but in relation to hollow core slabs there are further points of interest:

- a) The shear tests were unable to fully distribute the shear load across the width of the beams which led to central webs carrying greater loads than the outer webs and failing first. This problem was compounded by the inconsistencies in the widths of the webs.
- b) Because of the above effect the shear capacity of a hollow core slab is less than the sum of the shear capacity of each of the individual web components. This observation needs to be taken into account in design.

### **10.3.3 Transverse flexure**

The transverse flexural strength of hollow core slabs was investigated because like shear it is difficult to place traditional reinforcement to prevent a transverse

flexural failure. Two types of test were performed with slabs either simply-supported in the transverse or longitudinal direction.

There was no evidence from any of the tests to suggest that fibres increase the transverse flexural strength of hollow core slabs. This is because the lower flange depth is too shallow for fibres to have any effect in resisting propagation of the flexural crack. It was also observed that fibres do not resist the propagation of cracks along the longitudinal length of the slab.

The transverse flexural cracking strength of plain and fibre reinforced concrete in hollow core slabs was found to equal the splitting tensile strength of cylinders, as opposed to the higher flexural tensile cracking strength of prisms. This is because the voids in the slab do not allow for the plastification of concrete which occurs in prisms.

#### **10.3.4 Anchorage and flexural cracking**

It was not initially intended to investigate the longitudinal flexural cracking strength of prestressed fibre reinforced concrete beams or slabs. However, since some of the more lightly prestressed elements failed in this manner, a brief discussion was made on this failure mode.

As was expected, fibres had little or no effect on the longitudinal flexural cracking strength. For both plain and fibre reinforced concrete in hollow core slabs the flexural cracking strength was calculated to be approximately equal to 1.1 times the splitting tensile strength of plain concrete. This is again due to the lack of plastification due to the presence of the core.

The ductility of flexural anchorage failures is largely dependant on the pull-out of the prestressing wires from the matrix. Since fibres have little effect on the wire slip behaviour, it was observed that the ductility of flexural failures is little affected by the presence of fibres. Anchorage failures in FRC can be therefore be designed against using the same methods as plain concrete.

It was seen that the flexural cracking strength of hollow core slabs increases linearly with the  $a/d$  ratio up to a maximum value of the  $a/d$  ratio. This maximum value equates to the transfer length and was measured to be approximately  $55\phi$ , which



corresponds to values of the transfer length obtained from direct pull-out tests on un-tensioned prestressing strands.

## 10.4 Design equation

A semi-empirical equation for predicting the ultimate shear capacity of PFRC beams was presented, and given in two forms: the first is related to the methods by which the shear capacity of prestressed concrete is predicted in BS 8110 and by other European codes, and is given as:

$$V_{cou} = \frac{Ib}{Ay} \sqrt{f_{ct,sp}^2 + 0.67\sigma_{cpX}f_{ct,sp}} \quad .. 10-1$$

where  $\sigma_{cpX}$  is the centroidal prestress at the critical section, and the splitting tensile strength ( $f_{ct,sp}$ ) can be calculated as either:

$$f_{ct,sp} = 0.5\sqrt{f_{cu}} + 0.37f_{fl,eq,300} \quad .. 10-2$$

or

$$f_{ct,sp} = 0.6f_{fl} + 0.37f_{fl,eq,300} \quad .. 10-3$$

where  $f_{cu}$  is the compressive cube strength,  $f_{fl,eq,300}$  is the equivalent flexural strength up to a deflection of span/300 and  $f_{fl}$  is the modulus of rupture of equivalent plain concrete.

This makes use of the equivalent flexural strength which is generally believed to be the most suitable single material property for including FRC in design formulae to account for both the increased post-cracking capacity and ductility. However, as an alternative to using the equivalent flexural strength, the benefit of fibres can be estimated by use of the ultimate fibre bridging stress (i.e.,  $0.37 f_{fl,eq,300} = \eta_{\theta} \lambda_f \tau_f V_f$ ). Equation 10-1 can also be easily be adapted in to the form used by ACI and PCI.

The second form is consistent with the methods of predicting the shear capacity currently being encouraged for use with steel fibres in reinforced concrete, i.e., as a fibre shear contribution ( $V_b$ ), to give

$$V_{cou} = V_{co} + V_b \quad \text{.. 10-4}$$

where  $V_{co}$  is the shear capacity of an equivalent plain prestressed element given by

$$V_{co} = \frac{Ib}{Ay} \sqrt{f_{ct}^2 + \sigma_{cpx} f_{ct}} \quad \text{.. 10-5}$$

with  $f_{ct} = 0.5\sqrt{f_{cu}}$ , and with  $V_b$  is given as

$$V_b = \frac{Ib}{Ay} (0.37 f_{f,eq,300} - 0.1\sigma_{cpx}) \quad \text{.. 10-6}$$

In deriving Equations 10-3 and 10-6 it was shown that increases in the ultimate splitting tensile strength of FRC over that of plain concrete can be related to the ultimate fibre bridging stress. This fibre bridging stress which is partly a function of the fibre-matrix interfacial bond strength was shown to increase with the compressive strength of the matrix whilst fibre pull-out was the principal failure mechanism. In addition, it was shown that for any fibre type there is a critical value of  $f_{cu}$  corresponding to a maximum fibre bridging stress when fibre rupture occurs.

While the proposed equations are satisfactory for use with prestressed concrete beams, it is necessary to implement an overall reduction factor on the predicted shear capacity of hollow core slabs. This is because of the problems relating to uneven load distribution across the slab width and inconsistent web widths.

## 10.5 Future Work

The work reported in this thesis has concentrated on the contribution of steel fibre reinforcement on elements (beams, slabs, cylinders and prisms) of 150 to 200 mm depth. Since it is known that there is a size effect in the testing of concrete structures it is imperative that future work deals with smaller and larger elements. The results of these studies should then be related to the semi-empirical equations developed and compared with the observations on the 150 to 200 mm deep elements.

In the shear tests reported, the hollow core slabs and x-beams were tested as single simply-supported units. This provides a worse-case scenario for shear, but does not simulate actual concrete practice. Some tests should consider the strength of fibre reinforced hollow core slabs cast as a floor with transverse ties, and *in situ* cast to the bearing.

Pajari and Yang (1995) have introduced the problem of shear failures in hollow core slabs cast as a floor when simply-supported on flexible supports. Following on from the work on shear reported in this thesis, full-scale tests using fibre reinforced hollow core slabs should be carried out to ascertain whether fibres can overcome this problem.

Finally, Chapter 1 refers to a number of secondary benefits which fibres may bring to hollow core slabs. These include the use of shotfired ceiling fixers, reduction in damage due to transporting and building-in, and smaller deflections due to delayed cracking. These points should be investigated.

## REFERENCES

- Adebar, P., Mindess, S., St-Pierre, D. & Olund, B., 1997; "Shear Tests on Fiber Concrete Beams without Stirrups," ACI Structural Journal, Vol. 94, No. 1, pp 68-76
- Åkesson, M., 1994; "Fracture Mechanics Analysis of the Transmission Zone in Prestressed Hollow Core Slabs," Publication 93:5, Division of Concrete Structures, Chalmers University of Technology, Gothenburg, Sweden, 62 pp
- American Concrete Institute, Committee 544, 1978; "Measurement of Properties of Fiber Reinforced Concrete," ACI Materials Journal, Vol.75 No.7 pp 283-289
- American Concrete Institute, Committee 544, 1988; "Measurement of Properties of Fiber Reinforced Concrete," ACI 544.2R-88, ACI Materials Journal, Vol.85 No.6 pp 583-593
- American Concrete Institute, Committee 544, 1993; "Guide for Specifying, Proportioning, Mixing, Placing, and Finishing Steel Fiber Reinforced Concrete," ACI 544.3R-93, ACI Materials Journal, V.90, No.1, pp 94-101
- American Society for Testing and Methods, 1985; "Standard Specification for Steel Fibers for Fiber Reinforced Concrete," ASTM A 820-85, ASTM Annual Book of Standards, Vol.04.02
- American Society for Testing and Methods, 1995; "Standard Specification for Fiber-Reinforced Concrete and Shotcrete," ASTM C 1116-95, ASTM Annual Book of Standards, Vol.04.02, pp 574-581
- American Society for Testing and Methods, 1994; "Standard Test Method for Flexural Toughness and First-Crack Strength of Fiber-Reinforced Concrete (Using Third-Point

Loading),” ASTM C 1018-94b, ASTM Annual Book of Standards, Vol.04.02, pp 501-508

Anderson, A.R. & Anderson, R.G., 1976; “An Assurance Criterion for Flexural Bond in Pretensioned Hollow Core Units,” ACI Journal, Vol. 73, No. 8, pp 457-464

Armelin, H.S. & Helene, P., 1995; “Physical and Mechanical Properties of Steel Fiber Reinforced Dry Mix Shotcrete,” ACI Materials Journal, V. 92, No. 3, pp 258 - 267

Ashour, S.A., Hasanain, G.S. & Wafa, F.F., 1992; "Shear Behaviour of High-Strength Fiber Reinforced Concrete Beams," ACI Structural Journal, Vol. 89, No. 2, pp 176-184

Austin, S.A. & Robins, P.J., 1995; “Sprayed Concrete: Properties, Design and Application,” Whittles Publishing, 382 pp

Balaguru, P.N., 1994; “Fiber Reinforced Concrete for Structural Components: A State-of-the-Art,” Wokshop on Fibre Reinforced Cement and Concrete, University of Sheffield, 28-30 July 1994, pp 362-372

Balaguru, P.N. & Ezeldin, A.S., 1987; “Behaviour of Partially Prestressed Beams made with High Strength Fiber Reinforced Concrete,” ACI SP 105 - Fiber Reinforced Concrete Properties and Applications, pp 419-434

Balaguru, P.N. & Shah, S.P., 1992; “Fiber-Reinforced Cement Composites,” McGraw-Hill, 530 pp

Balázs, G.L., Erdélyi, L. & Kovács, I., 1997; "Fiber Reinforced Prestressed Concrete," The Concrete Way to Development, FIP Symposium, Johannesburg, South Africa, 9-12 March 1997

Batson, G.B., 1994; “State-of-the-Art of Steel Fiber Reinforced Concrete,” Wokshop on Fibre Reinforced Cement and Concrete, University of Sheffield, 28-30 July 1994

- Bekaert, 1995; "Background Document to Explain the Shear Formulas of the Dramix Guideline," Document 4, 4pp
- Bentur, A. & Mindess, S., 1990;. "Fibre Reinforced Cementitious Composites," Elsevier Applied Science, 449 pp
- Bernander, K-G., 1986; "Tests with Fibre Reinforced Extruded Hollow Core Slabs," Test Report, AB Strängbetong, Nacka, Sweden, 4 pp
- Boucheret, J-M., 1994; "Concretes and Mortars Reinforced with Fibraflex Metallic Amorphous Fibres," Paper presented at Wokshop on Fibre Reinforced Cement and Concrete, University of Sheffield, 28-30 July 1994
- Boucharet, J-M., 1997; Personal Communication. (Product Manager, Fibraflex, France)
- Brooks, M.D., Gerstle, K.H. & Logan, D.R., 1988; "Effect of Initial Strand Slip on the Strength of Hollow-Core Slabs," PCI Journal, Vol. 33, No. 1, pp 90-111
- BS 12, 1991; "Specification for Portland Cements," British Standards Institution.
- BS 882, 1992; "Specification for Aggregates from Natural Sources for Concrete," British Standards Institution.
- BS 1881, 1983; "Methods of Testing Concrete," British Standards Institution.
- BS 3892, Part 1, 1993; "Specification for Pulverized-Fuel Ash for use with Portland Cement," British Standards Institution.
- BS 8110, 1985; "Structural Use of Concrete, Part 1.," Code of Practice for Design and Construction," British Standards Institution.

Casanova, P., Rossi, P. & Schaller, I., 1997; "Can Steel Fibers Replace Transverse Reinforcements in Reinforced Concrete Beams?," ACI Materials Journal, Vol. 94, No. 5, pp 341-354

✓ Chen, L., Mindess, S. & Morgan, D.R., 1994; "Specimen Geometry and Toughness of Steel Fibre Reinforced Concrete," ASCE Journal of Materials in Civil Engineering, Vol. 6 No. 4 pp 529-541

Criswell, M.E., 1994; "Reinforced Fiber Reinforced Concrete and Issues for its Inclusion in Structural Design Codes," Paper presented at Workshop on Fibre Reinforced Cement and Concrete, University of Sheffield, 28-30 July 1994

Della Bella, B. & Querin, E., 1997; "Developments of Deep Section Slide-Forming: New Technology for the Production of "Jumbo-Sized" Hollow Core Slabs and Beams up to 900 mm," The 4th International Symposium on Noteworthy Developments in Prestressing and Precasting, 3 - 4 July 1997, Singapore, pp 44-48

Demeke, A. & Tegos, I.A., 1994; "Steel Fiber Reinforced Concrete in Biaxial Stress Tension-Compression Conditions," ACI Structural Journal, Vol. 91, No. 5, pp 579-584

Den Uijl, J.A., 1995; "Transfer Length of Prestressing Strand in HPC," Progress in Concrete Research, Faculty of Civil Engineering, Delft University of Technology, The Netherlands, Vol. 4, pp 75-90

Den Uijl, J.A., 1997a; Personal Communication. (Professor, Faculty of Civil Engineering, Delft University of Technology, Netherlands)

Den Uijl, J.A., 1997b; "Bond Modelling of Prestressing Strand," Paper presented at the 1997 Spring Convention, American Concrete Institute, Seattle, Washington, U.S.A., 5-10 April 1997

Divakar, M.P., Fafitis, A. & Shah, S.P., 1987; "Constitutive Model for Shear Transfer in Cracked Concrete," *Journal of Structural Engineering, ASCE*, Vol. 113, No. 5, pp 1046-1062

Dramix Guideline, 1995; "Design of Concrete Structures. Steel Wire Fibre Reinforced Concrete Structures with or without Ordinary Reinforcement," Final Draft, 25pp

EFNARC, 1993; "Specification for Sprayed Concrete," Final Draft, European Federation of National Associations of Specialist Contractors and Material Suppliers to the Concrete Industry, UK, 35 pp

EFNARC, 1996, "European Specification for Sprayed Concrete," European Federation of Producers and Applicators of Specialist Products for Structures, UK, 30 pp

Elliott, K.S., 1996; "Multi-Storey Precast Concrete Framed Structures," Blackwell Science, Oxford, 602 pp

El-Shakra, Z.M. & Gopalaratnam, V.S., 1993; "Deflection Measurements and Toughness Evaluations for FRC," *Cement and Concrete Research*, Vol. 23, pp 1455-1466

Eurocode 2, 1994; "Design of Concrete Structures, Part 1: General Rules and Rules for Buildings," European Prestandard, ENV 1992-1-1 and, "Design of Concrete Structures, Part 1-3: General Rules – Precast Concrete Elements and Structures," European Prestandard, ENV 1992-1-3, CEN (Comité Européen de Normalisation).

Ezeldin, A.S. & Balaguru, P.N., 1989; "Bond Behaviour of Normal and High-Strength Fiber Reinforced Concrete," *ACI Materials Journal*, Vol. 86, No. 5, pp 515-524

Fattuhi, N., 1994; "Reinforced Corbels made with Plain and Fibrous Concrete," *ACI Structural Journal*, Vol. 91, No. 5, pp 530-536



Fibraflex, 1995; Company literature

FIP, 1988; "Precast Prestressed Hollow Core Floors," Recommendations, Fédération Internationale de la Précontrainte, Thomas Telford, London, 31 pp

FIP, 1996; "Precast Prestressed Hollow Core Floors," Recommendations, Part 2, Second Draft, Fédération Internationale de la Précontrainte

France, R., 1996; Personal Communication. (Quality Control Manager, Richard Lees Ltd., Derby)

Girhammar, U-A., 1992; "Design Principles for Simply-Supported Prestressed Hollow Core Slabs," Structural Engineering Review, Vol. 4, No. 4, pp 301-316

Girhammar, U-A. & Pajari, M., 1995; "Shear Capacity of Notched Prestressed Hollow Core Slabs with Circular Voids," Structural Engineering Review, Vol. 7, No. 2, pp 63-74

Glavind, M., Munch-Petersen, C. & Pedersen, E.J., 1994; "Framework Programme 1989-92 Fibre Reinforced Concrete," Nordic Concrete Research, Publication No. 14, 1/94, pp 6-25

Gopalaratnam, V.S., 1997; Personal Communication. (Associate Professor, Dept. of Civil Engineering, University of Missouri, U.S.A)

Gopalaratnam, V.S. & Gettu, R., 1994; "On the Characterisation of Flexural Toughness in FRC," Proceedings of Workshop on Fibre Cement and Concrete, University of Sheffield, 28-30 July 1994, pp 373-387

✓ Gopalaratnam, V.S., Shah, S.P., Batson, G.B., Ramakrishnan, V. & Wecharatana, M., 1991; "Fracture Toughness of fiber Reinforced Concrete," ACI Materials Journal, Vol.88, No.4, pp 339-353

Greenhalgh, J., 1995; Personal Communication. (Technical Sales Representative, Bekaert Building Products, Sheffield)

Hannant, D.J., 1978; "Fibre Cements and Fibre Concretes," John Wiley and Sons, 219pp

Hansen, E.Aa., 1996; "Determination of the Tensile Strength of Concrete," Nordic Concrete Research, Publication No. 17, pp 1-17

Hara, T., 1984; "Effects of Steel Fiber on Shear Transfer," Transactions of the Japan Concrete Institute, Vol. 6, pp 425-432

Hodgkinson, L., 1996; Personal Communication. (Product Manager, W.R. Grace Construction Products, Warrington)

Holmgren, J., 1985; "Advanced Tunnel Support using Steel Fibre Reinforced Shotcrete," Steel Fiber Concrete, US-Sweden Joint Seminar, Stockholm, 3-5 June 1985, pp 361-376

Imam, I., Vandewalle, L., Mortelmans, F. & Van Gemert, D., 1997; "Shear Domain of Fibre-Reinforced High-Strength Concrete Beams," Engineering Structures, Vol. 19, No. 9, pp 738-747

Japan Concrete Institute, 1983a; "Method of Making Fiber Reinforced Concrete in the Laboratory," JCI Standard SF1, JCI Standards for Test Methods of Fiber Reinforced Concrete

Japan Concrete Institute, 1983b; "Method of Test for Flexural Strength and Flexural Toughness of Fiber Reinforced Concrete," JCI Standard SF4, JCI Standards for Test Methods of Fiber Reinforced Concrete, pp 35-36

Japan Concrete Institute, 1983c; "Method of Tests for Compressive Strength and Compressive Toughness of Fiber Reinforced Concrete," JCI Standard SF5, JCI Standards for Test Methods of Fiber Reinforced Concrete

Johnston, C.D., 1982; "Definition and Measurement of Flexural Toughness Parameters for Fiber Reinforced Concrete," Cement, Concrete and Aggregates, CCAGDP, Vol.4, No. 2, pp 53-60

Johnston, C.D., 1985; "Toughness of Steel Fiber Reinforced Concrete," Steel-Fiber Concrete US-Sweden Joint Seminar, Stockholm, Sweden, 3-5 June 1985, pp 333-359

Juvas, K., 1996; "Superplasticizers for No-Slump Concrete," Proceedings - Nordic Concrete Research Meeting, Espoo, Finland, p 59

Khaloo, A.R. & Kim, N., 1997; "Influence of Concrete and Fiber Characteristics on Behaviour of Steel Fiber Reinforced Concrete under Direct Shear," ACI Materials Journal. Vol. 94, No. 6, pp 592-601

Lanu, M., 1995; "Testing Fibre-Reinforced Concrete in some Structural Applications," Report No. 237, Technical Research Centre of Finland, Espoo, Finland

Li, V.C., 1992; "Postcrack Scaling Relations for Fiber Reinforced Cementitious Composites," Journal of Materials in Civil Engineering, ASCE, Vol. 4, No. 1, pp 41-57

Li, V.C., Stang, H. & Krenchel, H., 1993; "Micromechanics of Crack Bridging in Fibre-Reinforced Concrete," Materials and Structures, Vol. 26, pp 486-494

Li, V.C. & Maalej, M., 1996; "Toughening in Cement Based Composites. Part II: Fiber Reinforced Cementitious Composites," Cement and Concrete Composites, Vol. 18, No. 4, pp 239-250

Lim, T.Y., Paramasivam, P. & Lee, S.L., 1987; "Analytical Model for Tensile Behaviour of Steel-Fiber Concrete," ACI Materials Journal, Vol. 84, No. 4, pp 286-298

Lin Yang, 1995; "Design of Prestressed Hollow Core Slabs with Reference to Web Shear Failure," Journal of Structural Engineering, ASCE, Vol. 120, No. 9, pp 2675-2696

Lorentsen, M., 1985; "Steel Fibre Concrete for Structural Elements," Steel Fiber Concrete, US - Sweden Joint Seminar, 3-5 June 1985, Stockholm, Sweden, pp 421-442

✓ Maalej, M. & Li, V.C., 1994; "Flexural Strength of Fiber Cementitious Composites," Journal of Materials in Civil Engineering, Vol. 6, No. 3, pp 390-406

Maidl, B.R., 1995; "Steel Fibre Reinforced Concrete," Ernst & Sohn, 292 pp

✓ Mangat, P.S. & Gurusamy, K., 1987; "Flexural Strength of Steel Fibre-Reinforced Cement Composites," Journal of Materials Science, Vol. 22, pp 3103-3110

Mansur, M.A., Ong, K.C.G. & Paramasivam, P., 1986; "Shear Strength of Fibrous Concrete Beams without Stirrups," Journal of Structural Engineering, ASCE, Vol. 112, No. 9, pp 2066-2079

Marshall, W.T., 1974; "Torsion in Concrete and CP 110," Structural Engineer, Vol. 52, pp 83-88

Martin, L.D. & Scott, N.L., 1976; "Development of Prestressing Strand in Pretensioned Members," ACI Journal, Vol. 73, No. 8, pp 453-456

Moens, J. & Nemegeer, D., 1991; "Designing Fibre Reinforced Concrete Based on Toughness Characteristics," Concrete International, Vol.13, No.11, pp 38-43

Morgan, D.R., Mindess, S. & Chen, L., 1995; "Testing and Specifying Toughness for Fibre Reinforced Concrete and Shotcrete," Second University - Industry Workshop on Fibre Reinforced Concrete and Other Advanced Composites, Toronto, Canada, 26-29 March 1995

Nammur Jr., G. & Naaman, A.E., 1989; "Bond Stress Model for Fiber Reinforced Concrete Based on Bond Stress-Slip Relationship," ACI Materials Journal, Vol. 86, No. 1, pp 45-57

Nanni, A., 1988; "Splitting-Tension Test for Fiber Reinforced Concrete," ACI Materials Journal, Vol. 85, No. 4, pp 229-233

Narayanan, R. & Darwish, I.Y.S., 1987a; "Shear in Prestressed Concrete Beams containing Steel Fibres," International Journal of Cement Composites and Lightweight Concrete, Vol.9, pp 81-90

Narayanan, R. & Darwish, I.Y.S., 1987b; "Use of Steel Fibres as Shear Reinforcement," ACI Structural Journal, Vol.84, No.3, pp 216-227

Narayanan, R.N. & Kareem-Palanjian, A.S., 1984; "Effect of Fibre Addition on Concrete Strengths," Indian Concrete Journal, Vol. 58, No. 4, pp 100-103

Narayanan, R.N. & Kareem-Palanjian, A.S., 1986; "Torsion, Bending, and Shear in Prestressed Concrete Beams Containing Steel Fibers," ACI Journal, Vol. 83, No. 3, pp 423-431

Nemegeer, D., 1995 & 1997; Personal Communication. (Bekaert Building Products, Zwevegem, Belgium)

Nemegeer, D. & Tatnall, P.C., 1995; "Measuring Toughness Characteristics of SFRC - A Critical View of ASTM C 1018," ACI SP-155 Testing of Fiber Reinforced Concrete.

Nemegeer, D. & Teutsch, M., 1993; "Advantages and Fields of Application of Concrete with Reinforcing Fibrous Steel," Concrete Precasting Plant and Technology, 11/1993, pp 74-80

Neville, A.M., 1981; "Properties of Concrete," 3rd Edition, Longman Scientific and Technical, 779 pp

Omar, W., 1990; "Diaphragm Action in Precast Concrete Floor Construction," PhD Thesis, University of Nottingham, 234 pp

Paine, K.A., 1995; "Prestressed Fibre Reinforced Concrete," Research Report SR 95 023, Department of Civil Engineering, University of Nottingham, 104 pp

Paine, K.A., 1996; "Trial Production of Fibre Reinforced Hollow Core Slab," Research Report SR 96 007, Department of Civil Engineering, University of Nottingham, 38 pp

Paine, K.A., Elliott, K.S. & Peaston, C.H., 1997; "Increasing the Shear Strength and Ductility of Prestressed Hollow Core Slabs using Metal Fibres," Fourth International Symposium on Noteworthy Developments in Prestressing and Precasting, Singapore, 3-4 July 1997, pp 116-124

Paine, K.A. & Peaston, C.H., 1997; Unpublished Compressive and Flexural Test Data on Crimped and Hooked-End Steel Fibre Reinforced Concrete, Department of Civil Engineering, University of Nottingham

Pajari, M., 1989; "Design of Prestressed Hollow Core Slabs," Research Report 657, Technical Research Centre of Finland, Espoo, Finland, 137 pp

Pajari, M., 1991; "Cracking and Shear Capacity of Prestressed Hollow Core Slabs," IABSE Colloquium (International Association for Bridge and Structural Engineering), Stuttgart, Germany, pp 697-702

Pajari, M. & Lin Yang, 1994; "Shear Capacity of Hollow Core Slabs on Flexible Supports," Research Report 1587, Technical Research Centre of Finland, Espoo, Finland, 137 pp

PCI, 1991; "Manual for the Design of Hollow Core Slabs," Buettner, D.R. and Becker, R.J., Precast/Prestressed Concrete Institute

Peaston, C.H., 1993; "Production, Properties and Design of Sprayed Fibre Concrete," PhD Thesis, Loughborough University of Technology

Peiffer, G., 1994; "Mix Design and Mechanical Properties of High Performance Concretes reinforced with Amorphous Metallic Fibres," CONCHEM International Conference, 22-24 November 1994, pp 139-151

Pisanty, A., 1992; "The Shear Strength of Extruded Hollow-Core Slabs," Materials and Structures, RILEM, Vol. 25, pp 224-230

Pisanty, A. & Regan, P.E., 1991; "Direct Assessment of the Tensile Strength of the Web in Prestressed Precast Hollow-Core Slabs," Materials and Structures, RILEM, Vol. 24, pp 451-454

prEN 1168, 1995; "Precast Prestressed Hollow Core Elements," CEN TC 229, European Standard, Comité Européen de Normalisation, 10th Draft, 52 pp

Rajagopal, R.S. and Siddappa, S., 1992; "Experimental Investigation on Fiber Reinforced Prestressed Concrete Beams under Shear," Fibre Reinforced Cement and Concrete -Proceedings of the 4th International Symposium held by RILEM, Sheffield, 20-23 July 1992, pp 554-570

Richardson, J.G., 1973; "Precast Concrete Construction," Cement and Concrete Association, 232 pp

RILEM Technical Committee 162, 1997; "Test and Design Methods for Steel Fibre Reinforced Concrete," Minutes of the 5th Meeting, Barcelona, Spain, 2-3 June 1997

Robins, P.J., Austin, S.A. & Jones, P.A., 1996; "Flexural Strength Modelling of Steel Fibre Reinforced Sprayed Concrete," *Sprayed Concrete Technology*, E & F N Spon, pp 107-114; "

Romualdi, J.P. & Mandel, J.A., 1964; "Tensile Strength of Concrete affected by Uniformly Distributed and Closely-Spaced Short Lengths of Wire Reinforcement," *ACI Journal*, V.61, No.6, pp 657-671

Rose, D.R. & Russell, B.W., 1997; "Investigation of Standardized Tests to Measure the Bond Performance of Prestressing Strand," *PCI Journal*, Vol. 42, No. 4, pp 56-80

Rossi, P., 1992; "Mechanical Behaviour of Metal-Fibre Reinforced Concretes," *Cement and Concrete Composites*, No. 14, pp 3-16

Sebaratnam, C.M. & Rangan, B.V., 1992; "Shear Strength of Extruded Prestressed Hollow Core Planks," *Transactions of The Institution of Engineers, Australia*, Vol. CE34, No. 2, pp151-157

Sharma, A.K., 1986; "Shear Strength of Steel Fiber Reinforced Concrete Beams," *ACI Journal*, Vol. 83, No. 4, pp 624-628

Shin, S.W., Oh, J.G. & Ghosh, S.K., 1994; "Shear Behaviour of Laboratory-Sized High Strength Concrete Beams Reinforced with Bars and Steel Fibers," *ACI SP 142 - Fiber Reinforced Concrete - Developments and Innovations*, pp 187-200

Soroushian, P. & Lee, C.M., 1990; "Distribution and Orientation of Fibers in Steel Fiber Reinforced Concrete," *ACI Materials Journal*, Vol. 87, No. 5, pp 433-439



Soroushian, P., Mirza, F. & Alhozaimy, A., 1994; "Bonding of Confined Steel Fiber Reinforced Concrete to Deformed Bars," ACI Structural Journal, Vol. 91, No. 2, pp 141-149

Sparrow, J., 1992; "Italian Precaster lead Development of Deep Section Slide Forming," Concrete Plant and Production, Jan. 1992

Stang, H., 1992; "Evaluation of Properties of Cementitious Materials," High Performance Fiber Reinforced Cement Composites, Proceedings of International RILEM/ACI Workshop, pp 388-406

Stang, H. & Aarre, T., 1992; "Evaluation of Crack Width in FRC with Conventional Reinforcement," Cement and Concrete Composites, Vol. 14, pp 143-154

Swamy, R.N. & Al-Noori, K., 1974; "Bond Strength of Steel Fiber Reinforced Concrete," Concrete, Vol. 8, No. 8, pp 36-37

Swamy, R.N. & Al-Ta'an, S., 1981; "Deformation and Ultimate Strength in Flexure of Reinforced Concrete Beams made with Steel Fibre Concrete," ACI Journal, Vol. 78, No. 5, pp 395-405

Swamy, R.N. & Bahia, H.M., 1979; "Influence of Fiber Reinforcement on the Dowel Resistance to Shear," ACI Journal, Vol. 76, No. 2, pp 327-355

Swamy, R.N. & Bahia, H.M., 1985; "The Effectiveness of Steel Fibers as Shear Reinforcement," Concrete International, Vol. 7, No. 3, pp 35-40

Swamy, R.N., Jones, R. & Chiam, T., 1993; "Influence of Steel Fibers on the Shear Resistance of Lightweight Concrete I-Beams," ACI Structural Journal, Vol. 90, No.1, pp 103-114

Taerwe, L., 1991; "Brittleness versus Ductility of High Strength Concrete," Structural Engineering International, No. 4, pp 40-45

Tan, K.H. & Mansur, M.A., 1990; "Shear Transfer in Reinforced Fiber Concrete," *Journal of Materials in Civil Engineering*, ASCE, Vol. 2, No. 4, pp 202-214

Tan, K.H., Murugappan, K. & Paramasivam, P., 1993; "Shear Behaviour of Steel Fiber Reinforced Concrete Beams," *ACI Structural Journal*, V.90, No.1, pp 3-11

Tan, K.H., Paramasivam, P. & Murugappan, K., 1995; "Steel Fibers as Shear Reinforcement in Partially Prestressed Beams," *ACI Structural Journal*, V.92, No.6, pp 643-652

Tassios, T.P. & Vintzeleou, E.N., 1987; "Concrete-to-Concrete Friction," *Journal of Structural Engineering*, ASCE, Vol. 113, No. 4, pp 832-849

Thompson, I., 1998; Unpublished Research on Fibres in Cement Bound Pavement Bases, University of Nottingham

Trottier, J-F. & Banthia, N., 1994; "Concrete Reinforced with Deformed Steel Fibers: Toughness Characterization and Bond-Slip Mechanisms," *Proceedings of Workshop on Fibre Cement and Concrete*, University of Sheffield, 28-30 July 1994, pp 212-236

Ueda, T. & Stitmannathum, B., 1991; "Shear Strength of Precast Prestressed Hollow Slabs with Concrete Topping," *ACI Structural Journal*, Vol. 88, No. 4, pp 402- 410

Valle, M. & Buyukozturk, O., 1994; "Behavior of Fiber Reinforced High Strength Concrete under Direct Shear," *ACI SP 142 - Fiber Reinforced Concrete - Developments and Innovations*, pp 201-233

Van de Loock, L., 1987; "Influence of Steel Fibers on the Shear Transfer in Cracks," *Proceedings of the International Symposium on Fibre Reinforced Concrete*, Madras, India, 16-19 December 1987, pp 1.102-1.113

Vandewalle, L. & Mortelmans, F., 1995; "Anchorage of Strands," PCI-FIP XIIth International Congress, Precast Prestressed Concrete Structures and Details, May 29 - June 2 1994, Washington D.C., U.S.A., Vol. 2, pp J16-J22

Walraven, J.C. & Mercx, W.P.M., 1983; "The Bearing Capacity for Prestressed Hollow Core Slabs," Heron, Vol. 28, No. 3, 46 pp

Weiler, B. & Grosse, C., 1996; "Pullout Behaviour of Fibers in Steel Fiber Reinforced Concrete," (Unknown source), pp 116-127

## APPENDIX A

### FIBRE CHARACTERISTICS

#### A.1. HS fibres

##### Dramix ZP 30/.5

produced by N.V. Bekaert

Description: Hooked-end steel wire fibres collated into bundles of about 30 with a water soluble adhesive

nominal length (mm)	diameter $d_f$ (mm)	aspect ratio $l/d_f$	tensile strength $f_m$ (N/mm <sup>2</sup> )	density (kg/m <sup>3</sup> )
30	0.5	60	1100 *	7800

\* strength of hook about 900 N/mm<sup>2</sup> (Nemegeer 1997)

##### A.1.1. Example calculation of critical fibre length for HS fibres

$$r = \frac{\pi d_f^2}{4} \cdot \frac{1}{\pi d_f} = 0.125$$

assuming  $\tau_f = 7$  N/mm<sup>2</sup> (Nemegeer 1997) then

$$l_{crit} = \frac{2rf_m}{\tau_f} = \frac{275}{7} = 39\text{mm} > l_f$$

and therefore  $\eta_1 = 0.5$  (Equation 2-3)

### A.1.2. Example calculation of critical fibre volume for HS fibres

Take concrete uniaxial tensile strength as 4 N/mm<sup>2</sup>. Can assume that Youngs modulus of fibre reinforced concrete and plain concrete matrix are equal, therefore

$$V_{f,crit} = \frac{\sigma_c}{\eta_0 \eta_l f_{fu}} = \frac{4}{0.41 * 0.5 * 1100} = 1.8\%$$

### A.2. AM fibres

**Fibraflex FF30L6**  
produced by Seva

Description: ribbon shaped amorphous metal fibre

nominal length (mm)	width w (mm)	thickness t (μm)	aspect ratio *	tensile strength (N/mm <sup>2</sup> )	density (kg/m <sup>3</sup> )
30	1.6	50	309	1400 - 2300 <sup>b</sup>	7200

<sup>b</sup> typical mean value of 1900 N/mm<sup>2</sup> (Boucharet, personal communication)

\* equivalent circular diameter taken as four-times cross-sectional area divided by fibre perimeter

Composition: (Fe,Cr)<sub>80</sub>(P,C,Si)<sub>20</sub>

#### A.2.1. Example calculation of critical fibre length for AM fibres

$$r = \frac{w \cdot t}{2(w + t)} = \frac{1.6 * 0.05}{2(1.6 + 0.05)} = 0.024$$

assuming a very conservative value of  $\tau_r = 4$  N/mm<sup>2</sup> then

$$l_{crit} = \frac{2 * 0.024 * 1900}{4} = 23mm < l_f$$

and therefore

$$\eta_l = 1 - \frac{l_{crit}}{2l_f} = 1 - \frac{23}{60} = 0.62 \quad (\text{Equation 2-3})$$

### A.2.2. Example calculation of critical fibre volume for AM fibres

Take concrete uniaxial tensile strength as 4 N/mm<sup>2</sup>. Can assume that Youngs modulus of fibre reinforced concrete and plain concrete matrix are equal, therefore

$$V_{f,crit} = \frac{\sigma_c}{\eta_\theta \eta_l f_{fu}} = \frac{4}{0.41 * 0.62 * 1900} = 0.8\%$$

## **APPENDIX B**

### **FLEXURAL TOUGHNESS TEST RESULTS**

**B.1 ASTM C 1018 Toughness Indices for pull-out bond and shear test mixes**

**B.2 Cracking, ultimate and equivalent flexural strengths for pull-out and shear test mixes**

### B.1. ASTM C 1018 Toughness Indices for pull-out bond and shear test mixes

	$I_5$				$I_{10}$				$I_{20}$				$R_{5,10}$				$R_{10,20}$			
	i	ii	iii	c.v.	i	ii	iii	c.v.	i	ii	iii	c.v.	i	ii	iii	c.v.	i	ii	iii	c.v.
B-1.0	3.6	4.7	5.2	18.7	7.8	9.7	10.7	15.4	17.3	18.5	21.3	10.9	85.2	100.4	109.2	12.3	94.4	87.6	106.4	9.9
B-1.5	4.4	4.8	4.8	12.2	9.2	10.4	10.2	6.6	18.4	21.6	20.3	8.0	95.0	112.6	109.4	8.9	92.0	111.5	100.5	9.7
B-2.0	4.7	5.5	5.9	11.2	11.0	12.6	13.1	8.9	23.6	26.7	27.7	8.4	126.0	143.2	144.0	7.3	125.6	140.7	146.4	7.8
PB9	4.0	4.4	4.4	6.1	8.1	9.4	9.6	9.0	16.4	19.8	18.3	9.4	83.2	99.7	104.5	11.7	82.8	103.9	86.4	12.4
PB10	4.4	5.1	4.2	9.5	9.8	10.4	10.3	3.2	18.3	21.1	21.8	9.1	108.3	107.5	120.8	6.6	85.1	106.9	115.0	15.1
PB11	4.4	5.6	5.3	12.9	10.0	11.9	11.3	8.8	20.4	27.0	23.3	14.0	112.0	125.3	120.5	5.6	104.3	151.5	120.3	19.1
PB12	6.2	4.9	4.9	13.7	12.1	11.3	9.6	11.6	25.7	22.6	19.5	13.7	117.9	126.5	94.6	14.6	136.3	113.7	99.0	16.2
PB13	5.0	5.1	4.9	2.2	12.4	10.1	11.7	10.3	25.1	19.0	25.1	15.3	147.6	99.0	136.7	20.0	127.2	89.4	133.8	20.5
PB14	4.2	4.8	5.2	10.4	9.4	10.3	10.1	4.8	19.5	20.0	20.8	3.3	104.1	110.4	98.2	5.9	100.7	97.4	107.0	4.8
PB15	4.9	5.3	4.6	6.3	11.9	11.9	10.1	9.2	23.7	25.5	20.7	10.4	140.0	132.3	109.6	12.4	118.2	136.3	105.8	12.8
PB16	4.6	4.5	4.9	3.7	8.6	8.5	8.4	1.2	18.6	17.5	16.8	5.1	78.6	78.2	70.4	6.1	100.7	90.2	84.2	9.1
PB17	3.8	4.4	-	10.1	7.5	8.7	-	10.5	14.3	17.1	-	12.6	72.6	85.8	-	11.8	68.9	83.9	-	13.9
PB19	3.5	4.7	-	21.2	6.5	8.5	-	18.9	12.1	15.2	-	16.1	60.0	76.3	-	16.9	55.6	66.7	-	12.8
PB20	2.6	2.4	-	4.0	3.4	3.1	-	6.5	3.9	3.5	-	7.6	15.4	12.8	-	13.0	5.4	4.0	-	21.1
PB21	3.8	4.1	4.6	10.2	6.0	6.4	7.3	10.1	9.6	9.8	-	1.5	44.1	45.3	53.8	11.1	-	31.8	25.0	16.9
PB22	4.7	4.3	4.6	4.4	9.0	9.6	9.2	3.3	14.2	14.8	14.2	2.4	87.3	106.5	91.6	10.6	51.3	52.1	50.0	2.1



## B.2. Cracking, ultimate and equivalent flexural strengths for pull-out and shear test mixes

	$f_{\Omega,cr}$				$f_{\Omega,ult}$				$f_{\Omega,eq,150}$				$f_{\Omega,eq,300}$			
	i	ii	iii	c.v.	i	ii	iii	c.v.	i	ii	iii	c.v.	i	ii	iii	c.v.
B-1.0	6.07	5.29	5.36	7.7	6.81	6.36	6.66	3.5	-	-	-	-	6.07	4.95	5.60	10.1
B-1.5	6.28	5.44	5.44	8.4	7.44	7.68	6.63	7.6	-	-	-	-	6.53	6.47	6.03	4.3
B-2.0	5.93	6.39	5.99	4.1	9.56	10.45	8.69	9.2	-	-	-	-	-	8.99	8.09	7.5
PB9	7.45	8.72	8.55	8.4	7.45	8.74	8.55	8.4	4.75	5.50	5.00	7.5	6.00	7.04	6.31	8.3
PB10	7.94	7.87	7.81	5.2	7.94	8.54	9.56	9.4	5.51	6.92	6.77	12.1	6.23	7.53	7.96	12.4
PB11	6.87	7.22	7.01	2.5	6.96	8.67	7.29	11.9	4.81	5.83	5.22	9.7	5.83	7.11	6.30	10.1
PB12	8.50	8.22	7.60	5.7	11.10	9.97	7.73	17.9	6.70	6.56	6.18	4.2	8.70	7.83	7.03	10.6
PB13	8.45	8.81	8.38	2.7	11.10	10.23	9.52	7.7	7.70	6.79	8.41	10.6	5.87	5.35	6.49	9.7
PB14	7.64	6.82	7.73	6.8	8.63	8.47	8.41	1.3	5.87	5.35	6.49	9.7	6.83	6.37	7.34	7.1
PB15	8.35	8.36	7.49	6.2	10.13	10.82	9.31	7.5	7.34	7.79	6.67	7.8	8.59	9.14	7.73	8.4
PB16	6.71	8.21	7.80	10.2	6.71	8.21	7.80	10.2	4.77	5.10	5.01	3.4	5.59	6.33	5.64	7.1
PB17	6.95	5.12	-	21.4	6.95	5.12	-	21.4	3.74	-	4.06	5.8	4.57	-	4.54	0.5
PB18	7.34	6.63	6.59	6.2	7.34	6.63	6.59	6.2	-	-	-	-	-	-	-	-
PB19	8.02	7.97	-	0.4	8.02	7.97	-	0.4	3.70	-	4.01	5.7	4.48	-	4.99	7.6
PB20	7.28	7.81	7.77	3.9	7.28	7.81	7.77	3.9	-	-	-	-	-	-	-	-
PB21	7.47	8.10	9.45	12.1	7.47	8.10	9.45	12.1	-	1.23	-	-	-	2.08	2.36	8.9
PB22	8.30	8.87	9.09	4.7	8.30	8.87	9.64	7.5	2.16	2.31	2.73	12.3	3.66	3.90	4.41	9.6

**APPENDIX C**

**MIX PROPORTIONS FOR  
MAIN TRIAL HOLLOW CORE SLABS**

**C.1**

Mixes 1, 2, and 3

**C.2**

Mixes 4, 5, and 6

**C.3**

Mixes 7 and 8

# C.1

## TRIAL 1

Fibre Reinforced Concrete Hollow Core Mixes.  
0.5 % HS fibres (all mixes)

Date: 12th September 1996

	Mix 1		Mix 2		Mix 3	
	Batch Weight (kg)	Weight per cubic metre (kg/m <sup>3</sup> )	Batch Weight (kg)	Weight per cubic metre (kg/m <sup>3</sup> )	Batch Weight (kg)	Weight per cubic metre (kg/m <sup>3</sup> )
Sand	463	709	473	724	480	735
10 mm aggregate	455	697	451	691	444	680
14 mm aggregate	337	516	339	519	338	518
RHPC	200	306	202	309	200	306
PFA	57	87	59	90	60	92
Water	88	135	82	126	79	121
Steel Fibres	26.8	39	26.8	39	26.8	39

	Mix 1	Mix 2	Mix 3
water/cementitious material	0.34	0.31	0.30
aggregate/cementitious material	4.89	4.85	4.85
sand/(sand and coarse aggregate)	0.37	0.37	0.38
coarse agg to total agg by volume	63%	62%	62%

## C.2

### TRIAL 2 Fibre Reinforced Concrete Hollow Core Mixes. 0.5 % HS fibres (Mixes 4 & 5), 1% HS fibres (Mix 6)

Date: 24th October 1996

	Mix 4		Mix 5		Mix 6	
	Batch Weight (kg)	Weight per cubic metre (kg/m <sup>3</sup> )	Batch Weight (kg)	Weight per cubic metre (kg/m <sup>3</sup> )	Batch Weight (kg)	Weight per cubic metre (kg/m <sup>3</sup> )
Sand	479	733	480	735	480	735
10 mm aggregate	442	677	440	674	449	688
14 mm aggregate	345	528	339	519	337	516
RHPC	202	309	200	306	202	309
PFA	60	92	58	89	60	92
Water	70	107	73	112	73	112
Steel Fibres	26.8	39	26.8	39	53.6	78

	Mix 4	Mix 5	Mix 6
water/cementitious material	0.27	0.28	0.28
aggregate/cementitious material	4.83	4.88	4.84
sand/(sand and coarse aggregate)	0.38	0.38	0.38
coarse agg to total agg by volume	62%	62%	62%

## C.3

### TRIAL 3

Fibre Reinforced Concrete Hollow Core Mixes.  
0.5 % HS fibres(Mix 7), 0.28% AM fibres(Mix 8)

Date: 19th December 1996

	Mix 7		Mix 8		Mix 9	
	Batch Weight (kg)	Weight per cubic metre (kg/m <sup>3</sup> )	Batch Weight (kg)	Weight per cubic metre (kg/m <sup>3</sup> )	Batch Weight (kg)	Weight per cubic metre (kg/m <sup>3</sup> )
Sand	517	792	508	778		
10 mm aggregate	444	680	443	678		
14 mm aggregate	329	504	339	519		
RHPC	234	358	236	361		
PFA	0	0	0	0		
Water	59	90	61	93		
Steel Fibres	26.8	41	13	20		

	Mix 7	Mix 8	Mix 9
water/cementitious material	0.25	0.26	
aggregate/cementitious material	5.52	5.47	
sand/(sand and coarse aggregate)	0.40	0.39	
coarse agg to total agg by volume	60%	60%	

## APPENDIX D

### GRILLAGE ANALYSIS OF HOLLOW CORE SLABS

#### D.1 Grillage Analysis

Grillage analysis<sup>1</sup> was carried out using QSE, a commercially available structural analysis package which uses a stiffness matrix method with Choleski decomposition.

The Grillage analysis used a planegrid structure. Since a 200 mm deep hollow core slab has seven webs, it was assumed that this could be modelled as seven independent members of geometrical property shown in C.3 in the y-plane. Transverse properties (x plane) are also shown in C.3. Material properties are given in C.2

#### C.2. Material properties

The following properties were assumed for fibre reinforced hollow core slabs

$$E = 36 \text{ kN/mm}^2$$

$$G = 13.8 \text{ kN/mm}^2$$

$$\mu = 0.2$$

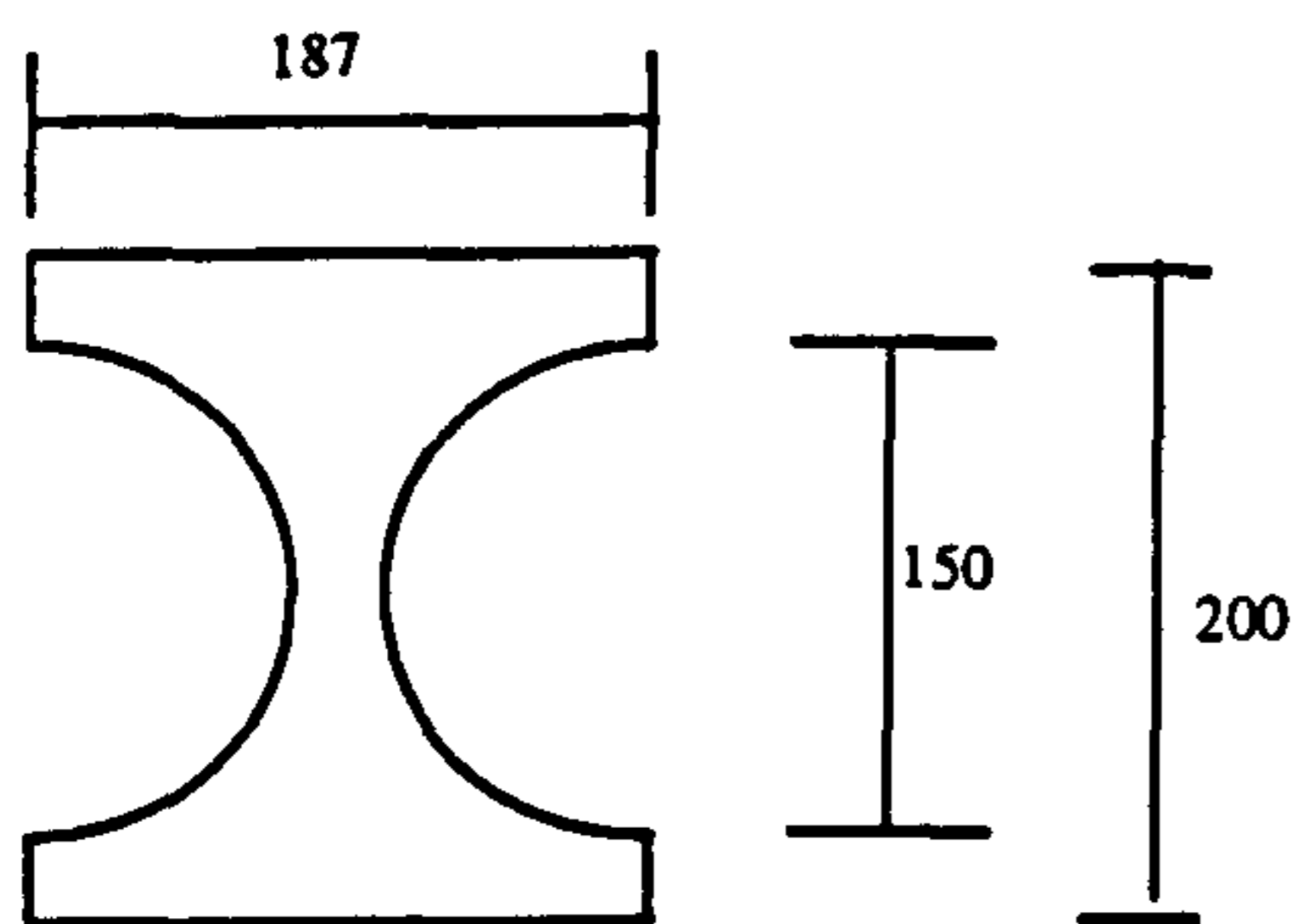
$$\text{density} = 2400 \text{ kg/m}^3$$

---

<sup>1</sup> see E.C. Hambly, "Bridge Deck Behaviour," Second Edition, 1991

### C.3 Geometrical properties

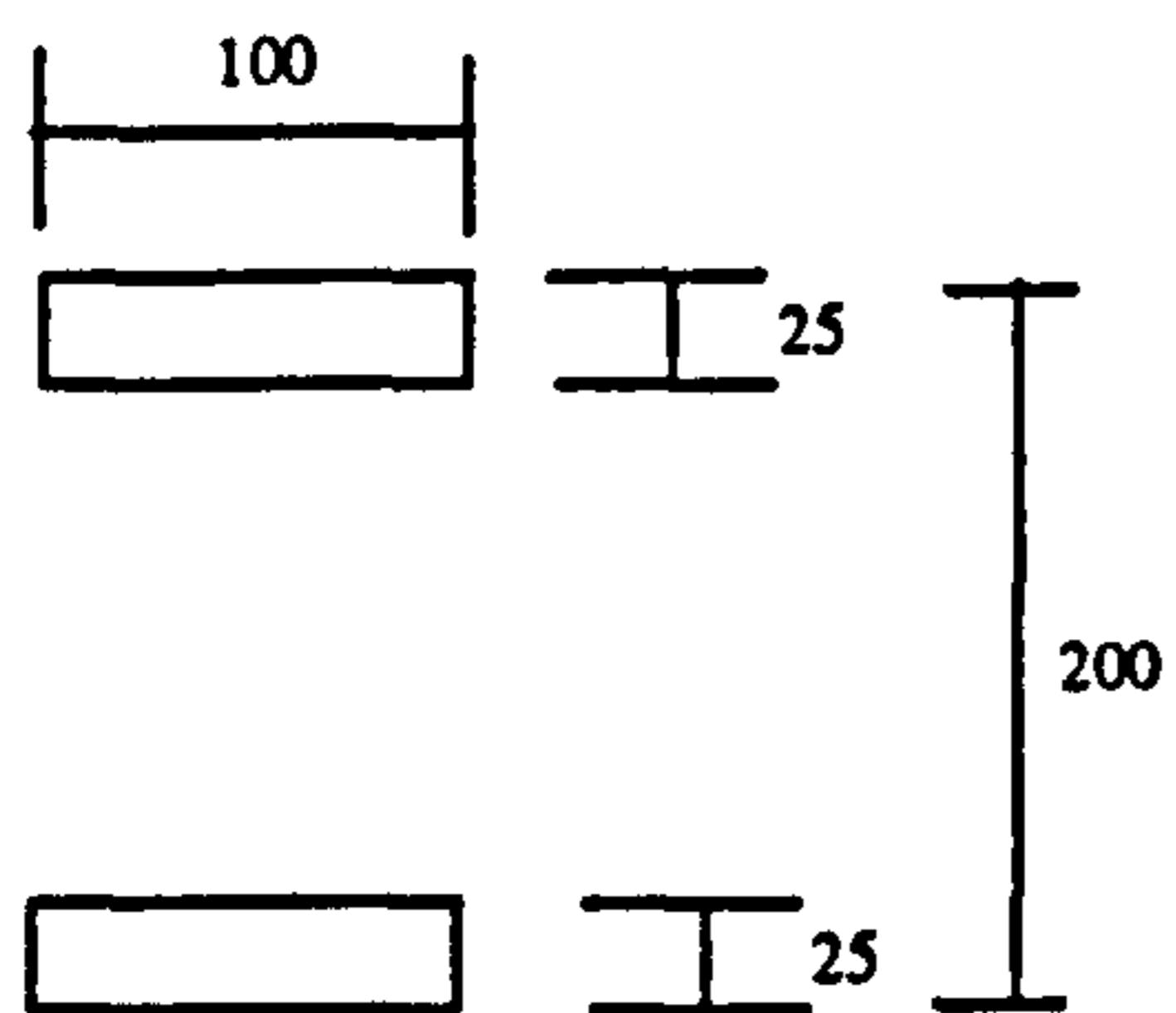
#### Y plane



$$I_x = 99.8 \times 10^6 \text{ mm}^4$$

$$J_x = 184 \times 10^6 \text{ mm}^4$$

#### X Plane



$$I_x = 38.5 \times 10^6 \text{ mm}^4$$

$$J_x = 40.6 \times 10^6 \text{ mm}^4$$

## APPENDIX E

### NET DEFLECTION OF SHEAR TESTS

#### E.1. Theoretical net deflection

A theoretical equation for the deflection ( $\delta_{th}$ ) of the beams and slabs in the shear tests was obtained from the theory of virtual work as a combination of a bending deformation ( $\delta_b$ ) and a shear ( $\delta_s$ ) deformation

$$\delta_{th} = \delta_b + \delta_s \quad \text{.. E-1}$$

where

$$\delta_b = \frac{P}{EI} \left( \frac{b^2 a^3}{3L^2} + a^2 b - a^3 - \frac{a^2 b^2}{L} + \frac{a^4}{L} + \frac{b^3 a^2}{3L^2} - \frac{a^5}{3L^2} \right) \quad \text{.. E-2}$$

$$\delta_s = \frac{6W}{5L^2} \left( \frac{ab^2 + a^2 b - a^3}{GA} \right) \quad \text{.. E-3}$$

where  $W$  = load,  $E$  = Young's modulus,  $G$  = shear modulus,  $a$  = shear span,  $l$  = span,  $b = l - a$ .

The theoretical net deflection of a 200 mm deep hollow core slab (Slab F9) over a 1.9 m span is shown in Figure E-1.



## **E.2. Experimental net deflection**

### **E.2.1 Ground LPs**

In all tests on slabs and x-beams, deflections were measured by recording the movement of the soffit by linear potentiometers (LP's) attached to the ground. This result gives a gross deflection since it does not account for settlement of the bearing, crushing of the specimen at the support and other extraneous deformations.

To try to obtain net deflections from these gross deflections, a load test was performed on the support and bearing plate to measure the amount of settlement under load. The average deformation (of four LP's) is shown in Figure E-2.

Figure E-3 shows the deformation as subtracted from the direct ground LP readings to give "net deflection". It can be seen that it does not closely relate to the theoretical net deflection. It was therefore not possible to obtain net deflections from these ground LP readings.

### **E.2.2 Deflection bar**

In later tests a deflection bar was hung from the slabs (Figure 7-1) to measure deflection independent of extraneous deformations. However, due to the test set-up this bar was not attached directly over the bearing point but approximately 75 mm into the span. The deflection obtained from the deflection bar is therefore lower than the actual net deflection.

To try to compensate for this, the theoretical extra deflection expected over a distance of 75 mm was estimated using the structural analysis package described in Appendix D. This deflection was then added to the deflection measured using the deflection bar. The results are shown in Figure E-4. Although this gives a much better result than the ground LP's it is still markedly lower than the theoretical net deflection.

### **E.2.2 LP's on top of slabs and beam**

Finally, for some tests LP's were situated on top of the slab directly over the bearing point as shown in Figure 7-1. The deflection measured in these LP's was then subtracted from the ground LP's to give net deflection. A typical result from laboratory-cast x-beam PB19 is shown in Figure E-5. It can be seen that this method of obtaining net deflection gives very similar results to the theoretical deflection obtained using Equation E-1.

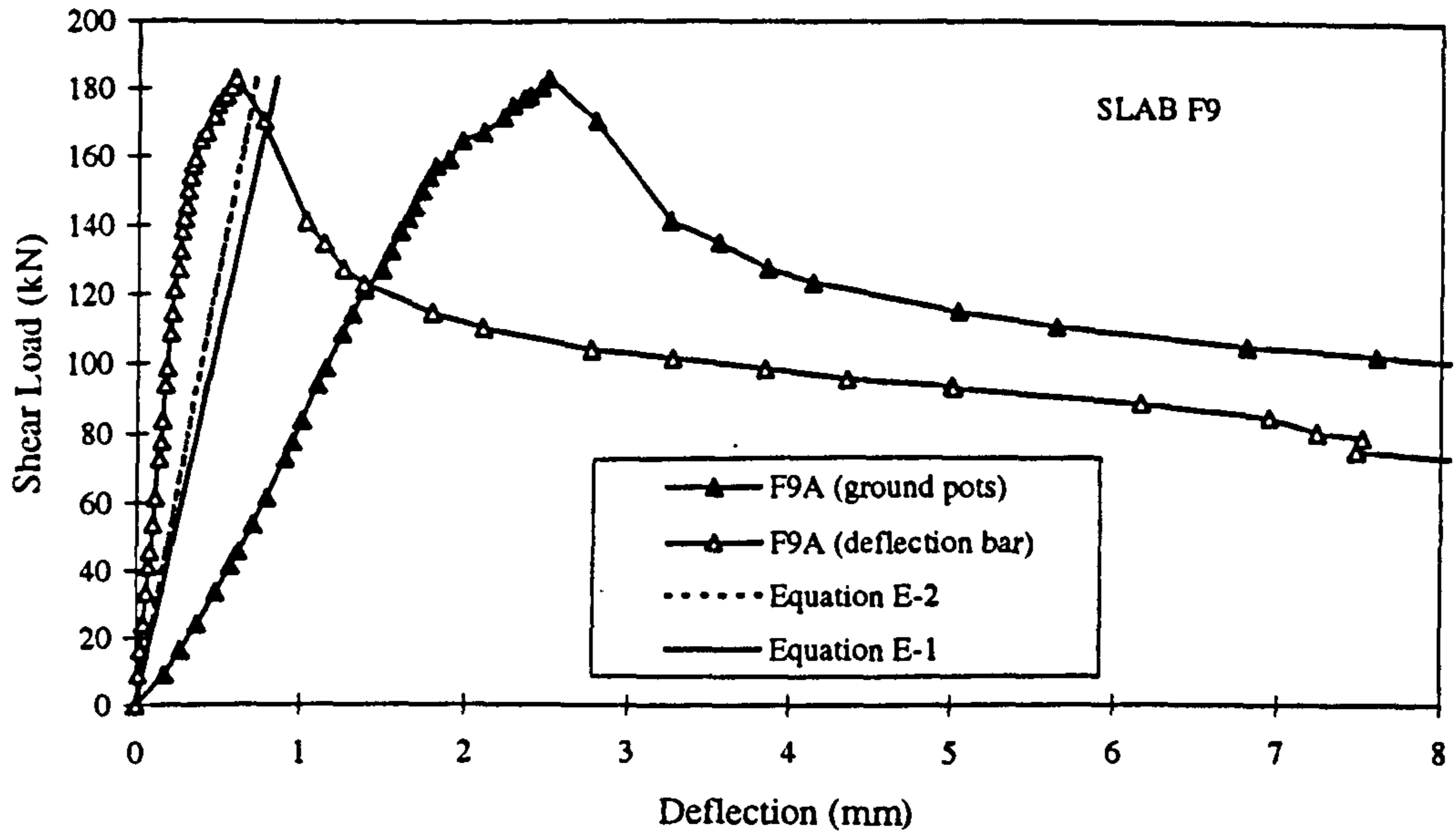


Figure E-1 Theoretical shear load versus net deflection compared with experimentally obtained results

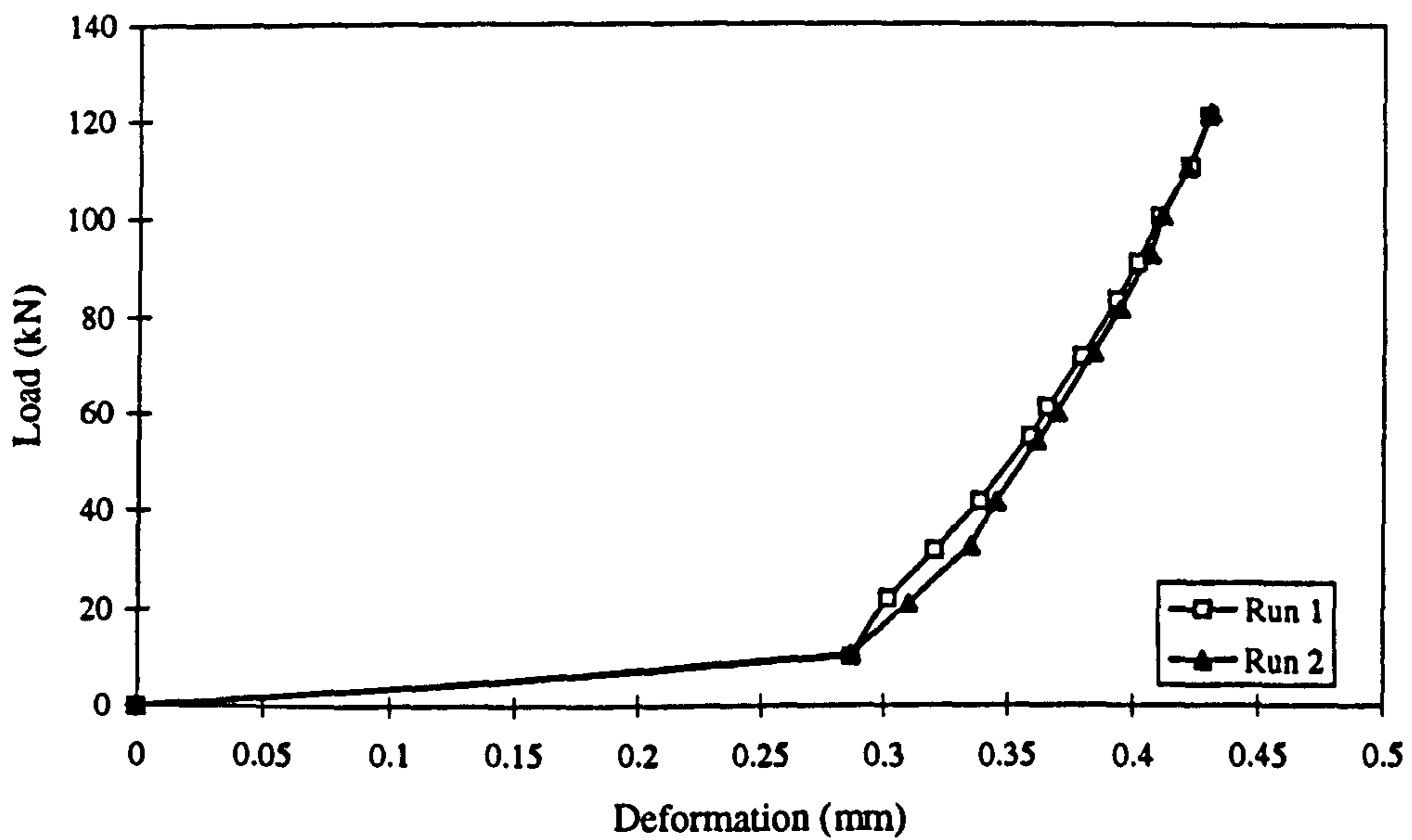


Figure E-2 Settlement of bearing plate under load

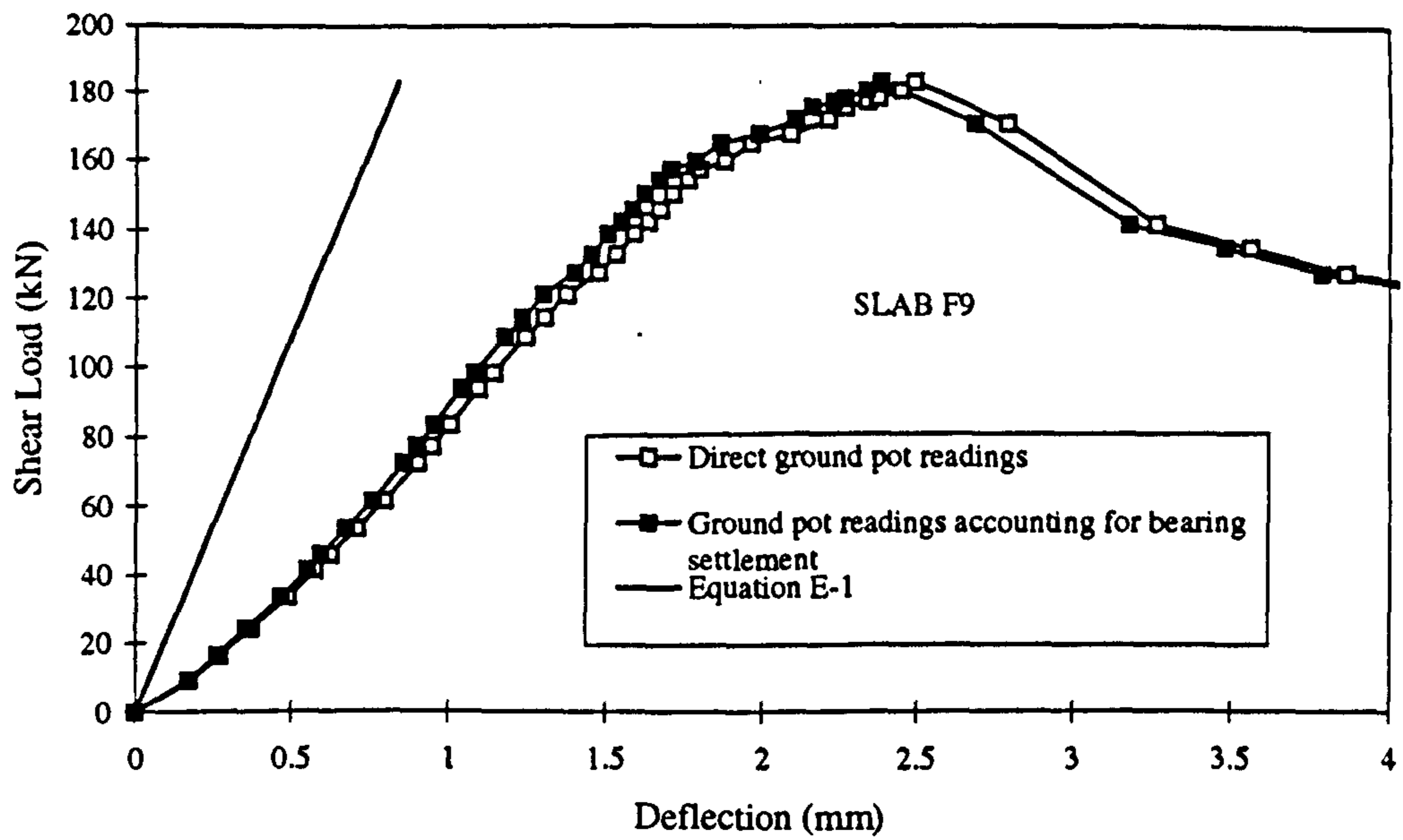


Figure E-3 Effect of bearing settlement on ground linear potentiometer readings

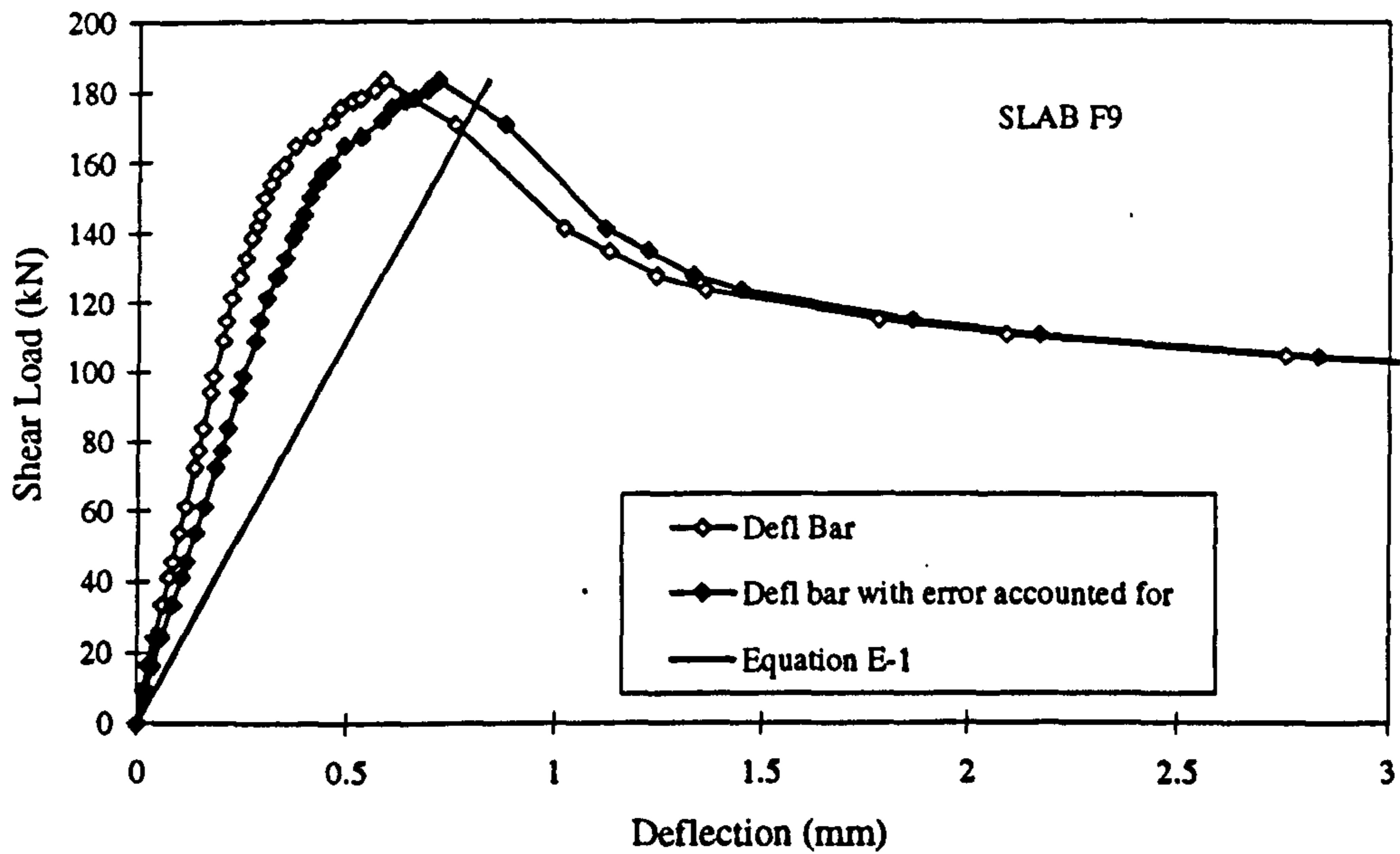
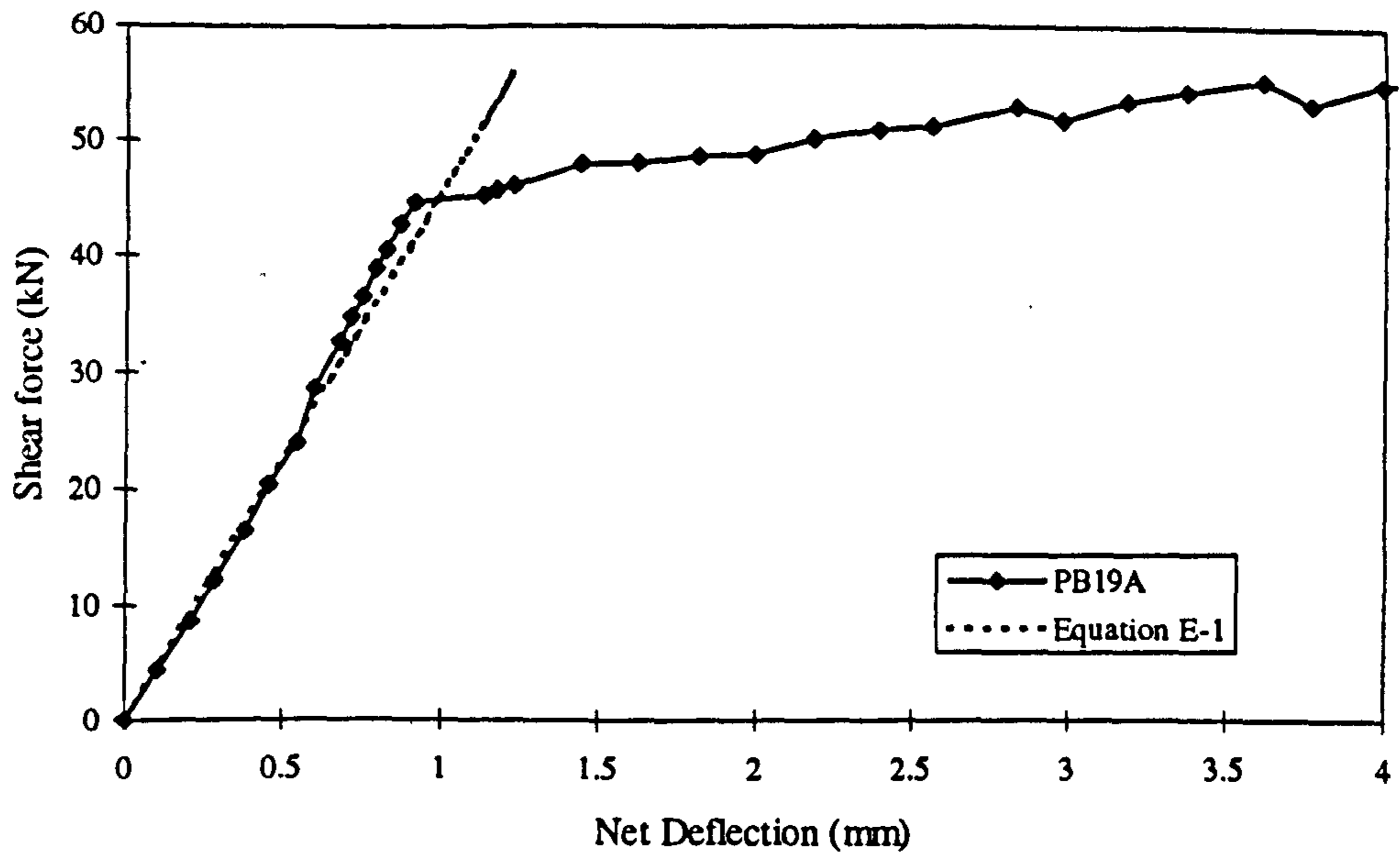


Figure E-4 Theoretical error associated with deflection bar readings



**Figure E-5 Comparison of Equation E-1 with experimentally obtained deflection using ground LPs and LPs above beam**

## APPENDIX F

### LOAD TEST ON SPREADER BEAM

Comparison of the shear strengths obtained in the full-width shear tests on hollow core slabs and the shear tests on single webs, suggested that there was not an even distribution of load across the width. This appendix describes a test performed on the spreader beam used in these full-width slab tests to analyse the degree of load distribution across the width of the slab.

The test was set-up with three 10 mm strain gauges attached to the beam. Two of the strain gauges (SG1 and SG3) were attached at a distance of 100 mm from the edge of the beam, which corresponds to a distance of 75 mm from the edge of the slab. The third strain gauge (SG2) was attached 30 mm from the centre line of the beam. All three strain gauges were placed at the mid height of the beam. Figure F-1 shows the strain readings for each of the strain gauges against load, showing a clear linear relationship. Both of the edge strain gauges show similar readings, whilst SG2 shows greater strains for the same load.

The distribution of these strain readings were analysed by fitting two possible strain distributions (triangular or parabolic) to the data points. Figure F-2 shows the parabolic stress distribution at a load of 100 kN with the maximum strain at the centre point of the beam. It can be seen that the maximum strain at the centre is approximately 1.18 times greater than the average strain across the section. Using a triangular strain distribution, the maximum strain is about 1.27 times greater than the average. The results of the QSE grillage analysis on the eccentrically loaded beams suggests that the parabolic distribution is probably the most accurate.

It can be concluded that the average cracking shear load measured in each of the shear tests on plain and FRC hollow core slabs is about 85% of the shear force which causes cracking in the slabs.

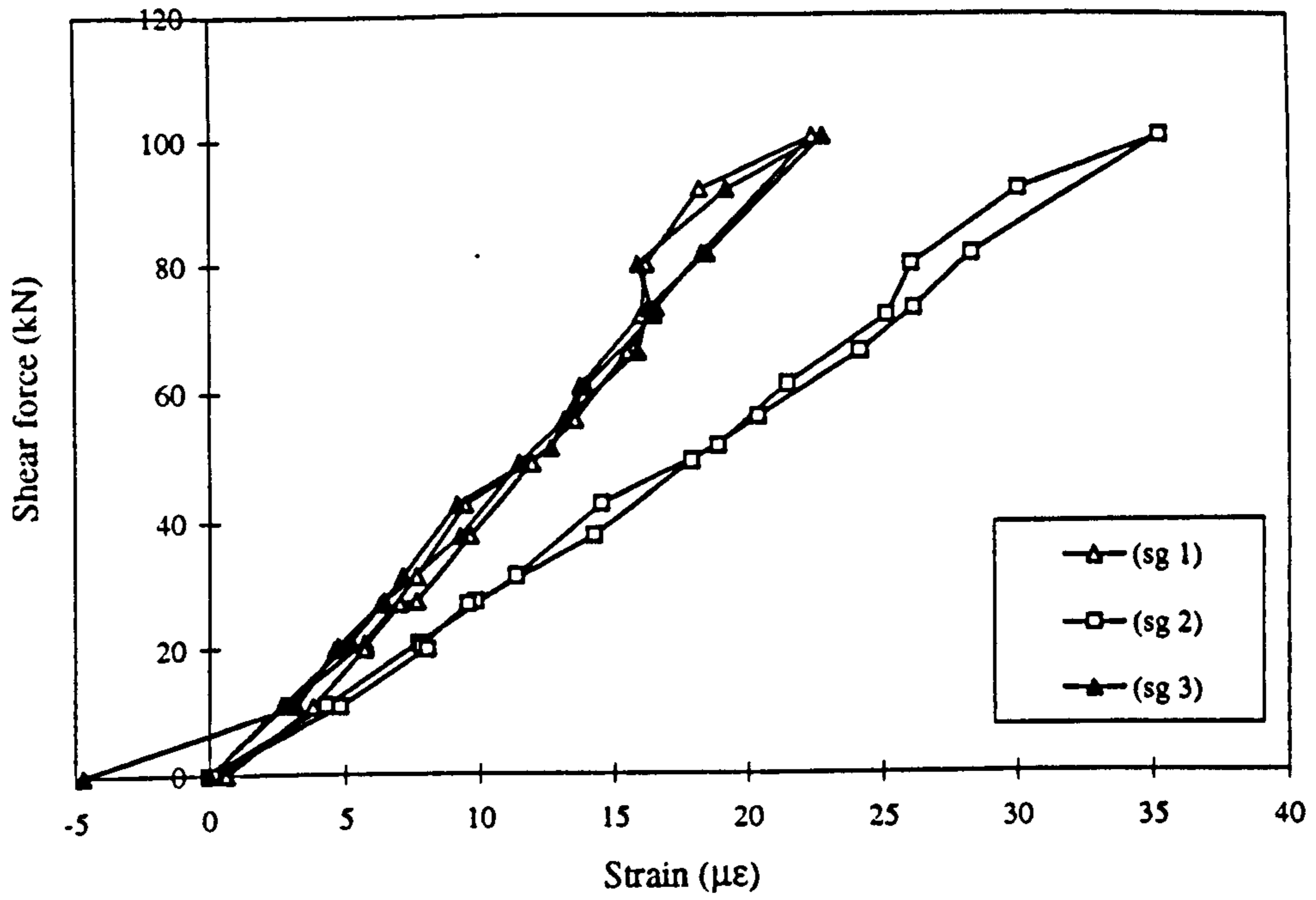


Figure F-1 Load v strain

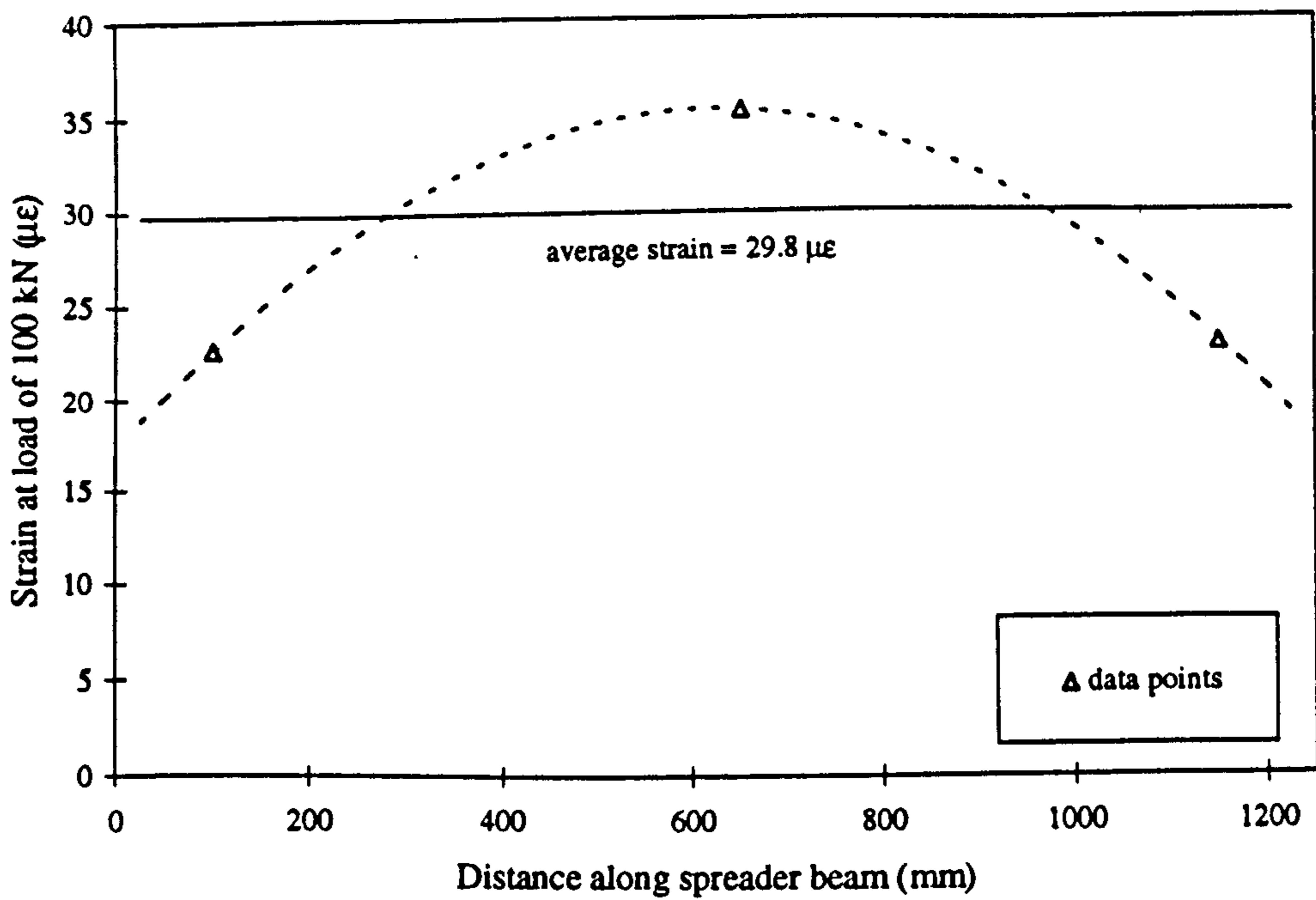


Figure F-2 Parabolic distribution of strain across the width of the beam at  $W = 100$  kN.